AD-A251 237



2

PL-TR-92-2059
SPECIAL REPORTS, NO. 267

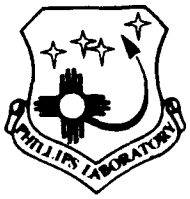
PROCEEDINGS OF THE 14TH ANNUAL REVIEW CONFERENCE ON ATMOSPHERIC TRANSMISSION MODELS, 11-12 JUNE 1991

EDITORS:
L. W. ABREU
F. X. KNEIZYS

DTIC
ELECTE
MAY 20 1992
S B D

26 FEBRUARY 1992

APPROVED FOR PUBLIC RELEASE; DISTRIBUTION UNLIMITED



PHILLIPS LABORATORY
AIR FORCE SYSTEMS COMMAND
HANSCOM AIR FORCE BASE, MASSACHUSETTS 01731-5000

92-13361



92 5 19 030

"This technical report has been reviewed and is approved for publication"

WILLIAM A. BLUMBERG, Chief
Simulation Branch
Optical Environment Division

ALAN D. BLACKBURN, Col, USAF, Director
Optical Environment Division

This report has been reviewed by the ESD Public Affairs Office (PA) and is releasable to the National Technical Information Service (NTIS).

Qualified requestors may obtain additional copies from the Defense Technical Information Center. All others should apply to the National Technical Information Service.

If your address has changed, or if you wish to be removed form the mailing list, or if the addressee is no longer employed by your organization, please notify GL/TSI, Hanscom AFB, MA 01731-5000. This will assist us in maintaining a current mailing list.

Do not return copies of this report unless contractual obligations or notices on a specific document requires that it be returned.

UNCLASSIFIED
SECURITY CLASSIFICATION OF THIS PAGE

REPORT DOCUMENTATION PAGE

Form Approved OMB No. 0704-0188

1a. REPORT SECURITY CLASSIFICATION UNCLASSIFIED	1b. RESTRICTIVE MARKINGS
2a. SECURITY CLASSIFICATION AUTHORITY	3. DISTRIBUTION / AVAILABILITY OF REPORT Approved for public release; distribution unlimited
2b. DECLASSIFICATION / DOWNGRADING SCHEDULE	
4. PERFORMING ORGANIZATION REPORT NUMBER(S) PL-TR-92-2059 SR, No. 267	5. MONITORING ORGANIZATION REPORT NUMBER(S)
6a. NAME OF PERFORMING ORGANIZATION Phillips Laboratory 6b. OFFICE SYMBOL (*If applicable*) GPO	7a. NAME OF MONITORING ORGANIZATION
6c. ADDRESS (*City, State, and ZIP Code*) Hanscom AFB, MA 01731-5000	7b. ADDRESS (*City, State, and ZIP Code*)
8a. NAME OF FUNDING / SPONSORING ORGANIZATION 8b. OFFICE SYMBOL (*If applicable*)	9. PROCUREMENT INSTRUMENT IDENTIFICATION NUMBER
8c. ADDRESS (*City, State, and ZIP Code*)	10. SOURCE OF FUNDING NUMBERS PROGRAM ELEMENT NO. 62101F; PROJECT NO. 7670; TASK NO 09; WORK UNIT ACCESSION NO. 10
11. TITLE (*Include Security Classification*) Proceedings of the 14th Annual Review Conference on Atmospheric Transmission Models.	
12. PERSONAL AUTHOR(S) L.W. Abreu and F.X. Kneizys	
13a. TYPE OF REPORT Reprint 13b. TIME COVERED FROM _____ TO _____	14. DATE OF REPORT (*Year, Month, Day*) 1992 February 26 15. PAGE COUNT 497
16. SUPPLEMENTARY NOTATION	
17. COSATI CODES FIELD / GROUP / SUB-GROUP	18. SUBJECT TERMS (*Continue on reverse if necessary and identify by block number*) Atmospheric Transmittance; Aerosols; Atmospheric Propagation; Clouds; Radiative Transfer; Optical Turbulence; Molecular Absorption; Ultraviolet; Visible; Infrared; Spectroscopy.

19. ABSTRACT (*Continue on reverse if necessary and identify by block number*)

Contains the viewgraphs and other materials for the 42 papers presented at the Fourteenth Annual Review Conference on Atmospheric Transmission Models held at the Geophysics Directorate, Phillips Laboratory (AFSC), Hanscom AFB, MA 11-12 June 1991

20. DISTRIBUTION / AVAILABILITY OF ABSTRACT ☒ UNCLASSIFIED/UNLIMITED ☐ SAME AS RPT. ☐ DTIC USERS	21. ABSTRACT SECURITY CLASSIFICATION UNCLASSIFIED
22a. NAME OF RESPONSIBLE INDIVIDUAL LEONARD W. ABREU	22b. TELEPHONE (*Include Area Code*) 617-377-2337 22c. OFFICE SYMBOL GPOS

DD Form 1473, JUN 86 *Previous editions are obsolete.*

SECURITY CLASSIFICATION OF THIS PAGE
UNCLASSIFIED

Contents

Introduction vii

Keynote viii

Session on Aerosols and Clouds

Summary of Session 1 1

"Boundary Layer Illumination Radiation Balance Model: BLIRB"
A. Zardecki 2

"Relations Between Giant Aerosols Near the Surface and Solar Aureole Brightness"
F.E. Volz 14

"The Computation of Radiative Transfer Through the Atmosphere Incorporating Various Aerosol Scenarios"
L.C. Rosen 17

"BACKSCAT Lidar Backscatter Simulation: Version 2.0"
J.R. Hummel, D.R. Longtin, N.L. Paul, J.R. Jones 28

"Cirrus Cloud Transmission Modelling"
W.M. Cornette, J.G. Shanks 34

"ICE-CLOUD - A Model for IR Transmittance Through Cirrus Cloud"
W.T. Kreiss, R. Vik 47

"The Status of the Navy Oceanic Vertical Aerosol Model"
S. Gathman 54

Session on Atmospheric Propagation Models

Summary of Session 2 61

"MODTRAN/LOWTRAN: Current Status, Future Plans"
L.W. Abreu, F.X. Kneizys, G.P. Anderson, J.H. Chetwynd 64

"FASCODE3: An Update"
G.P. Anderson, F.X. Kneizys, J.H. Chetwynd, L.W. Abreu, M. Hoke, S.A. Clough, R.D. Worsham, E.P. Shettle 73

"EOSAEL92"
A.E. Wetmore 86

"HITRAN'91: The Contemporary Spectroscopic Molecular Database"
L.S. Rothman 98

"SHARC, An Atmospheric Radiation and Transmittance Code for Altitudes from 50 to 300 km"
D. Robertson, L. Bernstein, J. Duff, J. Gruninger, R. Sundberg ,
R. Sharma, R. Healey 107

"Recent Developments of the GENLN2 Line-by-Line Model: Studies in Support of the UARS Project"
D.P. Edwards 119

"Present Status of Transmittances and Radiances Modelling at L.M.D."
N.A. Scott, A. Chédin, F. Chéruy, B. Tournier 129

"AURIC (Atmospheric Ultraviolet Radiance Integrated Code): an Update"
R. Huguenin, R. Hickey, K. Minschwaner, G.P. Anderson, L.A. Hall, R.E Huffman 130

"Ontar's PC Compatible LOWTRAN Package"
J. Schroeder, P. Noah 143

"Coupling Atmosphere and Background Effects"
W.M. Cornette 152

"SENTRAN7: A Sensitivity Analysis Package for LOWTRAN7 and MODTRAN"
D.R. Longtin, F.M. Pagliughi, N.L. Paul 165

"Atmospheric Models in the Strategic Scene Generation Model"
W.M. Cornette, D.C. Anding 173

"Review of the Chemical Kinetic Rate Constants Used in the SHARC Model"
V.I. Lang, A.T. Pritt, Jr. 188

Session on Measurements and Models

Summary of Session 3 200

"Atmospheric Ultraviolet Radiance and its Variations"
R. Link, D.J. Strickland D.E. Anderson, Jr. 202

"Photoabsorption Cross Sections in the Transmission Window Regions of the Schumann-Runge Bands of Oxygen"
K. Yoshino, J.R. Esmond, D.E. Freeman, W.H. Parkinson, A.S-C. Cheung 203

"Incorporation of LOWTRAN7 into the ACQUIRE Model"
S.G. O'Brien 211

"High-resolution Spectral Measurements of Upwelling and Downwelling Atmospheric Infrared Emission with Michelson Interferometers"
H.E. Revercomb 215

"Validation of HIS Spectral Measurements with the FASCODE Line-by-Line Model"
S.A. Clough, R.D. Worsham, W.L. Smith, H.E. Revercomb, R.O. Knuteson,
H.M. Woolf, G.P. Anderson, M.L. Hoke, F.X. Kneizys, M.V. Wagner, R.M. Goody 231

"Improved HNO_3 Band Model Parameters"
N. Jones, A. Goldman, D. Murcray, F. Murcray, W. Williams 242

"Line-by-line Calculations of Atmospheric Fluxes and Heating Rates"
S.A. Clough, M.J. Iacono, J.-L. Moncet 249

"Comparison of FASCOD2 and LOWTRAN7 Models with FIT Spectral Transmittance Measurements in the 3-12μm Region"
J.M. Thériault 263

"Spectral Solar Radiation Modeling, Measurement, and Data Base Activities at the Solar Energy Research Institute"
C.J. Riordan, R.L. Hulstrom 276

"LOWTRAN 7 Comparisons with Field Measurements"
R. Smith, N. McNabb, K. Hammerdorfer, T. Corbin 282

"Spectral Smoothing in the Fourier Domain: A Software Package for Line-by-Line Calculations"
W. Gallery, M. Esplin 314

"A Comparison of Computational Approaches for the Voigt Function"
F. Schreier 320

Topical Session on Spectral Line Shapes

Summary of Session 4 329

"Basis of the Water Vapor Continuum Coefficients in the GL Models"
S.A. Clough 333

"Water Vapor Continuum Absorption Measurements with Line Shape Interpretations"
M. Thomas 341

"Line Coupling for Microwave Oxygen Lines"
P.W. Rosenkranz 361

"Laboratory Measurements of Line Coupling in CO_2 and N_2O"
L.L. Strow 370

"Line Mixing: A Near Wing and Far Wing Problem"
J.-M. Hartmann 389

Contributed Papers

"Far-wing Lineshape Contribution to the Water Continuum in the Millimeter and Infrared Regions"
R.H. Tipping, Q. Ma 409

"Laboratory Measurements of the 60-GHz O_2 Spectrum in Air"
H.J. Liebe 419

"Line Coupling in Polar and Nonpolar Molecules"
A.S. Pine and J.P. Looney 429

"Study of CO_2 Blue Wing in the 4.1 μm Region"
C. Delaye, M. Thomas 441

"Theoretical Approach to the Line Wing Problem"
L. Sinitsa 449

Appendix

Call for Papers 457

Agenda 459

List of Attendees 465

Author Index 478

INTRODUCTION

The Fourteenth DoD Tri-Service Review Conference on Atmospheric Transmission Models was held at the Geophysics Directorate, Hanscom AFB, Massachusetts on 11-12 June 1991. The purpose of the meeting was to review progress in the modeling of radiation propagating through the earth's atmosphere, identify deficiencies in these models, and make recommendations for improvements.

Approximately 140 scientists and engineers, representing DoD, other government agencies, industry, and the academic community were in attendance. The agenda consisted of forty two papers with sessions on aerosols and clouds, atmospheric propagation models, measurements and models and an extended Topical session on spectral line shapes hosted by Michael L. Hoke which included invited papers and contributed papers.

This proceedings volume summarizes the technical presentations at the conference. The main part of the report consists of the abstracts and copies of the viewgraphs or slides and other material as provided by the authors for the presentations. Preceding the viewgraphs for each session is a commentary prepared by the co-chairpersons on each presentation within that session. The Appendix includes the original call for papers and invitation to the meeting, a copy of the Agenda for the meeting, a list of the attendees, and an author index.

A special thanks is extended to Ronald G. Isaacs, Betty Stenhouse and Atmospheric and Environmental Research, Inc.

Francis X. Kneizys
Leonard W. Abreu



Accession For
NTIS GRA&I ☑
DTIC TAB ☐
Unannounced ☐
Justification
By
Distribution/
Availability Codes
Dist | Avail and/or Special
A-1

KEYNOTE: Col. Grant Aufderhaar
USAF (OUSDA)
Pentagon
Washington, DC

DEFENSE CRITICAL TECHNOLOGIES PLAN

SUBMITTED ANNUALLY BY THE

DEPARTMENT OF DEFENSE

IN CONSULTATION WITH THE

DEPARTMENT OF ENERGY

TO THE

COMMITTEES ON ARMED SERVICES
UNITED STATES CONGRESS

CRITICAL TECHNOLOGIES PLAN

HISTORICAL CONTEXT

- QUALITATIVE SUPERIORITY PROVIDES UNDERPINNING TO NATIONAL SECURITY
- U.S. SUCCESSFUL IN DOING SO FOR FORTY YEARS (B-52, MINUTEMAN, POLARIS, U-2, AIRCRAFT TURBINES, SENSORS, ACCURACY IN TARGETING, SATELLITES, ETC.)

RECENT TRENDS

- DECLINE IN FUNDING FOR TECHNOLOGY BASE SINCE 1965:
  - — FEWER $ FOR BUDGET CATEGORIES 6.1, 6.2, 6.3A

CONSEQUENCES

- U.S. TECHNOLOGY BASE IS RUSTING
  - — CONSISTS OF 80's RESEARCH AND EARLY 80's TECHNOLOGY
- RADICALLY NEW CONCEPTS ARE DIFFICULT TO IMPLEMENT
  - — REGARDLESS OF MERIT
  - — NOT ENOUGH $ TO DEMONSTRATE NEW TECHNOLOGIES
- EXPECTATIONS ARE UNSUSTAINABLE

8231/32190/LY

CRITICAL TECHNOLOGIES PLAN

DEFENSE PLANNING GUIDANCE REQUIRES CONTINUED QUALITATIVE SUPERIORITY ...

... AND CONTINUED QUALITATIVE SUPERIORITY REQUIRES ARRESTING EROSION OF THE TECHNOLOGY BASE THROUGH:

- CLEAR REALISTIC LONG-TERM GOALS
- A HEALTHY INFRASTRUCTURE
- ADEQUATE RESOURCES
  - — TO DEVELOP NEW TECHNOLOGIES (6.1, 6.2)
  - — TO DEMONSTRATE NEW SYSTEMS CAPABILITY USING NEW TECHNOLOGIES (6.3A)
- AN EFFICIENT MECHANISM FOR TURNING CONCEPTS INTO SYSTEMS
  - — THAT ARE CAPABLE OF MEETING THE LONG-TERM GOALS

B231/321604 V

CRITICAL TECHNOLOGIES PLAN

CONGRESSIONAL MANDATE

- PL 101-189

"THE SECRETARY OF DEFENSE ... SHALL SUBMIT ... AN ANNUAL PLAN FOR DEVELOPING THE TECHNOLOGIES CONSIDERED ... MOST CRITICAL TO INSURING THE LONG-TERM QUALITATIVE SUPERIORITY OF UNITED STATES WEAPON SYSTEMS."

B231/321604.Y

CRITICAL TECHNOLOGIES PLAN

PRINCIPAL FEATURES OF THE PLAN

- LINKS CRITICAL TECHNOLOGIES TO DOD SCIENCE AND TECHNOLOGY STRATEGY
- SELECTS 20 CRITICAL TECHNOLOGIES
- PRIORITIZES THEM
- PROVIDES FUNDING ESTIMATES
- INDICATES MILESTONES TO 2005
- PROVIDES INTERNATIONAL COMPARISONS
- INCLUDES INDUSTRIAL BASE AND MANUFACTURING ISSUES

S231/32190/LY

CRITICAL TECHNOLOGIES PLAN

ADDITIONAL CONSIDERATIONS FOR THE FY 1990 PLAN

- BROADER CONGRESSIONAL TASKING
- INCREASED DISCUSSION OF MANUFACTURING ISSUES
- NEW SELECTION CRITERIA
  - — (INCLUDES: STRENGTHENING THE INDUSTRIAL BASE)
- FUNDING SHOWN OVER A DECADE (NOT JUST ONE YEAR)
- CRITICAL TECHNOLOGIES PRIORITIZED
- INTELLECTUAL CONSOLIDATION OF SOME CRITICAL TECHNOLOGIES
  - — EMPHASIZING *TECHNOLOGY* RATHER THAN *NEED*
  - — COMBINING CLOSELY RELATED TECHNOLOGIES

S231/32190/LY

ADDITIONAL REQUIREMENT FOR THE 1991 PLAN,
AS AMENDED IN
THE NATIONAL DEFENSE AUTHORIZATION ACT
FOR FY 1991 AND 1992, PL 101-510

"SEC.801. ANNUAL DEFENSE CRITICAL TECHNOLOGIES PLAN

(A) INCREASED INFORMATION RELATING TO FUNDING ...

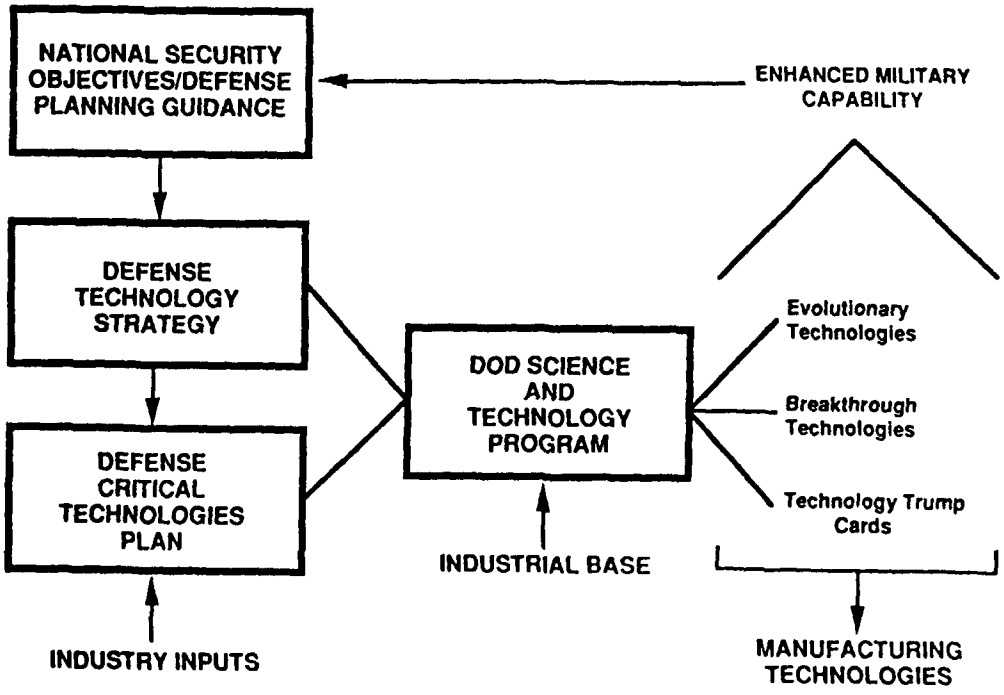
(3) IDENTIFY EACH PROGRAM ELEMENT ...

FOR WHICH FUNDS ARE BUDGETED FOR
THE SUPPORT OF THE DEVELOPMENT
OF ANY CRITICAL TECHNOLOGY IDENTIFIED
IN THE PLAN; AND

(4) FOR EACH SUCH ELEMENT --

(A) SPECIFY THE AMOUNT [IN FY92] INCLUDED
FOR EACH CRITICAL TECHNOLOGY COVERED
BY THE PROGRAM ELEMENT ... [AND
COMPARE] ... WITH THE AMOUNT ... FOR
THE [PRECEDING] FISCAL YEAR [FY91]..."

DEFENSE TECHNOLOGY STRATEGY AND PLANNING



CRITICAL TECHNOLOGIES PLAN

THE PARTICIPANTS

STEERING COMMITTEE: SENIOR S&T MANAGERS FROM DOD, SERVICES, DOE

WORKING GROUP: OSD (CHAIRMANSHIP)
ARMY
NAVY
AIR FORCE
DARPA
DIA
DNA
SDIO
JCS

DOE HEADQUARTERS

DOE NATIONAL LABORATORIES:
LAWRENCE LIVERMORE
LOS ALAMOS
SANDIA

9231/32199/LY

CRITICAL TECHNOLOGIES PLAN

SUBJECTS ADDRESSED IN THE REPORT

- DESCRIPTION OF THE TECHNOLOGY
- PAYOFF
- S&T PROGRAMS
- RELATED MANUFACTURING CAPABILITY
- R&D IN THE UNITED STATES
- INTERNATIONAL ASSESSMENT

9231/32199/LY

LIST OF DEFENSE CRITICAL TECHNOLOGIES

- SEMICONDUCTOR MATERIALS AND MICROELECTRONIC CIRCUITS
- SOFTWARE PRODUCIBILITY
- PARALLEL COMPUTER ARCHITECTURES
- MACHINE INTELLIGENCE/ROBOTICS
- SIMULATION AND MODELING
- PHOTONICS
- SENSITIVE RADARS
- PASSIVE SENSORS
- SIGNAL PROCESSING
- SIGNATURE CONTROL
- WEAPON SYSTEM ENVIRONMENT
- DATA FUSION
- COMPUTATIONAL FLUID DYNAMICS
- AIR-BREATHING PROPULSION
- PULSED POWER
- HYPERVELOCITY PROJECTILES
- HIGH ENERGY DENSITY MATERIALS
- COMPOSITE MATERIALS
- SUPERCONDUCTIVITY
- BIOTECHNOLOGY MATERIALS AND PROCESSES
- FLEXIBLE MANUFACTURING

Technologies not *in priority order*

CRITICAL TECHNOLOGIES PLAN

TECHNOLOGY OBJECTIVES

- SEMICONDUCTOR MATERIALS AND MICROELECTRONIC CIRCUITS:
  - — HIGH-SPEED COMPUTING AND SIGNAL PROCESSING, AUTOMATIC CONTROL, SENSITIVE RECEIVERS, MILLIMETER WAVE RADAR, PHOTONICS
- SOFTWARE PRODUCIBILITY:
  - — AFFORDABLE, TRUSTED SOFTWARE, AUTOMATIC SOFTWARE GENERATION, REUSABLE SOFTWARE
- PARALLEL COMPUTER ARCHITECTURES:
  - — ULTRA-HIGH-SPEED COMPUTING
- MACHINE INTELLIGENCE AND ROBOTICS:
  - — BUILD HUMAN INTELLIGENCE INTO MECHANICAL DEVICES, MANUFACTURING, MAINTENANCE
- SIMULATION AND MODELING:
  - — TESTING CONCEPTS AND DESIGNS WITHOUT EXPENSIVE REPLICAS, TRAINING FOR COMPLEX MILITARY SCENARIOS
- PHOTONICS:
  - — ULTRA-HIGH-DENSITY MEMORIES AND HIGH-VOLUME, HIGH-SPEED INFORMATION PROCESING
- SENSITIVE RADARS:
  - — NON-COOPERATIVE TARGET IDENTIFICATION, DETECTION OF LOW-OBSERVABLE TARGETS

8231/221995LY

CRITICAL TECHNOLOGIES PLAN

TECHNOLOGY OBJECTIVES (CONT.)

- PASSIVE SENSORS:
  - — SILENT SENSING OF TARGETS OR ENVIRONMENT, MONITORING EQUIPMENT (CONDITION SENSING)
- SIGNAL PROCESSING:
  - — PROCESSING SIGNALS FOR INFORMATION EXTRACTION, AUTOMATIC TARGET DETECTION/TRACKING/CLASSIFICATION/RECOGNITION
- SIGNATURE CONTROL:
  - — CONTROLLING PLATFORM OR WEAPON SIGNATURES (RADAR, OPTICAL, ACOUSTIC, ETC.) TO ENHANCE THEIR SURVIVABILITY
- WEAPON SYSTEM ENVIRONMENT:
  - — UNDERSTANDING OR PREDICTING THE BEHAVIOR OF THE ENVIRONMENT TO ENHANCE WEAPON EFFECTIVENESS
- DATA FUSION:
  - — COMBINING AND INTERPRETING DATA FROM SEVERAL SOURCES AND PRESENTING IT IN A CONVENIENT FORM TO THE HUMAN OPERATOR
- COMPUTATIONAL FLUID DYNAMICS:
  - — MODELING OF COMPLEX FLUID FLOW TO MAKE DEPENDABLE PREDICTIONS BY COMPUTING, THUS OBVIATING EXPENSIVE FACILITIES AND EXPERIMENTS

8231/32190/LY

CRITICAL TECHNOLOGIES PLAN

TECHNOLOGY OBJECTIVES (CONT.)

- AIR BREATHING PROPULSION:
  - — LIGHT-WEIGHT, FUEL EFFICIENT ENGINES
- PULSED POWER:
  - — COMPACT, LIGHT-WEIGHT, LOW-VOLUME DEVICES FOR HIGH-POWER MICROWAVES, HIGH-ENERGY LASERS, ELECTROTHERMAL GUNS, RADARS, ELECTROMAGNETIC LAUNCHERS, PARTICLE BEAMS
- HYPERVELOCITY PROJECTILES:
  - — TO PENETRATE HARDENED TARGETS
- HIGH ENERGY DENSITY MATERIALS:
  - — SAFE, TRANSPORTABLE, EFFICIENT ENERGETIC MATERIALS FOR EXPLOSIVES AND PROPELLANTS
- COMPOSITE MATERIALS:
  - — HIGH-TEMPERATURE, HIGH-STRENGTH, LIGHT-WEIGHT COMPOSITE MATERIALS FOR AEROSPACE APPLICATIONS
- SUPERCONDUCTIVITY:
  - — FABRICATION AND EXPLOITATION OF SUPERCONDUCTING MATERIALS
- BIOTECHNOLOGY:
  - — SYSTEMATIC APPLICATION OF BIOLOGY IN MILITARY ENGINEERING OR MEDICINE

8231/32190/LY

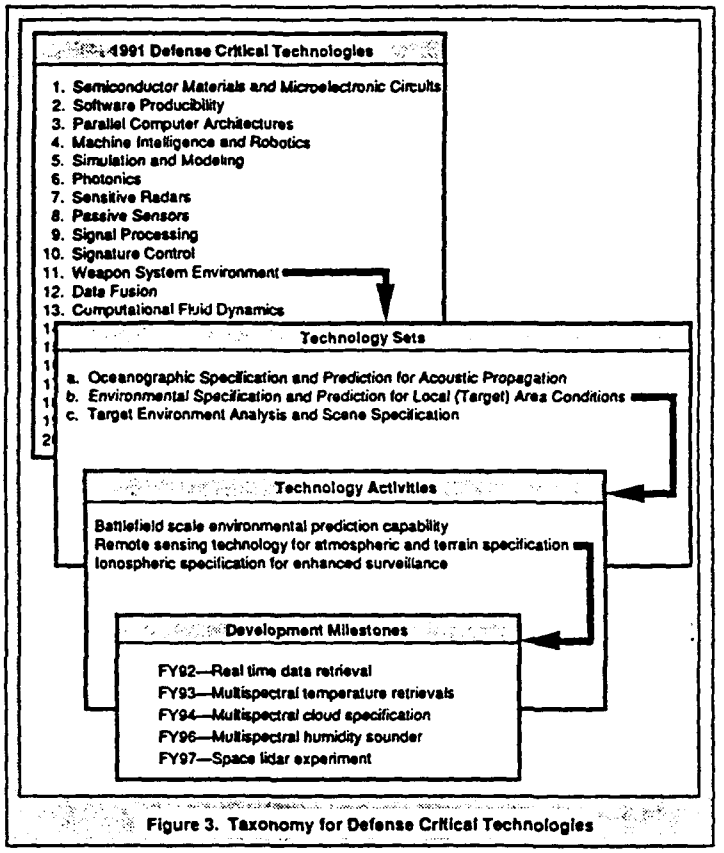


Figure 3. Taxonomy for Defense Critical Technologies

DEFENSE CRITICAL TECHNOLOGIES PRIORITIZED IN THREE GROUPS

(FY92 FUNDING ESTIMATES FOR S&T PROGRAMS IN $M)

A		B		C	
• COMPOSITE MATERIALS	$187	• AIR-BREATHING PROPULSION	$389	• BIOTECHNOLOGY	$ 40
• COMPUTATIONAL FLUID DYNAMICS	97	• MACHINE INTELLIGENCE AND ROBOTICS	151	• HIGH ENERGY DENSITY MATERIALS	86
• DATA FUSION	112	• PARALLEL COMPUTER ARCHITECTURES	169	• HYPERVELOCITY PROJECTILE	188
• PASSIVE SENSORS	528	• SENSITIVE RADARS	194	• PULSED POWER	83
• PHOTONICS	203	• SIGNATURE CONTROL	110	• SUPERCONDUCTIVITY	62
• SEMICONDUCTOR MATERIALS AND MICROELECTRONIC CIRCUITS	512	• SIMULATION AND MODELING	361		
• SIGNAL PROCESSING	245	• WEAPON SYSTEM ENVIRONMENT	393		
• SOFTWARE PRODUCIBILITY	185				

• FLEXIBLE MANUFACTURING

NOTE: TECHNOLOGIES ARE LISTED IN ALPHABETICAL ORDER WITHIN EACH GROUP.

CRITICAL TECHNOLOGIES PLAN

CAVEATS

- CRITICAL TECHNOLOGIES ARE NOT THE ONLY IMPORTANT TECHNOLOGIES
  - — THEY DO NOT EXIST IN ISOLATION
  - — THERE ARE OTHER IMPORTANT TECHNOLOGIES
  - — WHICH ARE DESCRIBED IN THE DOD S&T STRATEGY
- THEY ARE NOT TO BE CONFUSED WITH THE
  - — "MILITARILY CRITICAL TECHNOLOGIES LIST" USED FOR EXPORT CONTROL PURPOSES
- FUNDING ESTIMATES ARE JUST THAT, NOT BUDGET NUMBERS
- PRIORITY GROUPINGS SHOULD NOT BE OVEREMPHASIZED

8231/22190/LY

CRITICAL TECHNOLOGIES PLAN

FOREIGN TECHNOLOGICAL CAPABILITIES

Critical Technologies	USSR	NATO Allies	Japan
1. Semiconductor Materials and Microelectric Circuits	▪	□□	□□□□
2. Software Producibility	▪	□□	□□
3. Parallel Computer Architectures	▪	□□	□□
4. Machine Intelligence and Robotics	▪	□□□	□□□□
5. Simulation and Modeling	▪	□□□	□□□
6. Photonics	▪▪	□□	□□□□
7. Sensitive Radars	▪	□□	□□
8. Passive Sensors	▪▪	□□	□□
9. Signal Processing	▪▪	□□	□□
10. Signature Control	▪▪	□□	□□

8231/22190/LY

CRITICAL TECHNOLOGIES PLAN

FOREIGN TECHNOLOGICAL CAPABILITIES (CONT.)

Critical Technologies	USSR	NATO Allies	Japan
11. Weapon System Environment			
12. Data Fusion			
13. Computational Fluid Dynamics			
14. Air-Breathing Propulsion			
15. Pulsed Power			
16. Hypervelocity Projectiles			
17. High Energy Density Materials			
18. Composite Materials			
19. Superconductivity			
20. Biotechnology Materials and Processes			

8231/32198/LY

CRITICAL TECHNOLOGIES PLAN

FOREIGN TECHNOLOGICAL CAPABILITIES (CONT.)

LEGEND:

POSITION OF THE USSR RELATIVE TO THE UNITED STATES		CAPABILITY OF OTHERS TO CONTRIBUTE TO THE TECHNOLOGY	
	Significant leads in some niches of technology		Significantly ahead in some niches of technology
	Generally on a par with the United States		Capable of making major contributions
	Generally lagging except in some areas		Capable of making some contributions
	Lagging in all important aspects		Unlikely to make any immediate contribution

8231/32198/LY

DEFENSE CRITICAL TECHNOLOGIES PLAN

TO OBTAIN A COPY OF THE REPORT:

COMPANIES, ASSOCIATIONS, PRIVATE INDIVIDUALS:	*CALL*	**202-697-5737**
REPORTERS, PRESS:	*CALL*	**202-695-0192**
U.S. GOVERNMENT:	*CALL*	**202-695-0552**

TO OBTAIN THE REPORT FROM **DTIC**, *REGISTERED USERS MAY*

CALL **202-274-7633** *AND REFERENCE "AD" NUMBER* **AD-A219 300**

Session 1

Summary of the Session on Aerosols and Clouds

The session on Aerosols and Clouds included 7 papers. The first paper by Zardecki (Science & Technology Corp.) described the Boundary Layer Illumination Radiation Balance (BLIRB) model, which they are developing for the Army Atmospheric Sciences Laboratory (ASL), in support of the BTI/SWOE program. The model will calculate the direct and scattered sunlight reaching the ground through an atmosphere containing a 3-dimensional distribution of clouds and aerosols. The model, which is based on a modified version of LOWTRAN, includes some interactions between individual clouds, such as partial shadowing of the direct sunlight by an adjacent cloud.

There were two papers on cirrus clouds. The first of these by Cornette & Shanks (Photon Research Associates) reviewed the literature on modeling transmission through cirrus clouds. It provided a reasonable summary of the current research work. Kreiss & Vik (Horizon Technology Inc.) described the ICECLOUD cirrus transmittance model they are developing for AF Wright Labs as part of the IASPM (IR Atmospherics & Signature Prediction Model) project. This model is largely based on the Liou, Heymsfield et al. model in Applied Optics last May and presented at this meeting two years ago.

There were several papers on atmospheric aerosols and their effects on radiation. Volz (PL) showed that his observations of the brightness of the solar aureole are well correlated with the presence of large dust and pollen particles (5 to 50 μm) in the atmosphere. This aureole brightness has shown a steady decrease over the past twelve years, implying a corresponding decrease in the large aerosol particles in the atmosphere.

Rosen (LLNL) presented preliminary results on modeling the sensitivity of radiation in the atmosphere to different aerosol conditions using LOWTRAN. This work is being done in support of DOE's Atmospheric Radiation Measurements (ARM) program.

Hummel et al. (SPARTA, Inc.) described version 2 of the Lidar backscatter simulation computer code they developed for PL/OPA, named BACKSCAT. This code is written to run stand alone on a PC using the standard LOWTRAN aerosol and cirrus models, which are built in, and external molecular absorption profiles for the lidar wavelength (such as calculated by FASCODE). However, the scientific portion was written in FORTRAN, so it could be easily modified to be directly incorporated into FASCODE, or to run on other computers.

Gathman (NOSC) described the current status of the Navy Ocean Vertical Aerosol Model (NOVAM). This model describes the vertical structure of the optical IR properties of the atmospheric aerosols in the boundary layer above the ocean surface. It uses as input,the surface meteorological conditions and radiosonde profiles. The version of the Navy aerosol model which is currently implemented in LOWTRAN effectively applies the surface values of the NOVAM optical/IR properties to the entire boundary layer.

BOUNDARY LAYER ILLUMINATION RADIATION BALANCE MODEL: BLIRB

A. Zardecki
Science and Technology Corporation, 555 Telshor Blvd., Suite 200,
Las Cruces, NM 88001

BLIRB provides direct and diffuse solar insolation at the earth's surface in the spectral range 0.4 to 12 μm. The model is an extension of LOWTRAN 7 to 3-D cloud and aerosol distributions in the lower 5 km of the atmosphere. The propagation of radiation through clouds is formulated by a variant of the adding method, supplemented by a stochastic ray tracing algorithm to model the penumbra effect. With a spectral resolution of 20 cm^{-1}, the spatial mesh can reach the size of 40X40X40 grid points in a physical volume whose extent is specified by the user. The full AFGL aerosol data base, including 40 boundary layer aerosol models, can be combined with six model atmospheres and five season-dependent visual range options. LOWTRAN 7 supplies the gaseous transmission to BLIRB, which offers four cloud options including cloud-free, horizontally homogeneous clouds, rectangular clouds, and a Cloud Scene Simulation prototype model developed by TASC.

Boundary Illumination Radiation Balance Model: BLIRB

A. Zardecki, R. Davis, B. Rappaport
Science & Technology Corporation
Las Cruces, New Mexico

A. Wetmore, J. Martin
Atmospheric Sciences Laboratory
White Sands Missile Range, NM

Annual Review Atmos. Transmission Models 1991

Boundary Illumination Radiation Balance Model: BLIRB

- Cloud Options
- Radiative transfer through 3-D clouds
- Atmospheric/aerosol data base
- Example of computation

BLIRB: Cloud Options

- Cloud-free, aerosol loaded atmosphere
- Horizontally homogeneous clouds: cloudiness
- Rectangular clouds: composition
- Clouds Scene Simulation Model - TASC

Science & Technology Corp

BLIRB: Radiative Transfer through 3-D Clouds

- Two-stream approximation: Coakley-Chylek 1975
- Doubling method for diffuse radiation
- IR radiation: average flux
- Stochastic ray tracing: penumbra effect

Science & Technology Corp

Two-Stream Approximation

Reflection and transmission functions

$$R(\mu) = \frac{(Q+1)(Q-1)[E - E^{-1}]}{(Q+1)^2 E - (Q-1)^2 E^{-1}}$$

$$\tilde{T}(\mu) = \frac{4Q}{(Q+1)^2 E - (Q-1)^2 E^{-1}}$$

where

$$E = exp(\alpha\tau/\mu)$$

$$Q = \frac{[1 - \omega_0 + 2\omega_0\beta(\mu)]^{1/2}}{[1 - \omega_0]^{1/2}}$$

$$\alpha = [1 - \omega_0 + 2\omega_0\beta(\mu)]^{1/2}[1 - \omega_0]^{1/2}$$

Adding Method, Lacis & Hansen 1974

Let

$$S = \frac{R_1 R_2}{1 - R_1 R_2}$$

then transmission & reflection between layers

$$D = T_1 + ST_1 + Se^{-\tau_1/\mu}$$

$$U = R_2 D + R_2 e^{-\tau_1/\mu}$$

Diffuse reflection and transmission

$$R_{12} = R_1 + e^{-\tau_1/\mu}U + T_1 U$$

$$T_{12} = e^{-\tau_2/\mu}D + T_2 e^{-\tau_1/\mu} + T_2 D$$

Monochromatic emissivity

$$\epsilon(\nu) = 1 - exp(-\sigma_a z),$$

Flux transmissivity

$$t_F(\nu) = \frac{\int_0^1 exp(-\sigma_a z/\mu)\,\mu\,d\mu}{\int_0^1 \mu\,d\mu}$$

$$t_F(\nu) = e^{-\tau_a}(1 - \tau_a) + \tau_a^2 E_1(\tau_a)$$

where

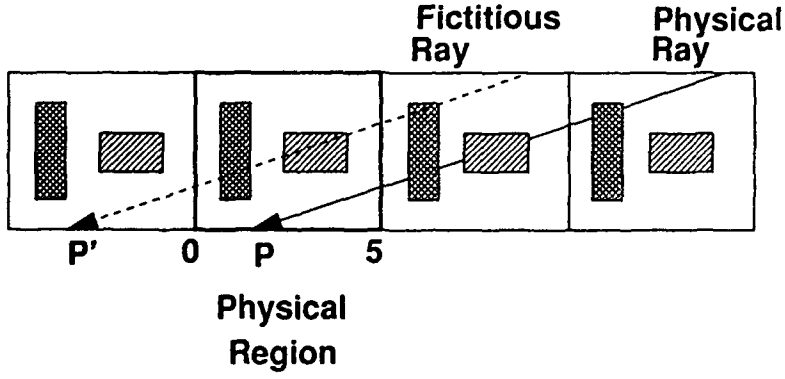
$$E_1(x) = \int_x^\infty s^{-1} exp(-s)\,ds$$

Average IR flux, w/o scattering

$$F\downarrow(\nu) = \int_{t_F}^1 B(\nu, T)\,dt_F$$

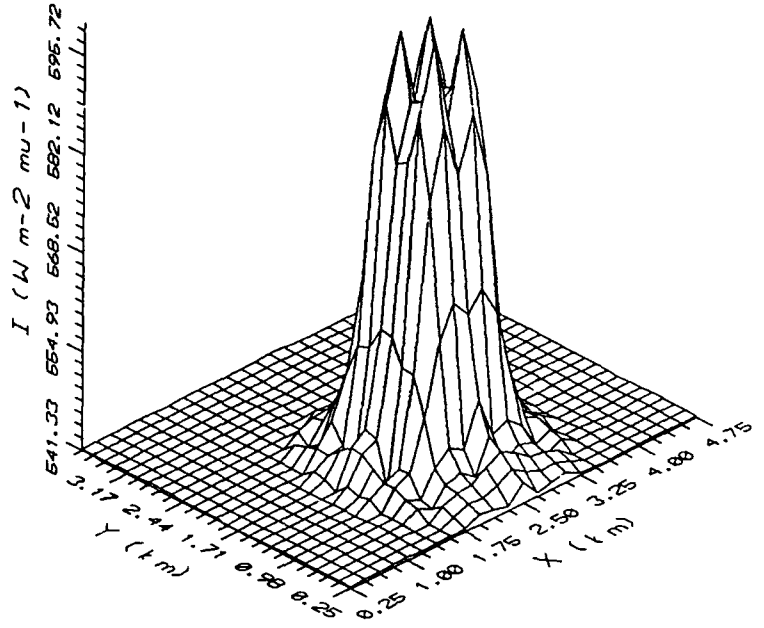
BLIRB: Stochastic Ray Tracing

- Random directions around the normal to earth's surface

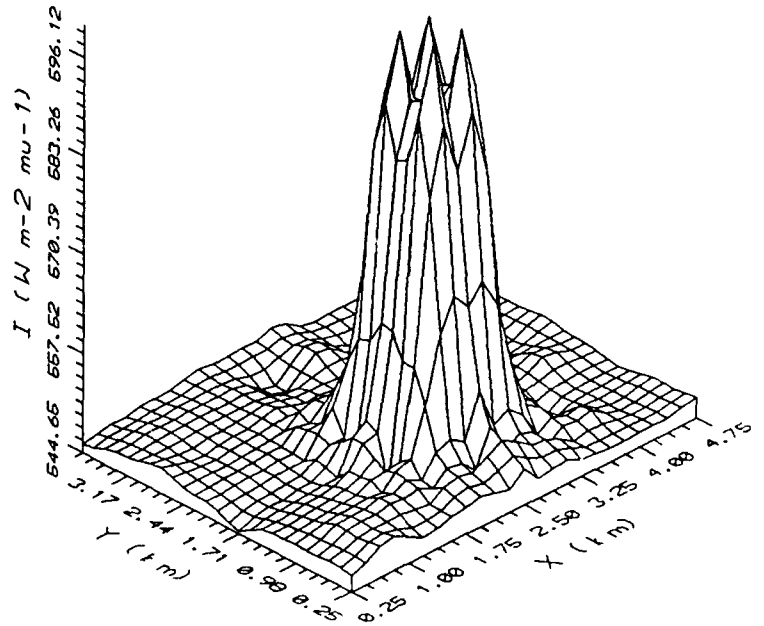


Science & Technology Corp

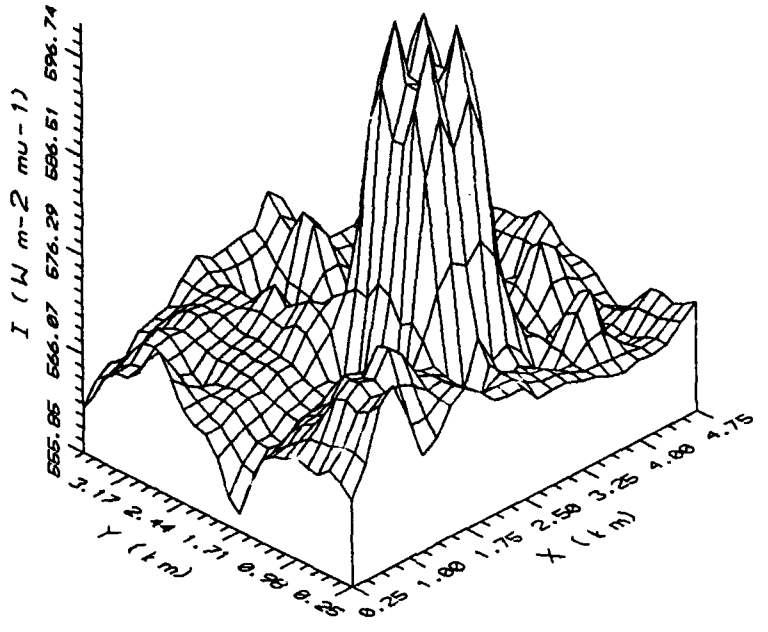
Angular Spread = 5 deg



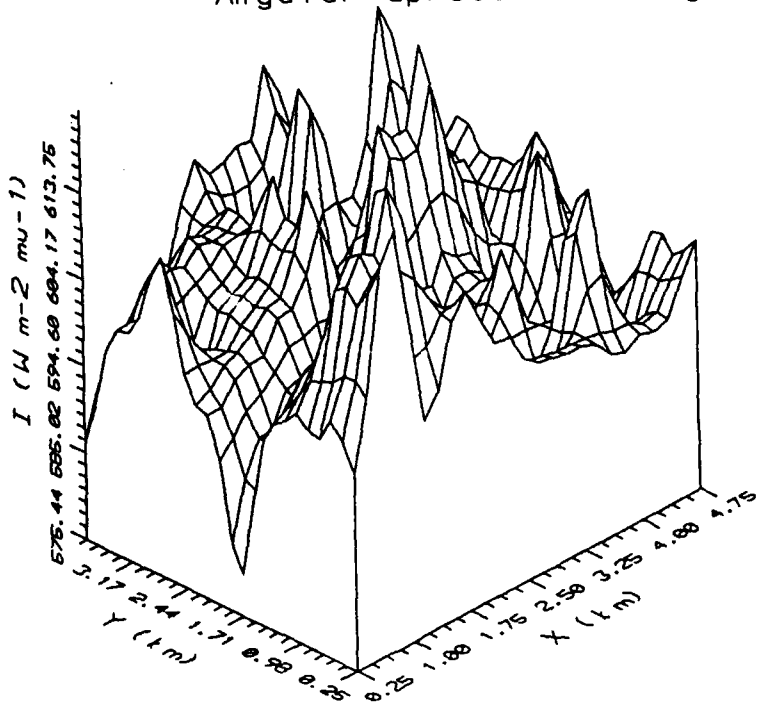
Angular Spread = 15 deg



Angular Spread = 30 deg



Angular Spread = 45 deg



BLIRB: AFGL Data Base

- Four layers with different aerosol types
- Rural, urban, maritime, tropospheric aerosols
- RH between 0 and 99%
- Only first two (up to 5km) layers used by BLIRB

Science & Technology Corp

BLIRB: Solar Radiation and Model Atmospheres

- Incident radiation: LOWTRAN 7/numerical fit
- Sky radiance - additional source
- Six temperature profiles
- Gaseous absorption from LOWTRAN 7

Science & Technology Corp

BLIRB: Rectangular Clouds

- Regions: ID and bounding coordinates
- Fine mesh structure: MHX(I), XMS(I)
- Material: a mixture of up to 3 aerosols
- Assignment of materials to regions
- PFNDAT phase function data base

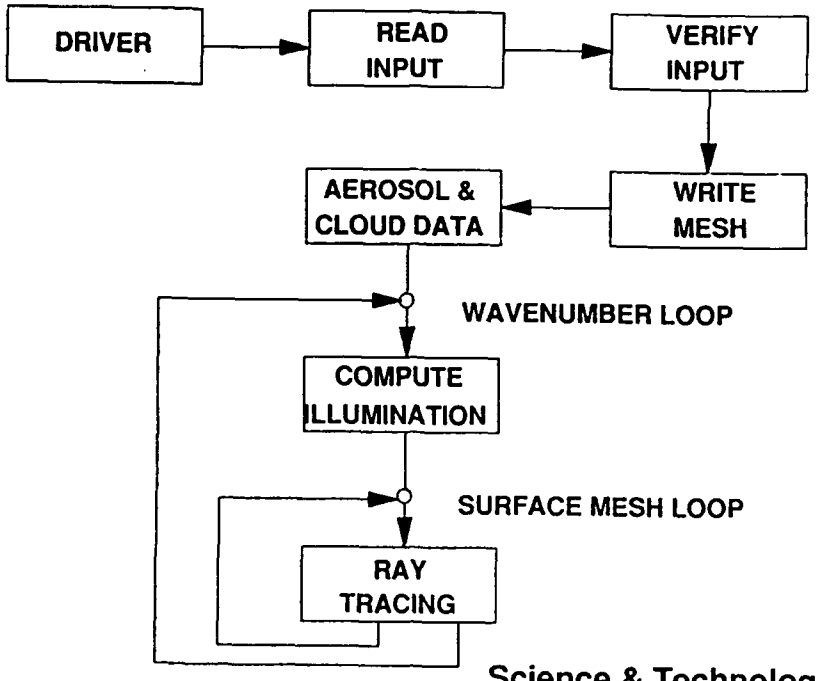
Science & Technology Corp

BLIRB: Surface Albedo

- Areas: ID and bounding coordinates
- Albedo: ID and value from input file
- Albedo: tabulated, wavelength-independent
- Spectral albedo arrays pending realistic data

Science & Technology Corp

BLIRB: Structure of the Code



Science & Technology Corp

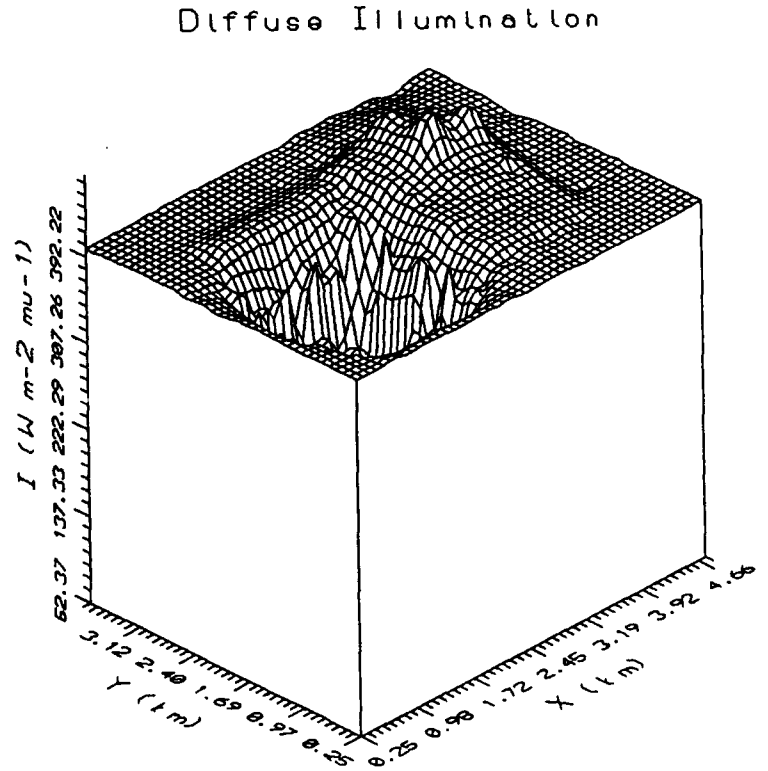
BLIRB: Examples of Computation

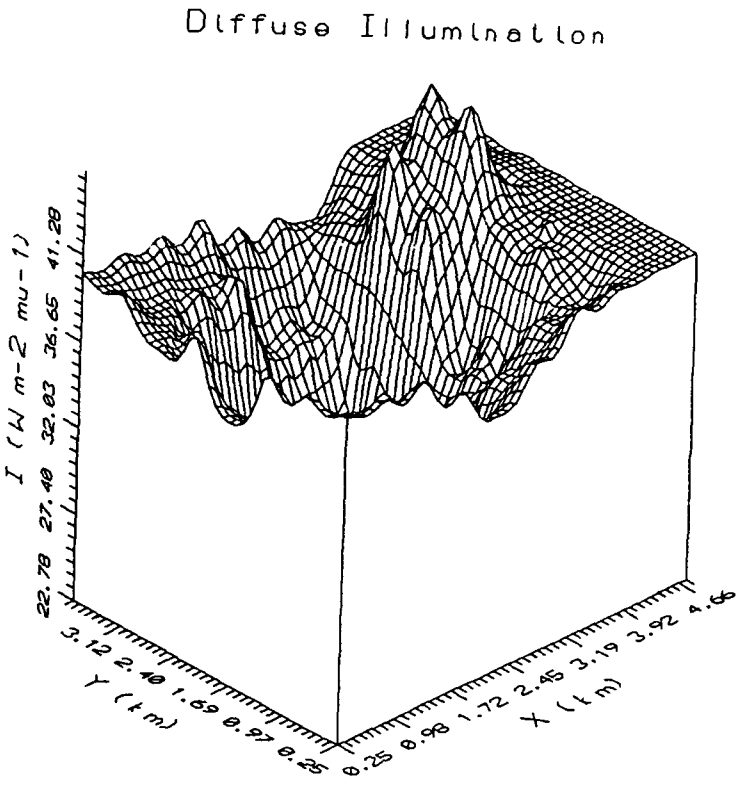
- Physical region w. Water Cloud 2x2x1 km
  - Visible radiation
  - Stochastic ray tracing: 10 rays
  - Surface albedo: 0.2, 0.4
- Nonuniform mesh
  - Two rectangular clouds
  - Cloud region: 10 mesh points/km
  - Background region: 2 mesh points/km

Science & Technology Corp

BLIRB: Input File

```
WAVL   0.55
VIS       1.0
BLIRB
MDL1          22.0000     6.0000     2.0000     0.0000     1.0000
MDL2           1.0000   292.0000    -1.0000    10.0000     0.0000
AREA           0.0000     5.0000     0.0000     4.0000     1.0000
AREA           3.0000     4.0000     2.0000     3.0000     2.0000
REGN           0.0000     5.0000     0.0000     4.0000     0.0000     5.0000     1.0000
REGN           1.0000     3.0000     1.0000     3.0000     3.0000     4.0000     2.0000
MESX          10.0000     5.0000
MESY          08.0000     4.0000
MESZ          10.0000     5.0000
ALBD           1.0000     0.2000
ALBD           2.0000     0.4000
MTRL           1.0000     0.1000     5.0000     0.1000     3.0000     0.0500
MTRL          -2.0000     3.0000     5.0000     0.1000
CLDS           2.0000     1.0000     1.0000
SUN           85.0000   000.0000     1.0000     1.0000
WAVN       18900.00   18940.00      20.0
RECL           1.0000
DONE
END
STOP
```





BLIRB: Conclusions

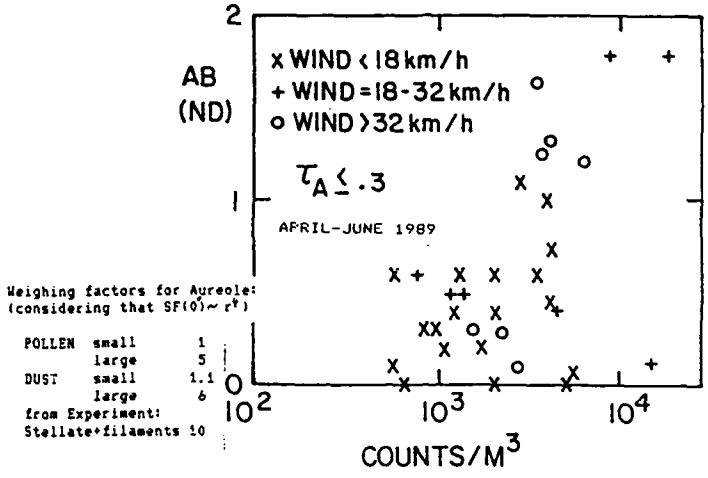
- **Integrates clouds, aerosols, and gas absorption**
- **Direct and diffuse radiation 0.4 - 12 micro-m**
- **RT based on adding method and ray tracing**
- **Mesh 40x40x40 grid points**
- **AFGL data base for background aerosols**
- **Four cloud models implemented**

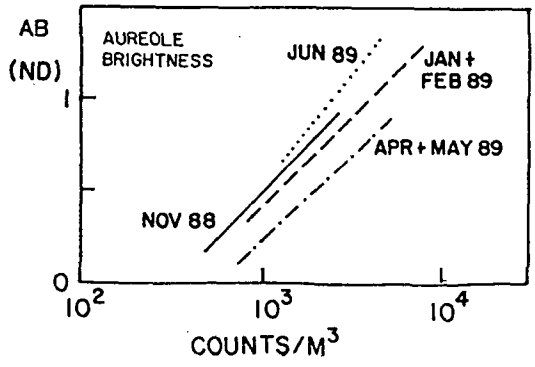
Science & Technology Corp

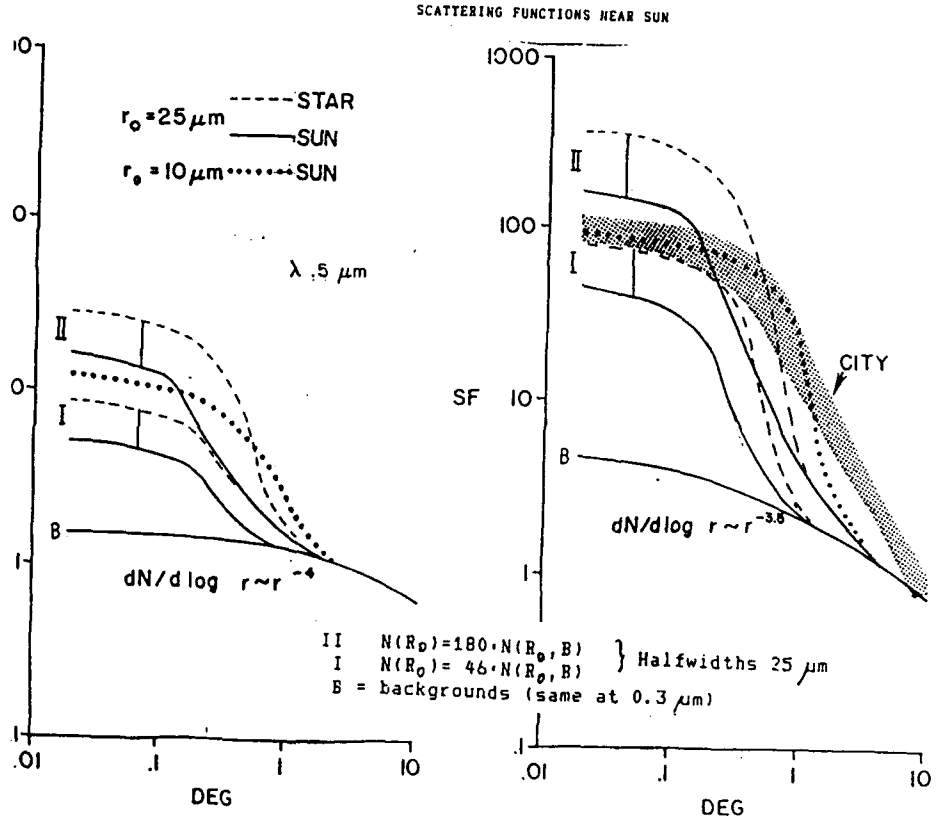
RELATIONS BETWEEN GIANT AEROSOLS NEAR THE SURFACE AND SOLAR AUREOLE BRIGHTNESS

F.E. Volz
Geophysics Directorate, Phillips Laboratory, Hanscom Air Force Base, MA 01731-5000

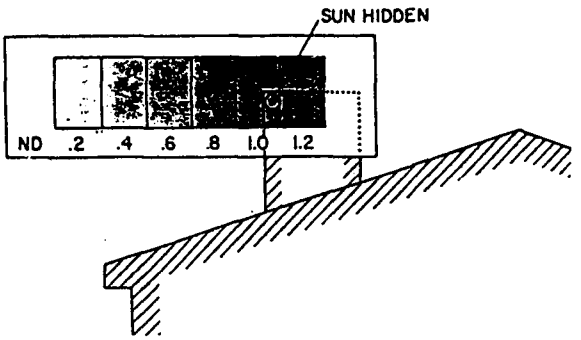
Observations of the sky brightness at the edge of the sun (aureole) to the west of Boston have shown a gradual decline since about 1979. The number of giant dust particles (with radii from 5 to 50 μm) suspended in the mixing layer at noontime appears to have decreased by more than a factor of ten. To correlate dust and pollen concentrations near the ground with simultaneous aureole data, those particles were collected by rotating impactor for over one year. Typical scattering functions for size distributions presented in the literature were calculated both for a point source and the sun; small-angle brightness of the latter is considerably lower.


AB
(ND)
x WIND < 18 km/h
+ WIND = 18-32 km/h
o WIND > 32 km/h
$\tau_A \leq .3$
APRIL-JUNE 1989
Weighing factors for Aureole:
(considering that SF(0)~ r^{-4})
POLLEN small 1
large 5
DUST small 1.1
large 6
from Experiment:
Stellate+filaments 10
COUNTS/M^3

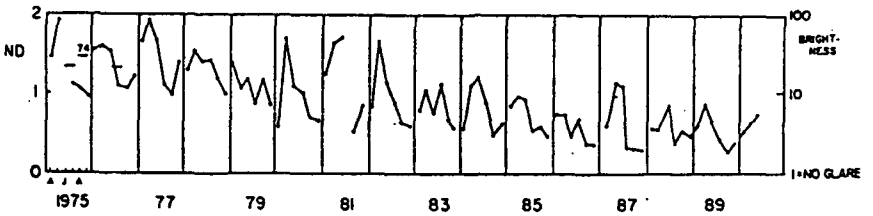

AB
(ND)
AUREOLE
BRIGHTNESS
JUN 89
JAN + FEB 89
APR + MAY 89
NOV 88
COUNTS/M^3

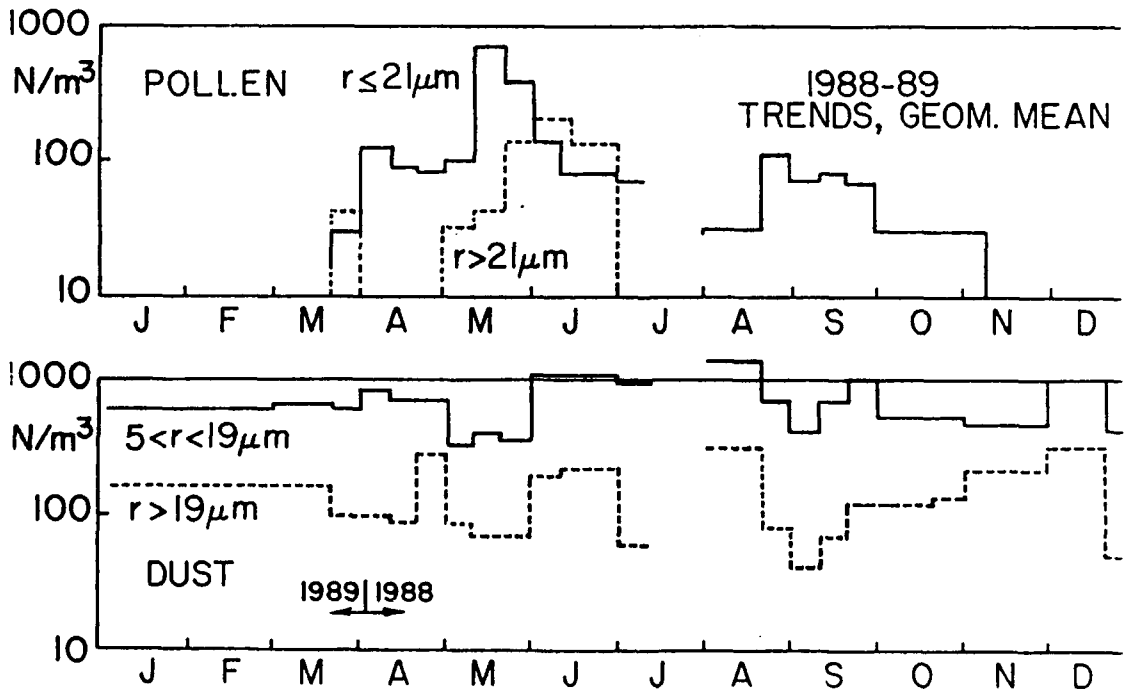

SCATTERING FUNCTIONS NEAR SUN
r_o = 25 μm STAR
SUN
r_o = 10 μm SUN
λ .5 μm
II
I
B
dN/d log r ~ r^{-4}
SF
CITY
dN/dlog r ~ r$^{-3.8}$
DEG
II N(R$_D$) = 180 · N(R$_o$, B)
I N(R$_D$) = 46 · N(R$_o$, B)
} Halfwidths 25 μm
B = backgrounds (same at 0.3 μm)

BASIS OF METHOD:
SKY BRIGHTNESS AT SUN'S EDGE (SOLAR AUREOLE), which is governed by particles 3 to 100 microns in size.
AUREOLE BRIGHTNESS is measured by neutral-density filter needed to suppress glare.
OBSERVATIONS at AFGL and at home (Lexington).
Probably the only continuous date base existing.



AIRBORNE GIANT AEROSOLS - STRONG DECLINE





THE COMPUTATION OF RADIATIVE TRANSFER THROUGH THE ATMOSPHERE INCORPORATING VARIOUS AEROSOL SCENARIOS*

L.C. Rosen
University of California, Lawrence Livermore National Laboratory,
Atmospheric & Geophysical Sciences Division, Livermore, CA 94550

The Atmospheric and Geophysical Sciences Division at the Lawrence Livermore National Laboratory is participating in the Atmospheric Research Measurements (ARM) Program. In order to evaluate radiative measurements affected by aerosol environments, calculations are performed utilizing various aerosol scenarios. Mie calculations are done employing appropriate indices of refraction associated with aerosol constituents to yield aerosol extinction coefficients and asymmetry parameters. These results are integrated over aerosol size distributions and are used as data input to the LOWTRAN 7 code. The MIE calculations and integration technique are discussed. The radiative transfer results computed from the LOWTRAN 7 code are compared for the aerosol scenarios. The importance of differing aerosol contributions is discussed.

*Work performed under the auspices of the U.S. Department of Energy by the Lawrence Livermore National Laboratory under Contract No. W-7405-ENG-48.

The Computation of Radiative Transfer through the Atmosphere Incorporating Various Aerosol Scenarios

June 11, 1991

L. C. Rosen
Atmospheric & Geophysical Sciences Division
University of California
Lawrence Livermore National Laboratory

Goals

- Develop a capability within the Atmospheric & Geophysical Sciences Division, Lawrence Livermore National Laboratory

- Advise Atmospheric Radiation Measurement (ARM) Program as to the importance of aerosols to measurement plan

Computational Procedure

For a Given Aerosol Scenario

- Calculate extinction and scattering coefficients, asymmetry parameters from MIE code.

- Integrate extinction and scattering coefficients, asymmetry parameters over size distributions in quadrature code.

- Input averaged extinction, absorption coefficients asymmetry parameters into LOWTRAN7 code to yield radiances and atmospheric transmittances.

MIE Code

- Input indices of refraction

- Output of extinction and scattering coefficients, asymmetry parameters, extinction and scattering efficiency factors.

Quadrature Code

- Input aerosol size distributions, extinction and scattering coefficients, asymmetry parameters, scattering efficiency factors, frequency.

- Output of aerosol extinction and absorption coefficients, asymmetry parameters as a function of frequency.

ARM Program — Goals

The ICRCCM and other GCM intercomparison programs have highlighted an important area of scientific need associated with the understanding and prediction of global climate change. From the findings of those programs, the following scientific requirements emerge as the most critical:

- A quantitative description of the radiative energy balance profile under important physical circumstances must be developed. The descriptions must come from field measurements.
- The processes controlling the radiative balance must be identified and investigated. Validation must come from a direct, comprehensive comparison of field observations with detailed calculations of the radiation field and its cloud and aerosol interactions.
- The knowledge necessary to improve parameterizations of radiative properties of the atmosphere used in GCMs must be developed. This requires intensive measurements at a variety of temporal, spatial and spectral scales.

A COMPARISON OF THE EFFECTS OF AEROSOLS AND RELATIVE HUMIDITY ON DIRECTLY TRANSMITTED SOLAR IRRADIANCE

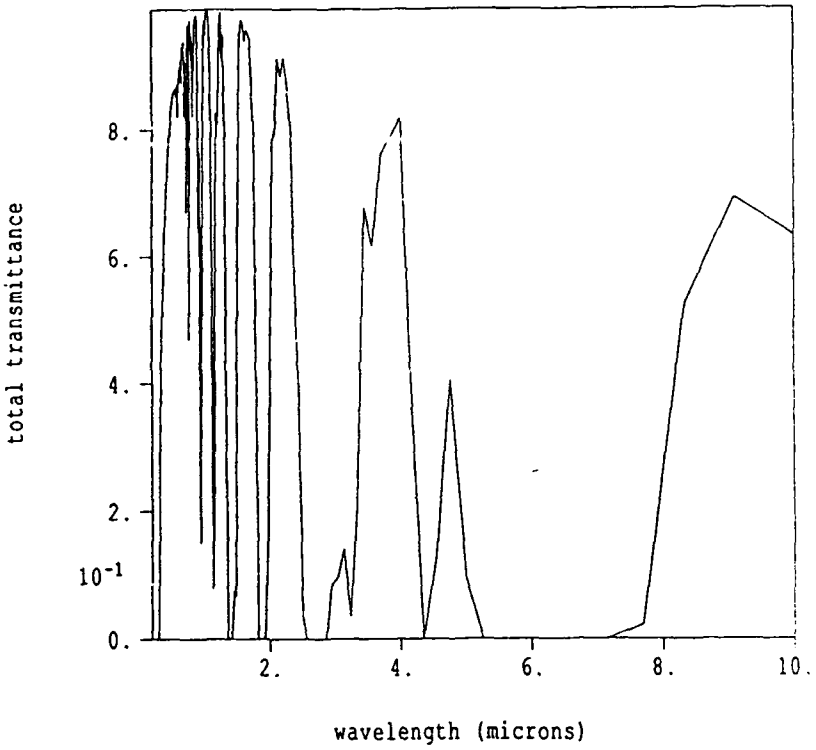
30° ZENITH, 0.2 μm TO 10.0 μm, MLS

AEROSOL	RELATIVE HUMIDITY (0-1 Km)	INTEGRATED IRRADIANCE (10⁻³ W/cm²) .20	.50	.76	AV. TRANSMITTANCE .20	.50	.76
NONE		1.0480	1.008	0.9598	0.4328	0.4173	0.4092
23 Km Vis.		0.8002	0.7658	0.7288	0.3185	0.3036	0.2963
5 Km Vis.		0.4284	0.4028	0.3912	0.1620	0.1524	0.1459

file 605 :midlatitude summer
no aerosol
observer= 0.000 zenith angle= 30.000

Relative Humidity = 76 %

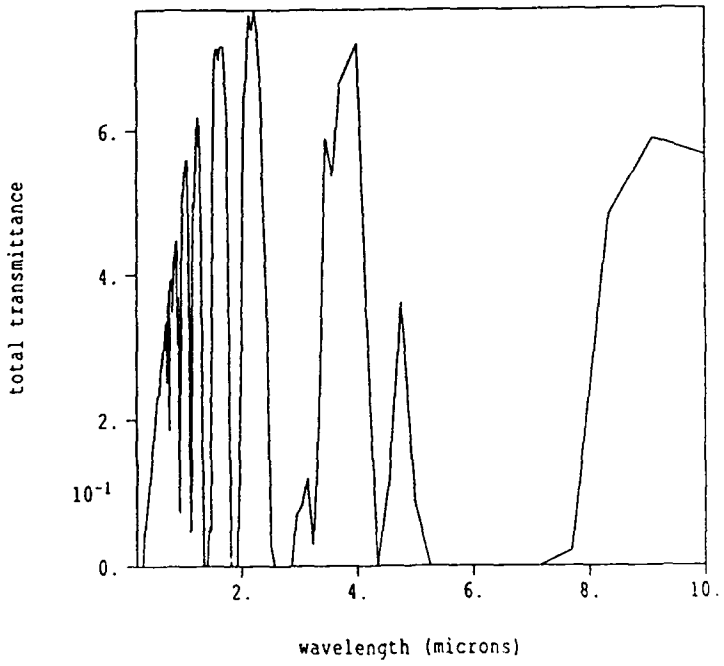
MIDLATITUDE SUMMER



file 605d :midlatitude summer
lowtran rural vis=5km
observer= 0.000 zenith angle= 30.000

Relative Humidity = 76 %

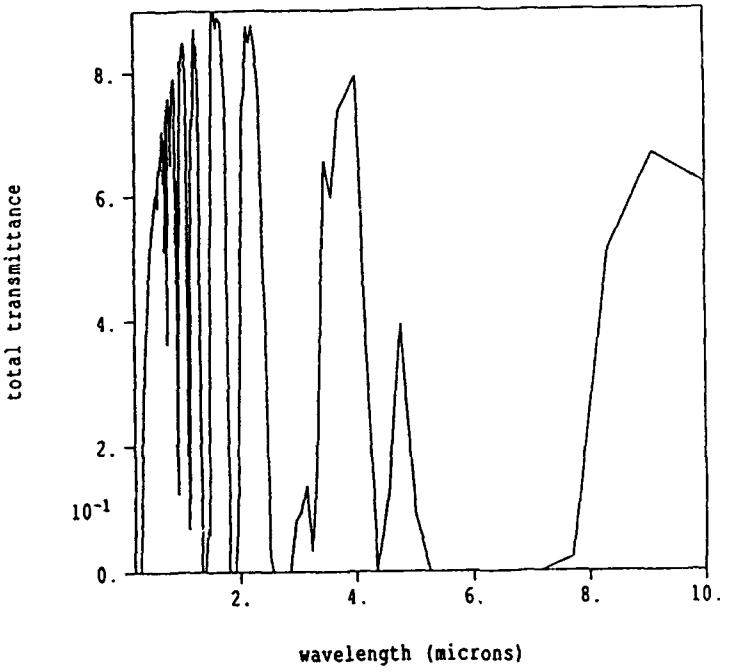
MIDLATITUDE SUMMER



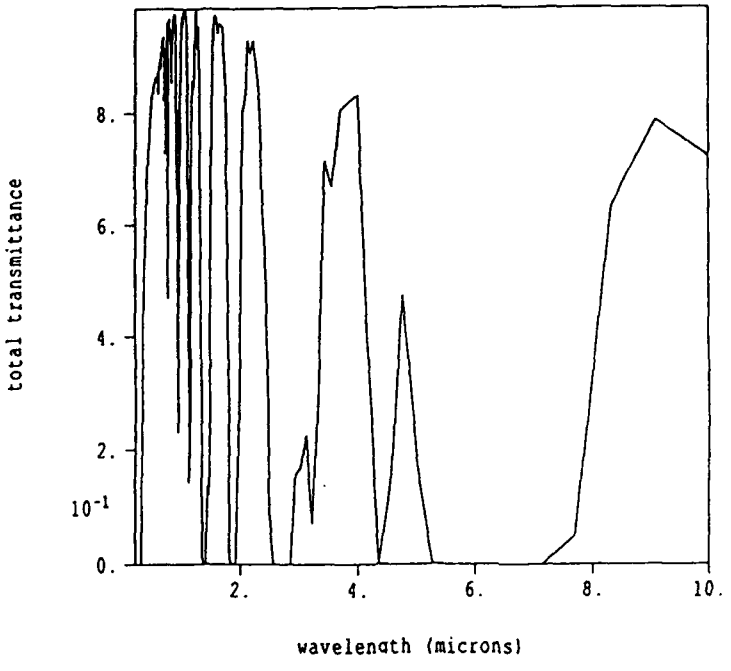
file 605b :midlatitude summer
lowtran rural vis=23km
observer= 0.000 zenith angle= 30.000

Relative Humidity = 76%

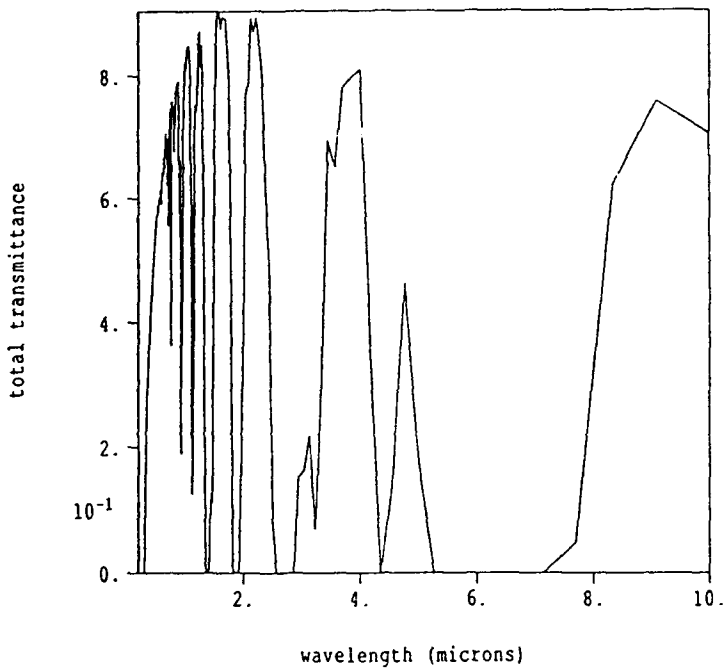
MIDLATITUDE SUMMER



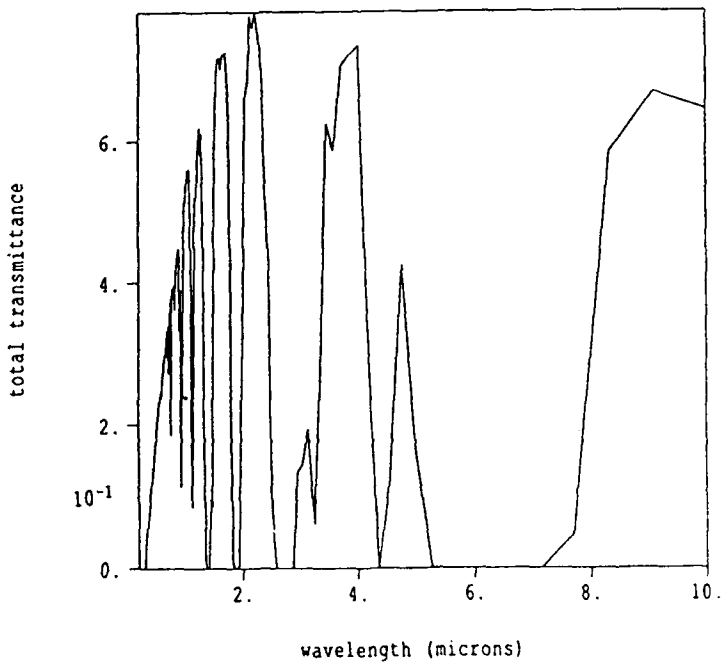
file 605i :midlatitude summer
no aerosol humidity=50%
observer= 0.000 zenith angle= 30.000



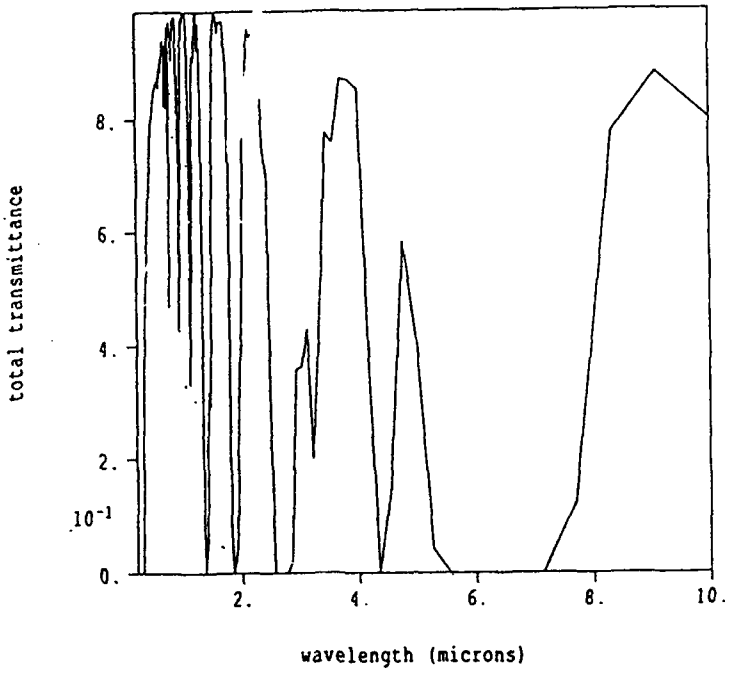
file 605j :midlatitude summer
lowtran rural vis=23km humidity=50%
observer= 0.000 zenith angle= 30.000



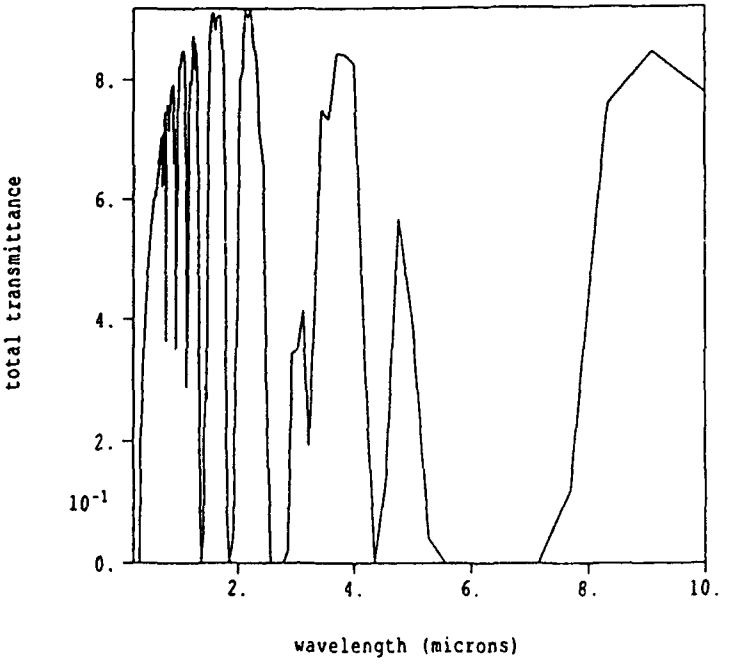
file 605k :midlatitude summer
lowtran rural vis=5km humidity=50%
observer= 0.000 zenith angle= 30.000



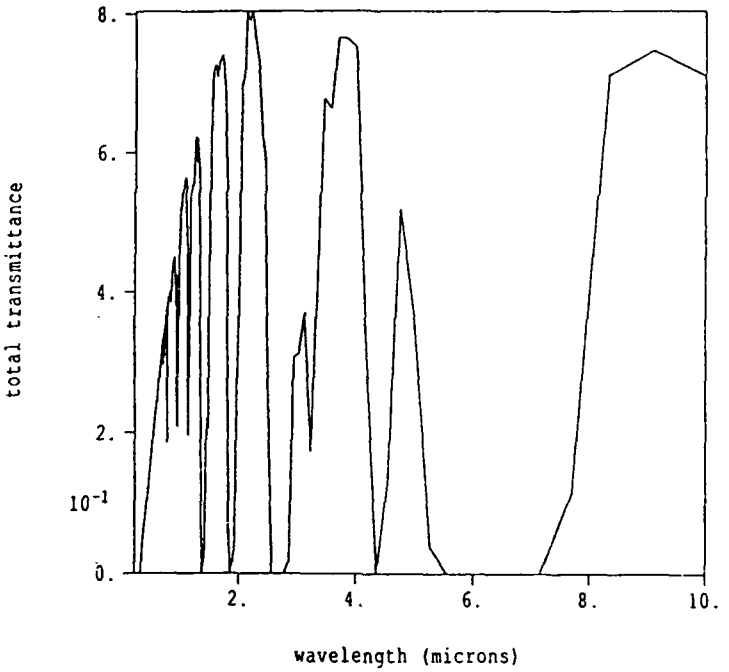
file 605f :midlatitude summer
no aerosol humidity=20%
observer= 0.000 zenith angle= 30.000



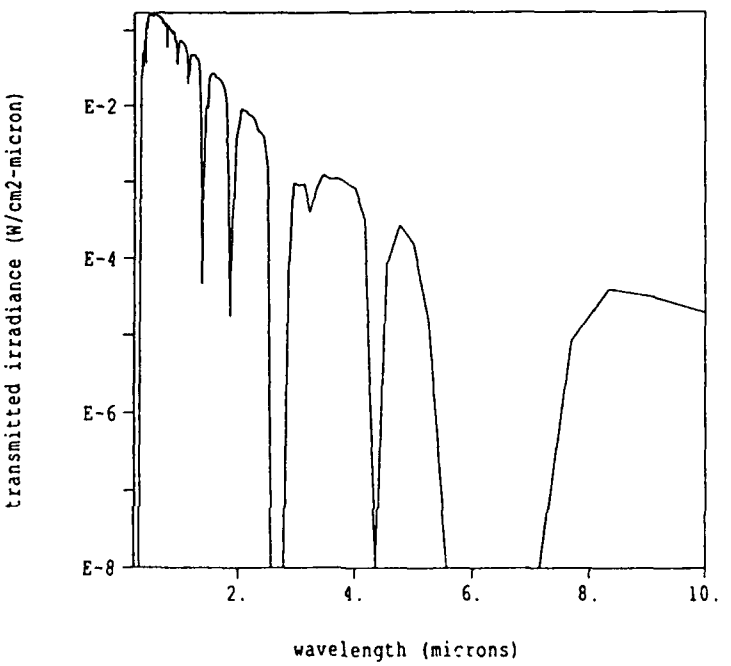
file 605g :midlatitude summer
lowtran rural vis=23km humidity=20%
observer= 0.000 zenith angle= 30.000



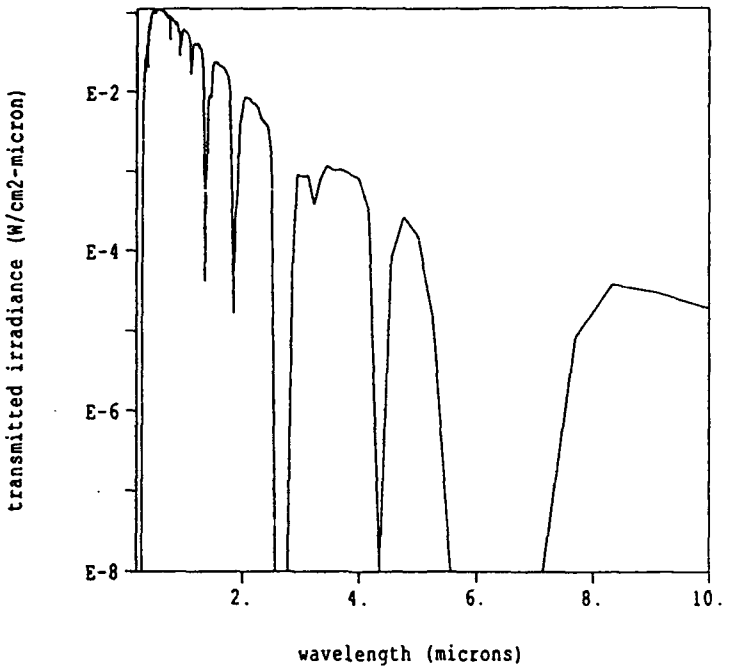
file 605h :midlatitude summer
lowtran rural vis=5km humidity=20%
observer= 0.000 zenith angle= 30.000



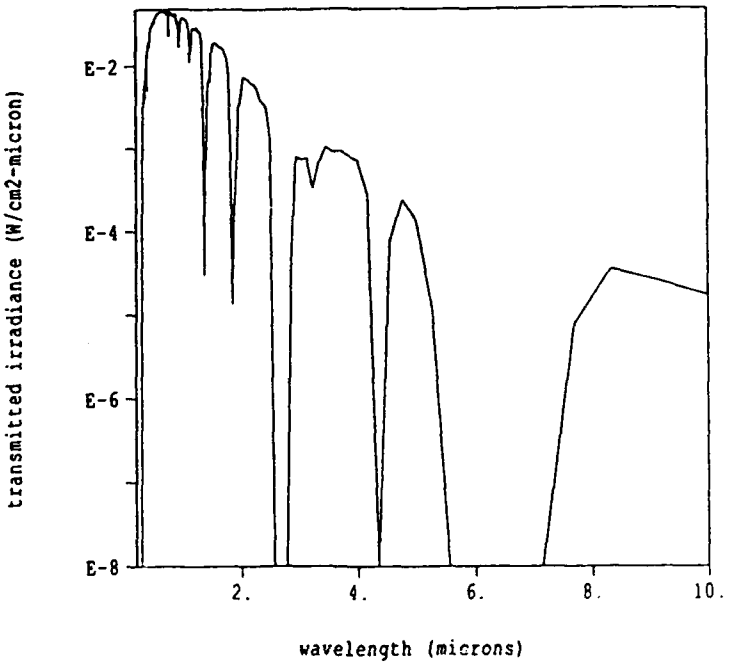
file 529.20.6:midlatitude summer RH = 20%
no aerosol
observer= 0.000 zenith angle= 30.000

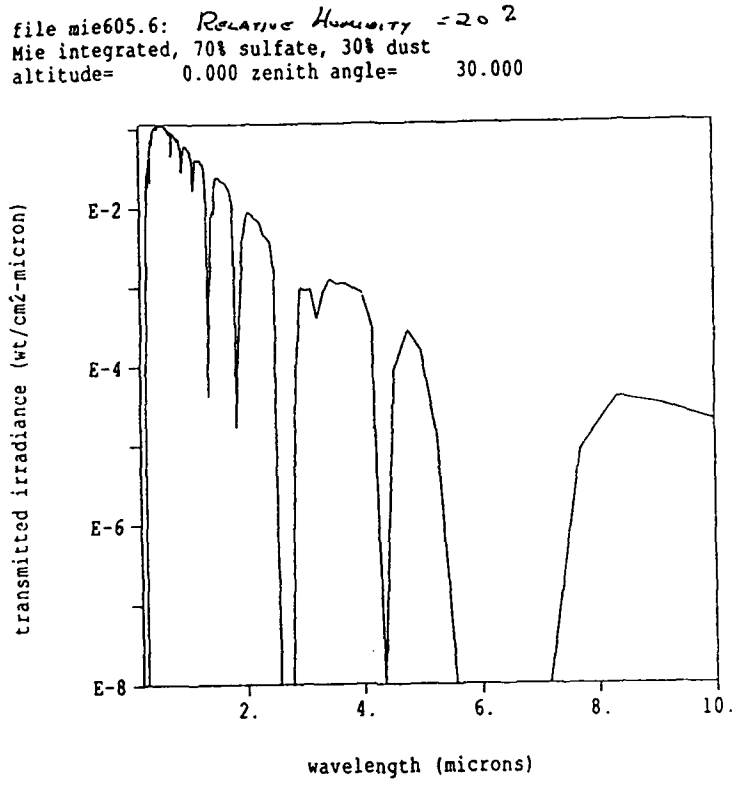


file 529b20.6:midlatitude s RH = 20%
lowtran rural vis=23km
observer= 0.000 zenith angle= 30.000



file 529d20.6:midlatitude summer RH = 20%
lowtran rural vis=5km
observer= 0.000 zenith angle= 30.000





Future Work

- Rural aerosol scenarios
- Marine aerosol scenarios
- Clouds
- Comparison of radiances and atmospheric transmittances

BACKSCAT LIDAR BACKSCATTER SIMULATION: VERSION 2.0

J.R. Hummel, D.R. Longtin, N.L. Paul, J.R. Jones
SPARTA, Inc., 24 Hartwell Avenue, Lexington, MA 02173

Backscatter from atmospheric aerosols can produce significant returns in monostatic laser radar (lidar) systems. The Geophysics Directorate of Phillips Laboratory is developing lidar systems that will measure this backscatter. To aid in the design and use of such systems, SPARTA has developed a lidar simulation program, BACKSCAT, that calculates the backscatter return for various lidar systems, viewing aspects, and atmospheric conditions. This paper describes a new version of the simulation system, BACKSCAT Version 2.0. BACKSCAT Version 2.0 has been totally redesigned. Additional aerosol models and cirrus cloud models have been added. In addition, an all new user interface has been developed.

BACKSCAT, LIDAR BACKSCATTER SIMULATION VERSION 2.0

By

John R. Hummel, David R. Longtin, Nanette L. Paul, & James R. Jones

11 June 1991

Annual Review Conference on Atmospheric Transmission Models

Hanscom AFB, Massachusetts

Contract F19628-88-C-0038



BRIEFING OUTLINE

- Background and Objectives of Work
- Overview of BACKSCAT
- New Features in BACKSCAT Version 2.0
- Summary and Recommendations for Future Work



BACKGROUND AND OBJECTIVES

BACKGROUND

- GL has Been Active in Developing and Fielding Atmospheric Backscatter Lidar Systems
- A Need Existed to Simulate the Aerosol Backscatter from Lidar Systems for Repesentative Atmospheric Conditions
- BACKSCAT Version 1.0 Was Developed to Meet That Need Using AFGL Atmospheric Models, circa LOWTRAN 6

OBJECTIVES

- Update BACKSCAT Aerosol Models to LOWTRAN 7 Levels
- Enhance BACKSCAT Based On User Feedback



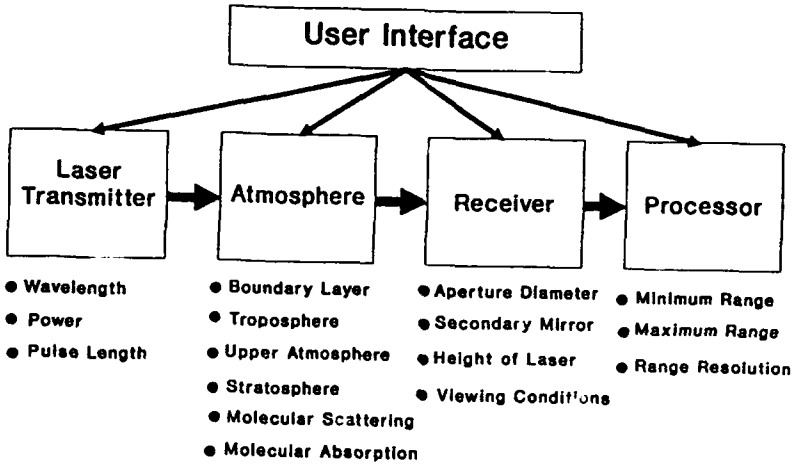
OVERVIEW OF BACKSCAT

- BACKSCAT Simulates the Aerosol Backscatter from a Backscatter Lidar Operating Under User Defined Lidar, Atmospheric, and Viewing Conditions
- A Menu Driven "Front End" Simplifies Operation
- Code Implemented for the IBM PC Environment in "C" (Menu System) and FORTRAN 77 (Science Portion)
- Atmospheric Conditions are User-Defined Employing:
  - Built-in Aerosol and Atmospheric Models
  - User-Supplied Propogation Profile

OVERVIEW OF BACKSCAT (Cont.)

SPARTA INC.

BACKSCAT Version 2.0



/backvg/061091

SPARTA INC.

NEW FEATURES IN BACKSCAT VERSION 2.0

- Addition of Cirrus Clouds and Wind-Dependent Desert Aerosol Models
- Molecular Scattering Profiles Based On:
  - Built-in GL Model Atmospheres
  - User-Supplied Radiosonde Data
- Built-in "Quick View" Graphics Package
- All-New Menu Interface System
  - Easier to Use
  - Improved Error Checking

/backfns/061091

SPARTA INC.

FEATURES OF BACKSCAT VERSION 2.0 (Cont.) - NEW MENU SYSTEM

BACKSCAT – LIDAR Backscatter Program

Atmospheric Parameters

Atmospheric Parameters File: *NONE* Read in new File? *N*
Seasonal Distribution: *FALL/WINTER*

Boundary Layer -	Height (km):	*2.00000*
	Type of Aerosols:	*RURAL*
	Relative Humidity (%):	*70.00*
	Visibility at the Surface (km):	*23.0000*
	Wind Speed at 10m (m/s):	*10.0000*
Troposphere -	Height (km):	*9.00000*
	Relative Humidity (%):	*70.00*
Stratosphere -	Height (km):	*29.0000*
	Type of Aerosols:	*STRATOSPHERIC*
	Aerosol Loading:	*BACKGROUND*
Upper Atmosphere -	Height (km):	*100.000*
	Type of Aerosols:	*METEORIC DUST*
	Aerosol Loading:	*NORMAL*
Cirrus Clouds -	**Cloud Type:**	*NONE*

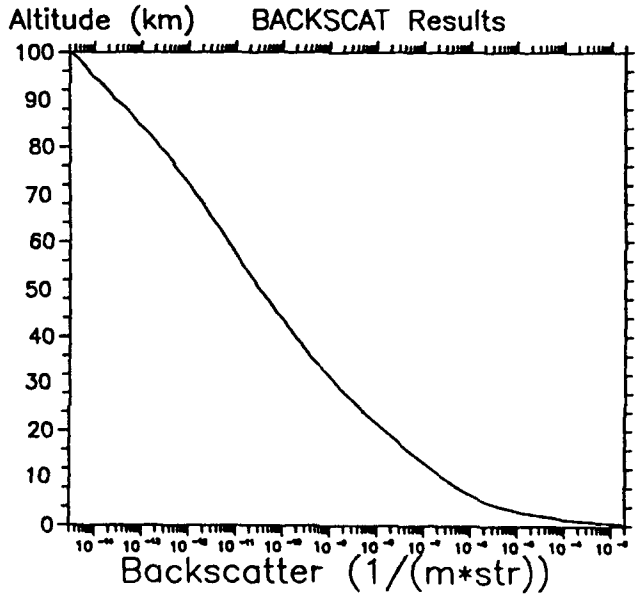
Cirrus Cloud Types:
NONE
STANDARD CIRRUS
SUBVISUAL CIRRUS

⇑, ⇓, Enter = Accpt Cirrus Cloud Type

/backfns/061091

SPARTA INC.

FEATURES OF BACKSCAT VERSION 2.0 (Cont.) - "QUICKVIEW OPTION"



FEATURES OF BACKSCAT VERSION 2.0 (Cont.) - RADIOSONDE DATA ENTRY

SPARTA INC.

RADIONSONDE DATA ENTRY

	ALTITUDE (m)	PRESSURE (mb)	TEMPERATURE (C)	MOISTURE (RH(%))
1	79.00	1003.50	23.90	74.00
2	110.00	1000.00	23.60	74.00
3	555.00	950.00	18.60	87.00
4	585.00	946.84	18.30	88.00
5	1017.00	900.00	15.00	96.00
6	1091.00	892.55	14.50	97.00
7	1328.00	867.92	13.50	96.00
8	1498.00	850.68	11.60	74.00
9	1500.00	850.00	11.70	71.00
10	1582.00	842.17	12.60	37.00
11	1717.00	828.93	18.10	11.00

Ctrl-ENTER To ACCEPT DATA
ESC from MAIN Menu
ALTITUDE REFERENCE *MSL*
UNITS: Alt → *m* , P → *mb* , T → *C* , M → *RH(%)*

SUMMARY AND RECOMMENDATIONS FOR FUTURE WORK

SPARTA INC.

SUMMARY

- A New Version of BACKSCAT, a Backscatter Lidar Simulation System, is Now Available
- New Features Include:
  - Addition of Cirrus Clouds and Desert Aerosol Models
  - User Defined Molecular Scattering Absorption Profiles
  - New Menu Interface System

RECOMMENDATIONS FOR FUTURE WORK

- Addition of Water Cloud Models
- Compute Aerosol Profiles Based on Fundamental Parameters (*ie.* Aerosol Size Distributions, Indices of Refraction)
- Extension of Simulation Capability to Other Lidar Systems (*ie.* Raman, Doppler)

CIRRUS CLOUD TRANSMISSION MODELLING*

W.M. Cornette, J.G. Shanks
Photon Research Associates, Inc., 9393 Towne Centre Drive, Suite 200,
San Diego, CA 92121

The modelling of transmission through a cirrus cloud is of significant concern to a wide variety of users, including IRSTs and satellite systems. A model of cirrus transmission involves a combination of characterizations of cirrus cloud properties and radiative transfer. This presentation will summarize an assessment of current cirrus transmission models, with recommendations for potential upgrades and additions to the existing models. Also, several aspects for modelling transmission through cirrus clouds are applicable to transmission through optically thick atmospheric layers by modelling scattering in the forward direction as being no scattering at all, thereby producing a much more reasonable result.

*This work was funded by the Air Force Geophysics Laboratory under Contract No. F08606-87-C-0035; Dr. Donald Grantham, Technical Monitor.

CIRRUS CLOUD TRANSMISSION MODELING

JUNE 1991

Presented at the 14th Annual Review Conference on Atmospheric Transmission Models
11-12 June 1991, Geophysics Directorate, Phillips Laboratory, Hanscom AFB, MA

Work Funded in Part by the Air Force Geophysics Laboratory
Under Contract No. F08606-87-C-0035; Dr. D. Grantham, Technical Monitor

Presented By:

Dr. William M. Cornette
Dr. Joseph G. Shanks

Photon Research Associates, Inc.
9393 Towne Centre Drive, Suite 200
San Diego, CA 92121

Photon Research Associates, Inc.

OUTLINE

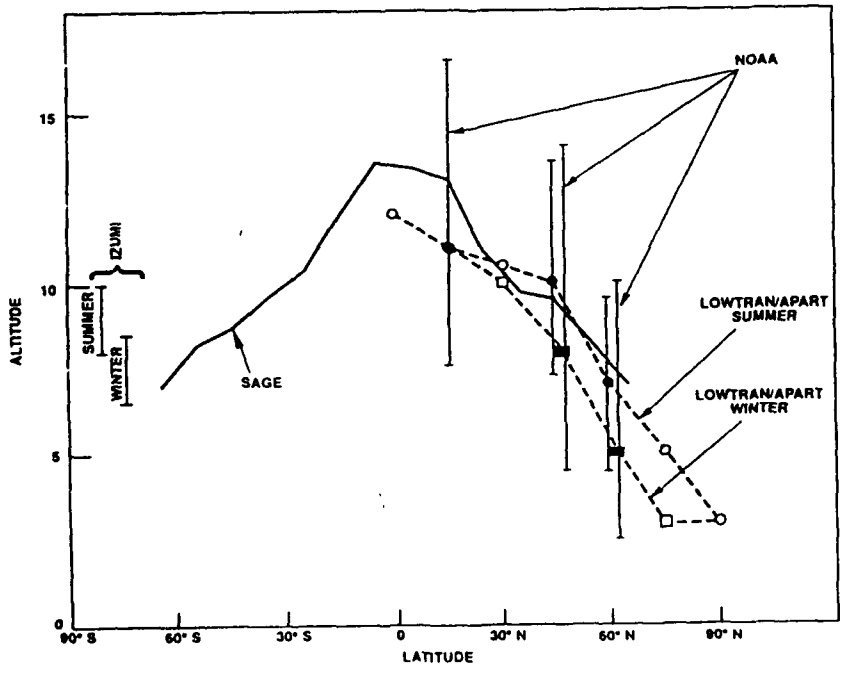
- Objective
- Cirrus Characterization
  - Mesoscale
  - Microscale
- Radiative Transfer
- Models

OBJECTIVE

To Assess the Current Capabilities in the Government, Contractor, and University Communities with Respect to the Present State of Technology in Cirrus Analysis and Attenuation Modeling.

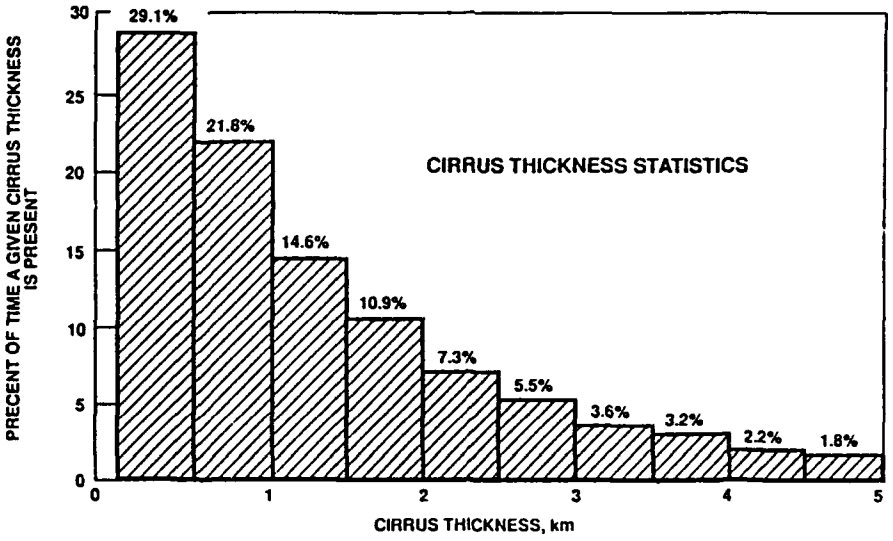
- **Cirrus (Ci)**
- **Cirrocumulus (Cc)**
- **Cirrostratus (Cs)**
- **Condensation Trails (Contrails)**
- **Nacreous (Stratospheric)**
- **Noctilucent (Mesospheric)**

CIRRUS CLOUD ALTITUDES



CIRRUS THICKNESS

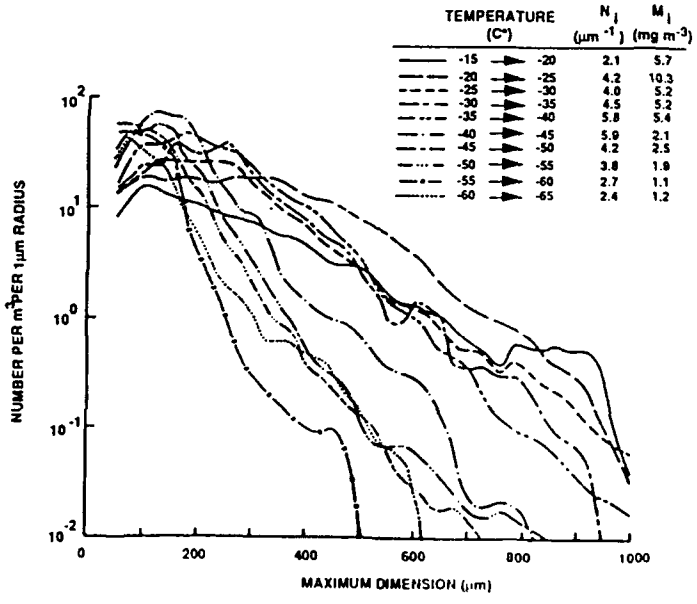
- Median Thickness = 1.0 km



Source: Hall et al. (1984)

OBSERVED SIZE DISTRIBUTIONS

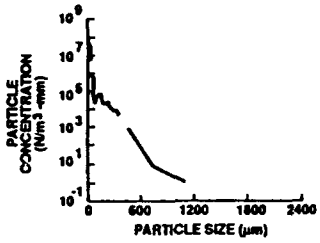
- Lidar Measurements



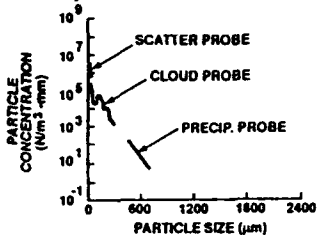
- Sassen, Starr and Uttal, 1989

PARTICLE SIZE DISTRIBUTIONS

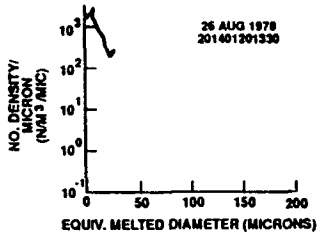
- **Opaque Cirrus**



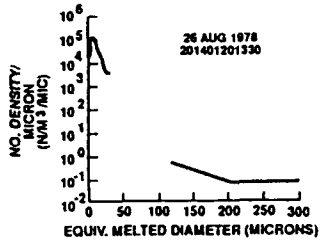
- **Thin, Translucent Cirrus**



- **Type 1 Subvisual Cirrus**

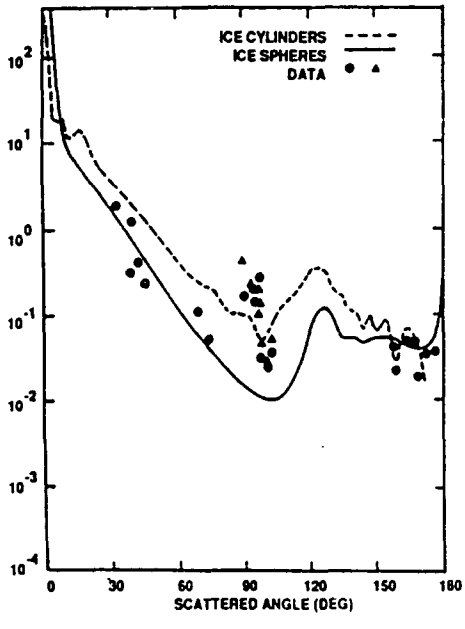


- **Types 1 & 2 Subvisual Cirrus**

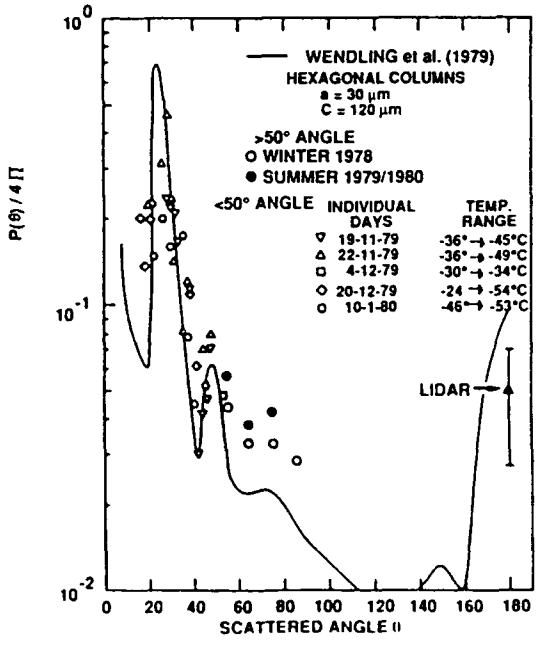


- **Barnes (1982)**

PHASE FUNCTIONS: OBSERVED



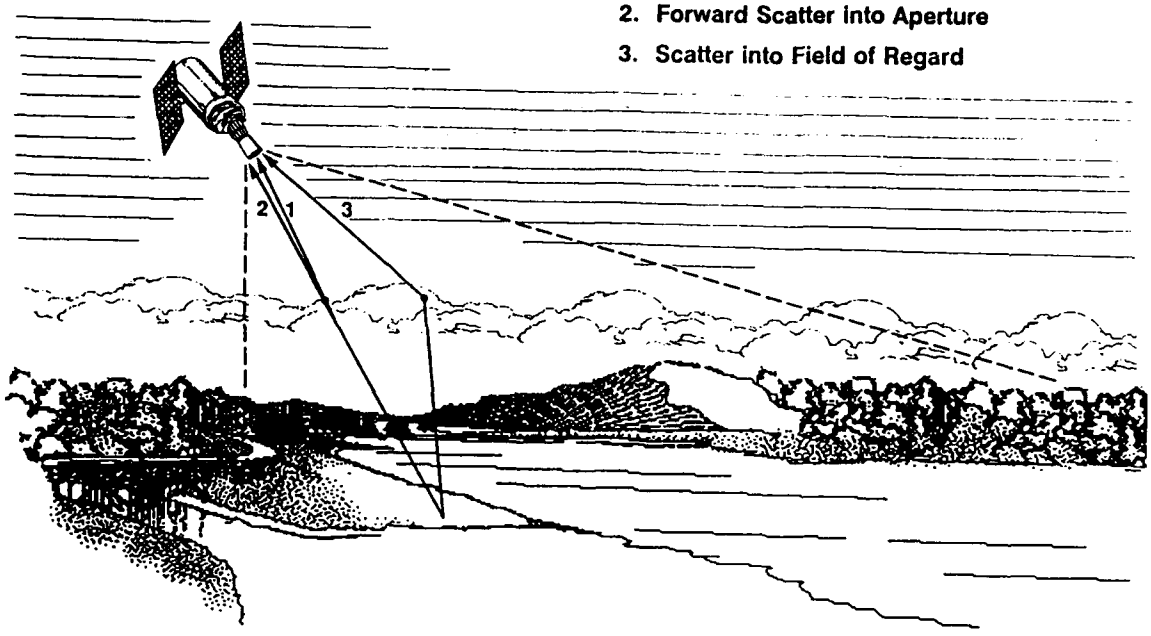
- **Lyons and Schummers; 1984**



- **Platt and Dilley; 1984**

FIRST-ORDER RADIATIVE TRANSFER

1. Direct Line-of-Sight
2. Forward Scatter into Aperture
3. Scatter into Field of Regard



CIRRUS CLOUD MODELS

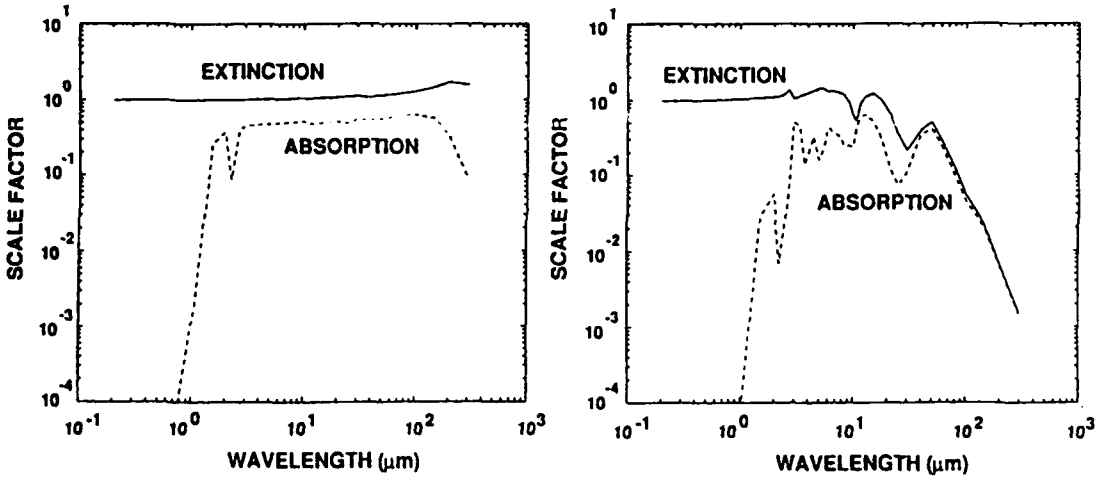
	RADIATIVE TRANSFER	PARTICLES	VERTICAL PROFILE	SIZE DISTRIBUTION
LOWTRAN	Beer's Law	Spherical	Uniform Layer	-
APART	Beer's Law and First Order Scattering	Spherical	Profile	-
SUBVIS	Beer's Law	Random Hexagonal	Uniform Layer	Temperature Dependent
Liou	Successive Order of Scattering	Random Hexagonal	Uniform Layer	Temperature Dependent
Rockwitz	Successive Order of Scattering	Oriented Hexagonal	-	-

MODELS

- "Comprehensive" Models
  - LOWTRAN 7
  - APART (Version 7.00)
  - SUBVIS and LOWTRAN
  - Liou
- "Element" Models
  - Pollack and Cuzzi
  - Liou, et al.
  - Rockwitz
  - Barnes
  - Hansen

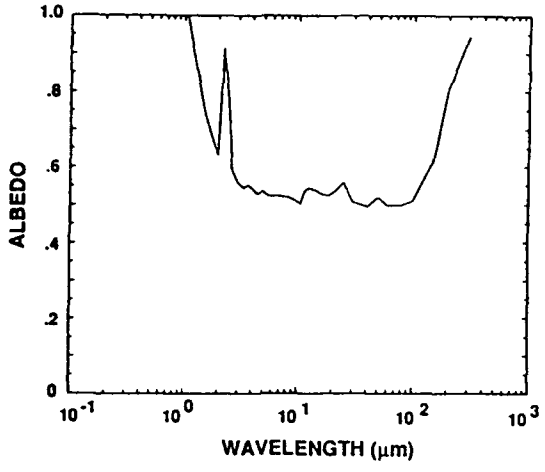
LOWTRAN/APART CIRRUS MODEL

- Standard
- Subvisual

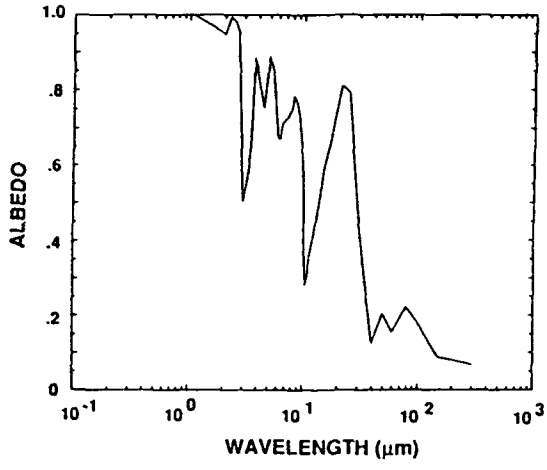


LOWTRAN/APART CIRRUS MODEL

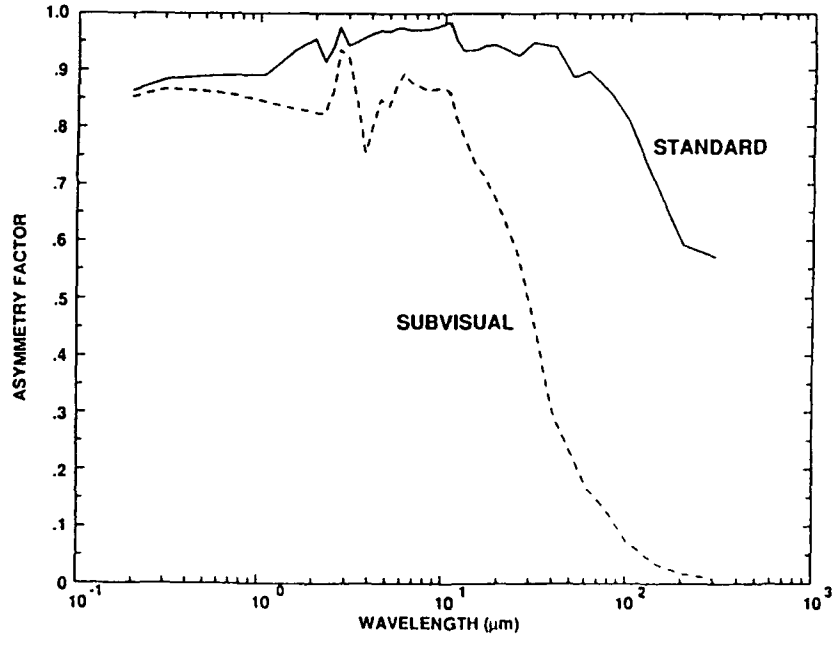
- Standard



- Subvisual



LOWTRAN/APART CIRRUS MODEL



PRA
Photon Research Associates, Inc.

LOWTRAN/APART MODEL DEFICIENCIES

- **LOWTRAN**
  - **Spherical Particles**
  - **Extinction Only**
    - **Multiple Scatter for Radiation Only, Not Transmittance**
  - **No Forward Scatter**
  - **Empirical Scaling Laws Not Based in Phenomenology**

- **APART**

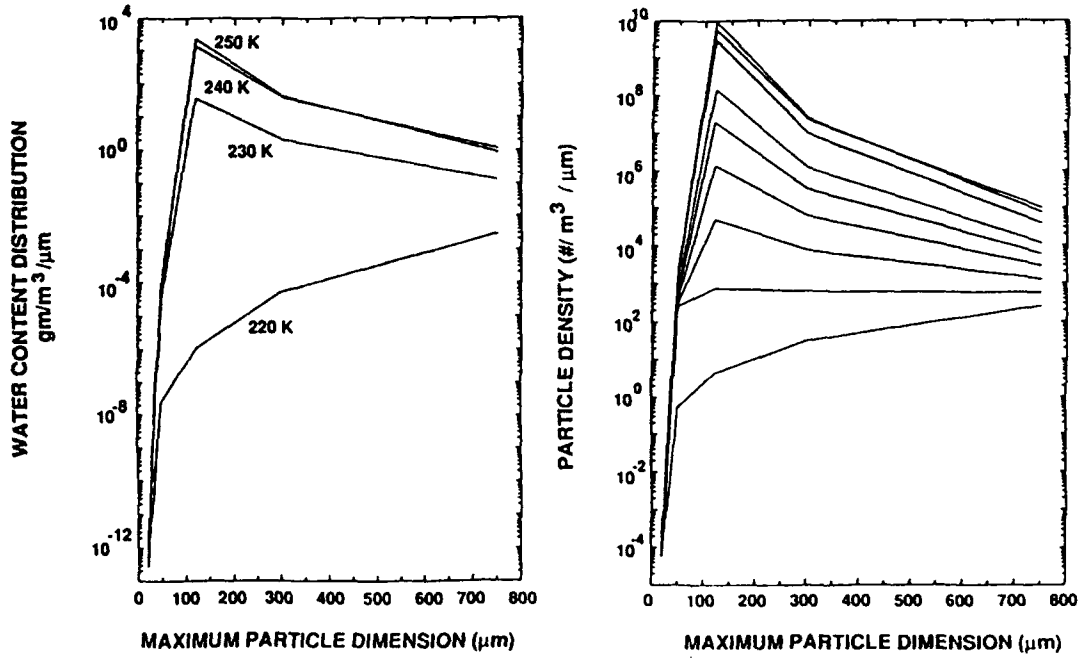
  - **Same as LOWTRAN**

- EXCEPT -

  - **Forward Scattering Correction Included for Single Scatter into Field-of-Regard and Aperture**

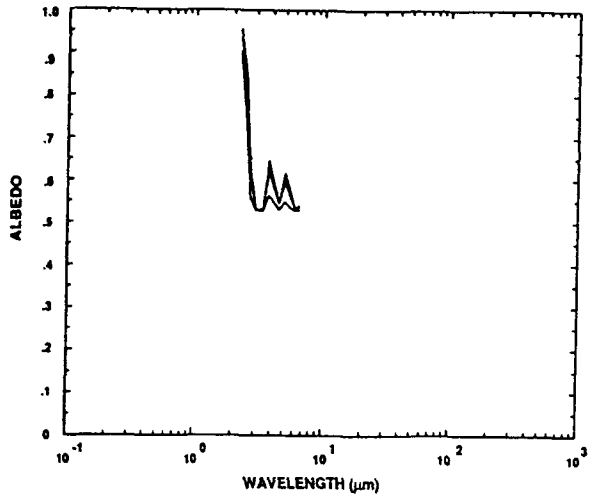
PRA
Photon Research Associates, Inc.

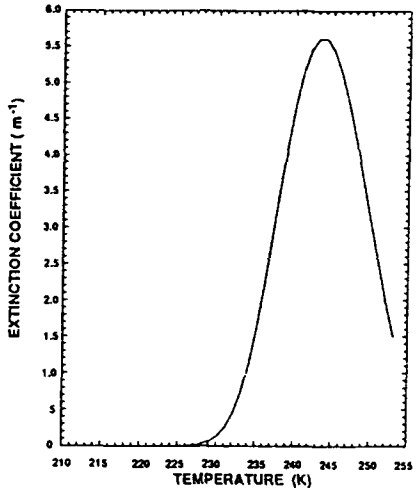
SUBVIS PARTICLE SIZE DISTRIBUTION



SUBVIS CIRRUS CLOUD

- 220, 230, 240, 250 K
- Geometrical Limit





SUBVIS MODEL DEFICIENCIES

- No Phase Functions
- No Multiple Scattering

} Input to LOWTRAN

- Limited Spectral Region (2.2 - 6.2 μm)
- Geometric Limit on Extinction
  - No Particles Less Than 20 μm Diameter
- Particles Randomly Oriented

CORRECTION FOR FORWARD SCATTER

- Replace

  $\sigma_{EXT} = K_{ABS} + \sigma_{SCAT}$

  with

  $\sigma_{EXT} = K_{ABS} + K\sigma_{SCAT}$

  Where g is Asymmetry Factor

- Sample Values of k
  - Hansen (1 - g) $\approx$ 0.49
  - Liou $\approx$ 0.83
  - APART $\approx$ 0.82 - 0.84

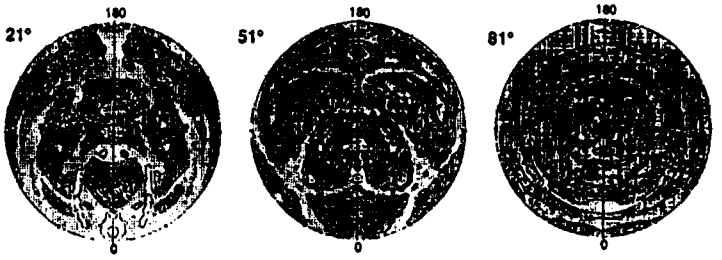
LIOU MODEL DEFICIENCIES

- Apparently Not Available
- Unknown Spectral Region
- Probable Geometric Limit
  - No Particles Less Than 20 μm Diameter
- Particles Randomly Oriented
- Unknown Term in Paper

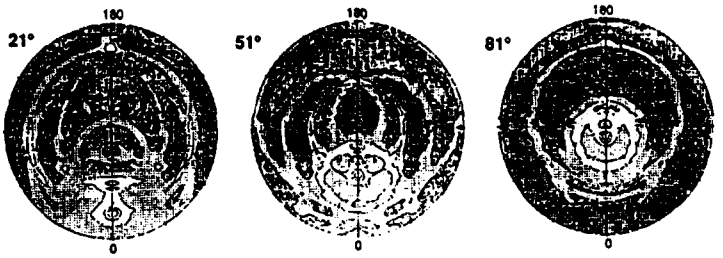
PRA
Photon Research Associates, Inc.

SINGLE SCATTERING DIAGRAMS

- **Upward Scattered Radiation**



- **Downward Scattered Radiation**



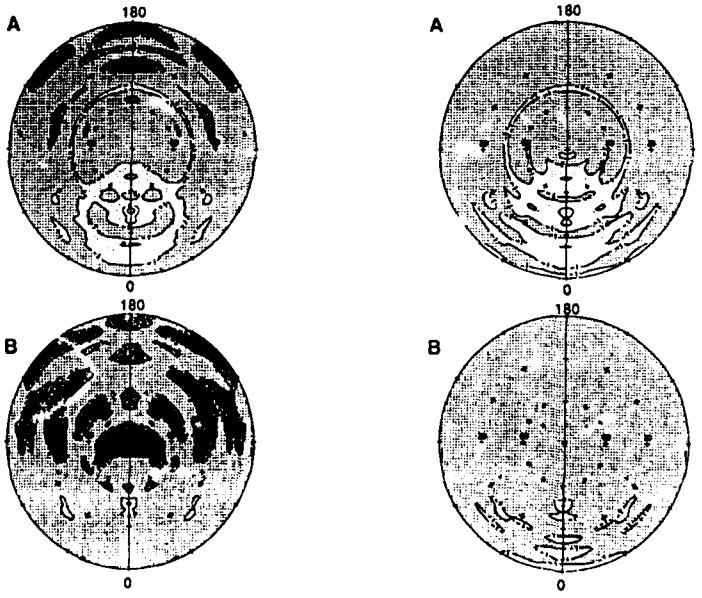
PRA
Photon Research Associates, Inc.

DUAL/TRIPLE SCATTERING DIAGRAMS

- **Dual Scattered**
- **Triple Scattered**

Upward 45°

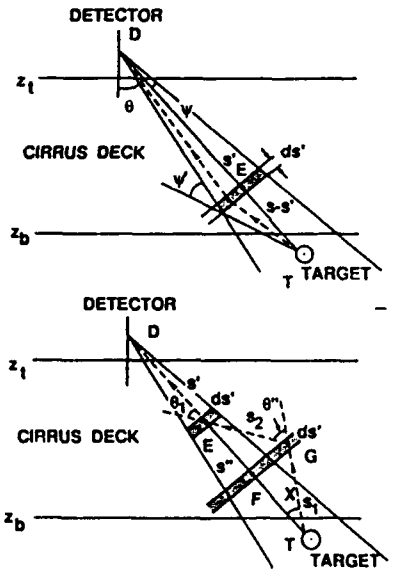
Downward 45°



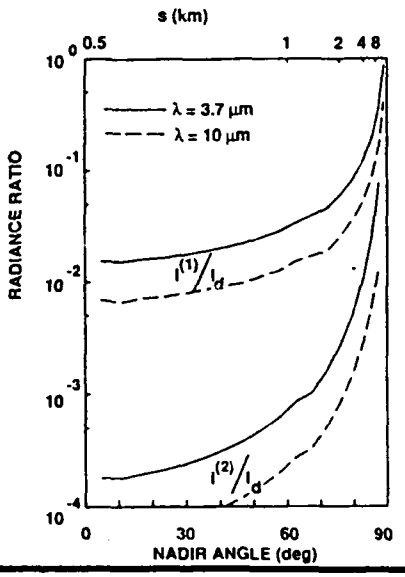
RECOMMENDATIONS

- Incorporate Capabilities into APART/MODTRAN
  - SUBVIS Cirrus Model
  - Forward Scatter Correction (MODTRAN)
  - Different Size Distributions
- Upgrade Capabilities
  - Empirical Phase Function
  - Oriented Particles
  - Small Particle Sizes
- Perform Sensitivity Study

MULTIPLE SCATTERING (LIOU)



- Midlatitude Winter
- Sensor IFOV = 2^o
- Cloud Top 8.5 km
- Cloud Thickness 0.5 km



ICE-CLOUD
A MODEL FOR IR TRANSMITTANCE THROUGH CIRRUS CLOUD

W.T. Kreiss, R. Vik
Horizons Technology, Inc., 3990 Ruffin Road, San Diego, CA 92123

ICECLOUD is a model for transmission of IR through cirrus clouds developed for the IASPM project. This task outlines the physical ideas on which the procedure is based. The model sets criteria for the occurrence of ice water and sets parameters defining the number, density and size distribution of the ice particles present. The ice particles are assumed to be hexagonal cylinders. Single particle optical scattering parameters appropriate to these particles (calculated using geometric optics) are used. The model represents transmission through dense cirrus clouds in a narrow region of the IR spectrum. The model can be improved, however, to broaden its applicability.

ICECLOUD

A MODEL FOR TRANSMITTANCE THROUGH CIRRUS CLOUD

BY

ROBERT C. VIK AND WILLIAM T. KREISS
HORIZONS TECHNOLOGY, INC.
3990 RUFFIN ROAD
SAN DIEGO, CA 92123-1826
(619) 292 8331

PRESENTED AT

THE ANNUAL REVIEW CONFERENCE ON ATMOSPHERIC MODELS
11-12 JUNE, 1991
GEOPHYSICS DIRECTORATE, PHILLIPS LABORATORY
SCIENCE CENTER, BUILDING 1106
HANSCOM AIR FORCE BASE
BEDFORD, MASSACHUSETTS 01731-5000

This work is being supported by the Tri-Services and the Department of Defense under the Defense Nuclear Agency Contract DNA001-90-C-0162.

CIRRUS CLOUDS CAN HAVE SIGNIFICANT EFFECTS ON LONG-RANGE IR SENSOR PERFORMANCE

- IADM/IRSTS FLIGHT TESTS
  - ANOMALOUS DEGRADATION
  - SUBVISUAL CIRRUS POSSIBLE CAUSE
- LIDAR/RADIOMETER TEST PROGRAM
  - CHARACTERIZED CIRRUS AS AN IR ENVIRONMENT
  - POINTED TO USE OF LOWTRAN7 CIRRUS MODELS
- CONCLUSIONS
  - BACKGROUND RADIANCE IMPORTANT (AS WELL AS PATH TRANSMITTANCE)
  - LOWTRAN7 MODELS ARE USEFUL, BUT:
    - EMPLOY SPHERICAL PARTICLES
    - PROVIDE OPTICAL DEPTH FROM GEOMETRICAL THICKNESS
- REQUIREMENT FOR A BETTER CIRRUS MODEL FOR IASPM

- **REQUIREMENTS FOR A CIRRUS MODEL IN IASPM**
  - **MUST INCLUDE SUBVISUAL CIRRUS**
  - **MUST TREAT NON-SPHERICAL ICE PARTICLES**
  - **OPTICAL DEPTHS MUST BE DETERMINED FROM OBSERVATIONAL DATA**

- **EXISTING KNOWLEDGE**
  - **OCCURANCE AND MICROPHYSICS OF CIRRUS CLOUDS (NCAR)**
  - **HEXAGONAL ICE PARTICLE OPTICAL PROPERTIES (UTAH)**

- **"ICECLOUD" MODEL**
  - **GOOD FOR THE TIME**
  - **WE KNOW HOW TO BUILD A BETTER MODEL NOW**

```
      PROGRAM ICECLOUD
C*****************************************************************
C
C        NCAR MODULES BY JOANNE PARRISH, NCAR, JULY 1986
C        UTAH MODULES BY LIOU AND TAKANO, LIOU AND ASSOCIATES, AUG 1988
C
C*****************************************************************

      REAL TREP, ICE
C                 TREP and ICE are the average temperature (deg K)
C                 and ice-water density (Gm/M**3) in the ice cloud.
      INTEGER IBOT,ITOP,ML,ICL,NCL
C           ML is the no. of LAYER's, and NCL is the no. in the cloud.
C                    ICL is the index of the first ice cloud LAYER.
C               IBOT and ITOP are, respectively, the indices of
C                    the bottom and top LEVEL's of the ice cloud.

      CHARACTER*64 INNAME, OUTNAM
      CHARACTER*72 TITLE
      PARAMETER (MAXP=1000,MAXL=34)

      IOS = 0
      OUTNAM = 'LOCARD'
      INNAME = 'MOD1.INP'

      OPEN(UNIT=1,FILE=INNAME,STATUS='OLD',IOSTAT=IOS)
c        Unit 1 is the input file

      CALL READSND

      CLOSE(UNIT=1)

      CALL PROFILE(ICL,IBASE,CBASE,ITOP,CTOP)

      ML = 34

      IF( ICL.NE.0 ) THEN
C               PROFILE returns ICL = 1 if there is an ice cloud.
        CALL CLOUD(IBASE,IBOT,ITOP,TREP,ICE)
      END IF

      IF ( ICL.NE.0 .AND. ICE.GT.1.E-06 ) THEN
        CALL LAYERS(ML,IBOT,ITOP,ICL,NCL)
        CALL BEBA(TREP)
      ELSE
        CALL NOICE(ML)
      END IF

      CALL NEWCOM

      CALL ARISPM(ML, ICE, OUTNAM)

      STOP

1000  FORMAT (A64)

      END
```

Figure 1. ICECLOUD main program

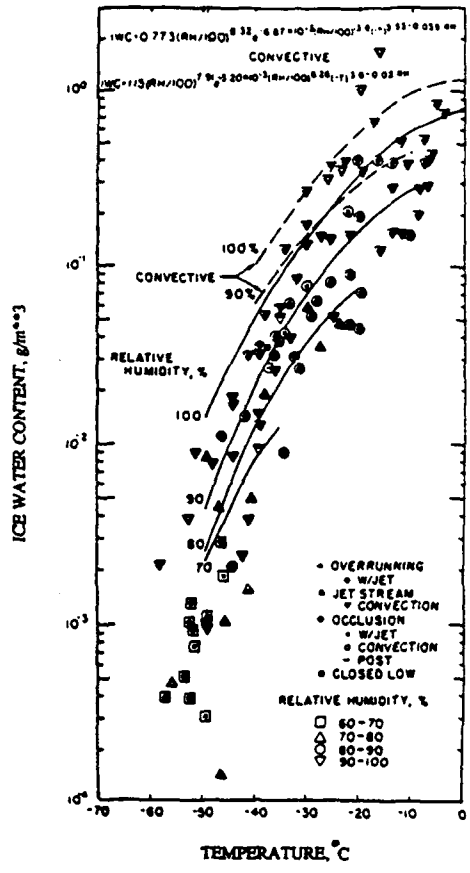
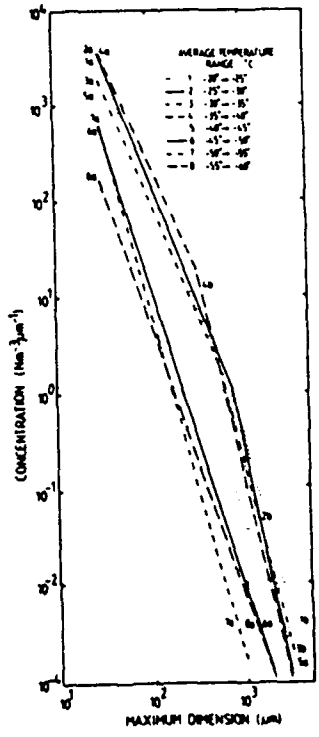
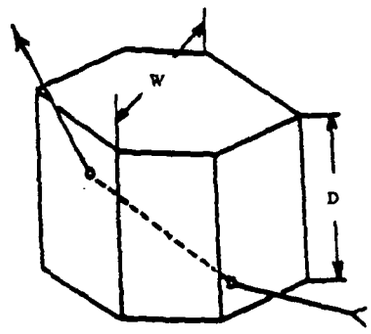


Figure 2. Cirrus cloud ice water content plotted against temperature and parameterized in terms of relative humidity according to convective regions. (Inside symbol: synoptic type ; Outside symbol: relative humidity).



$N = AD^{B}$

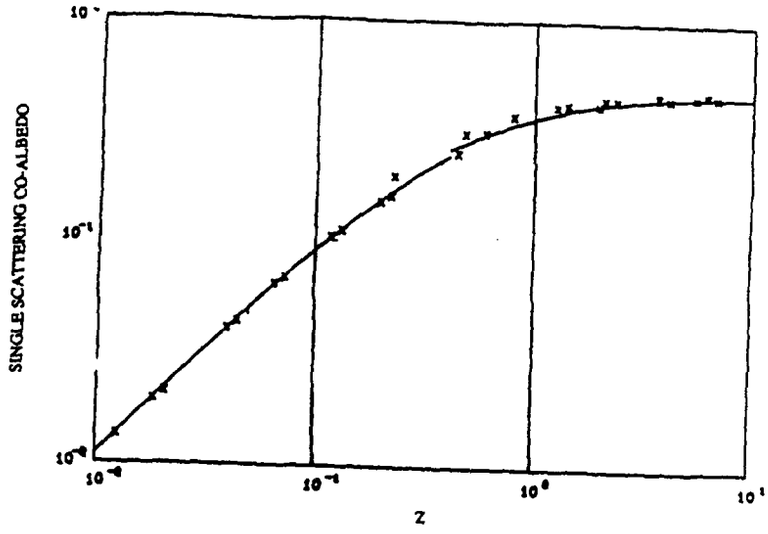
Figure 3. Curves fitted to the average spectra for each temperature range.



The extinction cross-section, averaged over look angles is:

$$C_e = 3/2\,(W/2)^2\,(\sqrt{3} + 4D/W)$$

Figure 4. Definition of extinction cross-section.



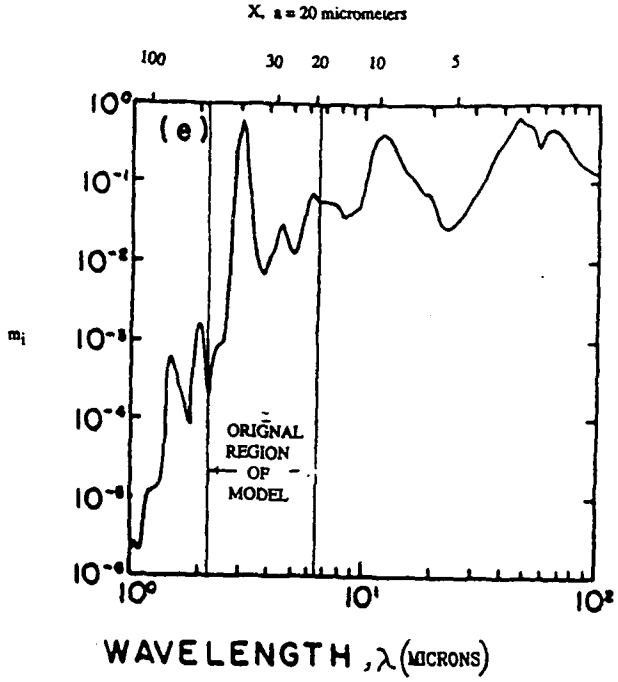
$z = 2\,m_i\,x$

m_i = imaginary part of the refractive index

x = size parameter:

$$x = \frac{2\pi}{\lambda}\,\frac{W}{2}\,\left(\frac{3\sqrt{3}\;D/W}{\sqrt{3} + 4\,D/W}\right)$$

Figure 5. Single scattering co-albedo.



C_e is valid for larger x (smaller λ) *a' forteriori*

$\tilde{\omega}$ is derived from calculations in the region $0.4 < \lambda < 2.5$ microns

Figure 6. Regions of validity of ICECLOUD.

"ICECLOUD" DEFICIENCIES

- DOES NOT APPLY TO SUBVISUAL CIRRUS
- APPLIES ONLY TO NARROW WAVELENGTH REGION
- SINGLE LAYER TRANSMITTANCE ONLY
- HIGH ALTITUDE WATER VAPOR MEASUREMENTS ARE DIFFICULT

ELECTO-OPTICAL MODEL FOR AERIAL TARGETING (EMAT)
(SUCCESSOR TO IASPM)

EMAT MODEL NEEDS

- BACKSCATTERING (BACKGROUND SCENES)
- PATH TRANSMITTANCE
- PATH RADIANCE
- MUST APPLY TO THIN AND SUBVISUAL CIRRUS
- CIRRUS CLIMATOLOGY/MORPHOLOGY
- A "PRESCRIBED" MODEL (STATISTICAL
- FULL WAVELENGTH COVERAGE

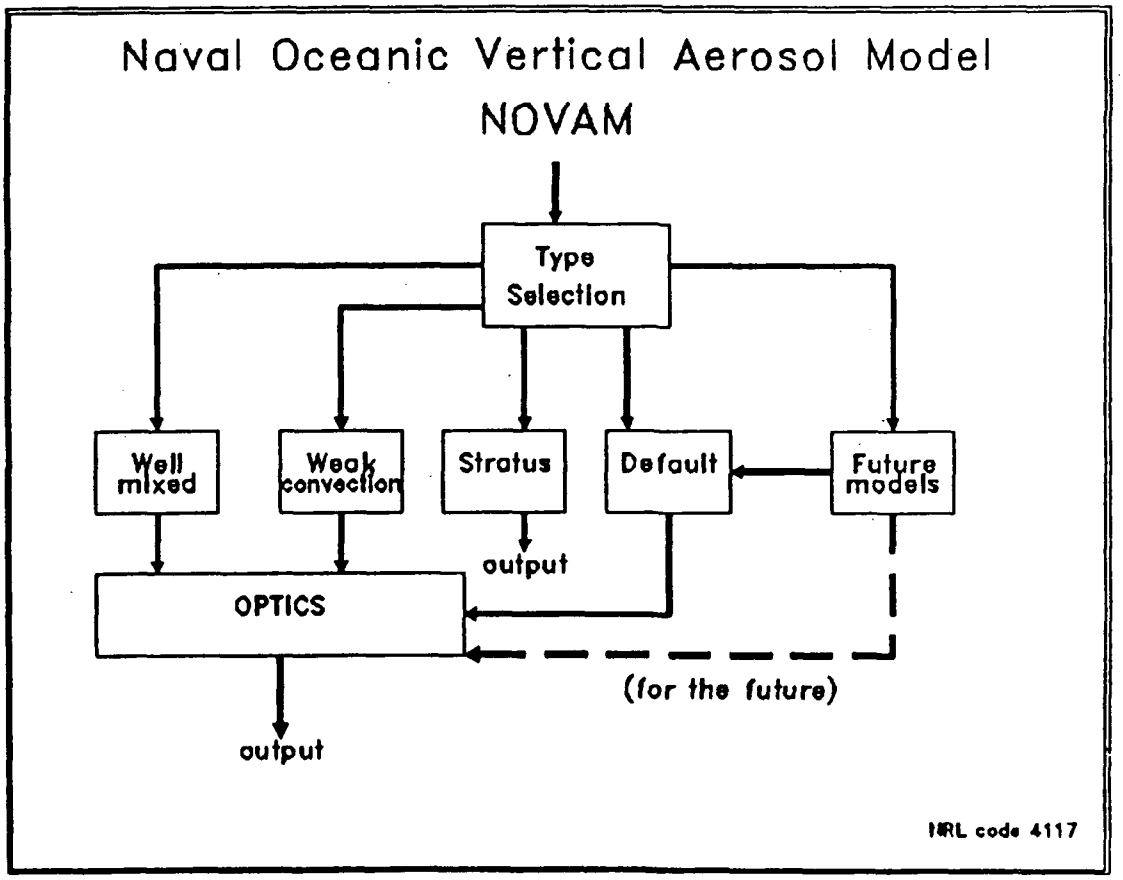
THE STATUS OF THE NAVY OCEANIC VERTICAL AEROSOL MODEL

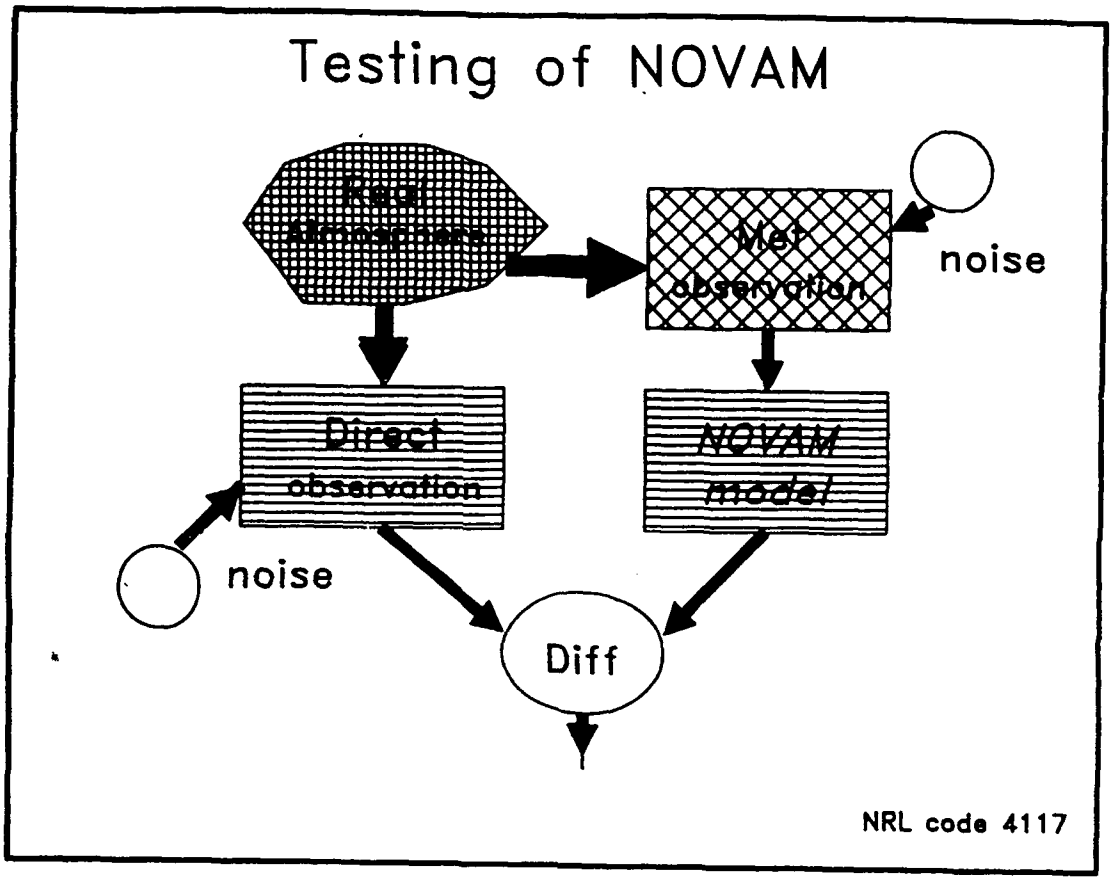
S. Gathman
Ocean and Atmospheric Sciences Division, Naval Ocean Systems Center,
San Diego, CA 92152

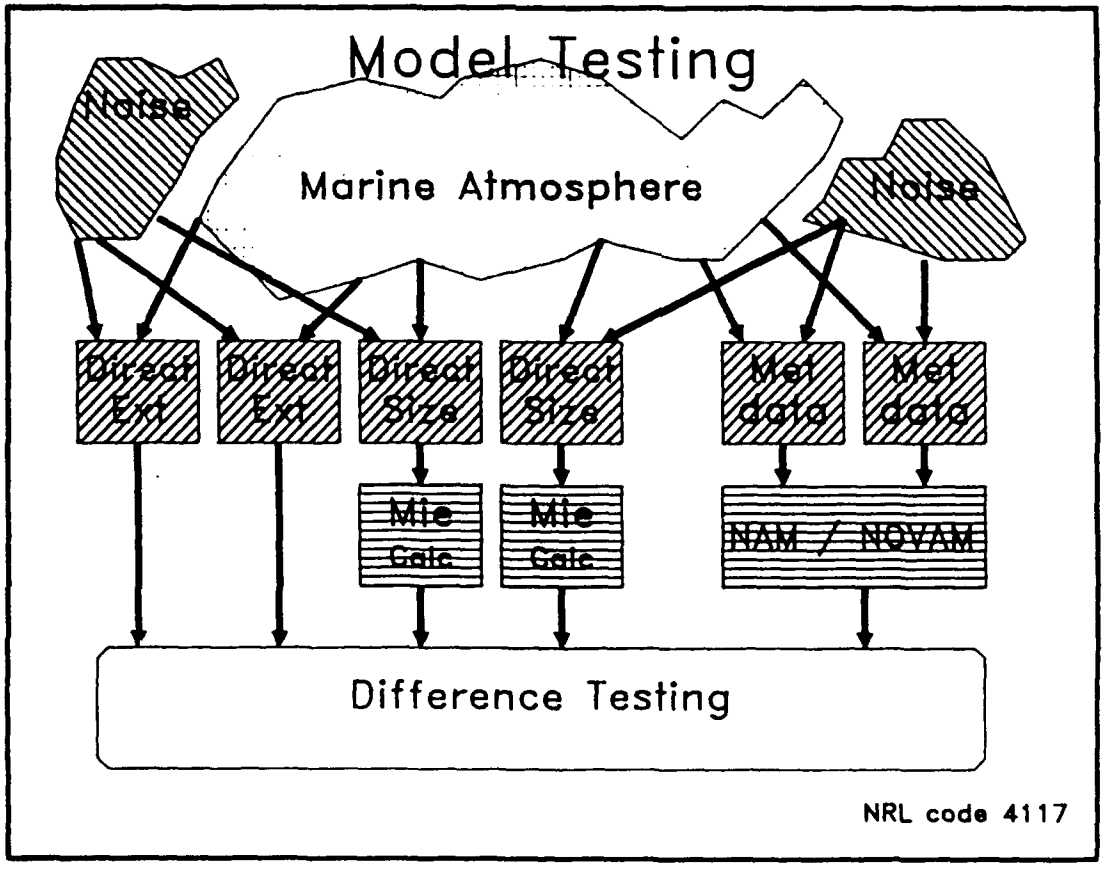
The Navy has been working on the development of a vertical aerosol model called NOVAM for several years. This model uses the navy aerosol model as a kernel for estimation of optical / IR properties of the atmosphere near the ocean surface and provides vertical structure of these properties specifically matched to oceanic conditions. The model utilizes surface meteorological data and radiosonde data as input. The model has been tested off of the California coast during the FIRE experiment and in the tropics during the KEY 90 experiment. This paper shows some of the results of these tests where predicted extinction profiles are plotted along side of measured extinction profiles.

The Status of the Navy Oceanic Vertical Aerosol Model

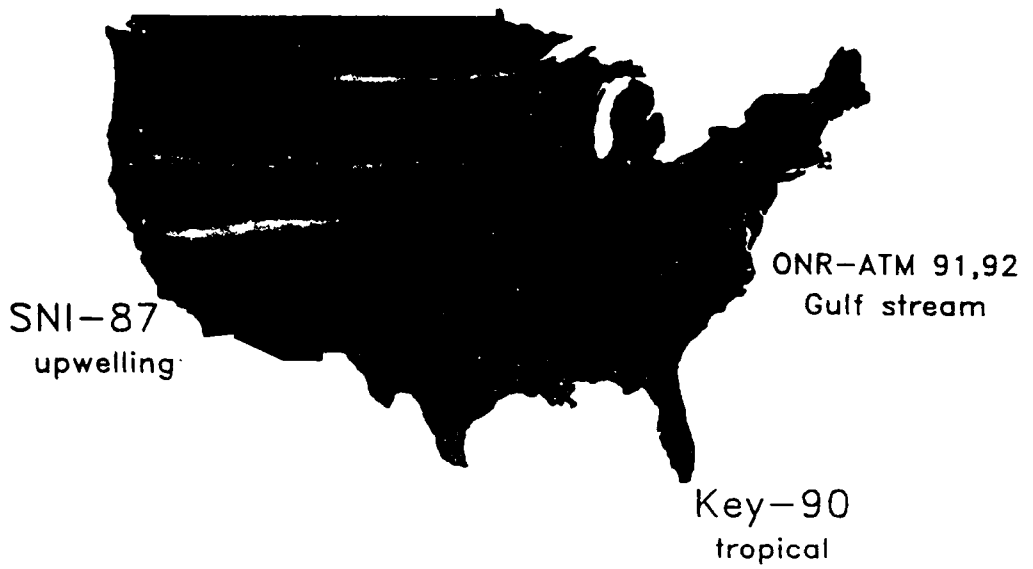
Stuart G. Gathman
NOSC code 543
San Diego, CA




Testing of NOVAM
Real Atmosphere
Met observation
noise
Direct observation
NOVAM model
noise
Diff
NRL code 4117


Model Testing
Noise
Marine Atmosphere
Noise
Direct Ext
Direct Ext
Direct Size
Direct Size
Met data
Met data
Mie Calc
Mie Calc
NAM / NOVAM
Difference Testing
NRL code 4117

NOVAM Testing



NRL code 4117

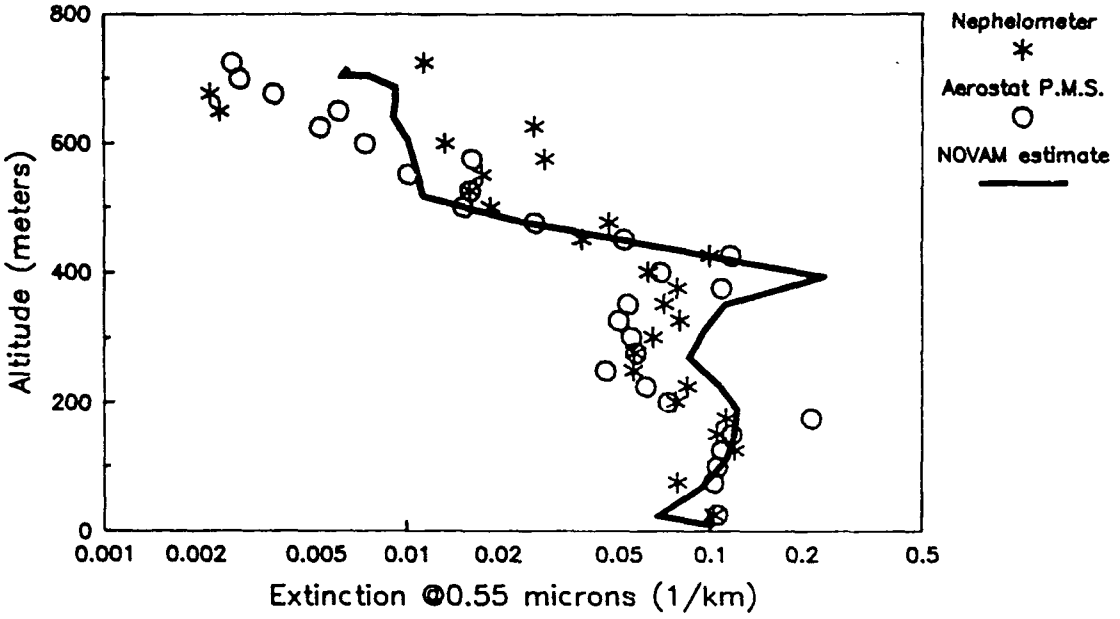
Testing Experiments

Field tests of NOVAM

- FIRE experiment at San Nicolas Island, CA. 1987
  - Tethered Aerostat Balloon
  - NOSC Navajo aircraft
  - NPS on the ship, *Point Sur*
- KEY–90 experiment Marathon Florida, 1990
  - Fishing boat for surface data
  - NOSC Navajo aircraft
  - NRL P–3A aircraft with LIDAR
  - Shore base LIDAR
- East Coast Experiment – plans for 91/92
  - Cooperation with IRAMMP, Summer 91
  - Cooperation with ONR/NRL ATI, FALL 91/92

NOSC code 543

Aerostat Measurements SNI–87
(flight 1814)

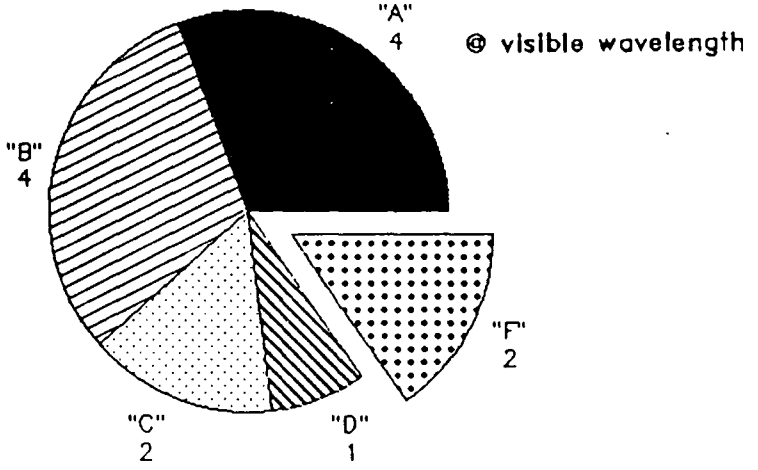


NRL code 4117

NOVAM Grades

"A"= within data envelope 90% of time

"B"= within data envelope 50% of time



"C"= within 2X data envelope 90% of time

"D"= within 2X data envelope 50% of time

(SNI 1987)

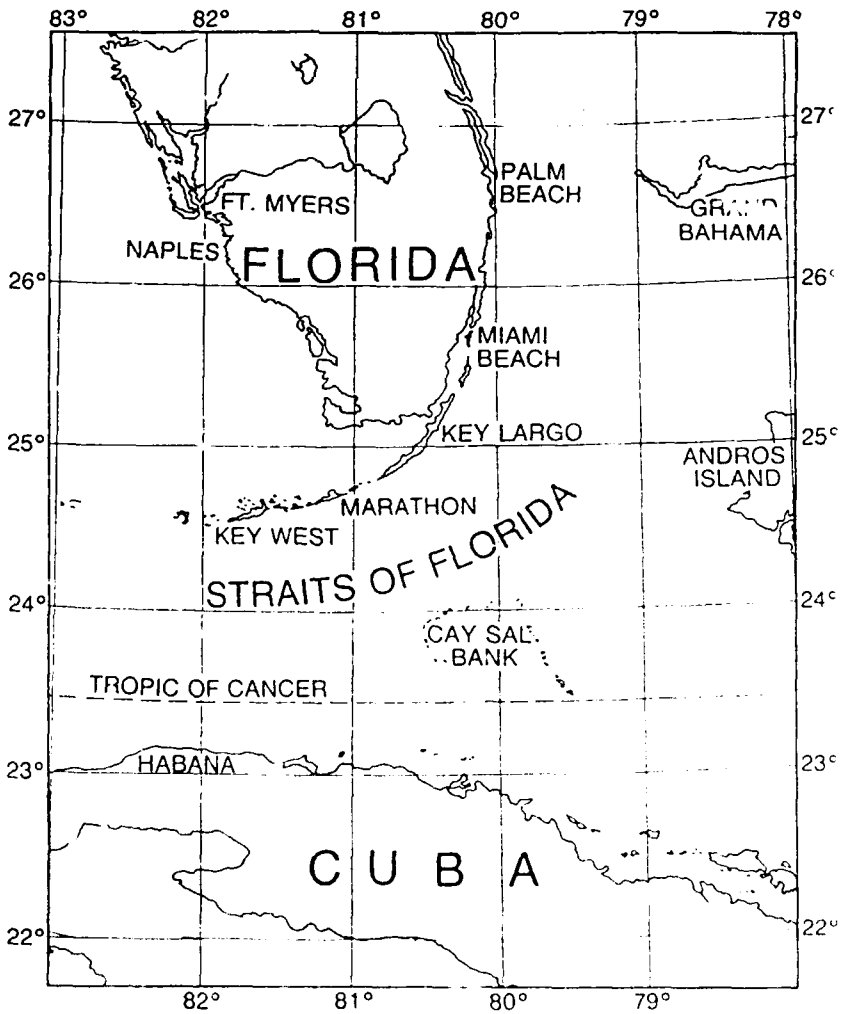
NRL code 4117

KEY-90 – Verification of NOVAM in a "tropic like" environment

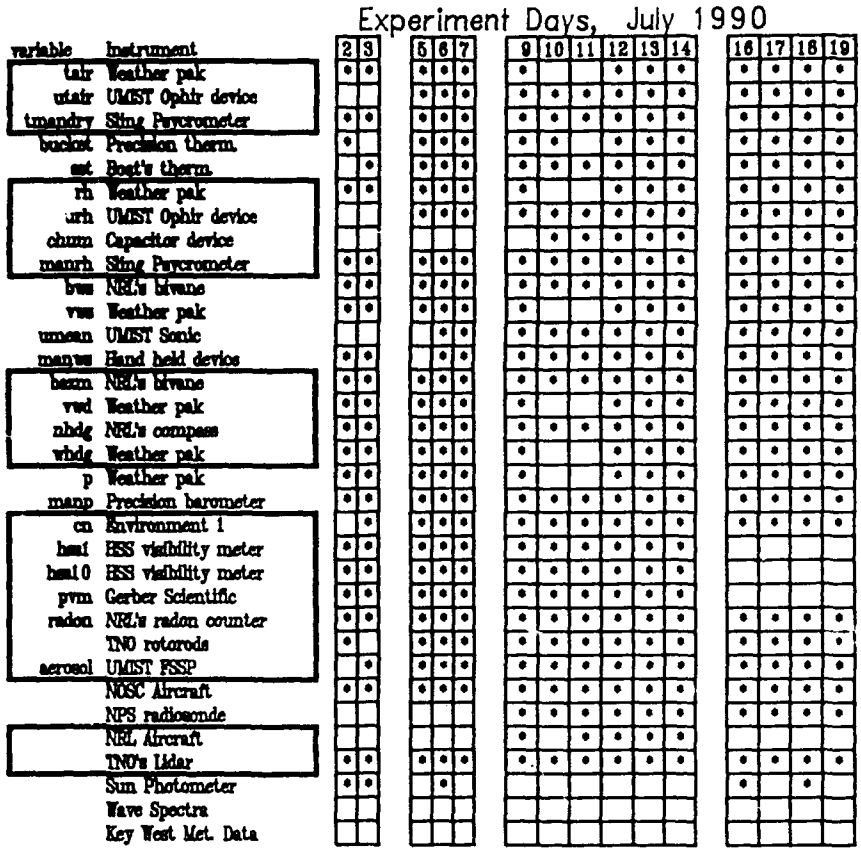
MEASURED EXTINCTION PROFILE

- **Measured profile of Aerosol size distribution**
  (Extinction calculated from Mie theory)
  NOSC aircraft with PMS probes
- **Surface Aerosol size distribution**
  Boat: UMIST PMS probe + TNO rotorod.
  (Extinction calculated from Mie theory)
- **Surface extinction @ 3–5 and 8–12 bands**
  Boat: PVM instrument.
- **Downward looking lidar using aureole measurement.**
  NRL P3 aircraft.
- **TNO's lidar using the Kunz calibration.**
  Shore based measurement.

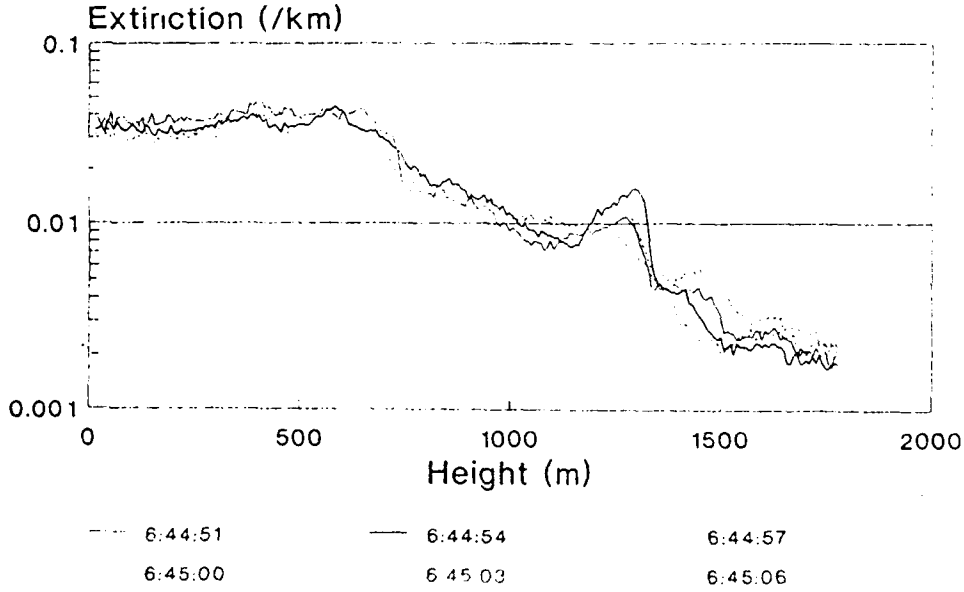
NRL code 4117



KEY - 90



Extinction Profiles (for NRL lidar)



7/14/90;shots:726-730;24°38′N,80°58′W

Session 2

Summary of the Session on Atmospheric Propagation Models

The status of atmospheric propagation models is steadily improving. Problems that once appeared intractable are now being implemented on PCs. LOWTRAN has become a tri-service/industrial standard that is now commercially available. Other codes are also following suit. The increased resolution of new codes has allowed for examination of different problem areas. In particular, Non-LTE and other upper atmospheric problems are now being considered. This has brought attention to the altitude mismatch in results between various codes that work in the lower atmosphere and those which have been designed to operate in the upper atmosphere. This problem is being worked and should be resolved in the near future.

Comments on specific presentations:

MODTRAN/LOWTRAN: CURRENT STATUS, FUTURE PLANS
Presented by L. Abreu

MODTRAN compares well with SHARC. Favorable comparisons have also been done with LOWTRAN7 and FASCOD3. Improvements in MODTRAN will be in the area of radiative transfer (multiple scattering algorithms). World wide model atmospheres will be added, and the code will be made more modular. MODTRAN and APART will be integrated for work on spectral backgrounds.

FASCODE3: An Update
Presented by G. Anderson

The history of FASCODE development was presented. Currently FASCODE is trying to produce "exact" results in an optimized fashion (e.g. mathematical line shape, layer selection, etc.). Improvements underway currently consist of improving the portability, radiance algorithm, cross-sections, HITRAN capability, and dealing with non-local thermodynamic equilibrium (NLTE) and transitions from LTE to NLTE. Finally FASCODE3 has not been released because too many corrections/additions were needed.

EOSAEL 92
Presented by A. Wetmore

The 1992 version of the Electro-Optical Systems Atmospheric Effects Library (EOSAEL) will leave unchanged the following modules: NMMW, CLTRAN, COPTER, GRNADE, MPLUME, OVRCST, FCLOUD, ILUMA, FASCAT, LASS, GSCAT, NOVAE, and RADAR. The following modules will be upgraded: LOWTRN, LZTRAN, KWIK, XSCALE, TARGAC, COMBIC. The SABRE and MSCAT modules will be dropped. Four new modules will be added: BITS - to be used for broad-band integrated transmittance; FASCODE - GD's model; NBMSCATT - a radiative transfer approximation; and UVTRANS - a UV transmission, fluorescence, and lidar program. The various modules are also being made interactive.

HITRAN '91: The Contemporary Spectroscopic Molecular Database
Presented by L. Rothman

Major molecular parameter updates have been done for H_2O, CO_2, O_3, methane, CO, NO, NO_2, HNO_3, and the hydrogen halides (HCl, HF, HI, HB). There have been minor changes in the trace gases (H_2O_2, C_2H_2, HCH_6, SF_6) and COF_2 is being added. Provisions are also being made to convert HITRAN to run on a PC.

SHARC, An Atmospheric Radiation and Transmittance Code for Altitudes from 50 to 300 km
Presented by D. Robertson

SHARC was initially developed for SDIO for modeling radiance in the upper atmosphere. SHARC will handle Non-LTE conditions found in the upper atmosphere (50 - 300 km) in either ambient or auroral conditions. Current resolution is .5 inverse centimeters at wavelengths from 2 to 40 microns. A manual is currently being printed and will be available shortly.

Recent Development of the GENLN2 line–by-line model: studies in support of the UARS project
Presented by D. Edwards

GENLN2 is a line-by-line Non-LTE atmospheric transmittance and radiance code. It contains six GD model atmospheres, is modular, and will produce plots using NCAR graphics. Comparisons with ATMOS have been favorable, with reasonably good transmission over a variable spectral grid.

Present status of Transmittances and Radiances Modeling at L.M.D.
Presented by N. A. Scott

L.M.D. is investigating the impact of high resolution measurements for/on signatures. The fast-running, versatile codes compute transmittance and/or radiance for a variety of conditions.

AURIC (Atmospheric Ultraviolet Radiance Integrated Code): An Update
Presented by R. Huguenin

AURIC is being developed as an atmospheric UV spectral transmission and solar irradiance code. MODTRAN is the starting point; AURIC's structure will try to stay with MODTRAN's. The initial release will not include airglow, will have a resolution of 1 wavenumber with interpolation to .5 wavenumber. Optimum methods are being employed, particularly in the temperature dependent model, in order to have the code run faster.

ONTAR's PC Compatible LOWTRAN7 Package
Presented by J. Schroeder

ONTAR entered into a cooperative R & D agreement with GP in 1988. Since then, ONTAR has released various versions of GP's LOWTRAN code. The most recent version, release 3.8, has the full LOWTRAN7 implemented. Online help is available with this interactive version of LOWTRAN as are plotting routines which include overlays for different runs.

ONTAR's LOWTRAN7 has been certified by GP and runs in 640K on a PC with no memory extender required: however, a coprocessor is recommended.

Coupling Atmospheric and Background Effect
Presented by W. Cornette

The development of a computer model to determine thermal clutter in a scene with changing atmospheric conditions was described. The model is sensitive to solar radiation and includes numerous terrain materials for background effects. Terrain scenes and several cloud models at varying altitudes are included.

SENTRAN7: A Sensitivity Analysis Package for LOWTRAN7/MODTRAN
Presented by D. Longtin

SENTRAN7 was described as a user active analysis code designed to perturb various input parameters of LOWTRAN7 or MODTRAN. Graphical outputs are created in 2D and 3D formats. The code is currently designed to operate on VAX/VMS and SUN Unix systems. A complete description of the user input commands and the graphical requirements required was presented.

Atmospheric Models in the Strategic Scene Generation Model
Presented by W. Cornette

The Strategic Scene Generation Model was described in detail with special emphasis on the atmospheric propagation models currently implemented in the code. The background scene modules APART, GENESIS and CLDSIM were described with 2D simulations of terrain and cloud scenes. Simulations on varying resolution of transmittance, calculations were shown and some subtle differences between MODTRAN and APART were explained.

Review of the Chemical Kinetic Rate Constants Used in the SHARC Model
Presented by A. Pritt

As the title indicates, this was a comprehensive review of the chemical kinetic rate constants being used in the SHARC model. A basic explanation of SHARC and NLTE conditions was given, along with an explanation of the derivation of H_20 and CO rate constants. The presenter showed numerous comparisons between SHARC and a large and impressive series of measurements.

MODTRAN/LOWTRAN: CURRENT STATUS, FUTURE PLANS

L.W. Abreu, F.X. Kneizys, G.P. Anderson, J.H. Chetwynd
Geophysics Directorate, Simulation Branch (OPS),
Hanscom Air Force Base, MA 01731-5000

MODTRAN (public release: November 1990) is a 2 parameter (P&T) band model code with moderate spectral resolution (2 cm^{-1} full width-half maximum). The MODTRAN band model parameters were calculated by utilizing the HITRAN-86 data base. The code is fully compatible with LOWTRAN 7 and the results can be degraded to between 2 and 50 wavenumber spectral resolution.

Future plans include an improved more accurate multiple scattering algorithm as well as a realistic modelling of the atmosphere-to-background-to-atmosphere coupling technique. A definitive set of worldwide model atmospheres is presently under development.

MODTRAN/LOWTRAN: CURRENT STATUS, FUTURE PLANS

L.W. ABREU, F.X. KNEIZYS, G.P. ANDERSON
and J.H. CHETWYND

ANNUAL REVIEW CONFERENCE ON ATMOSPHERIC TRANSMISSION MODELS

11-12 JUNE 1991

GEOPHYSICS DIRECTORATE
PHILLIPS LABORATORY

SOFTWARE DESCRIPTION FOR
ATMOSPHERIC PROPAGATION MODELS AND DATA BASE:

FASCODE, MODTRAN, LOWTRAN, HITRAN

o Common Elements:

Transmittance and Radiance
Geometry, thermal multiple scattering
Default atmospheric profiles
(molecular, aerosol, particulates)
Spectral range: 0 to 50,000 cm^{-1} (0.2μm to ∞)
Interpolation, Scanning, and Filter Functions

o FASCODE (FASCOD2-1986; FASCOD3-1990)

Resolution:	Line-by-line (high)
Physics:	"Exact", Voigt
Altitude Range:	0 to space
Applications:	High resolution simulations (LTE, NLTE, Laser, Lidar)
Comments:	Slow for large spectral ranges Requires external database (HITRAN) Requires NLTE specifications Recognized International Standard

o MODTRAN (1990)

Resolution:	2 cm^{-1} (moderate)
Physics:	2-parameter band model (P and T)
Altitude Range:	60 km
Applications:	Moderate resolution simulations, solar (direct and scattered)
Comments:	Moderate time consumption No NLTE Spectral database stored in 1 cm^{-1} bins

o LOWTRAN (1989)

Resolution:	20 cm^{-1} (low)
Physics:	1-parameter band model (P)
Altitude Range:	0 to 50 km (limited by band model)
Applications:	Broad band spectral simulations Solar (direct and scattered)
Comments:	Efficient (no time penalty) Loss of small scale spectral character Recognized International Standard

o HITRAN (HITRAN86-1987, HITRAN90-1990)

Resolution:	Infinite
Physics:	Complete spectroscopic parameters for over 350,000 transitions for 28 separate molecular species Molecular cross sections for 9 additional species
Application:	Source data for high resolution line-by-line synthesis of molecular absorption properties Used directly by FASCODE Source of derivative band models for MODTRAN and LOWTRAN
Comments	Recognized International Standard

THE LOWTRAN MODEL

ATMOSPHERIC TRANSMITTANCE/BACKGROUND RADIANCE
- 20 CM-1 RESOLUTION

33 LAYER ATMOSPHERIC MODEL
- CHOICE OF MODEL ATMOSPHERES, AEROSOL MODELS
- USER DEFINED

GEOMETRY FOR ANY SLANT PATH
- LOOKING UP/DOWN
- TANGENT HEIGHTS
- HORIZONTAL PATHS

PRODUCT TRANSMITTANCE DUE TO
- MOLECULAR ABSORPTION (BAND MODEL)
- MOLECULAR SCATTERING
- AEROSOL EXTINCTION
- CONTINUUM ABSORPTION

THERMAL EQUILIBRIUM IN EACH ATMOSPHERIC LAYER

LOWTRAN7

ABSORBER	SPECTRAL RANGE (CM^{-1})
Water Vapor (H_2O)	0-17860
Ozone (O_3)	0- 200, 515- 1275, 1630- 2295, 2670-3260, 13000-24200, 27500-50300
Uniformly Mixed Gases.	
Methane (CH_4)	1065- 1775, 2345- 3230, 4110- 4690, 5865- 6135
Nitrous Oxide (N_2O)	0- 120, 490- 775, 865- 995, 1065- 1385, 1545- 2040, 2090- 2655, 2705- 2865, 3245- 3925, 4260- 4470, 4540- 4785, 4910- 5165
Oxygen (O_2)	0- 265, 7650- 8080, 9235- 9490, 12850-13220, 14300-14600, 15695-15955
Carbon Monoxide (CO)	0- 175, 1940- 2285, 4040- 4370
Carbon Dioxide (CO_2)	425- 1440, 1805- 2855, 3070- 4065, 4530- 5380, 5905- 7025, 7395- 7785, 8030- 8335, 9340- 9670

LOWTRAN7

ABSORBER	SPECTRAL RANGE (CM^{-1})
Trace Gases:	
Nitric Oxide (NO)	1700- 2005
Nitrogen Dioxide (NO_2)	580- 925, 1515- 1695, 2800- 2970
Ammonia (NH_3)	0- 2150
Sulphur Dioxide (SO_2)	0- 185, 400- 650, 950- 1460, 2415- 2580

LOWTRAN 7 BAND MODEL

TRANSMITTANCE FUNCTIONS

$$T = EXP\ [\ -\ (CW)^a\ ]$$

$$W = (P/P_o)^n \times (T_o/T)^m \times U$$

where:

a,n,m are BAND MODEL PARAMETERS

U = ABSORBER AMOUNT

C = BAND MODEL ABSORPTION COEFFICIENT

MODTRAN : Specific Attributes

* Moderate Spectral Resolution 2 cm^{-1} (FWHM)

* 2 Parameter Band Model (P,T)

  1 cm^{-1} Bins Stored On Tape

  Calculated From 1986 HITRAN Data Base (0 - 17900 cm^{-1})

* Internal Triangular Slit Function

  Degradable To Desired Spectral Resolution

* Atmospheric Molecules :

  H_2O O_3 CO_2 CH_4 N_2O CO N_2

  O_2 HNO_3 NO NO_2 NH_3 SO_2

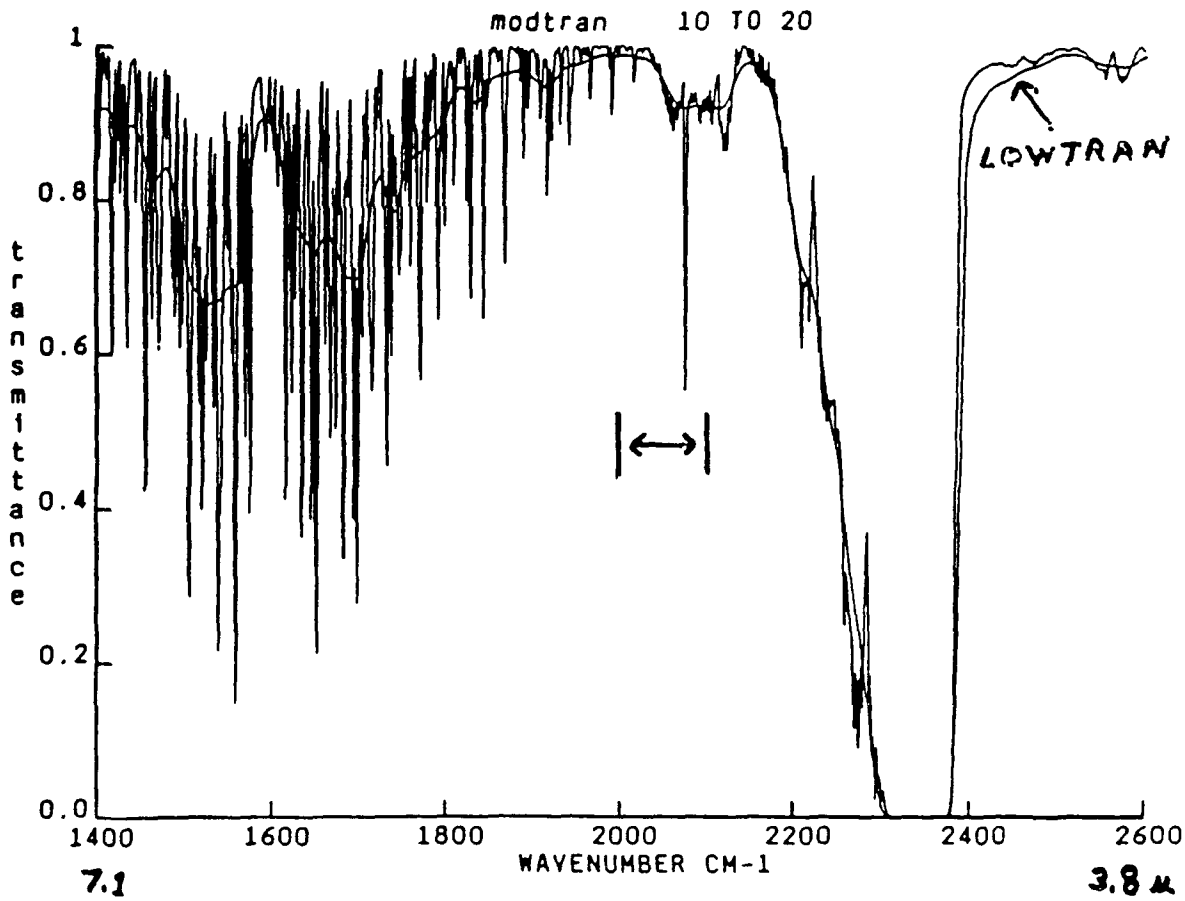
EXPANDED APPLICABILITY

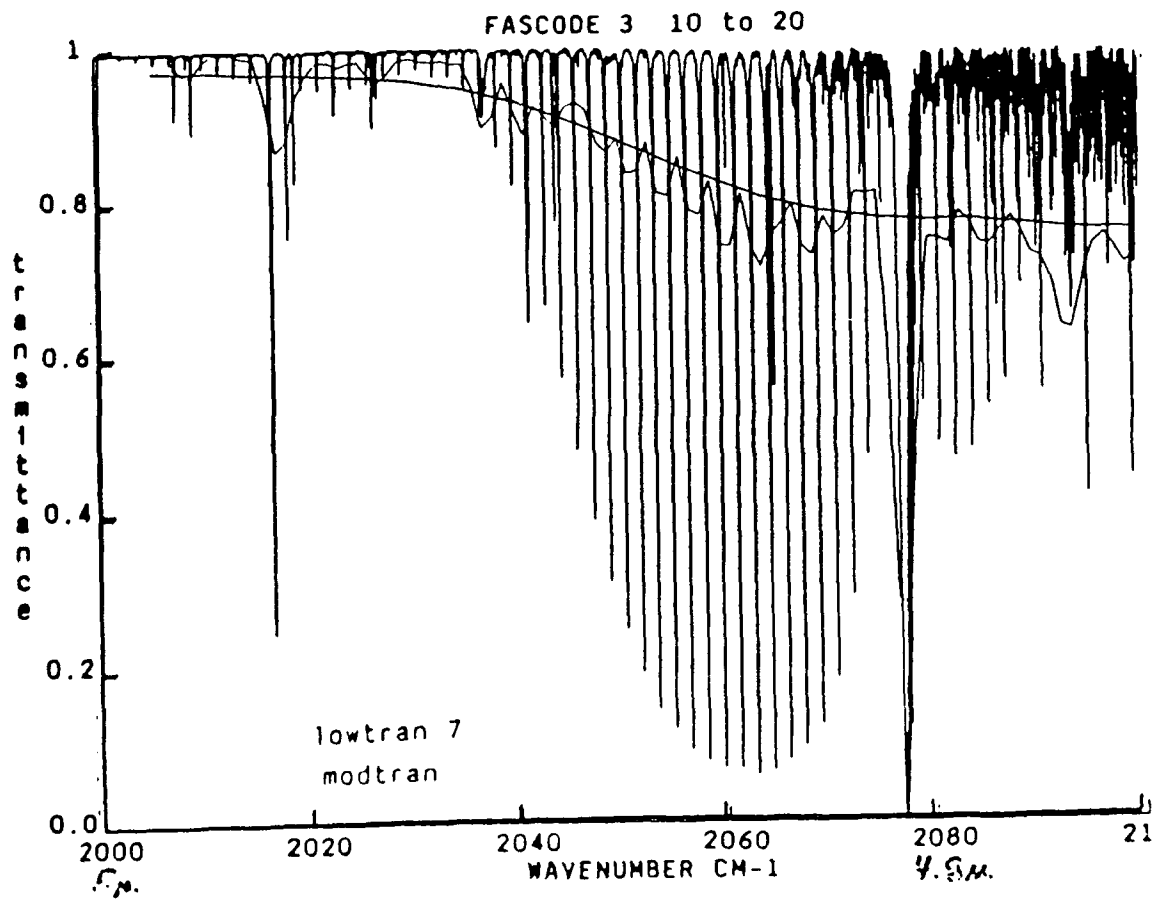
* MODTRAN IS BETTER SUITED THAN LOWTRAN FOR ATMOSPHERIC PATHS ABOVE 30 KM

  - Band Model Parameters Are Both Temperature and Pressure Dependent

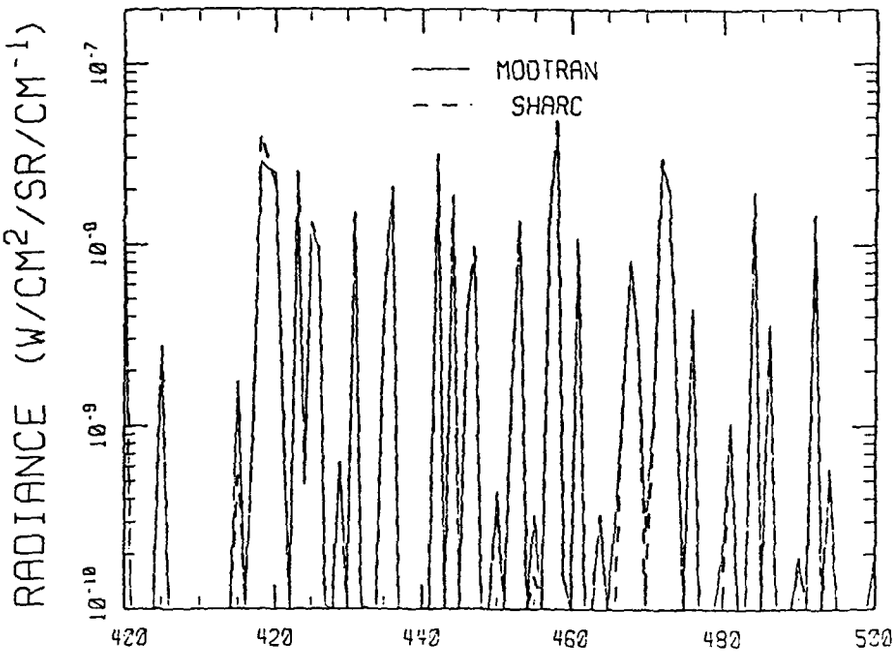
  - Transmittance Is Modeled With A Voigt Lineshape

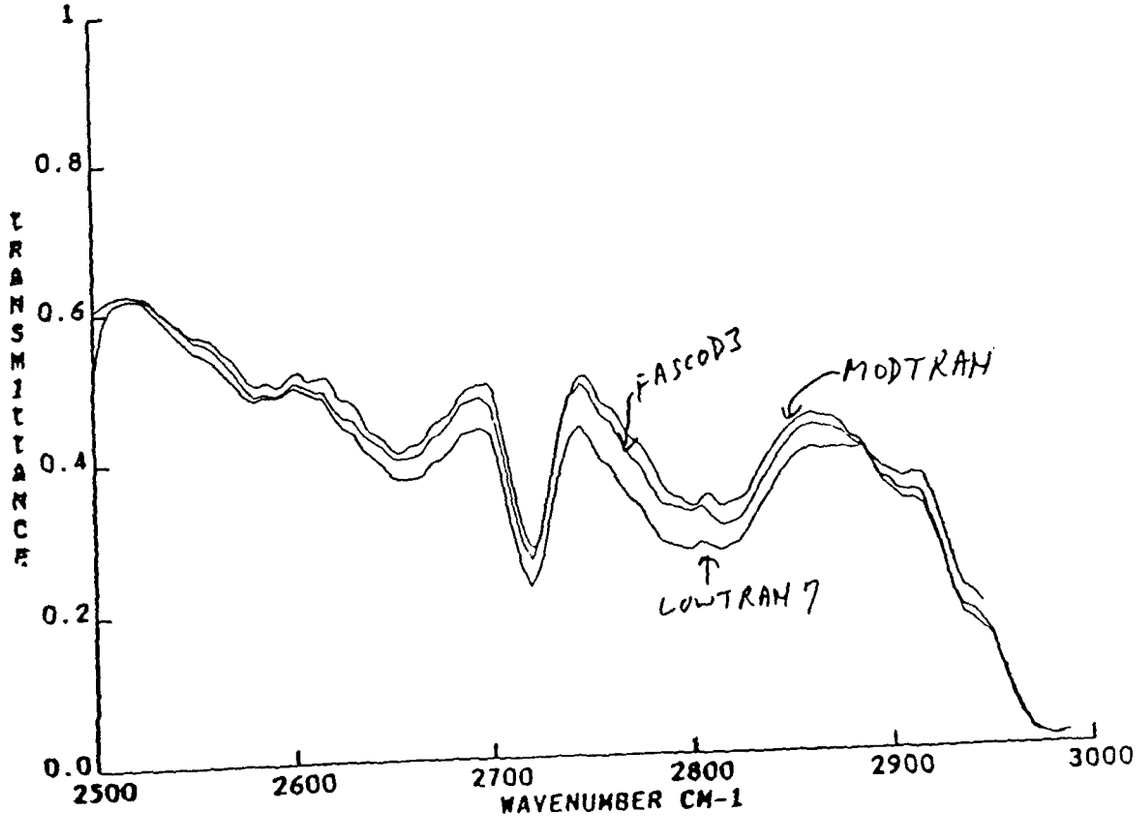
* HOWEVER, MODTRAN STILL ASSUMES LOCAL THERMODYNAMIC EQUILIBRIUM


modtran 10 TO 20
LOWTRAN
transmittance
1
0.8
0.6
0.4
0.2
0.0
1400
1600
1800
2000
2200
2400
2600
WAVENUMBER CM-1
7.1
3.8 μ


FASCODE 3 10 to 20
transmittance
1
0.8
0.6
0.4
0.2
0.0
lowtran 7
modtran
2000
2020
2040
2060
2080
21
WAVENUMBER CM-1

H_2O 60 KM LIMB





Range 8 km at SFC 20 gm/m³ H_2O

GL ATMOSPHERIC PROPAGATION MODELS

GENERAL PROPERTIES	FASCODE	MODTRAN	LOWTRAN
SPECTRAL RESOLUTION			
HIGH	X		
MODERATE	X	X	
LOW	X	X	X
CAPABILITIES			
TRANSMITTANCE	X	X	X
BACKGROUND RADIANCE			
THERMAL	X	X	X
SOLAR/LUNAR		X	X
NON-LTE	X		

SPECIFIC APPLICATIONS	FASCODE	MODTRAN	LOWTRAN
LASER PROPAGATION	X		
PLUME SIGNATURES	X	X	
TARGET CONTRAST	X	X	X
REMOTE SENSING	X	X	X

FUTURE PLANS

* IMPROVED MULTIPLE SCATTERING ALGORITHM BASED OI THE DISCRETE-ORDINATE-METHOD
* WORLD-WIDE DATA BASE OF MODEL ATMOSPHERES
* MODULARIZATION OF CODES
* INTEGRATION OF MODTRAN AND APART
* SPECTRALLY DEPENDENT BACKGROUNDS
* IMPROVED GEOMETRY ROUTINES FOR 32 BIT MACHINES

DOD POINT OF CONTACT FOR LOWTRAN 7 AND MODTRAN IS:

LEONARD W. ABREU
GL/OPS(AFSC)
HANSCOM AFB, MA 01731
(617) 377-2337 Autovon 478

DOD POINT OF CONTACT FOR FASCOD3 IS:

GAIL P. ANDERSON
GL/OPS(AFSC)
HANSCOM AFB, MA 01731
(617) 377-2335 Autovon 478

NOTE: DOD Contractors, please have your contract monitor make the request.

The codes are publicly available through:

National Climatic Data Center, NOAA
Environmental Data Services
Federal Building
Asheville, NC 28801

FASCOD3: AN UPDATE

G.P. Anderson, F.X. Kneizys, J.H. Chetwynd, L.W. Abreu, M.L. Hoke
Geophysics Directorate, Hanscom Air Force Base, MA 01731-5000

S.A. Clough, R.D. Worsham
Atmospheric and Environmental Research, Inc., 840 Memorial Drive, Cambridge, MA 02139

E.P. Shettle
Naval Research Laboratory, Code 6522, Washington, DC 20375

FASCOD3, a line-by-line atmospheric radiance-transmittance code, is currently available in a beta-test version. As with FASCOD2, the program is applicable to spectral regions from the microwave to the middle ultraviolet, employing standard spectroscopic parameters supplied from external line atlases. New FASCOD3 capabilities include: multiple scattering of thermal radiation, CO_2 and O_2 temperature-dependent line coupling for selected bands, UV diffuse absorption (0_2 and 0_3), improved weighting functions, enhanced non-local thermodynamic equilibrium (NLTE) calculations, and, perhaps most importantly, compatibility with the HITRAN91 database, including temperature-dependent cross sections. NLTE input requirements include LTE temperature and density profiles plus adequate descriptions of the NLTE population profiles for the specified excited vibrational states. Auxiliary NLTE line positions, halfwidths, strengths and vibrational-rotational assignments must also be provided.

FASCOD3: An Update

G.P. Anderson, F.X. Kneizys,
J.H. Chetwynd, L.W. Abreu, M.L. Hoke
(Geophysics Lab (AFSC))

S.A. Clough, R.D. Worsham
(Atmospheric and Environmental Research, Inc.)

E.P. Shettle
(Naval Research Laboratory)

Presented at the:

Annual Review Conference on Atmospheric Transmission Models
11-12 June 1991

FASCODE: Fast Atmospheric Signature Code

Version 3 - β

AFGL:	F.X. Kneizys	- Primary
	S.A. Clough[1]	- Primary
	G.P.Anderson	- UV, Constituent Profiles
	J.H. Chetwynd	- Programming, Validation
	L.W. Abreu	- LOWTRAN7 Compatibility
	W.O. Gallery[1]	- Geometry
	L.S. Rothman	- Line Atlas
	M.L. Hoke	- Line Coupling
	E.P. Shettle[2]	- Aerosols/Hydrometeors
	R.D. Worsham[3]	- X-sections, etc.

[1] currently at Atmospheric and Environmental Research, Inc.
[2] currently at Naval Research Laboratory
[3] at Atmospheric and Environmental Research, Inc.

Some thoughts on FASCOD3 presentation: 1 June 1991

1. Authorship 2. History/Contractor Support

3. FASCOD2/FASCOD3 in 1990 - "The Way We Were"

4. Delays in FSC3 release - why?

FASCODE: Fast Atmospheric Signature Code

Version 2 and Version 3-β

Visidyne:	H.J.P. Smith D.J. Dube M.E. Gardner	- contributions to FASCOD1C (1978)
	T.C. Degges	- NLTE theory (1977, 1985)
Sonicraft:	W.L. Ridgway R.A. Moose A.C. Cogley	- contributions to FASCOD2 (1985)
AER, Inc.:	R.G. Isaacs	- multiple scattering (1987)
	R.D. Worsham	- programming contributions to FASCOD3 & MS (1988-91)
	S.A. Clough	- radiance algorithm, etc. (1990-1991)

Introduction: (or "Just what is so difficult anyway?" and "Why bother?")

o Line-by-Line Radiance/Transmittance Model which attempts:

to provide "exact" solution to radiative transfer problem -
Beer's Law [T=exp(-a(i)*N(i))]
Planck Function [B=fn(T)]
Radiance Eqn [R=BdT]

to optimize mathematics for rapid solution

to account for realistic atmospheric lines-of-sight
(not including non-linear "seeing")

to maintain "state-of-the-art" spectroscopy

to unify physical description for all frequencies

to accommodate intrument design characteristics

o Limiting Considerations

Spectral sampling - governed by "true" line shape

Atmospheric layering - governed by Curtis-Godson approximation

Computer allocations - historic

o Solutions (?)

Optimize:
line shape per layer
layer selection
merging of adjacent layers

Provide "all" default options (realistic)

Maintain LOWTRAN compatibility for all non-molecular parameters

Support user-friendly I/O:
documentation, distribution, maintenance
user services

Basic Input/Output:

o INPUT

Mode

- optical depth
- transmittance
- radiance

Spectroscopic variables for line-by-line calculations

- external data bases (HITRAN86, NLTE, coupling coef.)
  [driven by LNFL routines for FASCOD3;
  BCDMRG routines for FASCOD2]
- internal block data (mm with coupling coef.)
- line shape including far wings and continua

Spectral range and sampling

- 500 cm^{-1} limit
- "buffering" at boundaries
- monochromatic option (laser)
- "natural" frequency spacing
  dv = 4 pts/halfwidth
- "instrumental" frequency spacing
  scanning and filter options

Line-of-sight/geometry

- horizotal
- H1 to H2 (-/+90°)
- tangent
- layering (boundaries and/or selection criteria)

Path characterization

- pressure, temperature
- constituent (trace) profiles
- hydrometeor profiles (clouds, rain, fog)
- particulate profiles (aerosols, dust, etc.)

FASCODE2/3: Fast Atmospheric Signature Code

Basic Input/Output:

o OUTPUT

Echo all input parameters

Path description

- layer selection
  pressure, temperature
  atmospheric constituent profiles*
  aerosol/hydrometeor profiles
  line shape, halfwidth

- geometry
  path type
  bending
  integrated amounts (layer, total)
  particulate absorption (layer, total)

Spectroscopic

- number of lines/species
- layer specific
  v_1, v_2, dv(natural)
  optical depth, transmittance, radiance
- total path
  (same)
- scanned
  dv(scan), type (triangular, rectangular, etc.)
- filtered
  v_1, v_2, shape
- plotted (all of above)
- layer boundary info: T/p(l), T/p(l-1), etc.

FASCOD3: Fast Atmospheric Signature Code

Version 3

Generic Capabilities:

- o Line-by-line molecular spectroscopy including line coupling
- o Uniform physical definitions (0-50000cm-1)
- o Full geometric path flexibility, 0-120+km,
  all lines of sight with spherical refraction
- o Access to arbitrary databases (HITRAN91/86, NLTE, etc.)
- o Voigt line shape at all altitudes and/or pressures
- o Mathematical optimization for
  layering and spectral sampling algorithms
- o Default or user-supplied atmospheric profiles,
  p, T, and mixing ratios for 28 constituents
- o Absorption x-section implementation from HITRAN86/90
- o Additional default & user specifications for 10 green-house gases
- o Default or user-supplied aerosol and hydrometeor profiles;
  full LOWTRAN7 compatibility
- o Laser (monochromatic) options
- o Non-local thermodynamic equilibrium; NLTE populations must be provided
  from outside source (i.e. Degges, SHARC, AARC, etc.)
- o Weighting functions, merge options, ground reflection
- o Thermal multiple scattering, layer fluxes
- o Standard "user" options (plot, scan, filter, etc)

4. Delays in FSC3 release - why?

90/91 SCIENCE:

i. improved radiance algorithms:
   Tbar(l) replaced by weighted (T(b)+T(b+1))
   [non-compatible with m.s. algorithm??]
   Default "fine" layer at observer
ii. x-sections including:
   p-broadening, T-dependence,
   default profiles from M. Allen, 1990
iii. "linear" Planck function interpolation
iv. HITRAN91 compatibility:
   Line coupling and cross sections
v. TIPS: Total Internal Partition Sum
   from Gamache & Rothman, with FSC3 extrap.
vi. isotopic implementation
vii. revised NLTE coding,
   including efficient 4th function
viii. dayside NLTE populations from SHARC (Sharma
   and Robertson), ARC (Wintersteinner &
   Picard), and HAIRM (Degges) (composite)
iix. nightside NLTE populations being explored
ix. H2O continuum extrapolation altered in near IR
   (based on measurements at 1.06 microns)
x. new defaults:
   simple CO2 mixing ratio modification:
   330ppmv can be replaced with single option
   default alpha(0) adjust. for line coupling:
   0.04cm-1 instead of 0.08 at 1 atm STP
   default line rejection values:
   fraction of Optical Depth & Continuum
xi. possible inclusion of GL/NRL Constituent
   Climatologies (CIRA-based)

90/91 CODE ENHANCEMENTS:

i. scanning/interpolation upgrades:
   SINC, SINC**2, fixed sampling
   FTS simulations/functions (Gallery)
ii. much improved "weighting function" options:
   renamed "sequential" transmittance/radiance
   reduced storage requirements, E/O systems
   compatibility
iii. improved efficient 4th function sampling
iv. corrected FASLOW compatibility (layering)
v. I/O improvements: ASCII/binary options
vi. portability!!
   UNIX, IBM, CRAY(?), Workstation, Apollo, etc.
   NCAR/IDL Graphics

90/91 OTHER:
i. future directions - ? (let's get there first!)

SPECIAL OPTIONS:

o Thermal multiple scattering - (Radiance ONLY)

encouraged for long slant paths at moderate to high pressure (i.e. below 15km) in the presence of scatterers (aerosols and/or clouds)
10-20% effect in IR
activated by IMS=1
directionally dependent
increases total radiance when looking down
decreases " " " " up
strong function of viewing angle
function of scattering opacity vs total opacity
** increases FASCOD3 runtime by at least a factor of 2-3
modularized coding (if IMS=0, normal FASCOD3 execution occurs)
new input parameters - surface T and emissivity
- min and max altitudes for calc.

o Non-local thermodynamic equilibrium (NLTE) - Radiance

appropriate for spectral ranges and altitudes where "hot" bands occur

potentially large effects, particularly for paths above 50km
activated by HIRAC=4
new input parameters - vibrational ID's
- vibrational T's or populations
- standard line parmeters (S, v)
modularized coding
improved line shape for far wings
increases runtime in proportion to no. of lines

SPECIAL OPTIONS (con't #1):

o Line coupling - Optical depth, transmittance, and radiance

important in vicinity of strong Q-branches and other "dense" band systems for which coupling coefficients are available (CO2 and O2 for now)
moderate effects (contamination of remote sensing channels leading to T-determinations with errors > 5-10K)
default option; activated whenever coef. are supplied
new input parameters - coupling coef. as a fn(T) (recognized by LNFL routines)
embedded coding
modifies line shape and continua
small effect on runtime

o Weighting Functions (Sequential Calculations)

instrument design tool for ascertaining signature source regions as a fn(distance from observer)
calculates cumulative transmittance from observer to points (layer boundaries) along the line-of-sight
activated by IMRG = 3-8, 13-18, 23-28
saves "layer-defined" monochromatic transmittances at dv(natural) for IMRG = 3-8; can consume large amnts of storage for moderate spectral range
for IMRG = 13-18, will save only spectrally scanned cumulative transmittances while preserving proper line-by-line calculation
for IMRG = 23-28, will save only filtered (spectrally integrated) cumulative transmittances, while preserving proper line-by-line calculation
coding dependent on viewing geometry:

	line-by-line calc	
	original	pre-stored
ground to space	(IMRG = 4, 14, 24	6, 16, 26)
space to ground	(IMRG = 3, 13, 23	5, 15, 25)
tangent	(IMRG = 7, 17, 27	8, 18, 28)

timing increases minimal to moderate
does NOT work with IAERSL = 1,7 or IMS = 1

SPECIAL OPTIONS:

o Cross Section Capability - Radiance and Transmittance

(activated by: **IXSECT = 1**)

Currently reads HITRAN86 cross sections
Will read HITRAN90 T-dependent cross sections
Incorporates cross section into layer optical depths
at the coarsest resolution possible:
i.e. Function 1 ($\pm 4\alpha$)
Function 2 ($\pm 16\alpha$)
Function 3 ($\pm 64\alpha$)
Function 4 (± 25 cm^{-1})
** Pressure broadened with Lorentzian convolution**
Layer-dependent
10 New default profiles for important greenhouse gases
(based on M. Allen, 1990 photochemistry)

Recent Comparisons/Validation:

o Theoretical

WMO Intercomparison of Transmittance and Radiance Algorithms (ITRA) - 1985-1988 and 1990-1991

- compared with 6 line-by-line codes for limb, nadir, and microwave test cases
- IR and mm wavelengths
- line shape (including continua)
- layering algorithm
- transmittance, radiance, and weighting functions

SHARC - Strategic High Altitude Radiance Code for NLTE comparisons (Sharma & Robertson)
ARC/NLTE - Atm. Radiance Code (Picard & Wintersteiner)

o Laboratory (partial list; historic validation)

Line coupling (Lafferty & Hoke, 1986-87)
etc.

o Atmospheric Instruments

SCRIBE (Stratospheric Cryogenic Interferometric Balloon Experiment, AFGL) 1984-1988; multiple balloon flights with very high spectral resolution ($0.06cm^{-1}$); limb and nadir radiance

HIS (High-Resolution Interferometer Sounder, Univ. of Wisconsin) 1985-1988; multiple airborne (balloon, aircraft, and shuttle) flights with high spectral resolution ($0.5cm^{-1}$); limb and nadir radiance

ATMOS (Atmospheric Trace Molecule Spectroscopy instrument, JPL/NASA) 1985; spacelab (shuttle) flight with very high spectral resolution ($0.01cm^{-1}$); solar occultation (transmittance)

IMORL (Infrared Mobile Optical Radiation Laboratory,NRL) 1976-1979; ground-based Fourier-transform spectrometer with very high resolution ($0.06cm^{-1}$); transmittance

FASCOD3: Fast Atmospheric Signature Code

Version 3

Applications:

o Laser Propagation/
Ground Based Laser

o Plume Signature/
Infrared Search and Track

o Target Contrast/
Tactical Decision Aids

o Remote Sensing/
Inproved Point Analysis Models

o Data Simulation/
UV, Visible, IR, microwave
NLTE, line coupling

o Instrument design & development/
Information content, etc.

o Heating-Cooling Rate Calculations/
Greenhouse gas absorption described by x-sections

DOCUMENTATION:

- o "Instant" User Instructions (upon release)
  - Read tape
  - Unpack
  - Machine conversions
  - I/O "Parameter" definitions
  - Test cases
  - Sample output
  - Database access
  - (File management)

- o User's Manual (release plus 5 months)
  - Expansion of "Instructions"
  - Scientific definitions
  - References
  - Description/justification of "default" choices
  - Subroutine descriptions and flow charts
  - Segment load file
  - File management

- o Scientific Report (release plus 10 months)
  - All of the above AND:

  - Philosphy/history of FASCODE
  - Algorithm descriptions
    - Line-by-line functions *
    - Line shape *
    - Line coupling
    - Continua *
    - Diffuse functions
    - Geometry *
    - Layering selection *
    - Layer merging *
    - Weighting functions
    - Standard profiles (p, T, constituent) *
    - Aerosol/hydrometeor profiles (LOWTRAN7)
    - NLTE
    - Multiple scattering
    - X-sections (greenhouse gases)
  - Test cases/templates
  - Validation
  - Comparisons
  - References
  - Hints/cautions
  - etc.

COMMON ELEMENTS: Model Atmospheres

Topics:

- o Available "default" profiles for pressure, temperature, density, and molecular constituents: FASCODE, LOWTRAN, and MODTRAN all employ the same set; see **AFGL Atmospheric Constituent Profiles (0-120km)**.

- o User input options for these parameters:
  Again, the same type of options are employed by all three codes. However, the details of the input procedures differ, based primarily on the number of constituent variables (28 for FASCODE, 12+ for LOWTRAN and MODTRAN) and historic usage.

- o New FASCOD3 "greenhouse" gas option:
  access to the molecular absorption cross sections available on the HITRAN86/90 databases has necessitated the addition of 10 new profiles.

- o Natural climatological variability:
  Near-term availability of climatologically varying profiles and their statistical evaluation.

GREENHOUSE GAS PROFILES: New FASCOD3 Default Options

- o HITRAN86/90 provides molecular absorption cross sections for: ClONO2, HNO4, CHCl2F, CCl4, CCl3F, CCl2F2, C2Cl2F4, C2Cl3F3, N2O5, HNO3, and CF4

- o FASCOD3 now includes "default" profiles for these gases, plus the capability to implement layer-by-layer optical depth/transmittance calculations.

- o These profiles are based on a "one/two-dimensional photochemical model" with upgraded 1990 chemistry and/or measurements. (M. Allen, JPL)

EOSAEL92

A.E. Wetmore
U.S. Army Atmospheric Sciences Laboratory,
White Sands Missile Range, NM 88002-5501

The U.S. Army Atmospheric Science Laboratory (ASL) is planning to release the next version of the Electro-Optical Systems Atmospheric Effects Library (EOSAEL) during the first quarter of fiscal year 1992. This paper reports what the EOSAEL users have to look forward to. The climatology (CLIMAT) database has been expanded to include the continental United States and most of Canada. The aerosol phase function database (PFNDAT) database used by the EOSAEL has been expanded to include models of desert aerosols and lidar backscatter coefficients. A new Narrow Beam Multiple Scattering code will replace many of the previous scattering codes. An ultraviolet transmission and lidar code is being included. We are replacing LOWTRAN-6 with LOWTRAN-7 and including the capability of calculating contrast transmission. The target acquisition (TARGAC) and natural aerosol extinction (XSCALE) model have been improved and laser transmission (LZTRAN) should have several new wavelengths added. Several of the modules will sport an interactive interface.

EOSAEL92

Alan E. Wetmore
U.S. Army Atmospheric Sciences Laboratory
White Sands Missile Range, New Mexico 88002-5501, USA

FALL 1991 DISTRIBUTION

The U.S. Army Atmospheric Sciences Laboratory (ASL) is planning to release the next version of the Electro-Optical Systems Atmospheric Effects Library (EOSAEL) during the first quarter of fiscal year 1992. There will be new models, upgrades to existing models, and obsolete models. Distribution will continue to be on magnetic tape and free to qualified recipients.

UNCHANGED MODELS

Many of the modules are unchanged in their physics. These are the near millimeter wave (NMMW), cloud transmission (CLTRAN), obscuration due to helicopter lofted snow and dust (COPTER), self-screening applications (GRNADE), missile smoke plume obscuration (MPLUME), contrast transmission (OVRCST) and contrast transmission (FCLOUD), natural illumination under realistic weather conditions (ILUMA), fast atmospheric scattering (FASCAT), large area screening systems applications (LASS), nonlinear aerosol vaporization and breakdown effects (NOVAE), and millimeter wave system performance (RADAR) modules.

UPGRADES TO EXISTING MODELS

- atmospheric transmittance and radiance (LOWTRN)
- laser transmission (LZTRAN)
- climatology (CLIMAT)
- munition expenditure module (KWIK)
- natural aerosol extinction (XSCALE)
- target acquisition (TARGAC)
- combined obscuration model for battlefield-induced contaminants (COMBIC)

LOWTRAN 7

- ASL researchers are incorporating the Geophysics Laboratory's (GL's) latest upgrades to LOWTRAN 7, modifying the input routines to use the EOSAEL record order independent routines, and making some changes to improve portability.
- The largest upgrades are the vertical structure algorithms. Bob Fiegel described this work last year.
- We are writing *The Complete LOWTRAN Manual.*
- Much of our time time has been spent increasing the portability and putting reasonable limits and checks on many mathematical operations.

LZTRAN

- Several new laser wavelengths will be added.
- It is not too late to request that your favorites be added.
- Remember that LZTRAN is a near earth transmission code.

CLIMAT

- Data for Canada and the continental United States has been added.
- An option to print out the summary data for all climate classes was added.

US ARMY
LABORATORY COMMAND

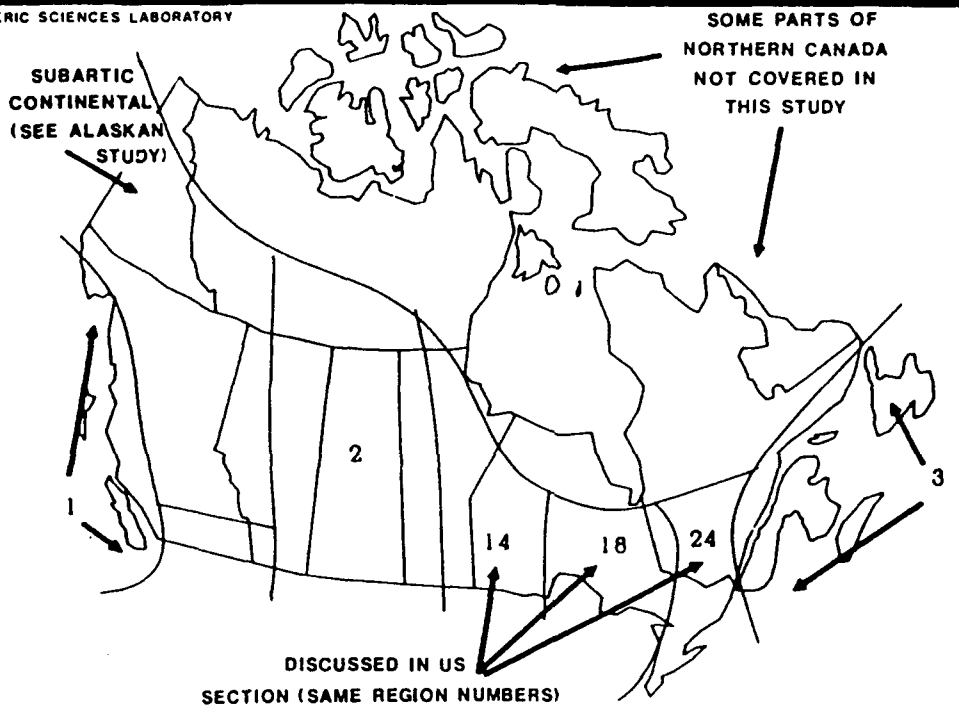
ATMOSPHERIC SCIENCES LABORATORY



CANADA

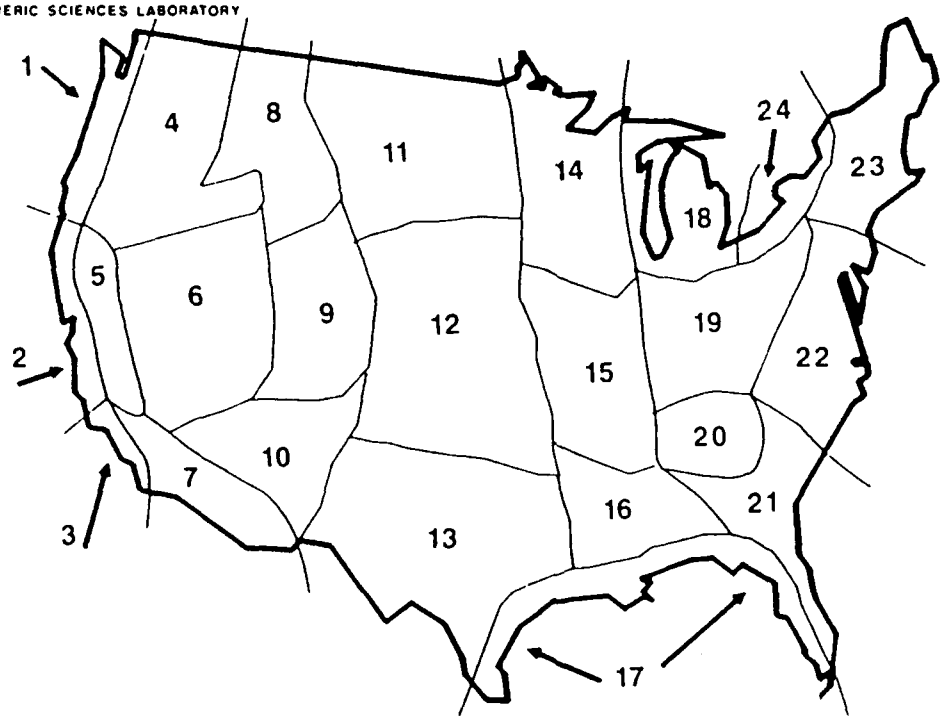
ATMOSPHERIC SCIENCES LABORATORY

US ARMY LABORATORY COMMAND



ATMOSPHERIC SCIENCES LABORATORY

US ARMY LABORATORY COMMAND



KWIK

- No new smoke munitions.
- Refinements to the calculation of extinction coefficients.
- The values of transmission reported by XSCALE are modified to better agree with experimental data.

XSCALE

- Increased speed in the calculations using the vertical structure models.
- The inversion–haze case has been compared with field data; good agreement was obtained.
- XSCALE now calculates transmission through thin cloud and haze layers. These paths may extend from above the layer, through the layer, to the ground below the layer.

TARGAC

- TARGAC has been upgraded to use the EOSAEL routine ILUMA. This replaces an independent routine that calculated illumination levels.
- A new thermal model (TCM2) for surfaces has been added. Turbulence and clutter calculations have been included in this model.
- An improved method of calculating the sky-to-ground ratio uses a delta Eddington model to account for path radiance and surface reflectance.

COMBIC

- COMBIC has had several modifications to fix minor bugs.
- A paper on using non-inventory smokes has been prepared.
- Instructions illustrating methodologies for adding "experimental" obscurants.

MODELS TO BE DROPPED

- The simulation of aerosol behavior in realistic environments (SABRE) and aerosol multiple scattering (MSCAT) modules will be dropped from the EOSAEL distribution.
- The SABRE model required too much customization to be used for different geographic sites.
- The MSCAT Monte Carlo code leaves far too many chances for misapplication. Most users who need a Monte Carlo code probably have their own. For those who were satisfied with MSCAT, the ASL will continue to supply it as a research code.

NBMSCAT

- NBMSCAT is a radiative scattering code developed by Luc Bissonnette of the Defence Research Establishment Valcartier, Canada.
- This code is an approximation to the radiative transfer equations suitable for narrow beams of light and observation points near the propagation axis.
- It handles arbitrary inhomogeneous obscurant clouds.

UVTRANS

- UVTRANS is an ultraviolet transmission, fluorescence, and lidar program developed for near earth applications.
- UVTRANS differs from LOWTRAN
  - flat earth and atmosphere approximations,
  - pressure parameterization valid for near earth only,
  - single aerosol model valid for visibilities less than 50 kilometers,
  - includes some different trace gasses.

USER INTERFACE IMPROVEMENTS

- We are developing an interactive user interface.
- There will be a demonstration available during the breaks.
  We would appreciate any comments on the work that is shown.
- We hope to have both a generic interface that can be used on any computer system and a more customized version for MS-DOS PC's.
- The interactive interface will also create a normal EOSAEL input file for later reuse or modification.

GRADE OF SOFTWARE

The ASL will be evaluating all of the modules to assign a grade.
These grades are not the same as "validating" the codes.

Research	Describes phenomena based on a physical or meteorological theory. Limited evaluations in the field or laboratory.
Developmental	Tailored version of a research model. Limits of applicability have been defined. At least "several" evaluations have been made.
Fieldable	Applicability has been defined. Confidence has been established throughout the community. "Many" evaluations have been "passed". The model has been verified for its stated usage.

AVAILABILITY

- EOSAEL92 is available to U.S. Department of Defense (DoD), specified allied organizations, and DoD authorized contractors at no cost. DoD agencies needing EOSAEL92 should send a letter of request, signed by a branch chief or division director, to the ASL. Contractors should have their DoD contract monitor send the letter of request. Allied organizations must request EOSAEL92 through their national representative.
- Please include, within security restrictions, your intended use(s). Also, indicate what type of nine-track tape your computer can read. We can make "ASCII" tapes, VAX VMS BACKUP tapes, and UNIX "tar" format tapes in either 1600 or 6250 bpi.
- (505) 678-5563 Commander/Director
FAX (505) 678-2432 U.S. Army Atmospheric Sciences Laboratory
DSN 258-5563 ATTN: SLCAS-AA-A (Dr. Wetmore)
awetmore@wsmr-emh73.army.mil White Sands Missile Range, New Mexico 88002-5501

BATTLEFIELD ATMOSPHERICS CONFERENCE

Formerly the EOSAEL/TWI Conference
2–6 December 1991
Fort Bliss, Texas

Mailing Address:

Commander/Director
U.S. Army Atmospheric Sciences Laboratory
ATTN: Battlefield Atmospherics Conference
White Sands Missile Range, New Mexico 88002-5501

HITRAN'91:
THE CONTEMPORARY SPECTROSCOPIC MOLECULAR DATABASE

L.S. Rothman
Geophysics Directorate, Optical Environment Division, Simulation Branch (OPS),
Hanscom Air Force Base, MA 01731-5000

The spectroscopic molecular database, HITRAN, is the DOD and international standard compilation of absorption parameters that enable the calculation of atmospheric spectral simulations from the microwave through the visible. A new edition of HITRAN has been made available in the first quarter of 1991. The current edition contains over 65 megabytes of high resolution data of transitions for 30 species and their atmospherically significant isotopic variants. In addition, there is a file of new cross-sections for heavy molecular species, with bands at several representative temperatures that should facilitate some quantitative retrievals. This task will summarize some of the major updates, improvements, and modifications.

HITRAN'91:
The Contemporary Spectroscopic Molecular Database

Laurence S. Rothman

Geophysics Directorate
Optical Environment Division
Simulation Branch (OPS)
Hanscom AFB, MA 01731-5000 USA

Abstract

The spectroscopic molecular database, **HITRAN**, is the DOD and international standard compilation of absorption parameters that enable the calculation of atmospheric spectral simulations from the microwave through the visible. A new edition of HITRAN has been made available in the first quarter of 1991. This current edition contains over 65 Megabytes of high resolution data of transitions for 30 species and their atmospherically significant isotopic variants. In addition, there is a file of new cross-sections for heavy molecular species, with bands at several representative temperatures that should facilitate some quantitative retrievals. This talk will summarize some of the major updates, improvements, and modifications.

Major Molecular Parameter Updates

- H_2O
- CO_2
- O_3
- CH_4
- CO, HNO_3, HCl, HF, HI, HBr...
- Cross-sections ($ClONO_2$, CFC's, N_2O_5...)

Water Vapor (H_2O)

	ν_{min}	ν_{max}	# bands	# lines
❶	*5904*	*7965*	*9*	*3112* *
❷	*8036*	*9482*	*9*	*1874*
❸	*9603*	*11 481*	*9*	*2484*
❹	*11 661*	*12 741*	*5*	*714* *
❺	*13 238*	*22 657*	*41 (39,2)*	*4608*
❻	*782*	*2745*	*2*	*

Water Vapor (H_2O)

All new regions have been taken at the Kitt Peak Solar Observatory using the FTS and long-path cell. These data replace older parameters that were observed using grating spectrometers and a path through the atmosphere. Most notable improvement in intensities of weak lines. In the case of data from Toth, a hybridization with '86 lines was used to supplement his data

❶ Toth, JPL

❷ Flaud & Camy-Peyret (FCP), Paris

❸ FCP

❹ Toth

❺ FCP | extends spectral range of compilation

❻ Toth

Carbon Dioxide (CO_2)

❶ **New Line Positions**: New fit of observed high resolution data by Hawkins & Rothman (including some DND points to supplement data). New data includes very high vibrational 4.3-μm observations of Bailly *et al.* (Orsay) and the 15-μm observations of Esplin *et al.* (GL)

❷ **New Intensities**: New intensity observations of Dana *et al.* (Paris) and Johns (NRC). Calculations by Wattson & Rothman for unobserved bands, include Herman-Wallis coefficients.

❸ **Revised Halfwidths**: Self- and Foreign-broadened halfwidths and temperature dependence now based on work at Ecole Centrale.

Ozone (O_3)

	ν_{min}	ν_{max}	# bands	# lines
❶	*557*	*900*	*2*	*12 085*
❷	*919*	*1271*	*18*	*42 500*
❸	*934*	*1178*	*4*	*13 590*
❹	*1319*	*2322*	*19*	*44 926*

Ozone (O_3)

❶ New data for ν_2 and $2\nu_2 - \nu_2$ from Pickett (JPL) *et al.*

❷ Revamping of 10-μm region. This time includes many new bands and hot bands.

❸ Isotopic bands of 10-μm region from FCP & Rinsland (NASA Langley)

❹ Many new combination bands from Goldman (Denver)

Methane (CH_4)

	ν_{min}	ν_{max}	# bands	# lines
❶	*0*	*6185*	*31 (21,6,4)*	*37 207*
❷	*2902*	*3147*	*3*	*309*

❶ Major improvement by Brown (JPL).

❷ Updated mono-deuterated methane bands by Brown.

Other Molecular Species

- CO (carbon monoxide): Update, primarily for HITEMP (*Tipping*)
- NO (nitric oxide): Update of fundamental (*Ballard*)
- NO_2 (nitrogen dioxide): Update of ν_3 region (*Perrin, FCP*)
- HNO_3 (nitric acid): Addition of new bands
  (fundamentals and combinations, 410 to 1400 cm^{-1})
  (*Goldman, Maki, Perrin, et al.*)
- HCl, HF, HI, HBr (hydrogen halides):
  Update, primarily for HITEMP (*Tipping, et al.*)

Other Molecular Species (continued)

- H_2O_2 (hydrogen peroxide): Update of ν_6 band, 138-1500 cm^{-1}
  (*Hillman*)
- C_2H_2 (acetylene): Addition of ν_5 band, 1192-1470 cm^{-1}
  (*Rinsland et al.*)
- C_2H_6 (ethane): Addition of ν_7 band, 2973-3000 cm^{-1}
  (*Goldman, Dang-Nhu, Bouanich*)
- COF_2, SF_6: New species on compilation
  (*Goldman, Rinsland, et al.*)
- OCS, N_2 ...

Updates generally include all parameters of HITRAN format.

Cross-sections (Supplemental files)

CFC's now at six temperatures: 203, 213, 233, 253, 273, and 293K. N_2O_5 at 233, 253, 273, and 293K. $ClONO_2$ at 213 and 296K.

Species	ν_{min}	ν_{max}	# lines
CFC-11 (CCl_3F)	830	860	
"	1060	1107	31 146
CFC-12 (CCl_2F_2)	867	937	
"	1080	1177	67 542
CFC-13 ($CClF_3$)	765	805	
"	1065	1140	
"	1170	1235	72 804
CFC-113 ($C_2Cl_3F_3$)	780	995	
"	1005	1232	5304

Cross-sections (continued)

Species	ν_{min}	ν_{max}	# lines
CFC-114 ($C_2Cl_2F_4$)	815	860	
"	870	960	
"	1030	1067	
"	1095	1285	146 418
CFC-115 (C_2ClF_5)	955	1015	
"	1110	1145	
"	1167	1260	76 038
N_2O_5	555	600	
"	720	765	
"	1210	1275	
"	1680	1765	1988
$ClONO_2$	740	840	
"	1240	1340	
"	1680	1790	26 622

SELECT OPTIONS

Input:

① ν_1 and ν_2 (Initial and final frequencies of selection)
② Molecule
③ Isotope
④ v', v" (upper and lower "global" quanta)
⑤ S_{crit} (Intensity cutoff)

Output:

- Batch file for input
- Files for input to subsequent programs
  (direct image; '82 format; user defined)
- Temperature Correction
- Hard copy listing
  (codes converted to spectroscopic and chemical notations;
  80 or 132 columns printers)

MAJOR CONTRIBUTORS

D. C. Benner
L. R. Brown
V. Dana
V. Malathy Devi
J.-M. Flaud
R. R. Gamache
A. Goldman
J. M. Hartmann
R. L. Hawkins
J. W. C. Johns
A. G. Maki
S. T. Massie (NCAR)
C. P. Rinsland
L. Rosenmann
M. A. H. Smith
R. Tipping
R. A. Toth
R. B. Wattson

SUMMARY

- ✯ New Edition of HITRAN published March 1991.
- ★ Improvements notable for remote sensing, laser transmission, climate modeling, use of heavy species...
- ✯ References and Error criteria now implemented.
- ✯ SELECT faster and more flexible.
- ☆ New media and structure for the database to materialize.
- ✱ HITEMP to be available in '91.

SHARC, AN ATMOSPHERIC RADIATION AND TRANSMITTANCE CODE FOR ALTITUDES FROM 50 TO 300 KM

D. Robertson, L. Bernstein, J. Duff, J. Gruninger, R. Sundberg
Spectral Sciences, Inc., 111 S. Bedford Street, Burlington, MA 01803

R. Sharma
Geophysics Directorate, Phillips Laboratory, Hanscom Air Force Base, MA 01731-5000

R. Healey
Yap Analytics, Inc., 594 Marrett Road, Lexington, MA 02173

The latest version of the Strategic High-Altitude Radiance Code (SHARC), SHARC-2, is now available. The new version contains significant upgrades, the most important being a fully integrated auroral model with time-dependent chemistry, extension down to 50 km altitude, and incorporation of the minor isotopes of CO_2. SHARC calculates atmospheric radiance and transmittance over the 2-40 μm spectral region and includes arbitrary paths within 50 and 300 km altitude. It models radiation due to NLTE (Non-Local Thermodynamic Equilibrium) molecular emission which are the dominant sources at these altitudes. It calculates molecular radiation on a line-by-line basis and has a spectral resolution of 0.1 cm^{-1}. SHARC uses an equivalent-width formalism to obtain the total transmittance for each line, thus alleviating the need for the usual numerical integration over the line shape.

SHARC

THE STRATEGIC HIGH-ALTITUDE RADIANCE CODE

BY

DAVID ROBERTSON, LARRY BERNSTEIN,
JAMES DUFF, JOHN GRUNINGER, ROBERT SUNDBERG,
SPECTRAL SCIENCES, INC.,

RAMESH SHARMA,
PHILLIPS LABORATORY/OPS

REBECCA HEALEY,
YAP ANALYTICS, INC.

11 JUNE 1991

OUTLINE

- SHARC-2 OVERVIEW
- MAJOR MODULES
  - RADIATIVE EXCITATION (NEMESIS)
  - AURORAL MODULE
- VALIDATION EXAMPLES
- ILLUSTRATIVE RUN TIMES
- CONCLUDING REMARKS

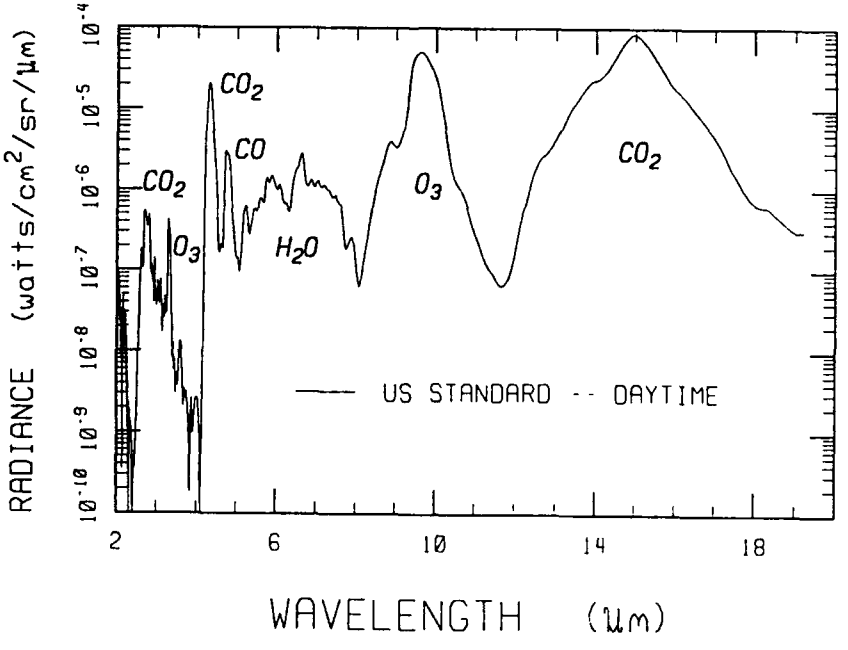
SHARC-2 OVERVIEW

- SHARC CALCULATES NLTE RADIATION FROM AMBIENT AND AURORAL ATMOSPHERES

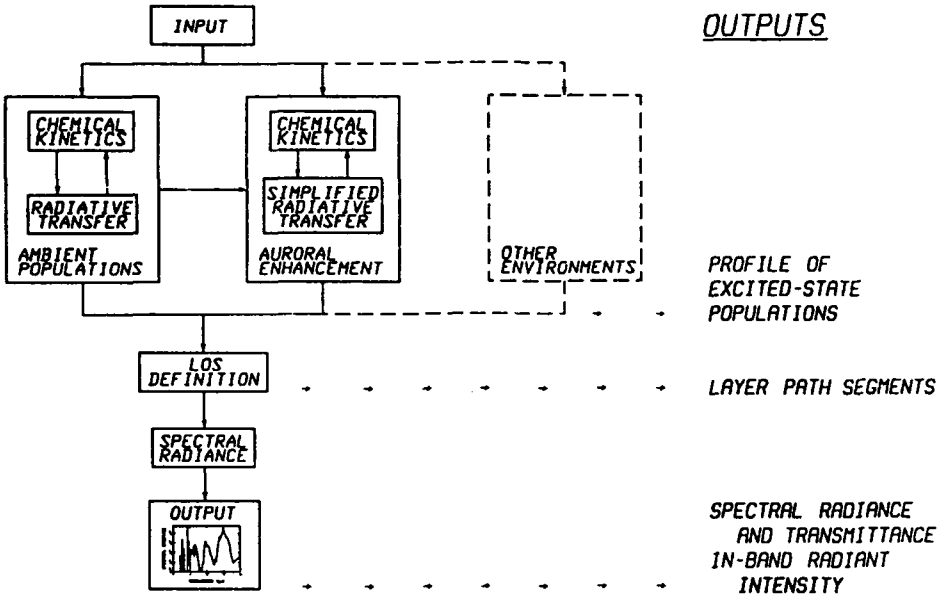
- BASIC FEATURES:
  - 50-300 km ALTITUDE REGIME
  - 2-40 μm WITH RESOLUTION OF 0.5 cm^{-1}
  - ARBITRARY VIEWING GEOMETRIES
  - INTERACTIVE INPUT MODULE WITH ERROR CHECKING
  - ADJUSTABLE CHEMICAL KINETICS MECHANISMS/RATES
  - AUTOMATICALLY INCLUDES LTE & NLTE CONTRIBUTIONS
  - AMBIENT MOLECULES INCLUDE: H_2O, O_3, CO, NO, OH, CO_2, ITS IMPORTANT ISOTOPES
  - AURORAL MODULE WITH: NO+, NO, CO_2
  - MULTIPLE OUTPUT OPTIONS
  - FORTRAN SOURCE CODE PROVIDED

ILLUSTRATIVE SHARC CALCULATION

- SPACE VIEWING THROUGH A 50km LIMB PATH



SHARC-2 FLOW CHART



AMBIENT POPULATIONS MODULE

- SYMBOLIC DESCRIPTION OF CHEMICAL KINETICS MECHANISM
  - BASED ON WIDELY USED SANDIA CHEMKIN CODE
  - EXAMPLE: $M + O + O_2 \rightarrow M + O_3(00\,0)$
    $M + O_3(00\,1) \rightarrow M + O_3(00\,0)$
    $O_3(00\,1) \rightarrow O_3(00\,0) + h\nu$
- RATE EQUATIONS SOLVED IN STEADY STATE
  - ASSUMES RATE EQUATIONS DEPEND LINEARLY ON VIBRATIONAL POPULATION
- MONTE CARLO CALCULATION FOR FIRST-ORDER RADIATIVE ENHANCEMENT
  - MULTIPLE APPLICATION YIELDS HIGHER ORDER ENHANCEMENTS

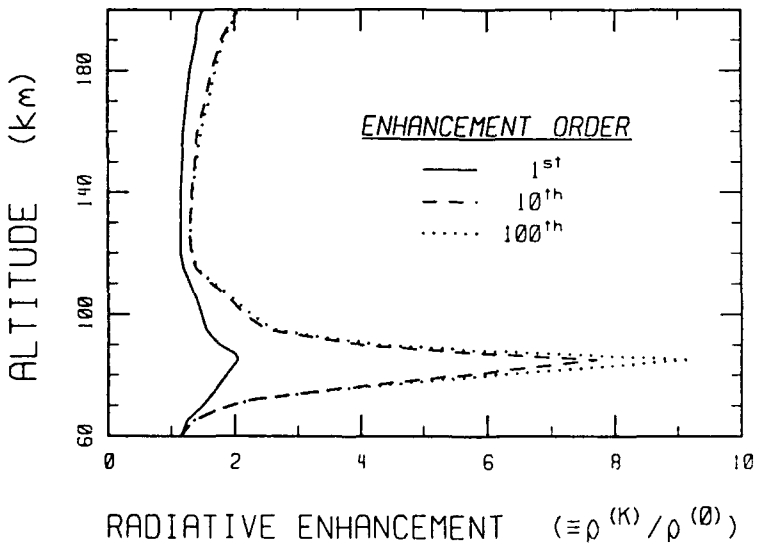
RADIATIVE EXCITATION MODULE (NEMESIS)

- RADIATIVE EXCITATION SIGNIFICANTLY ENHANCES THE EXCITED-STATE POPULATIONS OF STRONG BANDS AND HENCE THE STRENGTH OF THEIR EMISSIONS

- BASIC MODEL ASSUMPTIONS
  - SEMI-INFINITE PLANE-PARALLEL HOMOGENEOUS LAYERS
  - VOIGT LINESHAPE
  - TRANSLATIONAL-ROTATIONAL EQUILIBRIUM
  - COMPLETE LINE FREQUENCY REDISTRIBUTION
  - COMPLETE ROTATIONAL LEVEL REDISTRIBUTION
  - NO LINE OVERLAP

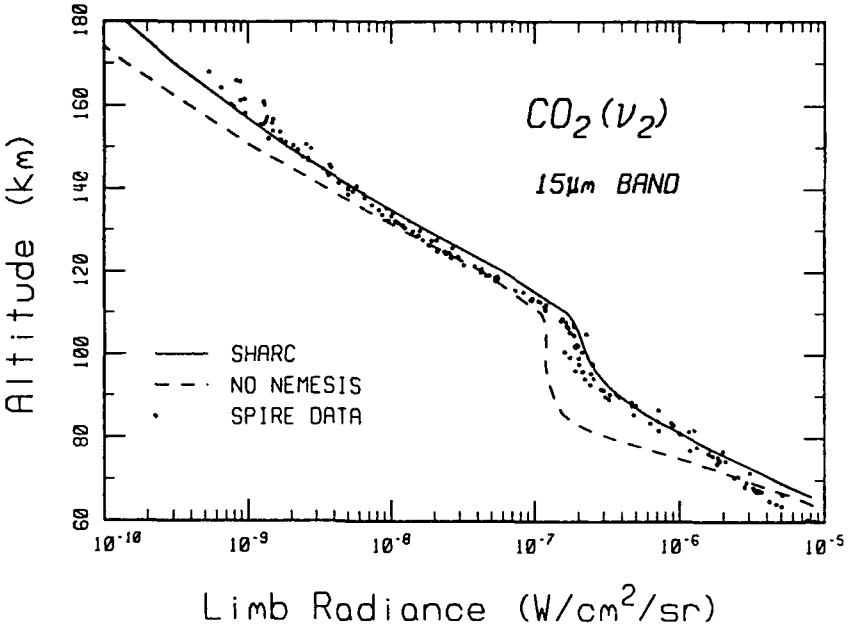
ENHANCEMENT OF $CO_2(\nu_2)$

- POPULATION ENHANCEMENT FACTOR DUE TO RADIATIVE EXCITATION



RADIATIVE ENHANCEMENT FOR CO_2

- NO-NEMESIS CALCULATION SKIPS RADIATIVE EXCITATION



SPECTRAL RADIANCE MODULE

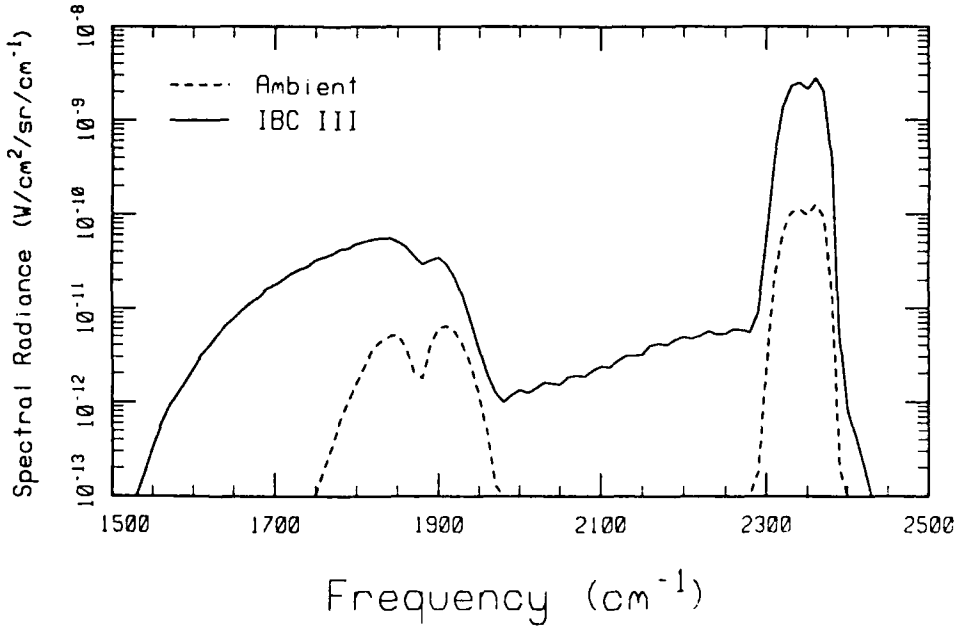
- RADIATION TRANSPORT CALCULATION PERFORMED FOR EACH MOLECULAR LINE
  - USES GL ATMOSPHERIC ABSORPTION LINE DATABASE (HITRAN)
- RODGERS-WILLIAMS APPROXIMATION FOR THE EQUIVALENT WIDTH (W) OF A SINGLE LINE WITH A VOIGT LINESHAPE
  - NASA HANDBOOK APPROXIMATION FOR W_D AND W_L
- LAYER-DEPENDENT LINE STRENGTHS
  - VIBRATIONAL AND ROTATIONAL TEMPERATURES
- CURTIS-GODSON APPROXIMATION
  - AVERAGING PROCEDURE FOR INHOMOGENEOUS PATHS
- LINE OVERLAP CORRECTION FOR DENSE REGIONS
- 50-70 TIMES FASTER THAN TRADITIONAL LBL APPROACH

SHARC AURORAL MODULE

- AURORAL PHENOMENOLOGY
  - STARTING POINT IS GL AARC CODE
  - ELECTRON DEPOSITION MODELS FOR DIFFERENT STRENGTH AURORAS: CLASS II, III, III+
  - SOLVES TIME/ENERGY DEPENDENT RATE EQUATIONS TO CALCULATE BOTH SECONDARY ELECTRON DISTRIBUTIONS AND THE KINETICS FOR IR RADIATORS
  - PRESENT IR MOLECULES ARE: NO, NO^+, CO_2
- SHARC AURORAL UPGRADE
  - GEAR'S STIFF ODE ALGORITHM USED AS REQUIRED
  - CAN ADD NEW RADIATORS VIA USER-DEFINED INPUT FILES
  - LOS CALCULATION COUPLED WITH AMBIENT REGION
- UPGRADED GEOMETRY MODEL INSURES THAT LOS TRAJECTORIES INTERSECT AURORA AS DESIRED

ILLUSTRATIVE AURORAL ENHANCEMENT

- RELATIVE STRENGTHS FOR PATH 90 km - SPACE

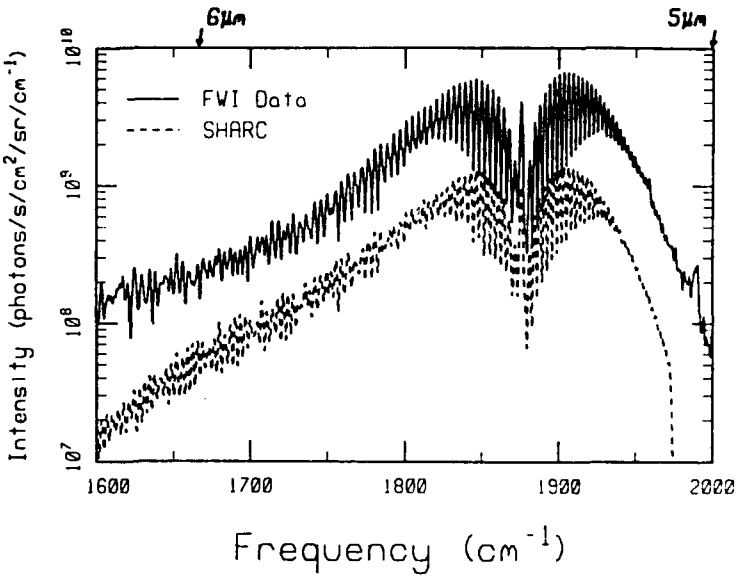


COMPARISON TO AURORAL FIELD DATA

- FWI DATA (FIELD WIDENED INTERFEROMETER)
- VERTICAL PATH TO SPACE FROM 90 KM
- CLASS II AURORA (~12 K RAYLEIGHS)
- SHARC CALCULATION FOR CLASS II (10 KR)
- MODEL CALCULATION USES A CONSTANT ELECTRON DOSE RATE

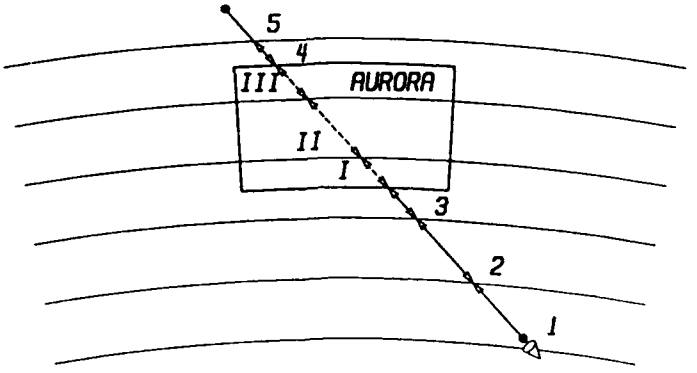
BUT

- AURORA IS LIKELY STRONGLY PREDOSED



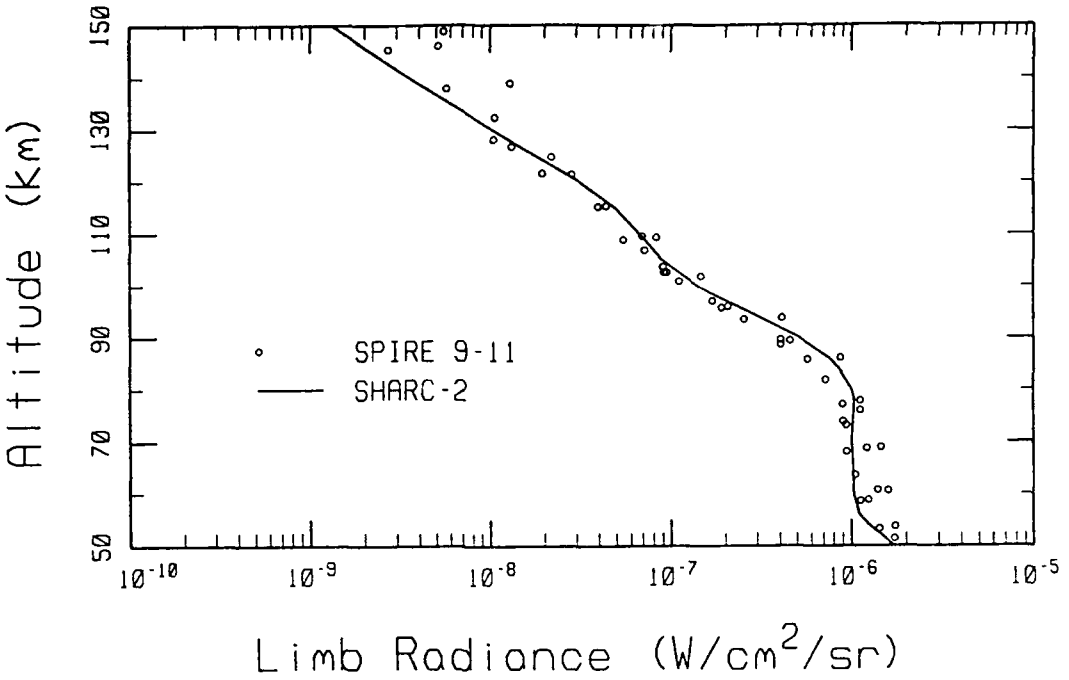
LOCALIZED ATMOSPHERIC REGIONS

- EXTENDED ATMOSPHERE PLUS LOCAL (AURORAL) REGIONS
  - POPULATIONS DEFINED IN EACH REGION
- LOS IS COMPOSED OF MULTIPLE HOMOGENEOUS SEGMENTS WITHIN EACH REGION



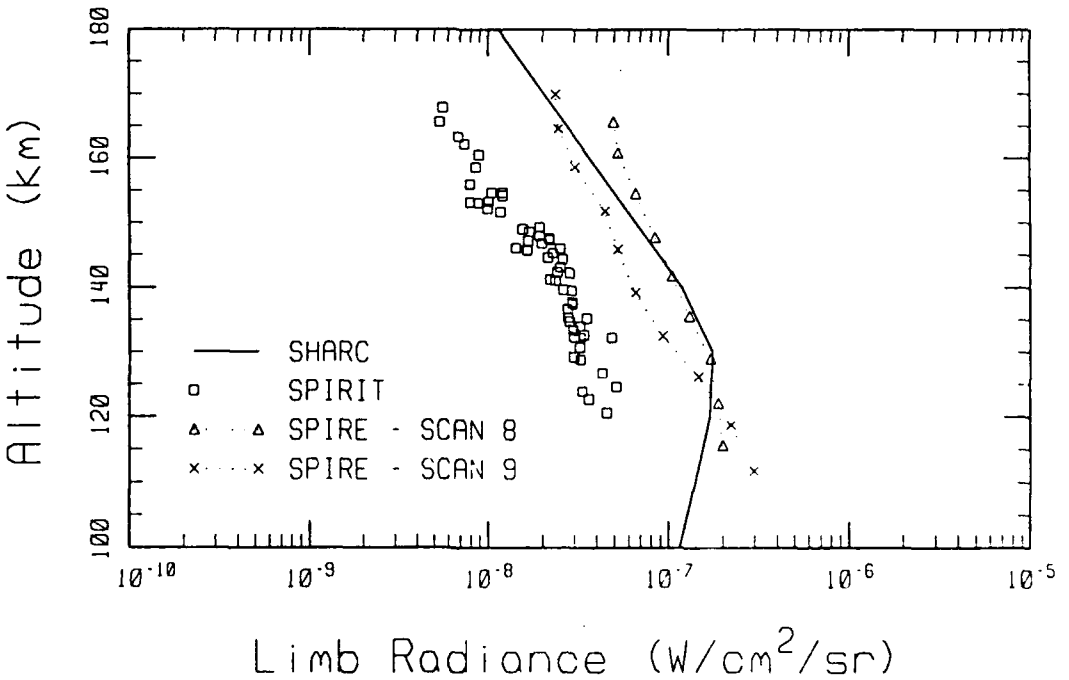
SPIRE: DAYTIME CO_2 (4.3 μm)

- STRONG SOLAR PUMPING VIA EXCITATION OF 2.7μm BAND



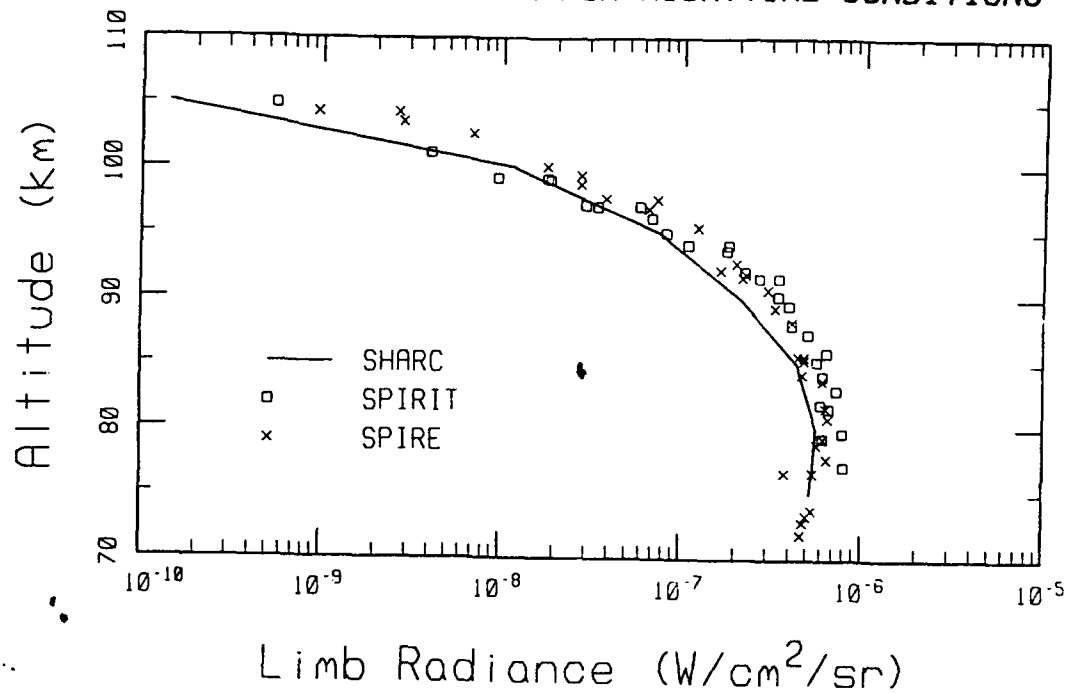
COMPARISON TO NO (5.3 μm) DATA

- SIGNIFICANT VARIABILIITY IN OBSERVED NO RADIANCES



COMPARISON TO O_3(9.6 μm) DATA

- SPIRIT 1 AND SPIRE DATA FOR NIGHTTIME CONDITIONS



RUN TIMES - CHEMISTRY

- CHEMISTRY ONLY REPEATED FOR MODIFIED ATMOSPHERE
- AMBIENT POPULATIONS
  - 89 BANDS OF H_2O, CO_2, O_3, CO, NO, OH
    26 OF WHICH REQUIRE RADIATION TRAPPING TREATMENT
  - 66 ATMOSPHERIC LAYERS FROM 50 TO 300 KM

  DATA GENERAL AViiON AV5100 (20 MIPS) : 15.2 MIN
  DEC VAX 8800 : 10.8 "
  DEC VAX 780 : 80.1 "

- AURORAL POPULATIONS (ADDITIONAL TO AMBIENT)
  - 31 VIBRATIONAL STATES: NO(13), NO^+(14), CO_2(4)
  - 37 RADIATING BANDS: NO(23), NO^+(13), CO_2(1)
  - 36 LAYERS FROM 80 TO 150 KM

  DATA GENERAL AViiON AV5100 (20 MIPS) : 7-12 MIN
  DEC VAX 8800 : 5- 8.5 "
  DEC VAX 780 : 37-64 "

RUN TIMES - LOS RADIANCE

- SPECTRAL RADIANCE - SINGLE BAND
  - 14-16 μm BAND OF CO_2 WITH 890 LINES
  - 131 LAYERS (50 KM LIMB)

DATA GENERAL AViiON AV5100 (20 MIPS)	:	5.2 SEC
DEC VAX 8800	:	3.7 "
DEC VAX 780	:	27.6 "

- SPECTRAL RADIANCE - MULTIPLE BANDS
  - 1-40 μm BANDPASS: H_2O, CO_2, O_3, CO, NO, OH
    84,000 LINES
  - 131 LAYERS (50 KM LIMB)

DATA GENERAL AViiON AV5100 (20 MIPS)	:	6.3 MIN
DEC VAX 8800	:	4.5 "
DEC VAX 780	:	33.4 "

SUMMARY

- SHARC WAS DEVELOPED TO MEET SDIO REQUIREMENTS FOR A HIGH-ALTITUDE RADIANCE MODEL
  - AURORAL AND QUIESCENT ATMOSPHERES
  - MODULARIZED STRUCTURE
  - ARBITRARY PATHS ABOVE 50 km
  - FULLY INTEGRATED & LOCALIZED AURORAL REGION
- COMPATIBLE WITH SSGM STRUCTURE
- VALIDATED WITH GL FIELD DATA

SHARC STATUS

- SHARC-2 WILL BE DISTRIBUTED IN JULY, 1991
  - CODE IS READY
  - MANUAL IS BEING PRINTED

- REQUEST (ON LETTERHEAD) FROM:

  DR. RAMESH SHARMA
  PHILLIPS LABORATORY(OL-AA)/GP/OPS
  HANSCOM AFB, MA 01731-5000

- ENCLOSE A 9-TRACK 1600-BPI TAPE

RECENT DEVELOPMENTS OF THE GENLN2 LINE-BY-LINE MODEL: STUDIES IN SUPPORT OF THE UARS PROJECT

D.P. Edwards
National Center for Atmospheric Research, Box 3000, Boulder, CO 80307

Recent developments of the general purpose line-by-line atmospheric transmittance and radiance model GENLN2 are described. Results will be presented of radiative transfer studies in support of algorithm development for the temperature sounding channels of infrared instruments aboard the Upper Atmosphere Research Satellite (UARS). The implications of spectral line shape modelling and line mixing have been considered for low altitude limb views and comparisons are made with spectra taken during the ATMOS experiment. The effect of high altitude non-LTE radiance in these channels has also been investigated.

GENLN2

Recent Developments and Studies in Support of the *UARS* Project

DAVID P. EDWARDS

Atmospheric Chemistry Division
National Center for Atmospheric Research
Boulder, CO

GENLN2 PROGRAMS

HITLIN

Purpose: Create fast access line data base.

- Binary, direct access line data base, allowing :-
- Fast search for first useful line
- Pointer on each line to next line of same gas
- Every 200 lines a record containing line number of next line of each gas
- Ability to merge new lines into data base
- Status number for each line indicating origin
- Line strength scaling to avoid underflow of weak lines.

GENLN2 PROGRAMS

LAYERS

Purpose: Perform atmospheric layering.

- Model or user supplied atmospheric profile
- User specified viewing geometry
- Layer structure calculated according to max ΔT and $\Delta\alpha_{Voigt}$ across a layer or user supplied
- Ray tracing accounting for atmospheric refraction and variation of g.
- Curtis–Godson mean values for T, p and gas amount.

GENLN2 PROGRAMS

GENLN2

Purpose: Line-by-line calculations.

- Spectral line shapes: Voigt (*Humlicek*, 1982), Doppler, Lorentz, Gross, Van-Vleck & Huber or user supplied
- CO_2 sub-Lorentzian line wings (*Cousin et al.*, 1985)
- Line mixing (*Edwards & Strow*, 1991)
- Water vapour continuum (*Clough et al.*, 1981)
- Heavy molecule absorption cross-sections (*McDaniel et al.*, 1991)
- N_2 and O_2 pressure induced continua (*Orlando et al.*, 1991)
- Temperature variation of line partition functions (*Gamach et al.*, 1990)
- Non-LTE model based on vibrational temperature profile input (*López-Puertas et al.*, 1986).

GENLN2 PROGRAMS

GENLN2

- Two stage line-by-line calculation: fine absorption grid close to line center, wider in the line wings
- Line cutoff at specified minimum intensity and at maximum value of $|\nu - \nu_0|$
- Vertical calculation: at any time the optical depth is known separately for each gas in every layer over a narrow wavenumber interval
- Parallel transmittance and radiance calculations
- Surface boundary options for radiance calculations
- Single gas emission studies for sensitivity calculations
- Gas-correlation, PMR and LMR calculation options.

GENLN2 PROGRAMS

GENGRP

Purpose: Graphics and spectra manipulation.

- Spectrum plotting based on NCAR graphics
- Spectra can be convolved with instrument function in the Fourier domain
- Boxcar, triangle, spectrometer (with apodizing functions) or user supplied instrument functions
- Spectrum convolution with broadband radiometer response
- Calculation of equivalent brightness temperatures.

Figure Captions

Fig. 1. A comparison of calculated transmittances and ATMOS spectra for a 22.4 km tangent height at the 617 cm^{-1} CO_2 Q-branch. The upper panel shows calculated transmittance spectra (dashed line for simple Voigt model, solid line for line mixing model with sub–Lorentzian line wings). The lower panel shows the differences between the calculated transmittances and the ATMOS spectra (dashed line for the Voigt model, chain line for line mixing model with Lorentzian line wings and solid line for the line mixing model and sub–Lorentzian line wings).

Fig. 2. A comparison of calculated transmittances and ATMOS spectra for a 13.6 km tangent height at the 791 cm^{-1} CO_2 Q-branch. The upper panel shows calculated transmittance spectra (dashed line for simple Voigt model, solid line for line mixing model with sub–Lorentzian line wings). The contribution of the CCl_4 band is also shown (dotted line). The lower panel shows the differences between the calculated transmittances and the ATMOS spectra (dashed line for the Voigt model, chain line for line mixing model with Lorentzian line wings and solid line for the line mixing model and sub–Lorentzian line wings).

Fig. 3. ISAMS channel 7.1 radiometer signal at different tangent heights for the Voigt model (dashed line) and the line mixing model with sub–Lorentzian line wings (solid line). The wide–band signals are shown left and the PMR signals right.

Fig. 5. Calculated radiance spectra for a 13.6 km tangent height at the 791 cm^{-1} CO_2 Q-branch. The upper panel shows calculated radiance spectra (dashed line for simple Voigt model, solid line for line mixing model with sub–Lorentzian line wings). The lower panel shows the CLAES blocker filter 8 etalon channel positions.

Fig. 6. CLAES blocker filter 8 etalon 3 channel radiance at different tangent heights for the Voigt model (dashed line) and the line mixing model with sub–Lorentzian line wings (solid line).

FIG. 1.

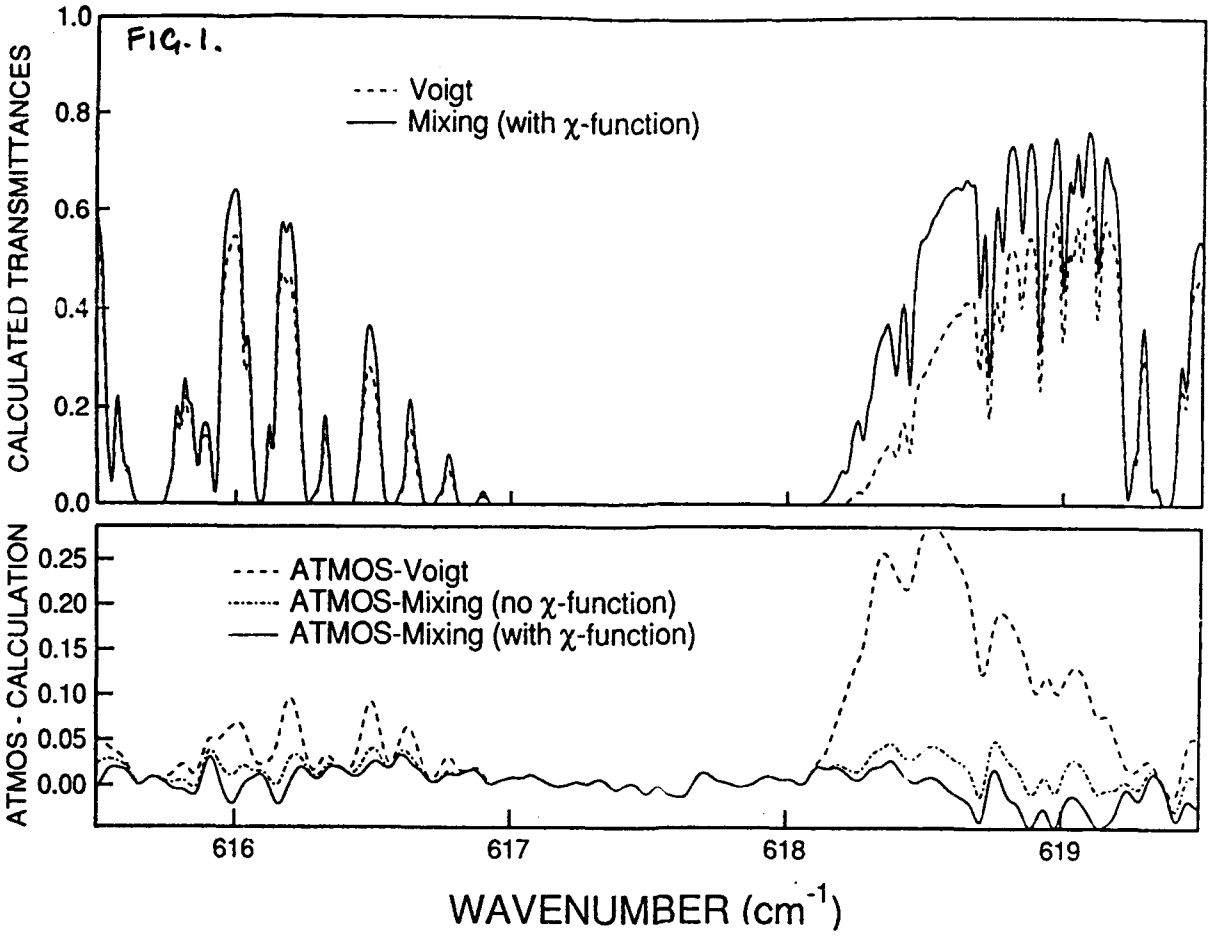
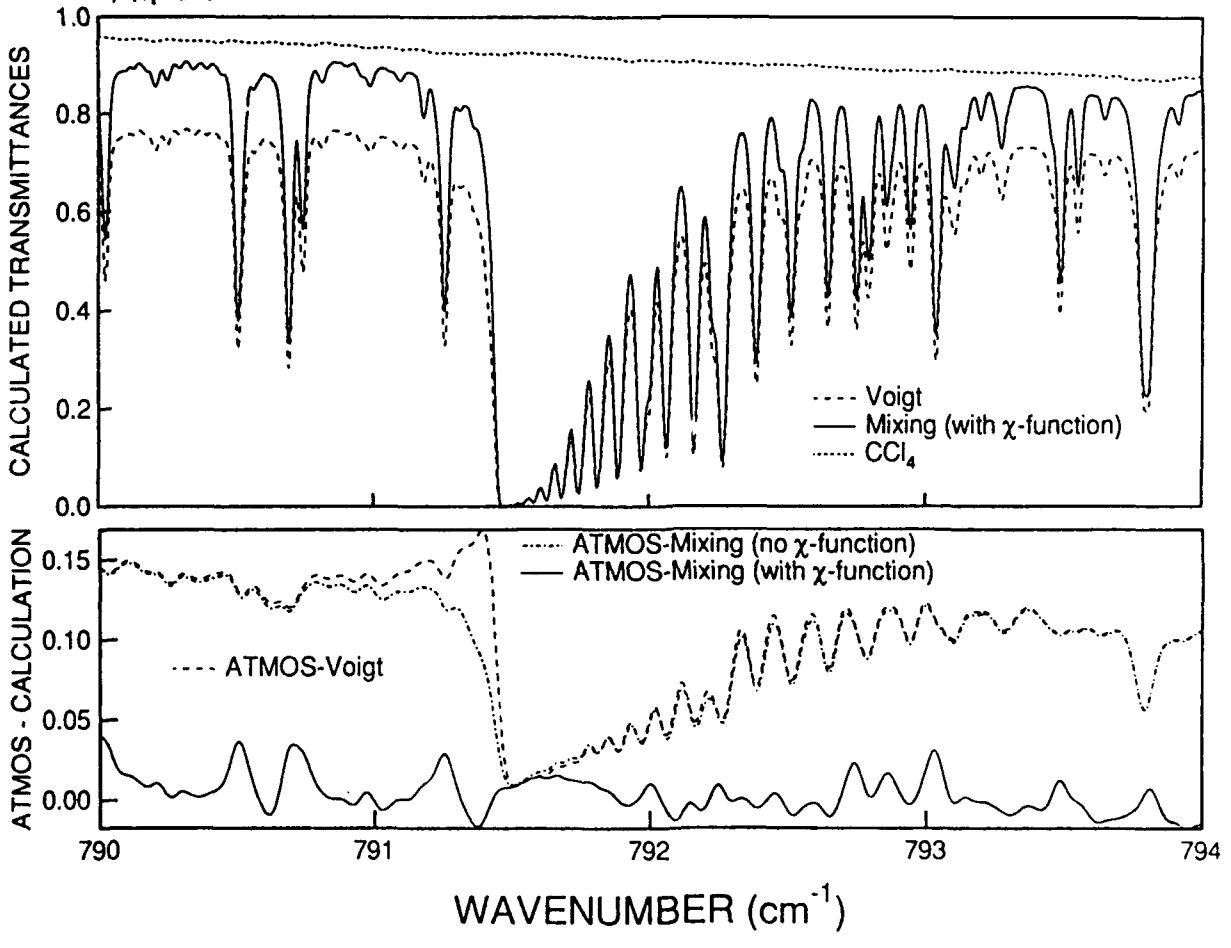
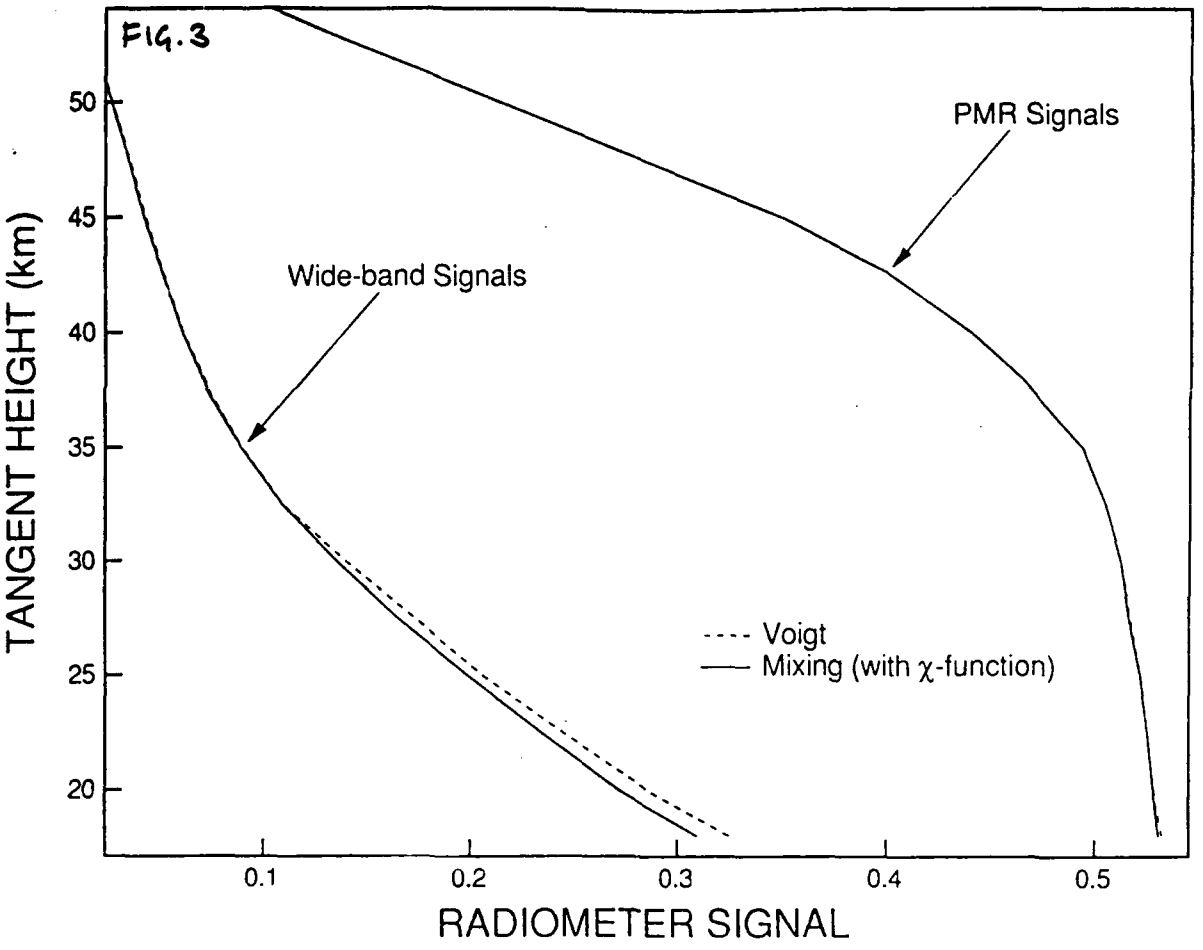

CALCULATED TRANSMITTANCES
1.0
0.8
0.6
0.4
0.2
0.0
Voigt
Mixing (with χ-function)
ATMOS - CALCULATION
0.25
0.20
0.15
0.10
0.05
0.00
ATMOS-Voigt
ATMOS-Mixing (no χ-function)
ATMOS-Mixing (with χ-function)
616
617
618
619
WAVENUMBER (cm-1)

FIG. 2.


CALCULATED TRANSMITTANCES
1.0
0.8
0.6
0.4
0.2
0.0
Voigt
Mixing (with χ-function)
CCl4
ATMOS - CALCULATION
0.15
0.10
0.05
0.00
ATMOS-Mixing (no χ-function)
ATMOS-Mixing (with χ-function)
ATMOS-Voigt
790
791
792
793
794
WAVENUMBER (cm-1)


Fig. 3
PMR Signals
Wide-band Signals
Voigt
Mixing (with χ-function)
TANGENT HEIGHT (km)
50
45
40
35
30
25
20
0.1
0.2
0.3
0.4
0.5
RADIOMETER SIGNAL

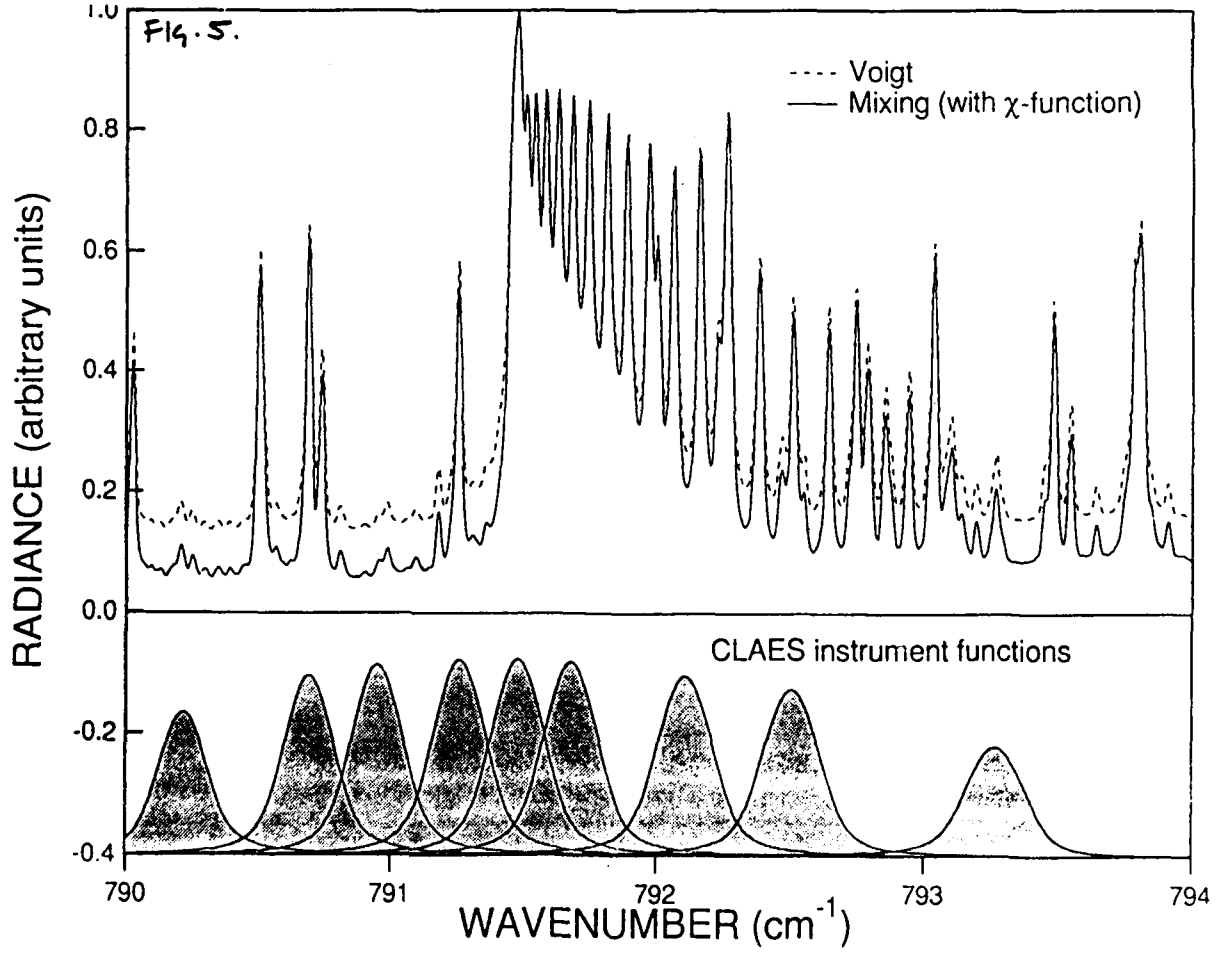
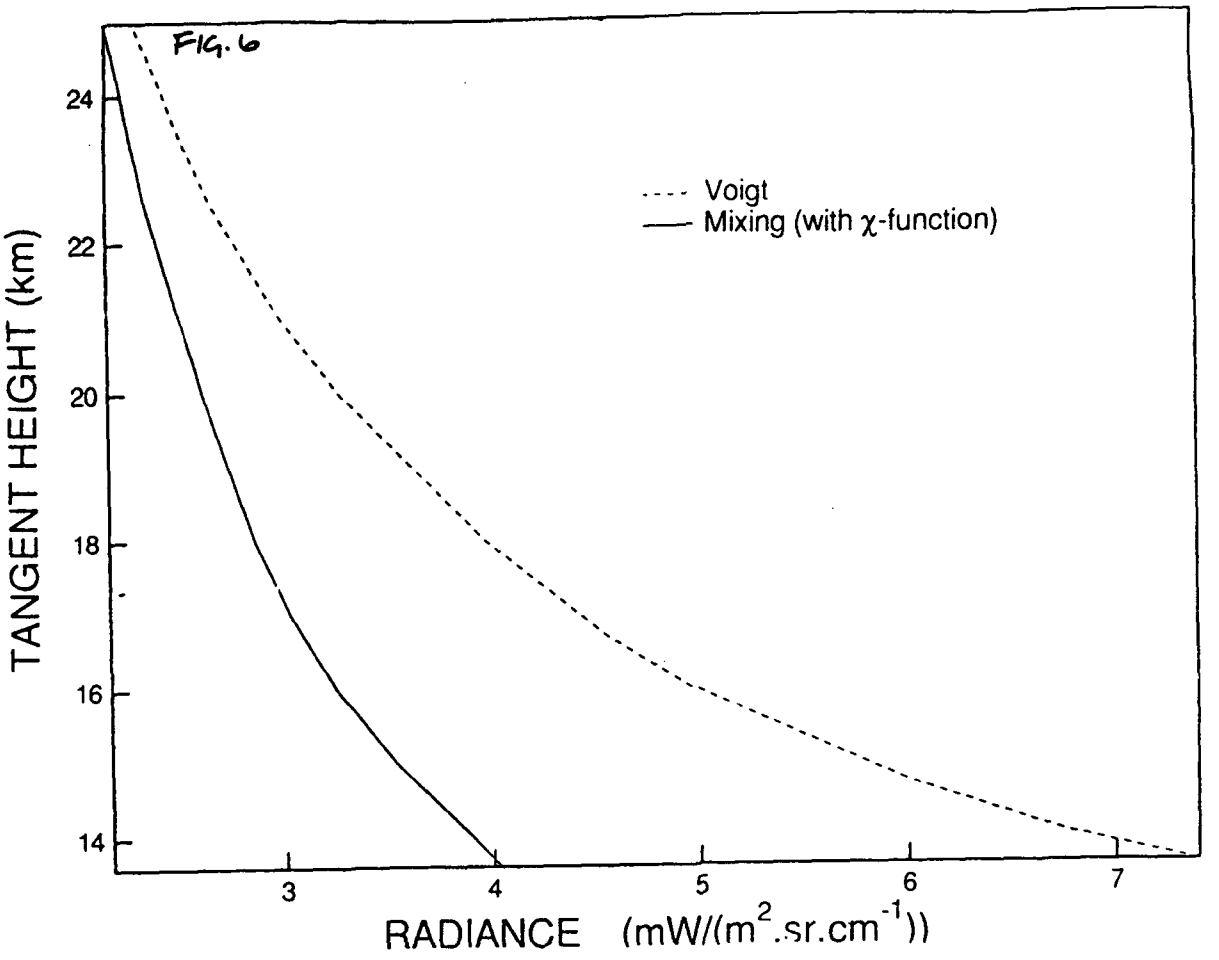
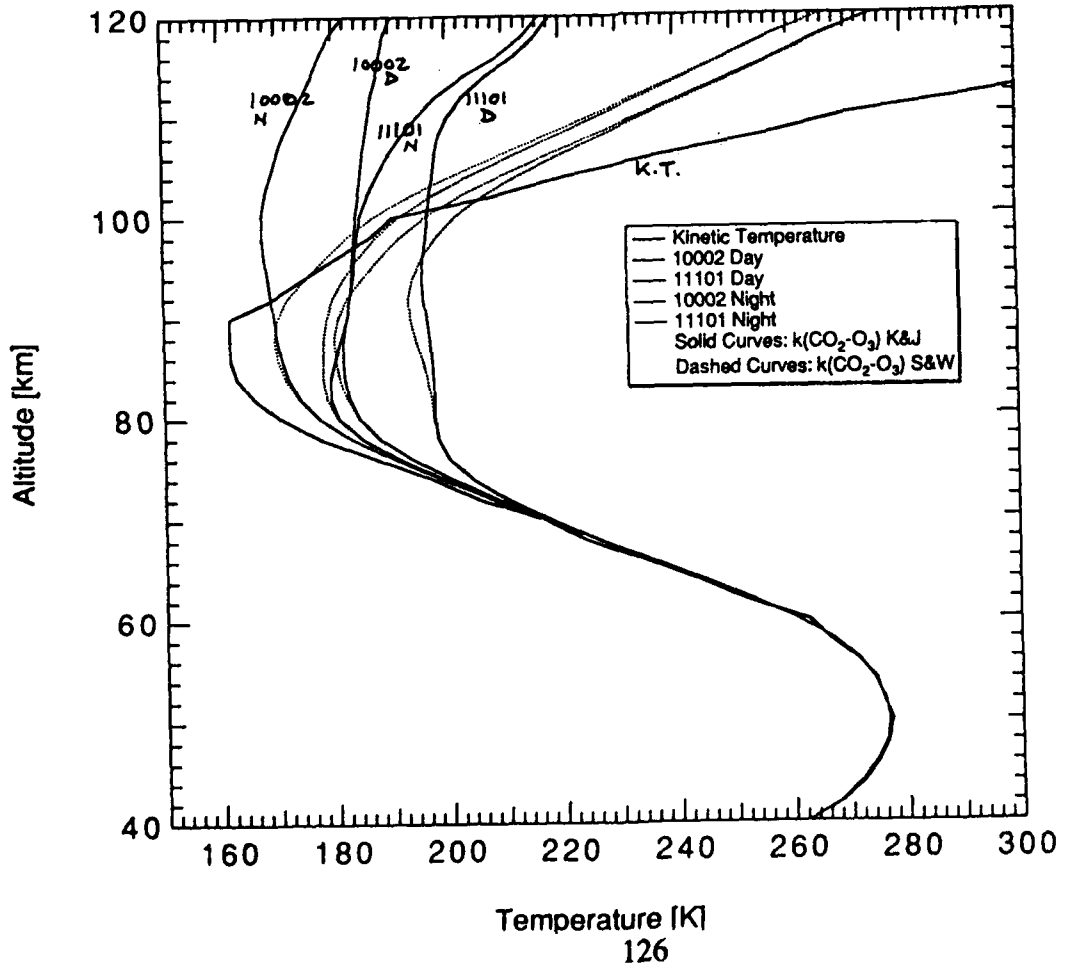

Fig. 5.
Voigt
Mixing (with χ-function)
CLAES instrument functions
RADIANCE (arbitrary units)
1.0
0.8
0.6
0.4
0.2
0.0
-0.2
-0.4
790
791
792
793
794
WAVENUMBER (cm-1)

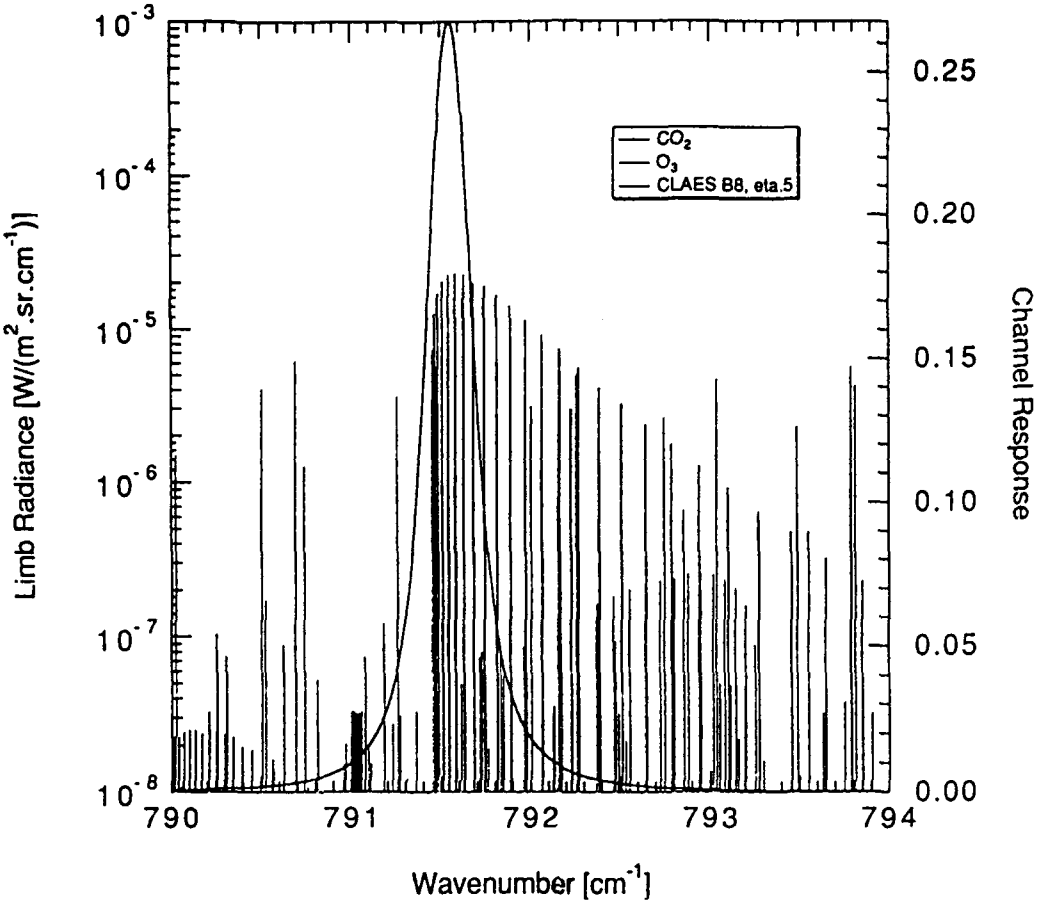
FIG. 6



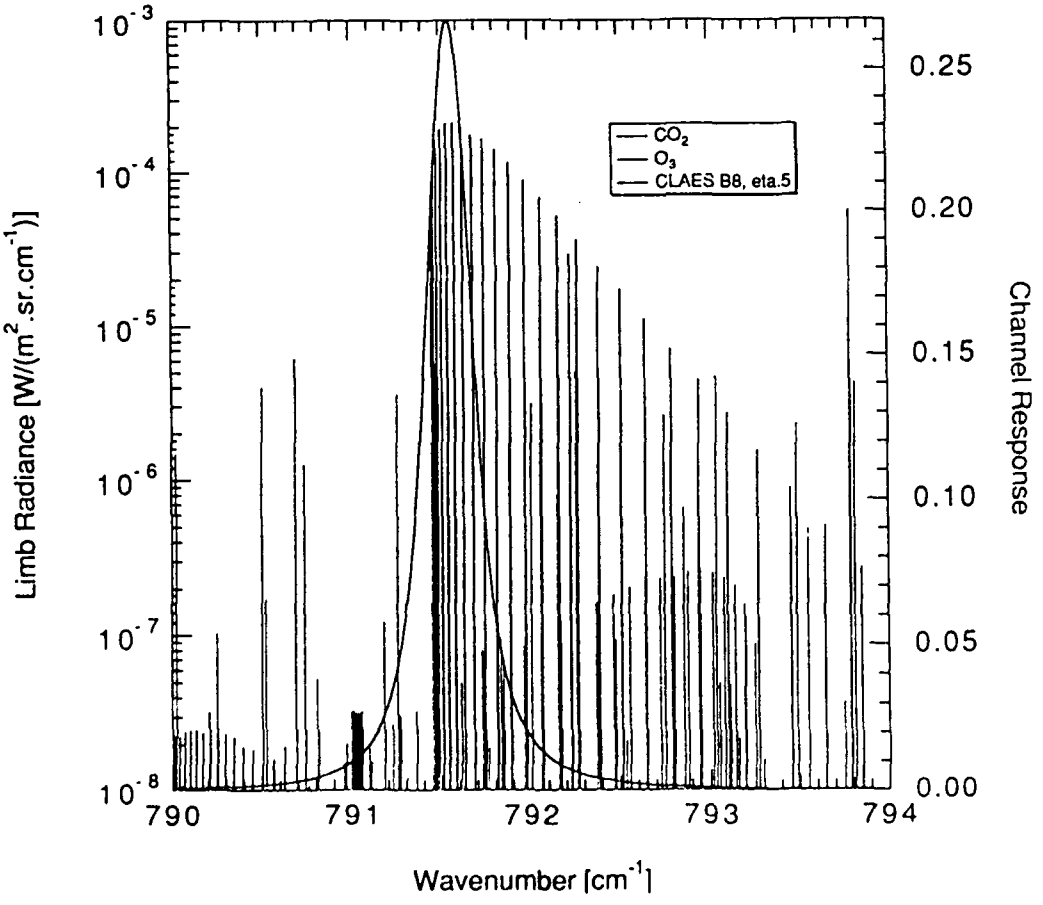
Vibrational Tempertures for CO_2 (11101)-(10002)



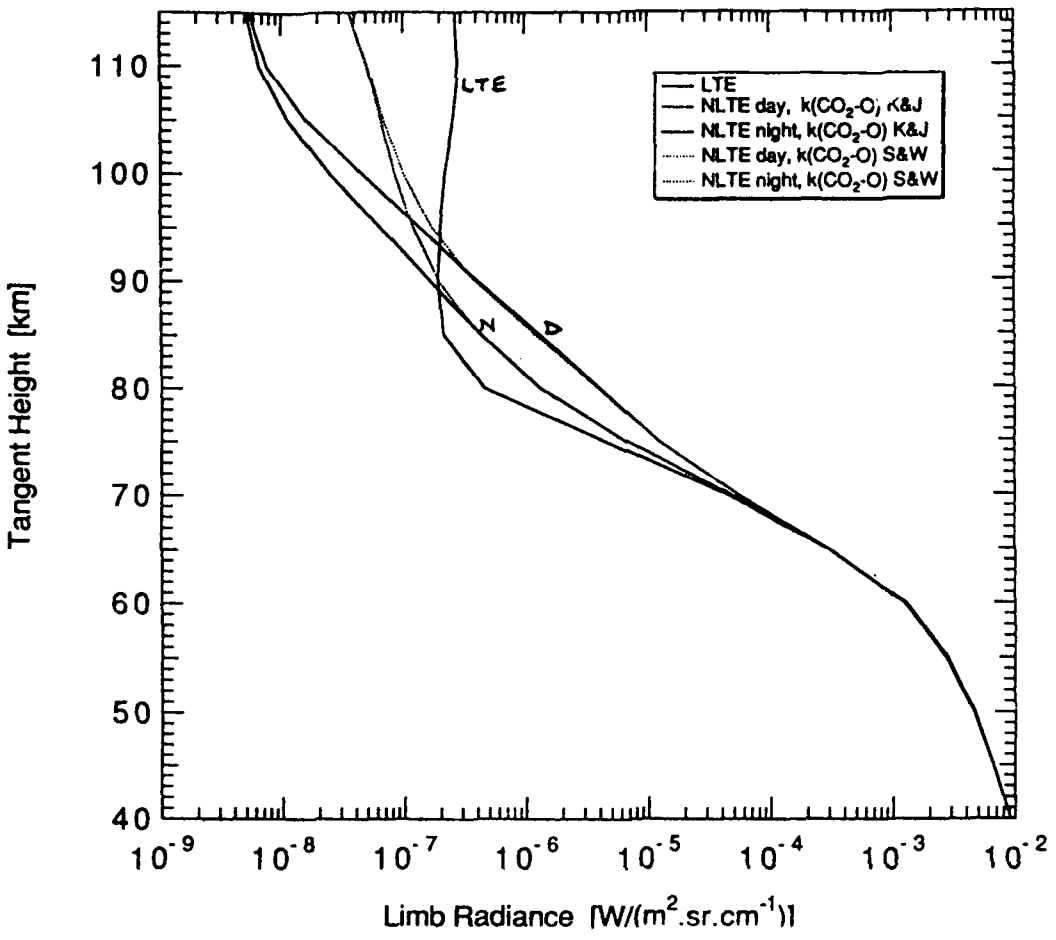
LTE 80km Limb Radiance: Subarc.Sum.#4.



NLTE 80km Day Limb Radiance: Subarc.Sum.#4, S&W.



CLAES High Altitude Radiance: B8, eta 5. Subarc.Sum.#4.



PRESENT STATUS OF TRANSMITTANCES AND RADIANCES MODELLING AT L.M.D.

N.A. Scott, A. Chédin, F. Chéruy, B. Tournier
(ARA/LMD) Ecole Polytechnique, 91128 Palaiseau Cedex, France

The ARA/LMD group has years of experience in the modelling of transmittances and radiances: STRANSAC (1974), 4A (Automated Atmospheric Absorption Atlas, 1981) and 3R (Rapid Radiance Recognition, 1986) represent three generations of forward radiative transfer models characterized by their increasing efficiency regarding the computation time. They have already been and are involved in several international campaigns of intercomparisons (ITRA: Intercomparison of Transmittance and Radiance Algorithms, IRC/IAMAP). STRANSAC and 4A are presently used within the context of the modelling of high spectral resolution radiance measurements (AIRS experiment of the NASA EOS - Earth Observing System - Programme, and IASI experiment of the CNES-GLOBSAT Programme).

A description of these models as well as a report on the work in progress will be given at the time of the Conference.

"AURIC (ATMOSPHERIC ULTRAVIOLET RADIANCE INTEGRATED CODE): AN UPDATE"

R. Hugeunin, R. Hickey
Aerodyne Research, Inc., 45 Manning Road, Billerica, MA 01821

M. Minschwaner
Harvard University, Cambridge, MA 02138

G.P. Anderson, L.A. Hall, R.E. Huffman
Phillips Laboratory, Hanscom Air Force Base, MA 01731-5000

AURIC is an atmospheric ultraviolet spectral transmission and solar irradiance code that is being developed as a modification of MODTRAN. The modification provides an extension of atmospheric structure to allow more than 34 layers, including layers above 100 km. The modification also provides an extension of wavelength to 100 nm. Atmospheric specification will allow compatibility with layer specifications in SHARC. A new O_2 Schumann Runge model is being developed for AURIC, but the initial release will not include airglow emissions.

AERODYNE RESEARCH, Inc.
SYSTEMS

ARI FILE NO. 1579-011
V6S/183

AURIC
(ATMOSPHERIC ULTRAVIOLET RADIANCE INTEGRATED CODE)
AN UPDATE

ROBERT HUGUENIN AND ROBERT HICKEY (AERODYNE RESEARCH, INC.)

KEN MINSCHWANER (HARVARD UNIVERSITY)

GAIL ANDERSON, AL HALL AND ROBERT HUFFMAN
(PHILLIPS LABORATORY/GEOPHYSICS DIRECTORATE/AF SYSTEMS COMMAND)

PRESENTED AT
ANNUAL REVIEW CONFERENCE ON ATMOSPHERIC MODELS
PHILLIPS LABORATORY/GEOPHYSICS DIRECTORATE
AFSC, HANSCOM AFB, MA

11-12 JUNE 1991

45 Manning Road
Billerica, Ma. 01821-3976
(508) 663-9500 Fax: (508) 663-4918

SYSTEMS

AURIC DEVELOPMENT PROGRAM

GOAL: DEVELOP AN ATMOSPHERIC ULTRAVIOLET SPECTRAL TRANSMISSION AND SOLAR IRRADIANCE CODE FOR DELIVERY TO SDIO BY 30 SEPTEMBER 1991

SYSTEMS

AURIC DEVELOPMENT PROGRAM

TECHNICAL APPROACH: MODIFY MODTRAN TO INCLUDE AN EXTENSION OF ATMOSPHERIC STRUCTURE AT ALTITUDES ABOVE 100 KM AND AN EXTENSION OF WAVELENGTH TO 100 NM. AIRGLOW EMISSIONS WILL NOT BE INCLUDED

SYSTEMS

HIGH ALTITUDE VERTICAL STRUCTURE EXTENSION

- MODTRAN/LOWTRAN7 CODE MODIFICATION TO REMOVE 33 LAYER LIMITATION
  - MODIFICATION OF EXISTING DIMENSION STATEMENTS
  - DEVELOPMENT OF N_{TH} ORDER INTERPOLATION ROUTINE FOR CONSTITUENT PROFILES
- USER-DEFINED N-LAYER SPECIFICATION
  - LAYERS CAN BE ADDED ABOVE 100 KM
  - NUMBER OF LAYERS CAN BE INCREASED BELOW 100 KM
  - ALLOWS COMPATIBILITY WITH SHARC LAYER SPECIFICATIONS
- CONSTITUENT PROFILES WILL BE EXTENDED TO 1000 KM
  - BLOCK DATA STATEMENT EXTENSIONS
  - PROFILE SPECIFICATION IN PROGRESS

SYSTEMS

HIGH ALTITUDE VERTICAL STRUCTURE EXTENSION (CONT'D)

- STORAGE REQUIREMENTS (VIRTUAL MEMORY USED)
  - TESTS PERFORMED ON MICROVAX WITH MODTRAN CONSTITUENT PROFILES

    MODTRAN - APPROXIMATELY 533 KBYTES
    AURIC (50 LAYERS) - APPROXIMATELY 558 KBYTES
    AURIC (100 LAYERS) - APPROXIMATELY 670 KBYTES
    AURIC (200 LAYERS) - ESTIMATED, APPROX. 1 MBYTE

- ALL CURRENT FUNCTIONALITY OF MODTRAN/LOWTRAN7 HAS BEEN RETAINED



SYSTEMS

EXOATMOSPHERIC SOLAR IRRADIANCE EXTENSION

- INITIAL WAVELENGTH EXTENSION TO 1205Å
  - USE OF SUSIM (4000 - 1205Å) TABLES PLANNED
  - NOMINAL 1Å RESOLUTION DATA WITH INTERPOLATION

- SELECTION OF SOLAR ACTIVITY MODEL IN PROGRESS



SYSTEMS

O_2 SCHUMANN-RUNGE MODEL UPGRADE

- BASED ON FIRST PRINCIPLES MODEL BY K. MINSCHWANER AND M. MCELROY (HARVARD UNIVERSITY)
- DEVELOPMENT OF FACTORABLE TEMPERATURE DEPENDENCE MODEL FOR COMPATIBILITY WITH MODTRAN/LOWTRAN TRANSMISSION FORMULATION



SYSTEMS

HARVARD SCHUMANN-RUNGE MODEL FEATURES

- $X^3\Sigma_g^-$ AND $B^3\Sigma_u^-$ ENERGY LEVELS FROM SPECTROSCOPIC CONSTANTS (VESETH AND LOFTHUS, 1974; CHEUNG ET AL, 1986)
- ROTATIONAL DEPENDENCE OF PREDISSOCIATION WIDTHS (CHEUNG ET AL, 1990; LEWIS ET AL, 1989)



HARVARD SCHUMANN-RUNGE MODEL FEATURES (CONT'D)

- BAND OSCILLATOR STRENGTHS (YOSHINO ET AL, 1983; LEWIS ET AL., 1986); HÖNL-LONDON FACTORS (TATUM AND WATSON, 1971); FULL BOLTZMAN CALCULATION TO DETERMINE INDIVIDUAL LINE STRENGTHS

- VIBRATION: $V' = 0, 1$ AND 2
  $V'' = 0$ TO 19

- ROTATION: $N'' = 1$ TO 51
  $N' = 0$ TO 50



SYSTEMS

HARVARD SCHUMANN-RUNGE MODEL FEATURES (CONT'D)

- 2 PRINCIPAL BRANCHES ($\Delta N = \Delta J = \pm 1$)
- 6 SATELLITE BRANCHES ($\Delta N = \pm 1$; $\Delta J = 0, \pm 1$; $\Delta N \neq \Delta J$)
- 2 FORBIDDEN LINES ($\Delta N = \pm 3$, $\Delta J = \pm 1$)
- ISOTOPIC OXYGEN LINES ^{16}O ^{18}O
- UNDERLYING HERZBURG, SCHUMANN-RUNGE CONTINUA INCLUDED



SYSTEMS

HARVARD SCHUMANN-RUNGE MODEL FEATURES (CONT'D)

- INPUT
  - O_2 SPECTROSCOPIC CONSTANTS
  - BAND OSCILLATOR STRENGTHS
  - LINE WIDTHS (FUNCTIONS OF UPPER STATE VIBRATIONAL /ROTATIONAL LEVELS)
  - TEMPERATURE
- CALCULATION
  - ENERGY LEVELS
  - POPULATION DISTRIBUTION
  - LINE POSITIONS
  - LINE STRENGTHS
- SPECTRAL CALCULATION

  $\sigma(\nu) = \Sigma$ ALL LINES WITHIN 500 CM^{-1}; VOIGT LINE PROFILES

- VALIDATION AT 79°K AND 300°K FROM MEASUREMENTS BY HARVARD-SMITHSONIAN GROUP

SYSTEMS

SCHUMANN-RUNGE TEMPERATURE DEPENDENCE MODEL

- MODTRAN/LOWTRAN TRANSMISSION FORMULATION

$$\tau_\nu = \exp\left\{-\sum_\ell (a_\nu + b_\nu T_\ell + C_\nu T_\ell^2)\, n_\ell\right\}$$

$$= \exp\left\{-a_\nu \underbrace{\sum_\ell N_\ell}_{U} - b_\nu \underbrace{\sum_\ell{}' T_\ell n_\ell}_{T} - c_\nu \underbrace{\sum_\ell{}' T_\ell^2 n_\ell}_{}\right\}$$

STORED COLUMN AMOUNTS

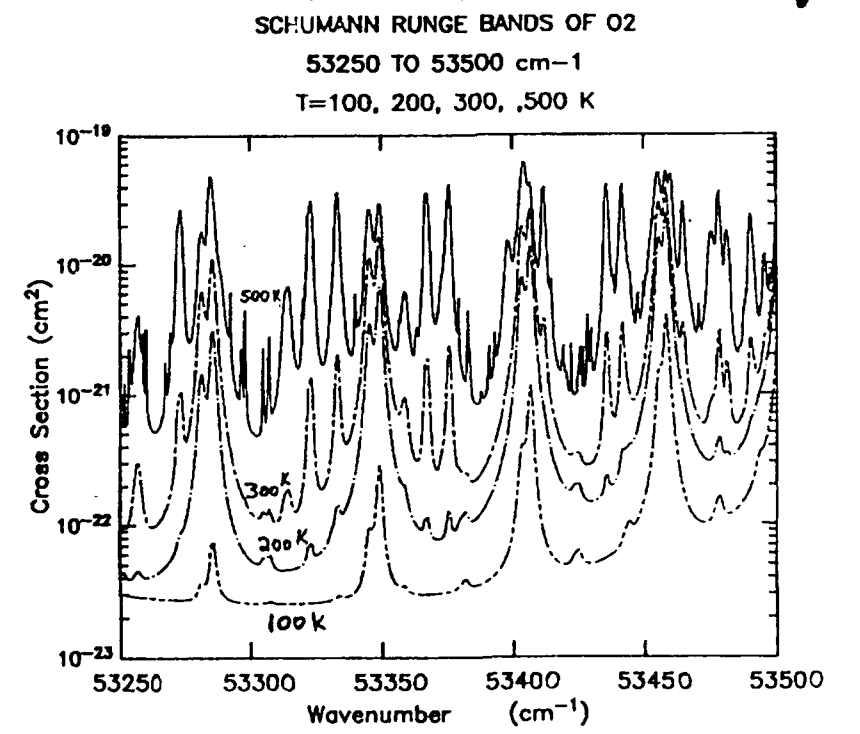
- TEMPERATURE DEPENDENCE MUST BE FACTORABLE, YIELDING (A_ν, B_ν, C_ν) vs. ν

eg $\sigma_\nu(T) = a_\nu + b_\nu T + c_\nu T^2$

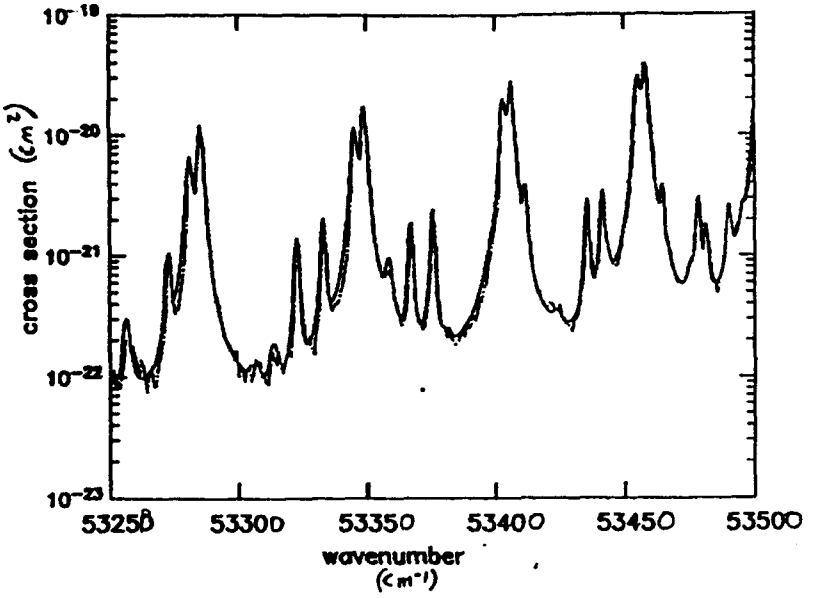
or $\sigma_\nu(T) = a_\nu + b_\nu T^2 + c_\nu T^4$

SCHUMANN-RUNGE TEMPERATURE DEPENDENCE MODEL (CONT'D)

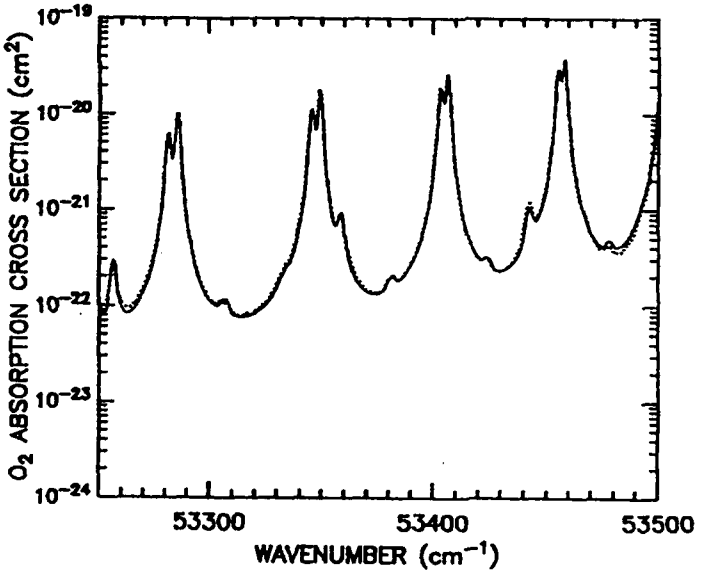
- WORK IS PROCEEDING TO DETERMINE THE BEST SET OF BASIS FUNCTIONS AND OPTIMAL FITTING PROCEDURES TO COVER TEMPERATURE RANGE OF 100 - 500°K
  - HOT AND COLD BANDS HAVE DIFFERENT TEMPERATURE DEPENDENCES
  - ATTEMPTING TO FIT CROSS-SECTIONS WITH POLYNOMIALS IN TEMPERATURES
  - DIFFERENT FITTING PROCEDURES REQUIRED ABOVE AND BELOW 275-300°K
  - DOUBLE QUADRATIC FIT, PINNED TO 275°K DATA POINT YIELDS PROMISING RESULTS

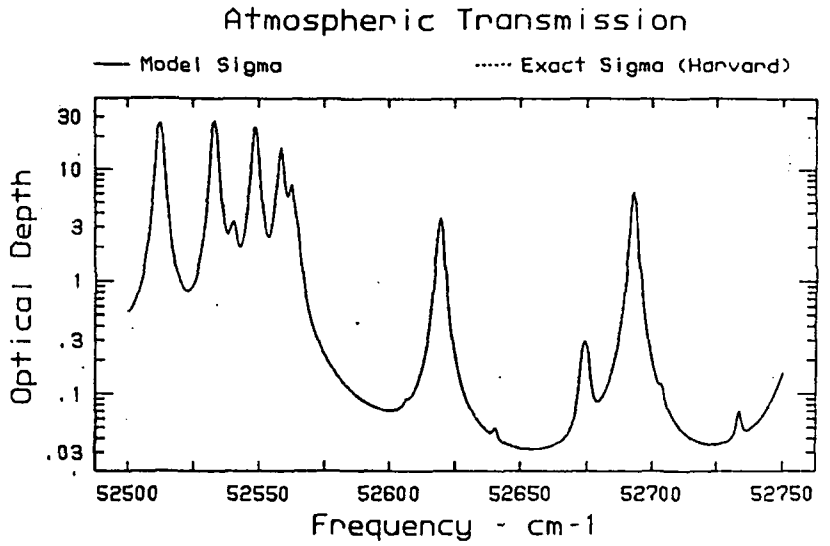


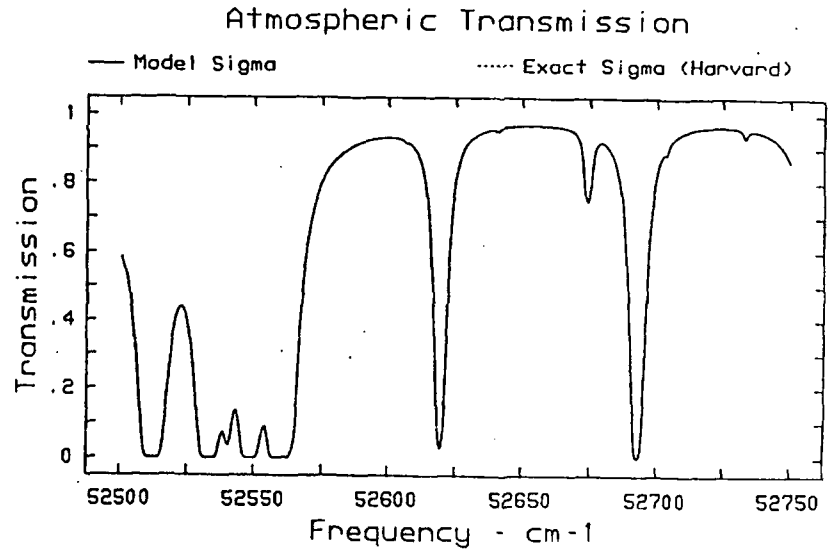
SCHUMANN–RUNGE BANDS OF O_2
53250–53500 cm^{-1}
T = 300 K



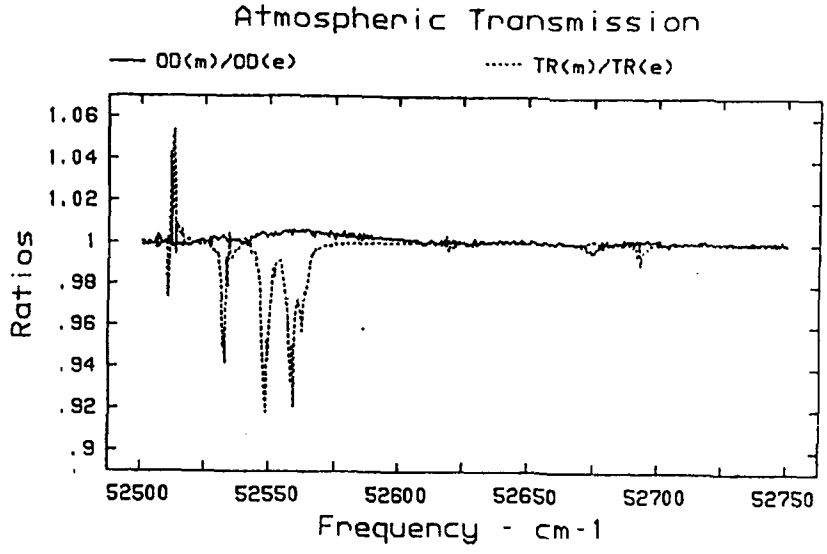
Schumann–Runge Bands of O_2, v''=0
53250 to 53500 cm^{-1}
T=300 K



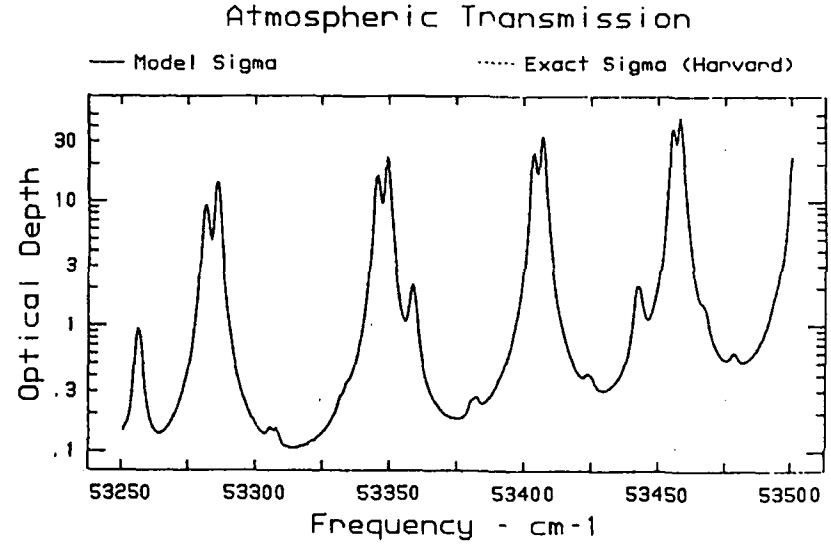

Atmospheric Transmission
Model Sigma
Exact Sigma (Harvard)
Optical Depth
30
10
3
1
.3
.1
.03
52500
52550
52600
52650
52700
52750
Frequency - cm-1

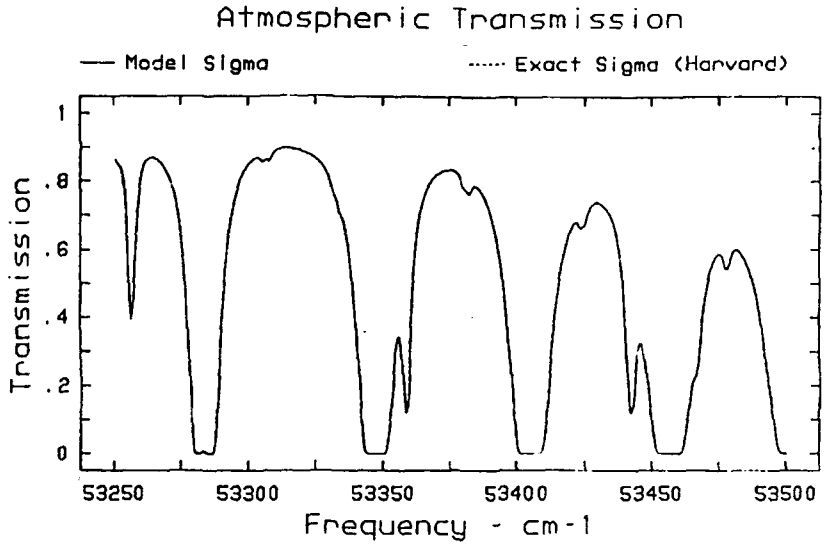

Atmospheric Transmission
Model Sigma
Exact Sigma (Harvard)
Transmission
1
.8
.6
.4
.2
0
52500
52550
52600
52650
52700
52750
Frequency - cm-1

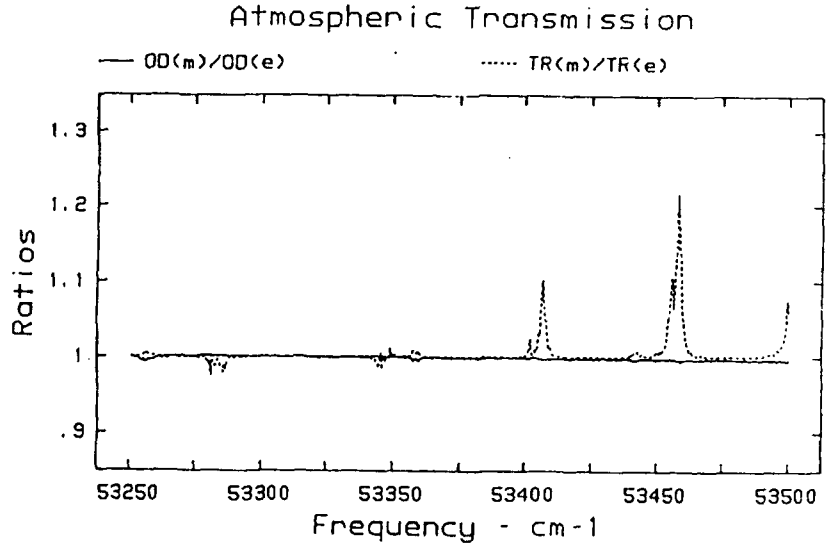
SYSTEMS



SYSTEMS




Atmospheric Transmission
Model Sigma
Exact Sigma (Harvard)
Transmission
1
.8
.6
.4
.2
0
53250
53300
53350
53400
53450
53500
Frequency - cm-1


Atmospheric Transmission
OD(m)/OD(e)
TR(m)/TR(e)
Ratios
1.3
1.2
1.1
1
.9
53250
53300
53350
53400
53450
53500
Frequency - cm-1

SUMMARY

- AURIC IS AN EXTENSION OF MODTRAN
  - EXTENDED ATMOSPHERIC STRUCTURE
    - 33 LAYER LIMITATION REMOVED
    - LAYERS CAN BE ADDED ABOVE 100 KM
    - CONSTITUENT PROFILES EXTENDED TO 1000 KM
  - WAVELENGTH RANGE EXTENDED TO 1205 Å
    - EXTENSION OF EXOATMOSPHERIC SOLAR IRRADIANCE
    - ADDITION OF IMPROVED O_2 SCHUMANN-RUNGE MODEL
  - FULL MODTRAN FUNCTIONALITY RETAINED
- AURIC PROVIDES ATMOSPHERIC SPECTRAL TRANSMISSION AND SOLAR IRRADIANCE
- AURIC 1.0 WILL NOT INCLUDE AIRGLOW EMISSIONS
- DELIVERY TO SDIO BY 30 SEPTEMBER 1991

ONTAR'S PC COMPATIBLE LOWTRAN7 PACKAGE

P.V. Noah, J. Schroeder
Ontar Corporation, 129 University Road, Brookline, MA 02146

PCTRAN7 is an implementation of the Phillips Laboratory/Geophysics Directorate's LOWTRAN7 model and associated software for the IBM and compatible family of personal computers. The package contains software for input generation, help for LOWTRAN7 parameters, an ASCII text file viewer for output files, screen graphics capability, and hard copy graphics. The software has been validated by the PL/GP under a cooperative IR&D agreement with Ontar.

This paper will describe PCTRAN7, Version 2a, and demonstrate the capabilities of the package.

PCTRAN 7 [c]: An Implementation of the GP's LOWTRAN 7 Model for the Personal Computer

USERS MODELING WORKSHOP
(LOWTRAN/MODTRAN/FASCODE-HITRAN)

PL/GP Hanscom AFB, MA

11 June 1991

Paul V. Noah and John Schroeder

Ontar Corporation

129 University Road

Brookline, MA 02146 - 4532

Tel: 617-739-6607 FAX: 617-277-2374



Cooperative R & D Agreement

With Geophysics Laboratory - Hanscom AFB, MA

September 1988

PC Implementation of a Software Package - LOWTRAN 7 - PCTRAN 7 [c]



LITERATURE AVAILABLE

SOFTWARE DEMONSTRATION

Ontar Corporation

129 University Road

Brookline, MA 02146 - 4532

Tel: 617-739-6607 FAX: 617-277-2374 Bulletin Board: 617-277-6299

ONTAR

PL/GP LOWTRAN 7 CODE

Computes Atmospheric Transmission and Radiance.

0 to 50,000 Cm^{-1} Spectral Coverage @ 5 to 20 Cm^{-1} Resolution.

All Viewing Geometries.

Default Atmospheric Profiles from Sea Level to 100 Km.

Capability for User Supplied Profiles.

Cloud, Rain and Aerosol Models.

Band Models for H_2O, O_3, N_2O, CH_4, CO, O_2, CO_2, NO, NO_2, NH_3 and SO_2. New UV parameters for O_2 (Schumann-Runge bands and Herzberg continuum) and updated O_3 Hartley and Huggins bands.

ONTAR

PCTRAN 7 [c] * Version 2a

PC Version of the PL/GP LOWTRAN 7 Atmospheric Radiance & Transmission Code

Complete Implementation of the LOWTRAN 7 Code - Release 3.8.

Installation Program.

Interactive User Input Software.

Help Screens for All Input Variables.

Screen and Hard Copy Graphics Output.

Tabular Output in ASCII Format.

Batch Processing Input Software.

Plotting from Different LOWTRAN Calculations.

Expert Help.

CERTIFIED for ACCURACY by the GEOPHYSICS DIRECTORATE.



Hardware and Software Requirements

Personal Computer - XT, AT, 80386, 80486 (Compatible, Clone)

1.2 Mbyte Diskette Drive, Hard Disk

640 Kbytes of Memory

CGA, EGA, or VGA Graphics Board and Monitor - for Screen Plots

Printer - for Hard Copy

Numeric Co-processor Highly Recommended



Setup Program

Semi-automatic Installation Procedure.

Copies all files to target drive.

Sets up Printer Support.

Defines Graphics Adapter Type.

Capable of Printer ONly Installation.

Checks Available Disk Space.

ONTAR Corporation, 129 University Road, Brookline, MA 02146, 617-739-6607



ONTAR's LOWTRAN Modules Program Suite -- Version 7.2a
LOWTRAN7/MODTRAN/SENTRAN

a. Input Shell
b. Execute Program
c. Data Plotting
d. Printer Plotting
e. View Data Output
f. View FILE7
g. View FILE8
h. Filter Input
i. Execute Filter Program
j. View Filter Output
k. Execute Scanning Program
l. Scanning Plotting
m. View FILE9
n. Multiple FILE7 Plots

o. Expert Help

x. Return to DOS

Input Function:



Initial Altitude (km)	1.500
Final Altitude/Tangent Height (km)	10.000
Initial Zenith Angle (degrees)	.000
Path Length (km)	.000
Earth Center Angle (degrees)	.000
Radius of Earth (km) [.000 - default]	.000
Type of Path	Short

Initial Frequency 2000.000 cm-1 Wavelength 4.000 m

Final Frequency 2500.000 cm-1 Wavelength 5.000 m

Frequency Increment (wavenumber) 5.000

Run # 2 of 4 LOWTRAN7 Cards 3 & 4



PC-TRAN7 Batch Mode Manager.

ESC - Quit LOWIN (write LOWIN and LOWPLT.DAT)
F2 - Edit current run.
F3 - Edit next run.
F4 - Edit previous run.
F5 - Add new run (to end) and go to that run
F6 - Delete current run.
F7 - Go to run.

Database name MCASE3

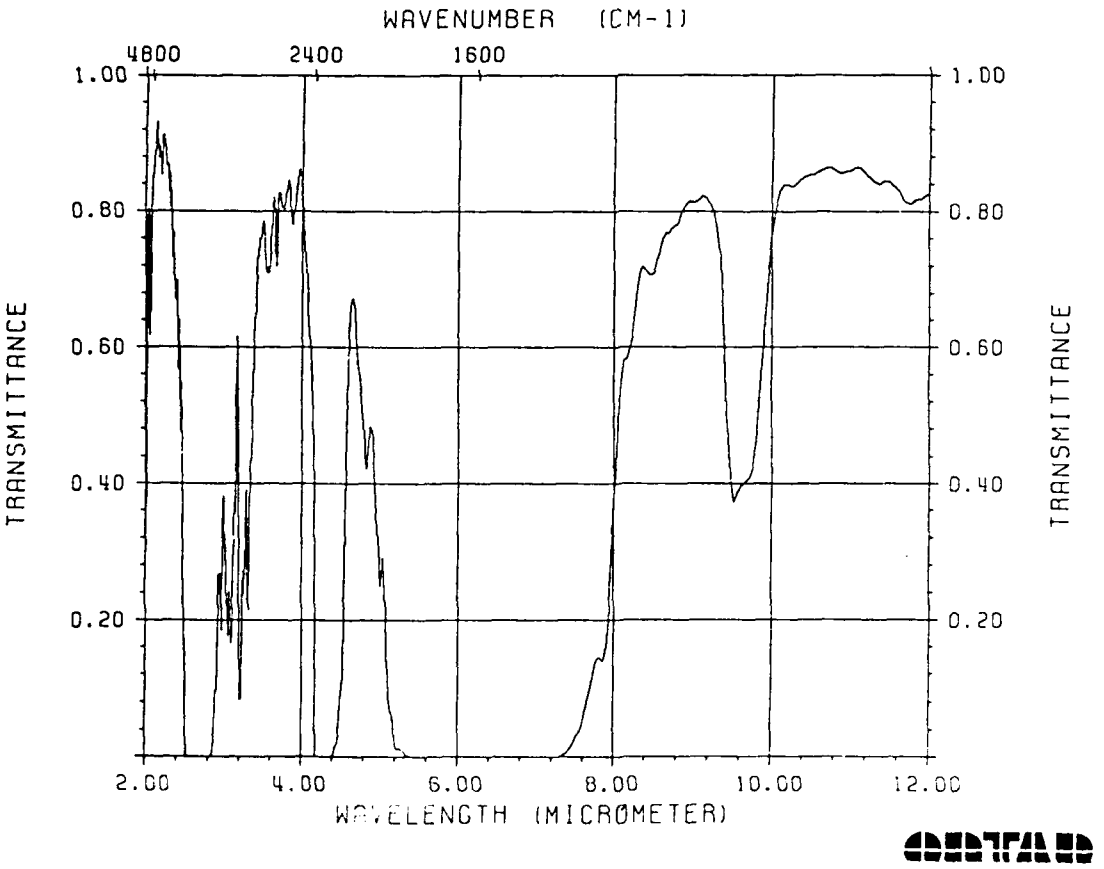
Number of runs in this database 4 Current run 3

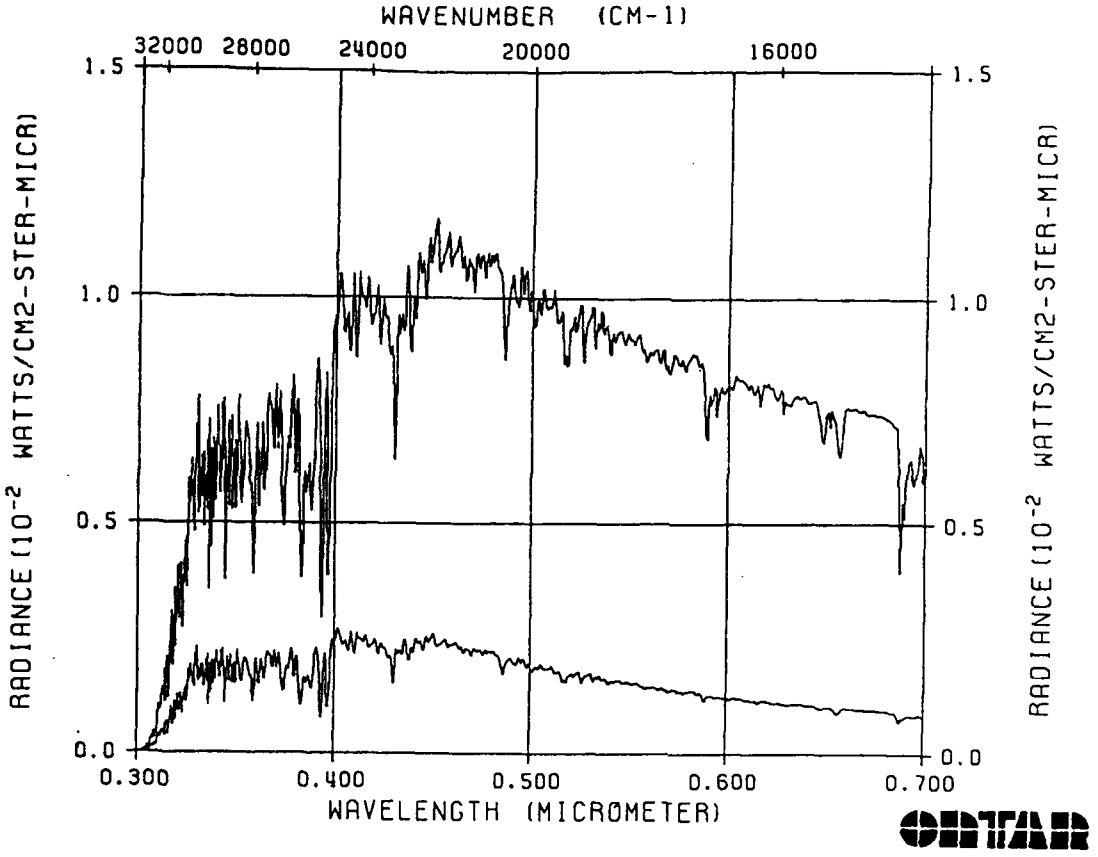
LOWTRAN7 Card 5



Plot Type	Transmittance in m
Type of X Axis	Linear
Type of Y Axis	Linear
Number of Decimal Digits for Y Axis	2
Length of X Axis (in inches)	7.0000
Beginning Wavenumber/Wavelength	4.0000 m
Ending Wavenumber/Wavelength	5.0000 m
X Axis Annotation Interval	.2000 m
X - Number of Minor Ticks / Division	5
Length of Y Axis (in inches)	6.0000
Autoscale Y Axis	No
Minimum Transmittance/Radiance	.00E+00
Maximum Transmittance/Radiance	1.00E+00
Y Axis Annotation Interval	2.00E-01
Y - Number of Minor Ticks / Division	5
Plot Grids (Graph Paper)	Coarse Grid

Run # 2 of 4 LOWPLT Scaling Plot # 1

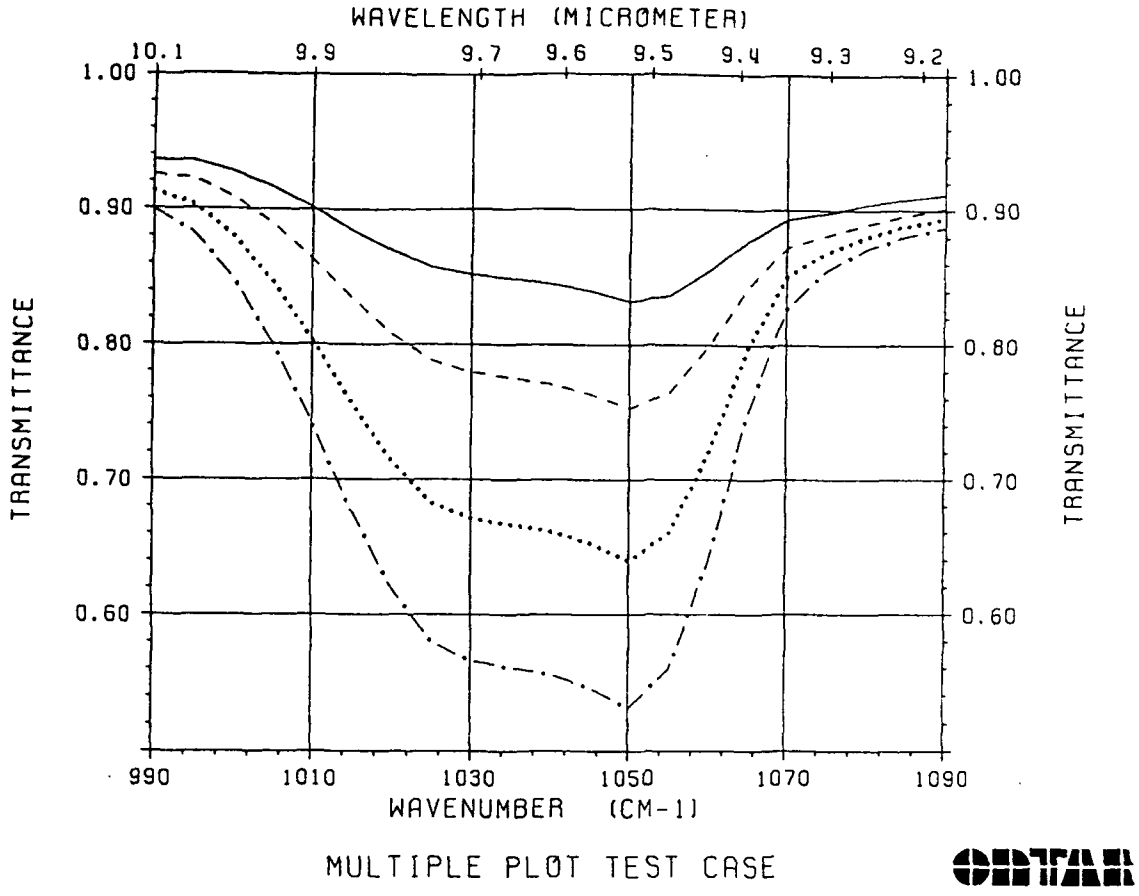




Multiple Run Plotting Inputs

Filename	Run	Plot Mode	Title
CASE-A	1	Transmittance	1976 U S STANDARD
CASE-A	2	Transmittance	SUBARCTIC WINTER
CASE-A	3	Radiance /w Scattering	SUBARCTIC SUMMER
CASE-A	4	Radiance	MIDLATITUDE SUMMER
CASE-B	1	Transmittance	1976 U S STANDARD
CASE-B	2	Radiance	TROPICAL MODEL
CASE-B	3	Radiance /w Scattering	MIDLATITUDE SUMMER
CASE-B	4	Transmittance	SUBARCTIC SUMMER
CASE-C	1	Transmittance	1976 U S STANDARD
CASE-C	2	Radiance	TROPICAL MODEL
CASE-C	3	Radiance /w Scattering	New Model Atmosphere
CASE-C	4	Transmittance	Met Data (Hor Path)

LOWMPIN Select Runs



PCTRAN7 Expert Help

Online Expert Help.

Guides you through common user problems.

Draws on over 5 years of PCTRAN user support.

Aides in selecting Appropriate Model:

- **LOWTRAN7**
- **MODTRAN**
- **SENTRAN**
- **FASCODE**

Helps in model parameter selection/setup.

COUPLING ATMOSPHERE AND BACKGROUND EFFECTS*

W.M. Cornette
Photon Research Associates, Inc., 9393 Towne Centre Drive, Suite 200,
San Diego, CA 92121

The available atmospheric transmission models typically represent the atmosphere in significant detail, but have traditionally modelled the background very simplistically, if at all. The impact that the atmosphere has on the background (e.g., convection, evaporation, condensation, evapotranspiration, radiative loading, cloud shadowing) has recently been modelled in some detail in a computer code developed for the U.S. Army Atmospheric Sciences Laboratory (ASL). This presentation will outline the model and will discuss some of the additional atmosphere-to-background and background-to-atmosphere coupling required (e.g., surface air heating by the background).

*This work was funded by the U.S. Army Atmospheric Sciences Laboratory under Contract No. DAAD07-90-C-0149; Dr. Patti Gillespie, Technical Monitor

COUPLING ATMOSPHERE AND BACKGROUND EFFECTS

JUNE 1991

Presented at the 14th Annual Review Conference on Atmospheric Transmission Models
11-12 June 1991, Geophysics Directorate, Phillips Laboratory, Hanscom AFB, MA

Work Funded in Part by the U.S. Army Atmospheric Sciences Laboratory
Under Contract No. DAAD07-90-C-0149; Dr. P. Gillespie, Technical Monitor

Presented By:

Dr. William M. Cornette

Photon Research Associates, Inc.
9393 Towne Centre Drive, Suite 200
San Diego, CA 92121

PRA
Photon Research Associates, Inc.

OBJECTIVE

Development of a Computer Model Which May be Used to Characterize the Amount of Thermal Clutter in a Scene Viewed by a Thermal Imager and How the Clutter Level Changes with Changing Atmospheric Conditions

ATMOSPHERIC EFFECTS ON BACKGROUND

- Temperature
  - Convection
  - Evaporation/Condensation/Evapotranspiration
- Radiative Loading
  - Direct Solar Loading
  - Scattered Solar Loading
  - Thermal Loading
  - Scattered Thermal Loading
- Background Type
  - Polar Regions
  - Mid-Latitudes
  - Deserts
  - Tropics

ENERGY FLUX

- Radiation
  - Emitted
  - Absorbed Solar
  - Absorbed Thermal
- Sensible (Direct)
  - Free Convection
  - Forced Convection
- Latent (Indirect)
  - Evaporation
  - Condensation
  - Evapotranspiration
- Ground/Submedium
  - Conduction
  - Convection (Water)

PRA
Photon Research Associates, Inc.

TERRAIN MATERIALS

- Water
- Snow
- Ice
- Broadleaf Trees*
- Pine Trees
- Irrigated Low Vegetation
- Meadow Grass
- Tundra*
- Scrub
- Sand
- Rock
- Packed Dirt
- Tilled Soil
- Urban Commercial
- Urban Residential
- Asphalt
- Concrete
- Metal Building Roof

* Summer and Winter Variations

PRA
Photon Research Associates, Inc.

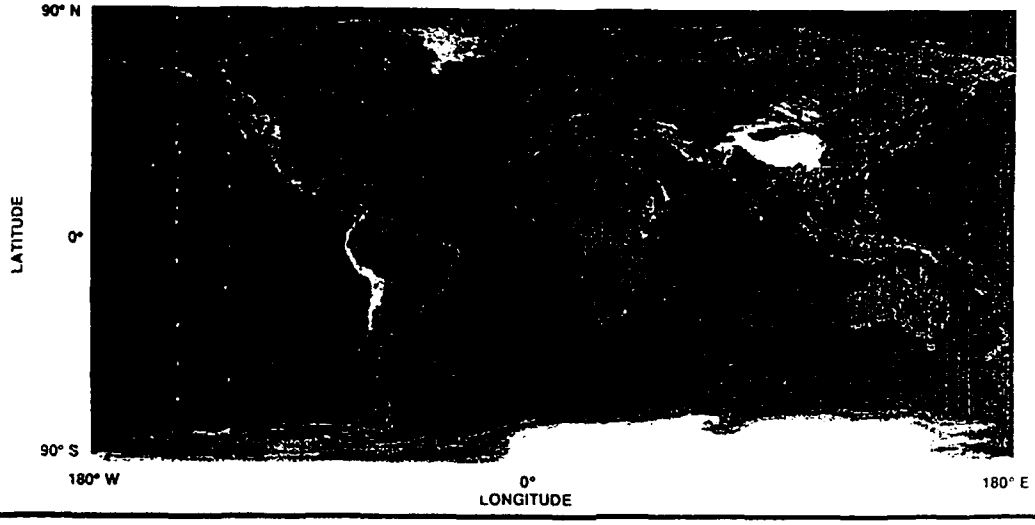
PARAMETERS

- Atmosphere
  - Pressure Profile
  - Temperature Profile
  - H_2O, CO_2, O_3 Profiles
  - Wind Speed
  - Cloud Cover and Altitude
- Background
  - Solar Absorptivity } From Reflectivity
  - Thermal Emissivity }
  - Thermal Conductivity
  - Submedium Temperature
  - Roughness
  - Density
  - Specific Heat
- General
  - Latitude
  - Time
  - Date

PRA
Photon Research Associates, Inc.

TERRAIN ALTITUDE MAP

- National Geophysical Data Center (NGDC) Global 10-Minute Terrain Data Base
- Resample with 1° Latitude and Variable Longitude Resolution



PRA
Photon Research Associates, Inc.

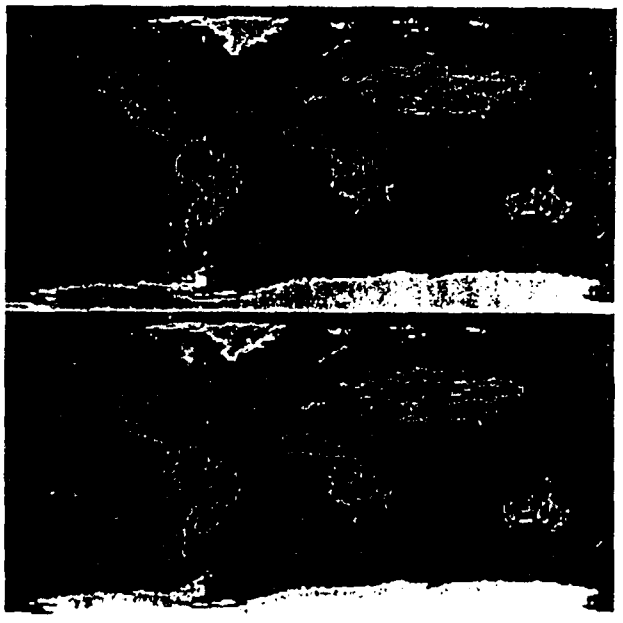
GLOBAL TERRAIN SCENES (DETERMINISTIC)

• City/Harbor Land/Sea Interface	San Diego, CA
• Arctic Tundra Land/Sea Interface	Point Barrow, AK
• Forested Low Relief Terrain	Wa Wa, Ontario, Canada
• Subarctic Rocky Land/Sea Interface	Trondheim, Norway
• Forested Terrain/Agricultural Terrain	Fulda, Germany
• Flat Agricultural	Alberta, Canada
• Desert Pavement with Dunes	Imperial Valley, CA
• Desert Land/Sea Interface	Salton Sea, CA
• Forested Mountains/Cultural	Santa Cruz, CA
• Multi-Year Sea Ice	Beaufort Sea
• Arctic Mountains with Scrub	Brooks Range, AK
• Arctic Tundra with Melt Lakes	-
• Open Ocean	-
• Mixed Farmlands/Orchards	Camarillo, CA
• Southern California Land/Sea Interface	Southern California

GLOBAL TERRAIN SCENES (MODIFIED)

- Tundra
- Pine Forest
- Mixed Forest/Farmland
- Grass Land - Savannah
- Scrub - Chaparral
- Scrub - Desert
- Urban
- Rural Land/Sea Interface
- Tropical Forest
- Tropical Savannah
- Tropical Desert
- Tropical Land/Sea Interface

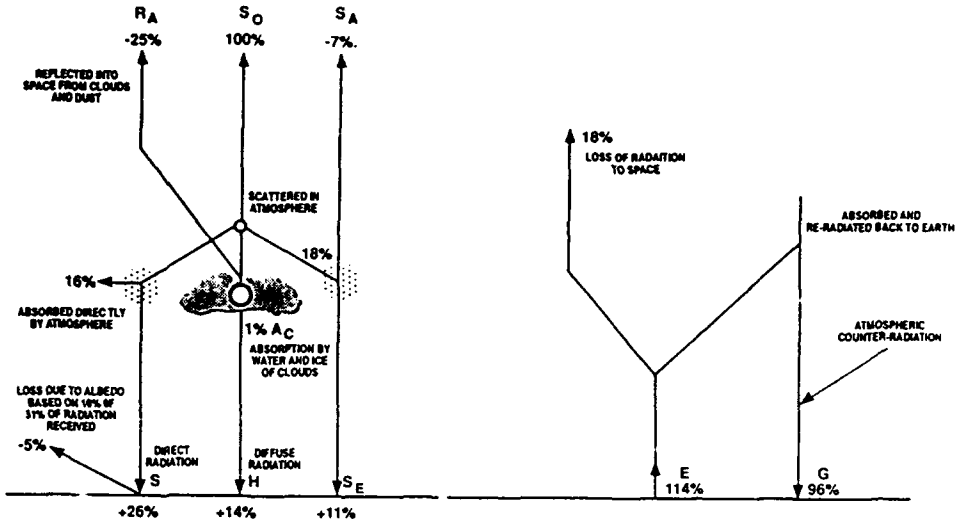
SCENE TYPE MAP



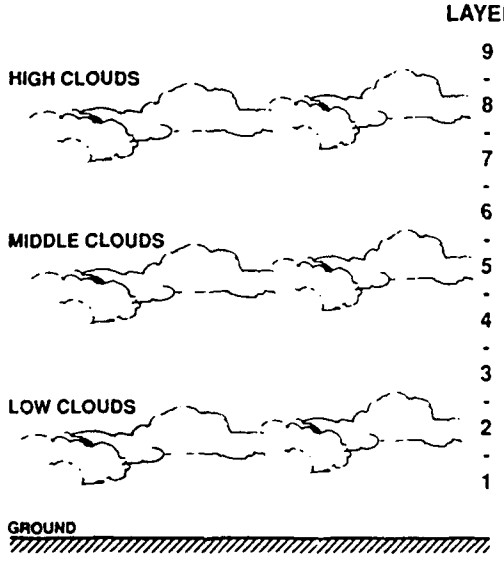
Blue	-	Ocean
Light Blue	-	Sea Ice
White	-	Continental Ice
Green	-	Tropical Forest
Tan	-	Grassland
Brown	-	Scrub Desert
Grey	-	Mixed Forest/Farmland
Red	-	Forested Mountains
Pink	-	Arctic Mountains
Purple	-	Tropical Savannah
Black	-	Other

HEAT BALANCE OF THE EARTH

- Solar Radiation
- Terrestrial Radiation



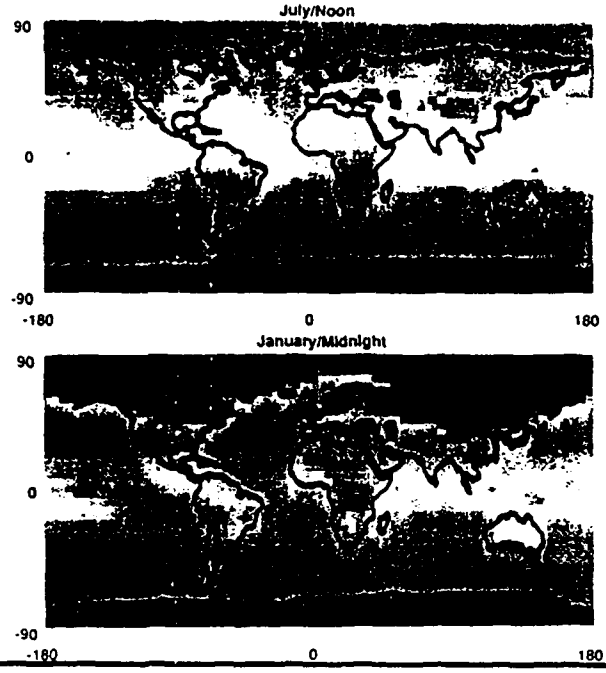
HEAT TRANSFER



- Short Wave (α_s)
  ($0.25 - 4.0\ \mu m$)
  - Direct Beam
  - Upward Diffuse
  - Downward Diffuse
- Long Wave (ϵ_{th})
  ($4.0\ \mu m - 25\ \mu m$)
  - Upward Diffuse
  - Downward Diffuse
- Multiple Scattered

PRA
Photon Research Associates, Inc

SURFACE TEMPERATURE MAPS



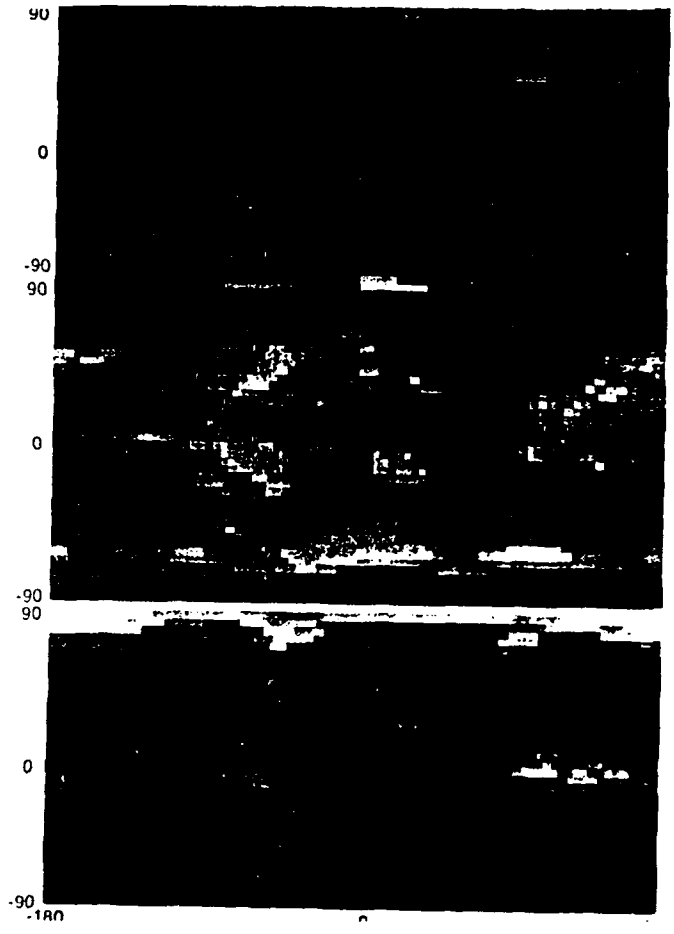
- NOAA Nimbus-7 C-Matrix Data Base
- Air Force Surface Temperature Analysis Base

PRA
Photon Research Associates, Inc

CLOUD COVER MAPS

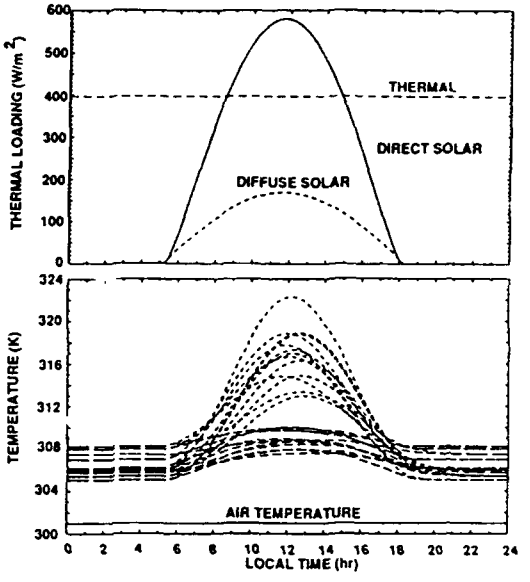
(NOAA NIMBUS-7 C-MATRIX DATA BASE)

JANUARY/MIDNIGHT



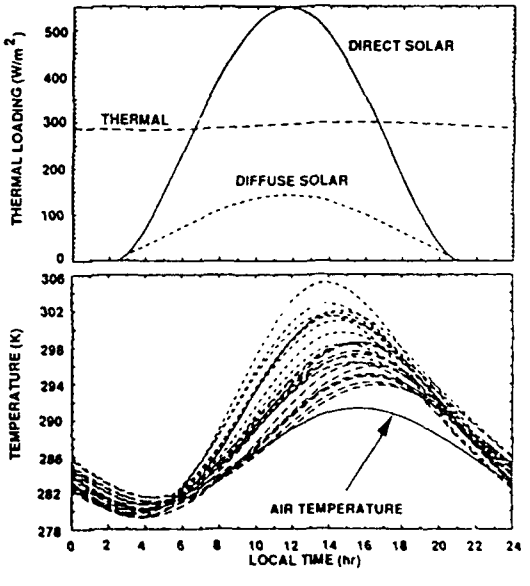
TROPICAL ATMOSPHERE

- Thermal Loading by Atmosphere Dominates at Night
- Heavy Cloud Cover Prevents Cooling at Night
- No Day-Night Air Temperature Variations



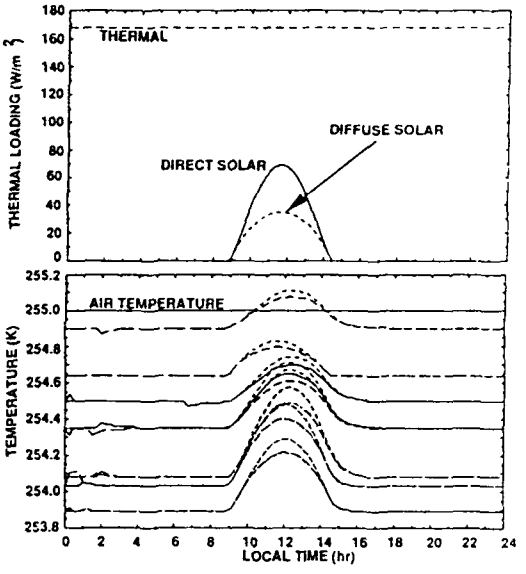
SUBARCTIC SUMMER ATMOSPHERE

- Driven by Local Air Temperature
- Cooling Observed at Night Below Local Air Temperature
- Large Day-Night Air Temperature Variations



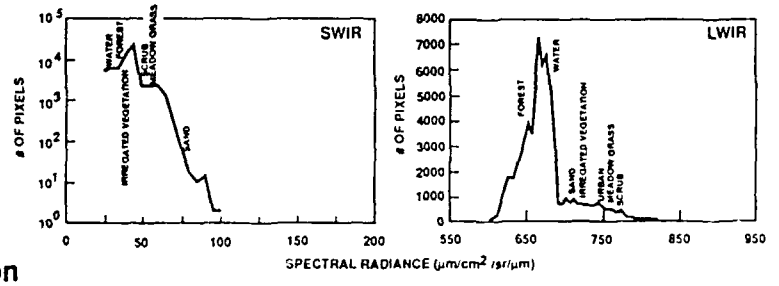
SUBARCTIC WINTER ATMOSPHERE

- Small Thermal and Solar Effects
- No Day-Night Air Temperature Variations
- Numerical "Noise" of Algorithm Seen in Temperature Curves

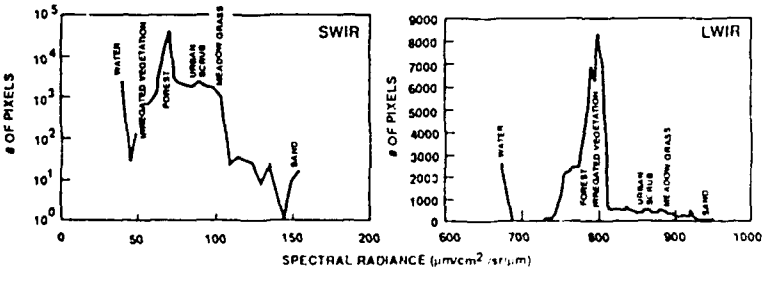


SANTA CRUZ, CALIFORNIA, SCENE

- Dawn Plus One Hour



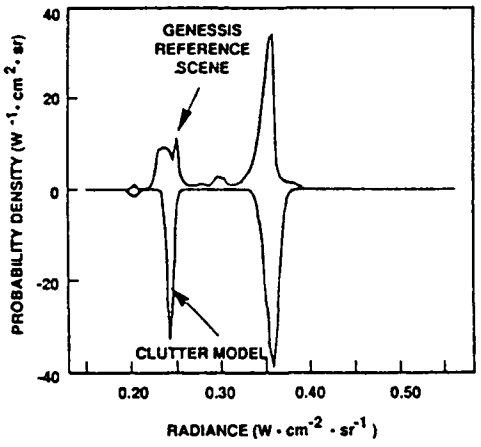
- Noon



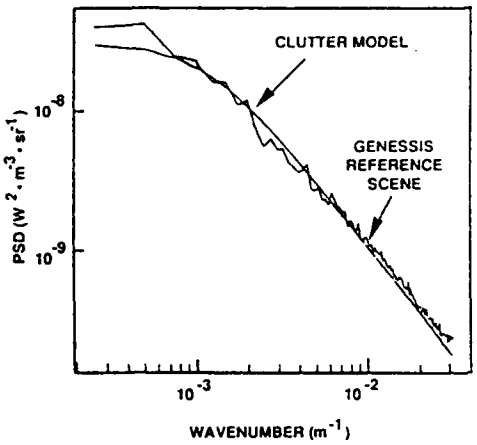
FULDA, GERMANY, SCENE

- Noon
- 3.7 - 4.1 μm

Probability Density Function



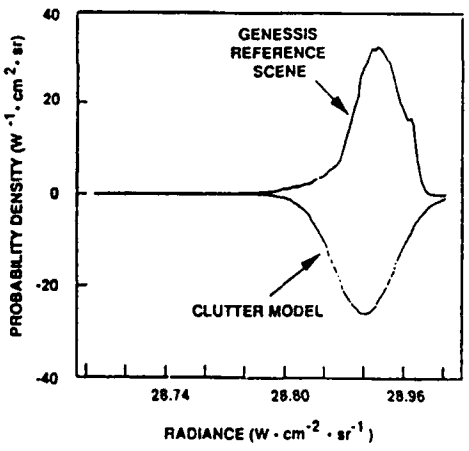
Power Spectral Density



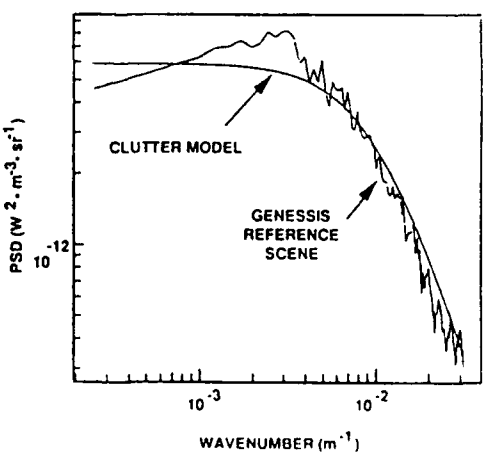
OPEN OCEAN SCENE

- 8 - 12 μm

Probability Distribution Function



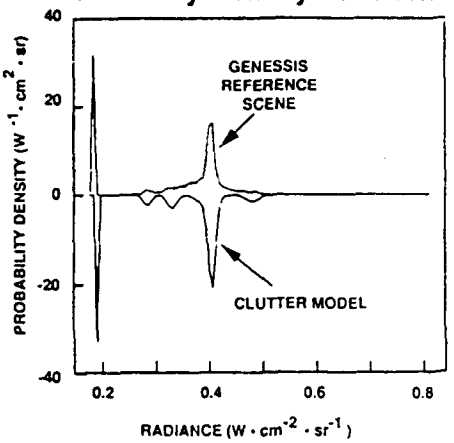
Power Spectral Density



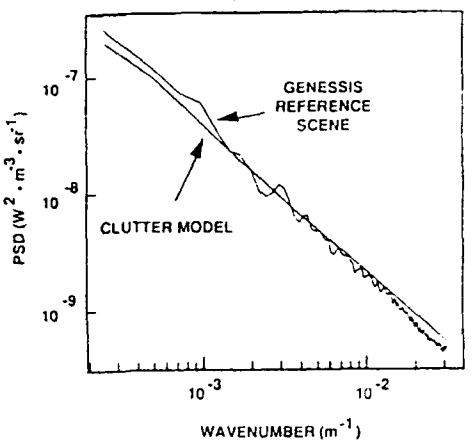
SAN DIEGO, CALIFORNIA, SCENE

- Noon
- 3.7 - 4.1 μm

Probability Density Function



Power Spectral Density

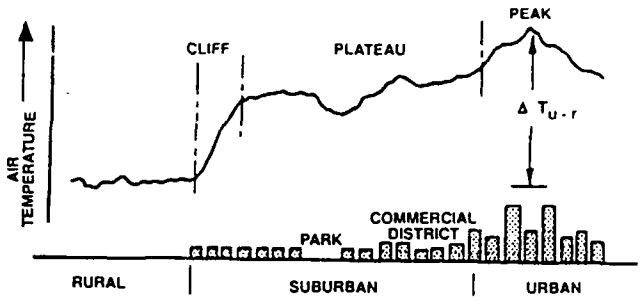


SKY NOISE

- Thermal Sky Noise
  - Due to Temperature Fluctuations
  - Derived from C_n^2 Profiles
  - Based on Work of Kent and Korf at AMOS
- Scatter Sky Noise (Pending)
  - Variations in Aerosol Number Density
  - Variations in Aerosol Particles
  - Variations in Molecular Density
  - Variations in Index of Refraction

BACKGROUND EFFECTS ON ATMOSPHERE

- Altitude/Profile
- Atmospheric Heating
- Free Convection
- Wind Speed and Direction
- Relative Humidity
- Pollutants
- Aerosols
- Turbulence
- Cloud Cover/Type/Altitude



CURRENT STATUS

- CLUTTR Code Developed
  - Calculates PDF's and PSD's
  - Includes Atmospheric Thermal Sky Noise
  - Includes Sensor Effects, Including Human Factors
- Future Development
  - Add Atmospheric Scatter Sky Noise
  - Improve Interfaces
  - Validate Algorithms and Data Bases
  - Extend Data Bases

SENTRAN7: A SENSITIVITY ANALYSIS PACKAGE FOR LOWTRAN 7 AND MODTRAN

D.R. Longtin, F.M. Pagliughi, N.L. Paul
SPARTA, Inc., 24 Hartwell Avenue, Lexington, MA 02173

The computer code SENTRAN, originally developed by researchers at The Pennsylvania State University, permits users to rapidly evaluate transmittances and radiances from LOWTRAN in response to perturbations of input atmospheric conditions. The code provides a friendly and efficient interface to create multiple LOWTRAN input decks as well as graphical representation of the output in both 2D and 3D formats.

In the current effort, SENTRAN has been upgraded for use with LOWTRAN 7 and MODTRAN. The new computer code is called SENTRAN7. As part of the upgrade, SENTRAN7 contains improved error checking on user inputs, an enhanced online help capability and smarter editing restrictions that reflect inputs from other LOWTRAN 7 or MODTRAN input cards. Additionally, users are able to graphically display results from the standard TAPE7 and TAPE8 files. New features of SENTRAN7 include the capability to run LOWTRAN 7 or MODTRAN internally, and screen display of available input files. Finally, the framework for a sensitivity package for FASCODE will be discussed.

SENTRAN7: A SENSITIVITY ANALYSIS PACKAGE FOR LOWTRAN7/MODTRAN

Presented at

The Annual Review Conference on Atmospheric Transmission Models

June 12, 1991

David R. Longtin, Nanette L. Paul and Frank M. Pagliughi

SPARTA, Inc.
24 Hartwell Avenue
Lexington, MA 02173

Contract F19628-88-C-0038



Acknowledgements

- We Wish to Thank the Following Individuals
  - Gail Anderson and Jim Chetwynd of The Geophysics Directorate
  - Charles Randall of The Aerospace Corporation
  - Charles Lo Presti of The Battelle Pacific Northwest Laboratory
  - Ken Tomiyama and Michael Hogan of The Pennsylvania State University



Outline of Talk

- Introduction to SENTRAN7
  - Software and Hardware Requirements
- Capabilities of SENTRAN7
  - Examples of Menus
  - New Features
- Ongoing Efforts
  - Sensitivity Package for FASCODE, SENCODE



What Is SENTRAN7?

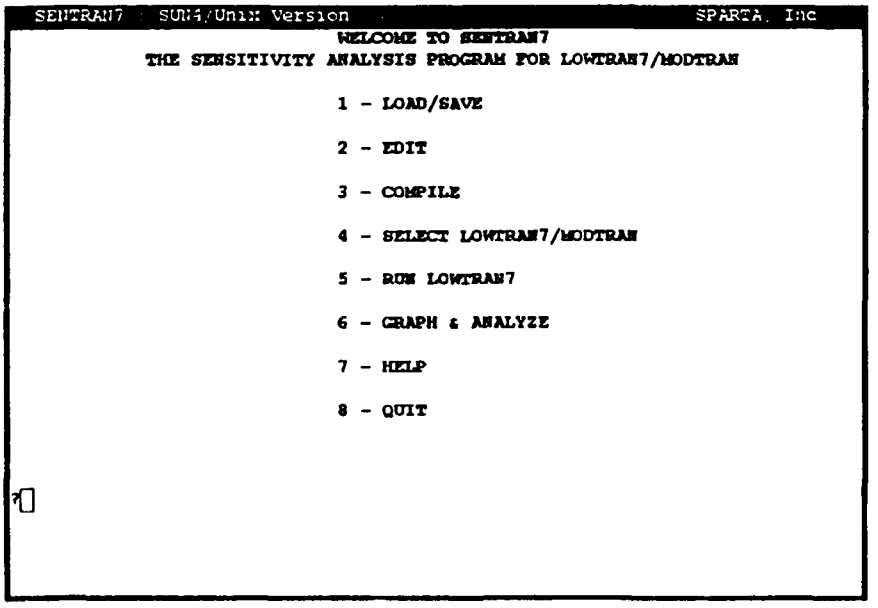
- User Interface System Designed to Evaluate the Sensitivity of LOWTRAN7/MODTRAN* Transmittances and Radiances to Input Variations
  - Interactive Input Module to Perturb LOWTRAN7/MODTRAN Input Parameters
  - Automatic Generation of LOWTRAN7/MODTRAN Input Decks
  - Autonomous Post-Processing of TAPE7 and TAPE8 Outputs
  - Graphical Representation of Output in 2D and 3D Formats
- Based on Original SENTRAN for LOWTRAN6 By K. Tomiyama and M. Hogan

* MODTRAN: *Moderate Resolution Model for* LOWTRAN7 Developed By Spectral Sciences, Burlington, MA

Software and Hardware Details For SENTRAN7

- Structural Design
  - SENTRAN7 Coded in Fortran-77
  - Graphics Consistent with Tektronix 4014 Standards
  - Terminal Control Follows ANSI Standards
- Hardware Requirements
  - Software Developed for VAX/VMS and SUN Unix Computer Systems
  - Interactive Viewing of SENTRAN7 Graphics Use VT240 Terminal or Emulator
  - Hard Copy Output Requires Tektronix 4014 Compatible Printer/Plotter **or** Device Able to Interpret Tektronix 4014 Files via Special Translating Programs
- SENTRAN7 Utilizes Standard Input and Output Formats from LOWTRAN7/MODTRAN Codes

Main Menu of SENTRAN7





Description of Main Modules

- LOAD/SAVE: Load or Save SENTRAN7 Methodology Files
  - Methodology Files Contain Images of LOWTRAN7 Input Cards and Directives for Their Perturbation
- EDIT: Interactive Editing Module for Specifying LOWTRAN7 Cards and Directives for Their Perturbation
  - Editor Emulates Logical Flow Through LOWTRAN7 Input Decks
  - Each LOWTRAN7 Input Described by a Nominal Value and an Optional Perturbation Directive
- COMPILE: Creates LOWTRAN7 Input Decks Based on Information in the EDIT Module
  - Provides List of Active Molecular Absorbers in the Spectral Interval of Interest



Description of Main Modules (cont.)

- SELECT LOWTRAN7/MODTRAN: Determines Code To Be Run
- RUN LOWTRAN7/MODTRAN: Executes Selected Code
- GRAPH AND ANALYZE: Generates Graphical Plots of Data
  - Screen or Files For Hard Copy Available
  - Additional Features Include Data Manipulation and Analysis
- HELP: Provides Information About and Examples For Most SENTRAN7 Commands
- QUIT: Exit SENTRAN7 Code

Edit Module: Editing Card 3

```
SENTRAN7 : SUN4/Unix Version                              SPARTA, Inc.
                        SENTRAN7 EDITING UTILITY

                              EDITING CARD 3

FOLLOWING PARAMS. USE A PERTURBATION VALUE

H1 ...        0.000   TO 20 STEP 2
H2 ...        0.000
ANGLE         0.000
RANGE         1.000   TO 10
BETA          0.000
RO ...        0.000

FOLLOWING PARAM. USES A PERTURBATION LIST (* IMPLIES PERTURBATION RESTRICTIONS)

LEN   *     0



ALL PARAMETERS FOR CARD 3 O.K. (Y/N) [Y]
```

Graph and Analyze Module

- Main Capabilities
  - Handles TAPE7 and TAPE8 Files from LOWTRAN7 Plus Raw X-Y-Z Data Files
  - Includes Tools for Data Analysis and Archiving
  - Generates Screen Plots of Data and Graphics Files for Hard-Copy Output
- 3-D Plotting Details
  - Permits User-Defined Rotation Angles
  - X and Y Axes Can Represent Wavenumber, or the First or Second LOWTRAN7 Variables Perturbed
  - Conversion to Micrometers Are Available
  - Plots For Layer-By-Layer Calculations from TAPE8 Always Make X-Axis the Wavenumber and and Y-Axis the Layer Number

Available Plots in SENTRAN7

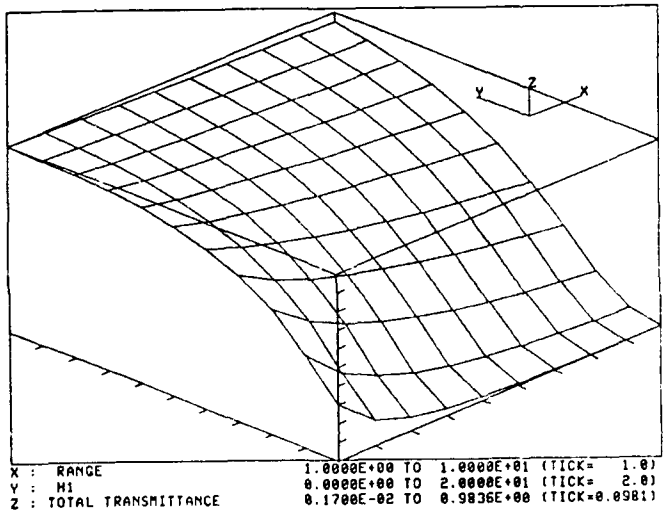
SPARTA INC.

PLOT CATEGORY[1]	SPECIFIC PLOTS
Raw-XYZ	
Transmittance	Transmittance: total, log of total, uniform mixed gases, trace gases, molecular scattering, H_2O, H_2O continuum, O_3, N_2 continuum, aerosol and hydrometeor, CO_2, CO, CH_4, N_2O, O_2, NH_3, NO, NO_2, SO_2, HNO_3 Aerosol and Hydrometeor Absorption
Thermal Radiance	Transmittance: total, log of total Atmospheric Radiance
Differential Transmittance and Black Body Function	*Differential Transmittance (DTAU), DTAU/layer thickness* DTAU*BB function, DTAU*BB function/layer thickness
Fluxes/Irradiance	Fluxes: upward total, upward solar, downward total, downward solar Direct Solar Irradiance
Solar/Lunar Radiance	Transmittance: total, log of total Radiance: total, atmospheric, path scattered, single scattered, total ground reflected, direct reflected
Direct Solar Radiance	Transmittance: total, log of total, solar irradiance Incident Solar Irradiance

[1] Plot Category Determined By Values of IEMSCT, IMULT, NOPRT

Example 3-D Plot From SENTRAN7

SPARTA INC.



Total Transmittance at 1300 cm^{-1} Versus H1 and RANGE for a Horizontal Path



Other Features of SENTRAN7

- Original SENTRAN Code Upgraded for Use with LOWTRAN7
  - Smarter Editing Restrictions That Reflect Previous User Inputs
  - Improved Error Checking on User Inputs
  - Refined Identification of Major Molecular Absorbers
- New Features in SENTRAN7
  - Compatibility with the Moderate Resolution Code, MODTRAN
  - Ability to Access LOWTRAN7/MODTRAN Codes Internally
  - Screen Display of Available Methodology and Other Input Files
  - Safeguards to Prevent Existing Files From Being Overwitten
  - Increased Portability Across Hardware Platforms
  - Online Help Available Within Editing Module
  - Tick Marks on Plots
  - Graphical Display of User-Defined Trace Gas Profiles, Card 2C Series



Ongoing Work: Sensitivity Package For FASCODE, SENCODE

- General Approach
  - Develop Parallel Package For FASCODE, But Retain SENTRAN7 Framework
  - Use Many of SENTRAN7's Supporting Routines
  - Limit Those FASCODE Input Cards That Can Be Perturbed
- Future Obstacles
  - Method of Effectively Dealing With FASCODE Output Files
  - Output May Exceed SENTRAN7's Plotting Capabilities
  - Some Sensitivity Studies May Grossly Interfere with FASCODE's Atmospheric Layering Package

ATMOSPHERIC MODELS IN THE STRATEGIC SCENE GENERATION MODEL*

W.M. Cornette, D.C. Anding
Photon Research Associates, Inc., 9393 Towne Centre Drive, Suite 200,
San Diego, CA 92121

The Strategic Scene Generation Model (SSGM) produces scenes of interest to a strategic space-based sensor, including terrain, clouds, earth limb, aurora, zodiacal light, and stars as background; and missile plumes and fuselages, post-boost and reentry vehicles as targets. In support of the various components of the SSGM are several atmospheric codes, which provide basic information regarding transmission and emitted and scattered path radiance, plus additional information required by the various background and target models. An overview of the SSGM will be presented, with emphasis on how the various atmospheric models are utilized. Comparisons between the codes will be presented, together with recommendations for upgrades to insure consistency.

*This work is being funded by the Naval Research Laboratory under Contract No. N00014-89-C-2283; H. Heckathorn, Technical Monitor.

ATMOSPHERIC MODELS IN THE STRATEGIC SCENE GENERATION MODEL

JUNE 1991

Presented at the 14th Annual Review Conference on Atmospheric Transmission Models
11-12 June 1991, Geophysics Directorate, Phillips Laboratory, Hanscom AFB, MA

Work Funded in Part by Naval Research Laboratory Under Contract No. N00014-89-C-2283
H. Heckathorn, Technical Monitor

Presented By:

Dr. William M. Cornette
David C. Anding

Photon Research Associates, Inc.
9393 Towne Centre Drive, Suite 200
San Diego, CA 92121

PRA Photon Research Associates, Inc.

STRATEGIC SCENE GENERATION MODEL (SSGM)

NAVAL RESEARCH LABORATORY

TASC

MRC

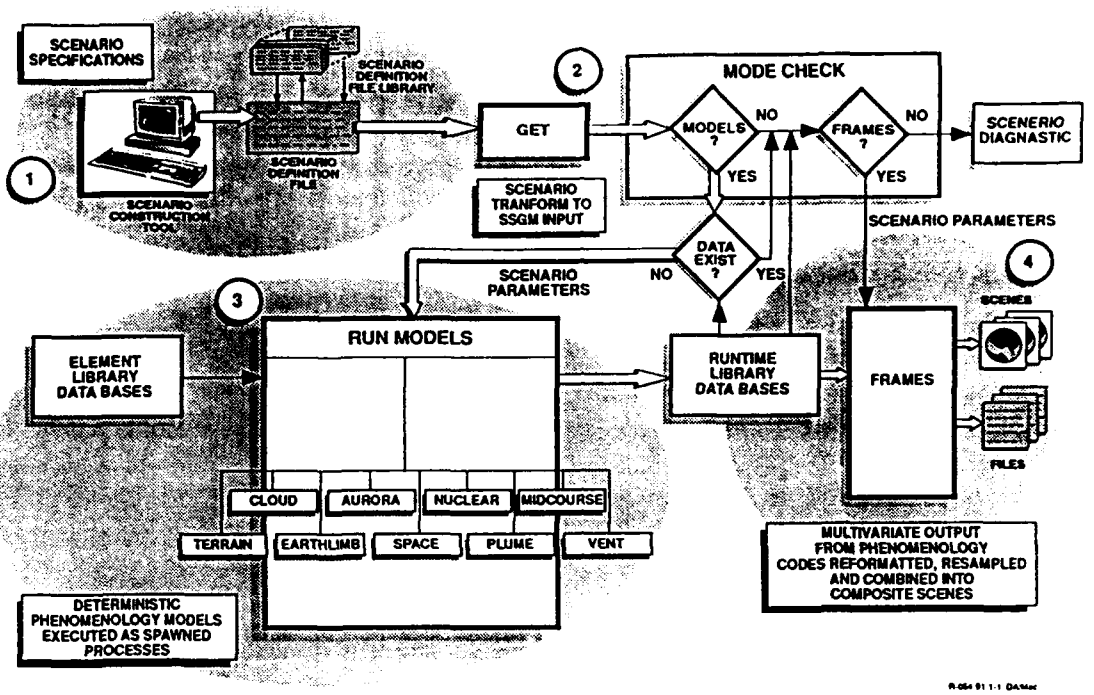
- **Definition**
  - Computerized Methodology Founded on State-of-Science Knowledge, Empirical Data Bases, Phenomenological Models to Generate LOS Radiometrics, 2-D Radiance Maps, Time-Sequenced Scenes, and Observables Data Bases for SDI Applications

- **Objectives:**
  - Provide Focus for SDIO Scene Generation Requirements
  - Serve as a Standard for Testing SDI Concepts and Designs Which is Traceable to a Consistent Set of Physical Assumptions, Conditions

- **Requirements:**
  - Phenomenology = Targets, Target Related Events, Natural and Nuclear Backgrounds
  - Scenarios = All Vehicle Types (Launch, Midcourse, Re-Entry)
  - Dimensions = Spatial, Temporal, Spectral Sampling Regimes
  - Geometry = All Sensor/Scene/Target Locations and Time-History Sequences
  - Connectivity = Event-Driven, Both Passive and Active (Illuminated) Signatures

PRA
Photon Research Associates, Inc.

SSGM FUNCTIONAL FLOW DIAGRAM DESIGN

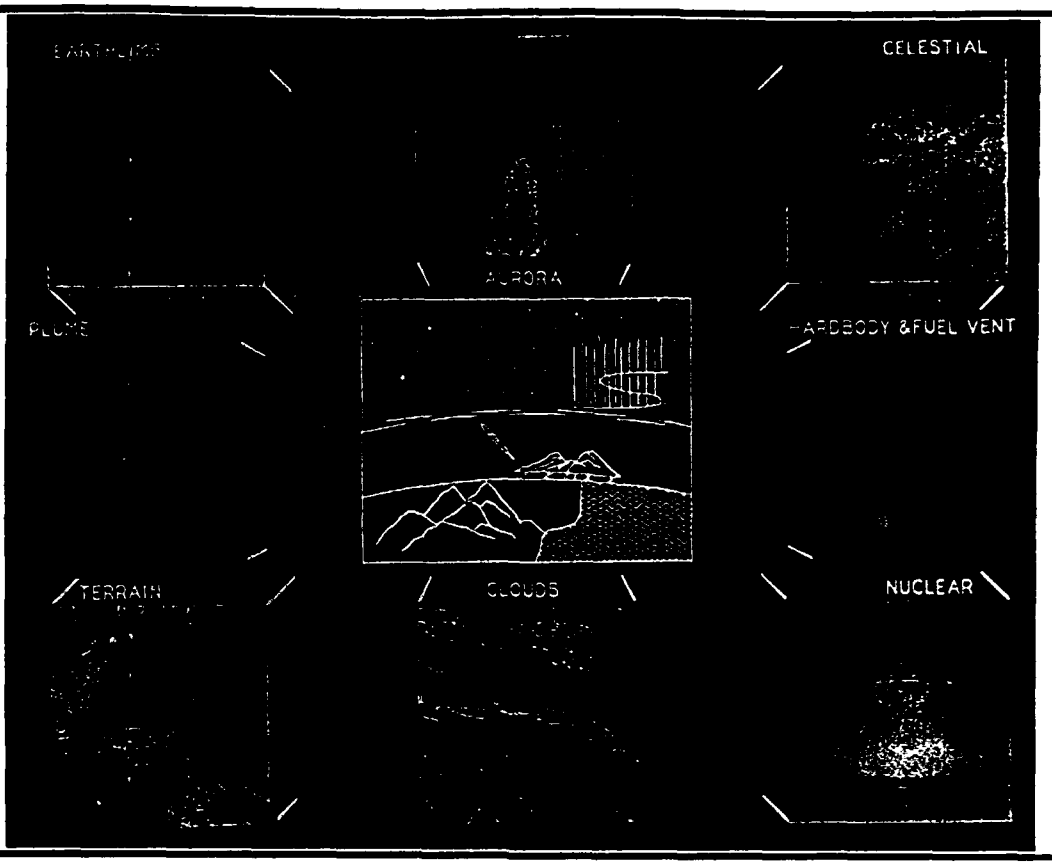


PRA
Photon Research Associates, Inc.

SSGM ATMOSPHERIC MODELS

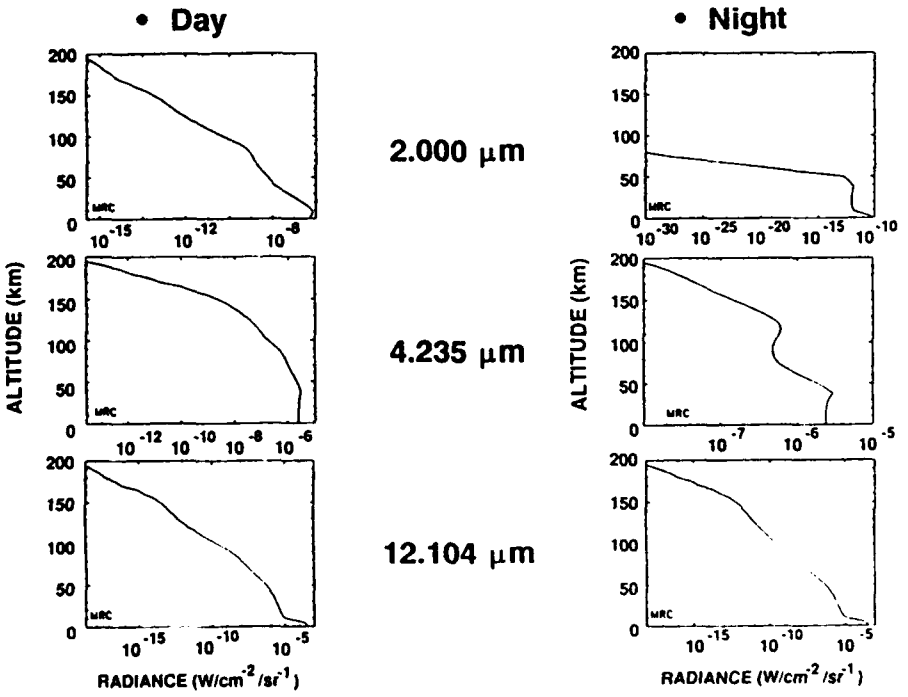
- Earthlimb
  - MODTRAN (<60 km)
  - SHARC (>60 km)
- Backgrounds
  - APART (Terrain)
  - APART (Clouds)
- Targets
  - APART (TARSIS)
  - SIRRM (Plumes)
  - Simple Extinctions (Plumes)

SSGM PHENOMENOLOGY



Photon Research Associates, Inc.

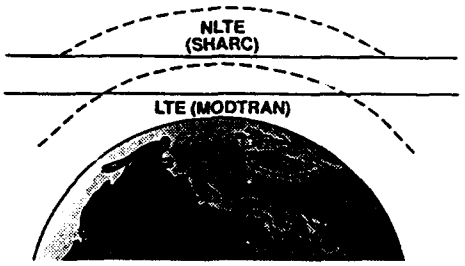
SSGM EARTH LIMB PROFILES

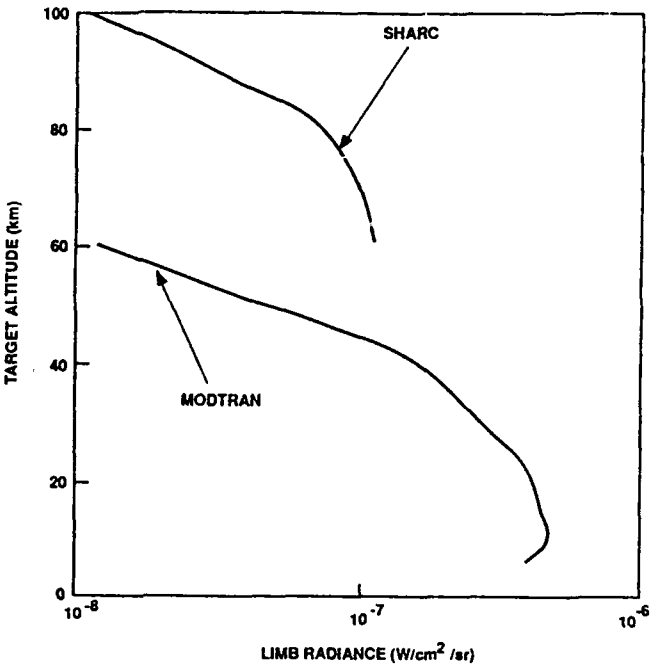


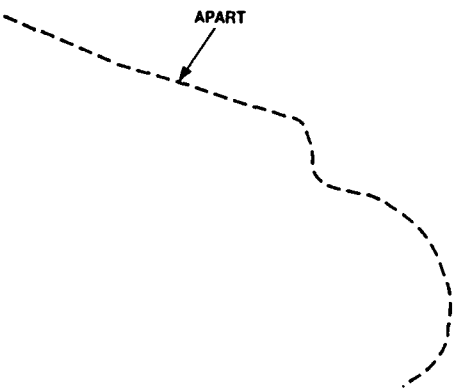
PRA
Photon Research Associates, Inc.

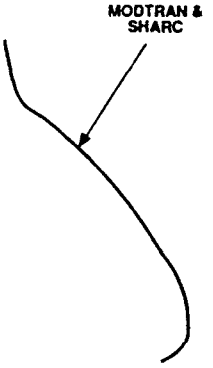
EARTH LIMB MODELING

- U.S. Standard Day
- 2.5 - 2.9 μm









PRA
Photon Research Associates, Inc.

BACKGROUND SCENE MODELS

- GENESSIS (Generic Scene Simulation Software) and CLDSIM (Cloud Simulation) are Collections of Computer Codes Which Generate 2-D Images of Terrestrial and Cloud Scenes

- GENESSIS Uses First-Principles Algorithms Which Include Those for:
  - Surface Temperature Heat Transfer
  - Solar-Viewer Shadowing and Scene Projection
  - Thermal Emission, Solar-Skyshine Reflection
  - Atmospheric Absorption, Scattering, Emission

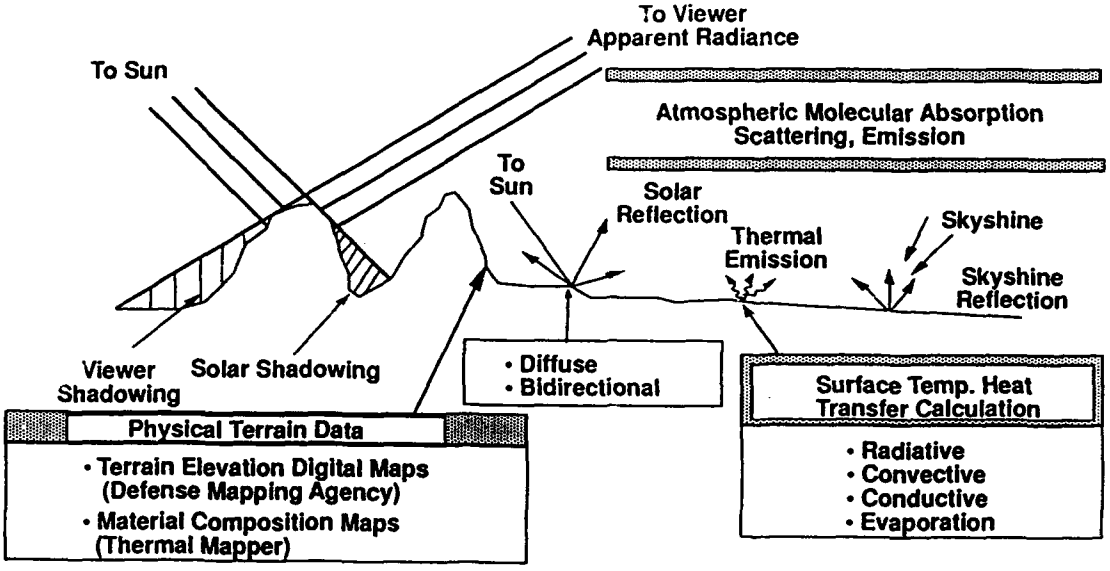
  Using an Input Scene Data Base Consisting of:
  - Digital Elevation Map
  - Earth Surface Material Assignment

- CLDSIM Uses the Following Assumptions and Treatments:
  - Cloud Tops are Treated as Surfaces, Emitting and Reflecting According to a Bidirectional Reflectance Function (BRDF). BRDF Varies with Cloud Optical Properties, Altitude, and Wavelength.
  - Clouds Can be Optically Thin and Transmit Radiation from Below
  - Cloud Top Temperatures Set Equal to Ambient
  - Skyshine Reflection Neglects Radiation from Neighboring Clouds

  Using an Input Scene Data Base Consisting of:
  - Digital Cloud Top Altitude Map
  - Cloud Types

PRA
Photon Research Associates, Inc.

GENESSIS TERRAIN SCENE MODEL



R-006-90.8 DA/Mac

PRA
Photon Research Associates, Inc.

GENESSIS SIMULATION OF SOUTHERN CALIFORNIA COASTLINE (NADIR VIEW)

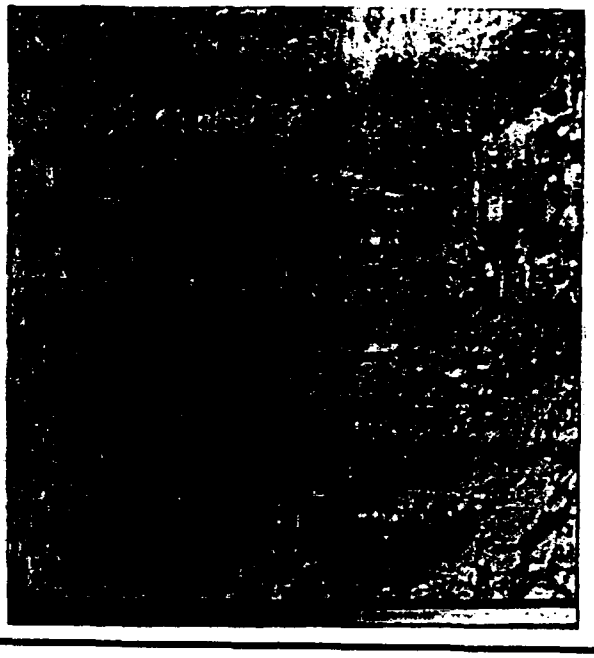
1024 x 1024 Pixels, 400 Meter Resolution, 10 - 12 μm



PRA
Photon Research Associates, Inc.

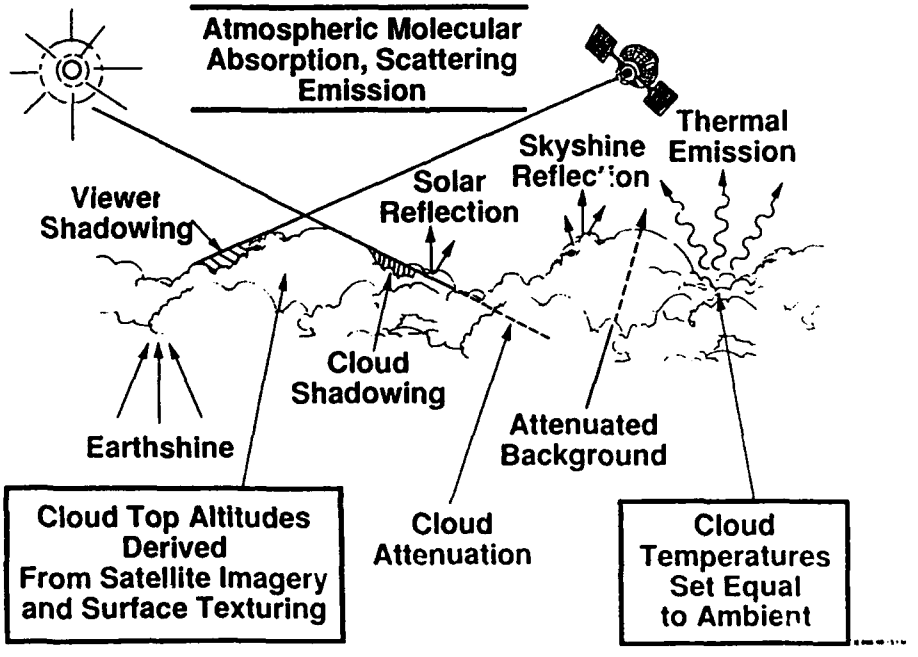
GENESSIS SIMULATION OF CAMARILLO, CALIFORNIA (NADIR VIEW)

512 x 512 Pixels, 30 Meter Resolution, 3.6 - 4.0 μm



PRA
Photon Research Associates, Inc.

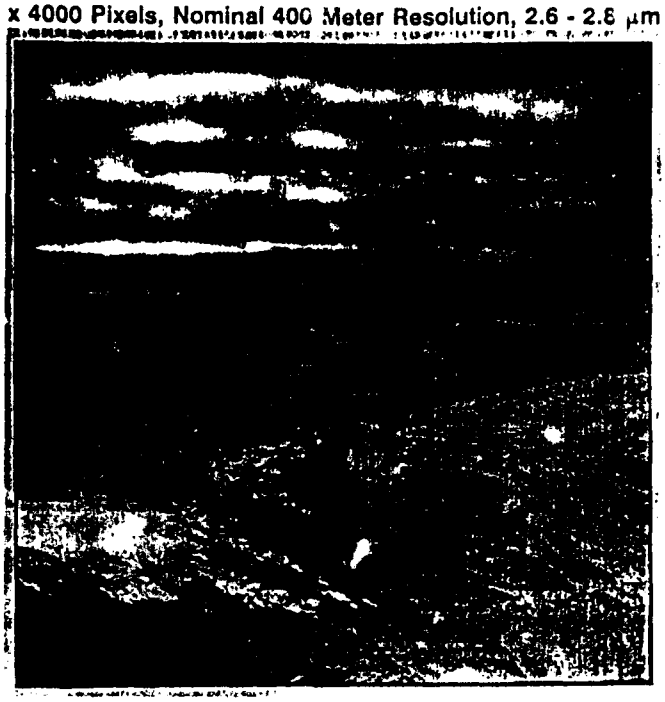
CLDSIM CLOUD SCENE MODEL



PRA
Photon Research Associates, Inc.

CLDSIM SIMULATION OF MULTIPLE CLOUD TYPE HORIZON SCENE

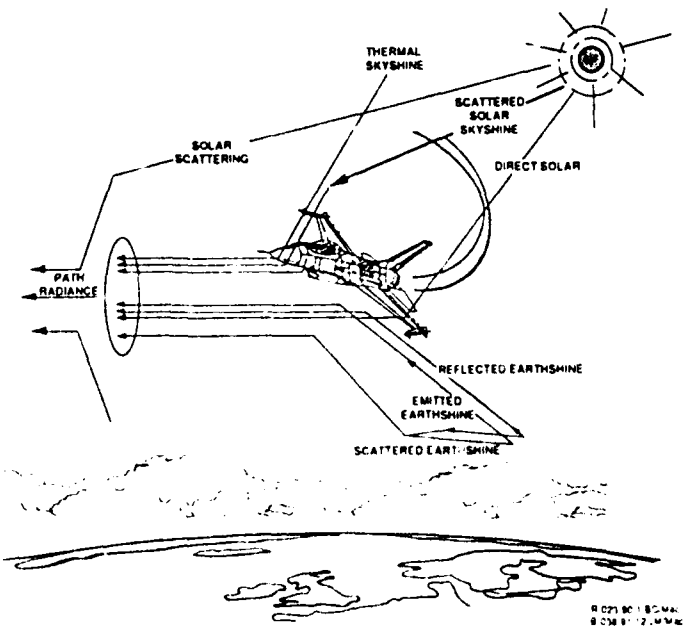
4000 x 4000 Pixels, Nominal 400 Meter Resolution, 2.6 - 2.8 μm



PRA
Photon Research Associates, Inc.

APART RADIATIVE ENVIRONMENT CODE

- Full LOWTRAN 7 Compatibility
- Observables-Driven Architecture
- Molecular Absorption
  - 5 cm^{-1} Resolution
  - 0.2-50 μm
  - Five Parameter Voight Model
- Five-Flux Multiple Scattering
- Turbulence/Sky Noise
- Forward In-Scatter
- Backgrounds
  - Contrast
  - Structured
  - Global Data Base
  - Bidirectional Materials
- Global Atmosphere Data Base
- Hydrometeors
  - Clouds (Water/Ice)
  - Fog
  - Rain
  - Snow



PRA
Photon Research Associates, Inc.

ATMOSPHERE MODELS

- Latitude Dependent
  - Equatorial (Summer/Winter)
  - Tropical (Summer/Winter/Annual)
  - Subtropical (Summer/Winter)
  - Midlatitude (Summer/Winter/Spring-Fall)
  - Subarctic (Summer/Winter/Special)
  - Arctic (Summer/Winter)
  - Polar (Summer/Winter)

- Special
  - U.S. Standard (1976)
  - Israeli Standard (Day/Night)
  - User-Defined

S-066-01.14

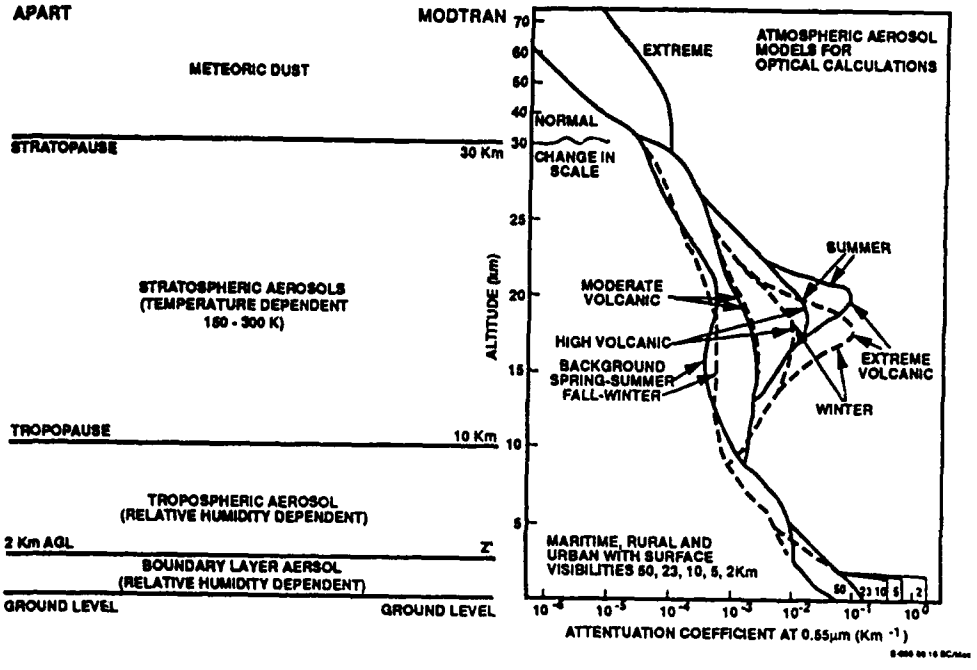
PRA
Photon Research Associates, Inc.

NORTHERN HEMISPHERE MODEL ATMOSPHERES

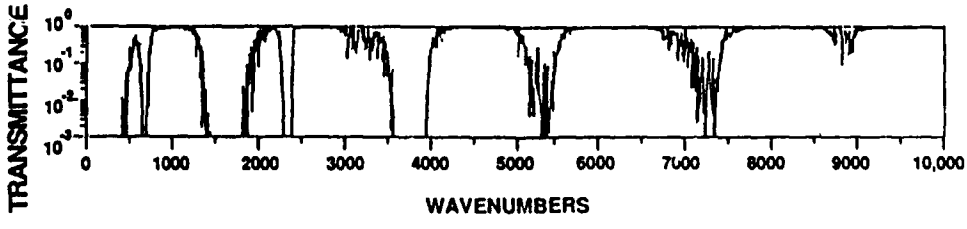
Type	Latitude	Seasons
Equatorial	0°	Summer Winter
Tropical	15°	Annual Summer Winter
Subtropical	30°	Summer Winter
Midlatitude	45°	Summer Winter Spring/Fall
Subarctic	60°	Summer Winter Winter (Cold) Winter (Warm)
Arctic	75°	Summer Winter Winter (Cold) Winter (Warm)
Polar	90°	Summer Winter
U.S. Standard	--	--
Israeli Standard	--	Day/Night

S-066-01.15

AEROSOL TYPES AND HAZE PROFILES



RADIATIVE TRANSFER

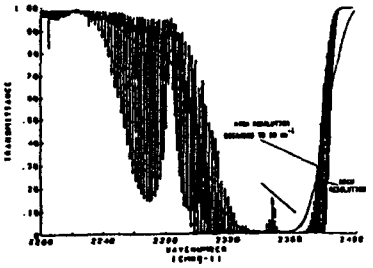


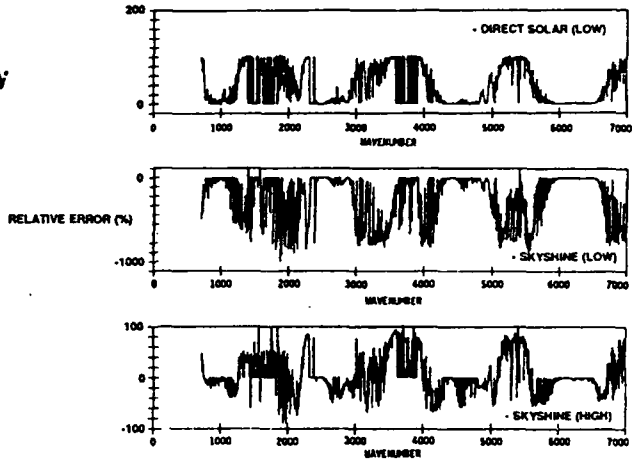
- Three Parameter Band Model
- Voight Line Shape
- Foreign-Broadened Line Wings
- Self-Broadened Line Wings
- Spectral Region 0.20 - 0.50 μm
- Band Parameters from 1986 AFGL Line Atlas
- User-Defined Resolution (5 - 200 cm^{-1})
- Molecular Oxygen Model Added in UV

PRA
Photon Research Associates, Inc.

BAND CORRELATION

- A Passive Observable Consists of
  - Thermal Emission
  - Solar Reflections
  - Skyshine Reflections
  - Earthshine Reflections
- Each Components Transmits Differently Due to Band Averaging

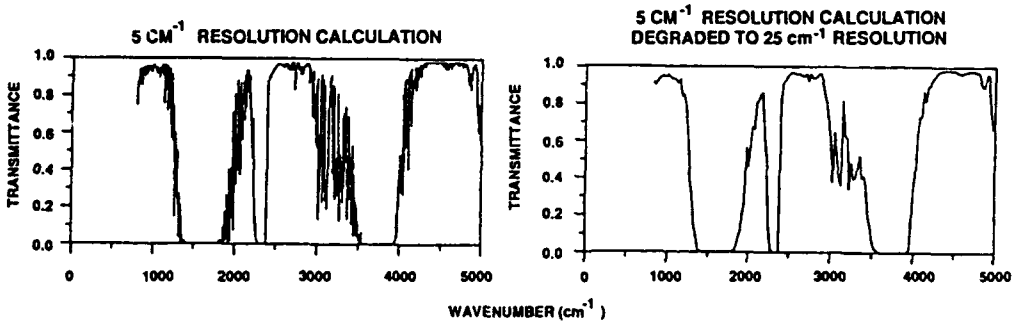


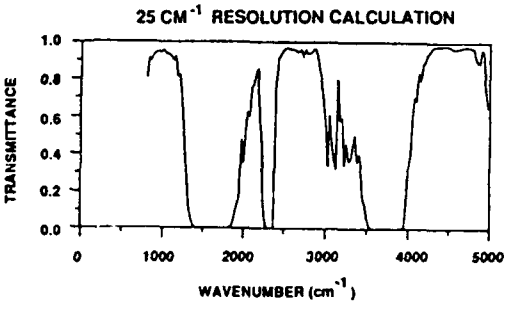


B-060-01.18

PRA
Photon Research Associates, Inc.

VARIABLE RESOLUTION





- Options
  - 5 cm^{-1} Resolution
  - Multiples of 5 cm^{-1} Resolution
  - "Constant" Wavelength Resolution

B-060-01.19

PRA
Photon Research Associates, Inc.

ATMOSPHERIC TURBULENCE EFFECTS

- Turbulence Induced Irregularities Cause Spatial and Temporal Variations of Atmospheric Index of Refraction
  - Spatial and Temporal Variations of Wavefront Amplitude → Scintillation
  - Spatial and Temporal Variations of Wavefront Phase → Image Blur
- Turbulence Induced Irregularities Also Cause Atmospheric Radiance Variations
  - Sky Noise
  - Increased Path Radiance
- These Effects Can be Estimated Using Weighted Integrals of C_n^2, the Index of Refraction Structure Parameter, Over the Propagation Path

PRA
Photon Research Associates, Inc.

APART/MODTRAN DIFFERENCES

- BAND PARAMETERS
  - Spectral Resolution
  - Spectral Range
  - Variable Resolution
  - Wavelength Resolution
- REFRACTIVITY
- RAY TRACING
- FULL SOLAR GEOMETRY
- SOLAR AND LUNAR EPHEMERIS
- MOLECULAR SCATTERING
- RELATIVE HUMIDITY (GOFF-GRATCH)
- MODIFIED PHASE FUNCTION
- ADDITIONAL MODEL ATMOSPHERES
- MULTIPLE SCATTER
  - Four-Stream
  - Exponential Sum Fit
  - Coupling
- EQUATION OF TRANSFER
- TEMPERATURE DEPENDENT BACKGROUND STRATOSPHERIC AEROSOL (150 - 300 K)
- HAZE PROFILE AND AEROSOL TYPE
  - Boundary Layer
  - Tropopause
  - Stratosphere
- HYDROMETEORS

PRA
Photon Research Associates, Inc.

ADDITIONAL APART CAPABILITIES

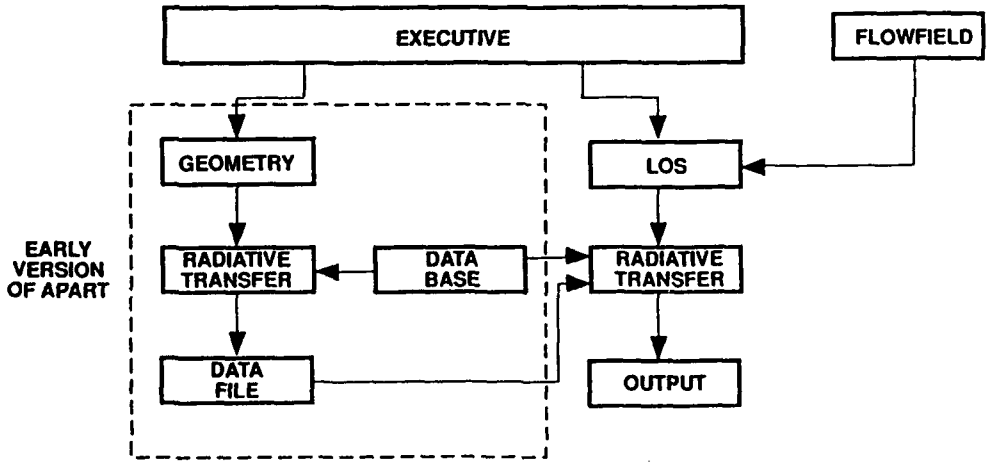
- TURBULENCE
  - Thermal Sky Noise
  - Scatter Sky Noise
  - Scintillation
- ATMOSPHERE
  - Diurnal Variations
  - Geographic Variations
- HEAT TRANSFER
  - Cloud Cover
  - Surface Temperature
  - Background Temperatures
- CORRECTION FOR LAYERING PROBLEM
- LINE CORRELATION
- INTEGRATION WITH OTHER CODES
  - Target
  - Plume
  - Terrain
  - Multiple Scatter
  - Heat Transfer
  - Cloud
- FORWARD SCATTER
- BACKGROUNDS
  - Space (Zodiacal, Stars, Galactic)
  - Global Scene Types
  - Materials
    - Diffuse
    - Directional
    - Bidirectional
  - Terrain Blockage
- USER-DEFINED
  - Atmosphere
  - Aerosol (Layered Species)
  - Hydrometeors
  - Background Scenes and Materials
- ULTRAVIOLET
  - O_2
  - O_3
  - H_2O
  - SO_2
  - N_2O
  - NO_2
  - N_2O_2
  - D_2O_2

8-066-81.22

PRA
Photon Research Associates, Inc.

SIRRM ATMOSPHERIC MODEL

- SIRRM Uses Early (1981) Version of APART



- Can Easily Upgrade SIRRM for Latest Version of APART

8-066-81.23

PRA
Photon Research Associates, Inc.

CONCLUSIONS

PROBLEM	CURRENT SOLUTION	DESIRED SOLUTION
LTE/NLTE "Discontinuity"	Interpolate	Single Code
Earthlimb vs. Backgrounds	None	Compatible or Single Code
Plume vs. Background	None	Compatible or Single Code

S-066-91.24

REVIEW OF THE CHEMICAL KINETIC RATE CONSTANTS USED IN THE SHARC MODEL

V.I. Lang, A.T. Pritt, Jr.
The Aerospace Corporation, PO Box 92957, Los Angeles, CA 90009

The SHARC (Strategic High Altitude Radiance Code) predicts the infrared (1-40 μm) radiance background of the Earth's atmosphere from 50 - 300 km for a variety of viewing geometries. At these altitudes the molecular species are no longer in thermodynamic equilibrium, requiring that the state populations of each emitter be calculated based on a steady state solution to a set of first-order differential equations describing the kinetic development of each emitter. Presented here is a review of the rate constants used to calculate specific vibrational level populations for H_2O, CO_2, and O_3 which are important molecular species emitting in the infrared.

REVIEW OF THE CHEMICAL KINETIC RATE CONSTANTS USED IN THE SHARC MODEL

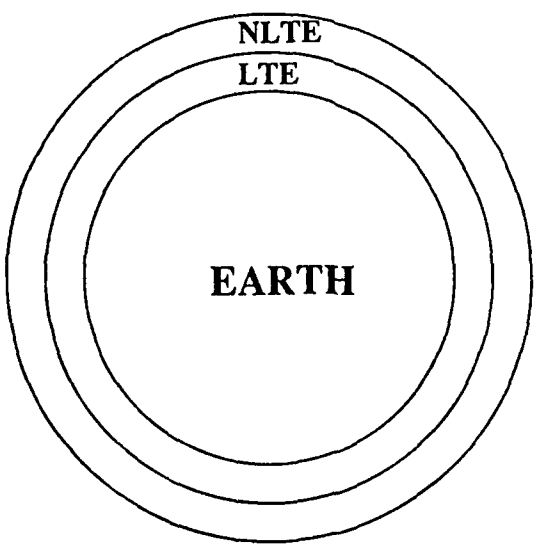
V. I. Lang and A. T. Pritt, Jr.
The Aerospace Corporation

prepared for the
Annual Review of Atmospheric Models
June 11 - June 12, 1991

work supported by the Geophysics Directorate, Phillips Laboratory
Dr. R. Sharma, Program Manager

STRATEGIC HIGH ALTITUDE RADIATION CODE (SHARC)

Features: NLTE Code
1 - 40 μm
50 - 300 km
Quiescent and Auroral
Vaious Viewing Geometries



OUTLINE

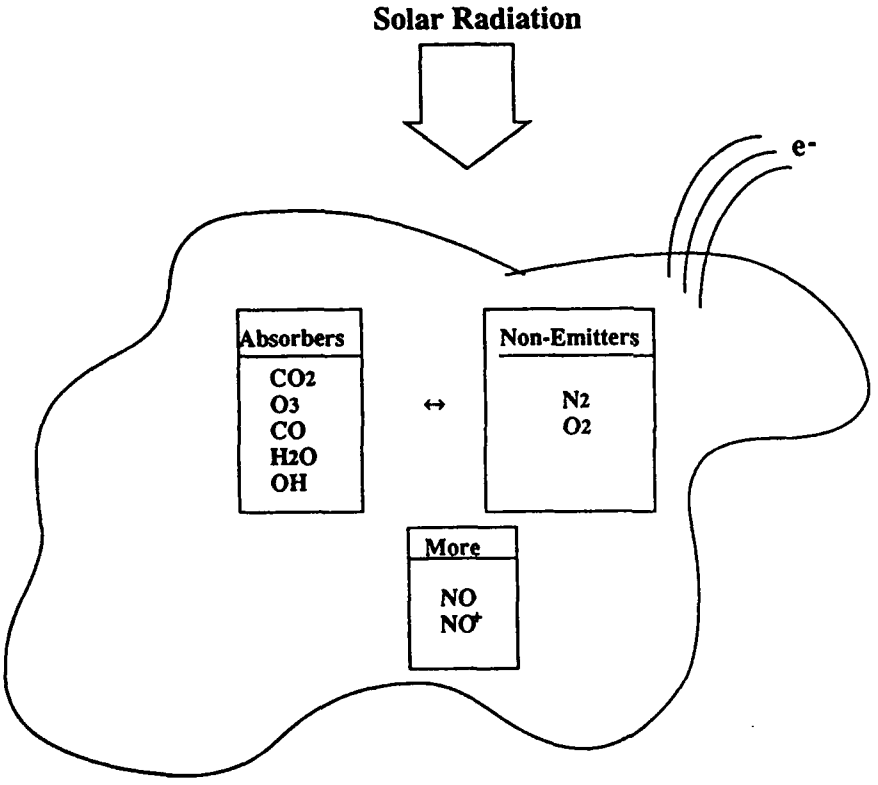
WHAT IS SHARC?

WHY AN NLTE MODEL?

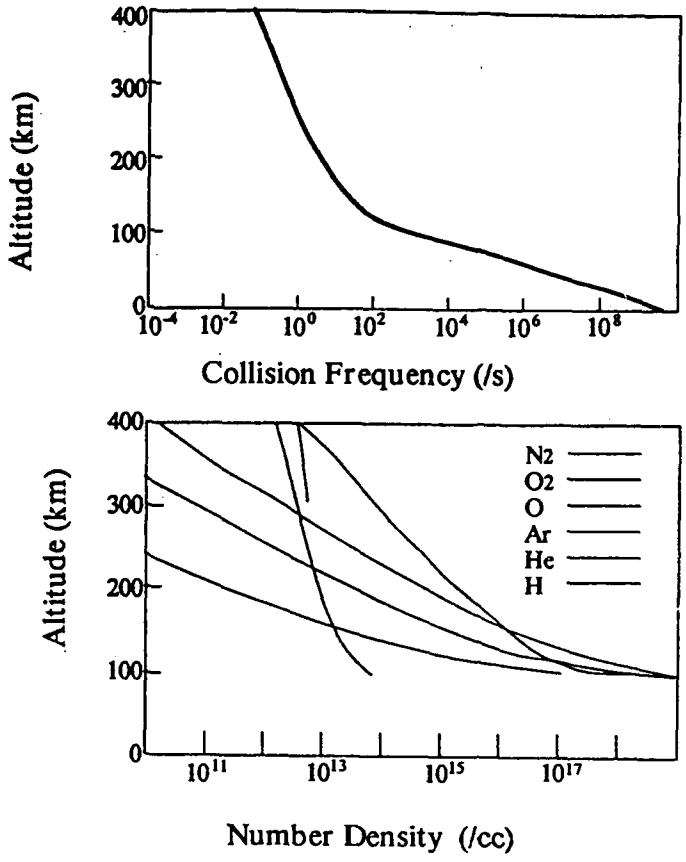
CO RATE CONSTANTS

H_2O RATE CONSTANTS

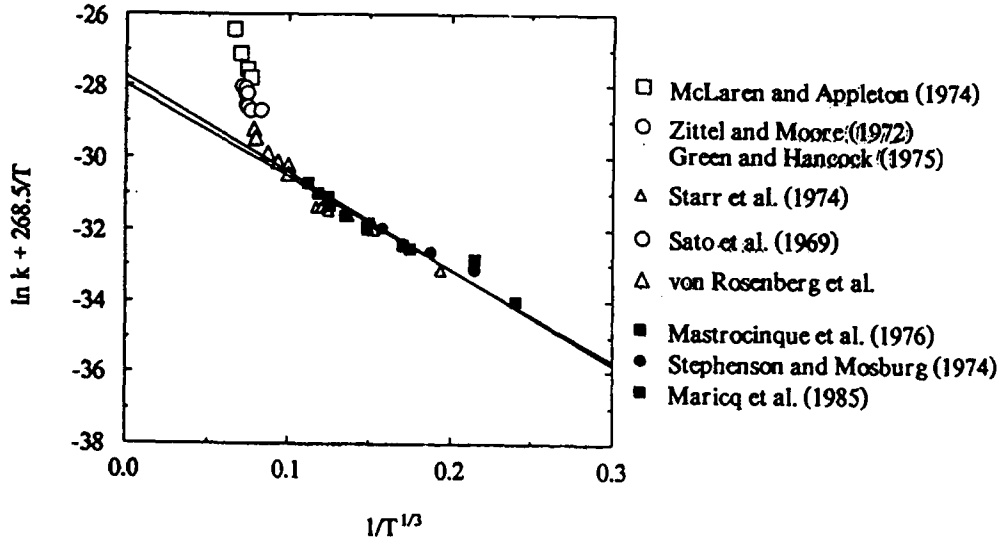
NEW WORK



EARTH'S ATMOSPHERE

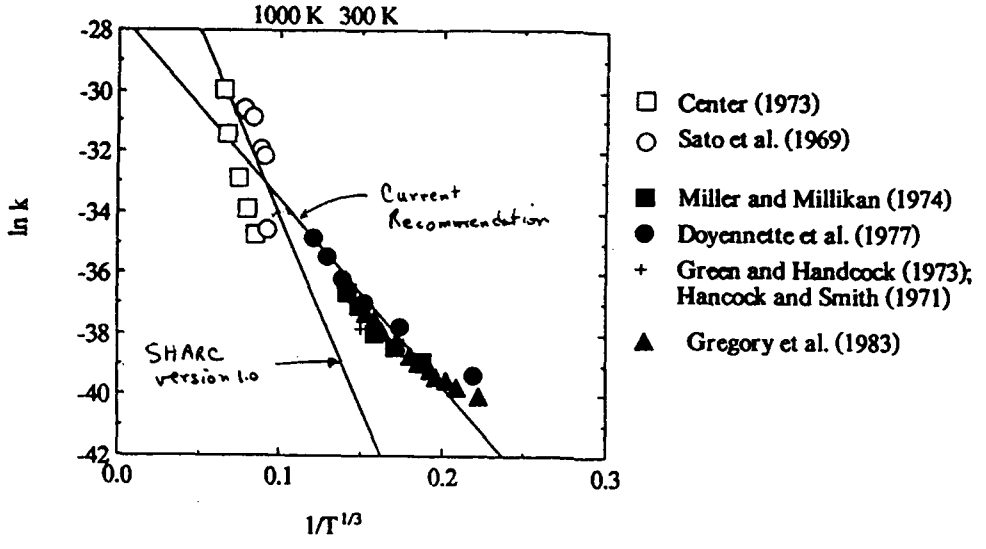


$$CO(1) + N_2(0) \rightarrow CO(0) + N_2(1)$$

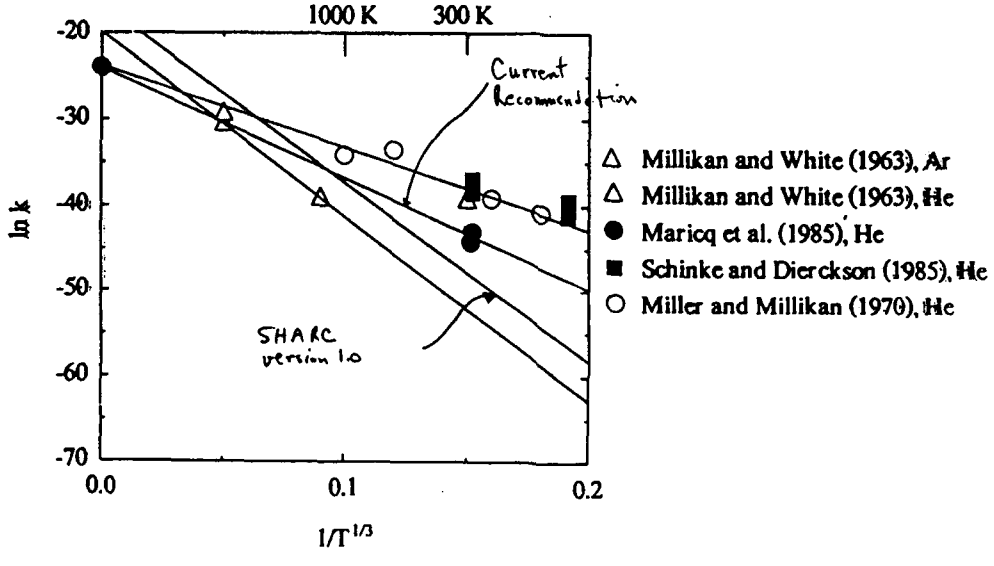


no change in rate constants.

$$CO(1) + O_2(0) \rightarrow CO(0) + O_2(1)$$



$$CO(1) + M \rightarrow CO(0) + M$$



$$CO(1) + O \rightarrow CO(0) + O$$

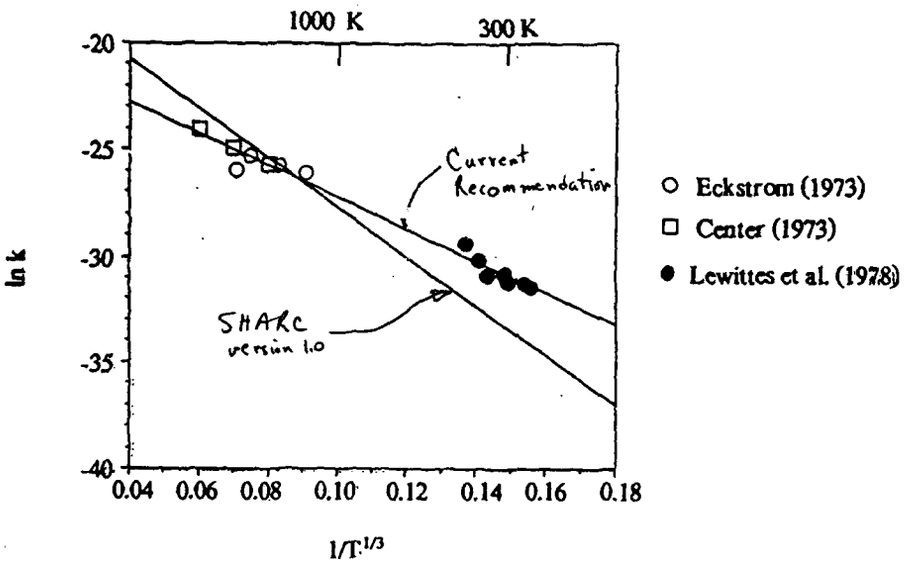


TABLE 1: Revisions to CO Kinetics

	Current SHARC Coefficients[a] A_i	C_i	D_i[b]	Revised Coefficients[a] A_i	C_i	D_i[b]
V-T Reactions[c],[d]						
M + CO(1) - M + CO(0) N_2/1.0/ O_2/1.0/	6.67e-08	208.3	0.0	3.78e-11	129.2	0.0
M + CO(0) - M + CO(1) N_2/1.0/ O_2/1.0/	6.67e-08	208.3	3083.7	3.78e-11	129.2	3083.7
M + CO(2) - M + CO(1) N_2/1.0/ O_2/1.0/	1.33e-07	208.3	0.0	7.56e-11	129.2	0.0
M + CO(1) - M + CO(2) N_2/1.0/ O_2/1.0/	1.33e-07	208.3	3045.6	7.56e-11	129.2	3045.6
M + CO(2) - M + CO(0) N_2/1.0/ O_2/1.0/	1.33e-07	208.3	0.0	7.56e-11	129.2	0.0
M + CO(0) - M + CO(2) N_2/1.0/ O_2/1.0/	1.33e-07	208.3	6129.3	7.56e-11	129.2	6129.3
O + CO(1) - O + CO(0)	9.90e-08	118.1	0.0	5.39e-11	48.8	0.0
O + CO(0) - O + CO(1)	9.90e-08	118.1	3083.7	5.39e-11	48.8	3083.7
O + CO(2) - O + CO(1)	1.98e-07	118.1	0.0	1.08e-10	48.8	0.0
O + CO(1) - O + CO(2)	1.98e-07	118.1	3045.6	1.08e-10	8.8	3045.6
O + CO(2) - O + CO(0)	1.98e-07	118.1	0.0	1.08e-10	48.8	0.0
O + CO(1) - O + CO(2)	1.98e-07	118.1	6129.3	1.08e-10	48.8	6129.3

TABLE 1 (cont.): Revisions to CO Kinetics

	Current SHARC Coefficients A_i	C_i	D_i	Revised Coefficients A_i	C_i	D_i
V-V Reactions[d]						
$CO(0) + N_2(1) - CO(1) + N_2(0)$	6.98e-13	25.6	0.0	2.20e-13	18.7	0.0
$CO(1) + N_2(0) - CO(0) + N_2(1)$	6.98e-13	25.6	268.5	2.20e-13	18.7	268.5
$CO(0) + O_2(1) - CO(1) + O_2(0)$	3.50e-10	124.0	844.4	1.68e-13	50.2	844.4
$CO(1) + O_2(0) - CO(0) + O_2(1)$	3.50e-10	124.0	0.0	1.68e-13	50.2	0.0
hv Emission[e]						
CO (1) - CO(0) + hv	30.96	0.0	0.0	30.96	0.0	0.0
CO (2) - CO(1) + hv	60.45	0.0	0.0	60.45	0.0	0.0
CO (2) - CO(0) + hv	1.03	0.0	0.0	1.03	0.0	0.0

a) Landau - Teller function $k = A_i\, T^{-Bi} \exp(-C_i\, T^{-.333} - D_i\, T^{-1})$; $B_i = 0$ for all reactions included here.
b) $D_i = \Delta E\ (cm^{-1})/1.44$
c) efficiences of collsion partner are listed below each reaction
d) rate units are cm^3 molecules^{-1} s^{-1}
e) rate units are s^{-1}; rates for reverse processes are zero

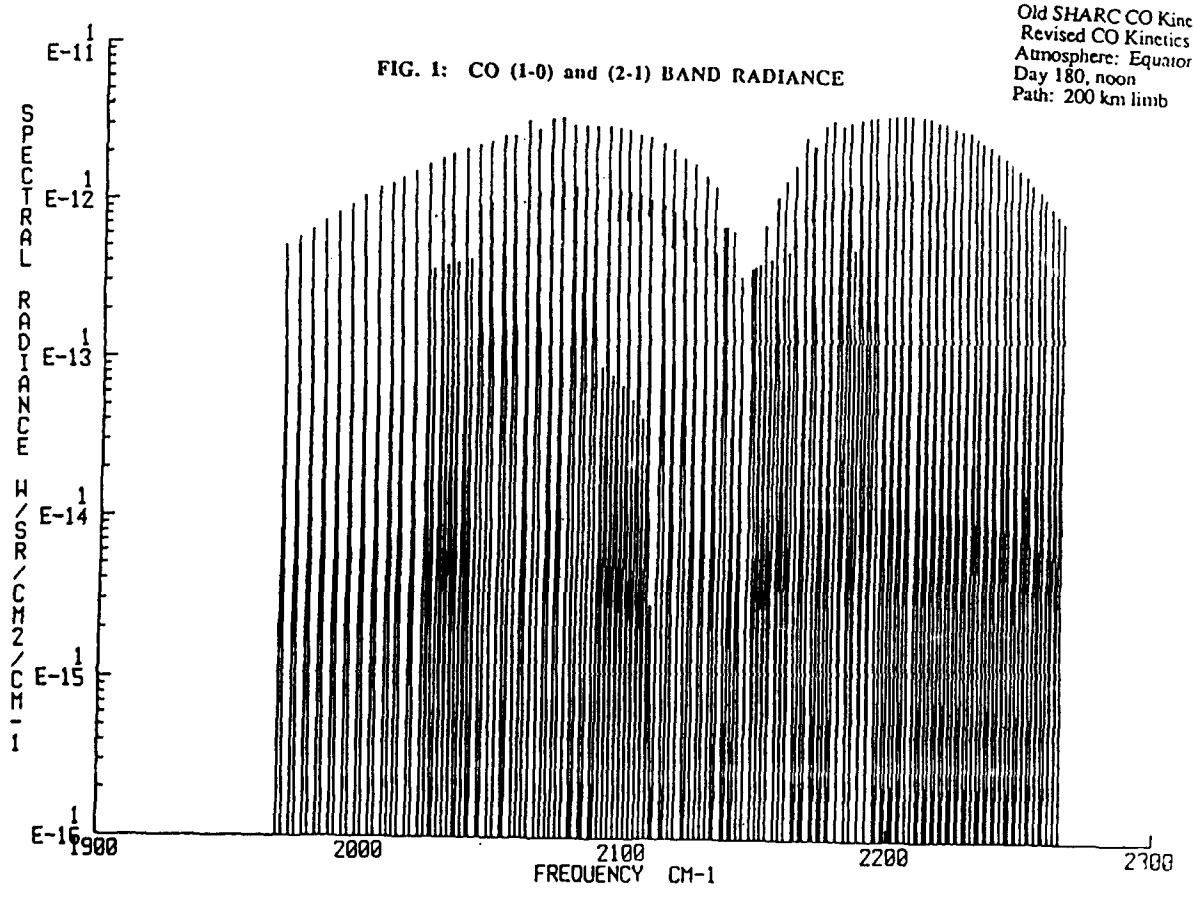
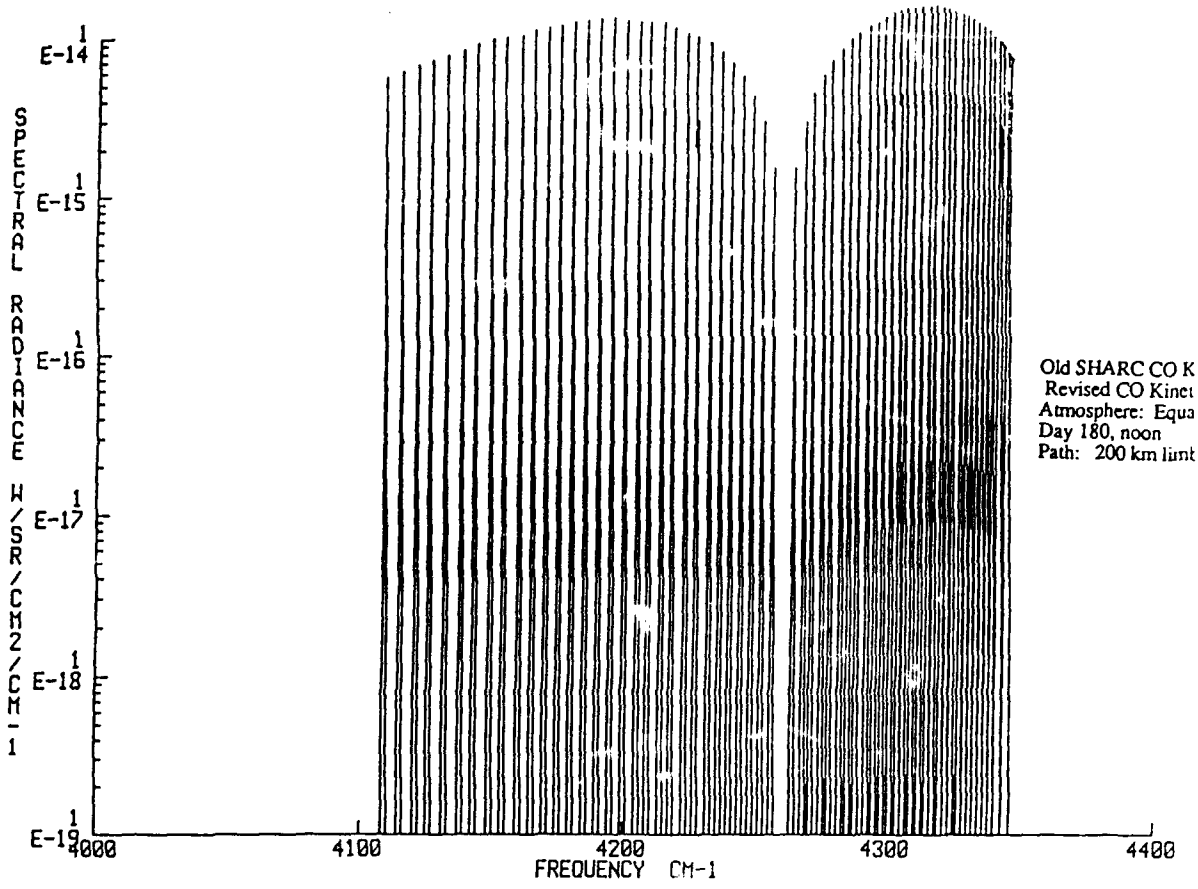


FIG. 1: CO (1-0) and (2-1) BAND RADIANCE

FIG. 2: CO (2-0) BAND RADIANCE



$$H_2O\ (010) + M \rightarrow H_2O\ (000) + M$$

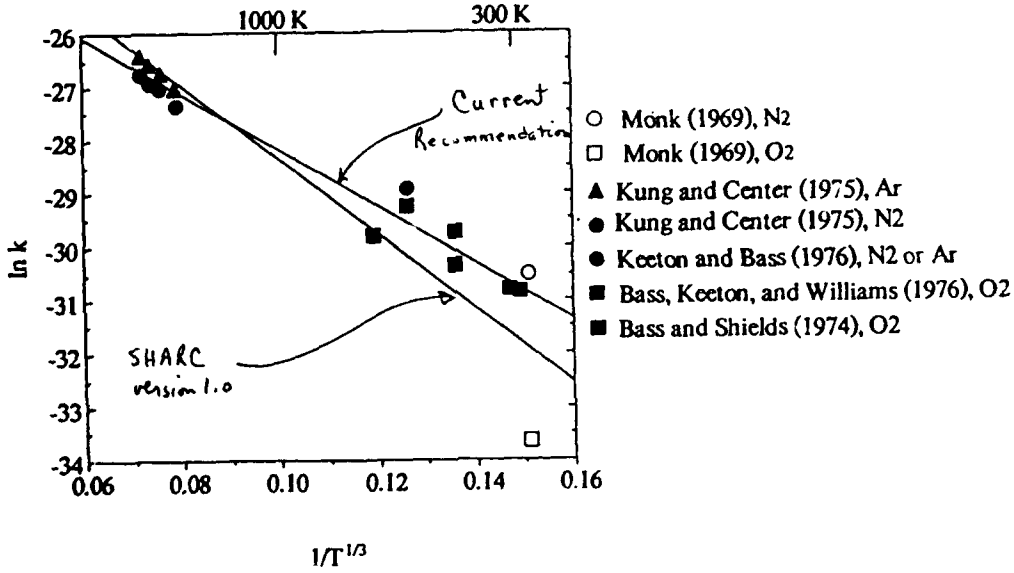


TABLE 1: Rate Coefficients for Relaxation of H_2O [$k_i = A_i T^{\beta_i} \exp(-C_i T^{-.333} - E_i/T]$

REACTIONS					REVISED RATE COEFFICIENTS A_i	β_i	C_i	**E_i
M + H2O(010) = M + H2O(000) N2/1.0/ O2/1.0/	5.37E-10	0.0	70.0	0.0	1.13E-10	0	52.5	0
M + H2O(100) = M + H2O(020) N2/1.0/ O2/0.7/	4.60E-13	0.0	0.0	0.0	*4.60E-13*	*0*	*0*	0
M + H2O(001) = M + H2O(020) N2/1.0/ O2/0.7/	4.60E-13	0.0	0.0	0.0	*4.60E-13*	*0*	*0*	0
M + H2O(020) = M + H2O(010) N2/1.0/ O2/1.0/	5.37E-10	0.0	70.0	0.0	2.26E-10	0	52.5	0
M + H2O(030) = M + H2O(020) N2/1.0/ O2/1.0/	5.37E-10	0.0	70.0	0.0	3.39E-10	0	52.5	0
M + H2O(110) = M + H2O(100) N2/1.0/ O2/1.0/	5.37E-10	0.0	70.0	0.0	1.13E-10	0	52.5	0
M + H2O(011) = M + H2O(001) N2/1.0/ O2/1.0/	5.37E-10	0.0	70.0	0.0	1.13E-10	0	52.5	0
M + H2O(110) = M + H2O(030) N2/1.0/ O2/0.7/	4.60E-13	0.0	0.0	0.0	*4.60E-13*	*0*	*0*	0
M + H2O(011) = M + H2O(030) N2/1.0/ O2/0.7/	4.60E-13	0.0	0.0	0.0	*4.60E-13*	*0*	*0*	0
O2(0) + H2O(010) - O2(1) + H2O(000)	1.00E-12	0.0	0.0	0.0	2.9E-12	0	0	0
O2(1) + H2O(000) - O2(0) + H2O(010)	1.00E-12	0.0	0.0	55.2	2.9E-12	0	0	55.2
O2(0) + H2O(020) - O2(1) + H2O(010)	1.00E-12	0.0	0.0	0.0	5.8E-12	0	0	0
O2(1) + H2O(010) - O2(0) + H2O(020)	1.00E-12	0.0	0.0	0.7	5.8E-12	0	0	0.7
O2(0) + H2O(030) - O2(1) + H2O(020)	1.00E-12	0.0	0.0	0.0	8.7E-12	0	0	0
O2(1) + H2O(020) - O2(0) + H2O(030)	1.00E-12	0.0	0.0	-59.3	8.7E-12	0	0	59.3
O2(0) + H2O(110) - O2(1) + H2O(100)	1.00E-12	0.0	0.0	0.0	2.9E-12	0	0	0
O2(1) + H2O(100) - O2(0) + H2O(110)	1.00E-12	0.0	0.0	31.0	2.9E-12	0	0	31.0
O2(0) + H2O(011) - O2(1) + H2O(001)	1.00E-12	0.0	0.0	0.0	2.9E-12	0	0	0
O2(1) + H2O(001) - O2(0) + H2O(011)	1.00E-12	0.0	0.0	27.3	2.9E-12	0	0	27.3
H2O(010) - H2O(000) + HV	18.350.0	0.0	0.0	0.0	20.33	0	0	0
H2O(020) - H2O(000) + HV	0.454	0.0	0.0	0.0	.567	0	0	0
H2O(100) - H2O(000) + HV	3.37	0.0	0.0	0.0	5.00	0	0	0
H2O(001) - H2O(000) + HV	78.40	0.0	0.0	0.0	76.58	0	0	0

REACTIONS (cont.)					REVISED RATE COEFFICIENTS A_i	B_i	C_i	D_i
H2O(030) - H2O(000) + HV	0.003	0.0	0.0	0.0	.0065			
H2O(110) - H2O(000) + HV	0.349	0.0	0.0	0.0	.7680	0	0	0
H2O(011) - H2O(000) + HV	17.22	0.0	0.0	0.0	17.23	0	0	0
H2O(020) - H2O(010) + HV	33.74	0.0	0.0	0.0	41.29	0	0	0
H2O(100) - H2O(010) + HV	0.612	0.0	0.0	0.0	1.36	0	0	0
H2O(001) - H2O(010) + HV	3.70	0.0	0.0	0.0	2.15	0	0	0
H2O(030) - H2O(010) + HV	1.11	0.0	0.0	0.0	1.21	0	0	0
H2O(110) - H2O(010) + HV	4.17	0.0	0.0	0.0	4.53	0	0	0
H2O(011) - H2O(010) + HV	65.98	0.0	0.0	0.0	71.49	0	0	0
H2O(030) - H2O(020) + HV	36.87	0.0	0.0	0.0	40.06	0	0	0
H2O(000) + HV - H2O(010)	0.0	0.0	0.0	0.0	--------	--	--	--
H2O(000) + HV - H2O(020)	0.0	0.0	0.0	0.0	--------	--	--	--
H2O(000) + HV - H2O(100)	0.0	0.0	0.0	0.0	--------	--	--	--
H2O(000) + HV - H2O(001)	0.0	0.0	0.0	0.0	--------	--	--	--
H2O(000) + HV - H2O(030)	0.0	0.0	0.0	0.0	--------	--	--	--
H2O(000) + HV - H2O(110)	0.0	0.0	0.0	0.0	--------	--	--	--
H2O(000) + HV - H2O(011)	0.0	0.0	0.0	0.0	--------	--	--	--
H2O(010) + HV - H2O(020)	0.0	0.0	0.0	0.0	--------	--	--	--
H2O(010) + HV - H2O(100)	0.0	0.0	0.0	0.0	--------	--	--	--
H2O(010) + HV - H2O(001)	0.0	0.0	0.0	0.0	--------	--	--	--
H2O(010) + HV - H2O(030)	0.0	0.0	0.0	0.0	--------	--	--	--
H2O(010) + HV - H2O(110)	0.0	0.0	0.0	0.0	--------	--	--	--
H2O(010) + HV - H2O(011)	0.0	0.0	0.0	0.0	--------	--	--	--
H2O(020) + HV - H2O(030)	0.0	0.0	0.0	0.0	--------	--	--	--

*Numbers in italics indicate that no change has been made from the original SHARC value
** The E_i terms (ie. the energy differences between levels) are not listed here for the V-T processes because these are obtained from the H_2OSTAT.DAT file in SHARC 2.0.

H_2O

TABLE 2: BAND RADIANCE COMPARISON

Transition	Frequency	Band Radiance (W/SR/cm^2) Old Kinetics	New Kinetics	Radiance Ratio Old:New
(010)-(000)	1594.750	0.37277e-6	0.35466e-6	1.05
(020)-(000)	3151.630	0.11184e-8	0.21412e-9	5.22
(100)-(000)	3657.053	0.87024e-9	0.47780e-9	1.82
(001)-(000)	3755.930	0.35921e-7	0.36124e-7	.994
(030)-(000)	4666.793	0.11070e-11	0.87792e-13	12.6
(110)-(000)	5234.977	0.63862e-11	0.24911e-11	2.56
(011)-(000)	5331.269	0.20763e-8	0.12812e-8	1.62
(020)-(010)	1556.880	0.39202e-7	0.75069e-8	5.22
(100)-(010)	2062.303	0.13254e-9	0.73330e-10	1.81
(001)-(010)	2161.180	0.16949e-8	0.16950e-8	1.00
(030)-(010)	3072.043	0.17710e-9	0.14089e-10	12.6
(110)-(010)	3640.227	0.39018e-10	0.15291e-10	2.55
(011)-(010)	3736.519	0.82490e-8	0.50967e-8	1.62
(030)-(020)	1515.163	0.32288e-8	0.25724e-9	12.6
Pure Rotational Lines		0.99151e-10	0.99151e-10	1.0
Total Overlap Corrected Band Pass Radiance		0.46488e-6	0.40686e-6	1.14

Model Atmosphere: DAYSUBAR.DAT
Lat. 0^0, Long. 0^0
Solar Zenith Angle 0^0

Limb View, 64 km Tangent

Fig. 1: Radiance Calculation Comparison (Including H_2O (020) Band; 3151.6 cm^{-1})

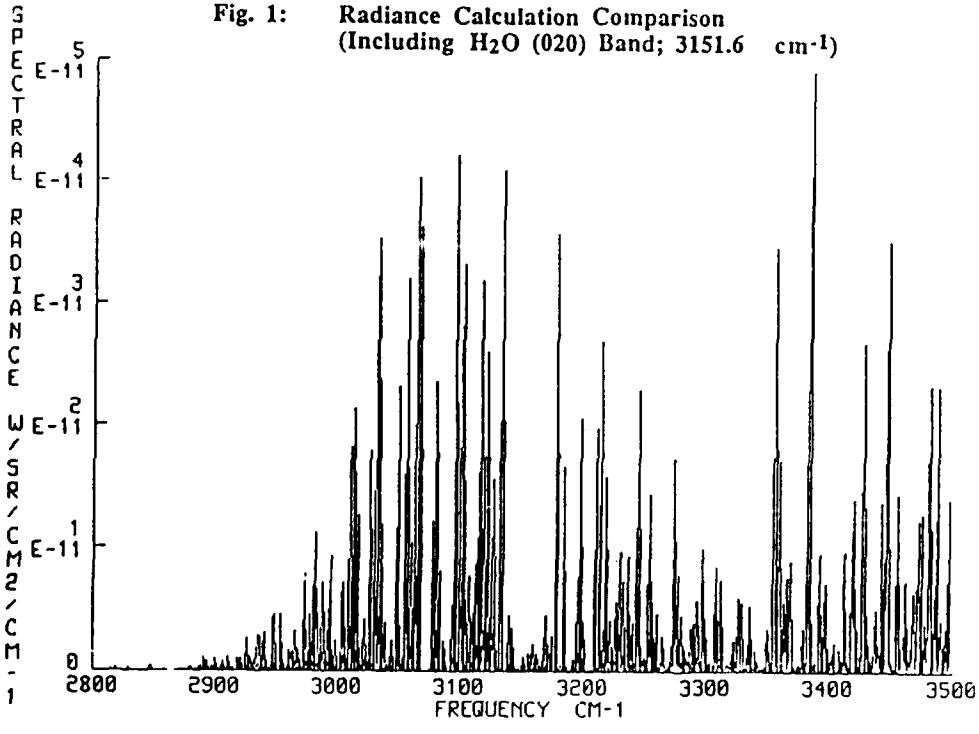


Fig. 2: Radiance Calculation Comparison (Including H_2O (030) Band; 4666.8 cm-1)

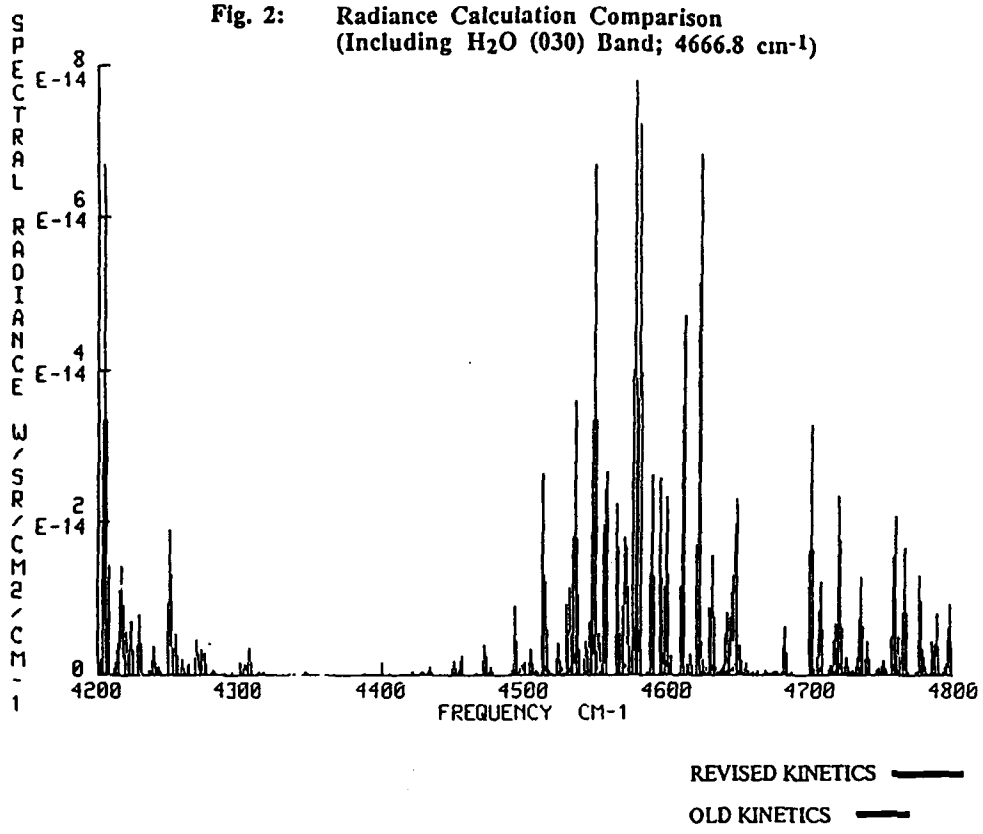
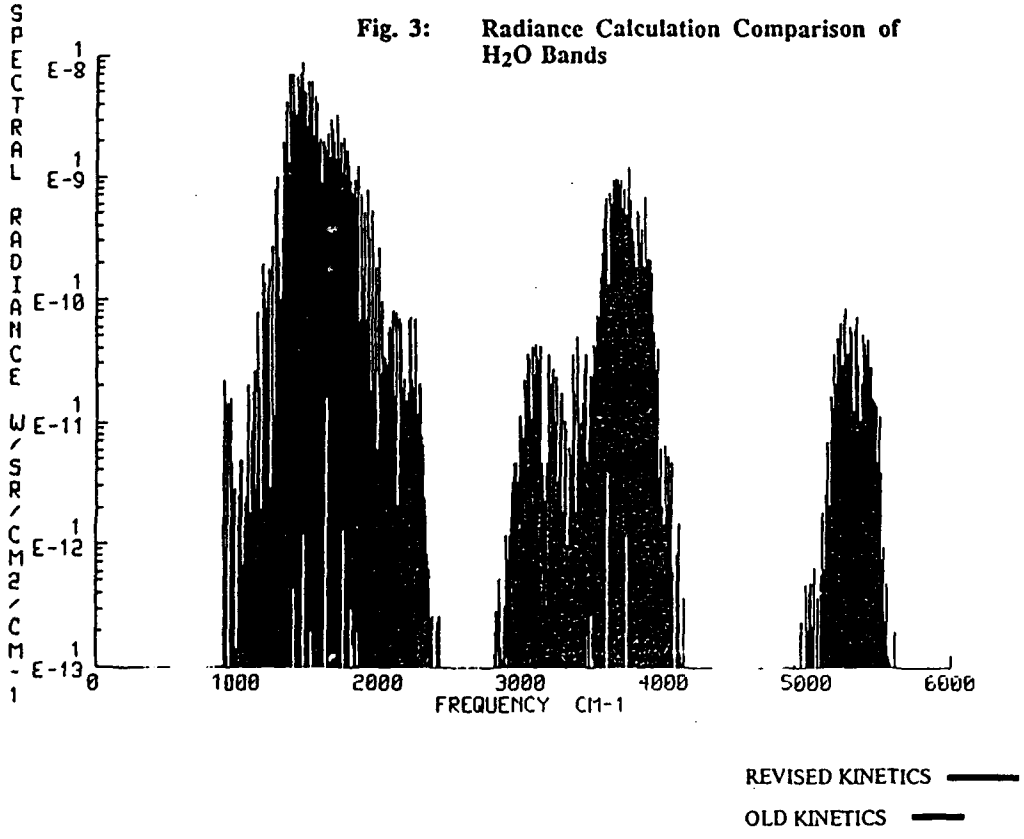


Fig. 3: Radiance Calculation Comparison of H_2O Bands



NEW WORK

OZONE RATE CONTANTS

NO RATE CONSTANTS

OH RATE CONSTANTS

LIMITATIONS OF KUYMER-JAMES MODEL

REVIEW ARTICLE

Session 3

Summary of the Session on Measurements and Models

This session addressed model applications, enhancements, validations, and potential new directions; the singular laboratory measurement paper described work on the UV Schumann-Runge bands. Because of the large number of separate issues covered, this synopsis is arbitrarily divided into two categories: "New Directions" and "Measurements and Validations".

NEW DIRECTIONS:

"Atmospheric Ultraviolet Radiance and its Variation": In the realm of new directions for PL/GP models, Computational Physics (CPI) outlined its approach to modeling UV/Visible airglow features and their variability. This modeling effort will eventually be merged with the lower atmosphere AURIC, MODTRAN, and SHARC (see previous papers, Huguenin et al.; Abreu et al.; Robertson et al.). Such syntheses will eventually produce a seamless code covering solar, thermal, and airglow features throughout the ultraviolet to far IR spectral ranges.

"Improved HNO_3 Band Model Parameters": Currently a full spectroscopic description for HNO_3 at 11.3 microns requires thousands of transitions. Implementing this system into a line-by-line algorithm consumes large amounts of time and storage; therefore, the authors propose an efficient temperature dependent band model, suitable for incorporation into LOWTRAN and MODTRAN.

"Line-by-Line Calculations of Atmospheric Fluxes and Heating Rates": Interest in Global Climate Change within the scientific community has driven the evolution of FASCOD3 into the arena of energy deposition within the atmosphere. AER has extended the code to produce heating and cooling rates for a variety of atmospheres, comparing those results to prior calculations (ICRCCM). The contour plots of line-by-line heating and cooling rates, as a function of both pressure and frequency, readily demonstrates the importance of correct detailed spectroscopy, particularly regarding "feature overlap" and the H_2O continuum, on potential global change predictions.

"A Comparison of Computational Approaches for the Voigt Function": F. Schreier of the Optoelectronics Institute, Germany, presents a comprehensive (and elegant) investigation of computational procedures for calculating the Voigt function. Coding implementation and subsequent timing runs were described.

"Spectral Smoothing in the Fourier Domain: A Software Package for Line-by-Line Calculations": With the growth of Fourier transform spectrometric techniques, used in both laboratory and field measurements (surface, airborne, balloon, shuttle, and satellite), the need for rapid FTS simulation capability became apparent. This new routine (developed at Optimetrics and Stewart Radiance Lab) provides a set of FTS scanning functions, including apodization, that can be used in conjunction with FASCOD3 output. The functions include sinc, $sinc^2$, Beer, Hamming, and Hanning.

MEASUREMENTS AND VALIDATIONS:

"Photoabsorption Cross Sections in the Transmission Window Regions of the Schumann-Runge Bands of Oxygen": This paper describes laboratory work done at Harvard-

Smithsonian to improve the measurements of the Schumann-Runge Band absorption in the window regions between stronger rotational lines, including the pressure dependence. These data are particularly important when calculating penetration of solar UV into the mesosphere and stratosphere. Eventually, full cross sections based upon the Harvard measurements will be incorporated into AURIC (see previous papers: Hugeunin et al., Link et al.).

"High-Resolution Spectral Measurements of Upwelling and Downwelling Atmospheric Infrared Emission with Michelson Interferometers": FASCOD3 validation is critically dependent upon good high-resolution radiance and transmittance measurements; the atmospheric data presented by the University of Wisconsin-Madison provide well calibrated IR radiances at both surface and aircraft altitudes (downwelling and upwelling). The data are of sufficient quality to infer necessary changes to CO_2 and H_2O spectral line parameters; independently those same parameters were updated for HITRAN91 based on laboratory data (see Rothman). The role of FTS data in interpreting the atmosphere (temperature, constituent, and particular profiles) is strongly reinforced by this excellent program.

"Validation of HIS Spectral Measurements with the FASCODE Line-by-Line Model": This is a companion paper to the Wisconsin (Revercomb et al., above) instrument presentation, further describing inferences drawn from comparisons between HIS atmospheric measurements and FASCOD3 calculations. Cloud (sub-visual cirrus) and fluorocarbon signatures, in addition to ozone, water, and carbon dioxide, are readily apparent, supporting the development of high resolution measurements in more operational modes.

"Comparison of FASCOD2 and LOWTRAN7 Models with FIT Spectral Transmittance Measurements in the 3-12 micron Region": The Canadian research group has compared high resolution interferometric transmittance measurements (winter and summer, high and low humidity) with both FASCOD2 and LOWTRAN7 (after degrading the data to LOWTRAN resolution; agreement is, in general, very good (<|8%|). However, their analyses point out some of the same problem areas in H_2O lines (updated in HITRAN91), along with concerns about the self and foreign continua. This latter problem is being addressed; see Special Session discussion.

"LOWTRAN7 Comparisons with Field Measurements": As the title indicates, the Army Night Vision Laboratory conducted an extensive set of comparisons of LOWTRAN7 with transmissometer measurements at 1.54, 3-5, and 8-12 micron frequencies. Measurements were made in Virginia, Panama, Alaska, and Utah. The quality of agreement was, in most cases, as good as the supporting meteorological data (humidity, etc.). An initial comparison of MODTRAN and high resolution Fourier transform transmissometer measurements also showed excellent agreement, furthering the arguments for the E/O community to convert from LOWTRAN to MODTRAN.

"Spectral Solar Radiation Modeling, Measurement, and Data Base Activities at the Solar Energy Resolution Institute (SERI)": SERI outlined their interest, motivation, and measurement program in the near UV through near IR spectral ranges. This program is driven by the need to assess performance of solar energy conversion devices. Both MODTRAN and LOWTRAN provide similar modeling capability, so the SERI development offers parallel validation of the DoD codes.

"Incorporation of LOWTRAN7 into the ACQUIRE Model": LOWTRAN7 has been modified for the Army to be compatible with EOSAEL 92; this has required changing the input to EOSAEL flexible formatting and adding target contrast calculations along with new aerosol and multiple scattering algorithms.

ATMOSPHERIC ULTRAVIOLET RADIANCE AND ITS VARIATIONS

R. Link, D.J. Strickland, D.E. Anderson, Jr.
Computational Physics, Inc., P.O. Box 788, Annandale, VA 22003

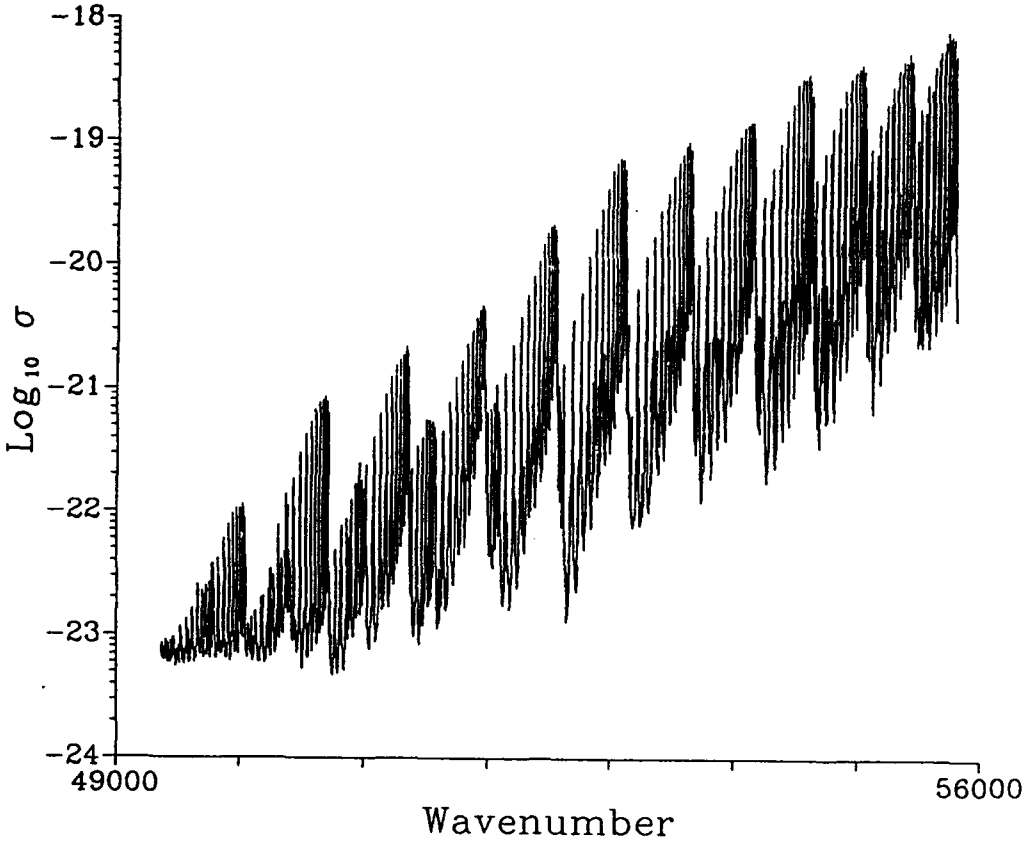
CPI is developing numerical codes for the Atmospheric Ultraviolet Radiance Integrated Code (AURIC) development effort of the Phillips Laboratory Geophysics Directorate in the area of Ionospheric Impact on Air Force Systems - Ultraviolet Remote Sensing. The modules will calculate thermospheric emission spectra and radiances in the 1000 - 6500 Å wavelength region for dayglow, nightglow, twilight and electron aurora, and will account for solar, photoelectron, auroral electron, and chemical excitation processes, pure and self absorption, and multiple scattering effects. The modules will provide the capability to calculate emission spectra as a function of wavelength and look angle, or provide radiances integrated over specified wavelength intervals for user-selected viewing geometries. An orbit code will be provided for satellite viewing geometries. An interface to MODTRAN will be provided for calculating Rayleigh scattering contributions. The integrand codes will provide the analyst with a powerful tool for predicting UV optical backgrounds, analyzing optical data, and designing sensors.

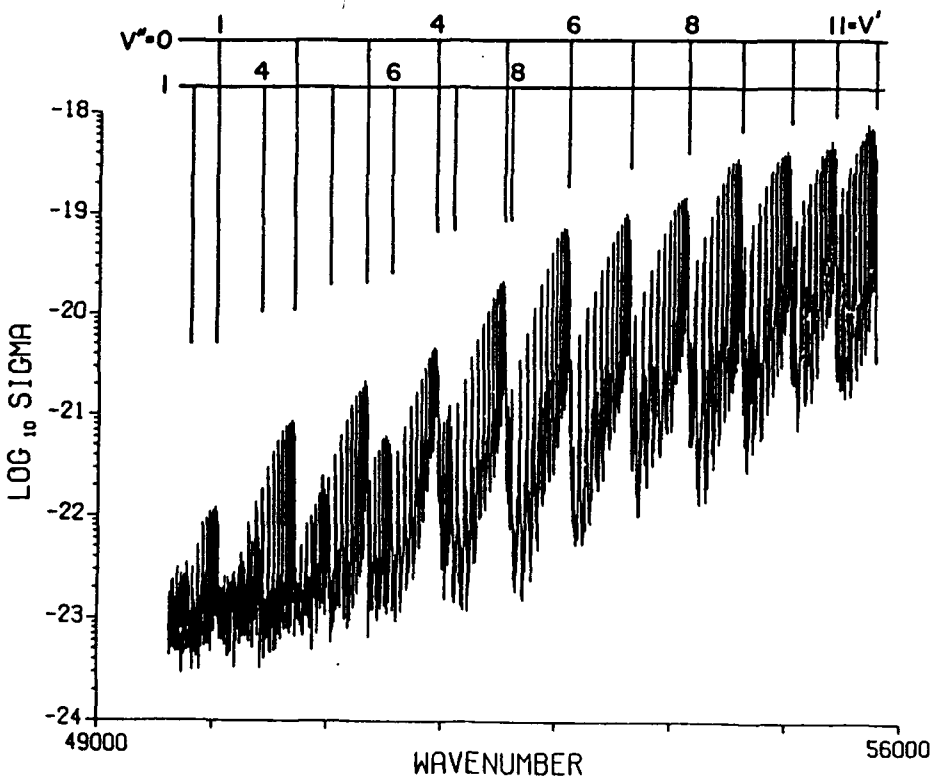
PHOTOABSORPTION CROSS SECTIONS IN THE TRANSMISSION WINDOW REGIONS OF THE SCHUMANN-RUNGE BANDS OF OXYGEN

K. Yoshino, J.R. Esmond, D.E. Freeman, W.H. Parkinson
Harvard-Smithsonian Center for Astrophysics, 60 Garden Street, Cambridge, MA 02138

A.S-C. Cheung
Chemistry Department, University of Hong Kong, Hong Kong

We have completed measurements of the absorption cross sections of the Schumann-Runge bands in the window regions between the rotational lines in the wavelength region 180-199 nm. The measurements have been done with many different pressures of oxygen, 50-76 torr, so that the pressure dependent absorption can be separated from the main cross sections. The measured cross section $\sigma_p(\lambda)$ at the window region is linearly dependent on the pressure P of O_2, $\sigma_p(\lambda) + \alpha(\lambda)P$. σ_2 is the cross section of O_2 extrapolated to zero pressure and $\alpha(\lambda)P$ is the cross section involving two molecules of O_2. They are used to eliminate the pressure dependent part of the cross sections from the measured cross sections in the transmission window regions. The absorption cross sections at the window region have been obtained for (2,0) - (12,0) bands. The total cross sections are obtained from the combination of the window cross sections here and the peak cross sections previously obtained by Yoshino et al. (1983).


-18
-19
-20
-21
-22
-23
-24
Log 10 σ
49000
56000
Wavenumber

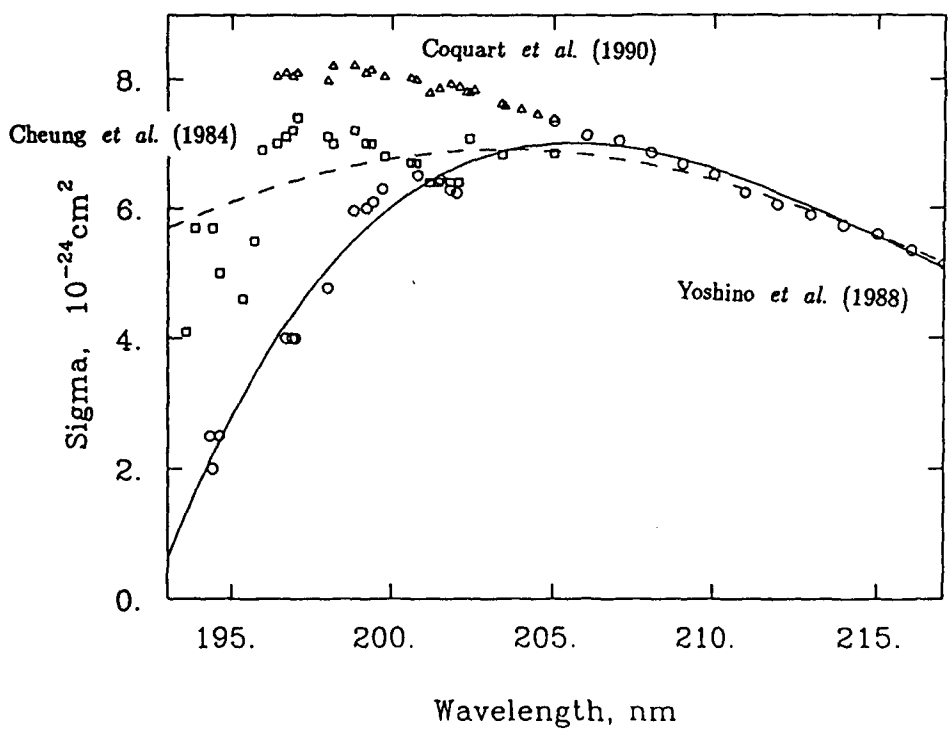

V"=0
1
4
6
8
11=V'
1
4
6
8
-18
-19
-20
-21
-22
-23
-24
LOG 10 SIGMA
49000
56000
WAVENUMBER

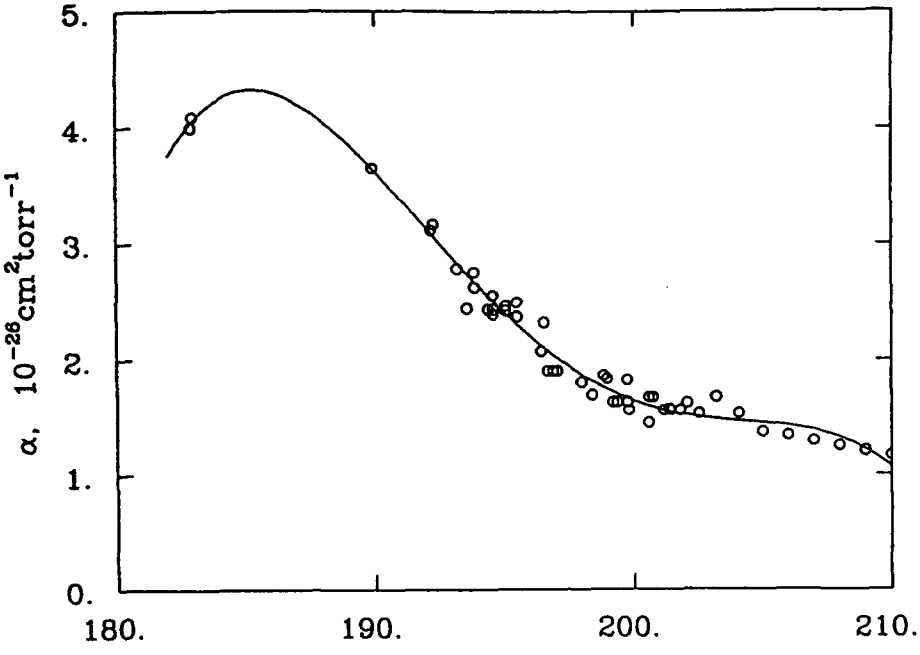
$$\sigma_P(\lambda) = \sigma_0(\lambda) + \alpha(\lambda)P$$

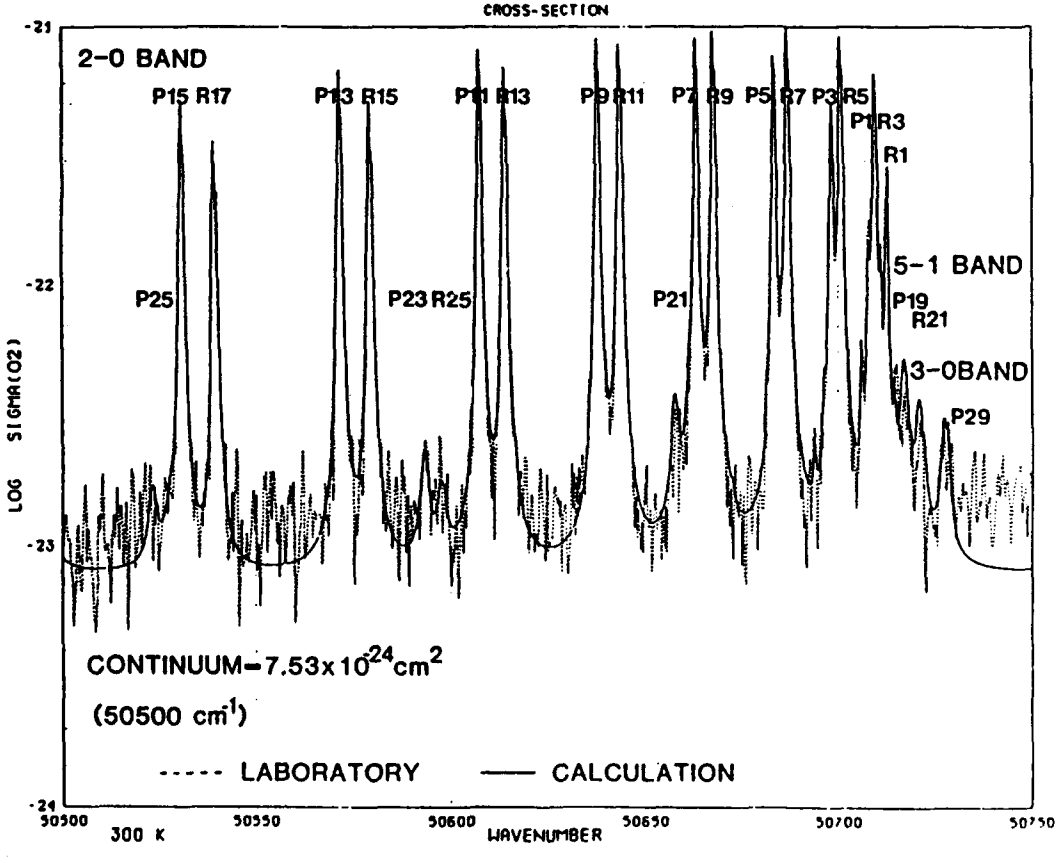
$$\sigma_0(\lambda) = \sigma_{SR}(\lambda) + \sigma_H(\lambda) + \sigma_R(\lambda)$$

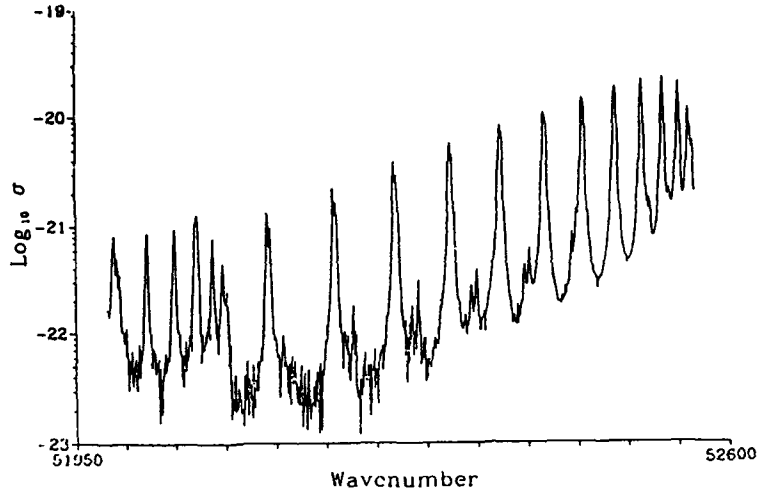
$\sigma_{SR}(\lambda)$: Wing effects of the Schumann-Runge bands
Temperature dependent
$\sigma_H(\lambda)$: Herzberg continuum
$\sigma_R(\lambda)$: Rayleigh scattering

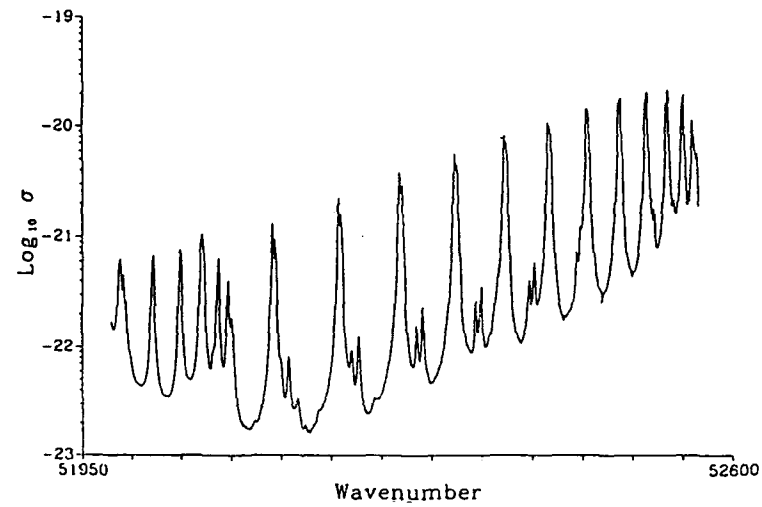
Herzberg Continuum Cross Sections, σ_H

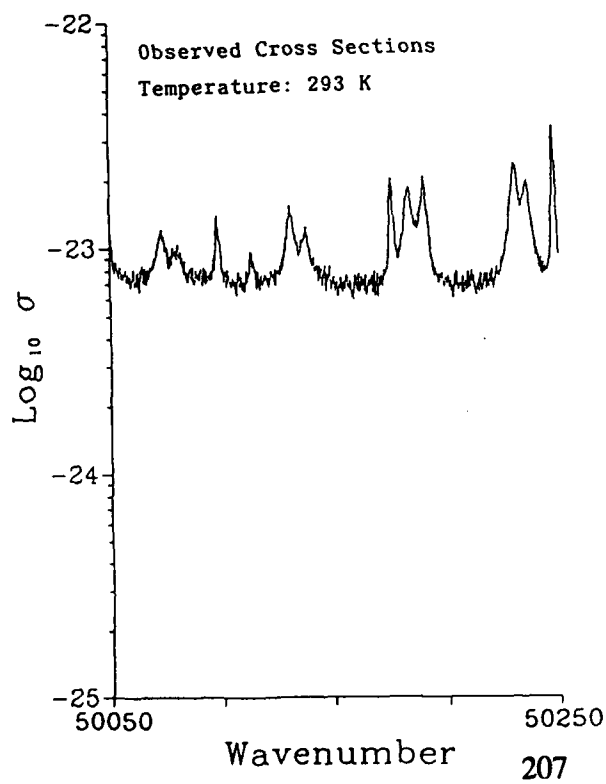


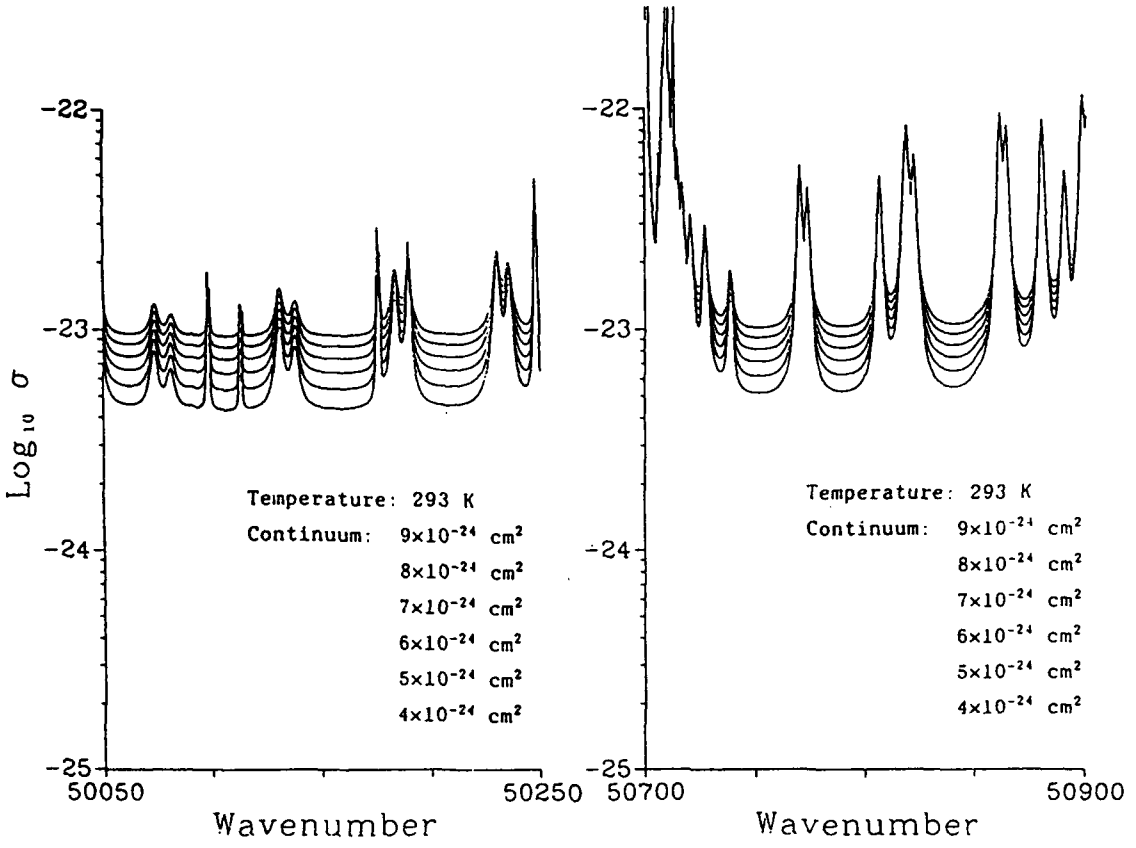

5.
4.
3.
2.
1.
0.
α, 10^{-26}cm^{2}torr^{-1}
180.
190.
200.
210.
Wavelength, nm

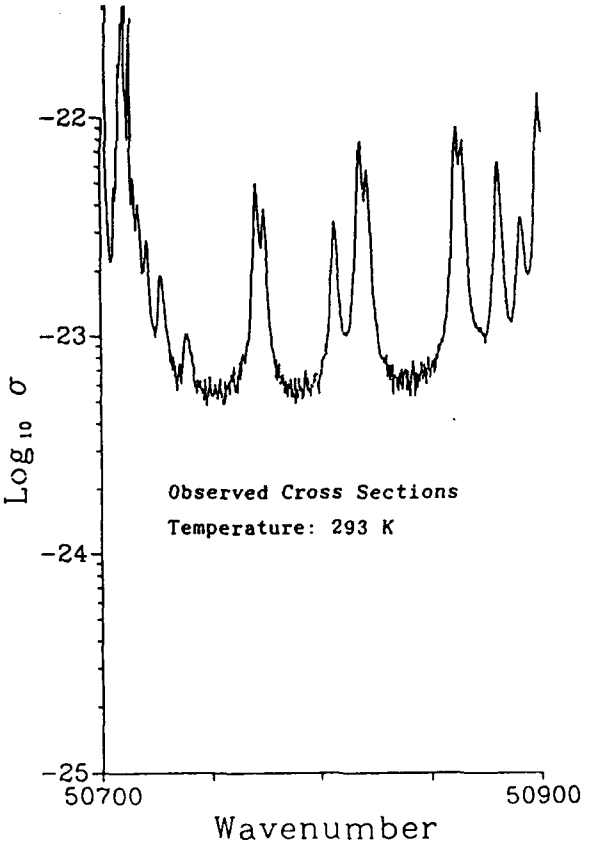

CROSS-SECTION
-21
-22
-23
-24
LOG SIGMA(O2)
2-0 BAND
P15 R17
P13 R15
P11 R13
P9 R11
P7 R9
P5 R7
P3 R5
P1 R3
R1
5-1 BAND
P25
P23 R25
P21
P19
R21
3-0BAND
P29
CONTINUUM=7.53x10^{-24}cm^2
(50500 cm^{-1})
----- LABORATORY
—— CALCULATION
50500
50550
50600
50650
50700
50750
300 K
WAVENUMBER

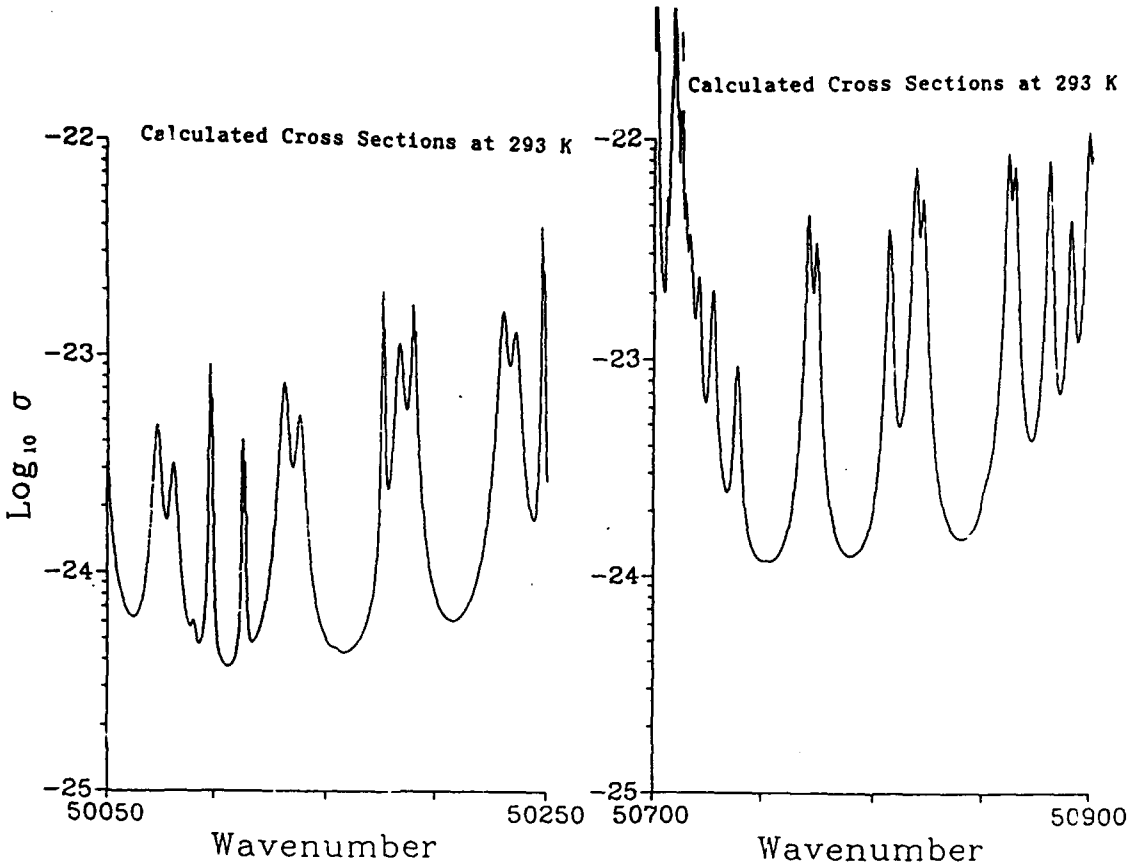

-19
-20
-21
-22
-23
Log10 σ
51950
52600
Wavcnumber

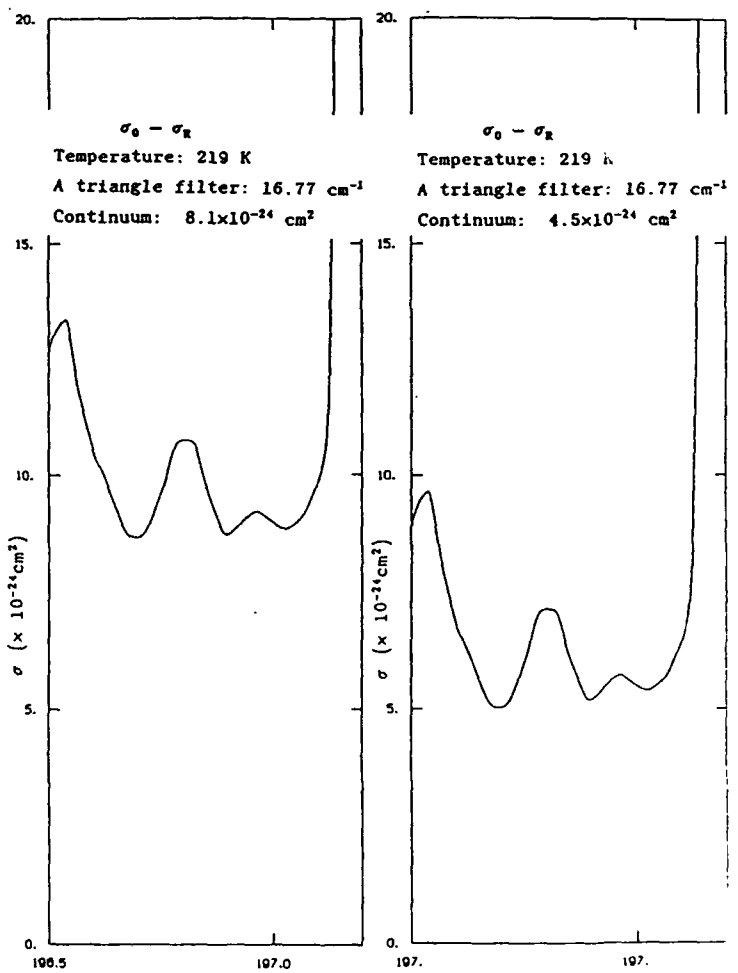

-19
-20
-21
-22
-23
Log10 σ
51950
52600
Wavenumber

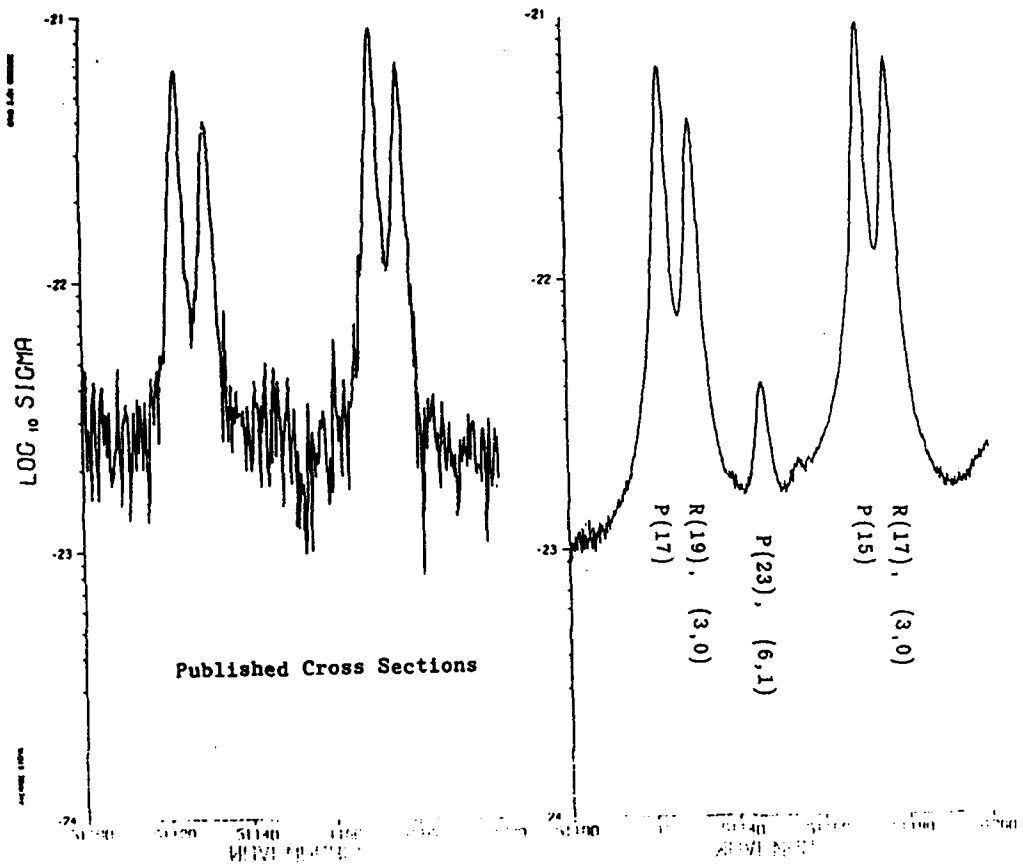

Observed Cross Sections
Temperature: 293 K
-22
-23
-24
-25
Log10 σ
50050
50250
Wavenumber


-22
-23
-24
-25
Log10 σ
Temperature: 293 K
Continuum: 9x10-24 cm2
8x10-24 cm2
7x10-24 cm2
6x10-24 cm2
5x10-24 cm2
4x10-24 cm2
50050
50250
Wavenumber
50700
50900
Wavenumber


-22
-23
-24
-25
Log10 σ
Observed Cross Sections
Temperature: 293 K
50700
50900
Wavenumber


Calculated Cross Sections at 293 K
Log10 σ
-22
-23
-24
-25
50050
50250
Wavenumber
Calculated Cross Sections at 293 K
-22
-23
-24
-25
50700
50900
Wavenumber


20.
σ0 − σR
Temperature: 219 K
A triangle filter: 16.77 cm-1
Continuum: 8.1x10-24 cm2
15.
10.
5.
0.
σ (x 10-24cm2)
196.5
197.0
20.
σ0 − σR
Temperature: 219 K
A triangle filter: 16.77 cm-1
Continuum: 4.5x10-24 cm2
15.
10.
5.
0.
σ (x 10-24cm2)
197.
197.


LOG 10 SIGMA
-21
-22
-23
Published Cross Sections
R(19), (3,0)
P(17)
P(23), (6,1)
R(17), (3,0)
P(15)

INCORPORATION OF LOWTRAN 7 INTO THE ACQUIRE MODEL

S.G. O'Brien
Las Cruces Scientific Consulting, 3373 Solarridge Street, Las Cruces, NM 88001

The Night Vision Laboratory ACQUIRE computer program is designed to calculate range performance predictions that are based upon results from the FLIR90 sensor performance model. ACQUIRE combines MRT data, target characteristics, and atmospheric conditions to predict the probability of accomplishing various acquisition tasks as a function of range. The addition of a modified version of LOWTRAN 7 to perform the atmospheric characterization task is described.

Incorporation of LOWTRAN 7 into the ACQUIRE Model

Sean G. O'Brien
Las Cruces Scientific Consulting

Incorporation of LOWTRAN 7 into ACQUIRE

Implementation

- Use ACQUIRE as the driver
- Input of negative transmission triggers LOWTRAN 7 execution
- Modified LOWTRAN 7 (EOSAEL LOWTRAN) already performs target contrast computation
- Modify ACQUIRE range performance algorithms to include contrast results

Incorporation of LOWTRAN 7 into ACQUIRE

Goals

- Use modified LOWTRAN 7 to calculate observer-target and observer-background transmissions and radiances in ACQUIRE, and calculate target contrast
- Modify ACQUIRE to adjust target acquisition results using LOWTRAN 7 target contrast results
- Test and document the resulting code

NVL ACQUIRE Model Input/Output

- Input
  - target: height, length, delta T
  - environment: atmospheric transmittance, smoke mass extinction coefficient, smoke concentration length, max range
  - device: # of MRT data points, number of resolvable cycles on target corresponding to 50% probability of performing tasks #1 and #2 (#2 is used for search detection task), WFOV/NFOV ratio, search time
- Output
  - echo of input
  - NFOV P(#1), P(#2), and P(#2,t) as functions of range
  - NFOV R(#1), R(#2) as functions of probability
  - Corresponding WFOV results (if any)

NVL ACQUIRE Model

- Uses FLIR90 model output as input
- FLIR90 predicts device-dependent performance parameters measurable in the laboratory
  - NETD (noise equivalent temperature difference)
  - MTF (modulation transfer function)
  - MRTD (minimum resolvable temperature difference)
- ACQUIRE accepts MRTD data and predicts field performance
  - probability of detection and recognition of military targets as a function of range
  - 2-D range performance
  - optional 1-D range performance
- NVL search model is embedded in ACQUIRE
  - allows time-dependent probability of detection analysis, given search period criterion

Modifications to LOWTRAN 7

- Adapted to be driven by EOSAEL 92 control program
- Change of input format to EOSAEL card order-independent format
- Addition of target contrast calculation
- Comparison to UV transmission models and data
- Documentation of LOWTRAN 7
  - upgrade to include new features:

    target contrast
    new aerosol models (e.g., desert model)
    multiple scattering of atmospheric radiance

HIGH-RESOLUTION SPECTRAL MEASUREMENTS OF UPWELLING AND DOWNWELLING ATMOSPHERIC INFRARED EMISSION WITH MICHELSON INTERFEROMETERS

H.E. Revercomb
University of Wisconsin - SSEC, 1225 W. Dayton Street, Madison, WI 53706

The University of Wisconsin Space Science and Engineering Center has developed instruments for the measurement of accurately calibrated atmospheric emission both from the ground and from an aircraft platform (NASA ER-2). These instruments have been used in recent field experiments to obtain extensive data sets of combined radiances and in-situ atmospheric measurements. Some of the interesting results from these experiments that will be presented include: clear air spectroscopic differences with line-by-line code, ice and liquid water cloud radiative signatures, and atmospheric state parameter retrievals from the infrared measurements. Results of comparisons of observations with FASCOD2 and Beta-FASCOD3 will be presented as well as the impact of improvements in the CO_2 line parameters over those found in HITRAN86.

COMPARISONS OF FASCODE SPECTRA WITH HIS OBSERVATIONS (II)

H.E. Revercomb, R.O. Knuteson, W.L. Smith,
H.M. Woolf*, and H.B. Howell*

University of Wisconsin
Space Science and Engineering Center
1225 West Dayton Street
Madison, WI 53706
USA

* NOAA/NESDIS Systems Design and Applications Branch,
1225 West Dayton Street, Madison, WI 53706

for
Annual Review Conference on
Atmospheric Transmission Models
Geophysics Laboratory
Hanscom AFB, MA

11-12 June 1991

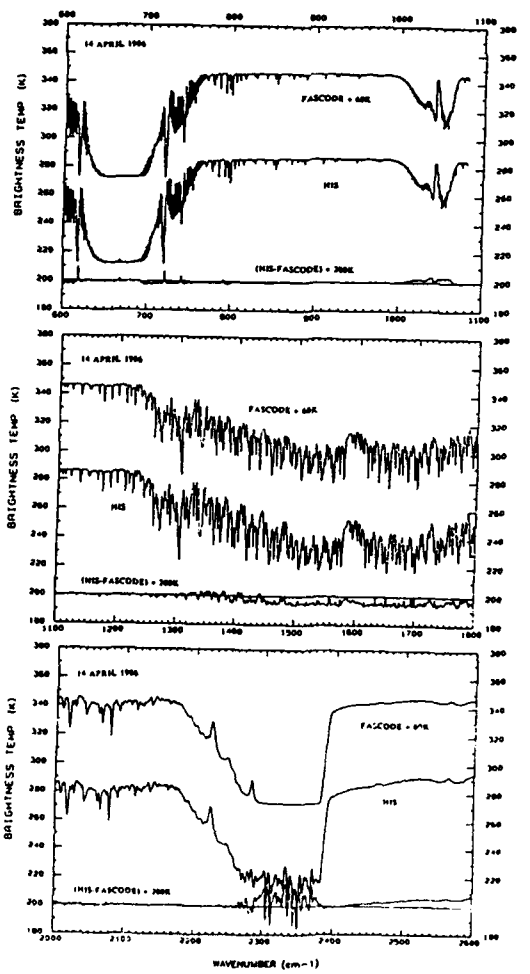
TOPICS

- HIS (High-resolution Interferometer Sounder) OBSERVATION HISTORY
- SUMMARY OF 1989 FASCOD2 / HIS COMPARISONS
- CO_2 RESULTS FROM FASCOD3
- NEW 1991 OBSERVATIONS

6-YEAR HISTORY OF ATMOSPHERIC OBSERVATIONS

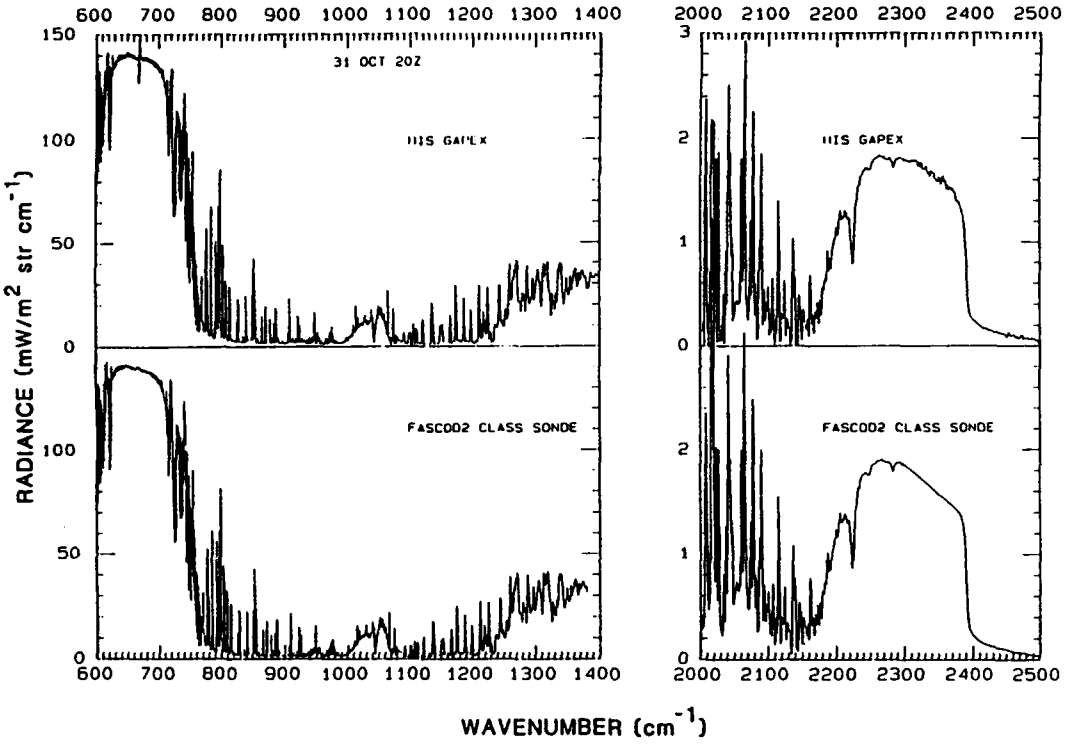
- NASA U2/ER2 AIRCRAFT (NADIR VIEWING)
  - KITT PEAK, APRIL 1986
  - COHMEX, JUNE / JULY 1986
  - FIRE, WISCONSIN, OCT / NOV 1986
  - NASA AMES, PACIFIC OCEAN, MAY 1991
  - CAPE, SERON, FIRE; 2ND HALF 1991
- NOAA P3 AIRCRAFT (NADIR VIEWING)
  - MIAMI, 1 TEST FLIGHT, NOV 1988
- GROUND BASED (ZENITH VIEWING)
  - MADISON, NOV 1986
  - GAPEX, DENVER, OCT / NOV 1988
  - MADISON / LIDAR, NOV / DEC 1989
  - WISP: COLORADO, FEB / MAR 1991
  - NSF SHIP, POINT SUR, MAY 1991

High-Altitude Aircraft Measurements of Upwelling IR Radiance

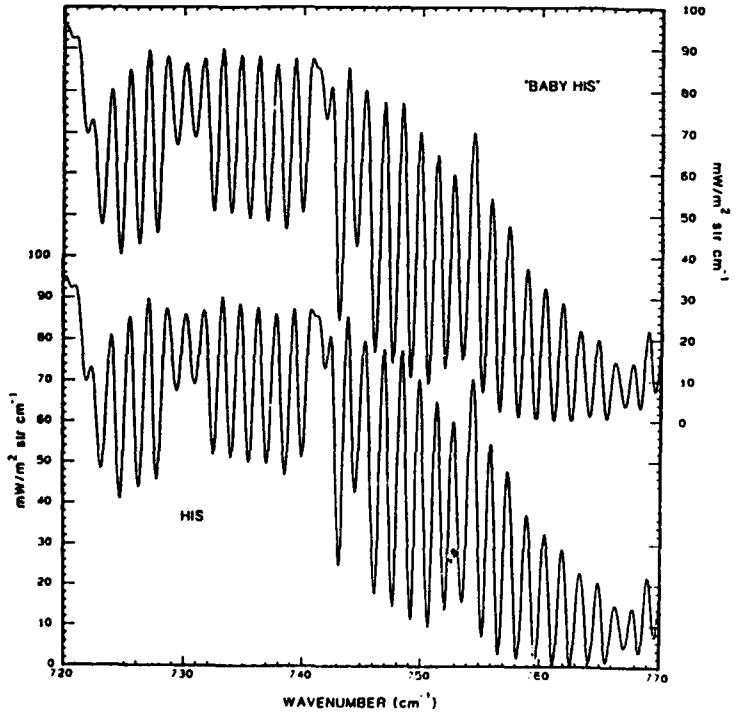


HIS GROUND-BASED OBSERVATIONS
(Downwelling Compared to FASCODE)

University of Wisconsin
Space Science and Engineering Center



University of Wisconsin
Space Science and Engineering Center

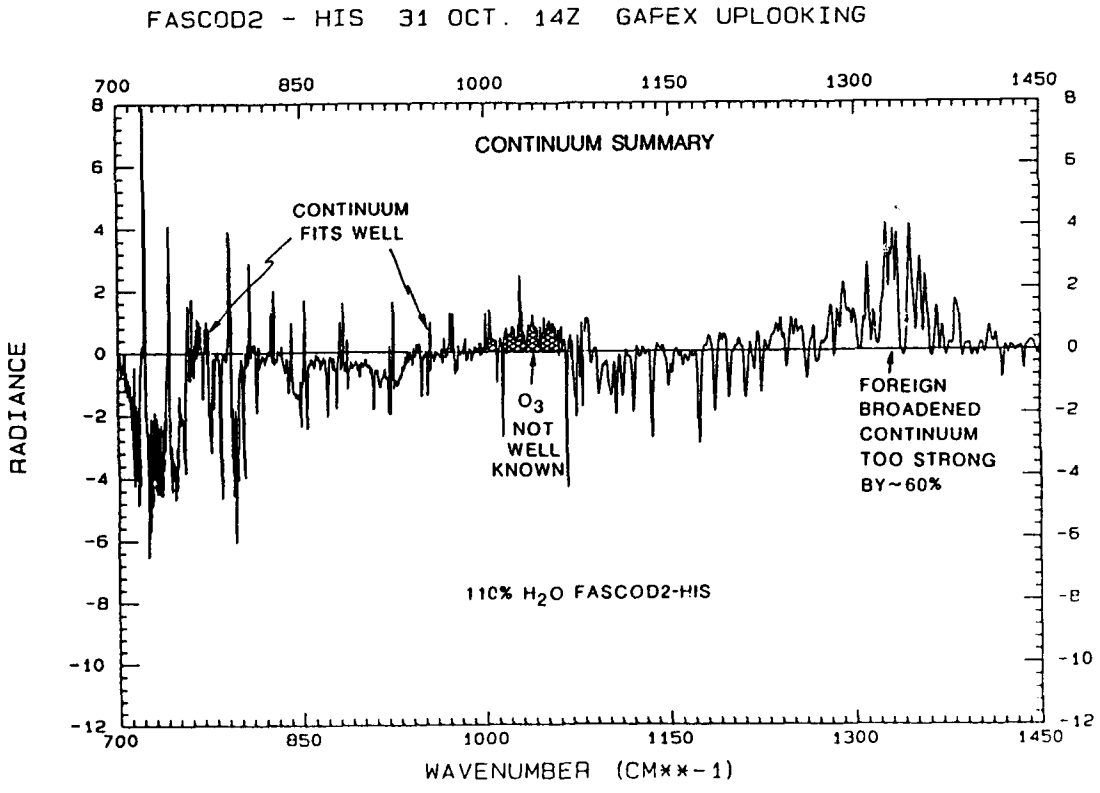


DEMONSTRATION OF ABSOLUTE RADIOMETRY
(Intercomparison of 2 different interferometric systems)

H_2O CONTINUUM: 1989 Summary

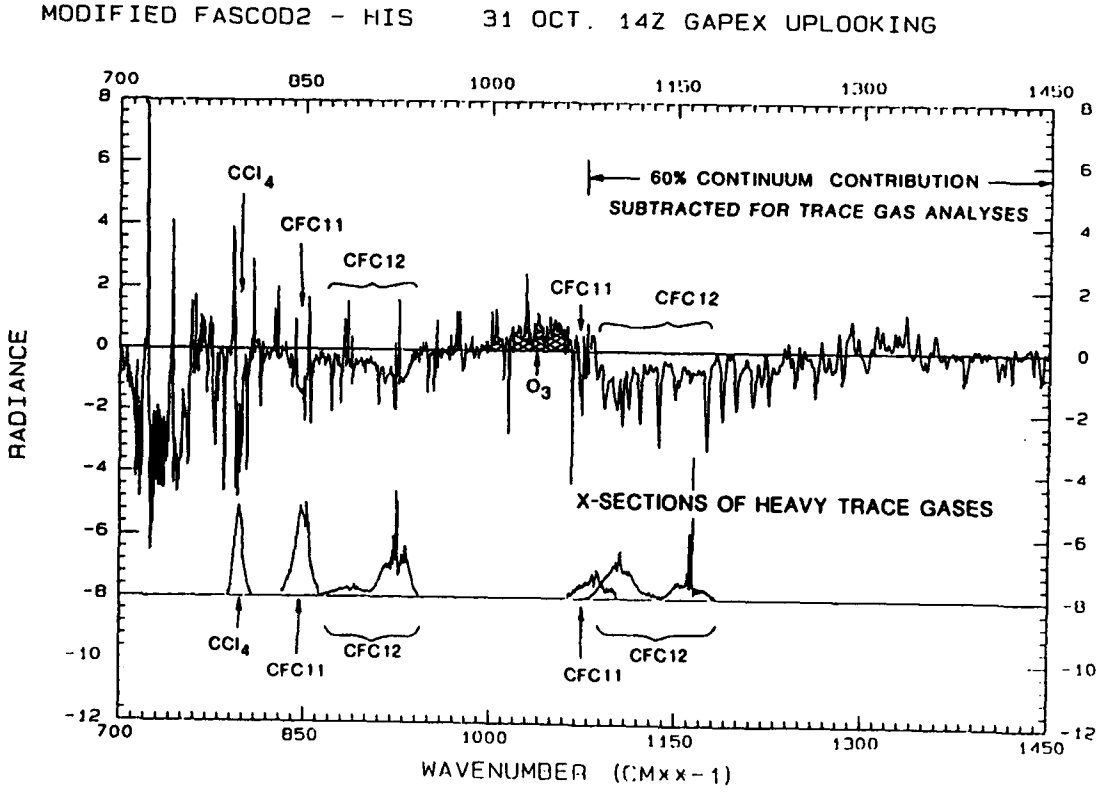
- HIS AGREES REASONABLY WELL WITH FASCOD2 FROM 750 TO 1000 cm^{-1} (10 TO 13 μm) (A 10% increase of the continuum strength would improve agreement)

- REDUCTION OF THE FOREIGN-BROADENING CONTINUUM BY 60% BETWEEN 1300 AND 1400 cm^{-1} (8 TO 9 μm) WOULD ACCOUNT FOR THE DISCREPANCY BETWEEN HIS AND FASCOD2 FOR DRY ATMOSPHERES.



TRACE GASES: 1989 Summary

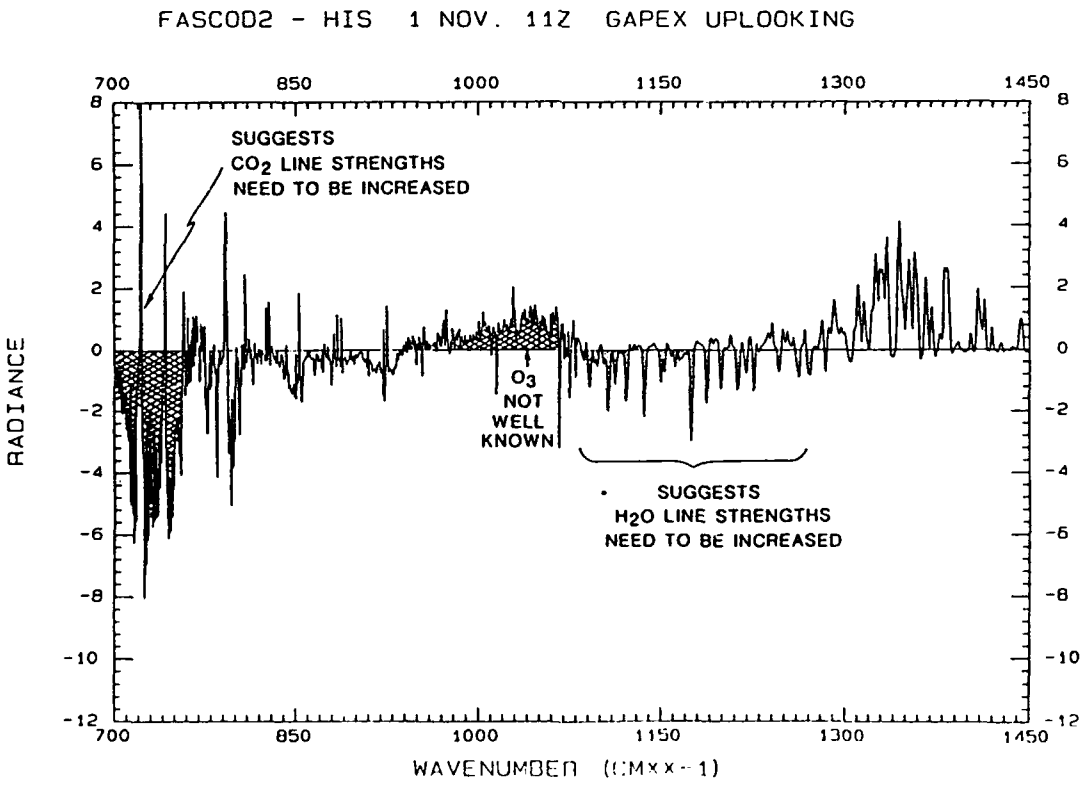
- CFC 11 AND CFC 12 ARE IDENTIFIABLE IN THE REGION FROM 1050 TO 1200 cm^{-1}, IN ADDITION TO THE REGION PREVIOUSLY IDENTIFIED FROM 840 TO 940 cm^{-1}
- CCl_4 IS IDENTIFIABLE CENTERED AT ABOUT 800 cm^{-1}



LINE STRENGTH ADJUSTMENTS:
1989 Summary

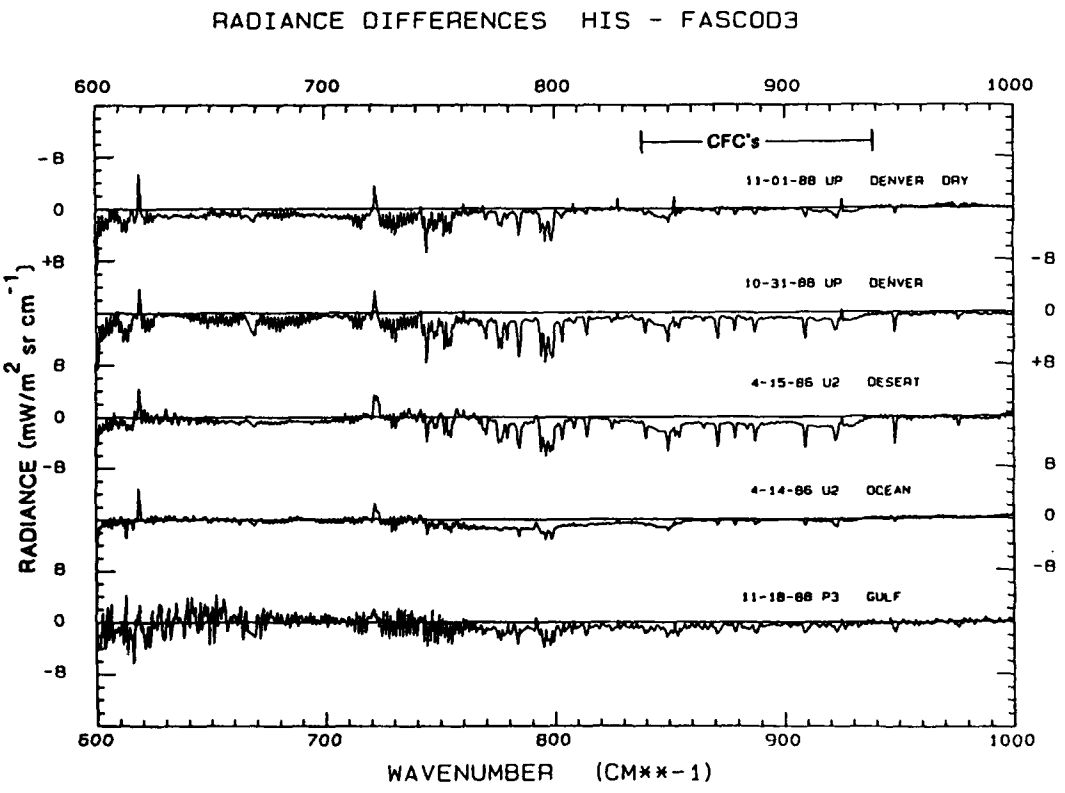
- H_2O LINE STRENGTHS FROM 1090 TO 1200 cm^{-1} NEED ABOUT 30% INCREASE

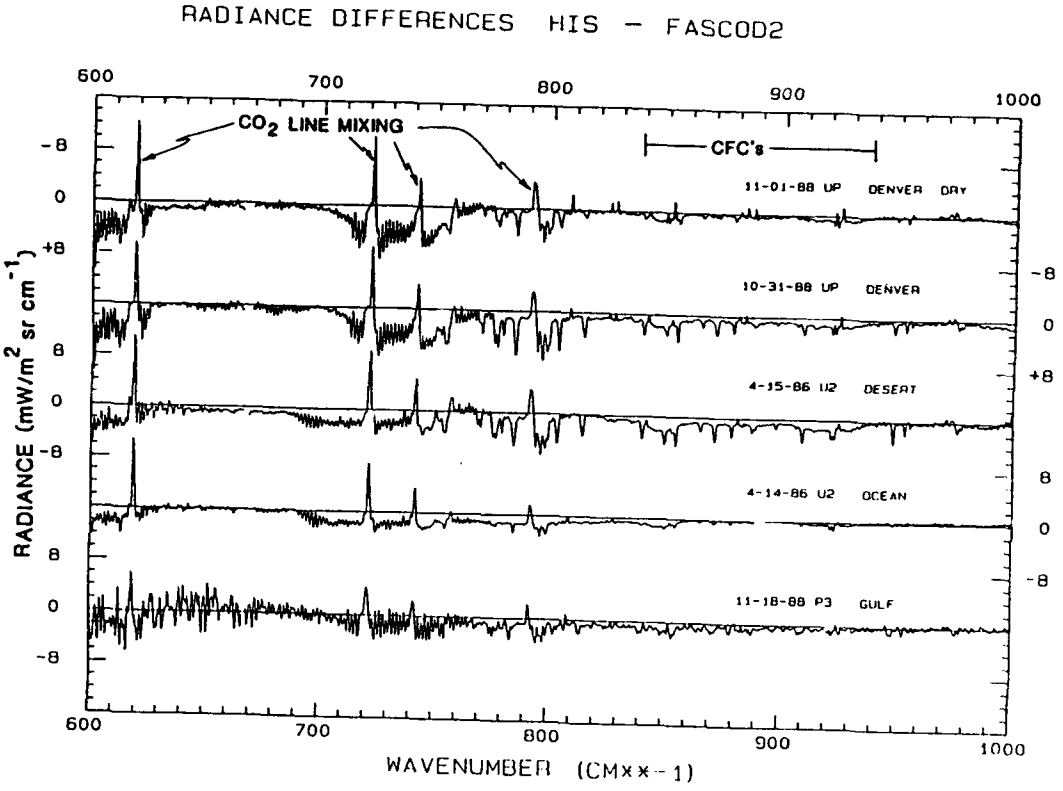
- CO_2 LINE STRENGTHS FROM ABOUT 700 TO 760 cm^{-1} NEED TO BE INCREASED



CO_2 RESULTS FOR FASCOD3

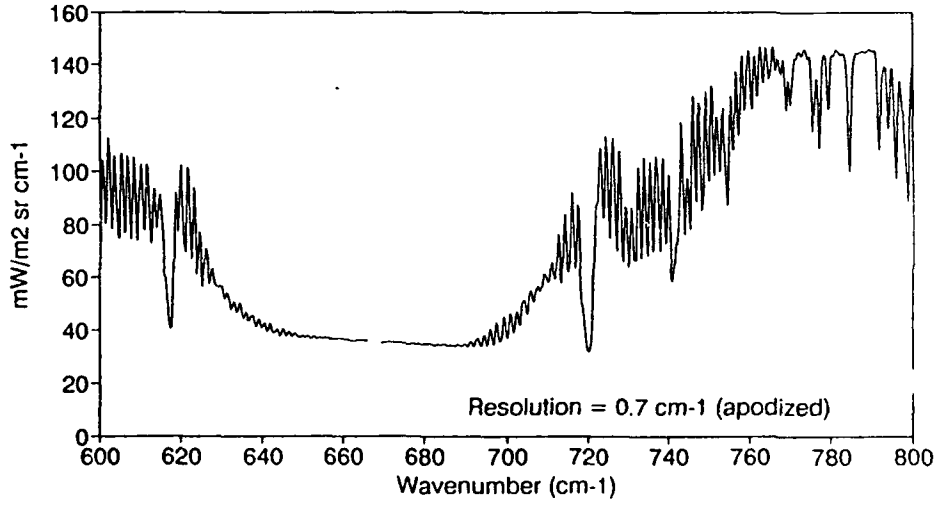
- AUGUST 1990 BETA TEST VERSION OF FASCOD3
- 1990 WATTSON / ROTHMAN CO_2 LINES
- RINSLAND H_2O LINES AUGMENTING HITRAN '86





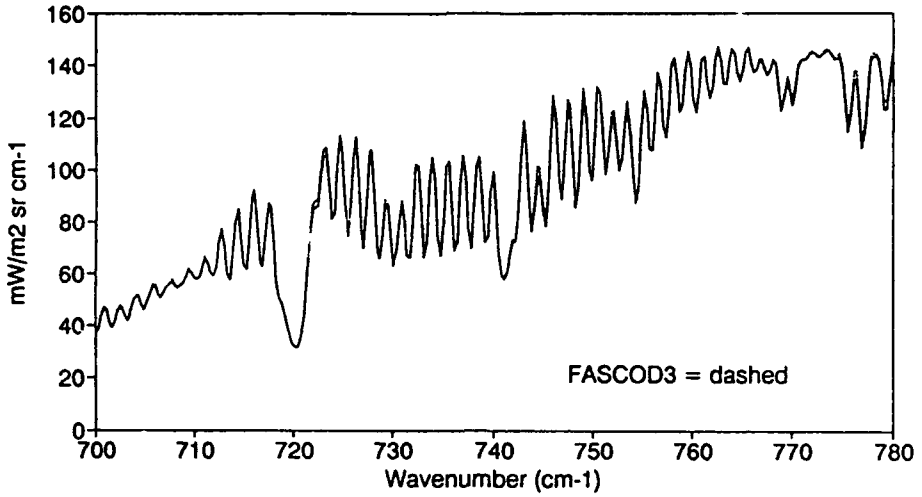
HIS

Downlooking: April 15, 1986



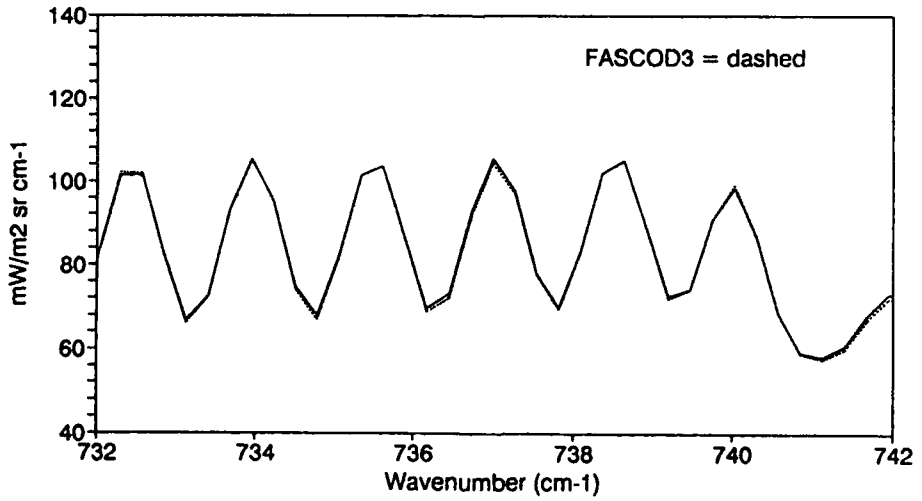
HIS & FASCOD3

Downlooking: April 15, 1986

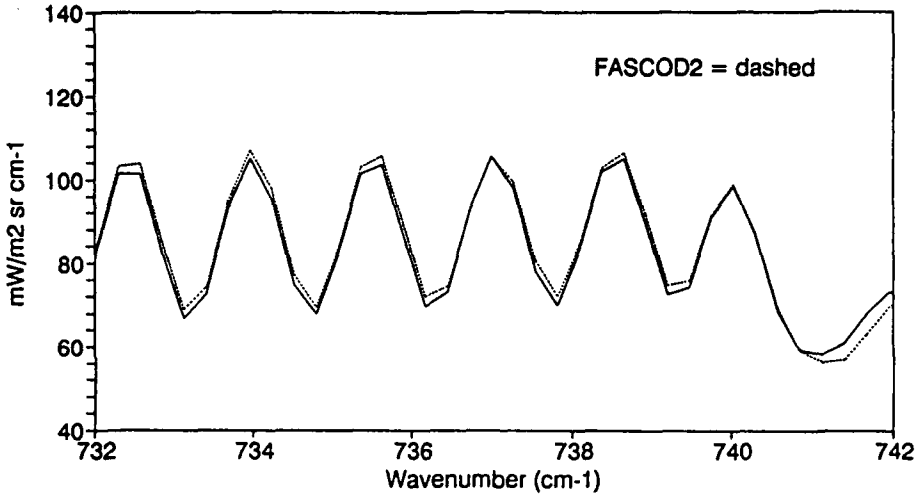


HIS & FASCOD3

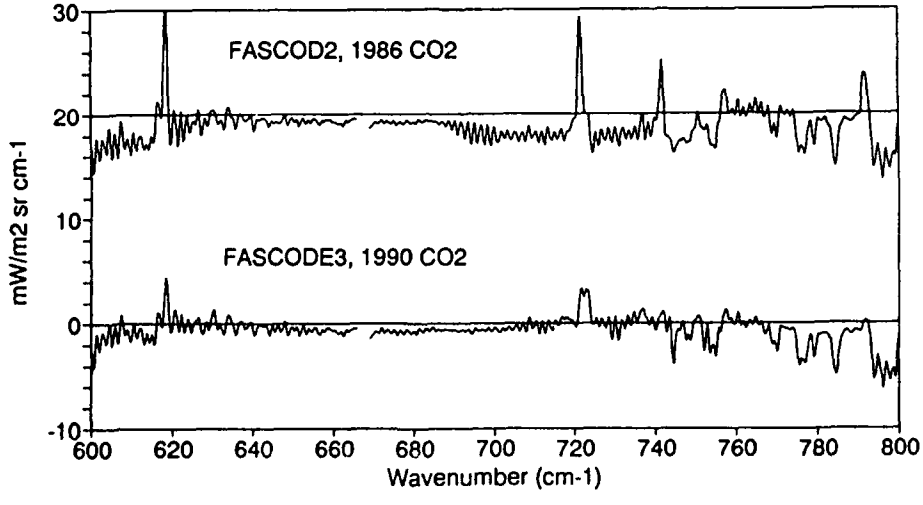
Downlooking: April 15, 1986



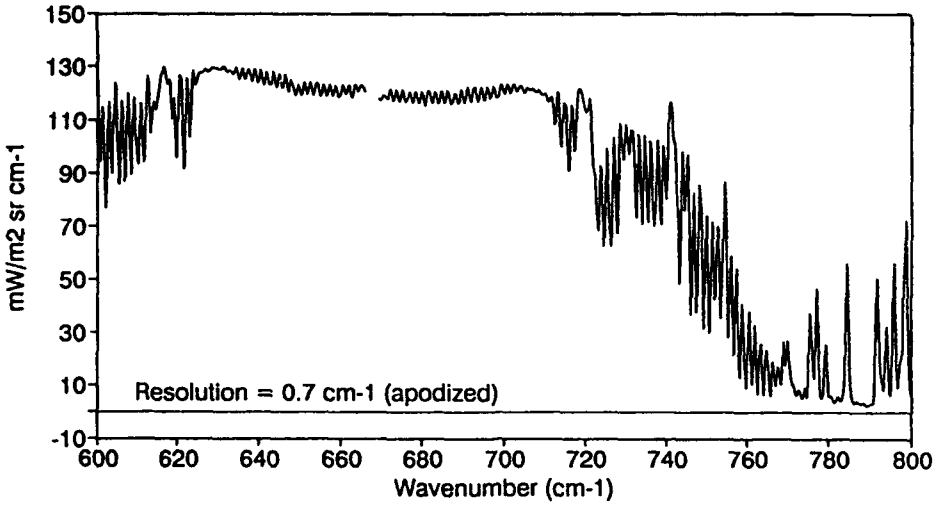
HIS & FASCOD2
Downlooking: April 15, 1986



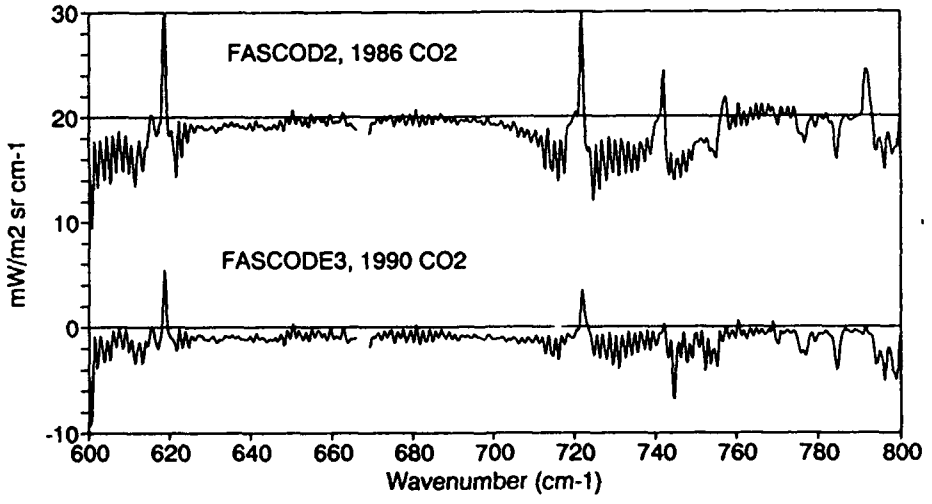
-FASCODE+ HIS
Downlooking: April 15, 1986



HIS
Uplooking: Nov 1, 1988 (11Z)

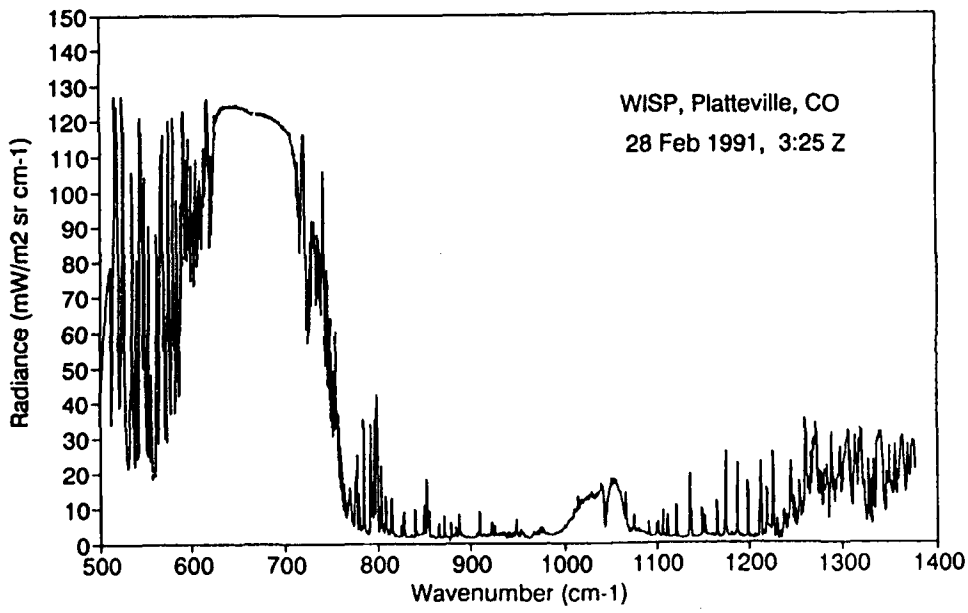


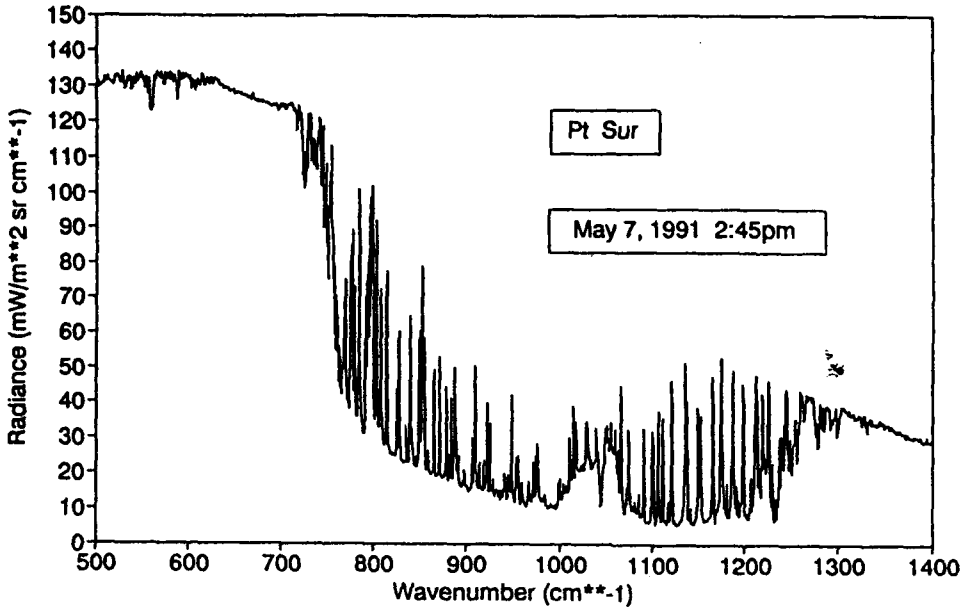
FASCODE - HIS
Uplooking: Nov 1, 1988 (11Z)

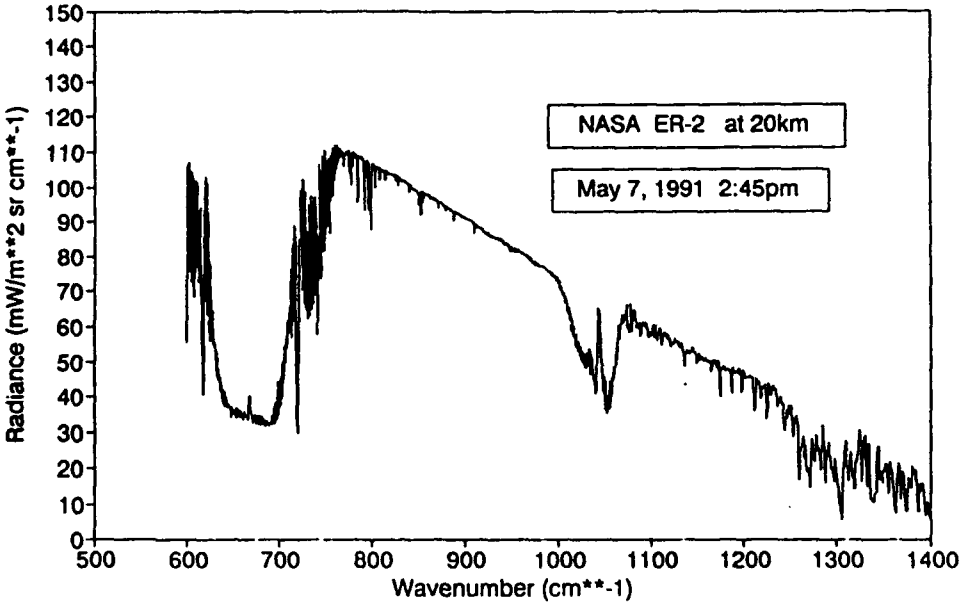


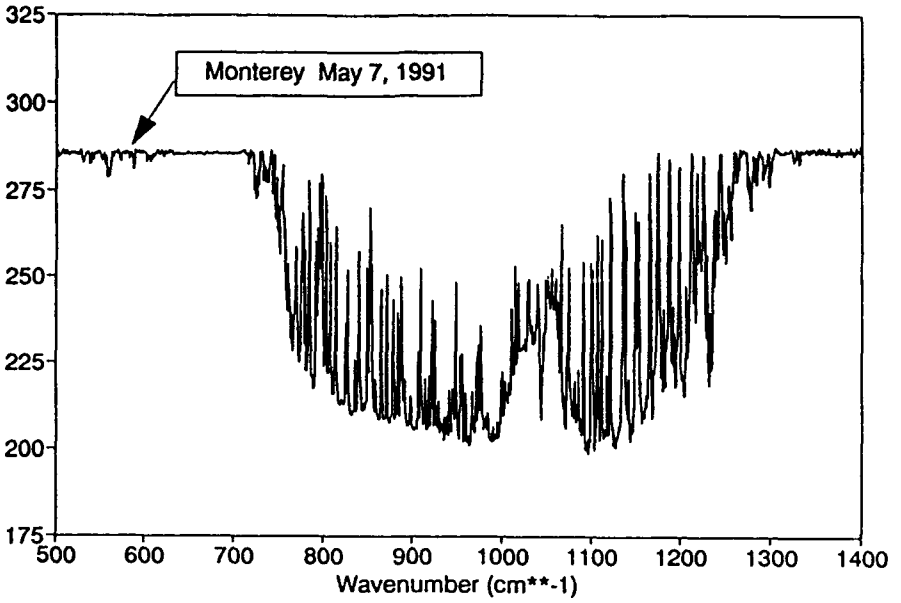
NEW 1991 OBSERVATIONS

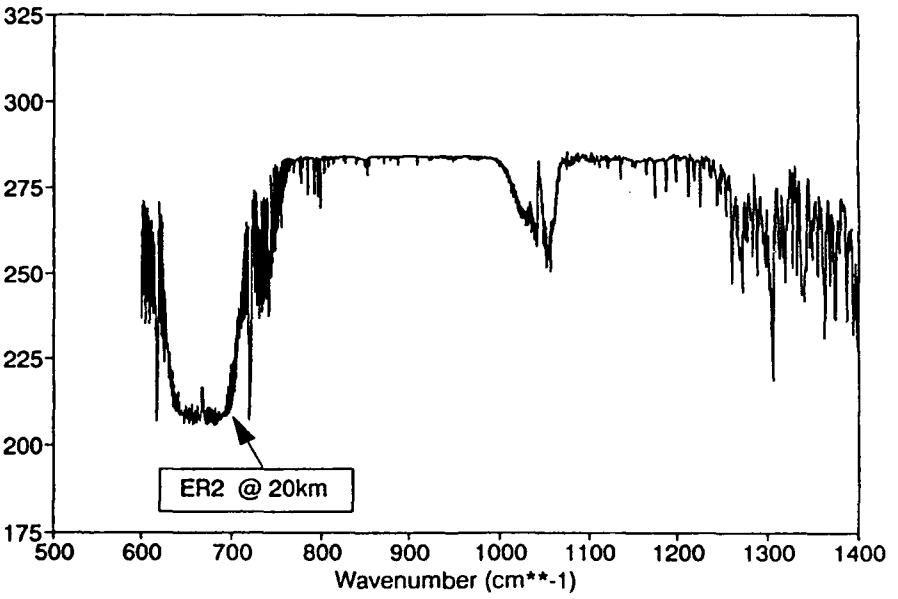
- PLATTEVILLE, COLORADO (WISP): UPLOOKING, VERY DRY, 26 FEB - 15 MAR 1991
- PACIFIC OCEAN, OFF MONTEREY: UPLOOKING FROM SHIP "PT SUR" & DOWNLOOKING FROM NASA ER2, VERY MOIST, 7-9 MAY 1991
- CAPE CANAVERAL (CAPE) & SOUTHEAST US (SERON): DOWNLOOKING FROM NASA ER2, JULY-AUGUST 1991
- COFFEYVILLE, KANSAS (FIRE & SPECTRE): DOWNLOOKING FROM NASA ER2 & UPLOOKING, NOV-DEC 1991




Pt Sur
May 7, 1991 2:45pm
Radiance (mW/m**2 sr cm**-1)
Wavenumber (cm**-1)
150
140
130
120
110
100
90
80
70
60
50
40
30
20
10
0
500
600
700
800
900
1000
1100
1200
1300
1400


NASA ER-2 at 20km
May 7, 1991 2:45pm
Radiance (mW/m**2 sr cm**-1)
Wavenumber (cm**-1)
150
140
130
120
110
100
90
80
70
60
50
40
30
20
10
0
500
600
700
800
900
1000
1100
1200
1300
1400


Monterey May 7, 1991
325
300
275
250
225
200
175
500
600
700
800
900
1000
1100
1200
1300
1400
Wavenumber (cm**-1)


ER2 @ 20km
325
300
275
250
225
200
175
500
600
700
800
900
1000
1100
1200
1300
1400
Wavenumber (cm**-1)

SUMMARY

- FASCOD3 WITH LINE MIXING AND THE NEW WATTSON / ROTHMAN CO2 LINES SUBSTANTIALLY IMPROVES AGREEMENT WITH HIS OBSERVATIONS IN THE 15 μm REGION.

- NEW HIS OBSERVATIONS FOR DIFFERENT ATMOSPHERIC CONDITIONS HAVE BEEN ACQUIRED DURING 1991 AND MORE ARE EXPECTED.

VALIDATION OF HIS SPECTRAL MEASUREMENTS WITH THE FASCODE LINE-BY-LINE MODEL

S.A. Clough, R.D Worsham
Atmospheric and Environmental Research, Inc., 840 Memorial Drive, Cambridge, MA 02139

G.P. Anderson, M.L. Hoke, F.X. Kneizys
Geophysics Laboratory (OP), Hanscom AFB, MA 01731

M. Wagner, R.M. Goody
Harvard University, Department of Applied Sciences, Pierce Hall, Cambridge, MA 02138

An extended version of FASCODE (Clough et al., 1986) has been utilized in conjunction with the GL HITRAN database (Rothman et al., 1987) and carbon dioxide line coupling coefficients (Hoke et al., 1988), to perform spectral radiance comparisons with data from the High-Resolution Interferometer Sounder (HIS; Revercomb et al., 1987). Validations have been performed with down viewing spectra from 19.6 km and up viewing spectra from the surface for the 600-1100 cm^{-1} spectral region. Effects that are observed include improvements relating to the 1991 HITRAN line parameters for water vapor and carbon dioxide, line coupling effects in carbon dioxide and absorption by anthropogenic molecules including CCl_4, CFC11, and CFC12. Of particular interest is the apparent effect of attenuation by sub-visual cirrus clouds and the correlation of the spectral residuals with carbon dioxide quantum number.



Validation of HIS Spectral Measurements with the FASCODE Line-by-Line Model

S.A. Clough — Atmospheric and Environmental Research, Inc.
R.D. Worsham

W.L. Smith — University of Wisconsin
H.E. Revercomb
R.O. Knuteson
H.M. Woolf

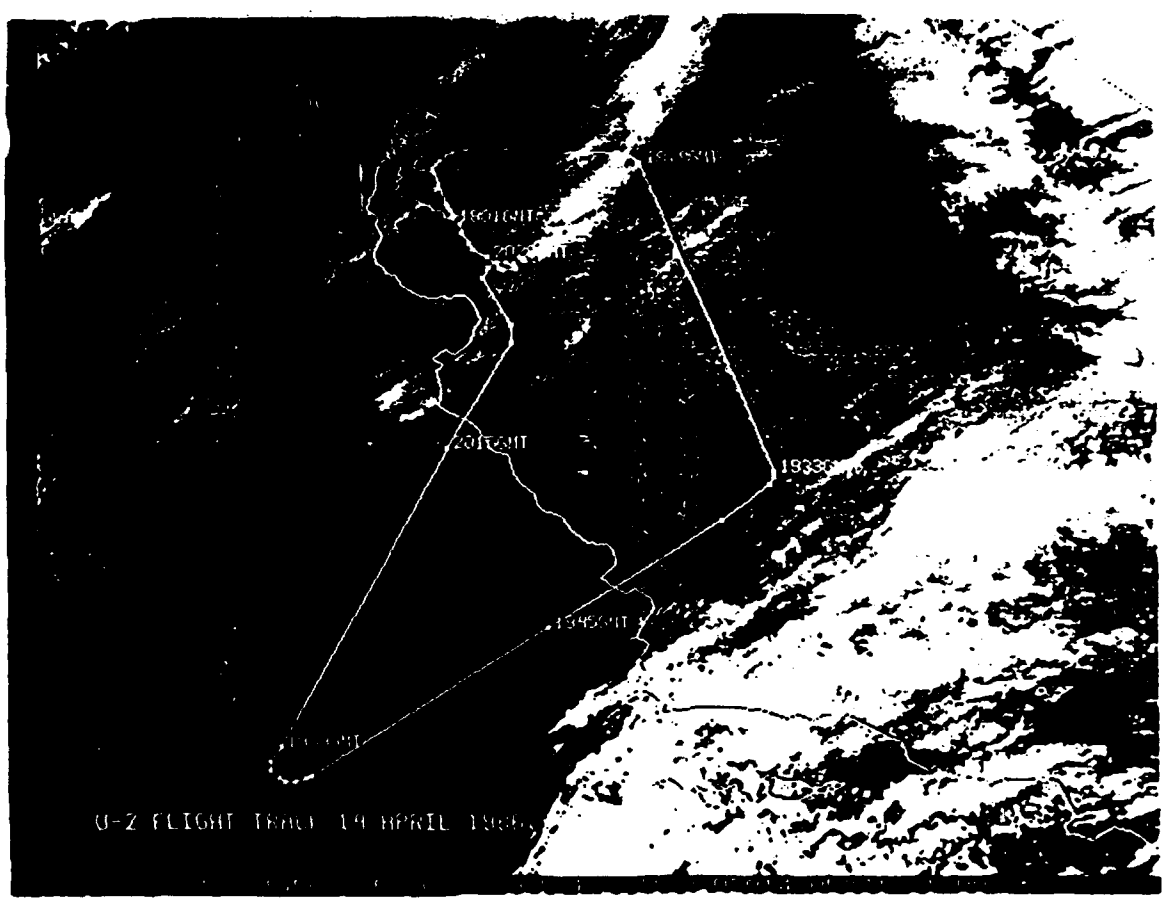
G.P. Anderson — Geophysics Directorate
M.L. Hoke
F.X. Kneizys

M.V. Wagner — Harvard University
R.M. Goody

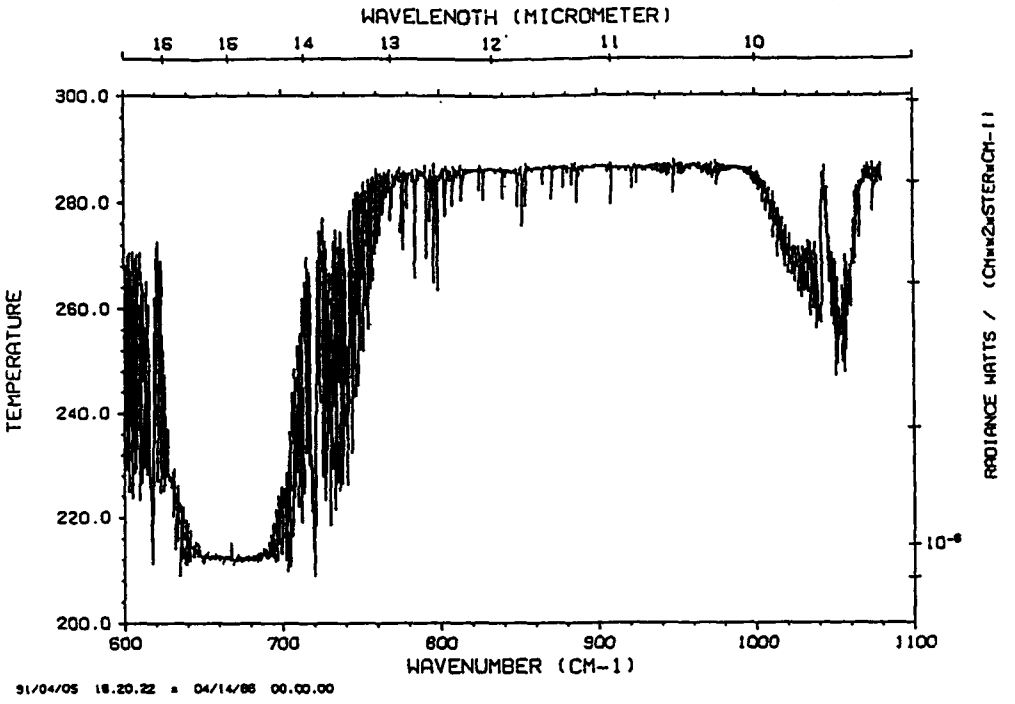


Platform	U2
Altitude	19.6 km
View	nadir
Surface	ocean
Instrument Temp.	ambient
Resolution (unappodized)	0.365 cm-1
Photometric Calibration	
absolute	~1K
relative	~0.5K




U-Z FLIGHT TRACK 19 APRIL 1988

Radiance spectrum in equivalent brightness temperature for the long wave spectral region from 600 to 1100 cm^{-1}. The data were taken with the U. of Wisconsin High-Resolution Interferometer Sounder (HIS), Smith et al. (1983).



aer

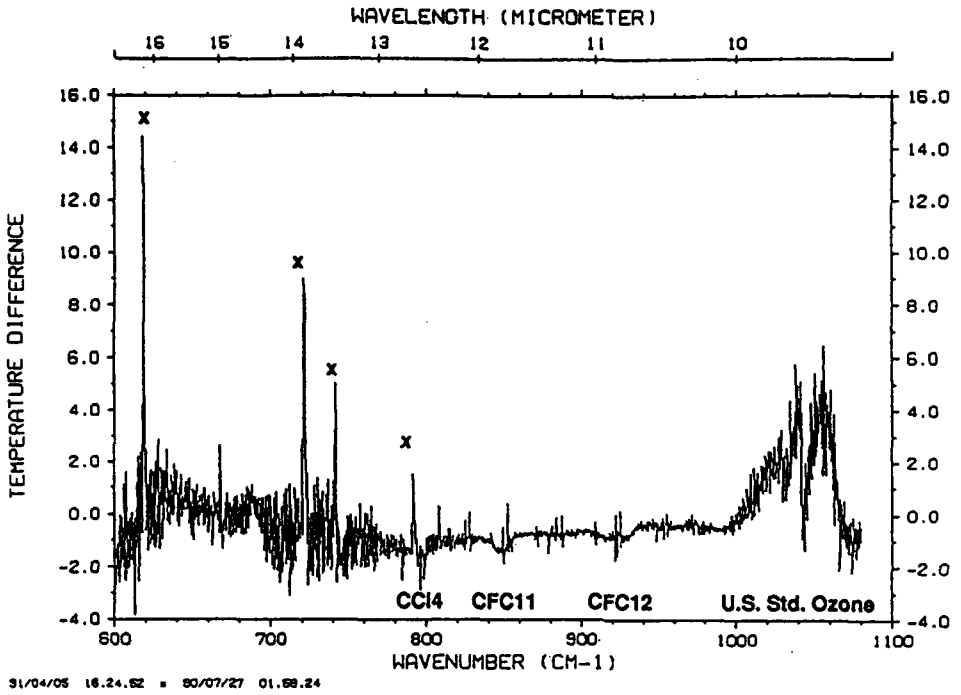
HIS/FASCODE Comparison

Data : unappodized
field of view correction in time domain
FFT to spectral domain

Calculation: line by line (FASCODE)
sinc scanning function
radiances at same spectral values as data

HIS - Calculated

HITRAN 86 Line Parameters

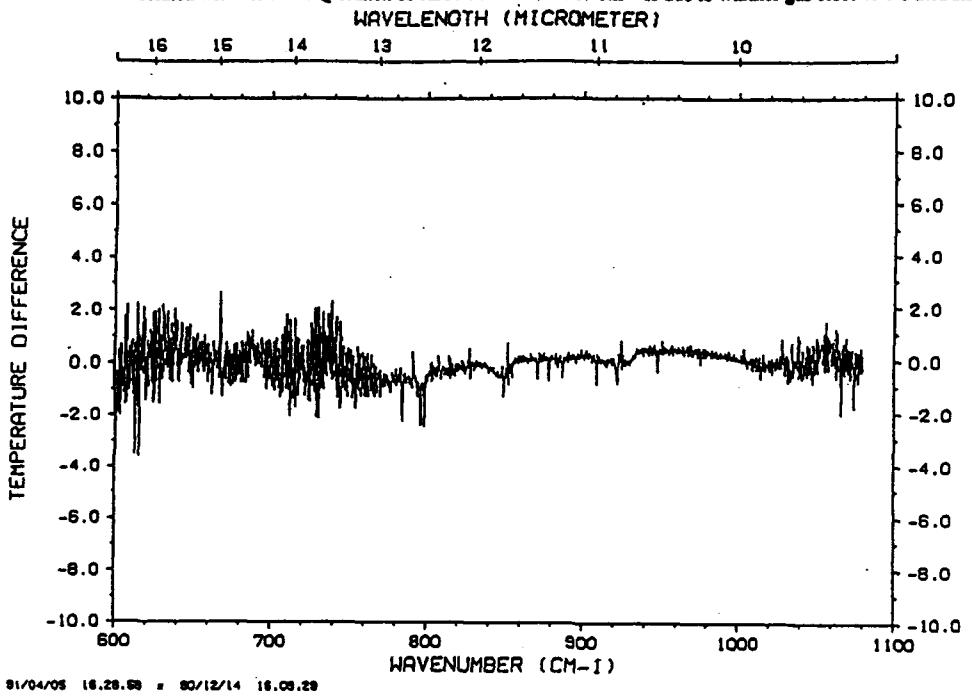


x - line mixing: CO2 Q branches

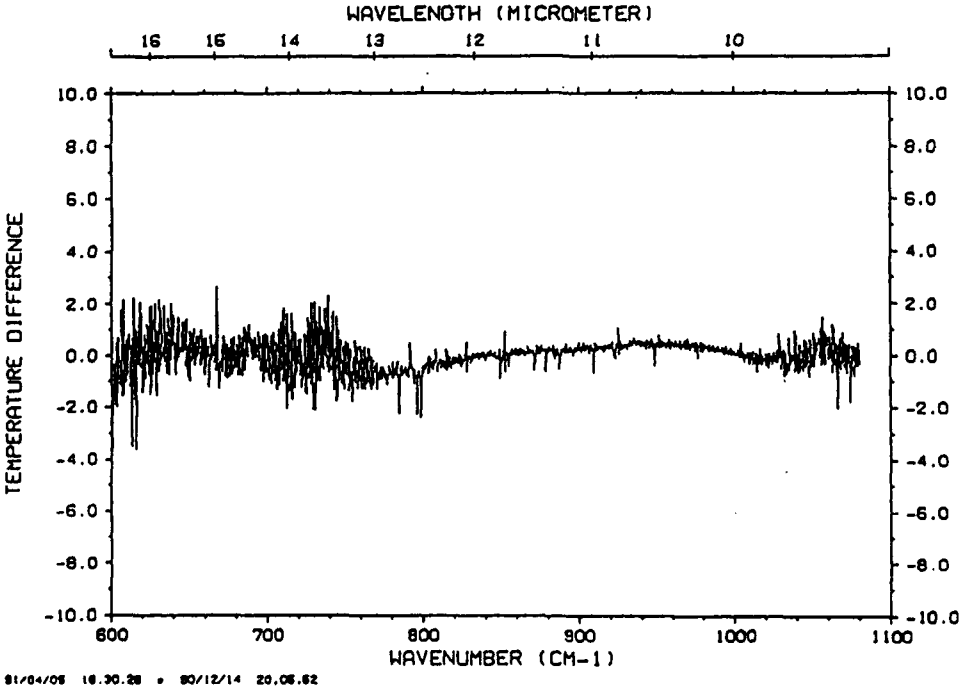
Parameters for FASCODE Calculation

Spectral parameters	**1986 HITRAN database**
Temperature profile	**radiosonde**
Water vapor profile	**radiosonde**
Ozone profile	**U.S. Standard profile**
Surface temperature	**obtained from window radiance**

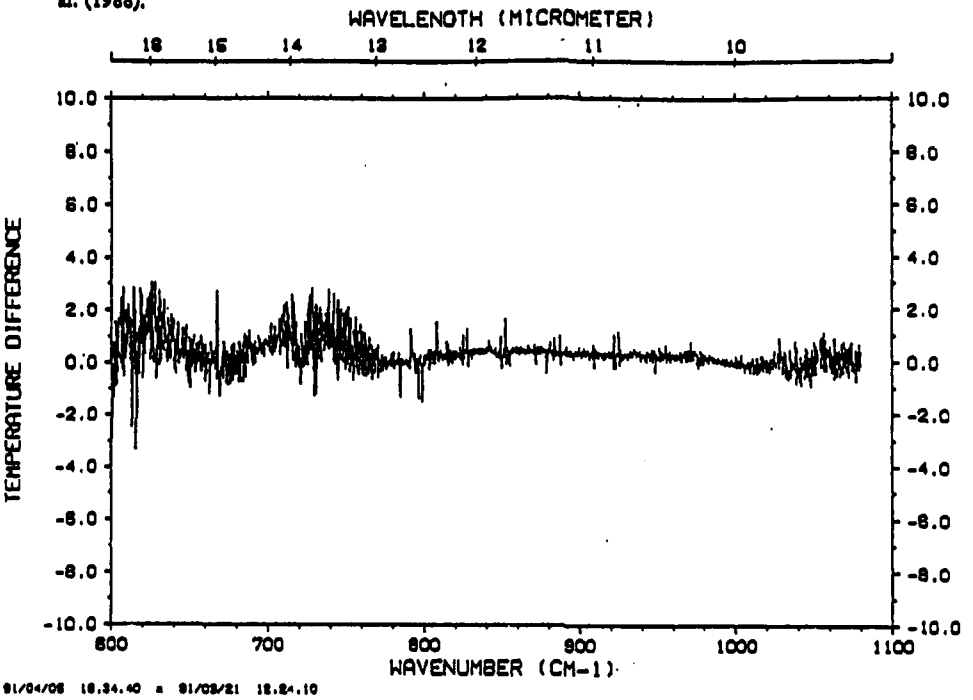
The effects of line coupling including its temperature dependence have been accounted for using the line coupling coefficients of Hoke et al. (1988) multiplied by a factor of 1.3 based on this and related spectra. Essential to these results are improved interim carbon dioxide line parameters provided by L.S. Rothman (1990). The improvements in the carbon dioxide line intensities are qualitatively consistent with those developed for ATMOS, Brown et al. (1987). The residuals for ozone have been reduced through the application of a retrieval algorithm to obtain an improved ozone profile. The remaining residual associated with the main Q-branch of carbon dioxide at 667 cm^{-1} is due to warmer gas close to the instrument.



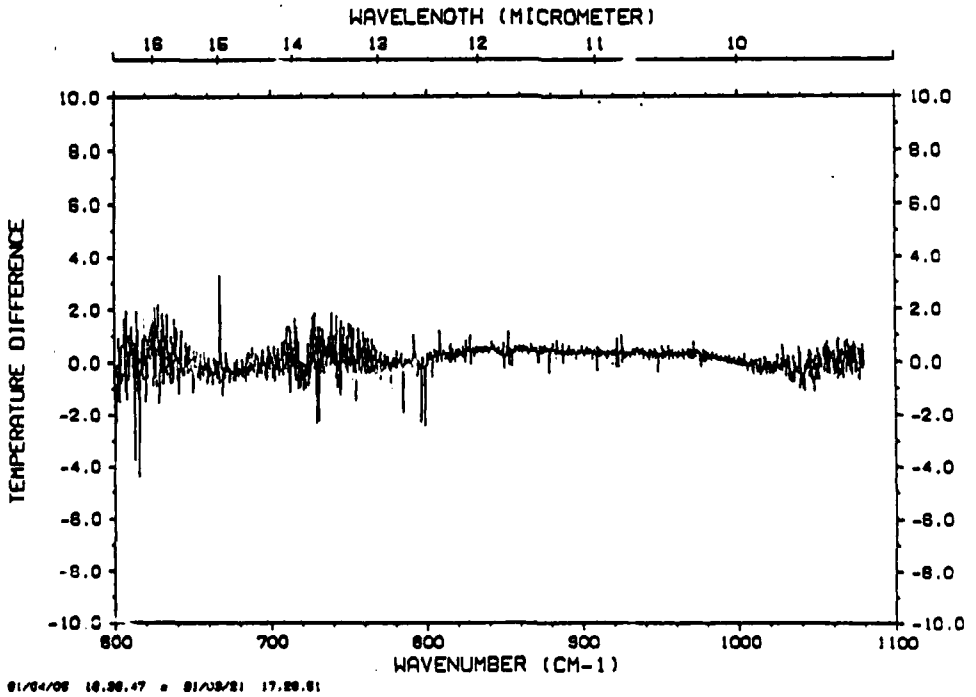
The same as the previous figure except that the effects of the absorption by the heavy molecules have now been included. This has been accomplished by using the cross sections of Massie et al. (1985) and the mixing ratios from the AER/NASA community model. The broad spectral features associated with CCl_4, CFC11 and CFC12 are well accounted for.



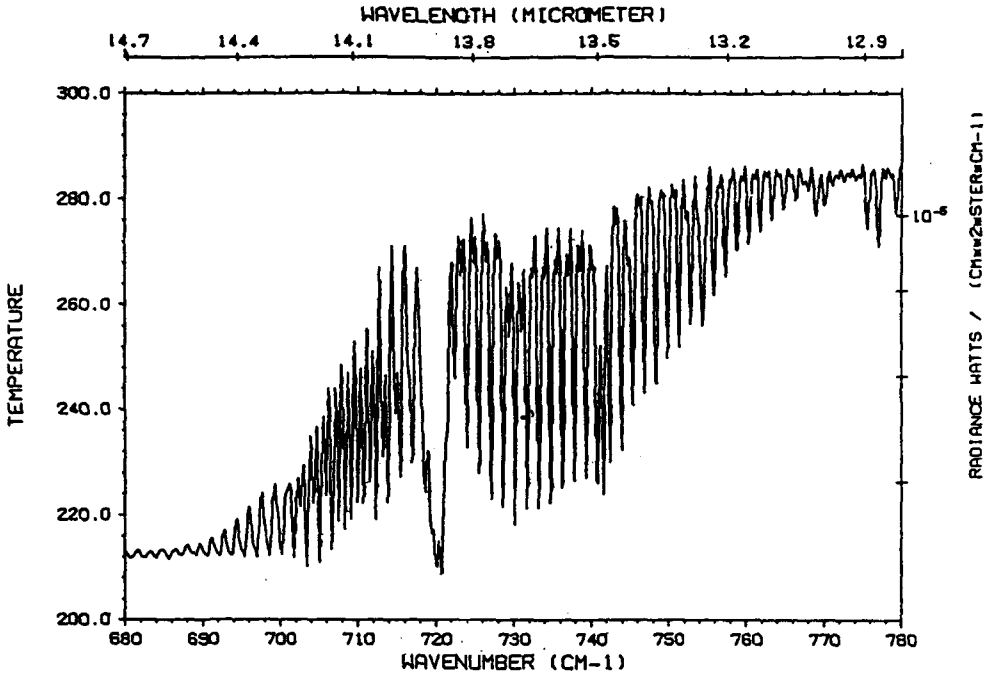
The same as the previous figures except that the effects of extinction due to a thin cirrus cloud at 13km have been included. The cloud has an optical thickness of 0.05 at 0.55 microns. For computational expediency conservative scattering has been invoked. The cloud model used for this example is one developed for LOWTRAN7 by Eric Shettle; spherical particles are assumed with a mode radius of four microns. The spectral characteristic of this cloud type provides a marked improvement in the spectral residuals. The idea of looking at this issue had its origins with the paper by Prabhakara et al. (1988).



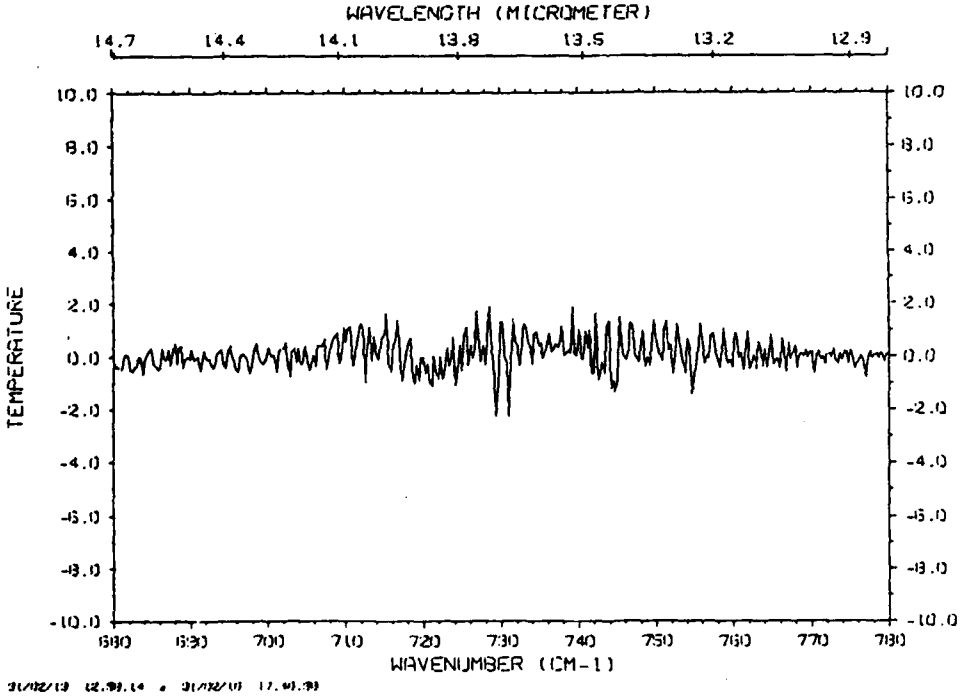
The effect on the spectral residuals of performing a temperature retrieval based on the spectral interval from 680-780 cm^{-1}. It may be noted that the mean error is improved from Fig. 5, but that the rms error about the mean is not greatly improved. Most of the irregular spaced residuals are due to incorrect intensities of pure rotational water lines.

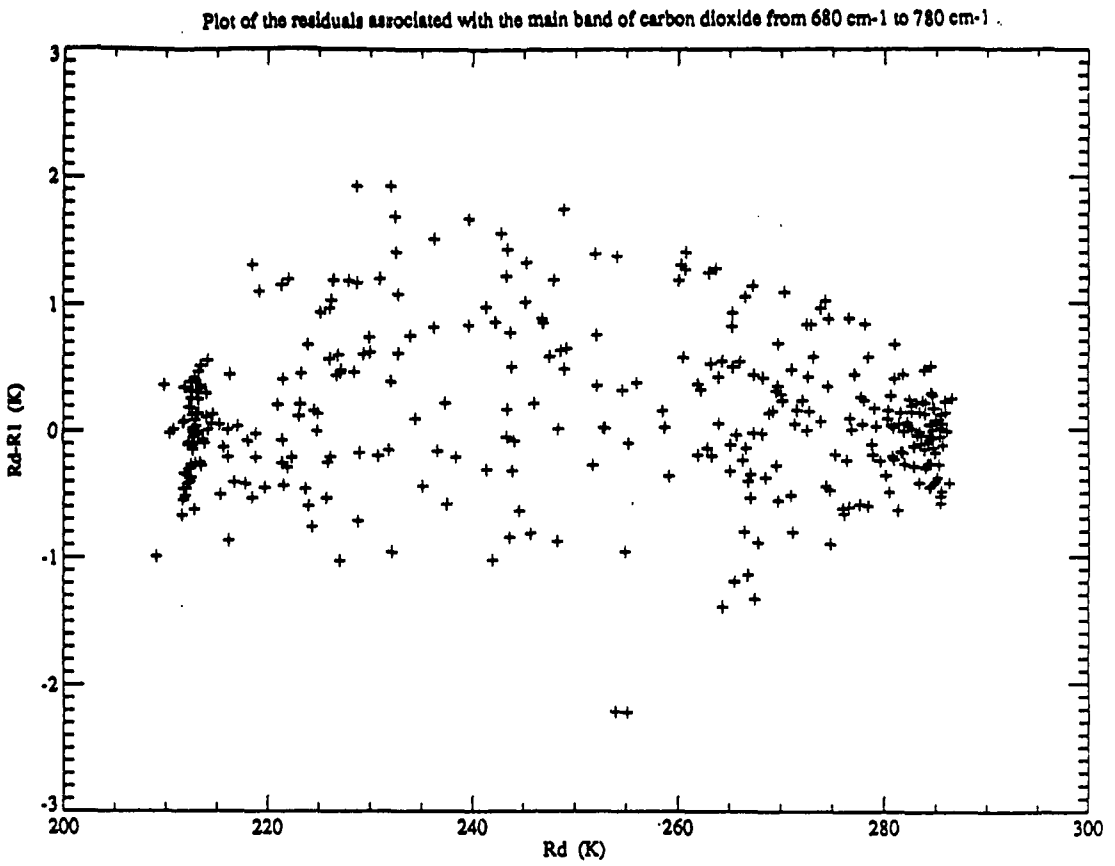


Radiance spectrum in equivalent brightness temperature for the long wave spectral region from 680 to 780 cm^{-1}. The data were taken with the U. of Wisconsin High-Resolution Interferometer Sounder (HIS), Smith et al. (1983).



The difference spectrum in equivalent brightness temperature between the HIS spectrum and a calculated spectrum using an advanced version of FASCODE.





aer

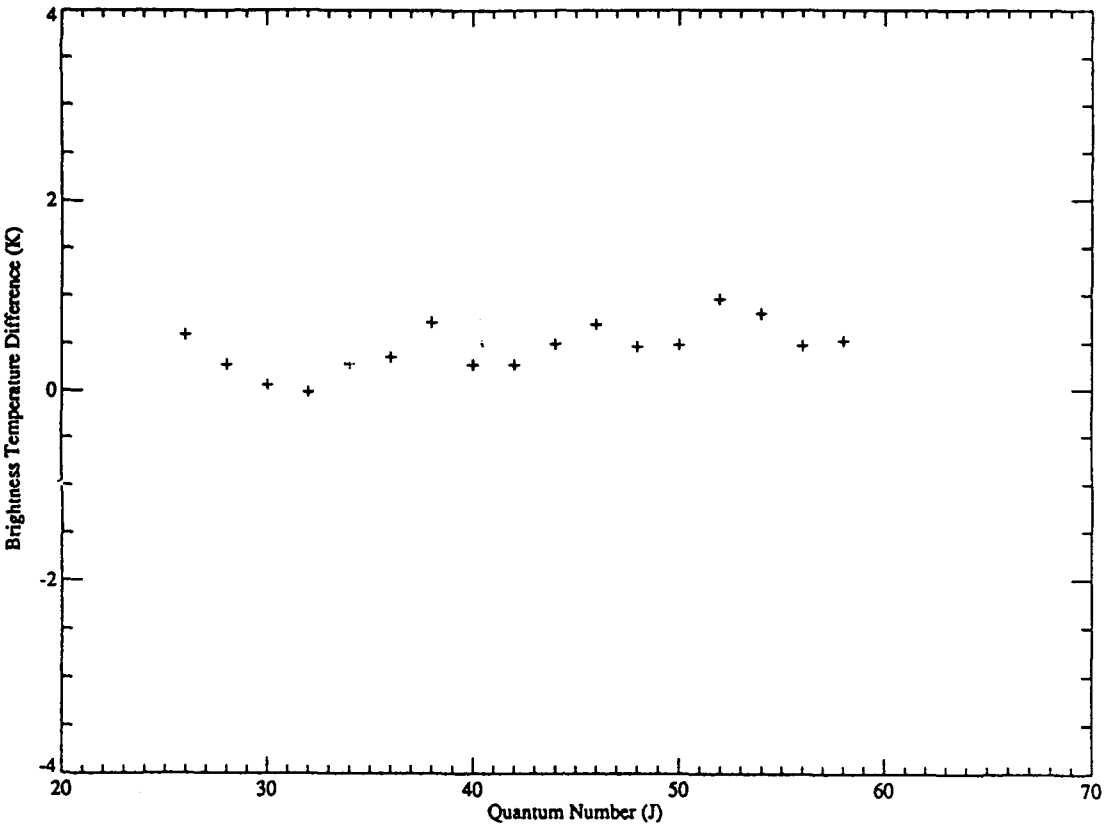
Residual Correlations

1) residuals vs. brightness temp. 680-780
   a) all points
   b) peaks
   c) valleys

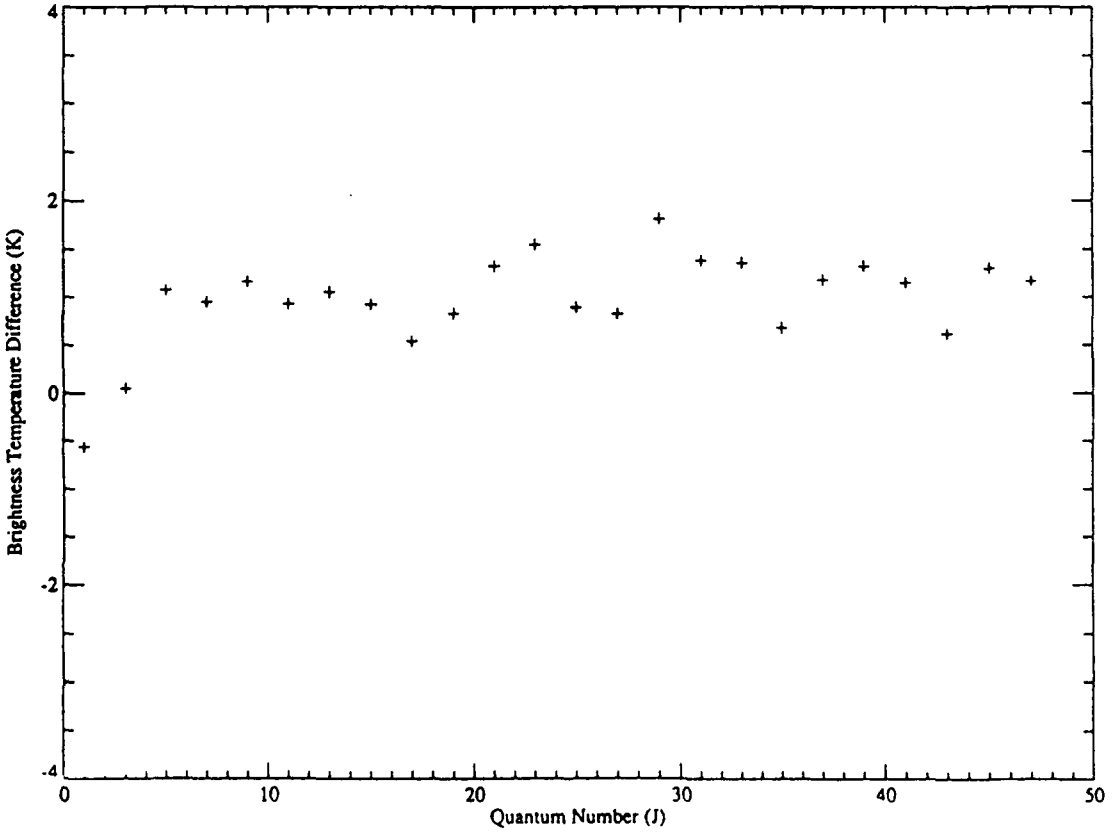
2) residuals vs. brightness temp. for reduced spectral regions

3) residuals vs. quantum number by band
   a) 667 2-1
   b) 720 5-2

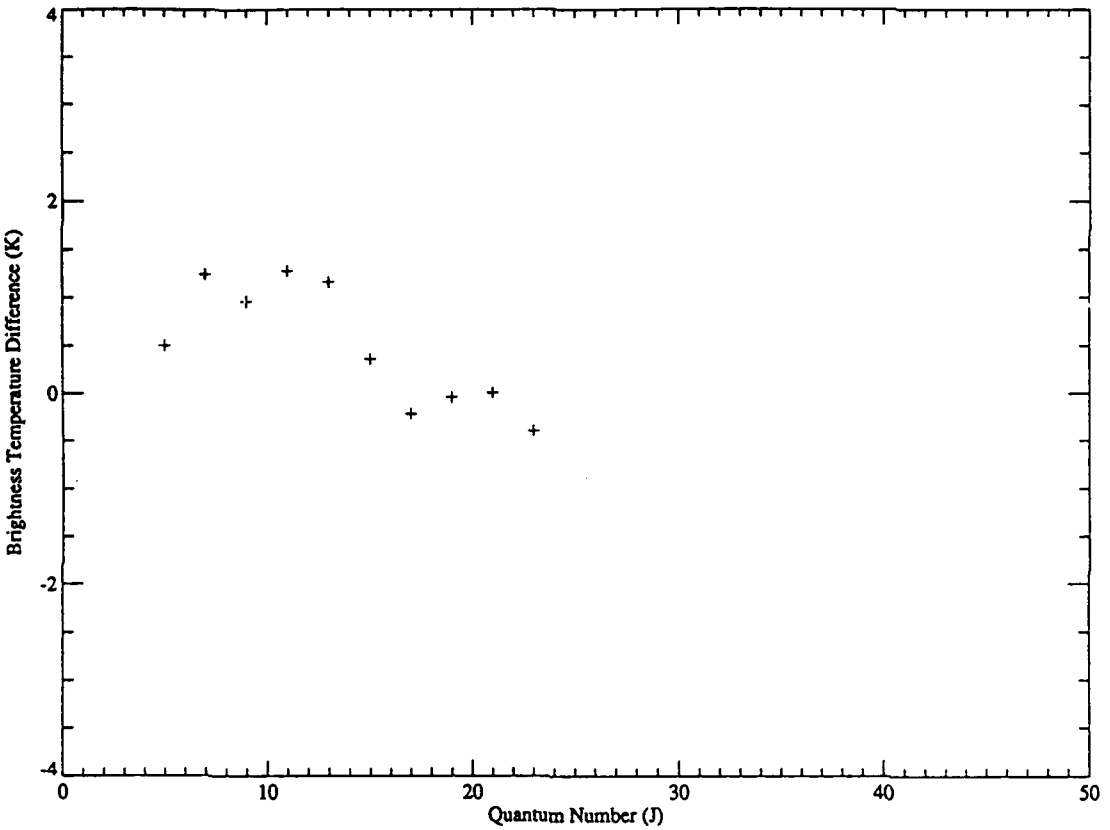
- residuals at the peak
  - doubly sampled data from U. of Wisconsin - 4 point interpolation
  - doubled the sampling frequency for calibration - 4 point interpolation



Band 2-1, R lines.



Band 5-2, R lines.



Band 5-2, P lines.

aer

Summary

Conclusions:

- data are extremely good
- '91 line parameters significantly better than '86
- line coupling (some remaining issues)
- cross sections
- effects of thin cloud (Prabhakara et al.)

Remaining Issues:

- residuals ~1-2 K in CO2 region
    - not calibration
    - not temperature profile
    - CO2 line parameters: widths, strengths?
    - additional intervening cloud?
- residuals associated with water vapor lines
    - pure rotation: strengths and widths

IMPROVED HNO_3 BAND MODEL PARAMETERS

N. Jones, A. Goldman, D. Murcray, F. Murcray, W. Williams
Department of Physics, University of Denver, Denver, CO 80206

Band model temperature dependent parameters for HNO_3 have been recalculated for the 11.3 μm bands using the best available molecular parameters and integrated band strengths. Parameters are calculated with a 1 cm^{-1} resolution and for several temperatures appropriate to the lower stratosphere. The new parameters should be suitable for both MODTRAN and LOWTRAN. A brief presentation of the calculations as well as sample results will be included.

IMPROVED HNO_3 BAND MODEL PARAMETERS FOR THE 11.3μ REGION

Nicholas Jones
Aaron Goldman
David Murcray
Frank Murcray and
Walter Williams

University of Denver
Department of Physics
Denver, CO 80208

Annual Review Conference
on
Atmospheric Transmission Models
Hanscom AFB

11-12 June, 1991

ABSTRACT

- HISTORY
- METHODS
- PRELIMINARY RESULTS
- COMPARISONS
- FUTURE WORK

HISTORY OF HNO_3 MODELS

Date	Group	Data Base	Model
1971	U of D	Lab Meas. Amb Temp	5 cm^{-1} B-M
1975	U of D	Lab Meas. Multi-Temp	5 cm^{-1} B-M
1978	G.L.	5 cm^{-1} B-M	LOWTRAN 4
1981	U of D NASA/Ames	Lab Meas. Multi-Temp	5 cm^{-1} B-M
1984	NASA/Ames U of D	Lab Meas. Multi-Temp	1 cm^{-1} B-M
1984/6	Maki et al	Lab Meas. High Res	Line-by-Line
1987	G.L.	Line-by-Line	HITRAN 1986
1991	U of D	Line-by-Line	1 cm^{-1} B-M w/Temp

HNO_3 BAND MODEL PARAMETERS
Method of calculation

- Calculate Band Model Coefficients for several temperatures using HNO_3 line parameters and Goodys' Statistical method

$$x/L = \frac{S^0}{2\pi\gamma^0} = \frac{1}{8}\,\frac{\left(\sum_{i=1}^{N} S_i^0\right)^2}{\left[\sum_{i=1}^{N} (S_i^0\,\gamma_i^0)^{1/2}\right]^2}, \qquad \beta = \frac{2\pi\gamma^0}{d} = \frac{8}{\Delta\nu}\,\frac{\left[\sum_{i=1}^{N} (S_i^0\,\gamma_i^0)^{1/2}\right]^2}{\sum_{i=1}^{N} S_i}.$$

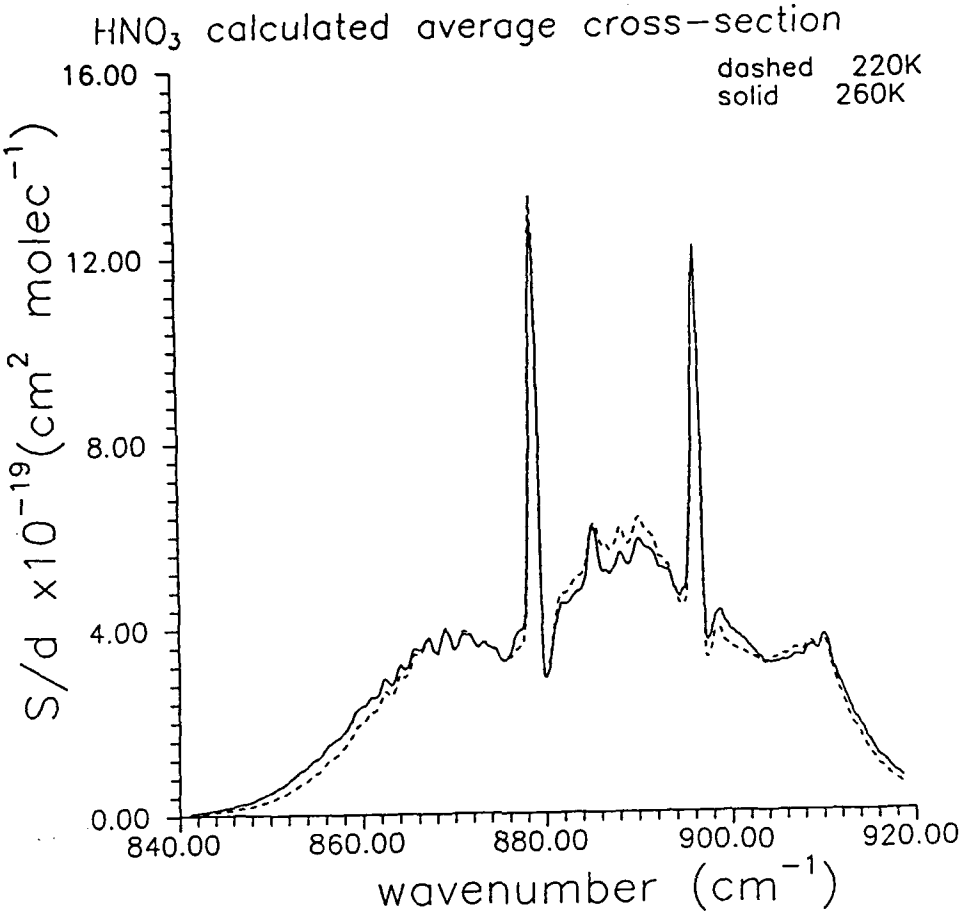
$$S^0/d = \left(\frac{2\pi\gamma^0}{d}\right)\,(x/L) = \frac{1}{\Delta\nu}\sum_{i=1}^{N} S_i^0$$

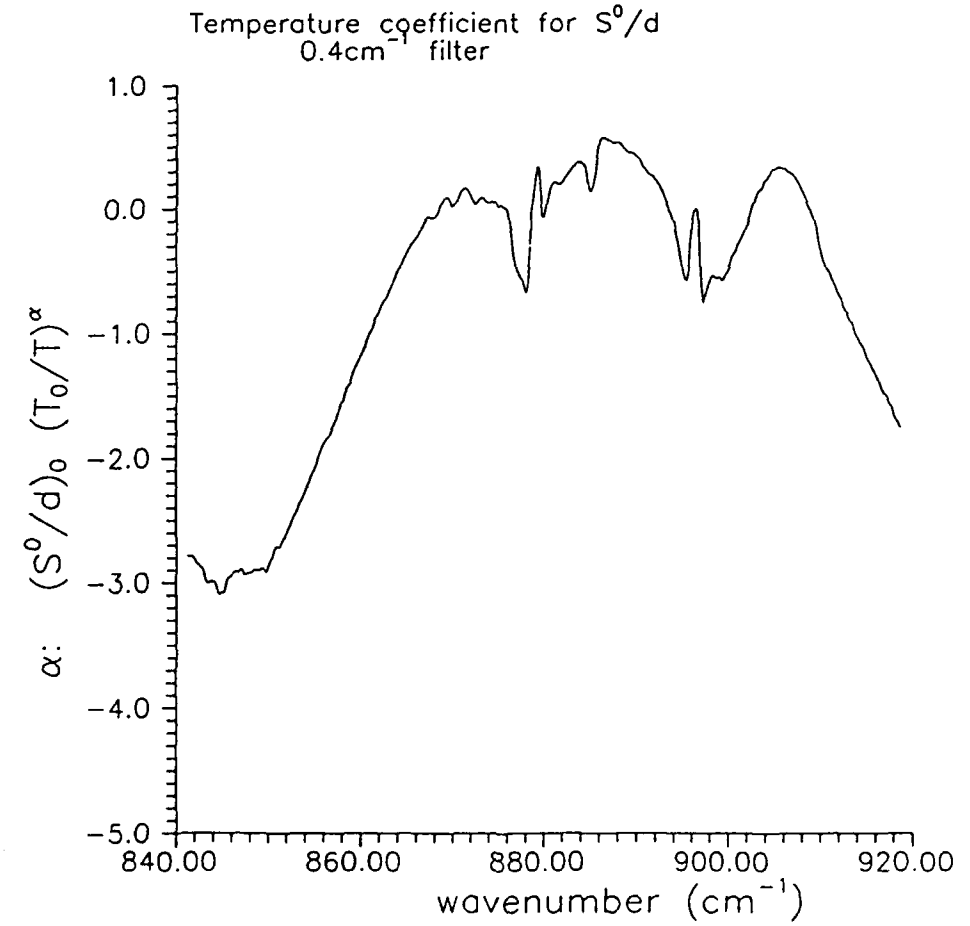
- Approximate Band Model Coefficients with Linear Coefficient

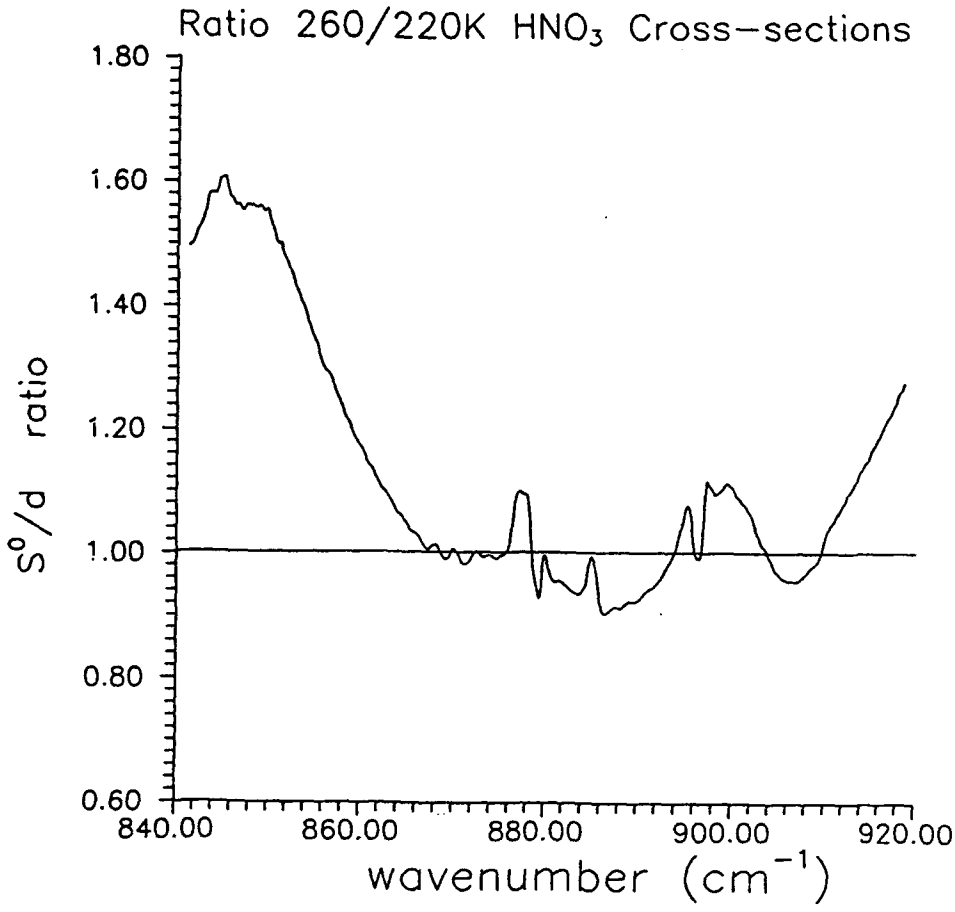
$K=S^0/d$

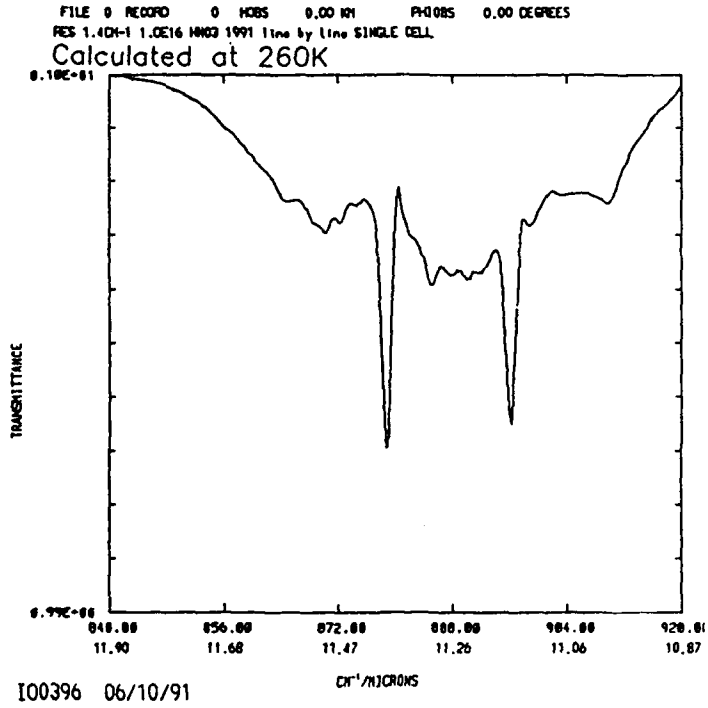
- Derive Temperature Dependent Linear Coefficients

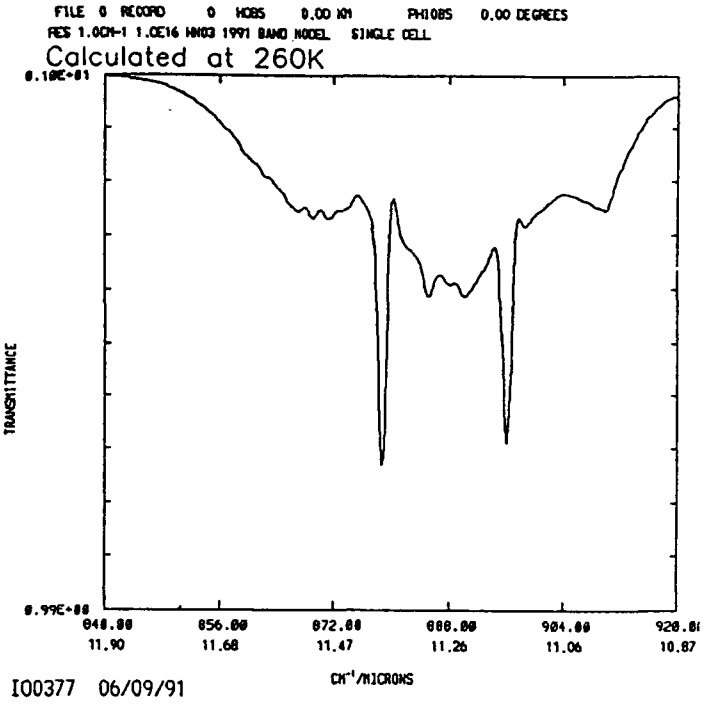
$K(T)\approx K_0(T_0)\,(T_0/T)^{\gamma}$

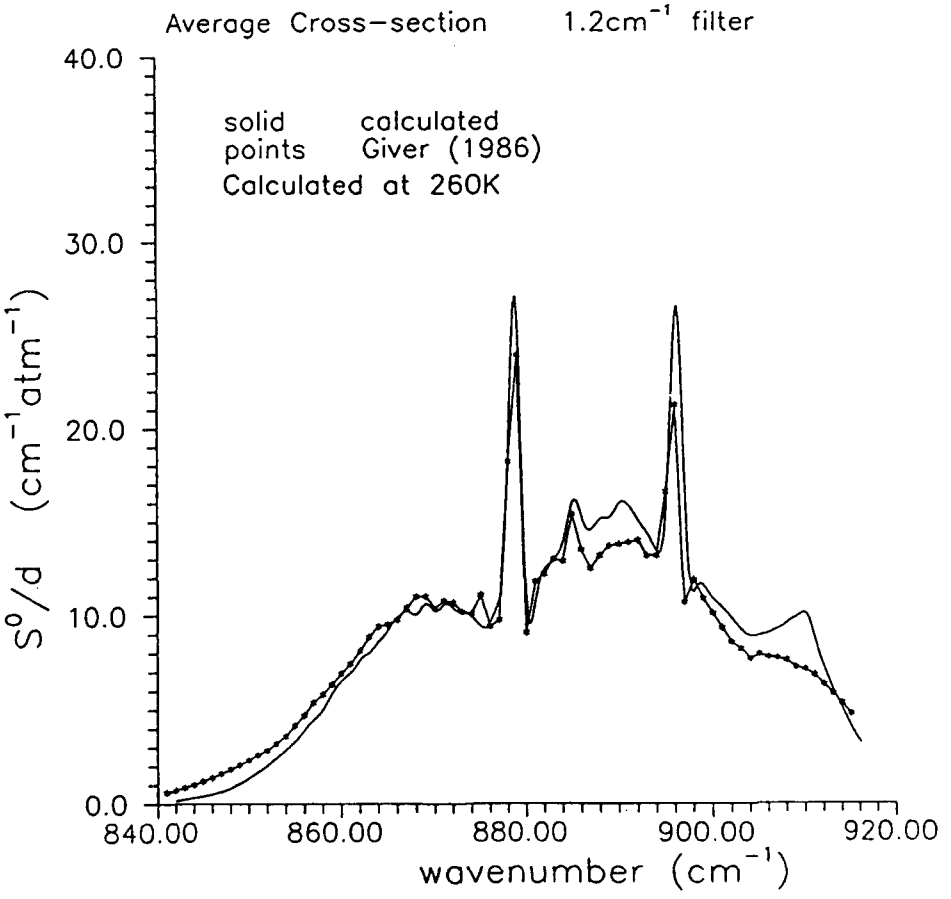

HNO3 calculated average cross-section
dashed 220K
solid 260K
16.00
12.00
8.00
4.00
0.00
S/d x10^-19(cm^2 molec^-1)
840.00
860.00
880.00
900.00
920.00
wavenumber (cm^-1)


Temperature coefficient for S°/d
0.4cm^-1 filter
1.0
0.0
-1.0
-2.0
-3.0
-4.0
-5.0
α: (S°/d)0 (T0/T)^α
840.00
860.00
880.00
900.00
920.00
wavenumber (cm^-1)


Ratio 260/220K HNO_3 Cross-sections
1.80
1.60
1.40
1.20
1.00
0.80
0.60
S^0/d ratio
840.00
860.00
880.00
900.00
920.00
wavenumber (cm^{-1})


FILE 0 RECORD 0 HOBS 0.00 KM PHOBS 0.00 DEGREES
RES 1.4CM-1 1.0E16 HNO3 1991 line by line SINGLE CELL
Calculated at 260K
TRANSMITTANCE
11.90
11.68
11.47
11.26
11.06
10.87
CM-1/MICRONS
I00396 06/10/91


FILE 0 RECORD 0 HOBS 0.00 KM PHIOBS 0.00 DEGREES
RES 1.0CM-1 1.0E16 HN03 1991 BAND MODEL SINGLE CELL
Calculated at 260K
TRANSMITTANCE
840.00 856.00 872.00 888.00 904.00 920.00
11.90 11.68 11.47 11.26 11.06 10.87
CM-1/MICRONS
I00377 06/09/91


Average Cross-section 1.2cm-1 filter
solid calculated
points Giver (1986)
Calculated at 260K
S°/d (cm-1atm-1)
40.0
30.0
20.0
10.0
0.0
840.00
860.00
880.00
900.00
920.00
wavenumber (cm-1)

SIGNIFICANCE OF TEMPERATURE DEPENDENCE

T-Dep Results

- Many Spectral Regions have ≤ 5% T-Dep
- Some Spectral Regions have ≥ 20% T-Dep
- Strongest T-Dep in Wings
- Incomplete "Hot Bands" Analysis

Applications

- Select Optimum Spectral Regions for HNO_3 Measurements:

  Regions w/wo Interference (F11, F12, H_2O)

  Regions w/wo T-Dep

- Verify T-Profile used for Analysis of Emission Data

REMAINING TASKS

- Extend Coefficients into the Wings
- Further Compare Line Parameters and Band Model Parameters with High Resolution and Low Resolution Lab Data
- Publish Results
- Make Data Base Available

LINE-BY-LINE CALCULATIONS OF ATMOSPHERIC FLUXES AND HEATING RATES

S.A. Clough, M.J. Iacono, J.-L. Moncet
Atmospheric and Environmental Research, Inc., 840 Memorial Drive,
Cambridge, MA 02139

A rapid and accurate radiance algorithm has been developed to provide enhanced capability for the line-by-line calculation of fluxes and heating rates using FASCODE for thermally inhomogeneous non-scattering atmospheres. First moment quadrature is utilized to obtain fluxes from the radiances, providing accuracies of 1% for two angles and 0.2% for three angles. Optical depths are calculated for a single zenith angle, generally the nadir. Extensive calculations have been performed for water vapor using the mid-latitude summer atmosphere in the context of the ICRCCM campaign. Comparisons with other line-by-line models have been conducted. Effects of line cutoff procedures have been studied in detail and will be discussed. The role of the water vapor continuum (Clough et al., 1989) will be described in detail. The heating rate and flux calculations are presented spectrally to provide insight into the correlation of the radiative effects between spectral domain and altitude. The importance of the 300-600 cm^{-1} region for the upper tropopause will be discussed. Calculations have also been performed for the tropical and subarctic winter atmospheres with important implications related to the water vapor continuum.

aer

Line-by-line Calculations of Atmospheric Fluxes and Heating Rates: Application to Water Vapor

S. A. Clough
M. J. Iacono
J.-L. Moncet
Atmospheric and Environmental Research, Inc.

12 June 1991

ICRCCM: InterComparisons of Radiation Codes for Climate Models

LBL: W.L. Ridgway - Goddard Laboratory for Atmospheres (GLA)

Model Atmospheres: Mid-Latitude Summer
Tropical 66 layers
Sub Arctic Winter

Line-by-Line Calculation
Advanced version of FASCODE.
G.P. Anderson & F.X. Kneizys Radiance Algorithm

Topics

Calculation:

heating rate:	**flux divergence**
flux:	**first moment quadrature**
radiance:	**inhomogeneous atmosphere**
spectral integration:	**box car**

Application:

spectral sampling error at high altitudes (GLA)
of quadrature points
spectral extent of line contributions
water vapor continuum
model atmospheres
spectral mapping of cooling rate vs. altitude

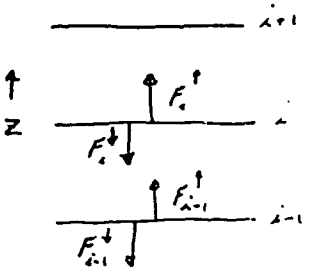
Heating Rate:

$$\left(\frac{\partial T}{\partial t}\right)_{IR} = -\frac{1}{c_p P}\frac{\Delta F}{\Delta Z}$$

F: net flux

$F_i = F_i^{\uparrow} - F_i^{\downarrow}$

$\Delta F = F_i - F_{i-1}$



Flux:

$$F_\upsilon^{\uparrow\downarrow} = \int_0^{2\pi}\int_0^{\pi/2} I_\upsilon(\theta,\phi)\cos\theta \sin\theta\, d\theta d\phi$$

I_υ: monochromatic radiance

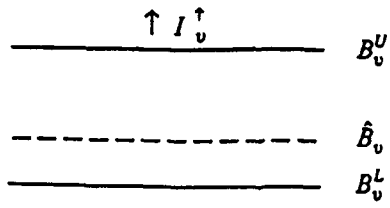
$$= 2\pi\int_0^1 I_\upsilon(\mu)\mu d\mu$$

μ: direction cosine

$$= 2\pi\sum_{j=1}^{N} w_{j,N} I_\upsilon(\mu_j)$$

$w_{j,N}$: first moment quadrature

Radiance Algorithm:



- Isothermal (old FASCODE)

$$I_\upsilon^\uparrow = \hat{B}_\upsilon(1-T_\upsilon)$$

T_υ: layer transmittance

T_υ: $\exp(-\tau_\upsilon)$

- linear in τ

$$I_\upsilon^\uparrow = B_\upsilon^U(1-T_\upsilon) - (B_\upsilon^L - B_\upsilon^U)T_\upsilon + \frac{B_\upsilon^L - B_\upsilon^U}{\tau_\upsilon}(1-T_\upsilon)$$

τ_υ: layer optical depth

- new algorithm (new FASCODE)

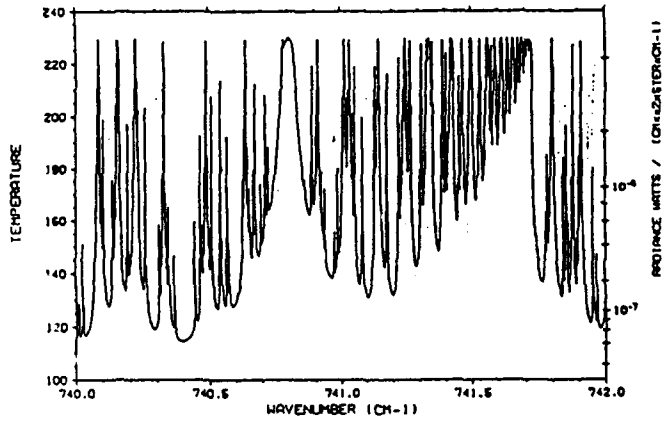
$$I_\upsilon^\uparrow = \left\{ \left(\hat{B}_\upsilon + a\tau_\upsilon B_\upsilon^U\right) / (1+a\tau_\upsilon) \right\} (1-T_\upsilon)$$

$a \sim 0.2$

- limits:

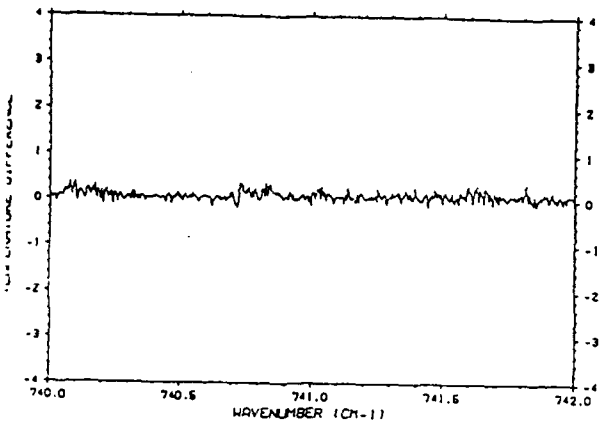
	isothermal	linear in τ	new
thin ($\tau \to 0$)	$\hat{B}_\upsilon \tau_\upsilon$	$\frac{B_\upsilon^U + B_\upsilon^L}{2} \cdot \tau_\upsilon$	$\hat{B}_\upsilon \tau_\upsilon$
thick ($\tau \to \infty$)	$\hat{B}_\upsilon$	B_υ^U	B_υ^U

Spectral Radiance

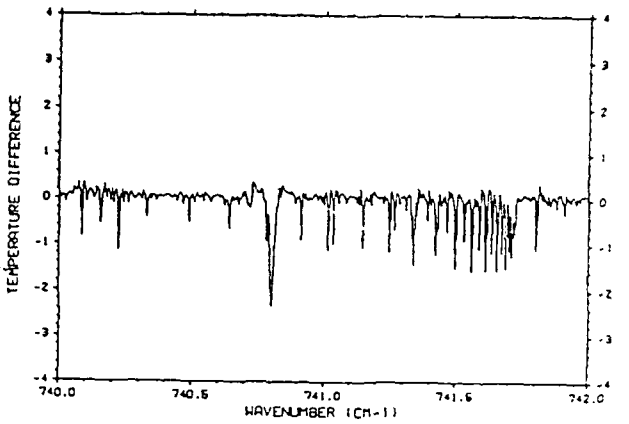


Approx. - 'Correct'

new algorithm

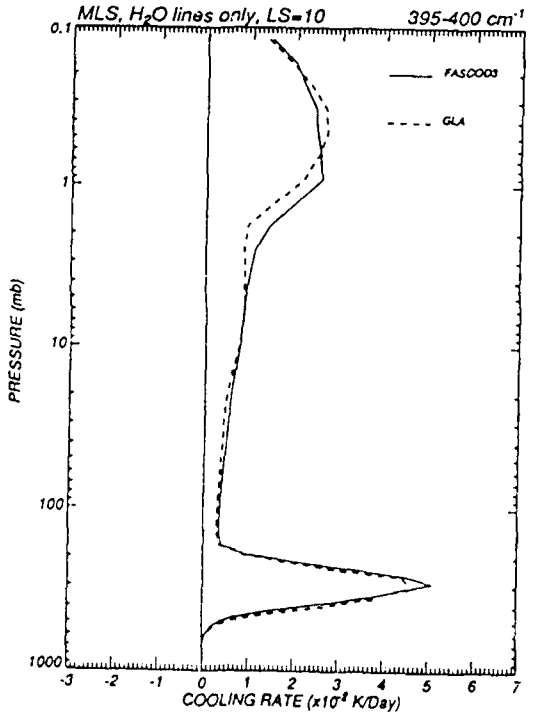


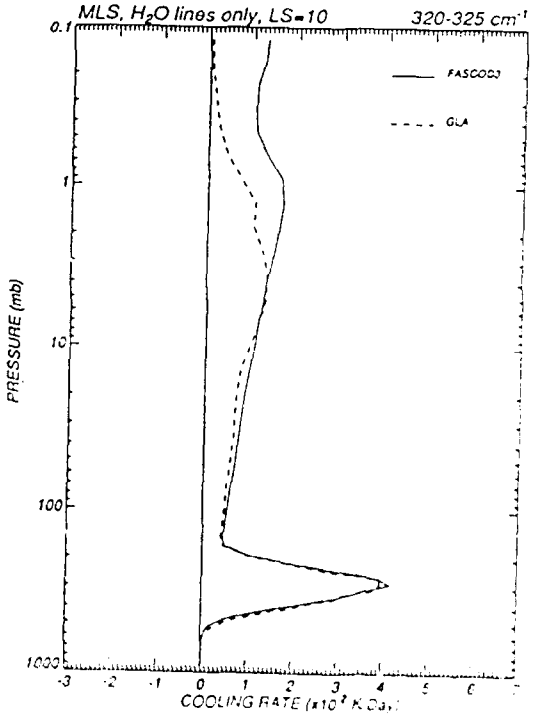
isothermal



Approx: 1 layer
2.5 km thick
5.2K differential

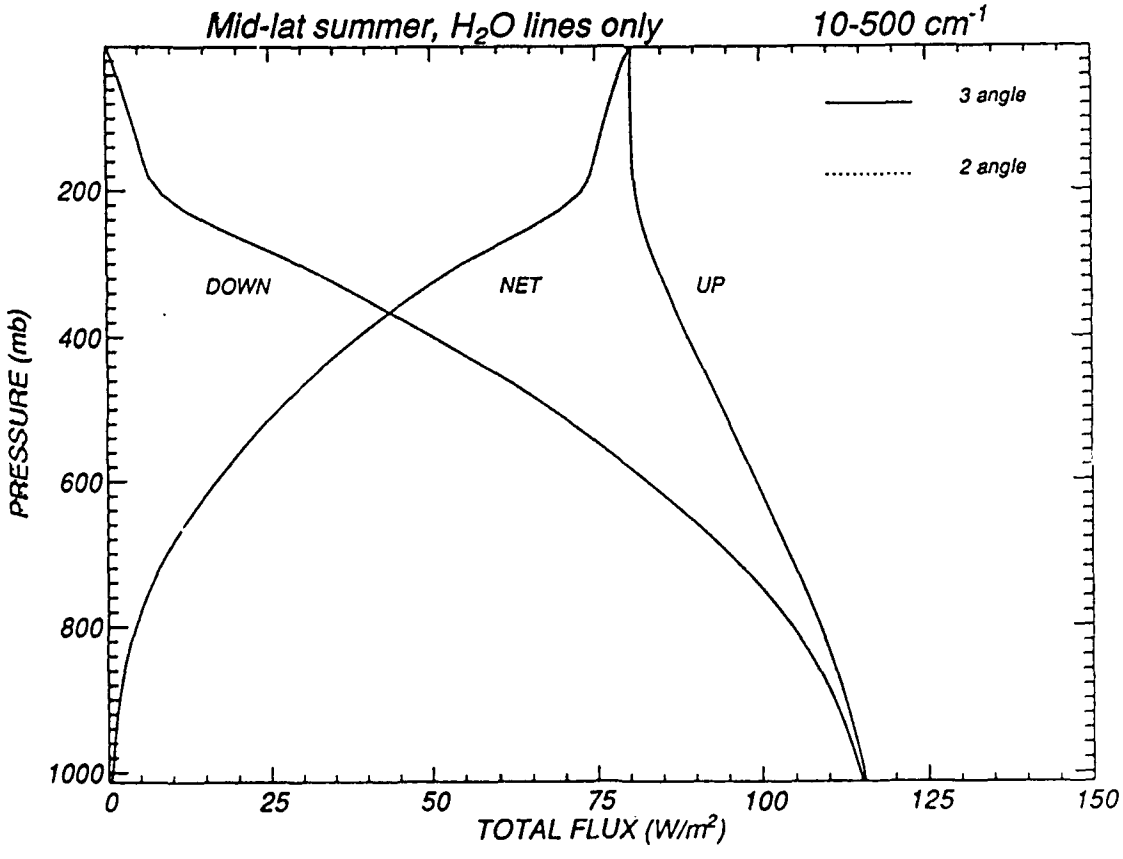
'Correct': 5 layers
each layer 0.5 km thick
uses new algorithm for radiance

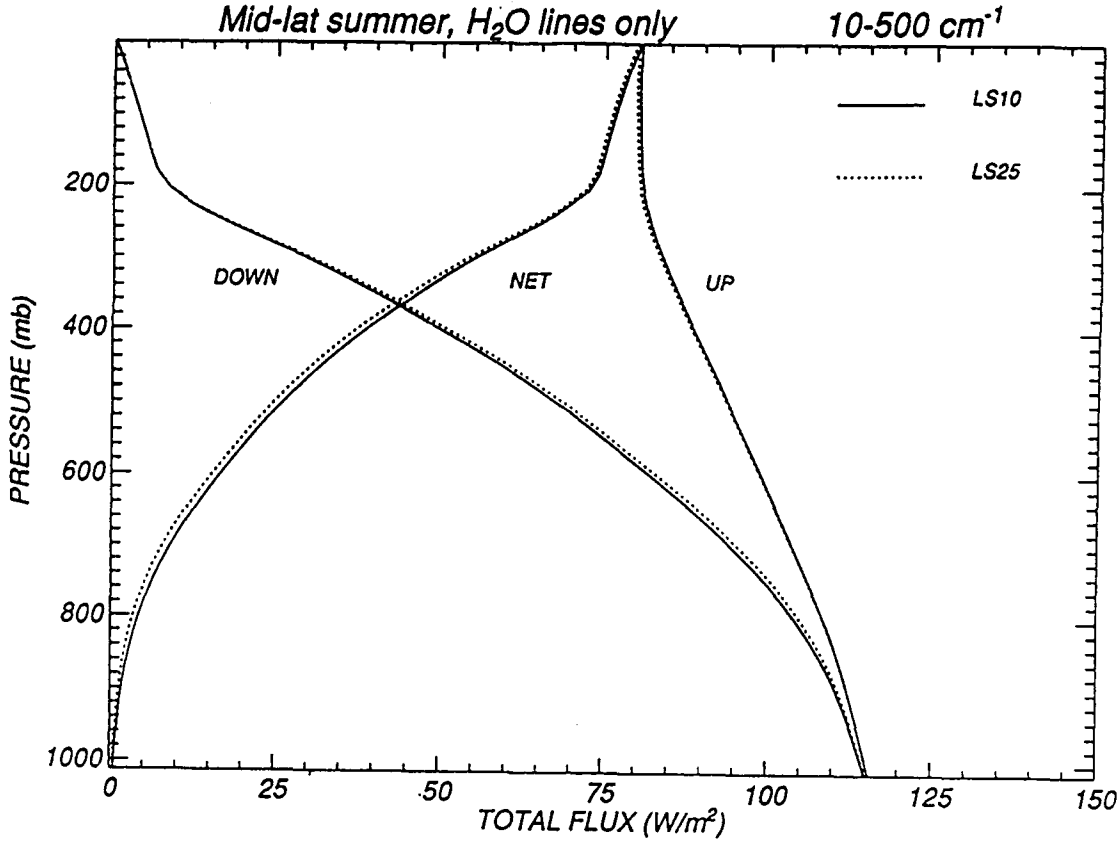


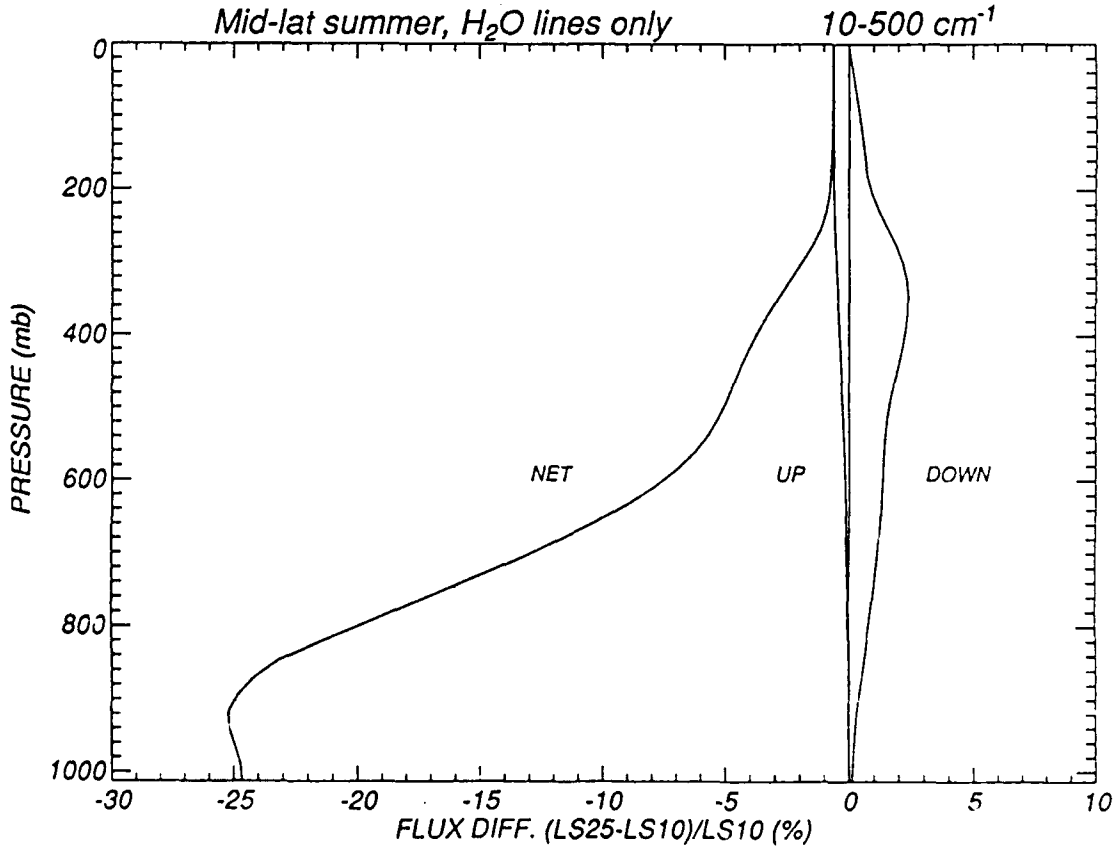


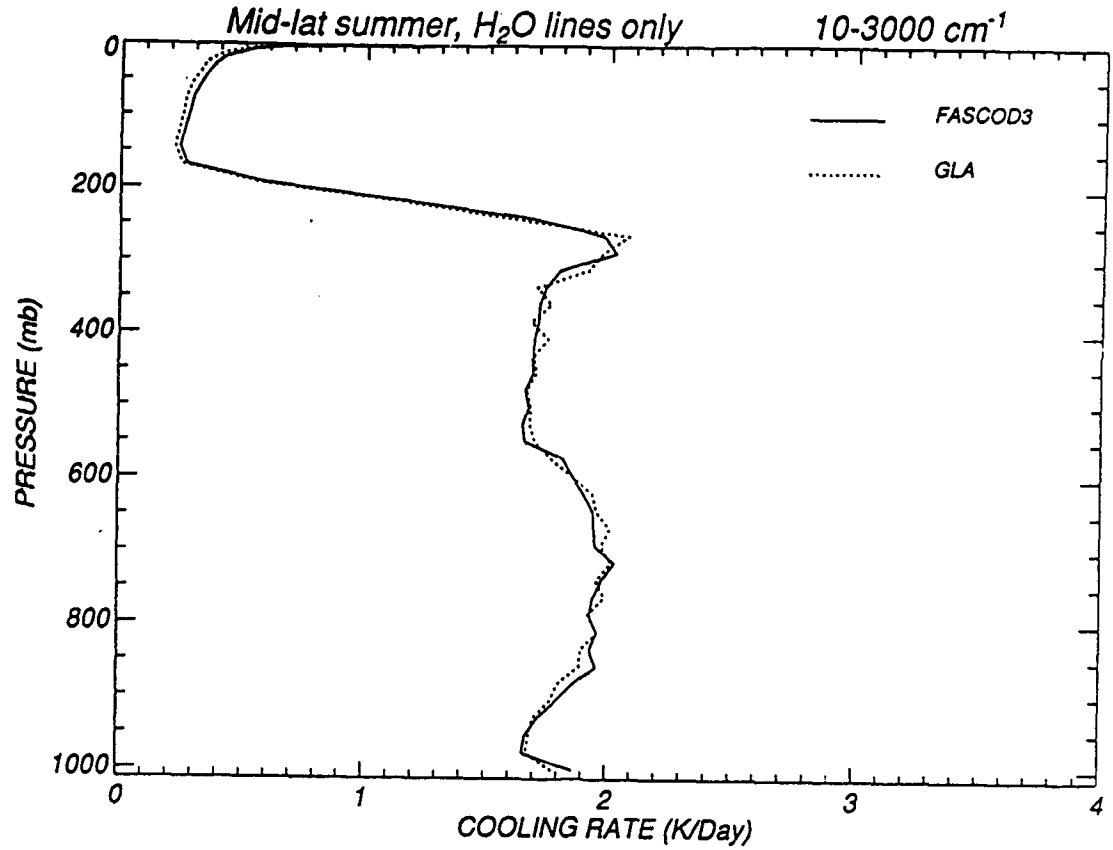
Flux Errors (%): Quadrature vs. 25 pt. trapezoidal

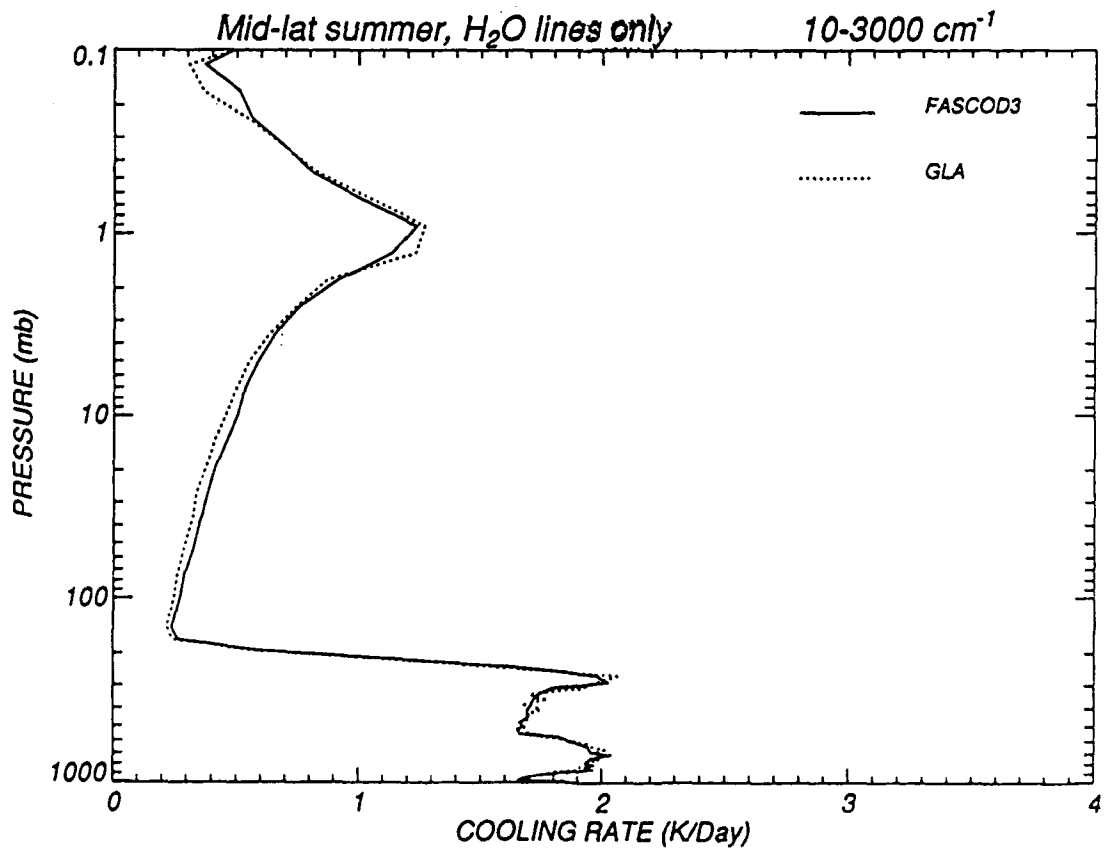
# angles	quadrature		first moment quadrature	
	up	down	up	down
1	-2.3	8.5	0.7	-4.5
2	-0.13	0.99	0.05	-0.58
3	0.006	0.16	0.007	-0.063
4	-0.009	0.04	0.003	0.020

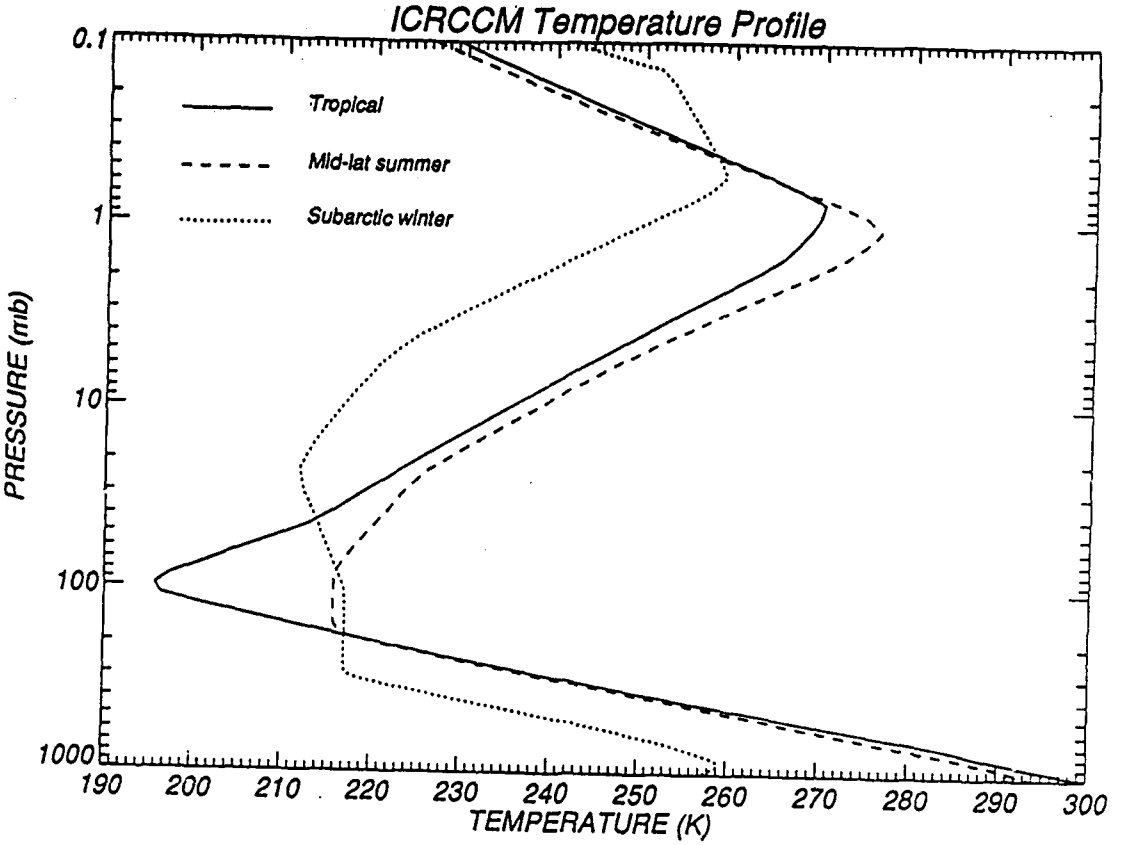


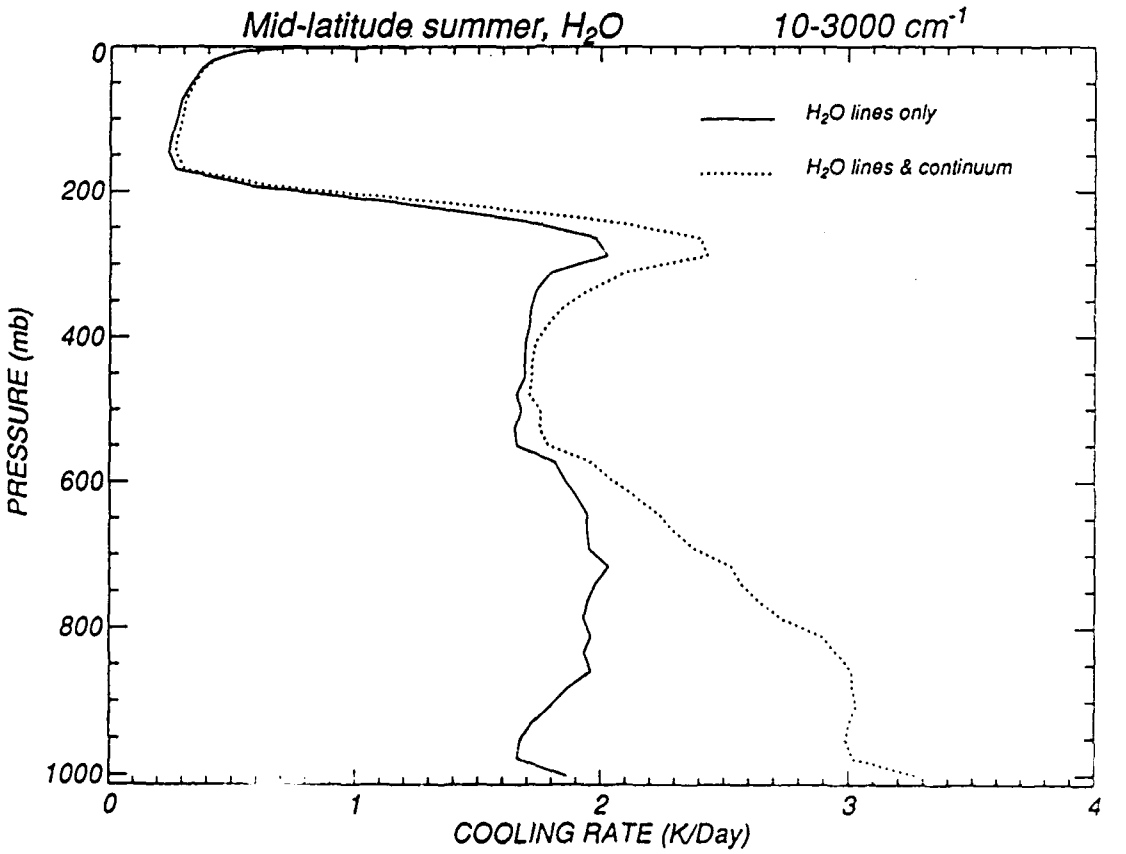

Mid-lat summer, H_2O lines only
10-500 cm^{-1}
LS10
LS25
DOWN
NET
UP
PRESSURE (mb)
200
400
600
800
1000
0
25
50
75
100
125
150
TOTAL FLUX (W/m^2)

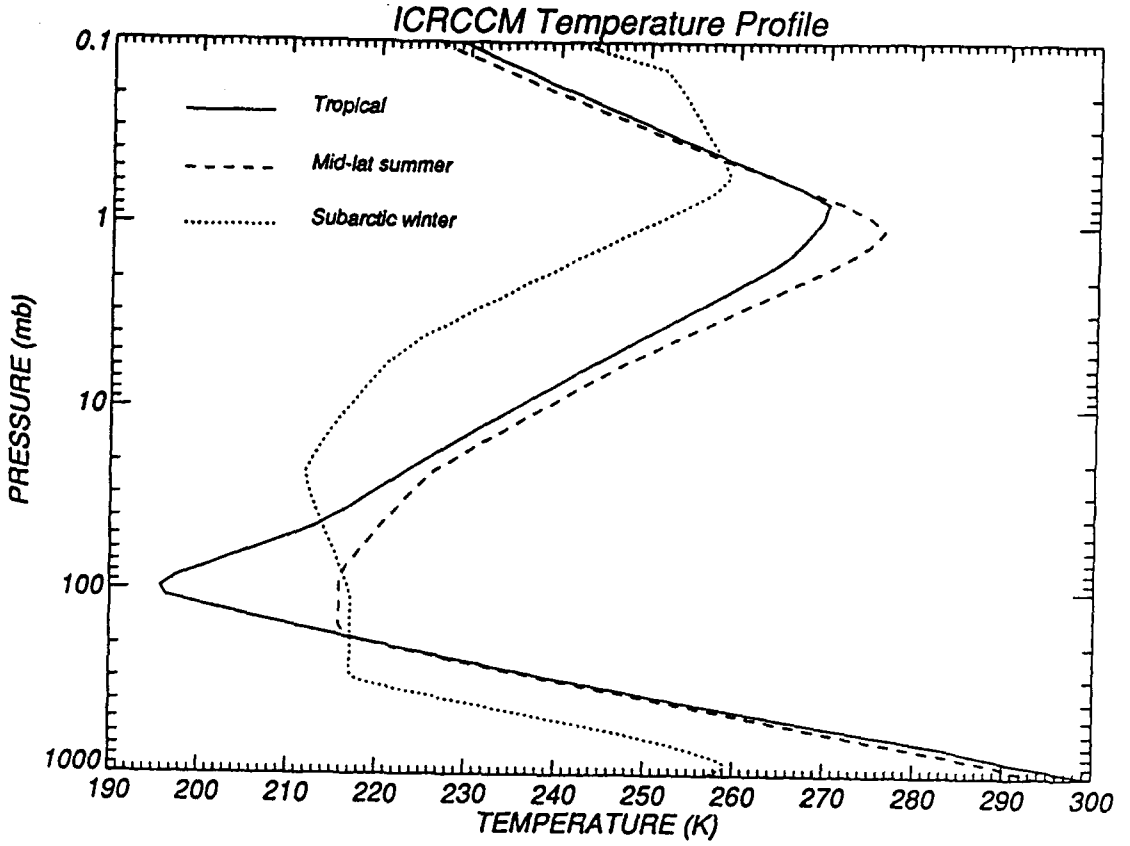

Mid-lat summer, H_2O lines only
10-500 cm^{-1}
NET
UP
DOWN
PRESSURE (mb)
0
200
400
600
800
1000
-30
-25
-20
-15
-10
-5
0
5
10
FLUX DIFF. (LS25-LS10)/LS10 (%)

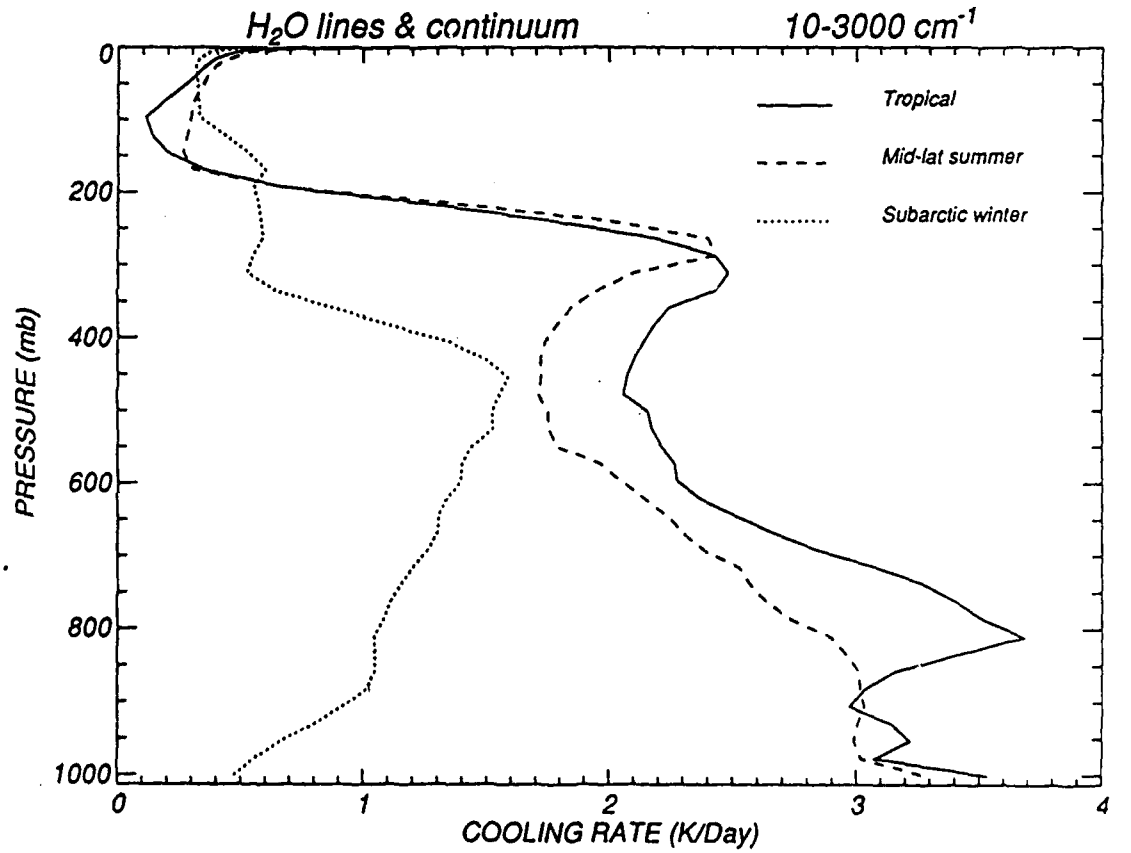

Mid-lat summer, H_2O lines only
10-3000 cm^{-1}
FASCOD3
GLA
PRESSURE (mb)
0
200
400
600
800
1000
0
1
2
3
4
COOLING RATE (K/Day)

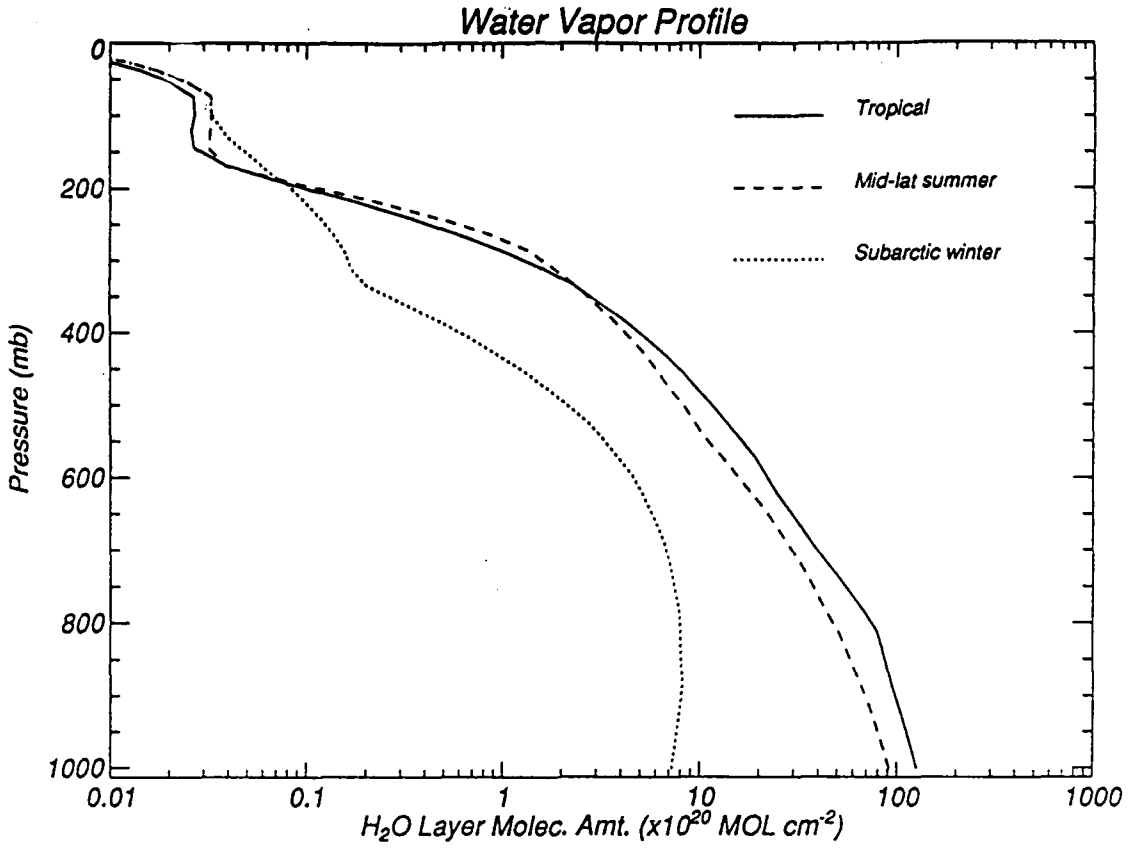

Mid-lat summer, H_2O lines only
10-3000 cm^{-1}
FASCOD3
GLA
PRESSURE (mb)
0.1
1
10
100
1000
0
1
2
3
4
COOLING RATE (K/Day)

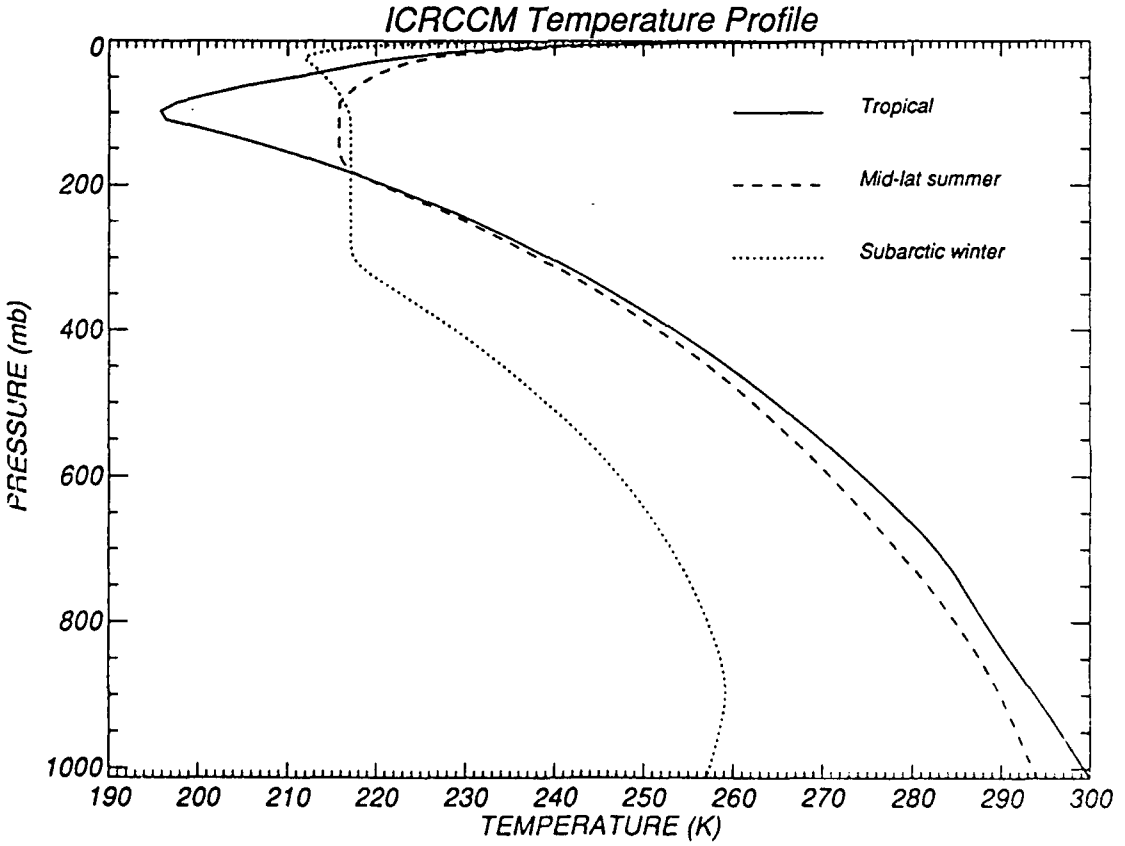

ICRCCM Temperature Profile
Tropical
Mid-lat summer
Subarctic winter
PRESSURE (mb)
0.1
1
10
100
1000
190
200
210
220
230
240
250
260
270
280
290
300
TEMPERATURE (K)

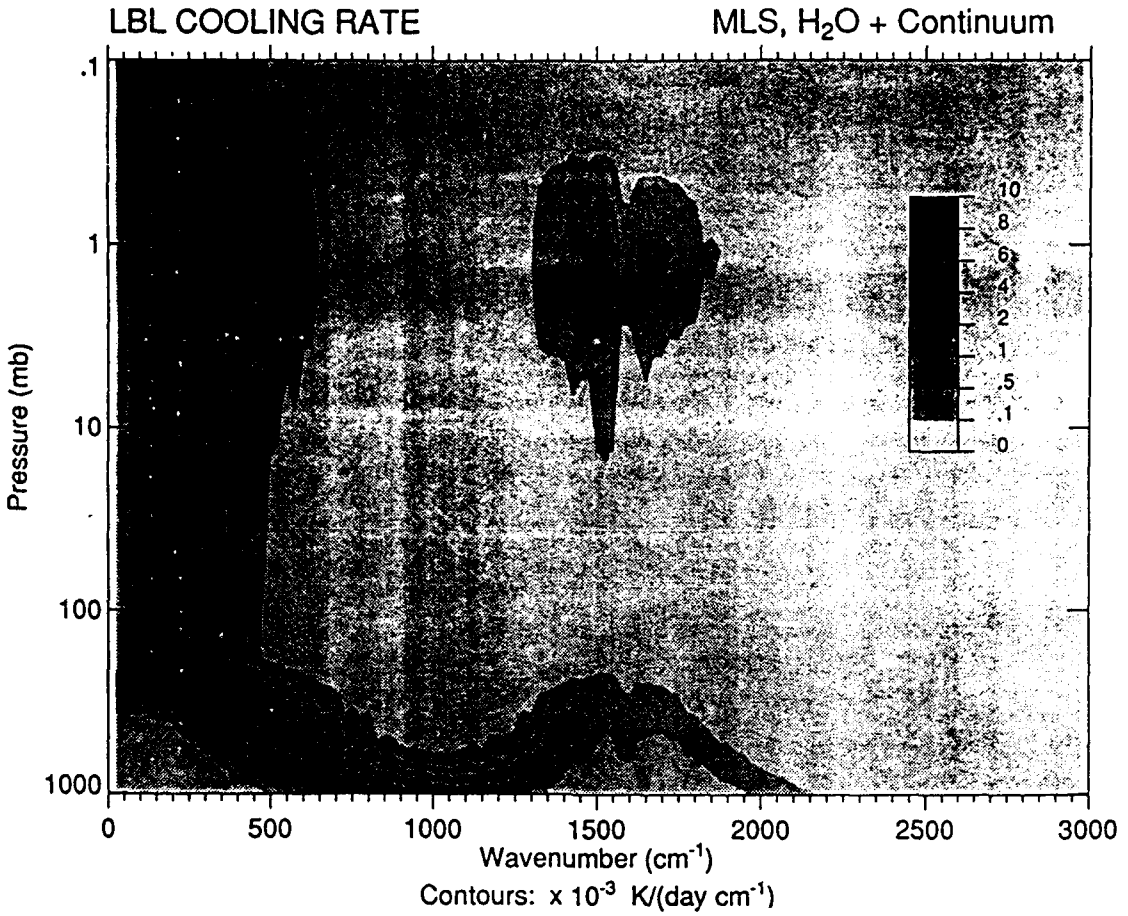

Mid-latitude summer, H_2O
10-3000 cm^{-1}
H_2O lines only
H_2O lines & continuum
PRESSURE (mb)
0
200
400
600
800
1000
0
1
2
3
4
COOLING RATE (K/Day)

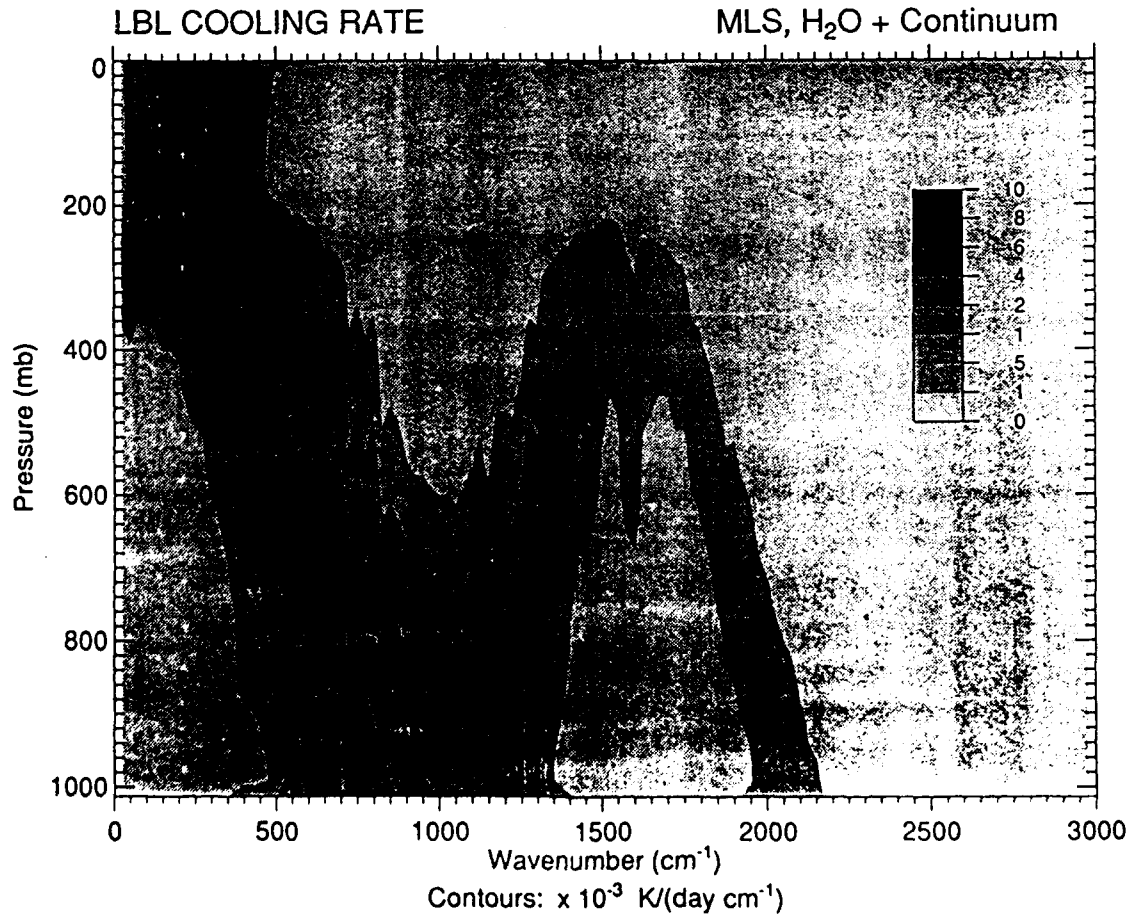

ICRCCM Temperature Profile
Tropical
Mid-lat summer
Subarctic winter
PRESSURE (mb)
0.1
1
10
100
1000
190
200
210
220
230
240
250
260
270
280
290
300
TEMPERATURE (K)

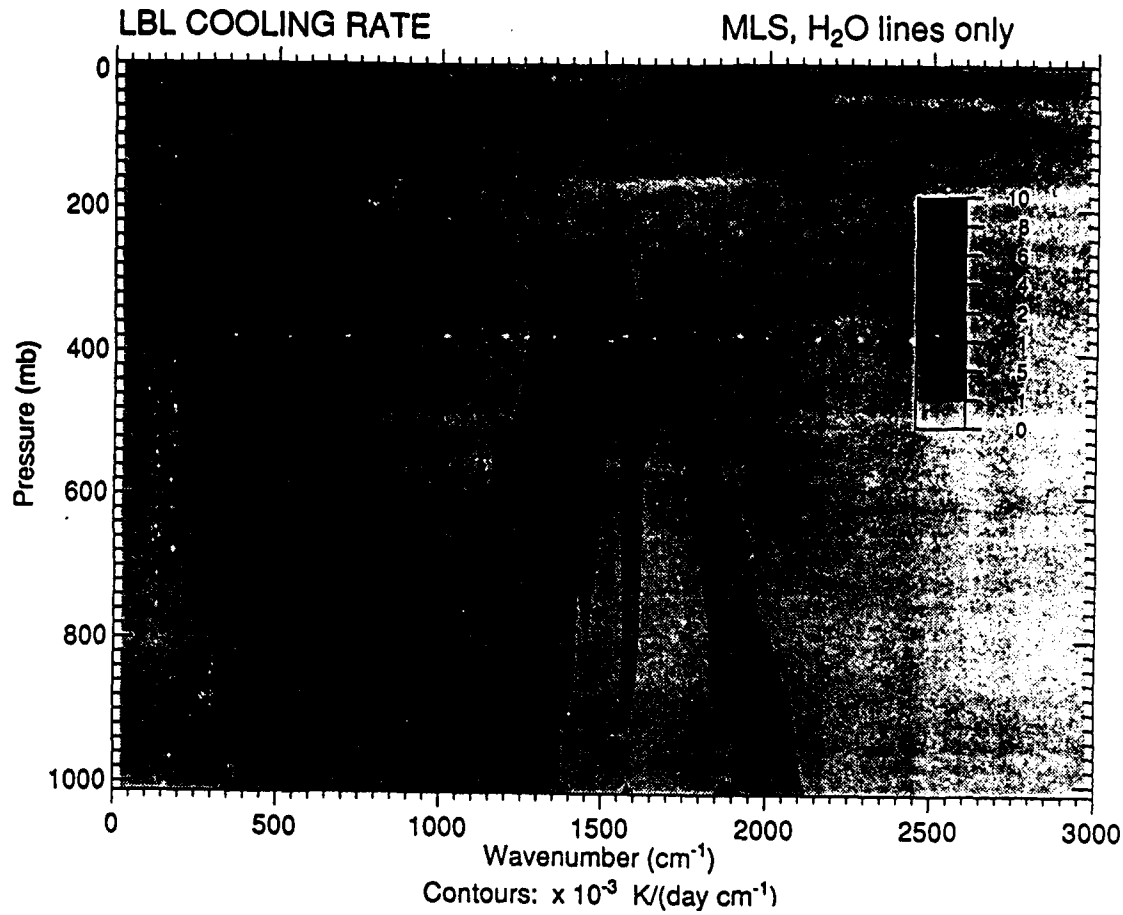

H2O lines & continuum
10-3000 cm-1
Tropical
Mid-lat summer
Subarctic winter
PRESSURE (mb)
0
200
400
600
800
1000
0
1
2
3
4
COOLING RATE (K/Day)

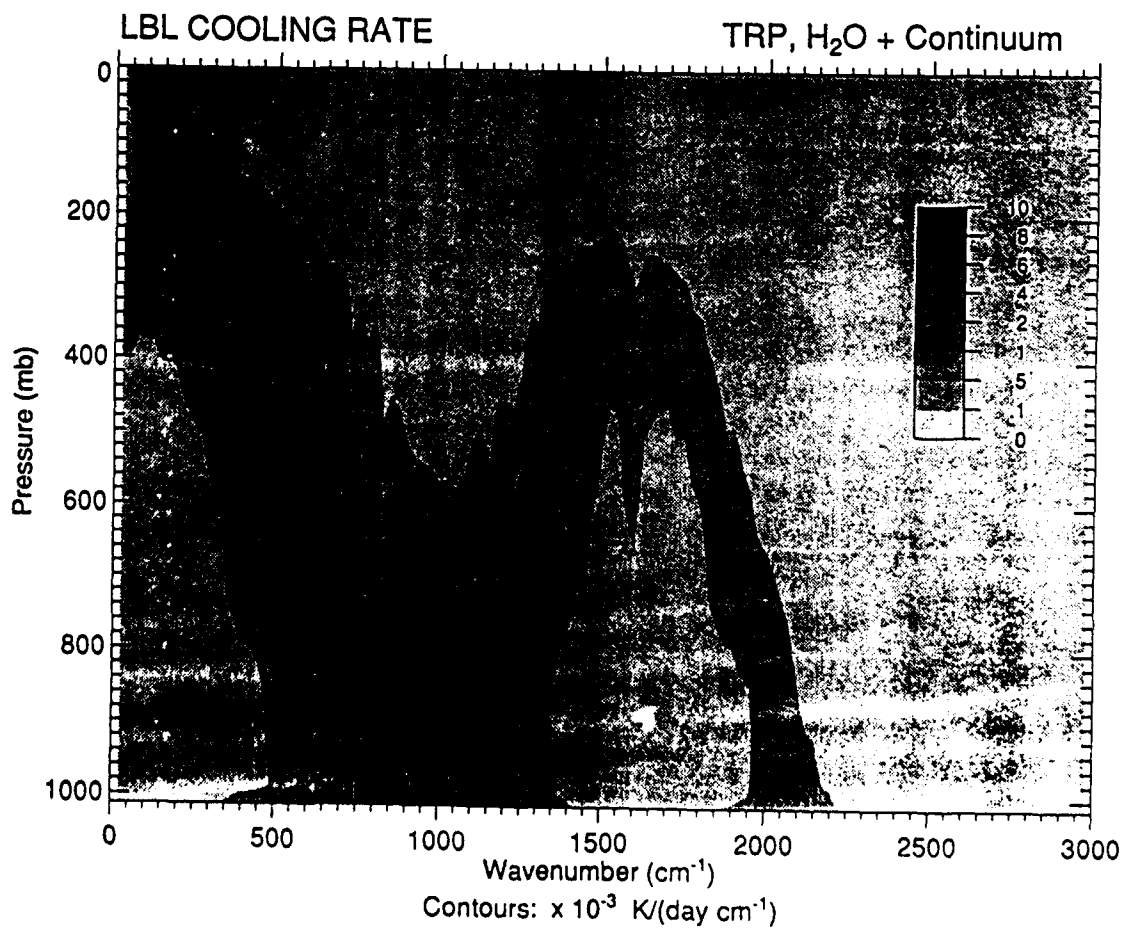

Water Vapor Profile
Tropical
Mid-lat summer
Subarctic winter
Pressure (mb)
0
200
400
600
800
1000
0.01
0.1
1
10
100
1000
H2O Layer Molec. Amt. (x10^20 MOL cm^-2)

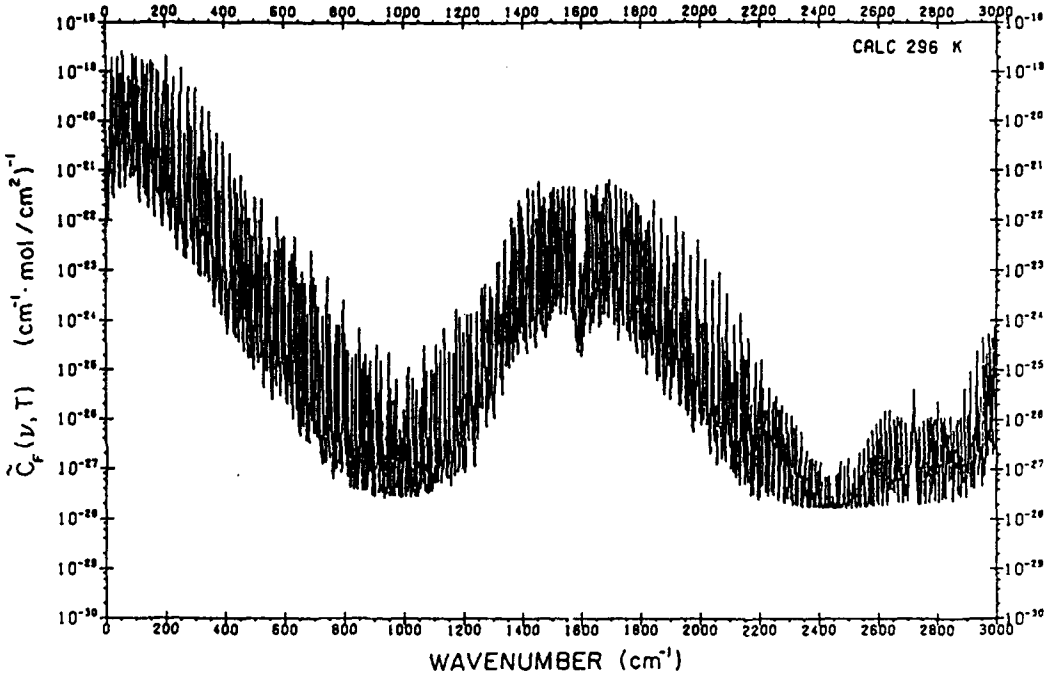

ICRCCM Temperature Profile
Tropical
Mid-lat summer
Subarctic winter
PRESSURE (mb)
0
200
400
600
800
1000
190
200
210
220
230
240
250
260
270
280
290
300
TEMPERATURE (K)


LBL COOLING RATE
MLS, H_2O + Continuum
Pressure (mb)
.1
1
10
100
1000
0
500
1000
1500
2000
2500
3000
Wavenumber (cm^{-1})
10
8
6
4
2
1
.5
.1
0
Contours: x 10^{-3} K/(day cm^{-1})


LBL COOLING RATE
MLS, H_2O + Continuum
Pressure (mb)
0
200
400
600
800
1000
0
500
1000
1500
2000
2500
3000
Wavenumber (cm^{-1})
10
8
6
4
2
1
.5
.1
.0
Contours: x 10^{-3} K/(day cm^{-1})


LBL COOLING RATE
MLS, H_2O lines only
Pressure (mb)
0
200
400
600
800
1000
0
500
1000
1500
2000
2500
3000
Wavenumber (cm^{-1})
10
8
6
4
2
1
.5
0
Contours: x 10^{-3} K/(day cm^{-1})


LBL COOLING RATE
TRP, H_2O + Continuum
Pressure (mb)
0
200
400
600
800
1000
0
500
1000
1500
2000
2500
3000
Wavenumber (cm^{-1})
10
8
6
4
2
1
.5
.1
0
Contours: x 10^{-3} K/(day cm^{-1})


CALC 296 K
$\tilde{C}_F(\nu, T)$ $(cm^{-1} \cdot mol/cm^2)^{-1}$
WAVENUMBER (cm^{-1})

COMPARISON OF FASCOD2 AND LOWTRAN7 MODELS WITH FIT SPECTRAL TRANSMITTANCE MEASUREMENTS IN THE 3-12 μm REGION

J.M. Thériault
DREV-Defense Research Establishment Valcartier,
P.O. Box 8800, Courcelette, Québec, Canada, GOA-1RO

A comparison is made between FASCOD2 and LOWTRAN7 predictions with experimental measurements carried out at DREV over a 5.7 km transmission path under a wide range of ambient temperature (-9° to 30° C) and humidity conditions (1.1 to 14.2 g/m^3). Following a brief review of the FIT instrumentation[1], low and high resolution measurements (20 and 1 cm^{-1}) of atmospheric transmittance in the 3-12 μm region are reported. The most significant differences have been recorded in winter and spring conditions. The analysis of the results suggests that the water vapor continuum modeling in the 7-12 μm region has some limitations at low ambient temperature in both models. Furthermore, the comparison of LOWTRAN7 with measurements has revealed an unexpected difference of 12%, independent of temperature and humidity conditions in the important transmission window near 3.6 μm. This difference is attributed to the modeling of the 3020 cm^{-1} absorption hand of methane.

[1]Theriault, J.M., Roney, P.L. and Reid, F., "Atmospheric Transmission in the 2.8-5.5 μm Region; Description of the Fourier Interferometric Transmissometer and Typical Result at Low Temperatures", Appl. Opt. 29, 3654-3666 (1990).

COMPARISON OF FASCOD2 AND LOWTRAN7 MODELS WITH FIT SPECTRAL TRANSMITTANCE MEASUREMENTS IN THE 3-12 μm REGION

J.-M. Thériault

DREV-Defence Research Establishment Valcartier
P.O. Box 8800, Courcelette, Quebec, Canada,
GOA-1RO

also with
(Mar. 91- Feb. 92)

CIMSS-Cooperative Institute for Meteorological
Satellites Studies
University of Wisconsin
Space Science and Engineering Center
1225 West Dayton Street
Madison, WI 53706

Presented at the
1991 Annual Review Conference on
Atmospheric Transmission Models, AFGL
11-12 June 1991

Propagation Group

High Resolution Atmospheric Transmission Measurement

- 5.7-km transmission range
- FIT-Fourier Interferometric Transmissometer
- Quebec city area : Wide range of ambiant temperature and humidity conditions

Current work:

- Transmissometer calibration techniques
- Water vapor and temperature effects
- Comparison with FASCOD2 and LOWTRAN7 predictions

FIT-Receiver :

1 - Parabolic Newtonian 17-in diameter F/4.6 telescope

2 - BOMEM DA2.02 field Interferometer:

- Resolution from 0.04 cm^{-1} to 64 cm^{-1}
- Clear optical beam cross section ~ 14 cm^2
- Bandpass: 2.8-12 μm MCT det. and BaF_2 beamsplitter

3 - System field of view: 0.5 mrad

FIT-Calibration :

$$T_{atm}(\nu) = \frac{1}{K(\nu)} \frac{P_d(\nu)}{P_{loc}(\nu)}$$

- Calibration factor:

$$K(\nu) = \frac{(R)}{d^2} \frac{A_m}{A_{ap}} \frac{f_1^2 f_3^2}{f_2^2} (RQ)$$

- In the Mid-IR : Verification of results with a wideband transmissometer (3.4-4.1 μm).

- In the Far-IR : Correction Factor $F_c(\mu) = R^2(\mu) \cdot Q$

Comparison of Measurements with FASCOD2 :

1 - Resolution of 1 cm^{-1}

2 - Spectral region: 850-3500 cm^{-1}

3 - Temperature Range: -8.55 to 29.4 C

4 - Humidity Range: 1.16 to 14.2 g/m^3

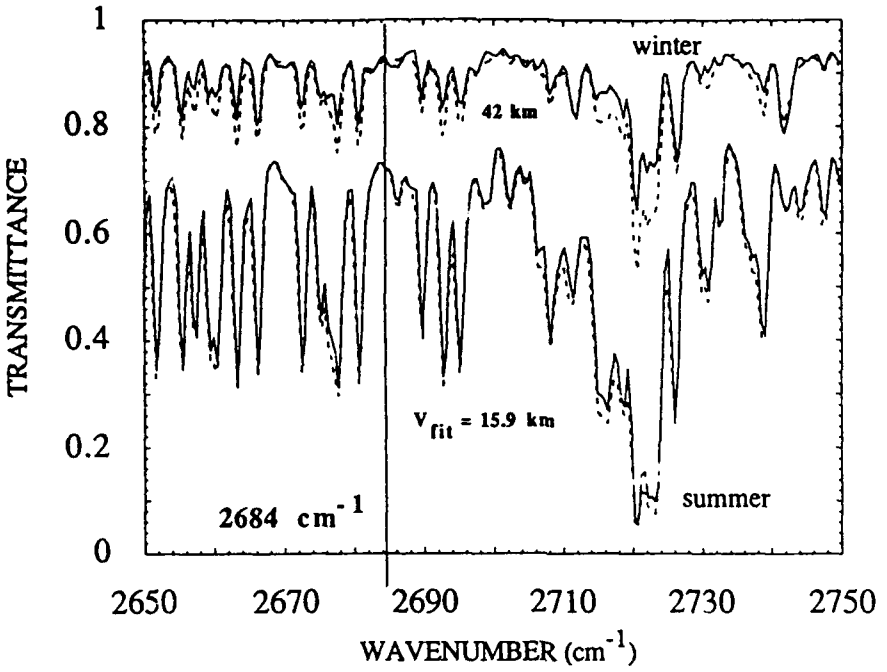
5 - HITRAN Database: 1986 Edition

6 - Contributions of other active molecules namely O_3, N_2O, CH_4, CO, O2, and N_2 : AFGL Mid-summer or Mid-winter conditons except for the CO_2 (350 ppm)

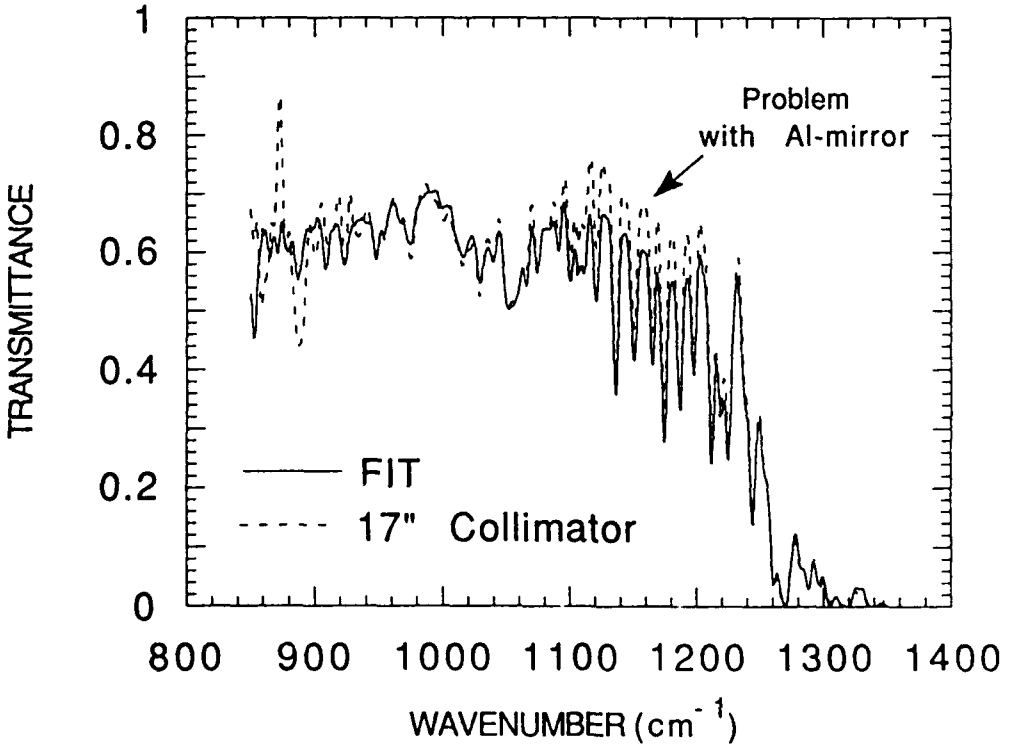
7 - Aerosol model: Rural Type

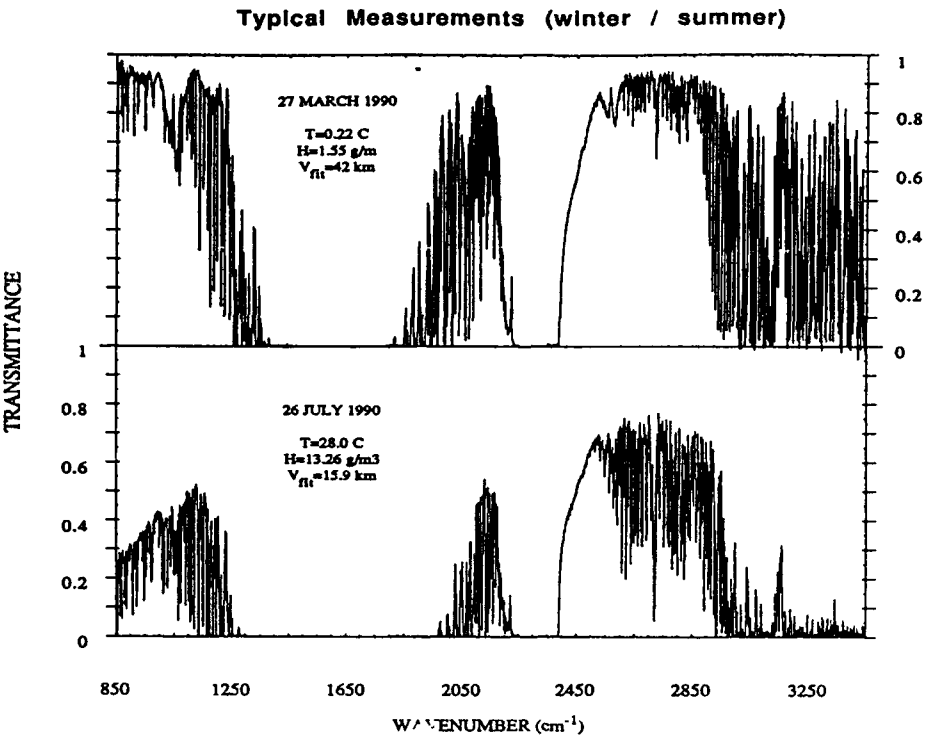
8 - Visibility evaluation: Matching FASCOD2 spectra with measurements at 2684 cm^{-1}

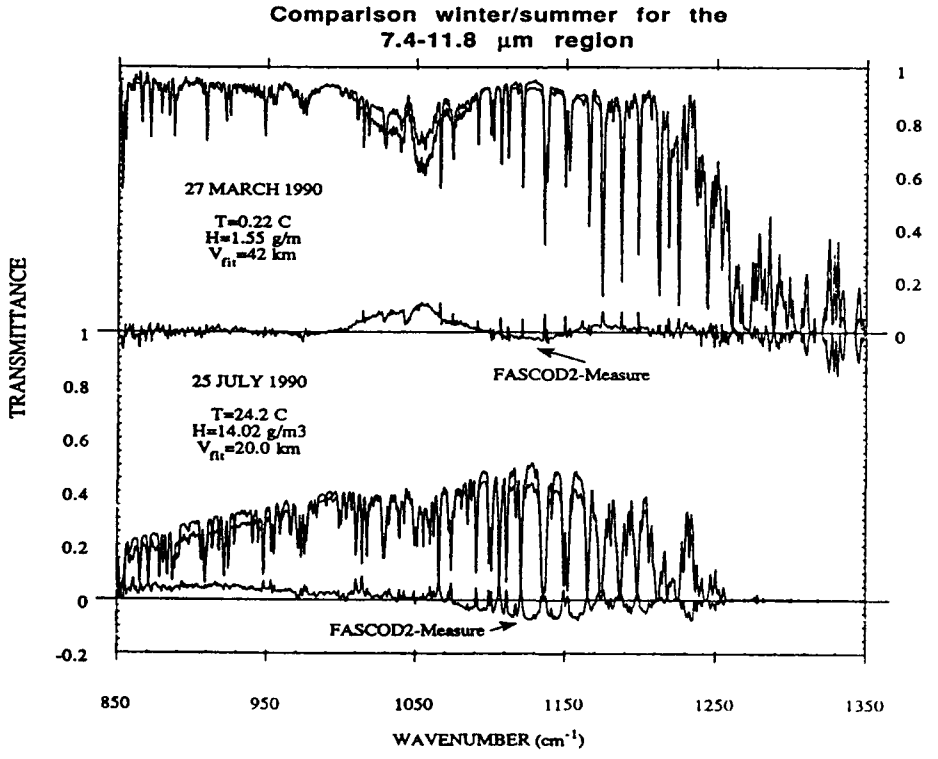
Visibility Evaluation

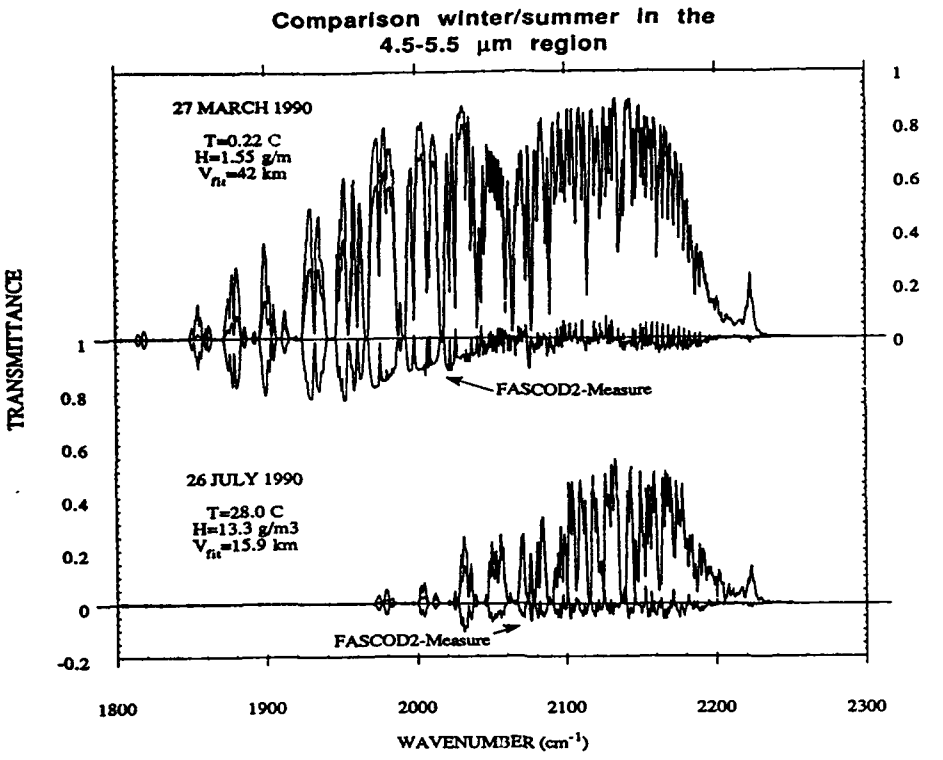


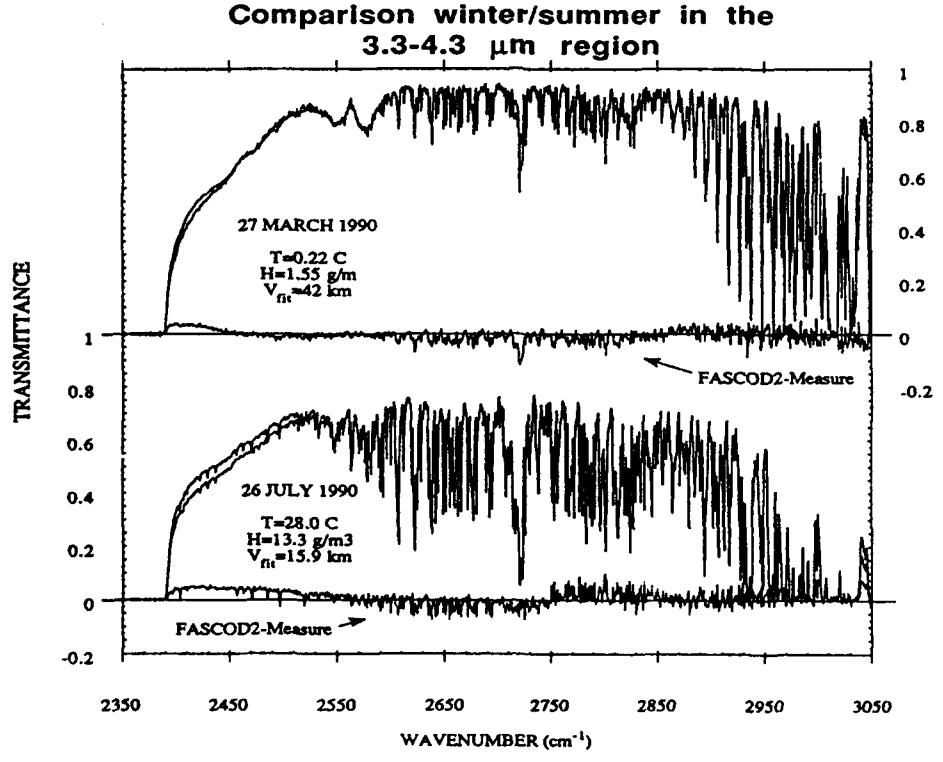
VALIDATION OF TRANSMITTANCE MEASUREMENTS

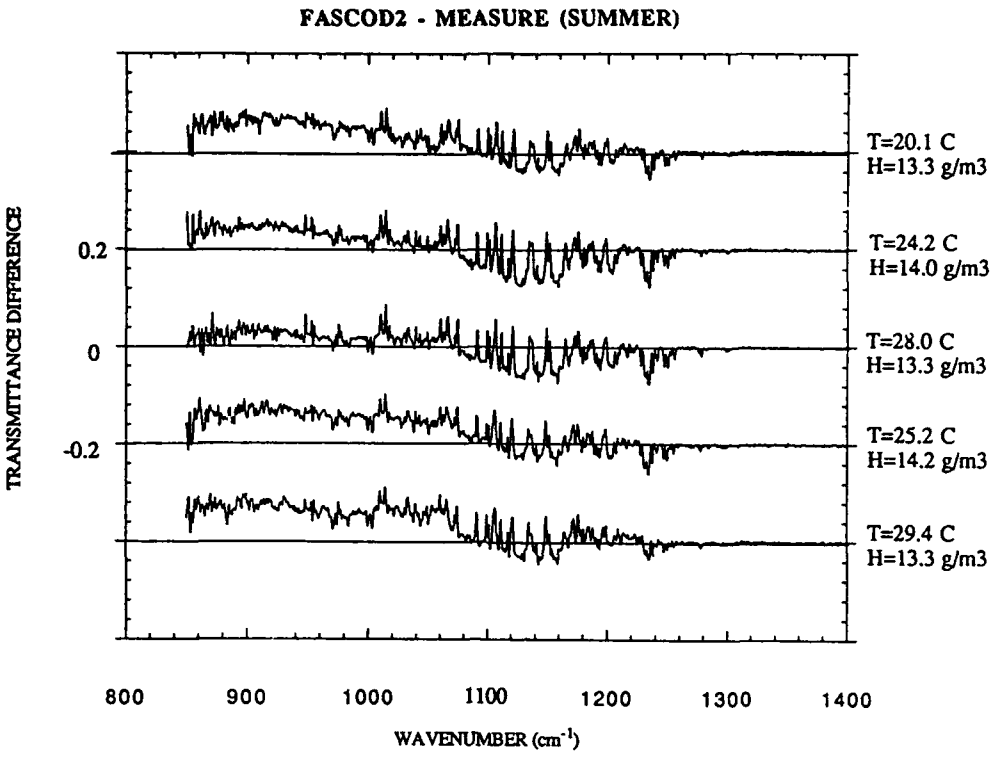


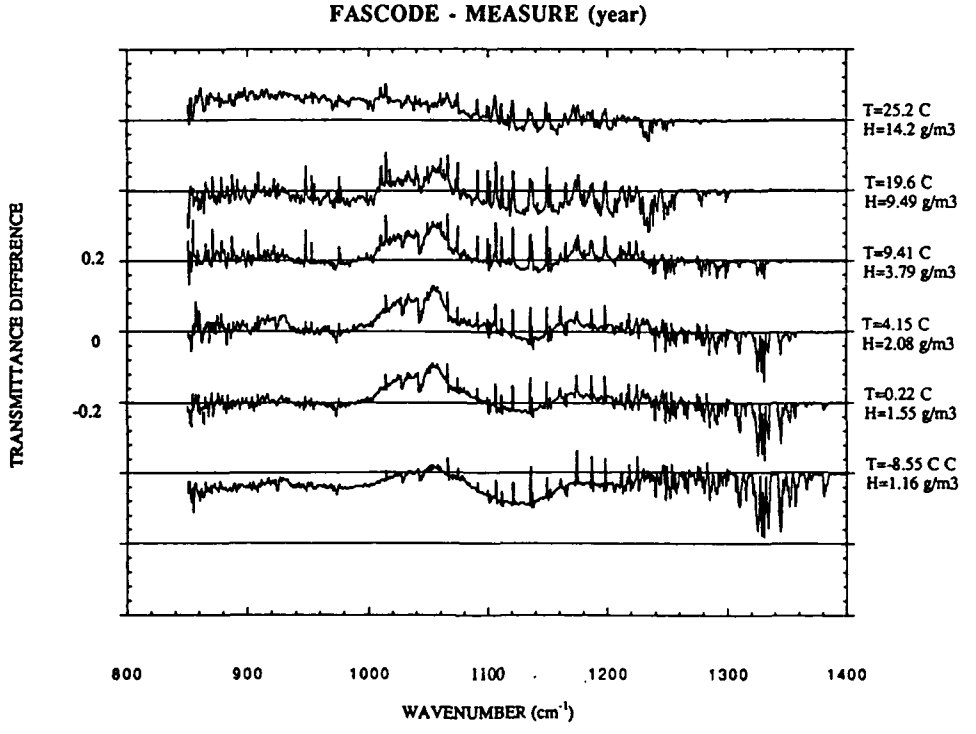

Typical Measurements (winter / summer)
27 MARCH 1990
T=0.22 C
H=1.55 g/m
V_fit=42 km
26 JULY 1990
T=28.0 C
H=13.26 g/m3
V_fit=15.9 km
TRANSMITTANCE
1
0.8
0.6
0.4
0.2
0
850
1250
1650
2050
2450
2850
3250
WAVENUMBER (cm-1)

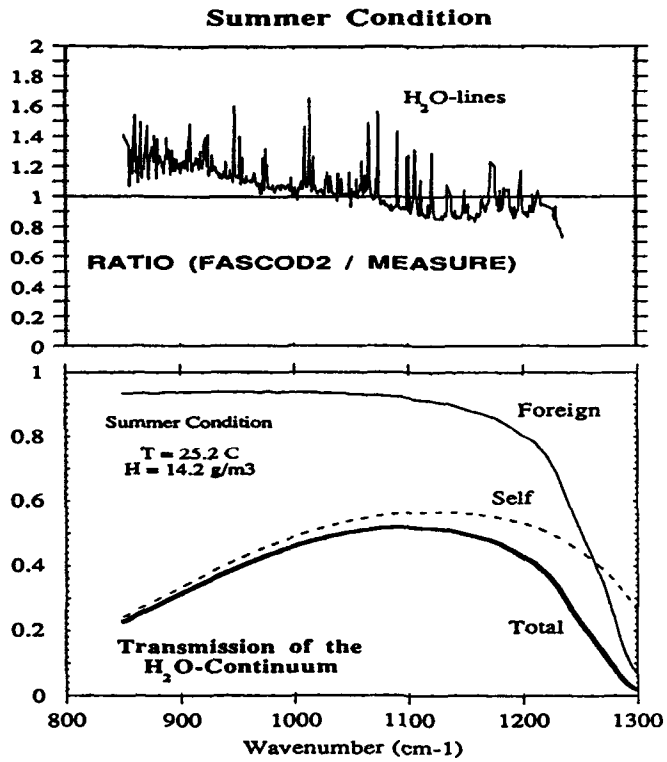

Comparison winter/summer for the
7.4-11.8 μm region
27 MARCH 1990
T=0.22 C
H=1.55 g/m
V_fit=42 km
FASCOD2-Measure
25 JULY 1990
T=24.2 C
H=14.02 g/m3
V_fit=20.0 km
FASCOD2-Measure
TRANSMITTANCE
1
0.8
0.6
0.4
0.2
0
-0.2
850
950
1050
1150
1250
1350
WAVENUMBER (cm-1)

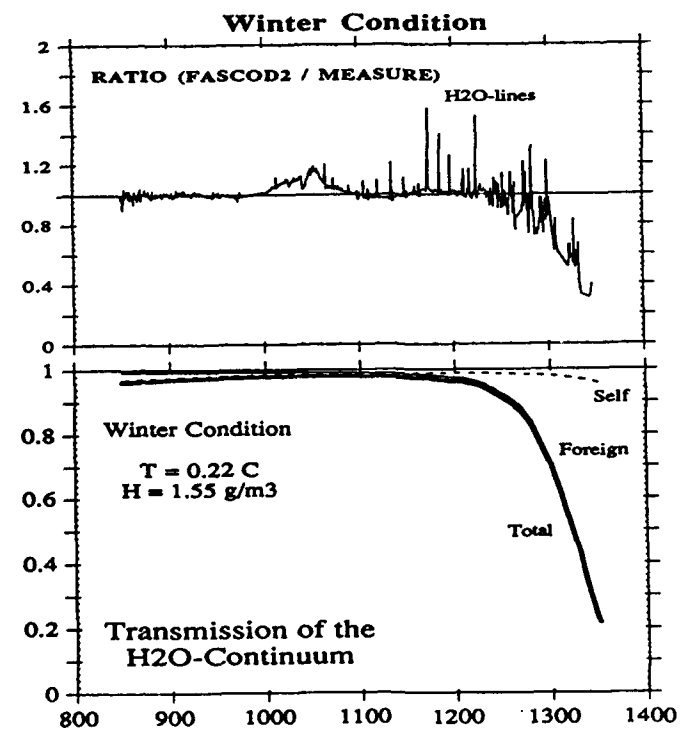

Comparison winter/summer in the
4.5-5.5 µm region
27 MARCH 1990
T=0.22 C
H=1.55 g/m
V_fit=42 km
FASCOD2-Measure
26 JULY 1990
T=28.0 C
H=13.3 g/m3
V_fit=15.9 km
FASCOD2-Measure
TRANSMITTANCE
WAVENUMBER (cm-1)
1800
1900
2000
2100
2200
2300


Comparison winter/summer in the
3.3-4.3 µm region
27 MARCH 1990
T=0.22 C
H=1.55 g/m
V_fit=42 km
FASCOD2-Measure
26 JULY 1990
T=28.0 C
H=13.3 g/m3
V_fit=15.9 km
FASCOD2-Measure
TRANSMITTANCE
WAVENUMBER (cm-1)
2350
2450
2550
2650
2750
2850
2950
3050

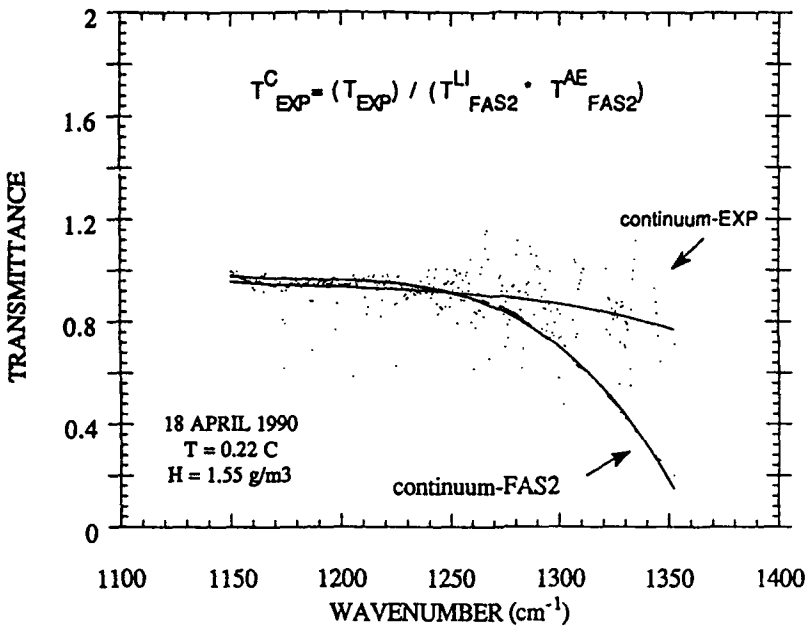

FASCOD2 - MEASURE (SUMMER)
TRANSMITTANCE DIFFERENCE
0.2
0
-0.2
T=20.1 C
H=13.3 g/m3
T=24.2 C
H=14.0 g/m3
T=28.0 C
H=13.3 g/m3
T=25.2 C
H=14.2 g/m3
T=29.4 C
H=13.3 g/m3
800
900
1000
1100
1200
1300
1400
WAVENUMBER (cm-1)


FASCODE - MEASURE (year)
TRANSMITTANCE DIFFERENCE
0.2
0
-0.2
T=25.2 C
H=14.2 g/m3
T=19.6 C
H=9.49 g/m3
T=9.41 C
H=3.79 g/m3
T=4.15 C
H=2.08 g/m3
T=0.22 C
H=1.55 g/m3
T=-8.55 C C
H=1.16 g/m3
800
900
1000
1100
1200
1300
1400
WAVENUMBER (cm-1)

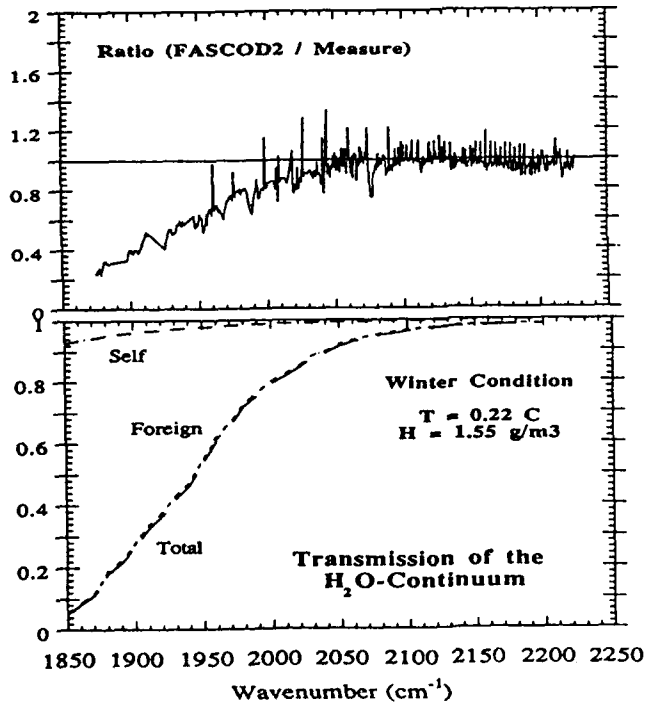

Summer Condition
H2O-lines
RATIO (FASCOD2 / MEASURE)
Summer Condition
T = 25.2 C
H = 14.2 g/m3
Foreign
Self
Total
Transmission of the
H2O-Continuum
Wavenumber (cm-1)


Winter Condition
RATIO (FASCOD2 / MEASURE)
H2O-lines
Winter Condition
T = 0.22 C
H = 1.55 g/m3
Self
Foreign
Total
Transmission of the
H2O-Continuum

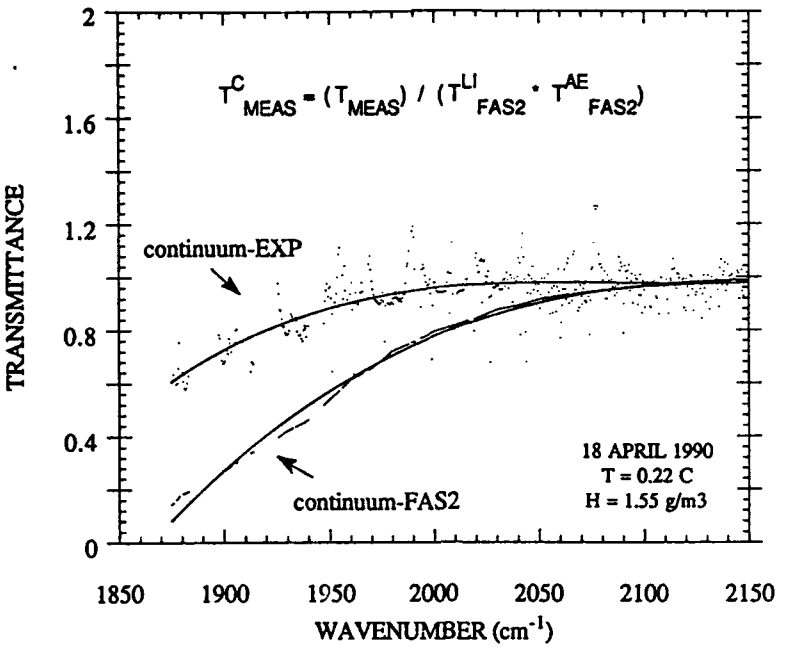
H_2O-continuum evaluation (cold conditions)

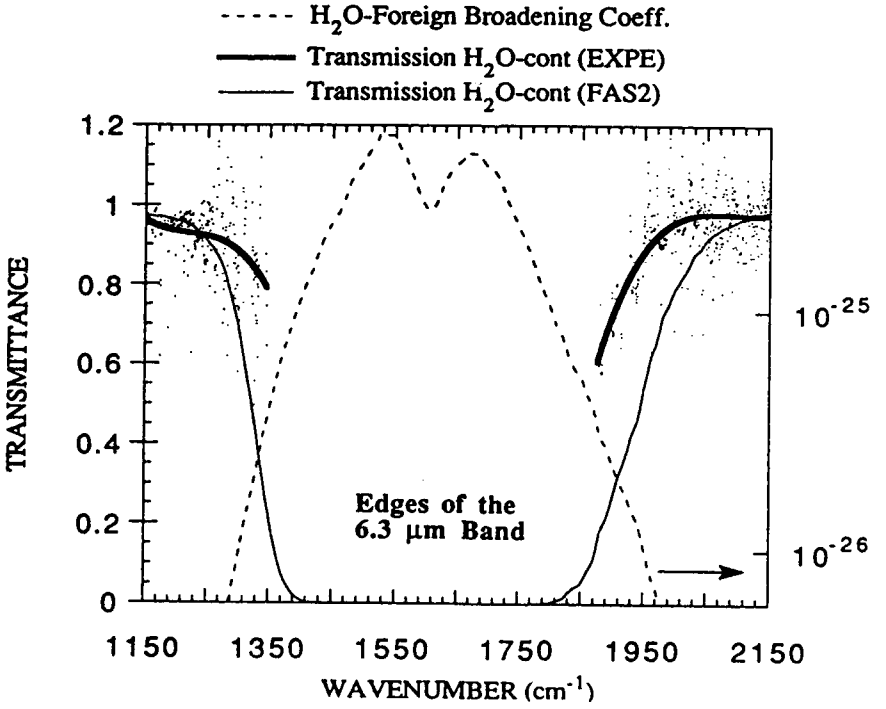


Winter Condition (4.5-5.5 μm)



H2O-continuum evaluation (cold conditions)





Comparison of Measurements with LOWTRAN7 :

1 - Resolution degraded to 20 cm^{-1}

2 - Spectral region: 850-3500 cm^{-1}

3 - Temperature Range: -8.55 to 29.4 C

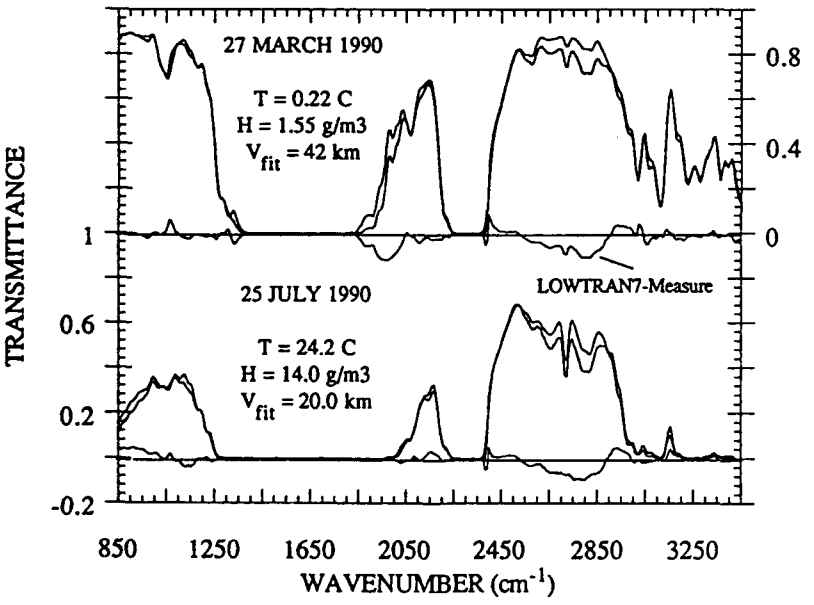
4 - Humidity Range: 1.16 to 14.2 g/m^3

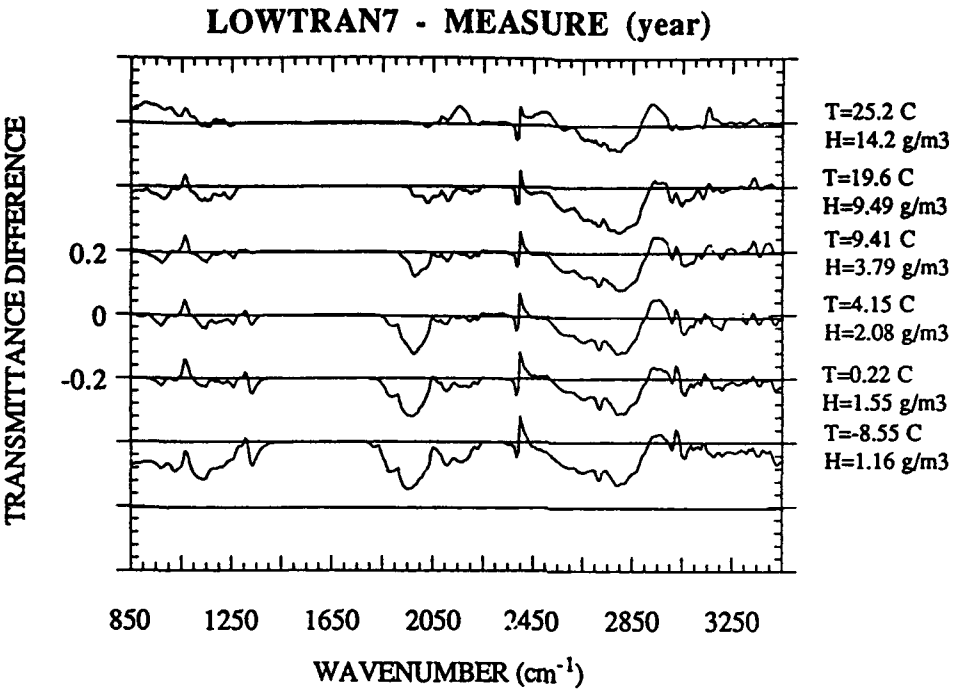
6 - Contributions of other active molecules namely O_3, N_2O, CH_4, CO, O2, and N_2 : AFGL Mid-summer or Mid-winter conditons except for the CO_2 (350 ppm)

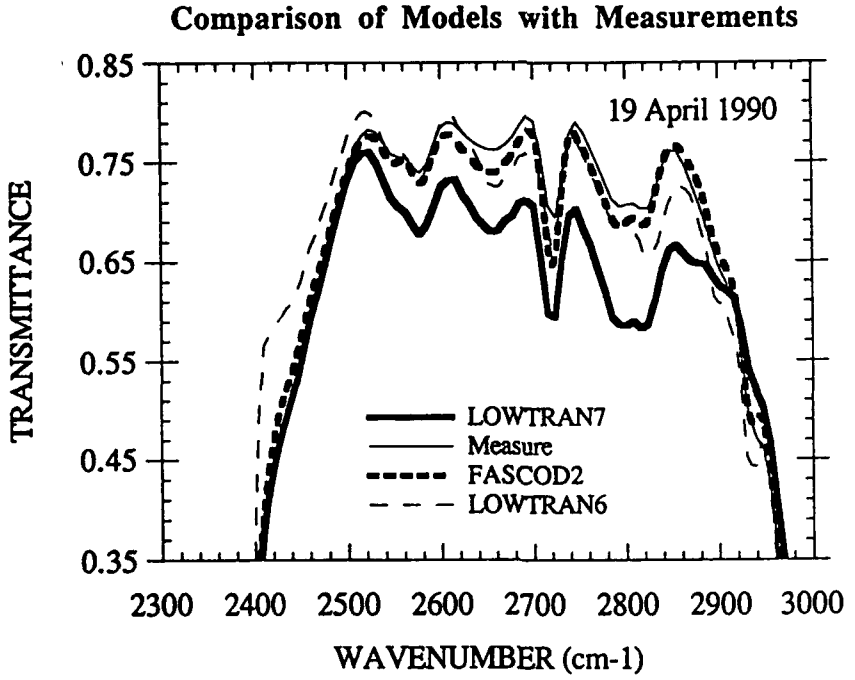
7 - Aerosol model: Rural Type

8 - Visibility evaluation: **Matching FASCOD2 spectra** with measurements at 2684 cm^{-1}

Comparison winter/summer for the 3-12 μm region




LOWTRAN7 - MEASURE (year)
TRANSMITTANCE DIFFERENCE
0.2
0
-0.2
T=25.2 C
H=14.2 g/m3
T=19.6 C
H=9.49 g/m3
T=9.41 C
H=3.79 g/m3
T=4.15 C
H=2.08 g/m3
T=0.22 C
H=1.55 g/m3
T=-8.55 C
H=1.16 g/m3
850 1250 1650 2050 2450 2850 3250
WAVENUMBER (cm-1)


Comparison of Models with Measurements
TRANSMITTANCE
0.85
0.75
0.65
0.55
0.45
0.35
19 April 1990
LOWTRAN7
Measure
FASCOD2
LOWTRAN6
2300 2400 2500 2600 2700 2800 2900 3000
WAVENUMBER (cm-1)

SUMMARY(FASCOD2)

1 - Overall agreement with measurements is very good. The average difference over the 3-12 μm region is generally smaller than 5% (ΔT/T). The remaining differences have been attributed to the water vapor and to the ozone.

2 - The analysis of results suggest that for

H_2O - The **self** broadening continuum absorption should be increased by approximately 10-15% in the 850-1000 cm^{-1}.

- The **Foreign** broadening continuum absorption should be reduced by approximately 50 % at the edges of the 6.3 μm absorption band (5.3 μm and 7.5 μm): Assuming that the lines parameters are perfect.

- The absorption of several **lines** in the 1100-1250 cm^{-1} region should be increased by approximately 20-50%.

O_3 - Generally for temperatures smaller than 10 C, the FASCOD2 transmittance of the ozone band at 9.6 μm is higher than the experimental one by approximately 10% on the average. Both the concentration and the absorption parameters may be the cause of this.

SUMMARY(LOWTRAN7)

1 - The average difference is generally smaller than 8%.

2 - The analysis of results suggest that for

H_2O - Continuum: (same remarks as for FASCOD2)

CH_4 - In the transmission window near 3.6 μm, LOWTRAN7 is always smaller than the measured one by approximately 12%, independently of the temperature and humidity conditions. It is attributed to the modeling of the 3020 cm-1 absorption band of methane.

SPECTRAL SOLAR RADIATION MODELING, MEASUREMENT, AND DATA BASE ACTIVITIES AT THE SOLAR ENERGY RESEARCH INSTITUTE

C.J. Riordan, R.L. Hulstrom
Solar Energy Research Institute, 1617 Cole Boulevard, Golden, CO 80401

The Solar Energy Research Institute uses atmospheric transmission codes and data to characterize spectral solar radiation (0.3-3.0 μm) at the earth's surface for designing and predicting the performance of spectrally selective solar energy conversion devices, such as solar electric cells (photovoltaics). We use a simple model called SPCTRAL2 that was developed at SERI using comparisons with more complex codes, such as LOWTRAN, and comparisons with limited measured data. We also maintain a data base with 3000 measured spectra, 0.3-1.1 μm at a 2-nm resolution. Our current activities include participation in a new International Energy Agency, Solar Heating and Cooling Program, Task 17 on Measuring and Modeling Spectral Radiation Affecting Solar Systems and Buildings. We will present an overview of all of our spectral solar radiation modeling, measurement, and data base activities at SERI.

Spectral Solar Radiation Modeling, Measurement, and Data Base Activities at the Solar Energy Research Institute

Carol Riordan and Roland Hulstrom

Solar Energy Research Institute
Golden, Colorado
303-231-1344 303-231-1220

June 1991

SERI

Objective

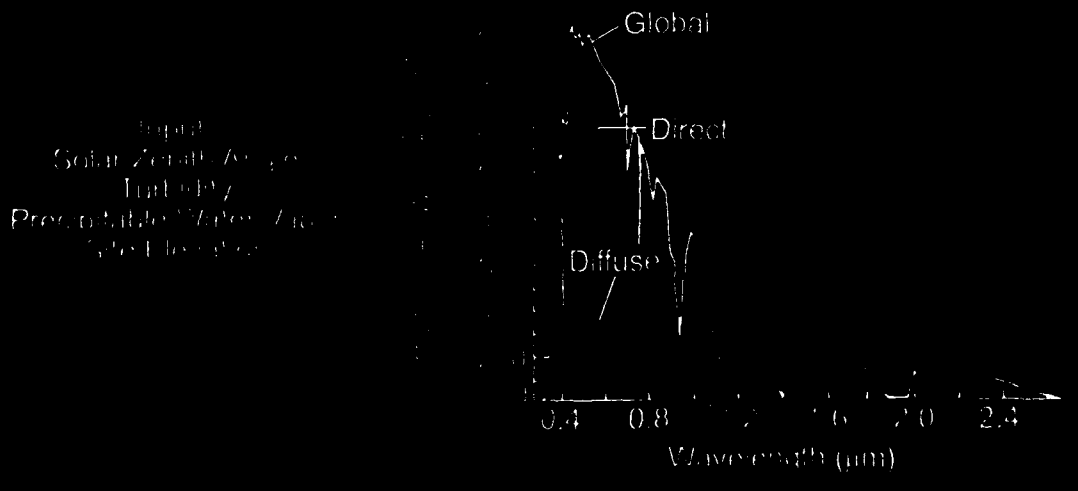
Briefly describe SERI's interests and activities in spectral solar radiation, and identify conference participants with similar interests

Tektronix

Interests

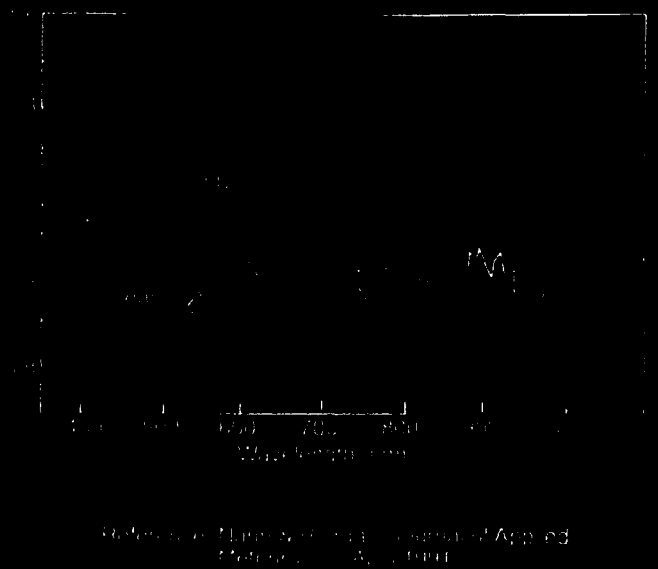
Spectral solar radiation at the earth's surface from 280 to 3000 nm at about 1-nm resolution for designing and predicting the performance of spectrally selective solar energy conversion devices (e.g.,photovoltaics)

Modeling



Modeling

Cloud Cover Modifier



Modeling - Measurements

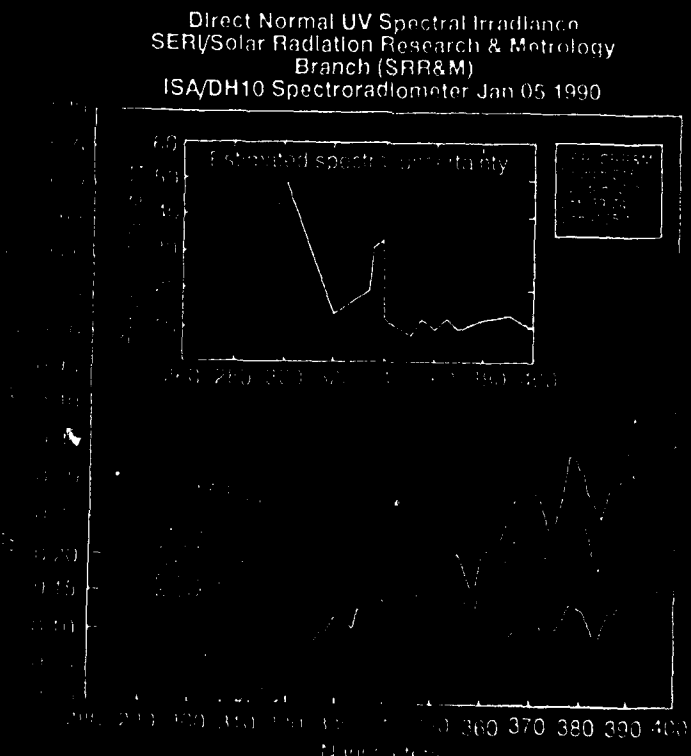
International Energy Agency
Solar Heating and Cooling Programme Annex 17
Measuring and modeling spectral
radiation affecting solar systems and buildings

A: Narrow-band spectral and broad-band infrared radiometry
B: Broad-band visible radiometry
C: Narrow-band spectral radiation data acquisition and analysis
D: Narrow-band spectral radiation modeling-SERI
E. Broad-band visible radiation data aquisition and analysis
F. Broad-band infrared radiation data aquisition and analysis

Measurements

Spectroradiometers

Geophysical Environmental Research	300-3000 nm
LI-COR LI-1800	300-1100 nm
Optronic Laboratories - 752D	200- 800 nm
Instruments S.A DH10	200- 800 nm



SERI

Measurements

Department of Energy
Atmospheric Radiation Measurement
(ARM) Program

Characterizing, evaluating, and calibrating instruments for measuring atmospheric properties and radiation at the Clouds and Radiation Testbed (CART) Sites

LOWTRAN 7 COMPARISONS WITH FIELD MEASUREMENTS

R. Smith, N. McNabb, K. Hammerdorfer, T. Corbin
TECOM Fort Belvoir Met Team, AMSTE-TC-AM (BE) CCNVEO,
Ft. Belvoir, VA 22060

This paper presents comparisons between LOWTRAN 7 and field measurements taken during a number of field tests conducted by the US ARMY Center for Night Vision and Electro-Optics. The data was taken by the TECOM Ft. Belvoir Meteorological Team. Transmission data in the .4 to .7 micron, 3 to 5 micron, and 8-12 micron bands were taken at Ft. A.P. Hill, VA in March and April 1991. Data at 1.54 micron was taken at Ft. Greely, AK in February and at Ft. Clayton, Panama during March and April 1991. A description of the equipment is provided along with the input values used for the LOWTRAN calculations.

LOWTRAN 7 COMPARISONS WITH FIELD MEASURMENTS

R.W.SMITH,T.CORBIN,N.MCNABB,K.HAMMERDORFER
TECOM FT BELVOIR METEOROLOGICAL TEAM

This paper presents comparisons between LOWTRAN 7 and field measurments taken during a number of field tests conducted by the US ARMY Center for Night Vision amd Electro-Optics at several different locations. The data was collected by the TECOM Ft Belvoir Meteorological Team. Data includes transmission at 1.54 microns,3-5 microns, and 8-12 microns. A brief description of the equipment and meteorological parameters are presented along with the measured transmission and calculations using LOWTRAN 7 and in one example, MODTRAN.

INTRODUCTION

One of the most important measurements made by this team in support of test operations is that of atmospheric transmission. It is essential to evaluate the performance of the many different articles our customers test ranging from R&D to operational evaluation. Transmission models are also of great importance to us. We use them in studies and we use them in field support. In field support, we often use LOWTRAN calculations whenever it is not possible or practical to use our measurement equipment due to size of the test or other considerations. For example, it is generaly not practical to provide support which takes four days to set up to support a one day test. At times, we must support one test with LOWTRAN while our equipment is in use on another test. We also use LOWTRAN to monitor the behavior of our measurement equipment by making real time calculations which our technicians compare to the measured data. In this manner, we can detect problems quickly and take corrective action. This is built into our automated run stream and serves as a great quality control mechanism. It is obvious then that we must have confidence in the transmission model in use and have a feel for how it performs under various conditions.

A few comments may be appropriate before we launch into the data. First is that this data was collected as part of testing programs with specific objectives and unfortunatly collecting nice clean data for these comparisons were not amoung them. So we have to live with real world problems of power,equipment changes, unwanted vehicle traffic, etc. These will be pointed out whenever possible. The second comment concerns the meteorological data. In some tests, we have to use locally collected data which is not designed to support E-O testing. Some problems with this will be pointed out. During large tests where we are collecting all data ourselves,we feel much more comfortable in its quality and representiveness.

The discussion will be organized with a brief description of our equipment at the beginning, then we will look at data collected at Ft AP Hill,Va in the 3 to 5 micron band and the 8-12 micron band. Visible data could not be obtained during this test because of a broken beam combiner at the transmissometer source.Next we will look at data taken for the Miniature Eyesafe Laser Infrared Observation System at 1.54 microns. This data was taken in Alaska, Panama, and Utah. Finally, and example involving MODTRAN will be presented. In all the comparisons,I must give credit to Major(Dr) Bob Hughes of the Wright-Patterson AFB Staffmet office for supplying the pc version of LOWTRAN7.I should point out that lowtran was run using 1.54 microns +/- 10 wave numbers.

1. INSTRUMENTATION:

The transmissometer system used for all the data except the section on modtran was a Barnes 4.5 inch research radiometer system with a 1000 C blackbody source for the 3-5 and 8-12 bands, an InSb detector for 3-5 microns and MCT for the 8-12 band. Both detectors are LN2 cooled. For the 1.54 transmission, a Germanium detector was used with a high intensity quartz halogen light source. Presision optics are used for even distribution of the energy and the beam is highly collimated. The system was calibrated by abutting the source and receiver to eliminate atmospheric and system effects. Then appropriate corrections for range and optics were applied. The result is a measurement of absolute transmission. Discussion of the equipment used for the higher resolution data is described in that section.

2. Ft A.P. Hill,Va Data

The following data was taken as part of the MultiSensor Automated Targeting field test. This data was taken over a two kilometer path with extensive meteorological measurements taken at both ends and optical turbulence measurements taken over the first kilometer of the path. Temperature and humidity measurements were done with Vaisala humicaps, visibility using a HSS visibility meter, rate of rain with a STI optical rainrate instrument,pressure by an AIR digital barometer and ceiling with a Vaisala Laser Ceilometer. Many other parameters were measured, such as soil temperature,solar radiation,and wind and are available on floppy disk. Meteorological data are collected on an automated system and represent 15 minute averages. Two days of data are presented. The data is presented in charts at the end of the text,hopefully in the correct order.

a. 20 Mar 91: This was a partly cloudy day with no clouds below 12000ft. Optical turbulence was in the light range so that data is not presented. Looking first at the met data, it is quite unexciting except for three spikes. These are periods were equipment was being changed or repaired causing a period of bad data (eliminated in the official test data base).Only site one data is included because site two data is identical.

The first comparison shows 3-5 microns. We had significant power stability problems due to cool weather with its use of heaters and due to the number of test particpants.During the period before 1400 our data read well below lowtran. We did not have a select amplifier in use on the 3-5 system so holding a good signal was difficult.We did achieve stable power by 1400 and the comparison to lowtran now becomes quite good.One minute data

shows the problems clearly especially the two periods when the lock-in amplifiers were turned off to reset the system.

The 8-12 system had a select amplifer so we actually obtained good data sooner. The one minute data indicates that while the data stabilizes easier, twiking the system takes longer.I should point out that the spike at about 0900 coincident with the met equipment problem is just that- coincidence.

b. 22 Mar 91: This day brings change with higher humidity and a period of rain. Site one data only for temperature and pressure are shown because they are identical.Both sites are shown for RH and visibility because differences are indicated. Note that differences in visibility increase with increasing visibility. That is common with the HSS instrument. But below 10 km the differences are real.Cloud height is shown as is a comparison of the rain rates (sites 3&4 are further down range). The difference between site one and two were verified by our observations. In this case we show our data compared to lowtran using data from both met sites. You are invited to make your own comparisons. I will say that these comparisons are consistent with what we usually observe.

3. Panama

Next we will travel south to Panama and look at the 1.54 micron region. Again we had a two kilometer path length but this time looking down some 300 meters and crossing the panama canal as shown on the map. Met data comes from the receiver site so its representiveness is in question. Two days are presented.

a.30 Mar 91: The only comment to be made about the met data is that the visibility was estimated by a human and is not representative of the path. Many fires from burning crops were in the area and especially dense during one afternoon period. The break in the measured data was caused by lunch. Note the very good agreement during the last hour.

b. 1 Apr 91: This day had no fires to contend with and the comparison is straight foward. Some of the difference is probably due to our detector band width.

4. Alaska

This was done with the cold weather testing of the MELIOS at the Cold Regions Test Center, Ft Greely, Alaska. Part of this test involved smokes. Again, met data was taken at the receiver site. The comparison chart shows mainly why were still in business. Between generator smoke and the obscurant smoke, comparisons are not really possible. For this paper, we will not discuss the type of obscurant used

5. Utah

The final stop on our support of MELIOS was the Dugway Proving Ground in Utah. Met data is again at the receiver site by a human,the path is two kilometers and very flat, but now the altitude is near 4000ft. In this case three days are shown.

a.21 May 91: The met data is included for reference. This was a clear warm day and had very strong optical turbulence, I would estimate in the 10E-12 range. The first comparison shows one hour averaged data with measured being somewhat lower that lowtran. Near the end of the day, dust from vehicles came over our path dropping the transmission but the observer could still see the top of the mountain 90 miles away. The fact that we could not see the base 10 miles away was not recorded. The effect of the turbulence can be seen on the one minute data.

b.22 May 91: This day was cloudy and cooler and the observed turbulence was slight. Now we have excellant agreement between measured and calculated. The one minute data captures a vehicle which kept crossing our line of sight, a problem we were able to resolve with our powers of persuasion.

c.23 May 91: This day was partly cloudy with moderate turbulence. Lack of turbulence measurments is a bother. But again in this case, with a uniform path and moderate turbulence, we found very good agreement with lowtran 7.

6. Summary

The above data gives us considerable confidence in using LOWTRAN7 as a tool of great usefullness. When one has good met measurements which describe the path, good comparisons can be obtained. As for scintillation, it most certainly is a factor in obtaining field measurements, but that is another topic which we intend to address in another paper.

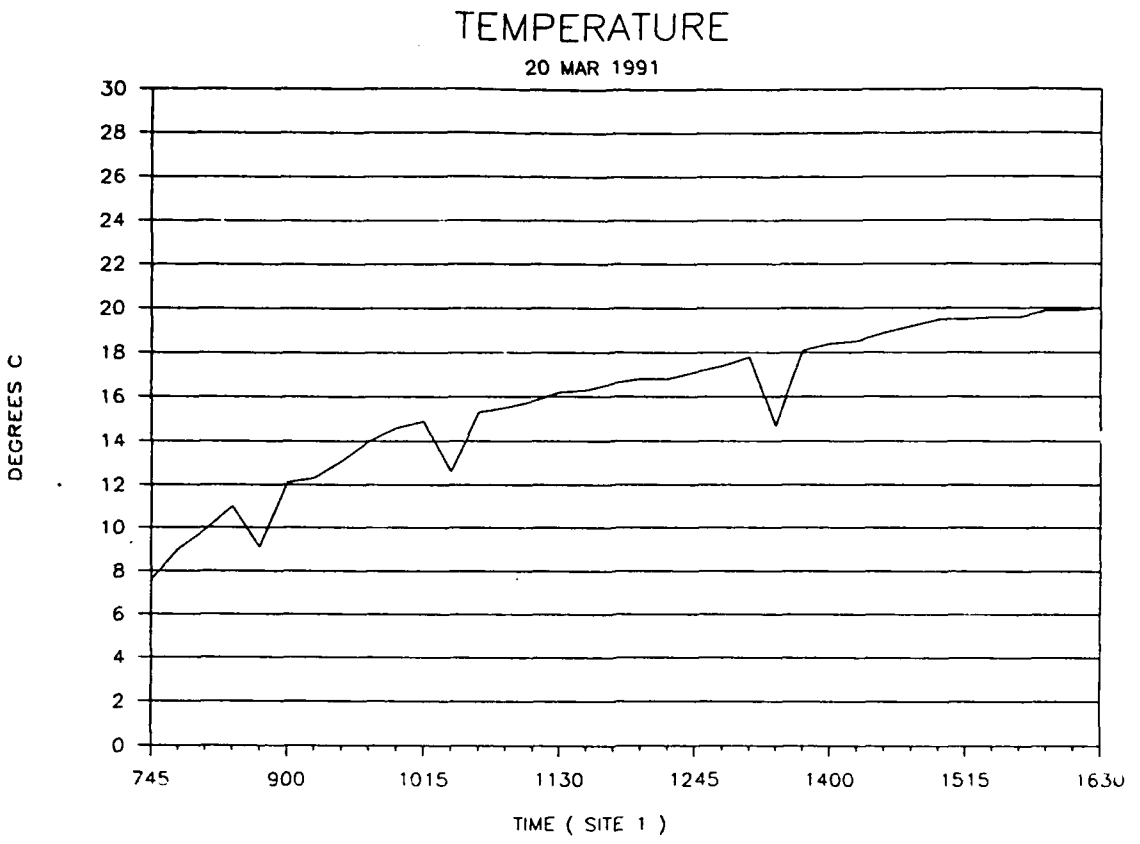
7. Bonus

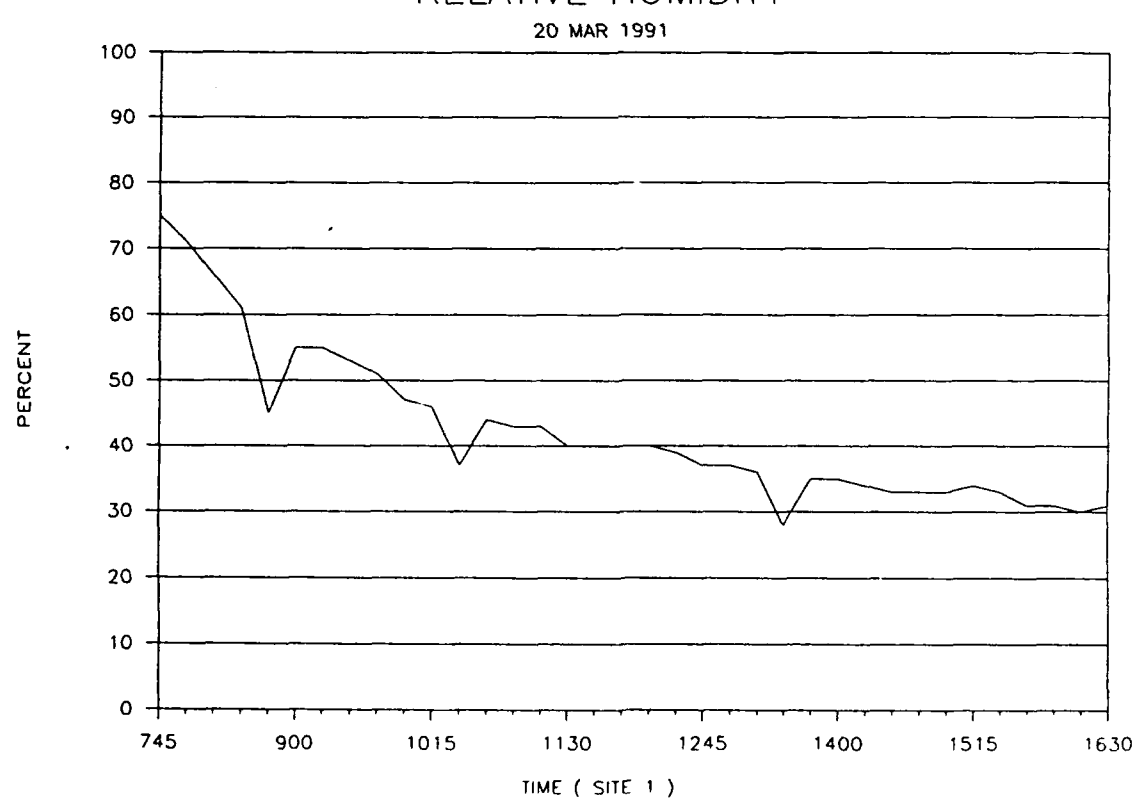
We would like to present some data we took in Germany in 1988 using our Nicolet FTIR transmissometer. This instrument has a MCTA detector with a ZnSe beamsplitter and can produce a two wave number resolution. The data were taken over a path of about 700 meters. The first chart shows the data obtained. The DF refers to distance and optics corrections. The second chart is a lowtran run using met data at both ends of the path including measured visibility. Incidently, that was also our data.The third chart shows a MODTRAN run of the same time. The agreement is very good, in fact remarkable considering our field conditions with the very sensitive FTIR.

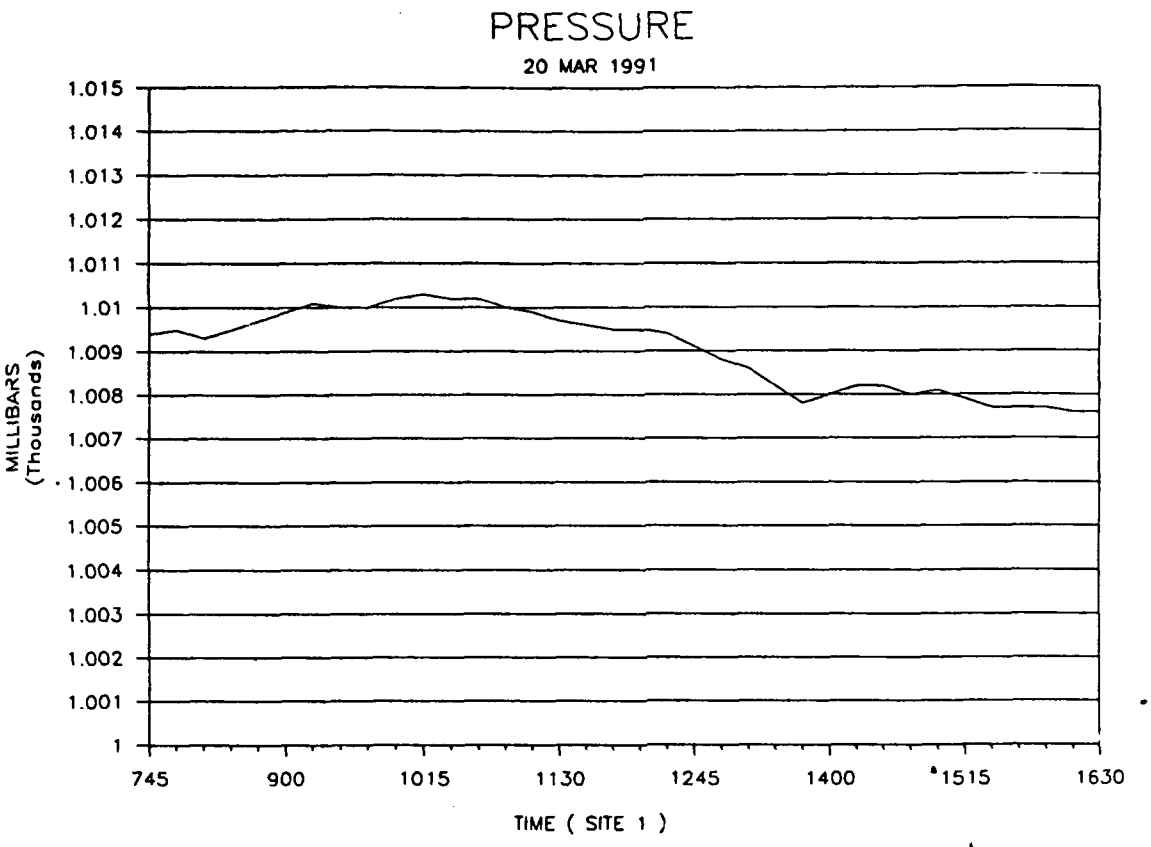
We are eagerly awaiting a pc version of MODTRAN and feel that it will eventually replace LOWTRAN in some of our support activities. Our manning and workload has interfered with our workwith the FTIR but we think that that will soon change.

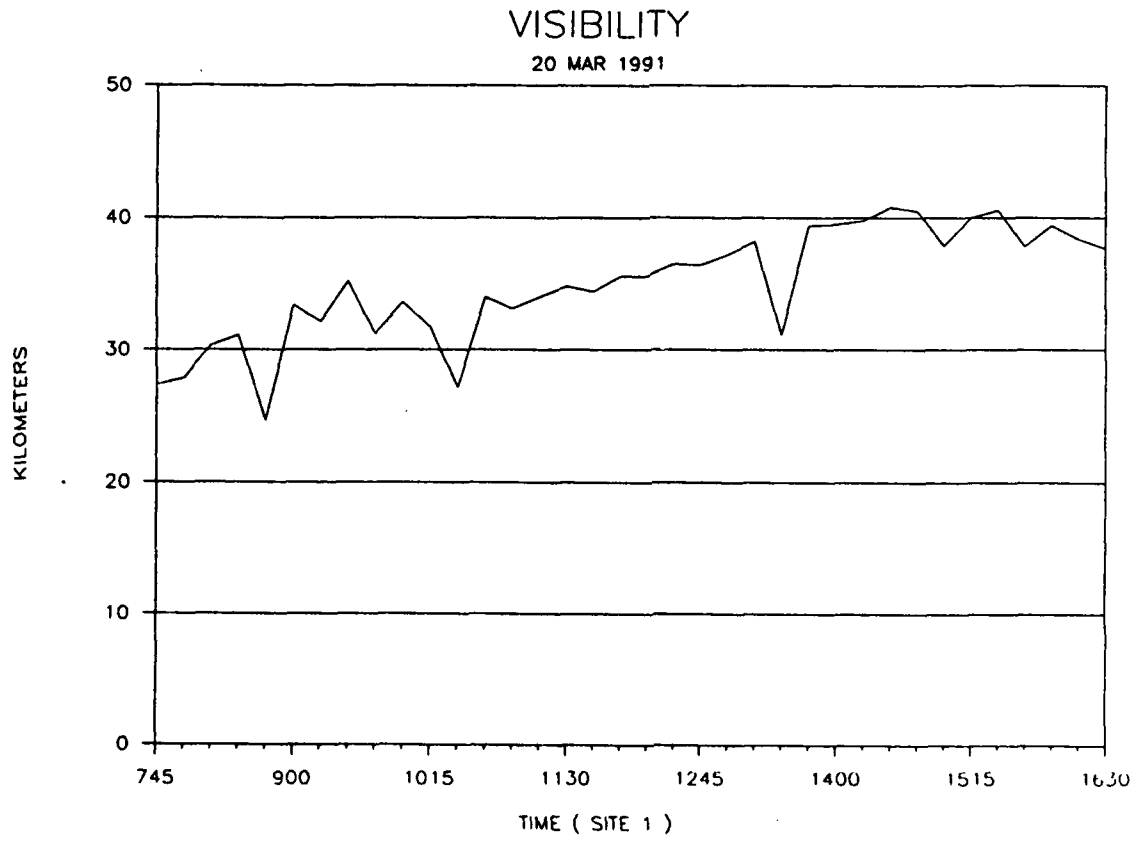
FINAL SUMMARY

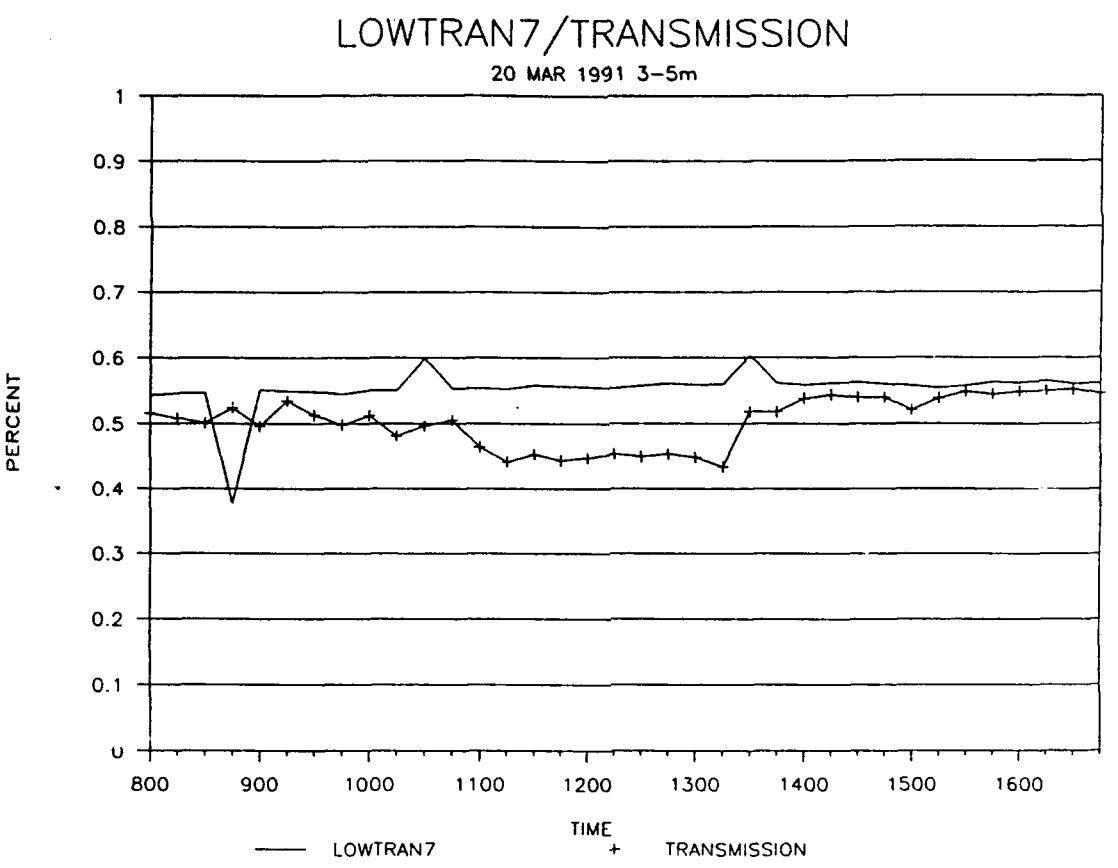
To provide support to our customers in the E-O world, we must have the capability for both measuring and calculating atmospheric transmission. We in fact use LOWTRAN7 as a quality control tool. Accordingly our confidence must be high that it is an accurate product. We feel that it is, at least to the accuracies we need and in our near the ground application. Our data shows that if the input data is accurate,so is the result.

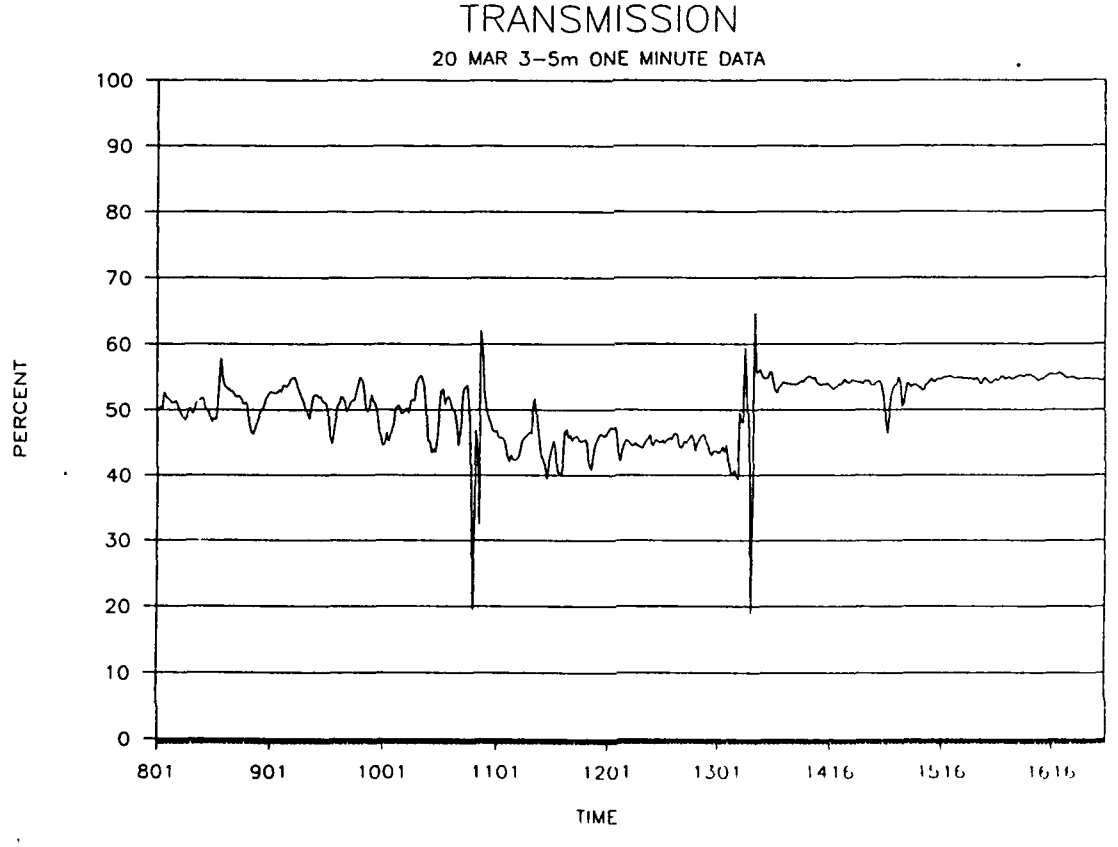

TEMPERATURE
20 MAR 1991
DEGREES C
30
28
26
24
22
20
18
16
14
12
10
8
6
4
2
0
745
900
1015
1130
1245
1400
1515
1630
TIME (SITE 1)

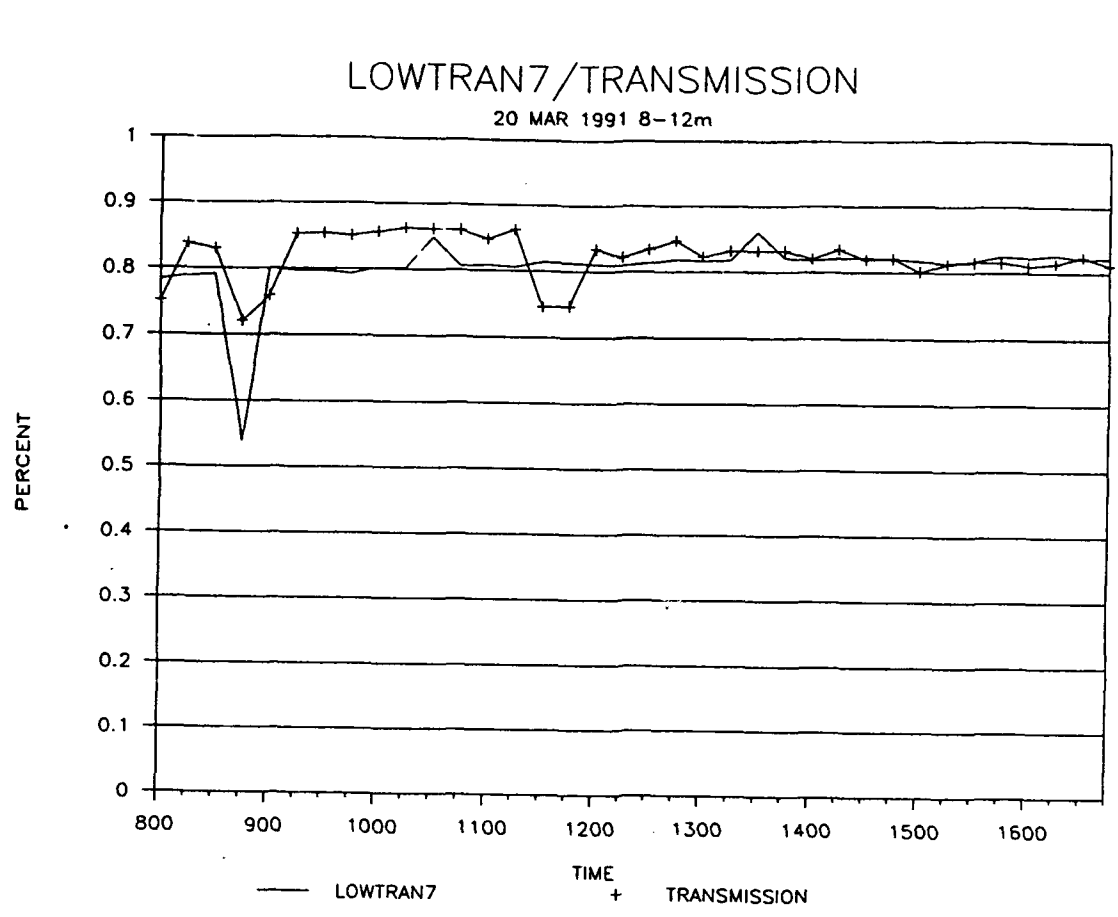

RELATIVE HUMIDITY
20 MAR 1991
PERCENT
100
90
80
70
60
50
40
30
20
10
0
745
900
1015
1130
1245
1400
1515
1630
TIME (SITE 1)

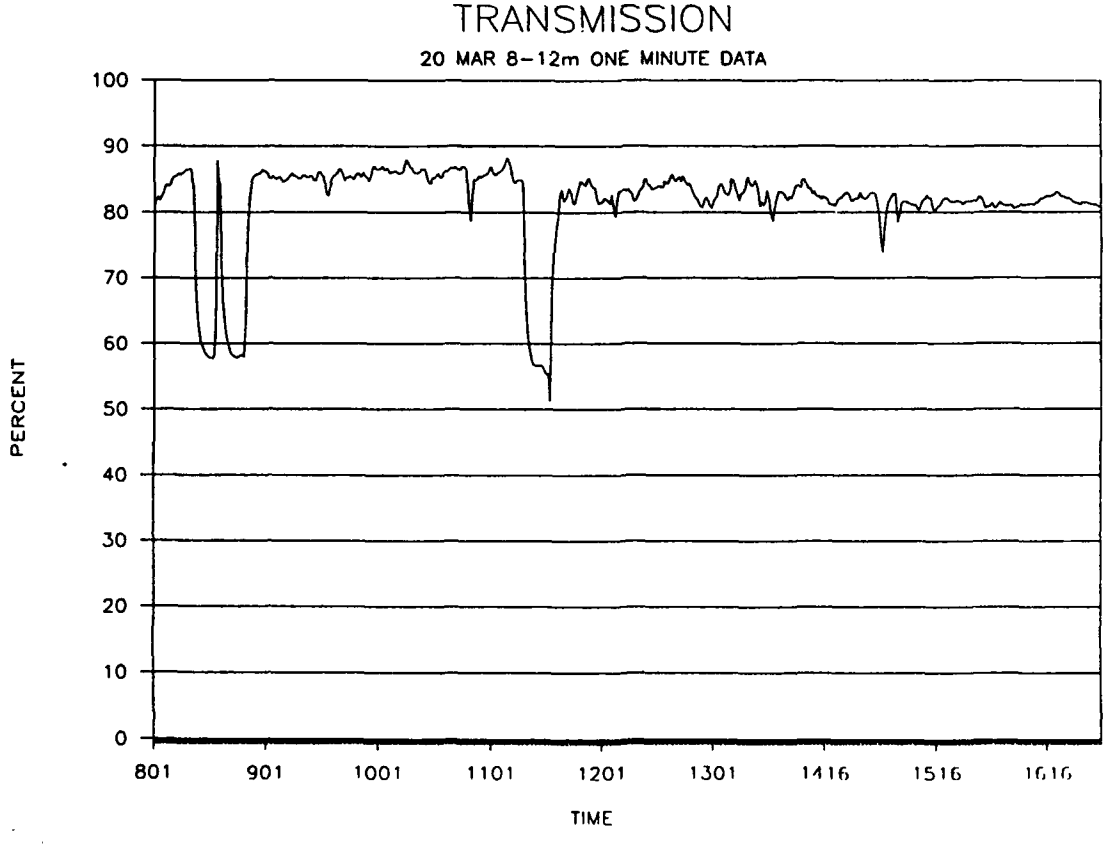

PRESSURE
20 MAR 1991
MILLIBARS (Thousands)
1.015
1.014
1.013
1.012
1.011
1.01
1.009
1.008
1.007
1.006
1.005
1.004
1.003
1.002
1.001
1
745
900
1015
1130
1245
1400
1515
1630
TIME (SITE 1)

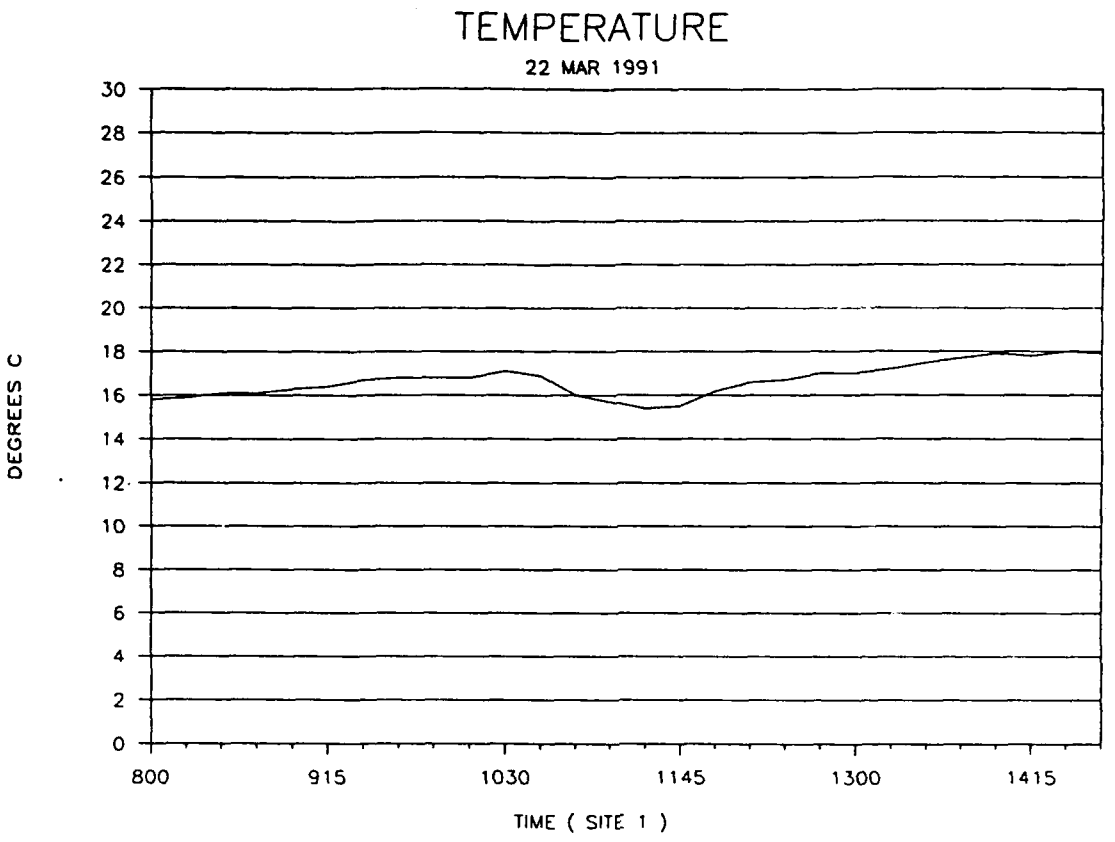

VISIBILITY
20 MAR 1991
KILOMETERS
50
40
30
20
10
0
745
900
1015
1130
1245
1400
1515
1630
TIME (SITE 1)

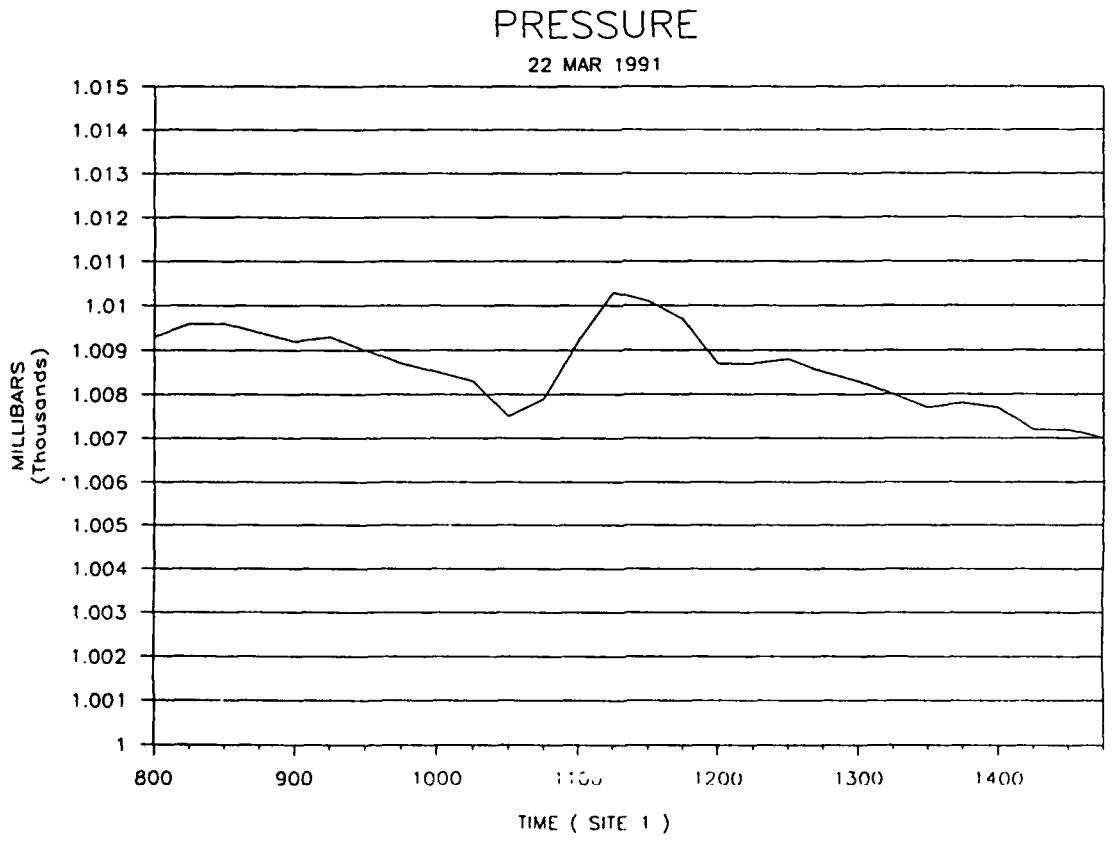

LOWTRAN7/TRANSMISSION
20 MAR 1991 3-5m
PERCENT
1
0.9
0.8
0.7
0.6
0.5
0.4
0.3
0.2
0.1
0
800
900
1000
1100
1200
1300
1400
1500
1600
TIME
LOWTRAN7
TRANSMISSION

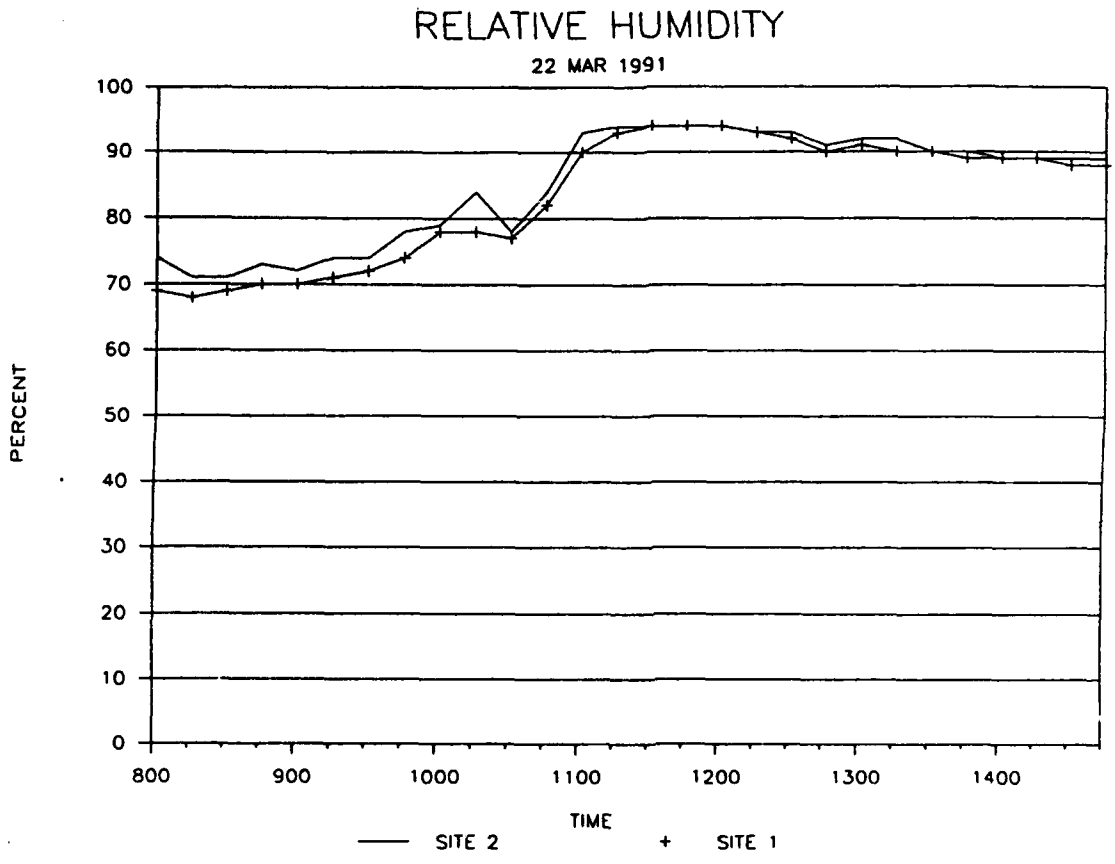

TRANSMISSION
20 MAR 3-5m ONE MINUTE DATA
PERCENT
100
90
80
70
60
50
40
30
20
10
0
801
901
1001
1101
1201
1301
1416
1516
1616
TIME

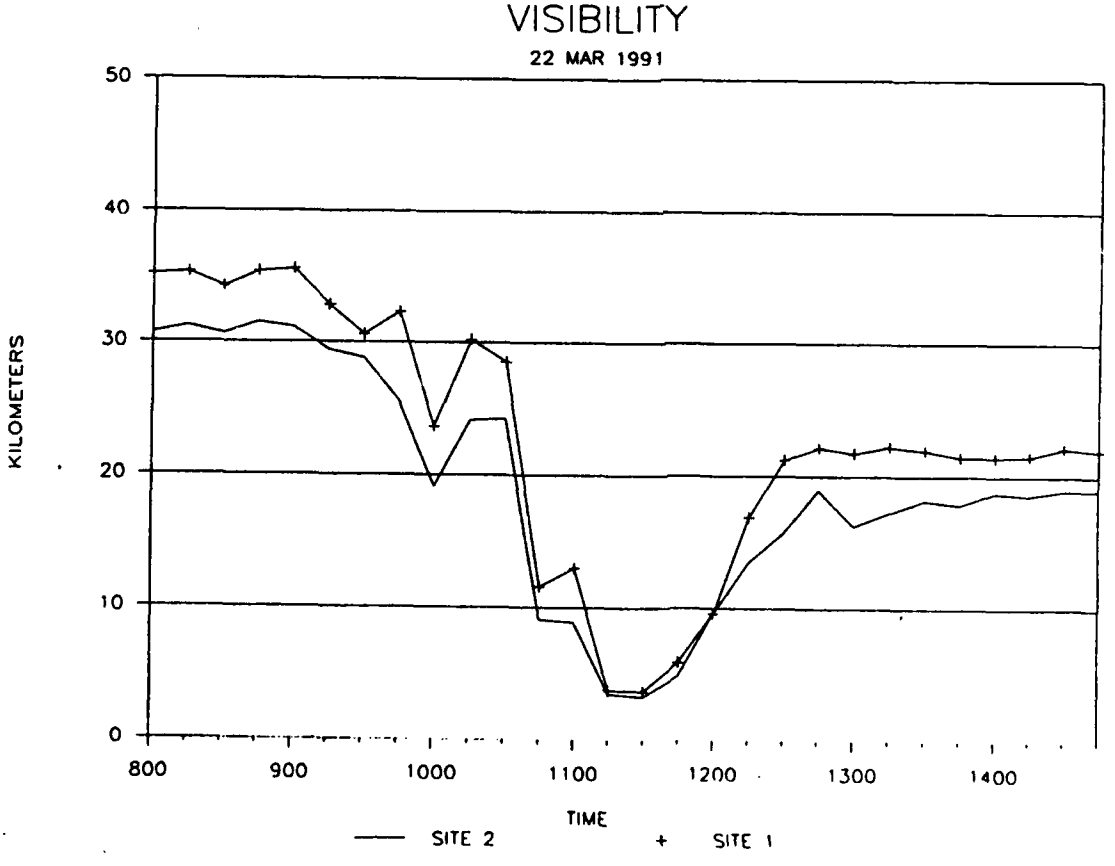

LOWTRAN7/TRANSMISSION
20 MAR 1991 8-12m
PERCENT
1
0.9
0.8
0.7
0.6
0.5
0.4
0.3
0.2
0.1
0
800
900
1000
1100
1200
1300
1400
1500
1600
TIME
LOWTRAN7
TRANSMISSION

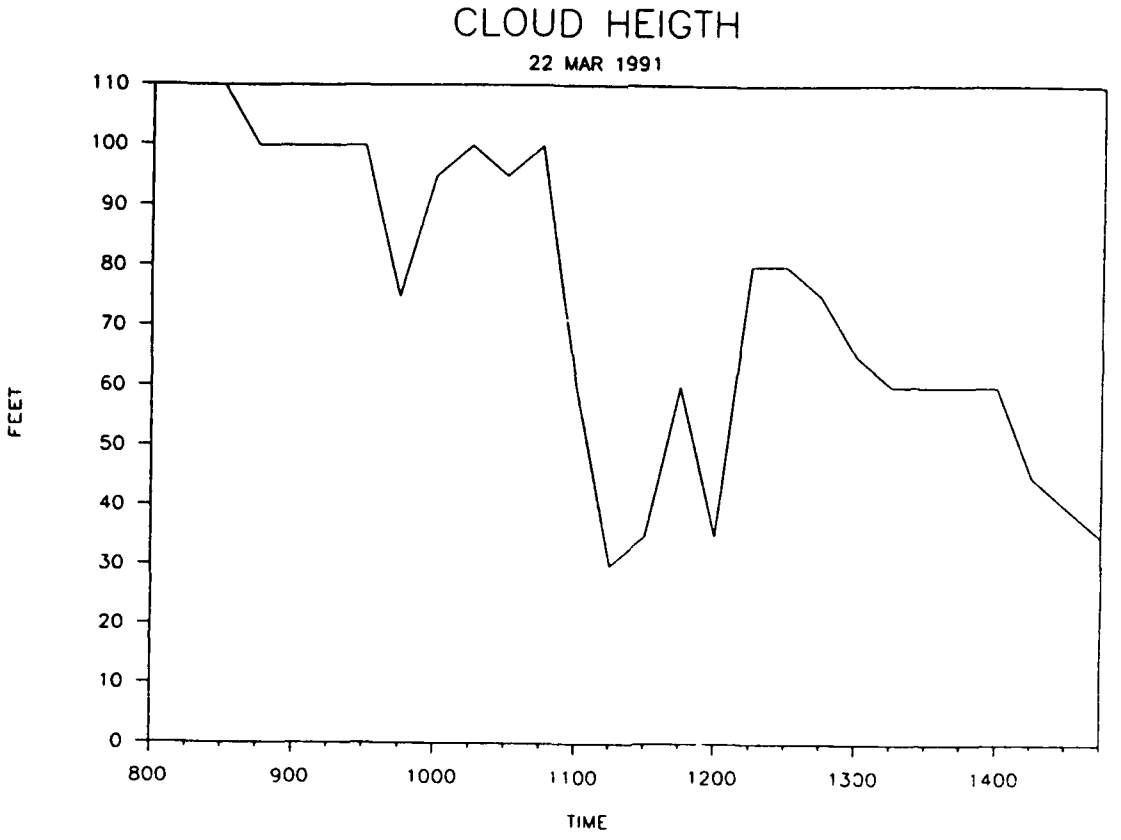

TRANSMISSION
20 MAR 8-12m ONE MINUTE DATA
PERCENT
100
90
80
70
60
50
40
30
20
10
0
801
901
1001
1101
1201
1301
1416
1516
1616
TIME

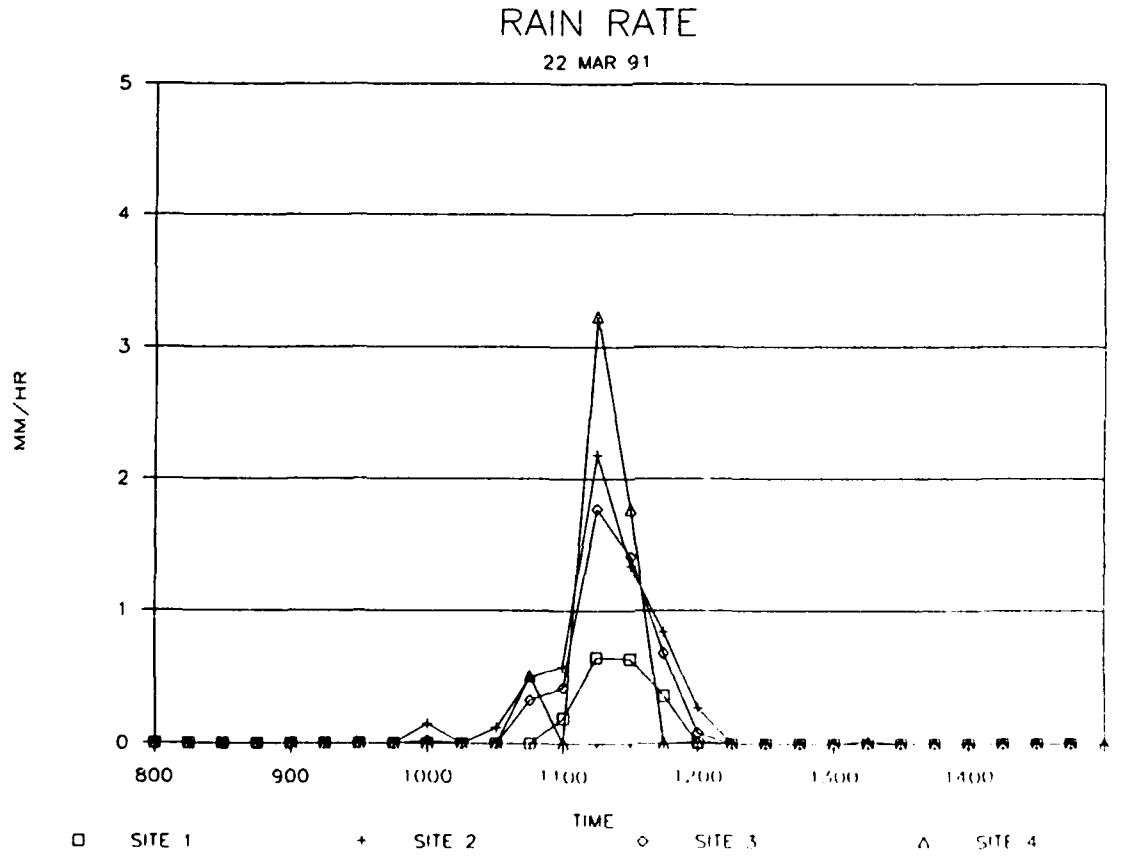

TEMPERATURE
22 MAR 1991
DEGREES C
30
28
26
24
22
20
18
16
14
12
10
8
6
4
2
0
800
915
1030
1145
1300
1415
TIME (SITE 1)

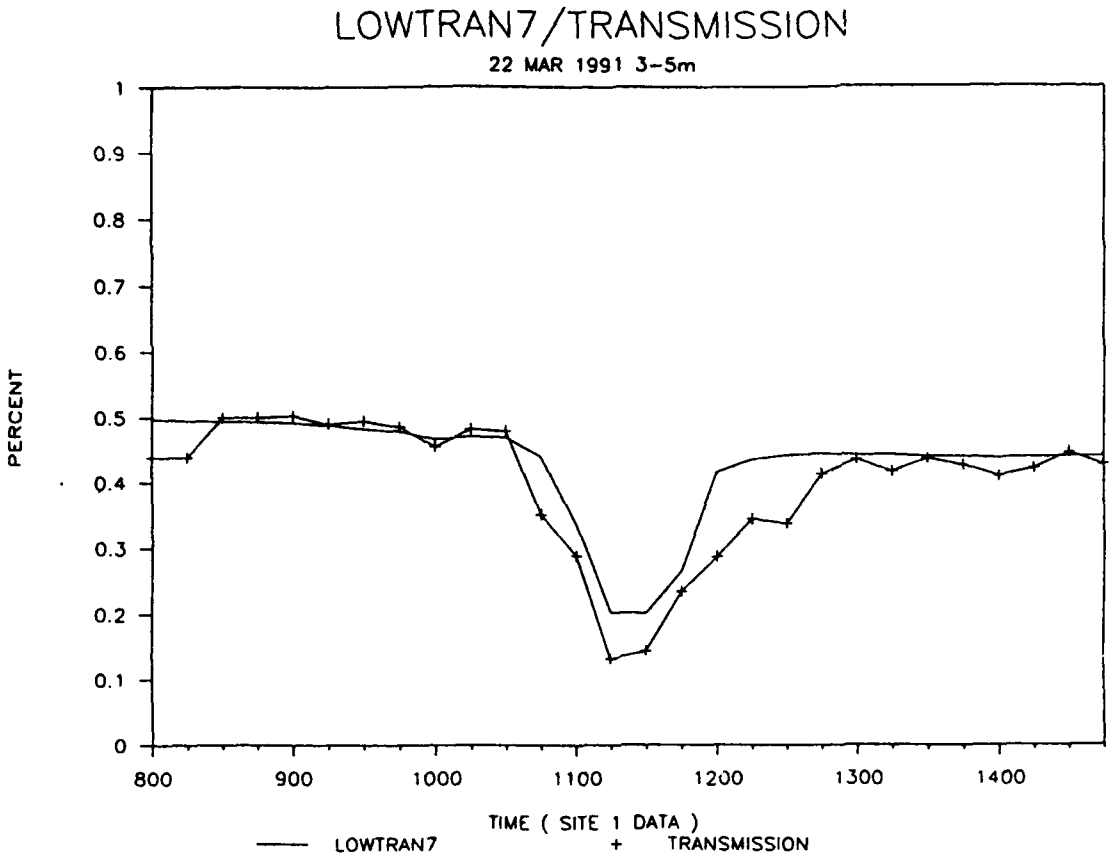

PRESSURE
22 MAR 1991
MILLIBARS
(Thousands)
1.015
1.014
1.013
1.012
1.011
1.01
1.009
1.008
1.007
1.006
1.005
1.004
1.003
1.002
1.001
1
800
900
1000
1200
1300
1400
TIME (SITE 1)

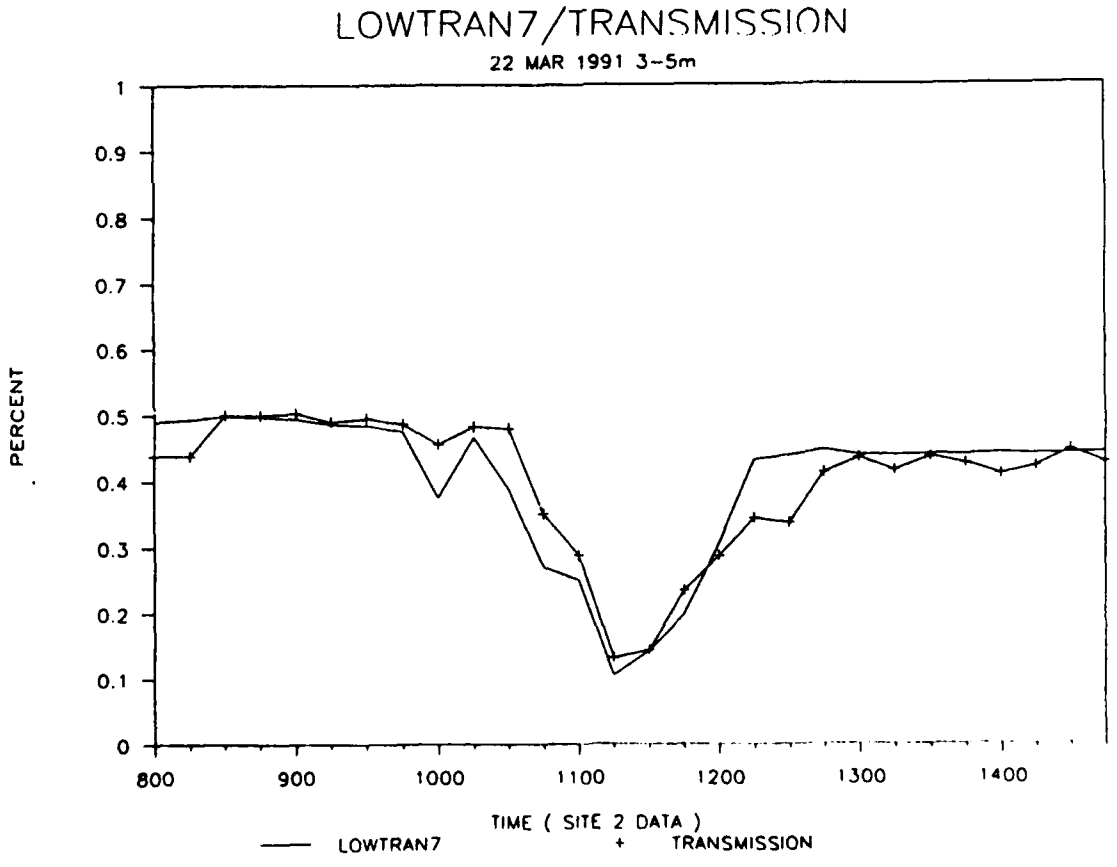

RELATIVE HUMIDITY
22 MAR 1991
PERCENT
100
90
80
70
60
50
40
30
20
10
0
800
900
1000
1100
1200
1300
1400
TIME
SITE 2
SITE 1

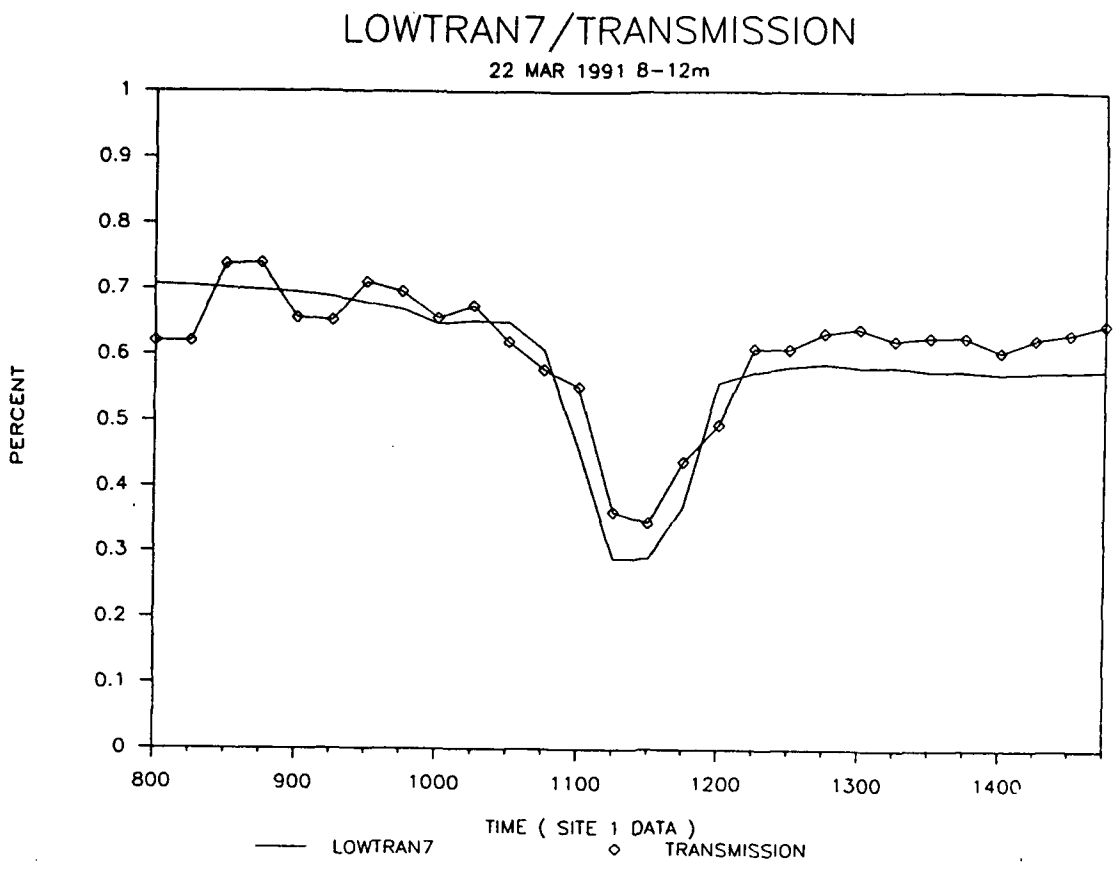

VISIBILITY
22 MAR 1991
KILOMETERS
50
40
30
20
10
0
800
900
1000
1100
1200
1300
1400
TIME
SITE 2
SITE 1

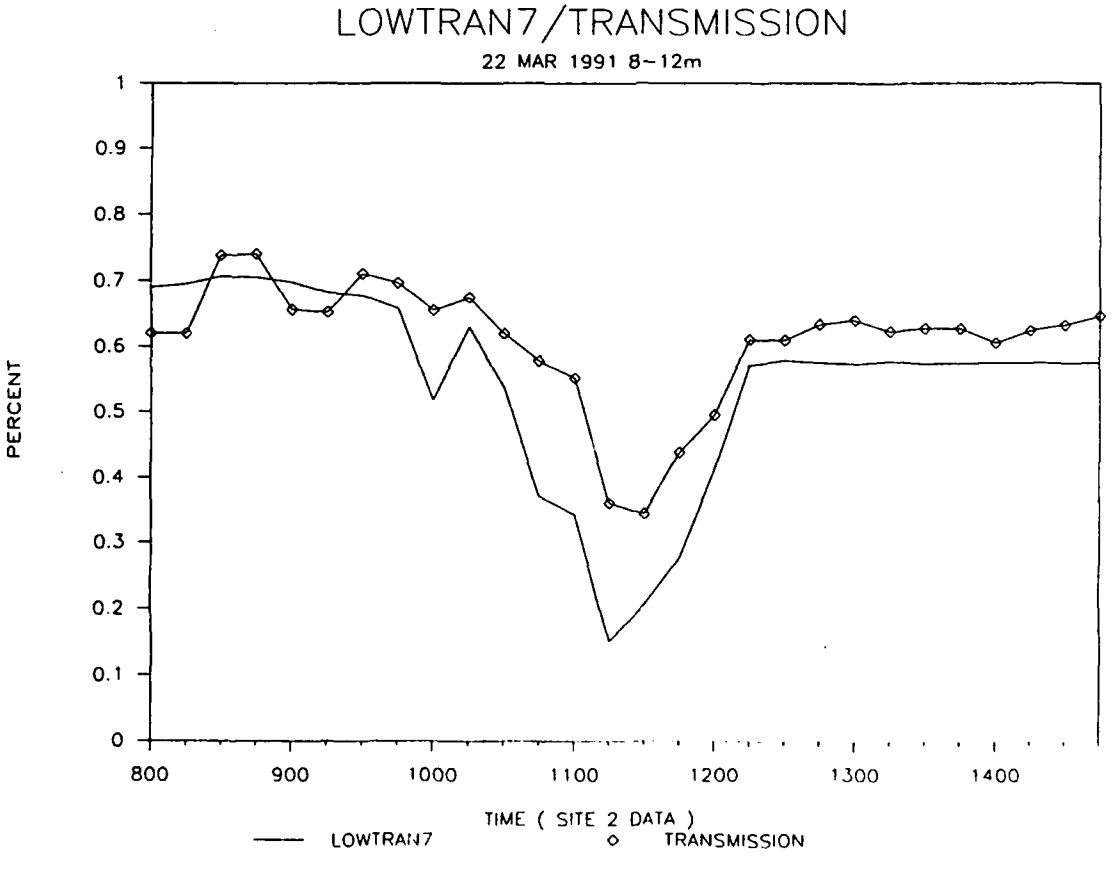

CLOUD HEIGTH
22 MAR 1991
FEET
110
100
90
80
70
60
50
40
30
20
10
0
800
900
1000
1100
1200
1300
1400
TIME

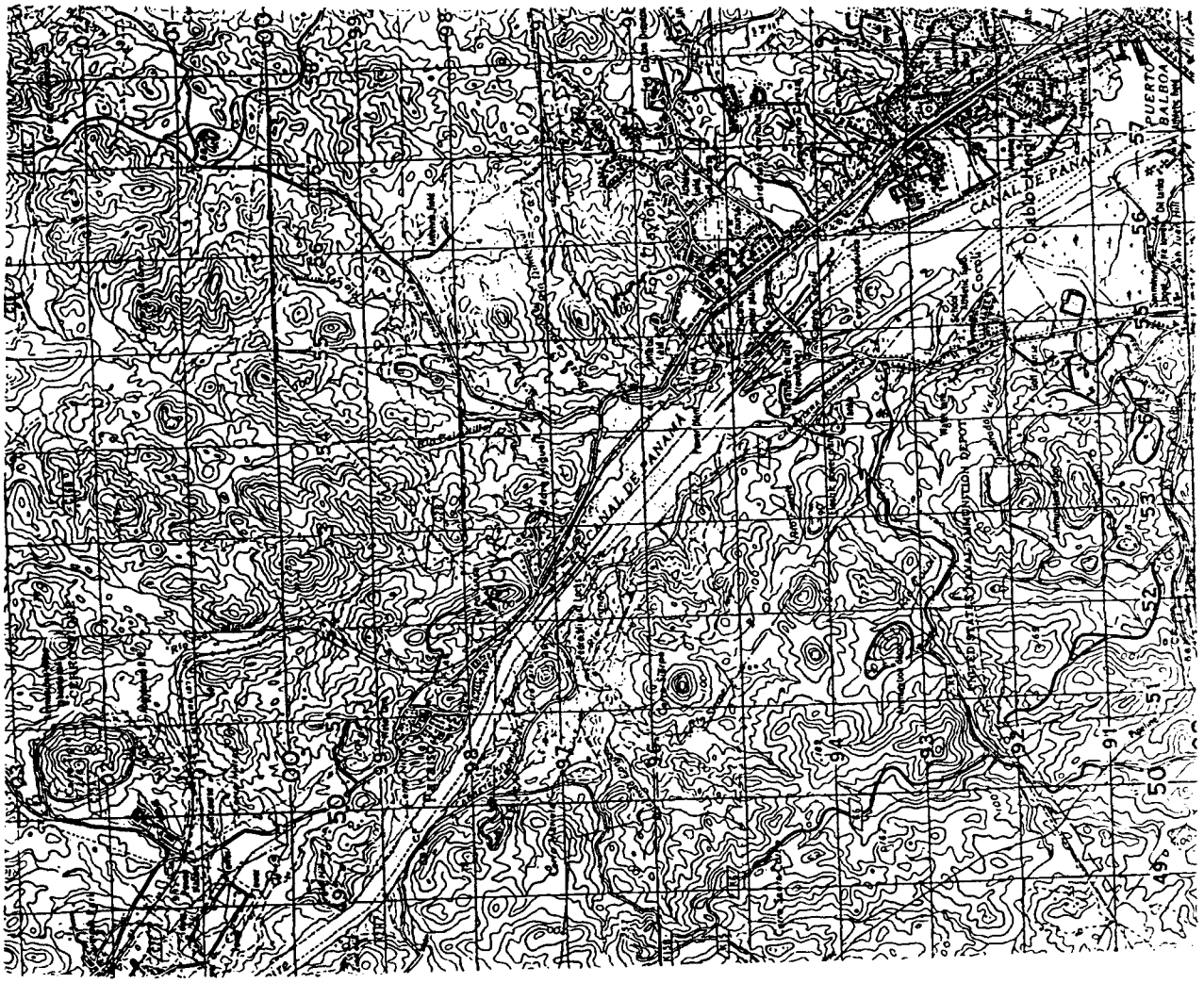

RAIN RATE
22 MAR 91
MM/HR
5
4
3
2
1
0
800
900
1000
1100
1200
1300
1400
TIME
SITE 1
SITE 2
SITE 3
SITE 4

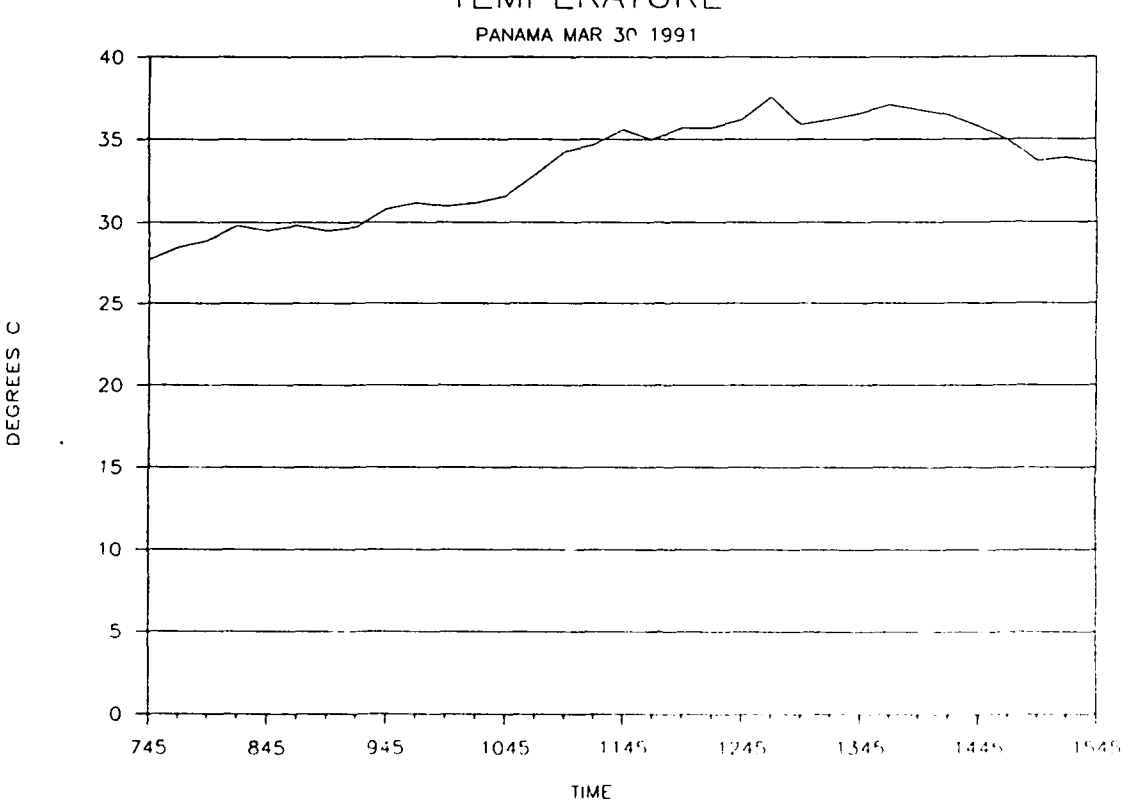

LOWTRAN7/TRANSMISSION
22 MAR 1991 3-5m
PERCENT
1
0.9
0.8
0.7
0.6
0.5
0.4
0.3
0.2
0.1
0
800
900
1000
1100
1200
1300
1400
TIME (SITE 1 DATA)
LOWTRAN7
+ TRANSMISSION

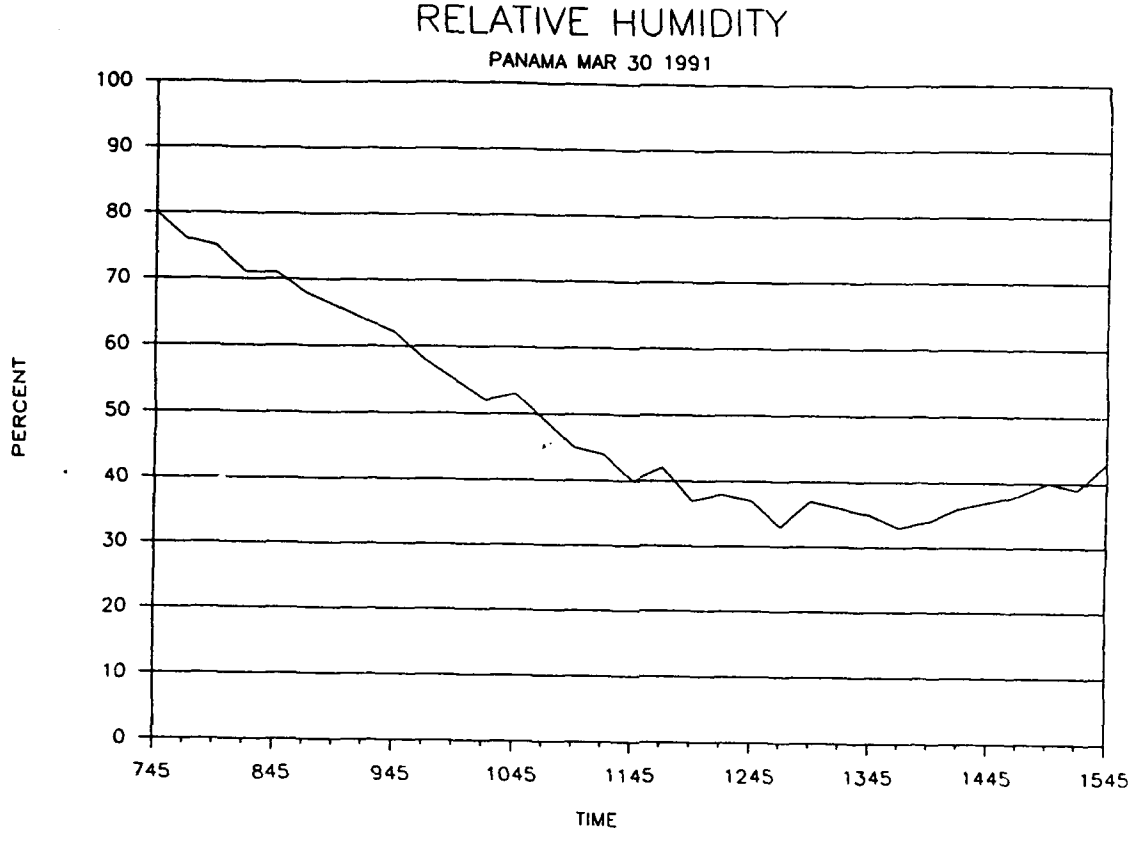

LOWTRAN7/TRANSMISSION
22 MAR 1991 3-5m
PERCENT
1
0.9
0.8
0.7
0.6
0.5
0.4
0.3
0.2
0.1
0
800
900
1000
1100
1200
1300
1400
TIME (SITE 2 DATA)
LOWTRAN7
+ TRANSMISSION

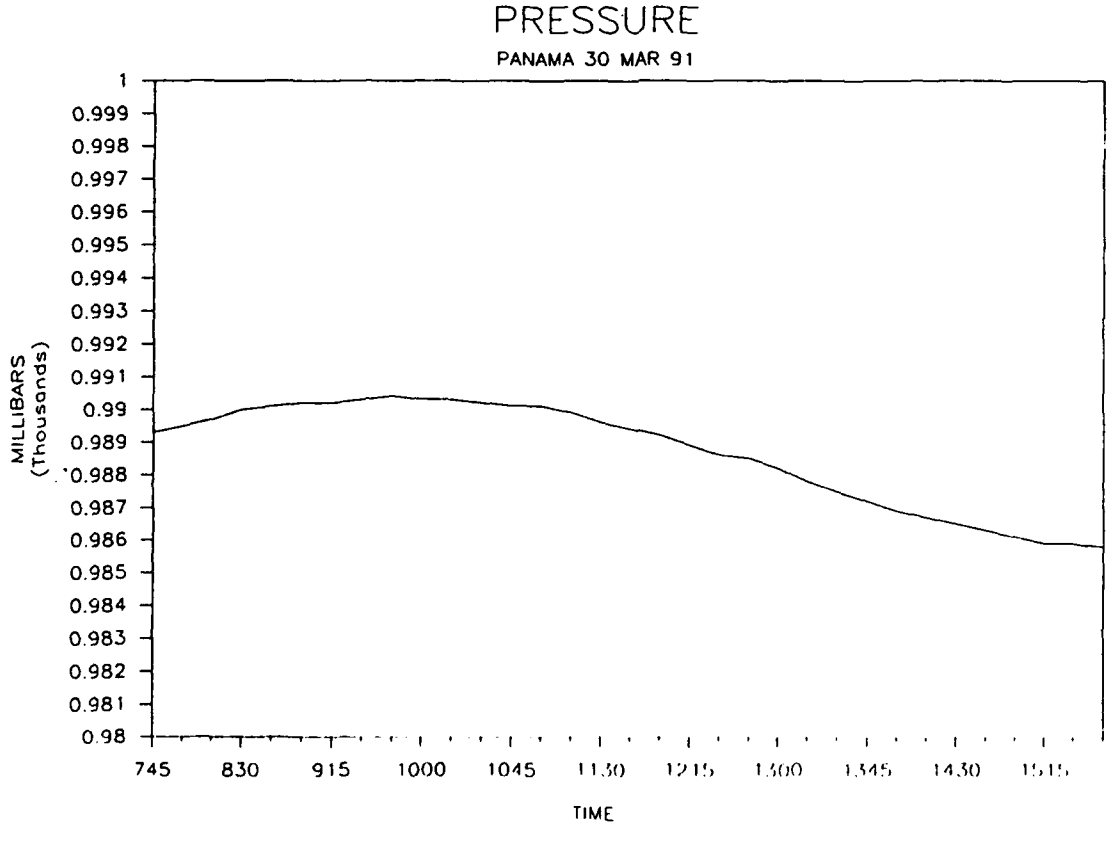

LOWTRAN7/TRANSMISSION
22 MAR 1991 8-12m
PERCENT
1
0.9
0.8
0.7
0.6
0.5
0.4
0.3
0.2
0.1
0
800
900
1000
1100
1200
1300
1400
TIME (SITE 1 DATA)
LOWTRAN7
TRANSMISSION

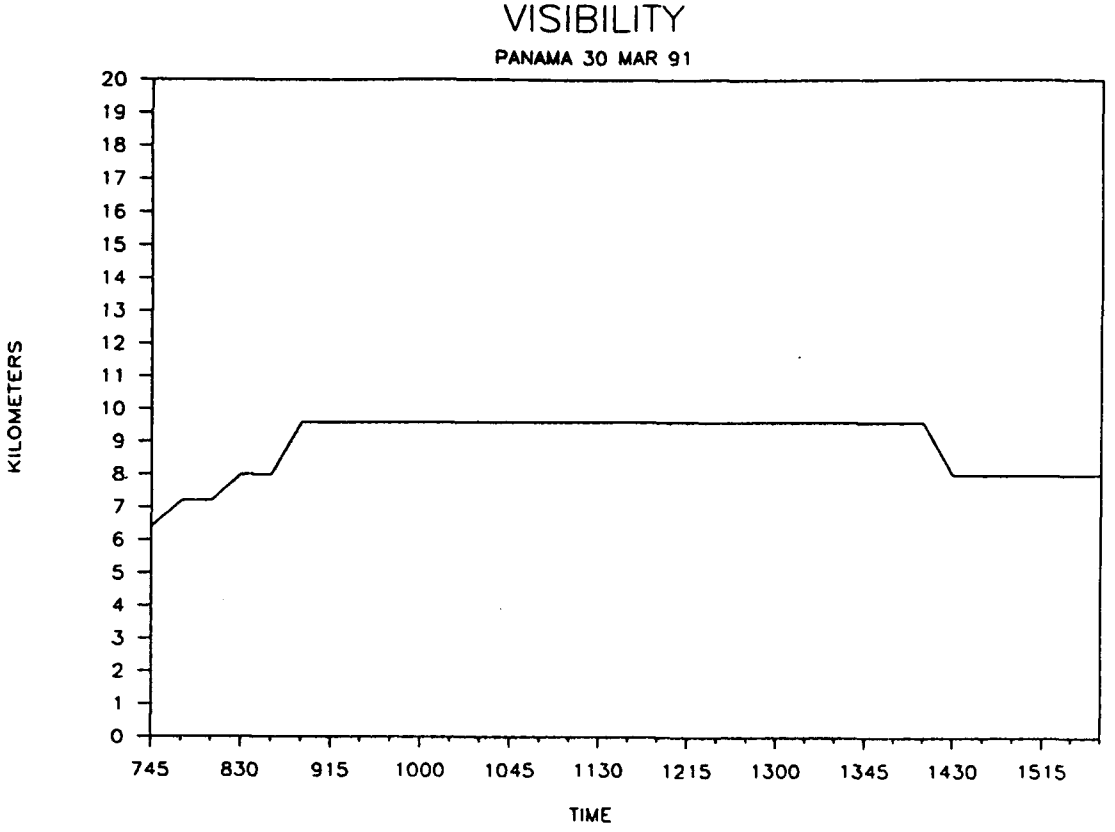

LOWTRAN7/TRANSMISSION
22 MAR 1991 8-12m
PERCENT
1
0.9
0.8
0.7
0.6
0.5
0.4
0.3
0.2
0.1
0
800
900
1000
1100
1200
1300
1400
TIME (SITE 2 DATA)
LOWTRAN7
TRANSMISSION

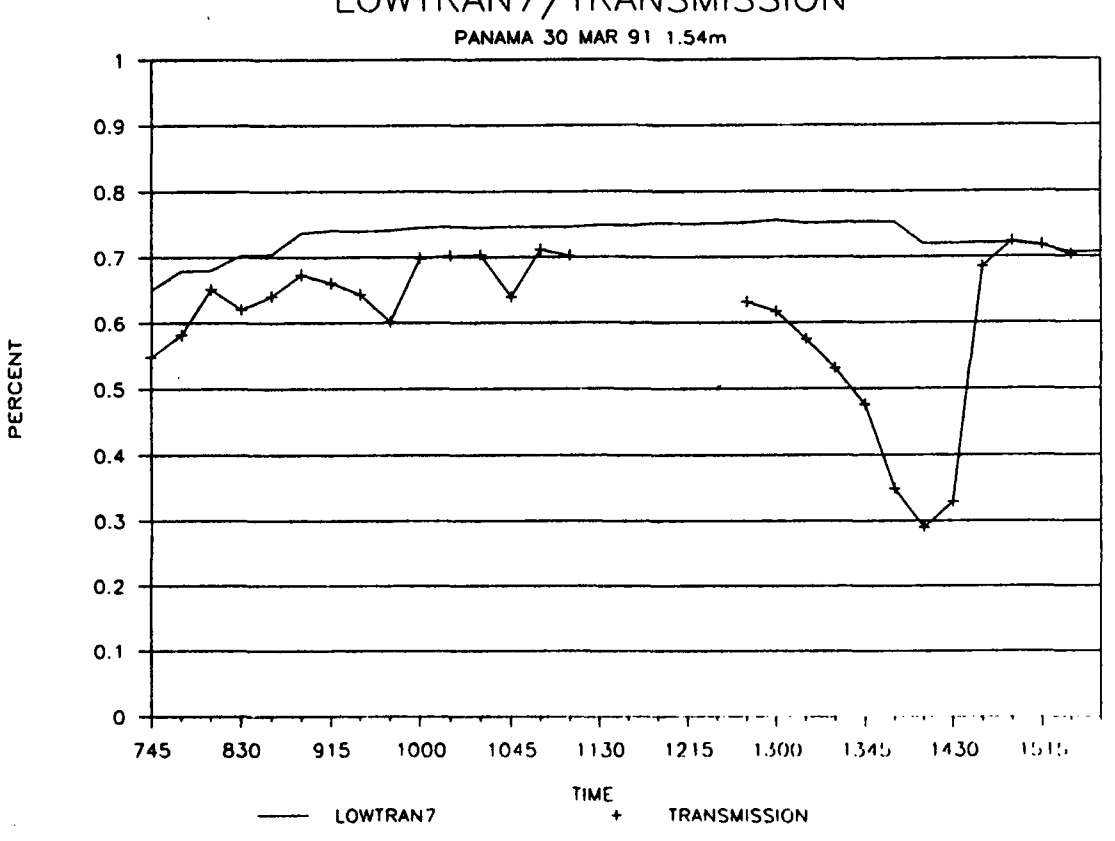

CANAL DE PANAMA
Diablo
PUERTO BALBOA

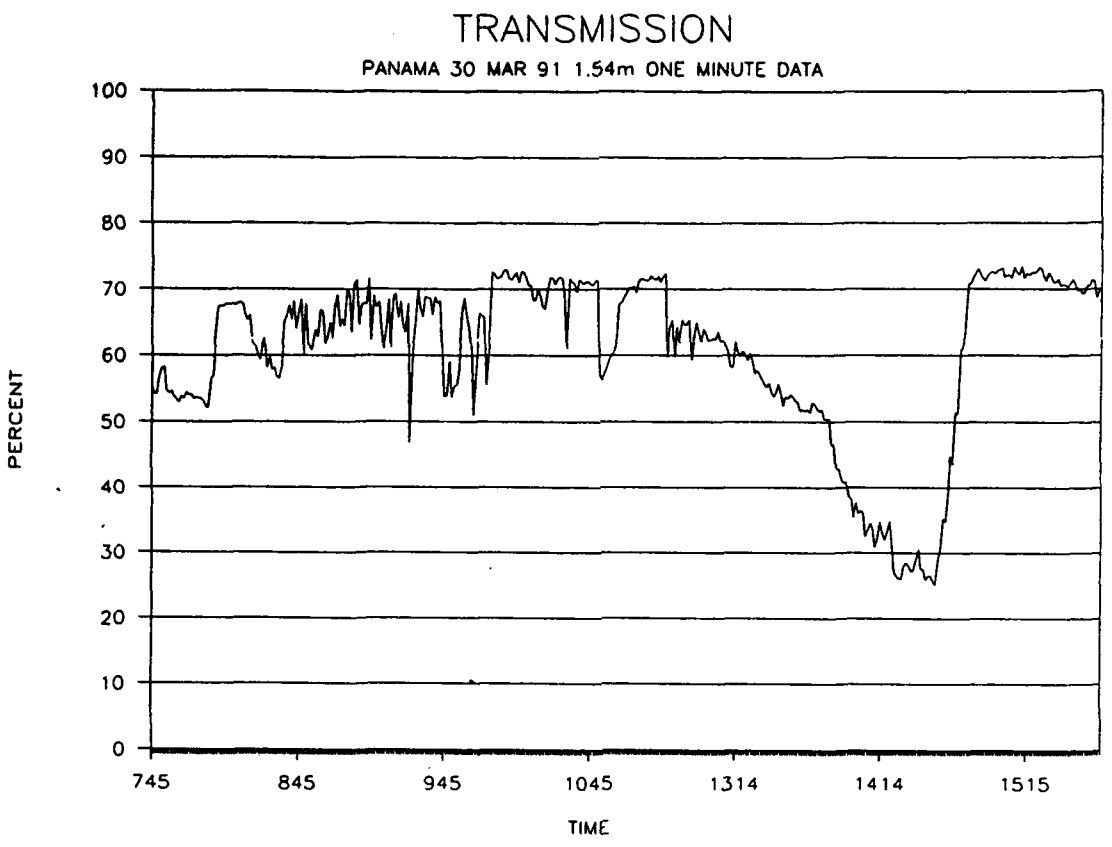

TEMPERATURE
PANAMA MAR 30 1991
DEGREES C
40
35
30
25
20
15
10
5
0
745
845
945
1045
1145
1245
1345
1445
1545
TIME

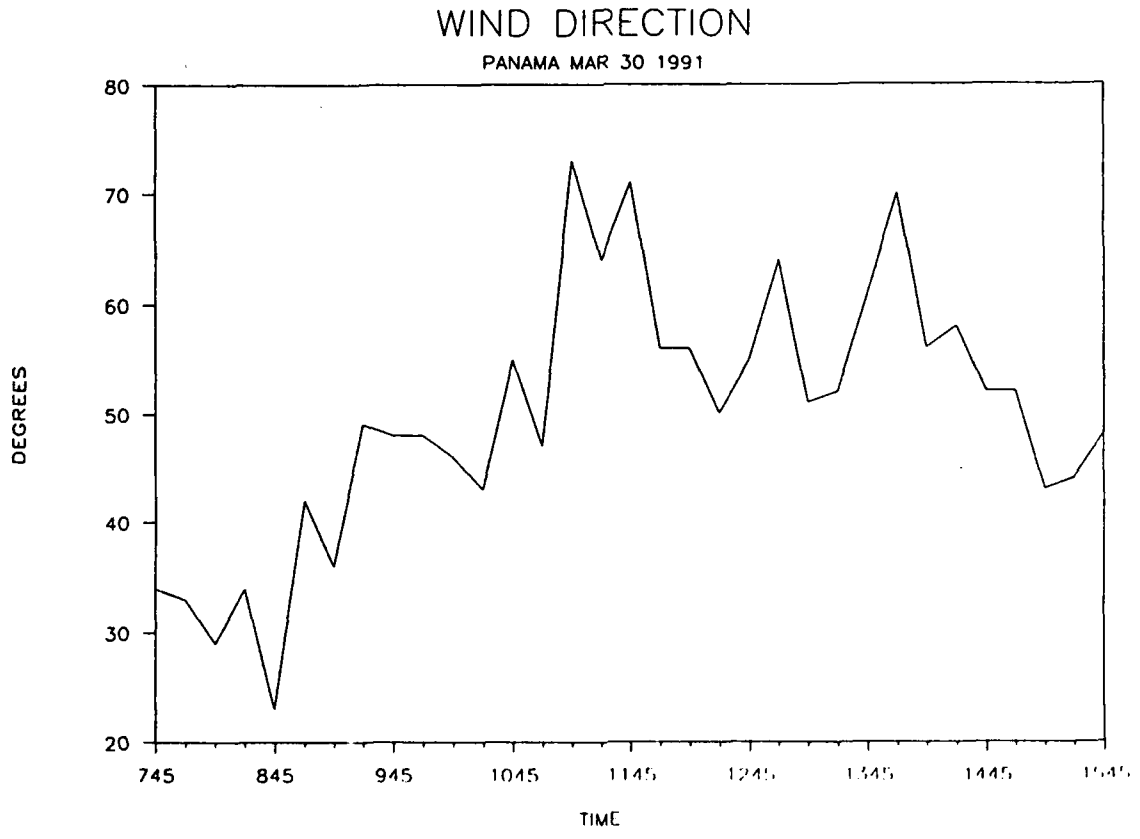

RELATIVE HUMIDITY
PANAMA MAR 30 1991
PERCENT
100
90
80
70
60
50
40
30
20
10
0
745
845
945
1045
1145
1245
1345
1445
1545
TIME

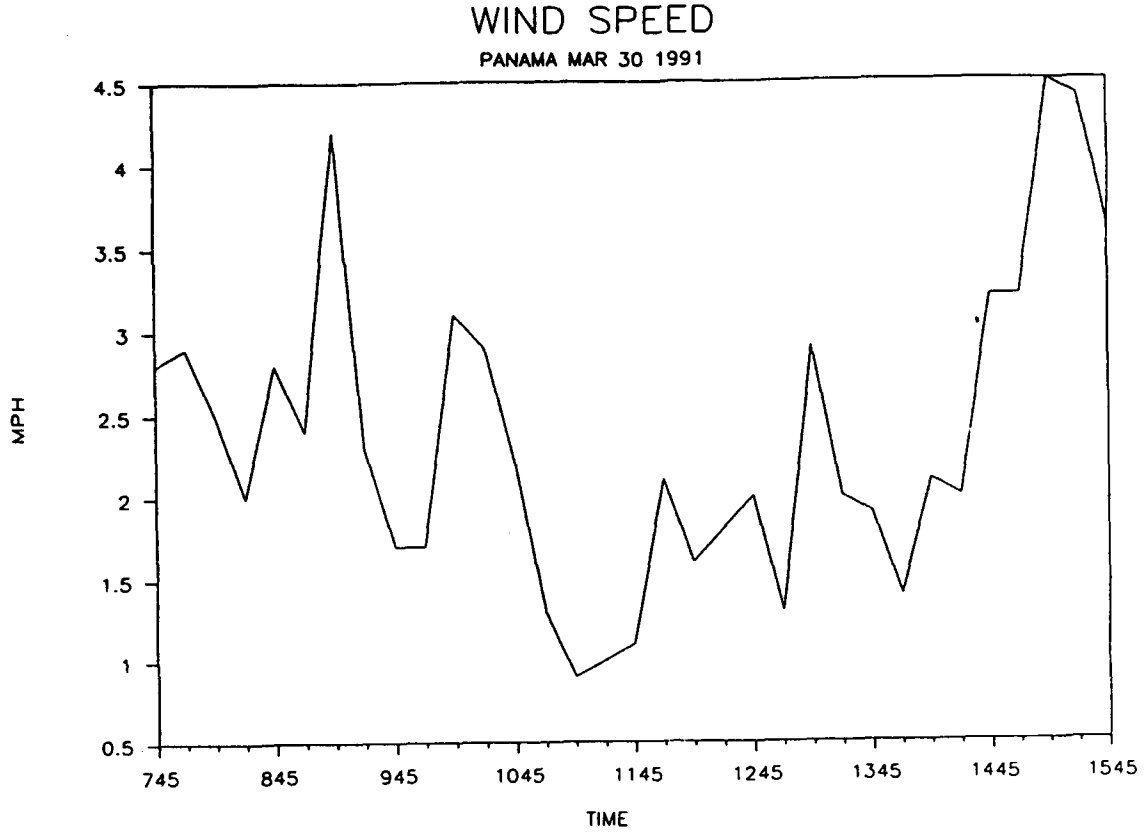

PRESSURE
PANAMA 30 MAR 91
MILLIBARS
(Thousands)
1
0.999
0.998
0.997
0.996
0.995
0.994
0.993
0.992
0.991
0.99
0.989
0.988
0.987
0.986
0.985
0.984
0.983
0.982
0.981
0.98
745
830
915
1000
1045
1130
1215
1300
1345
1430
1515
TIME

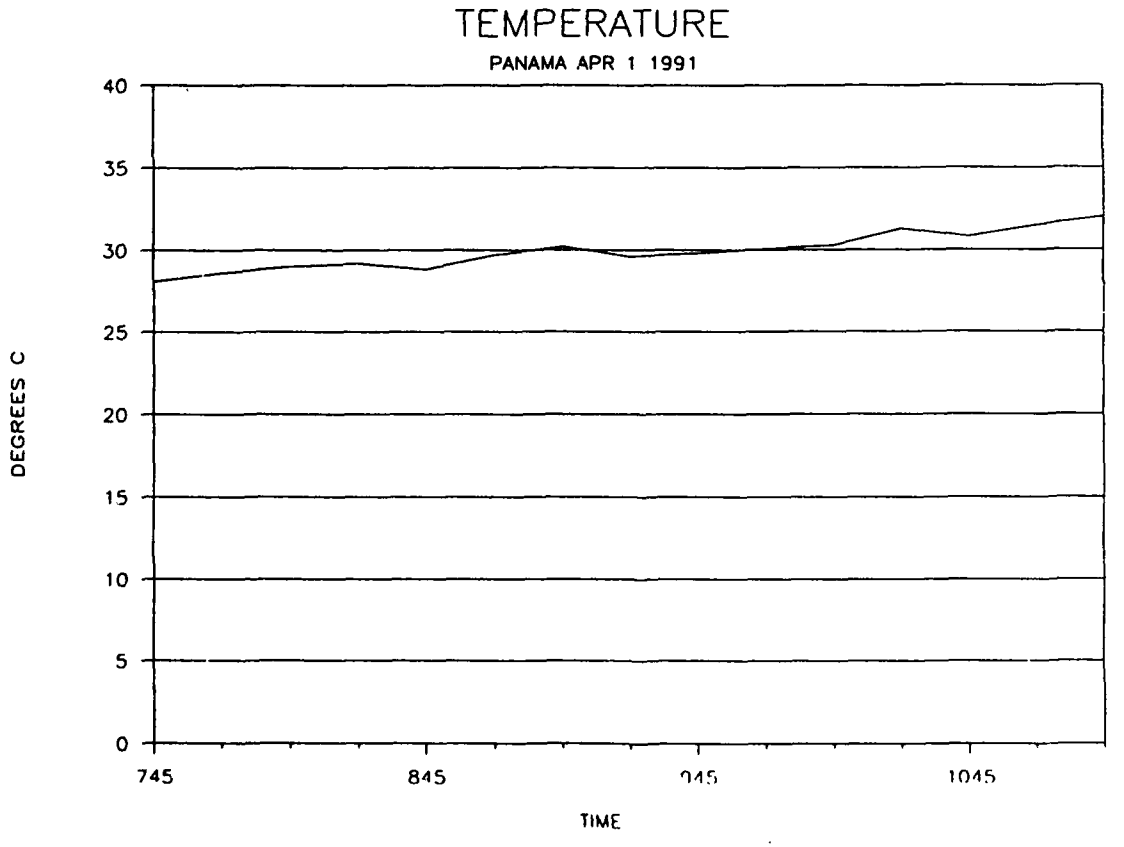

VISIBILITY
PANAMA 30 MAR 91
KILOMETERS
20
19
18
17
16
15
14
13
12
11
10
9
8
7
6
5
4
3
2
1
0
745
830
915
1000
1045
1130
1215
1300
1345
1430
1515
TIME

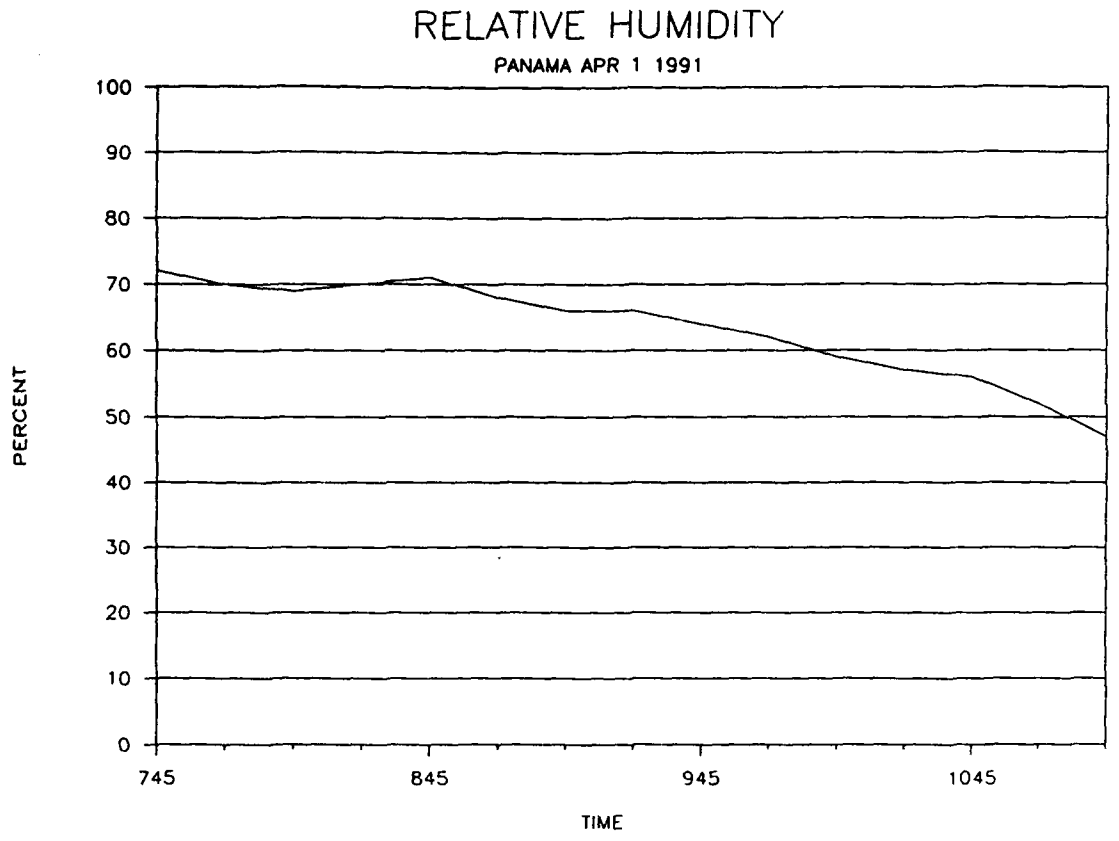

LOWTRAN7/TRANSMISSION
PANAMA 30 MAR 91 1.54m
PERCENT
1
0.9
0.8
0.7
0.6
0.5
0.4
0.3
0.2
0.1
0
745
830
915
1000
1045
1130
1215
1300
1345
1430
1515
TIME
LOWTRAN7
TRANSMISSION

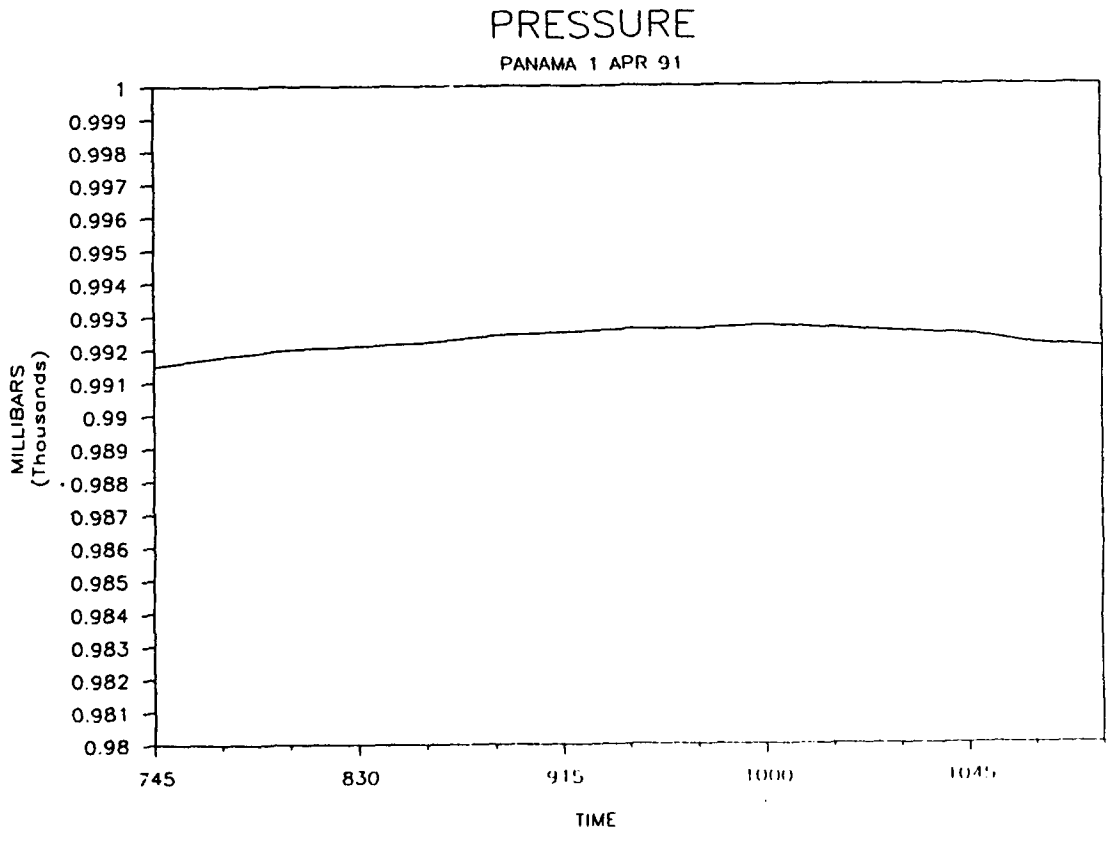

TRANSMISSION
PANAMA 30 MAR 91 1.54m ONE MINUTE DATA
PERCENT
100
90
80
70
60
50
40
30
20
10
0
745
845
945
1045
1314
1414
1515
TIME


WIND DIRECTION
PANAMA MAR 30 1991
DEGREES
80
70
60
50
40
30
20
745
845
945
1045
TIME


WIND SPEED
PANAMA MAR 30 1991
MPH
4.5
4
3.5
3
2.5
2
1.5
1
0.5
745
845
945
1045
1145
1245
1345
1445
1545
TIME

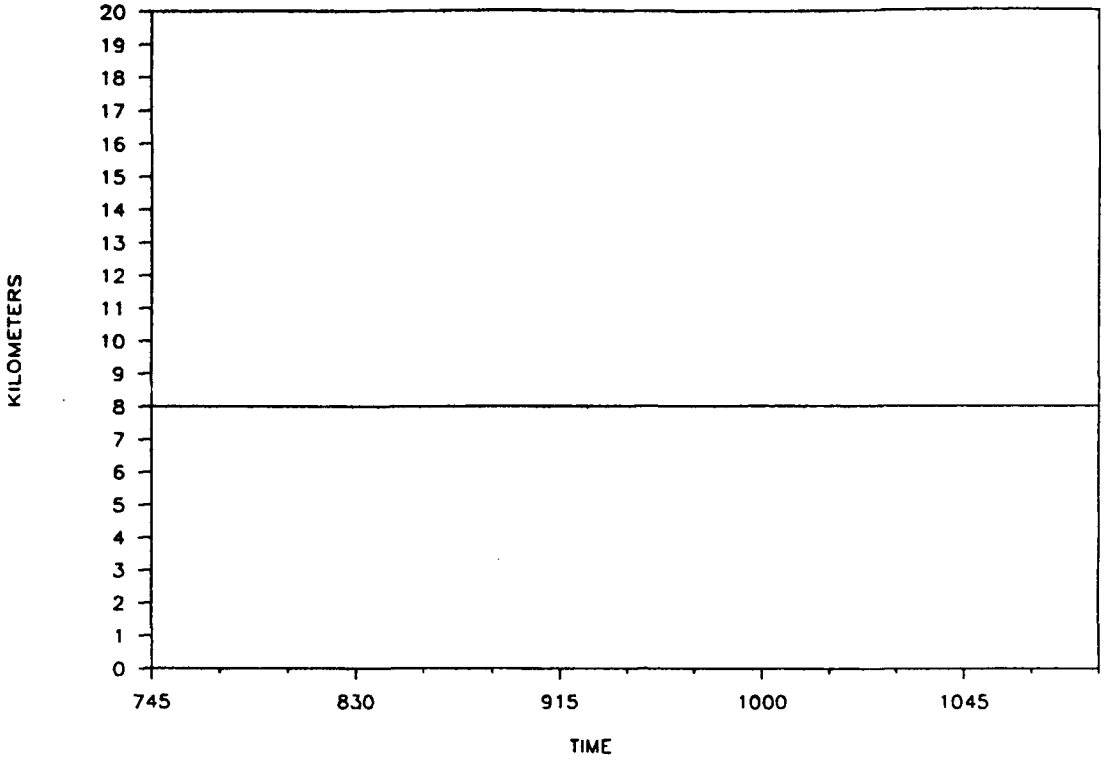

TEMPERATURE
PANAMA APR 1 1991
DEGREES C
40
35
30
25
20
15
10
5
0
745
845
945
1045
TIME


RELATIVE HUMIDITY
PANAMA APR 1 1991
PERCENT
100
90
80
70
60
50
40
30
20
10
0
745
845
945
1045
TIME


PRESSURE
PANAMA 1 APR 91
MILLIBARS (Thousands)
1
0.999
0.998
0.997
0.996
0.995
0.994
0.993
0.992
0.991
0.99
0.989
0.988
0.987
0.986
0.985
0.984
0.983
0.982
0.981
0.98
745
830
915
1000
TIME

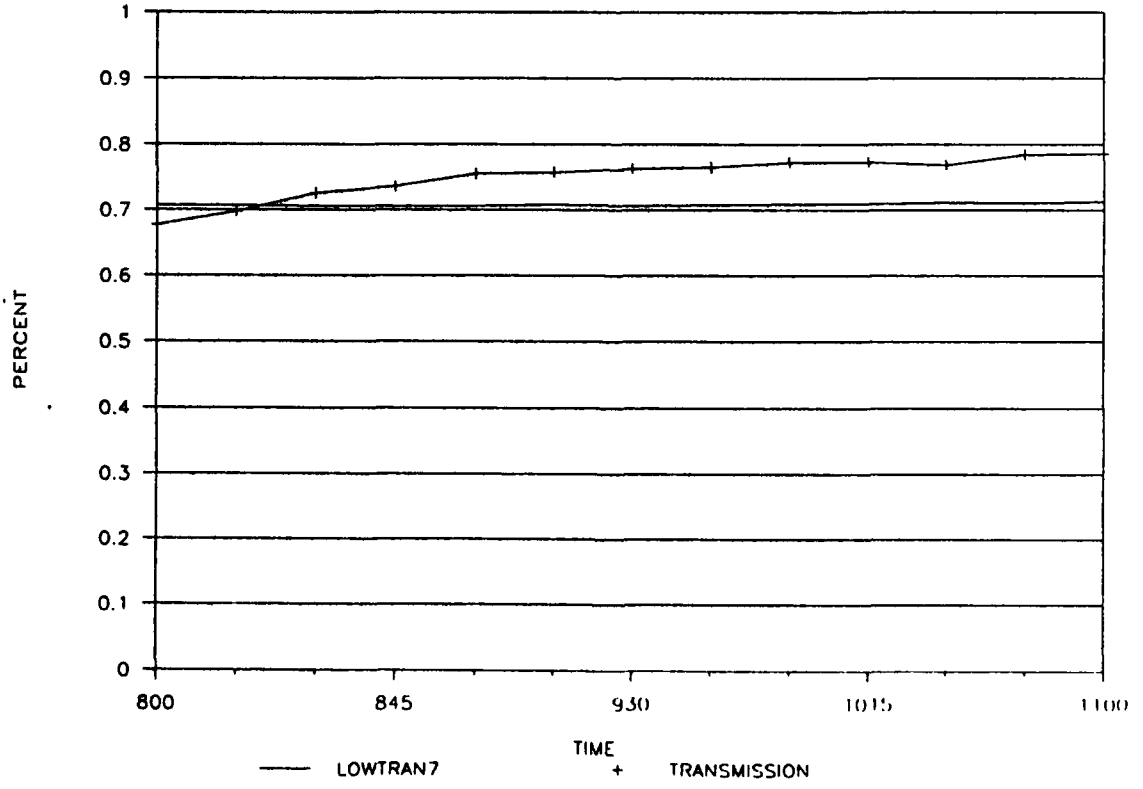
VISIBILITY

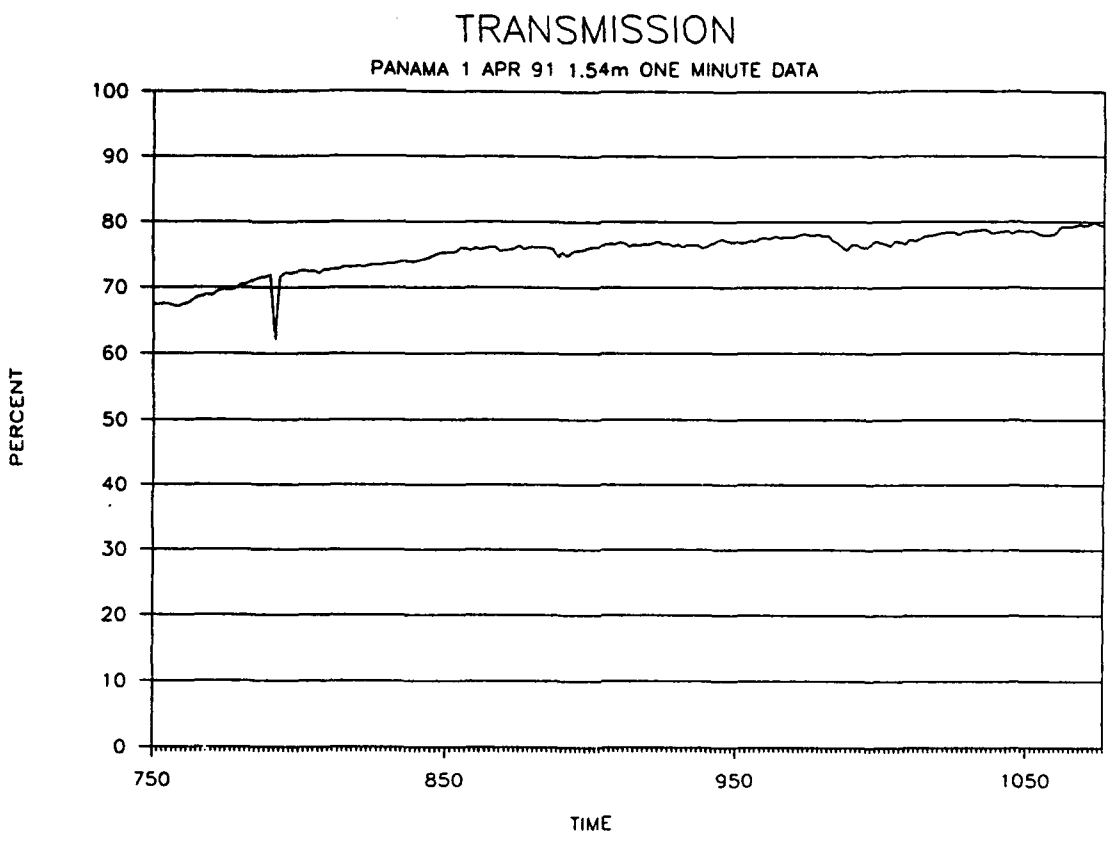
PANAMA 1 APR 91

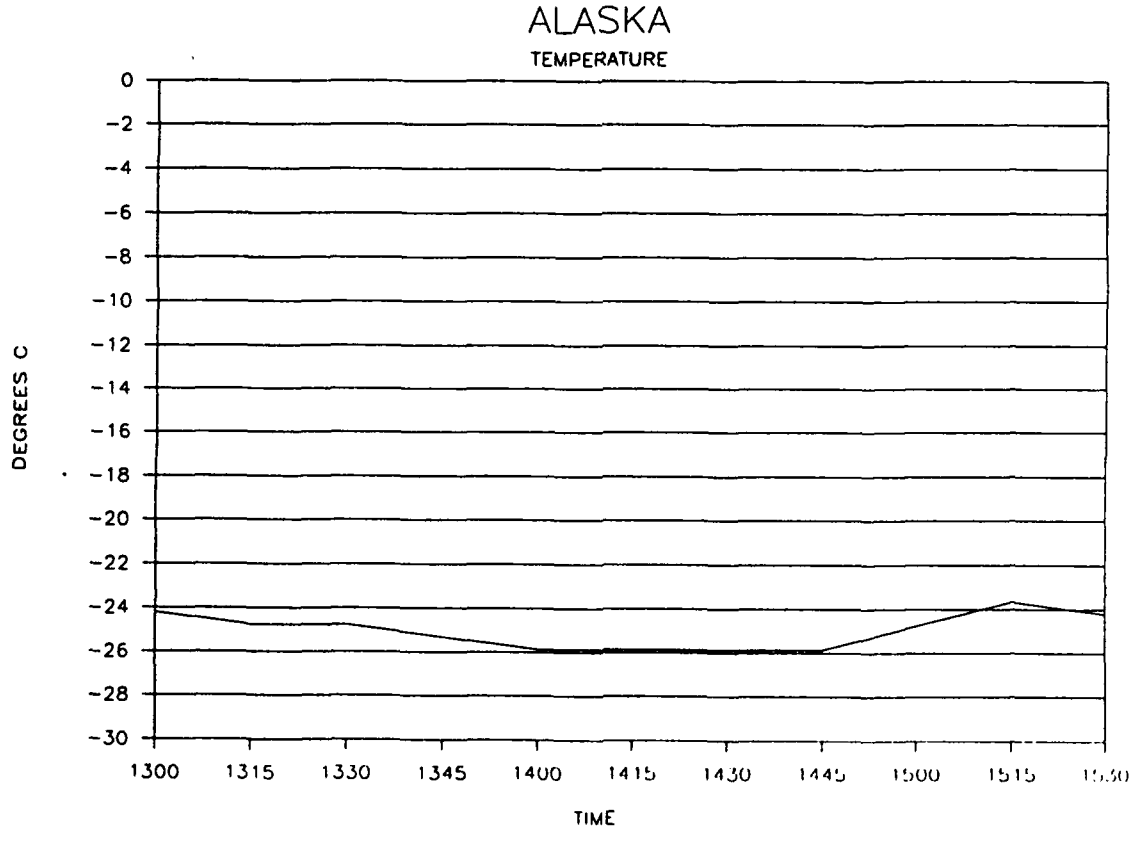


LOWTRAN7/TRANSMISSION

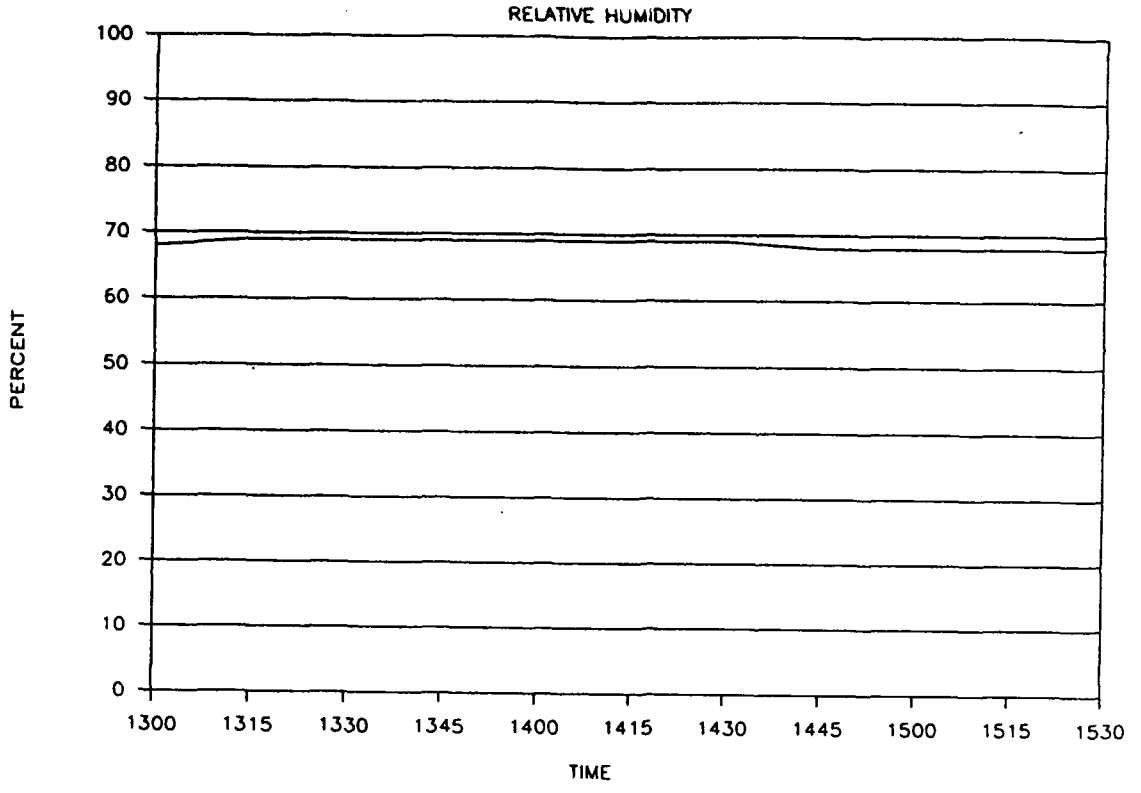
PANAMA 1 APR 91 1.54m



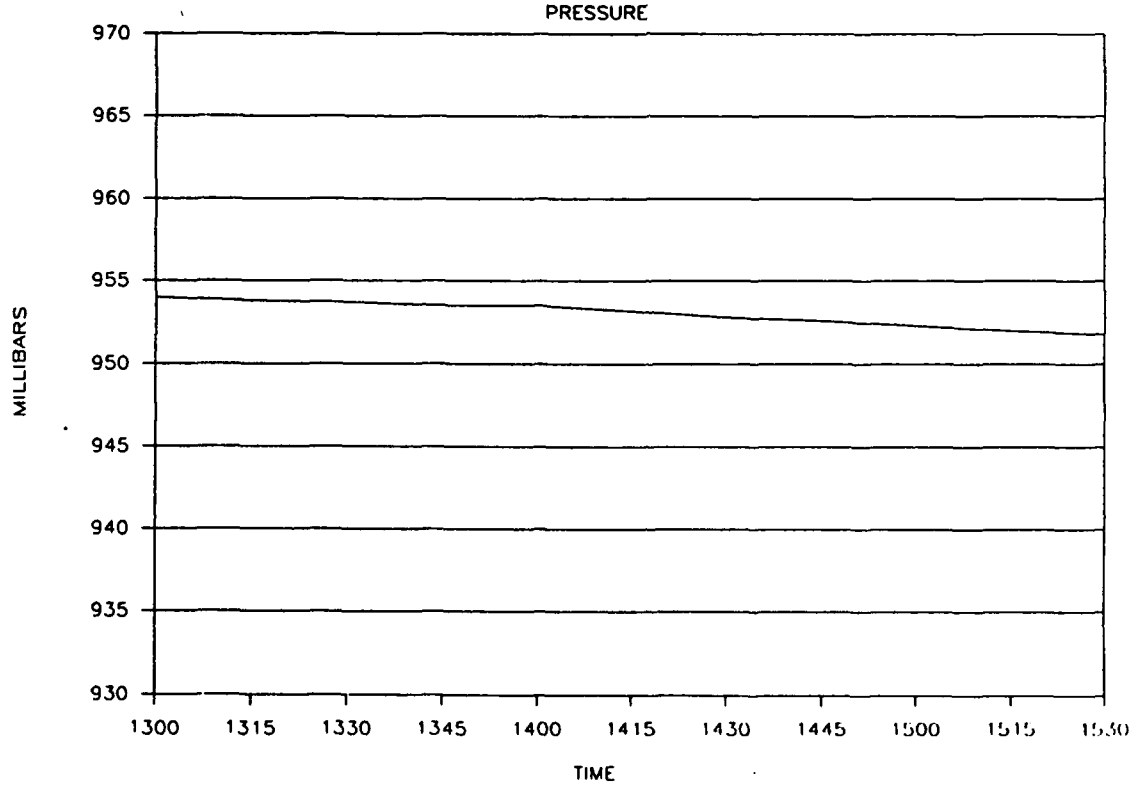

TRANSMISSION
PANAMA 1 APR 91 1.54m ONE MINUTE DATA
PERCENT
100
90
80
70
60
50
40
30
20
10
0
750
850
950
1050
TIME

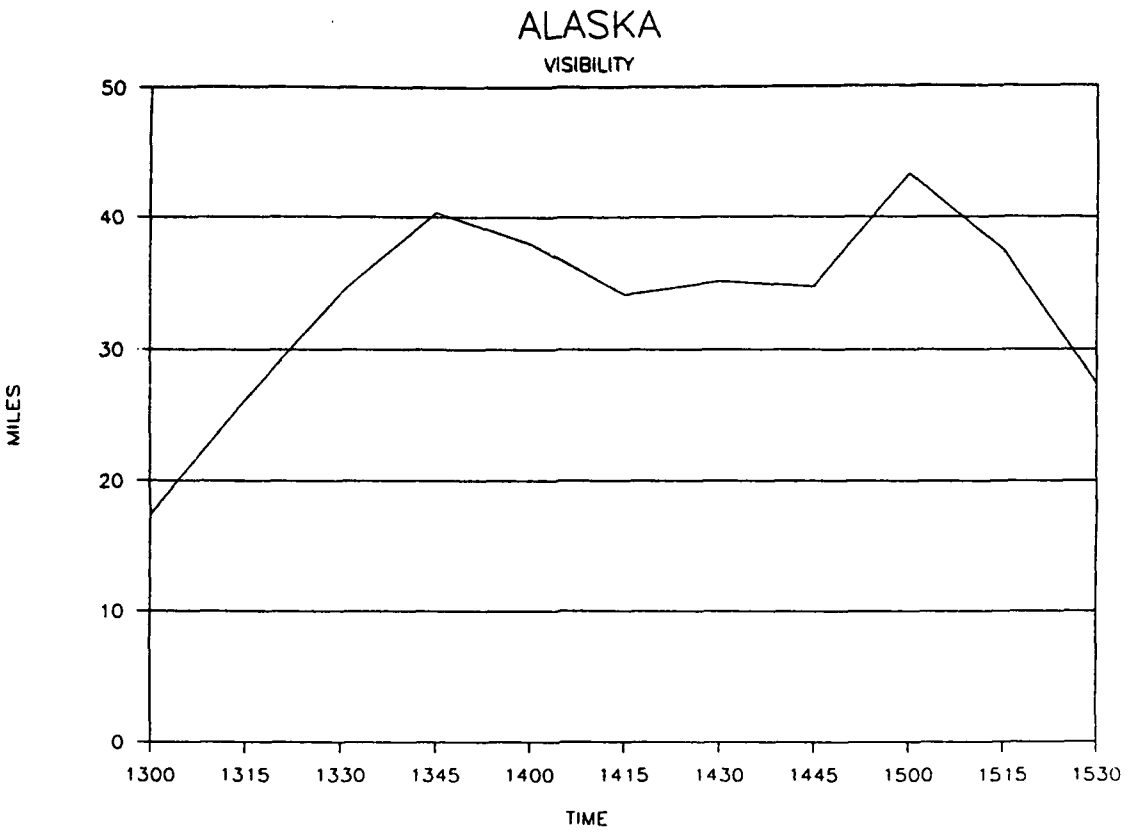

ALASKA
TEMPERATURE
DEGREES C
0
-2
-4
-6
-8
-10
-12
-14
-16
-18
-20
-22
-24
-26
-28
-30
1300
1315
1330
1345
1400
1415
1430
1445
1500
1515
TIME

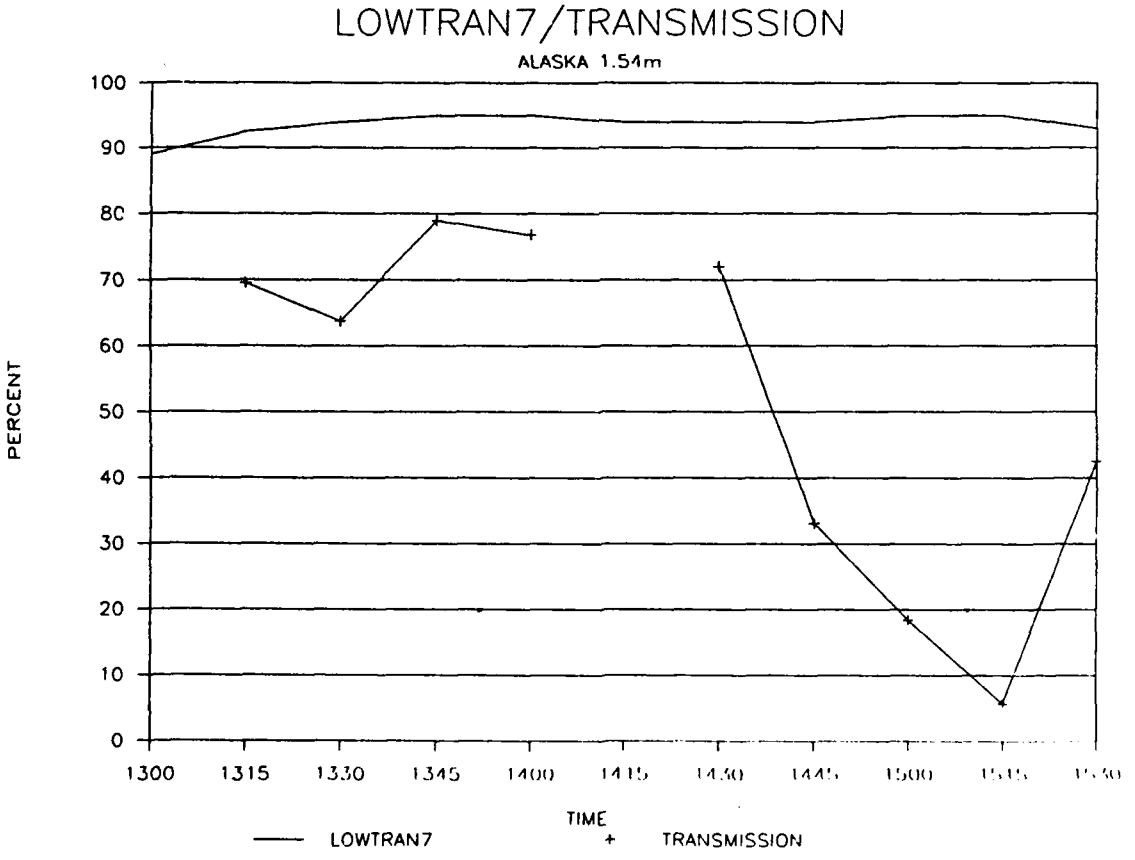
ALASKA

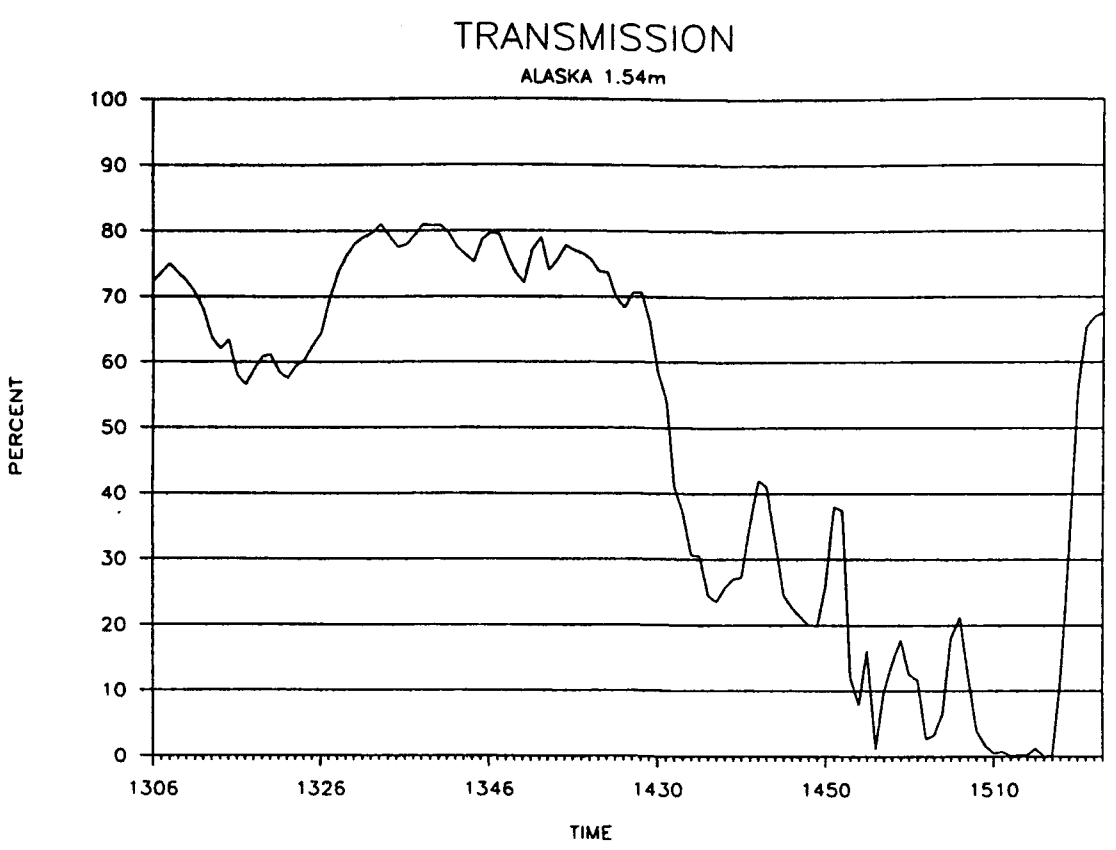


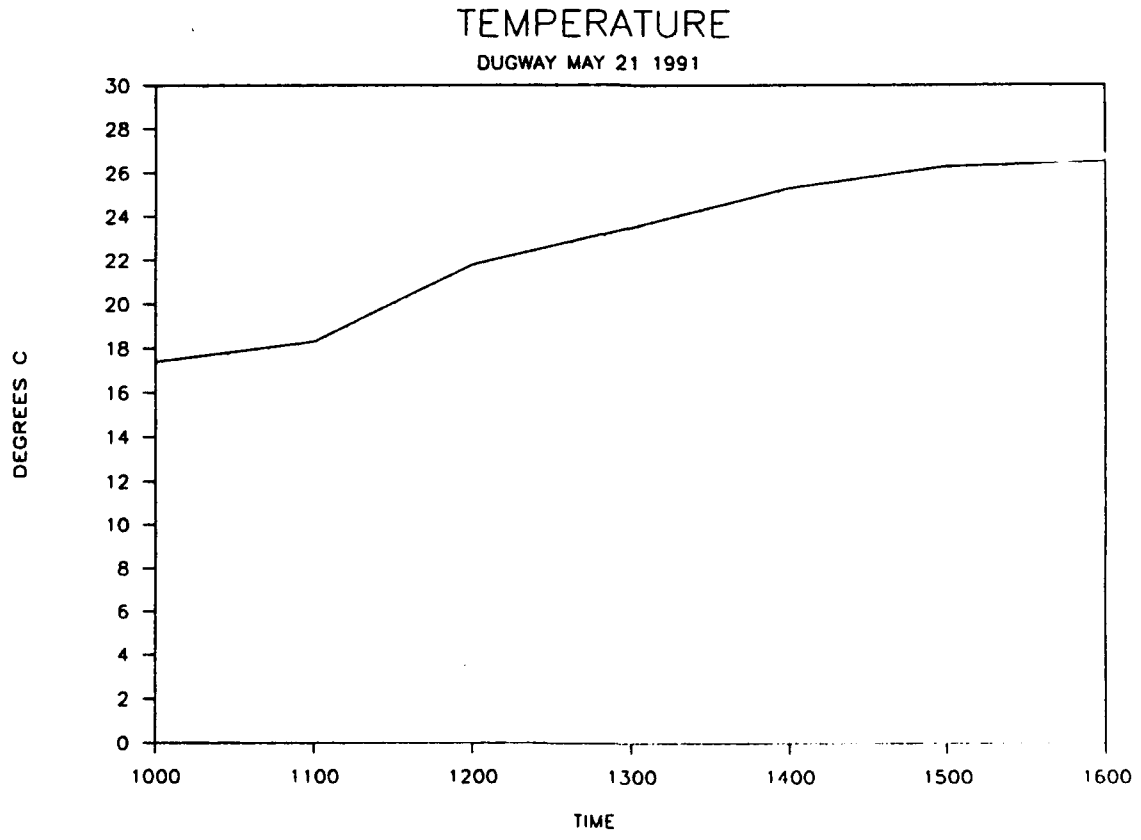
ALASKA

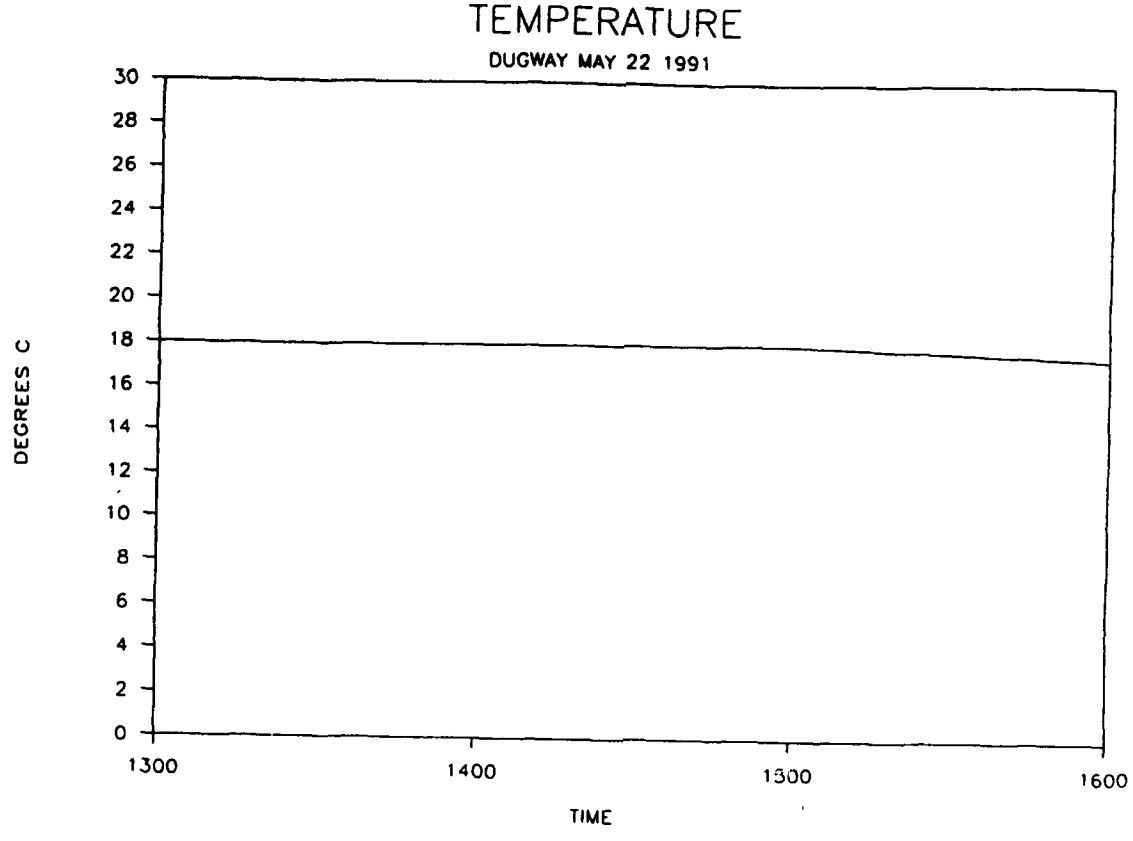


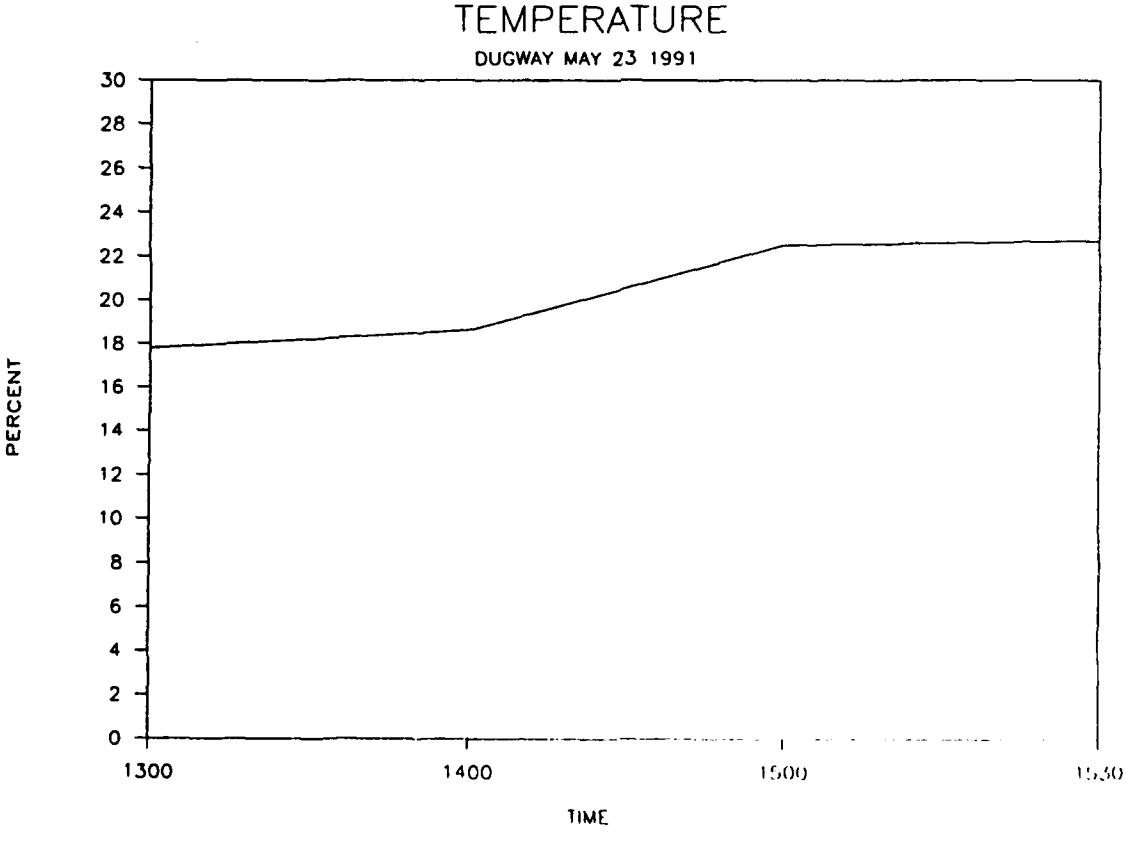

ALASKA
VISIBILITY
MILES
50
40
30
20
10
0
1300
1315
1330
1345
1400
1415
1430
1445
1500
1515
1530
TIME

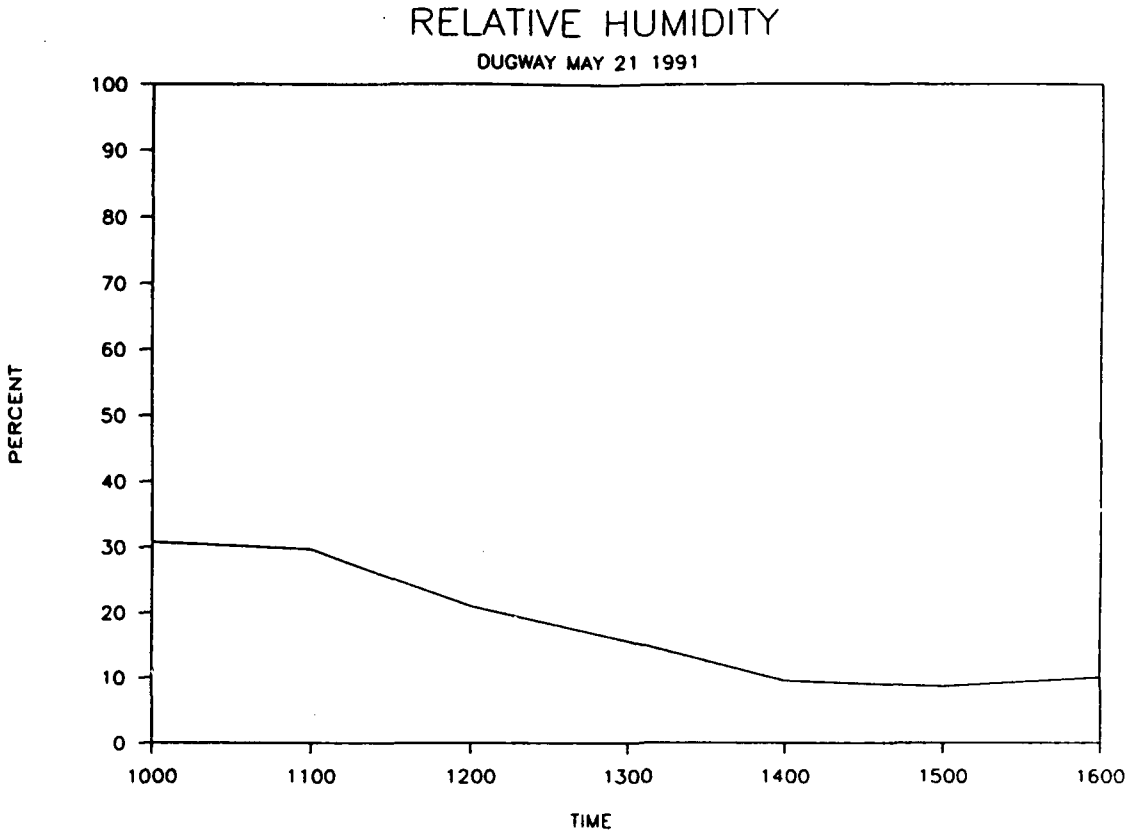

LOWTRAN7/TRANSMISSION
ALASKA 1.54m
PERCENT
100
90
80
70
60
50
40
30
20
10
0
1300
1315
1330
1345
1400
1415
1430
1445
1500
1515
1530
TIME
LOWTRAN7
TRANSMISSION

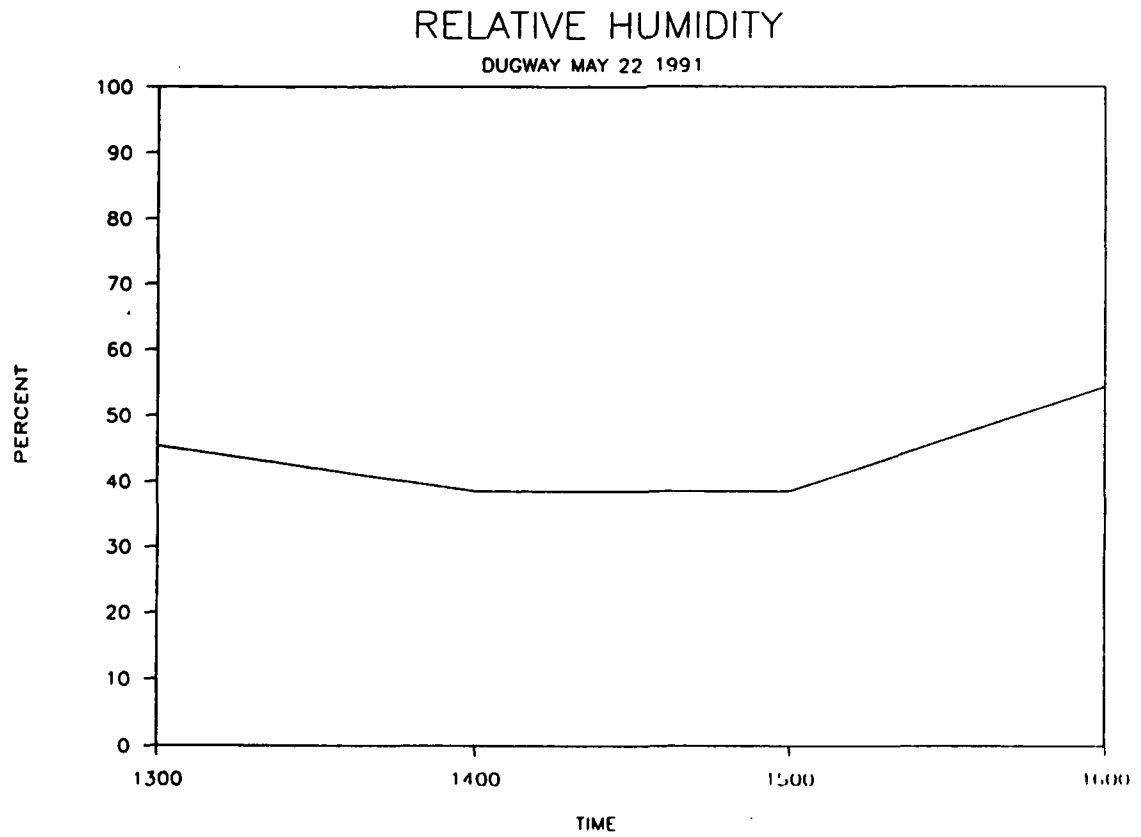

TRANSMISSION
ALASKA 1.54m
PERCENT
100
90
80
70
60
50
40
30
20
10
0
1306
1326
1346
1430
1450
1510
TIME

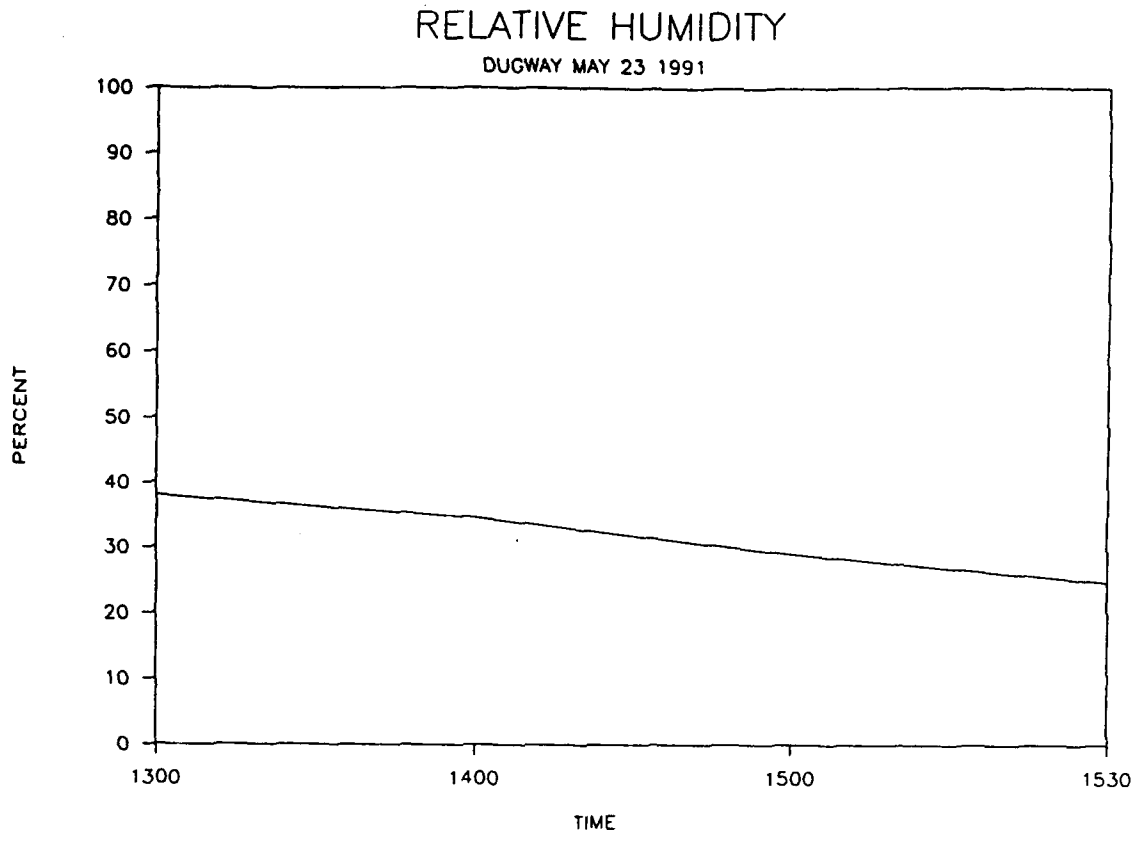

TEMPERATURE
DUGWAY MAY 21 1991
DEGREES C
30
28
26
24
22
20
18
16
14
12
10
8
6
4
2
0
1000
1100
1200
1300
1400
1500
1600
TIME

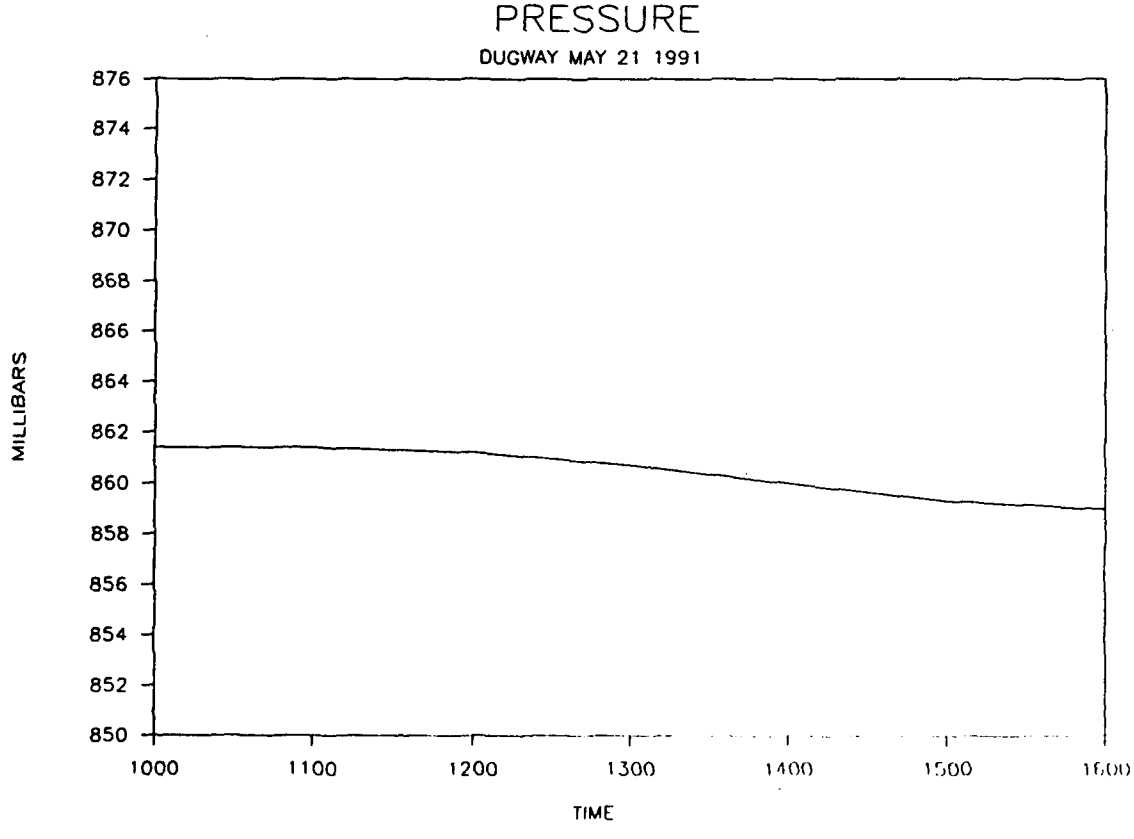

TEMPERATURE
DUGWAY MAY 22 1991
DEGREES C
30
28
26
24
22
20
18
16
14
12
10
8
6
4
2
0
1300
1400
1300
1600
TIME

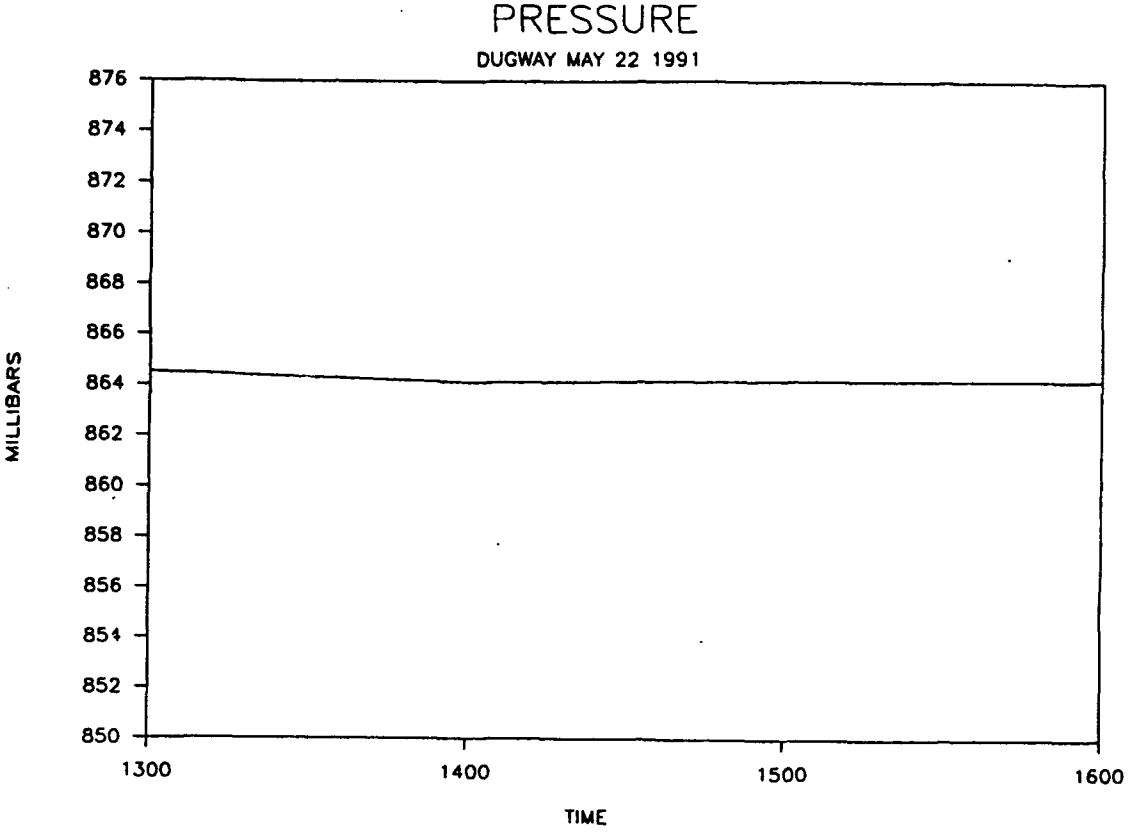

TEMPERATURE
DUGWAY MAY 23 1991
PERCENT
30
28
26
24
22
20
18
16
14
12
10
8
6
4
2
0
1300
1400
1500
1530
TIME

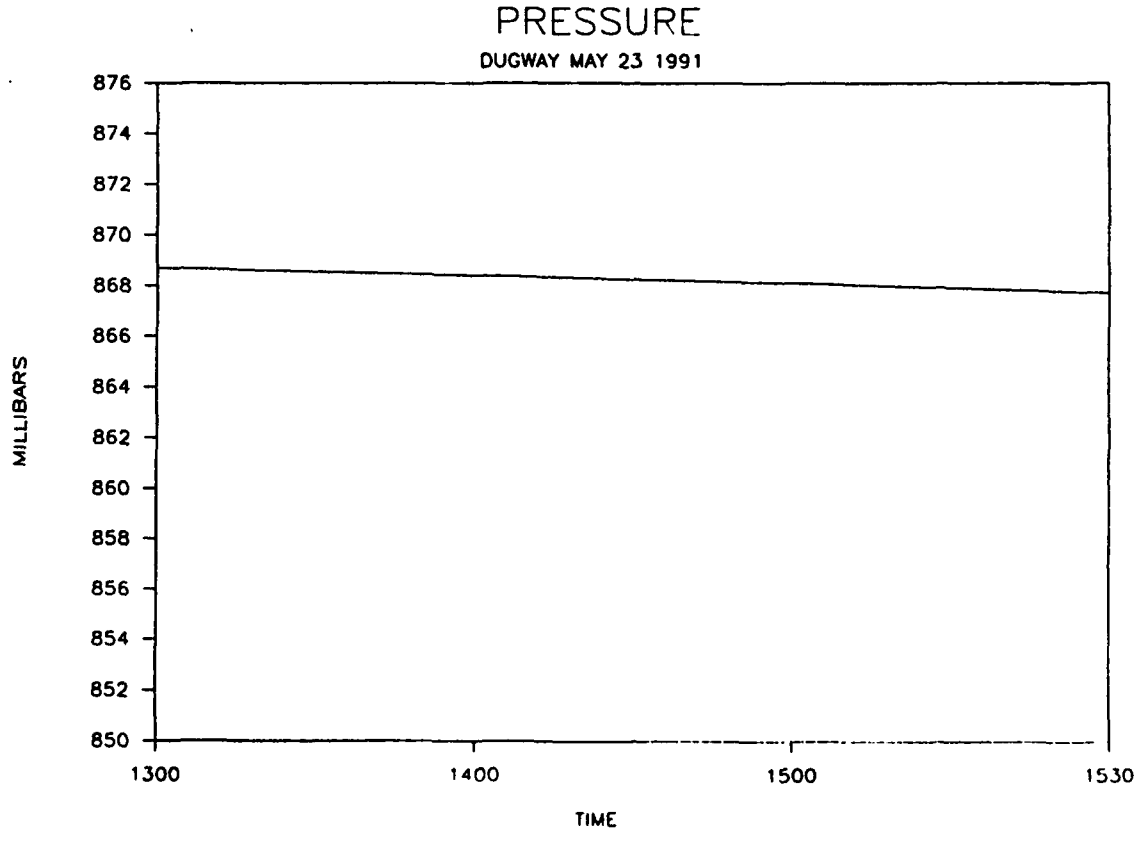

RELATIVE HUMIDITY
DUGWAY MAY 21 1991
PERCENT
100
90
80
70
60
50
40
30
20
10
0
1000
1100
1200
1300
1400
1500
1600
TIME

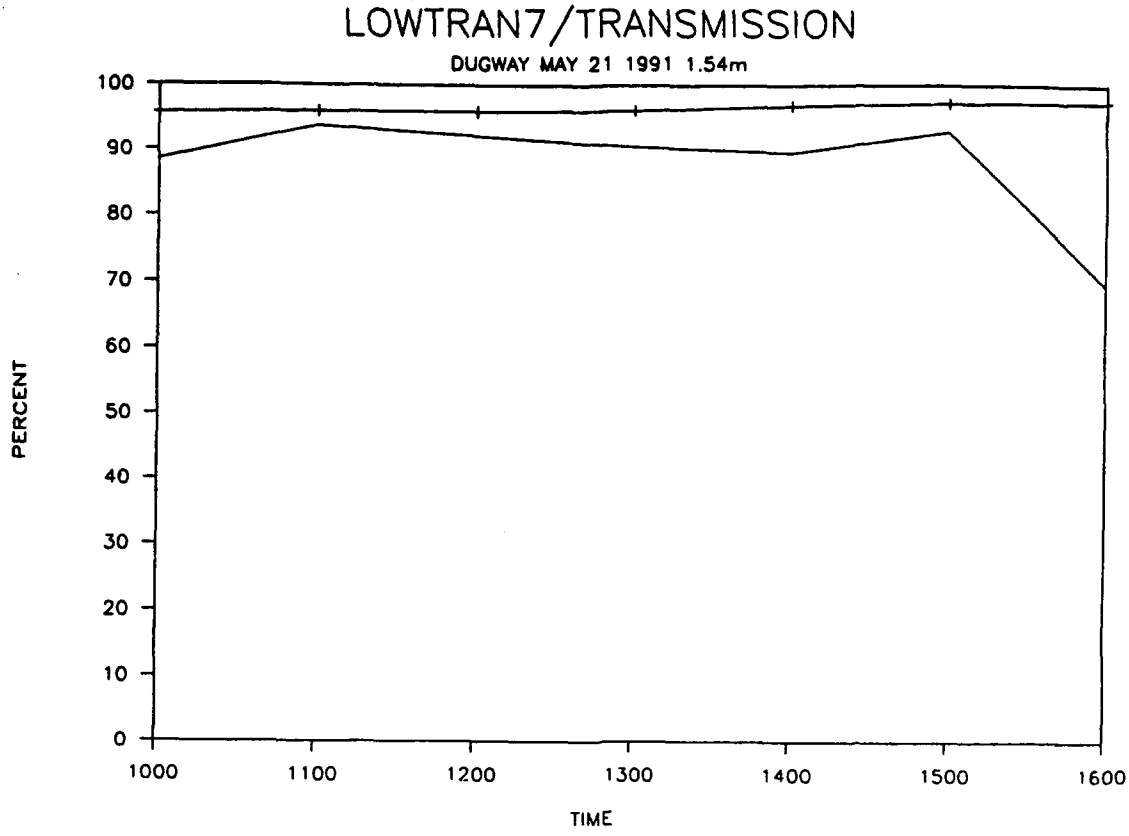

RELATIVE HUMIDITY
DUGWAY MAY 22 1991
PERCENT
100
90
80
70
60
50
40
30
20
10
0
1300
1400
1500
1600
TIME

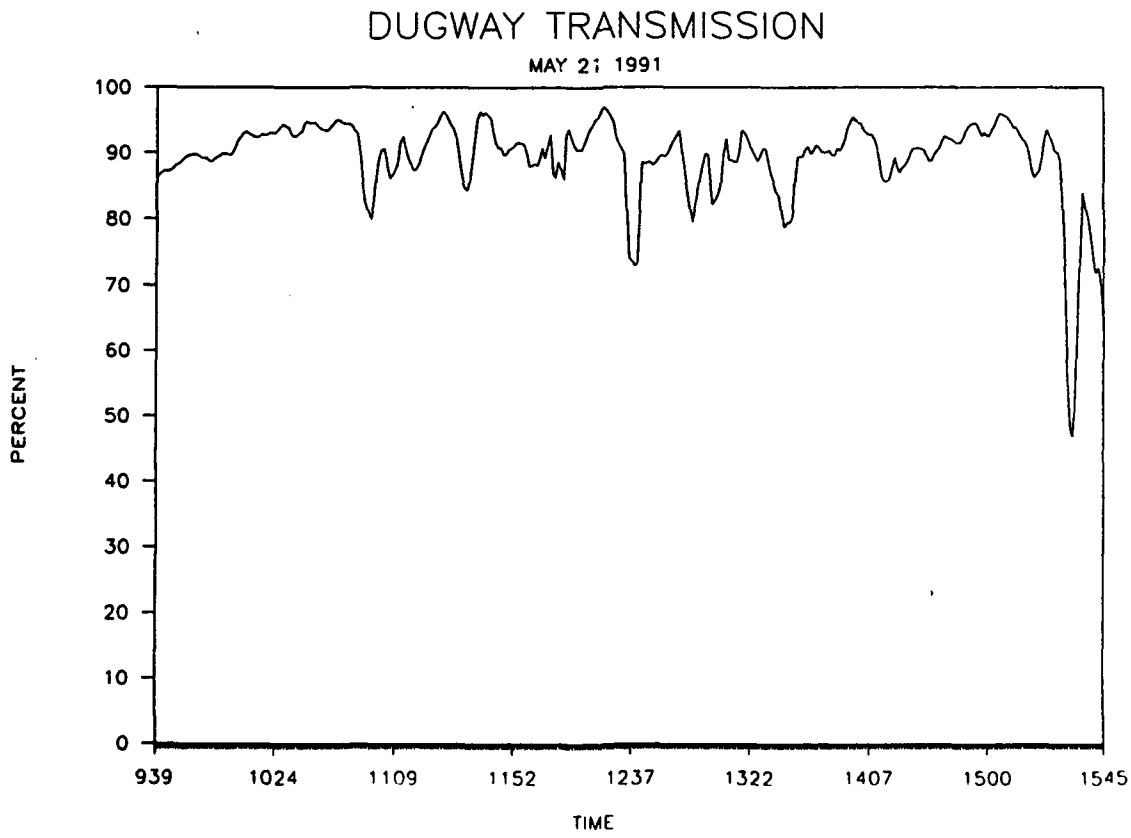

RELATIVE HUMIDITY
DUGWAY MAY 23 1991
PERCENT
100
90
80
70
60
50
40
30
20
10
0
1300
1400
1500
1530
TIME

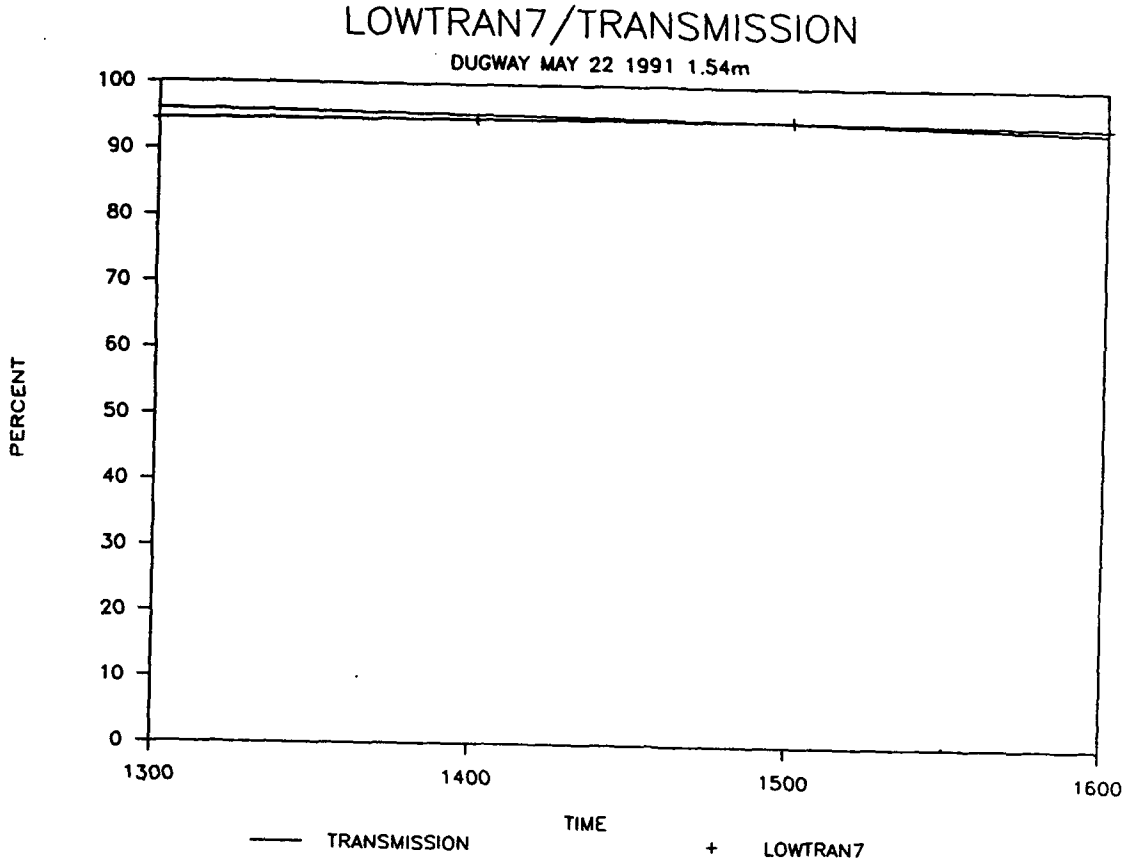

PRESSURE
DUGWAY MAY 21 1991
MILLIBARS
876
874
872
870
868
866
864
862
860
858
856
854
852
850
1000
1100
1200
1300
1400
1500
1600
TIME

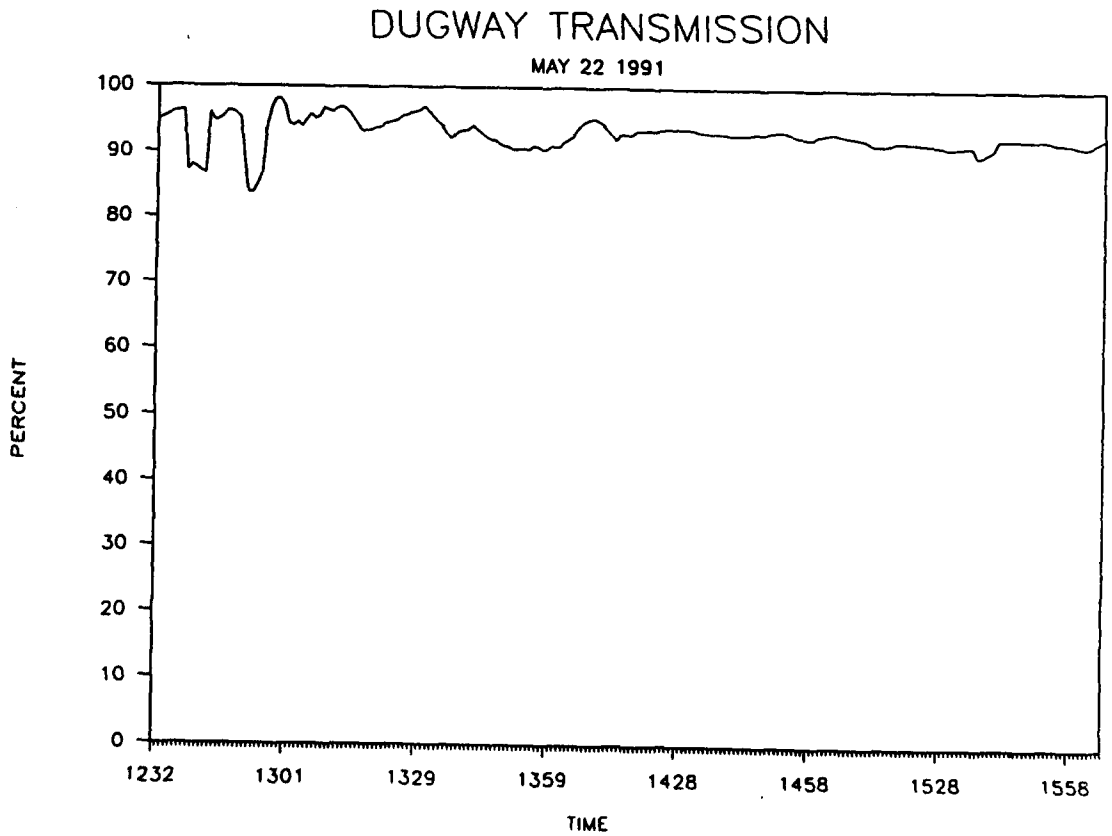

PRESSURE
DUGWAY MAY 22 1991
876
874
872
870
868
866
864
862
860
858
856
854
852
850
MILLIBARS
1300
1400
1500
1600
TIME

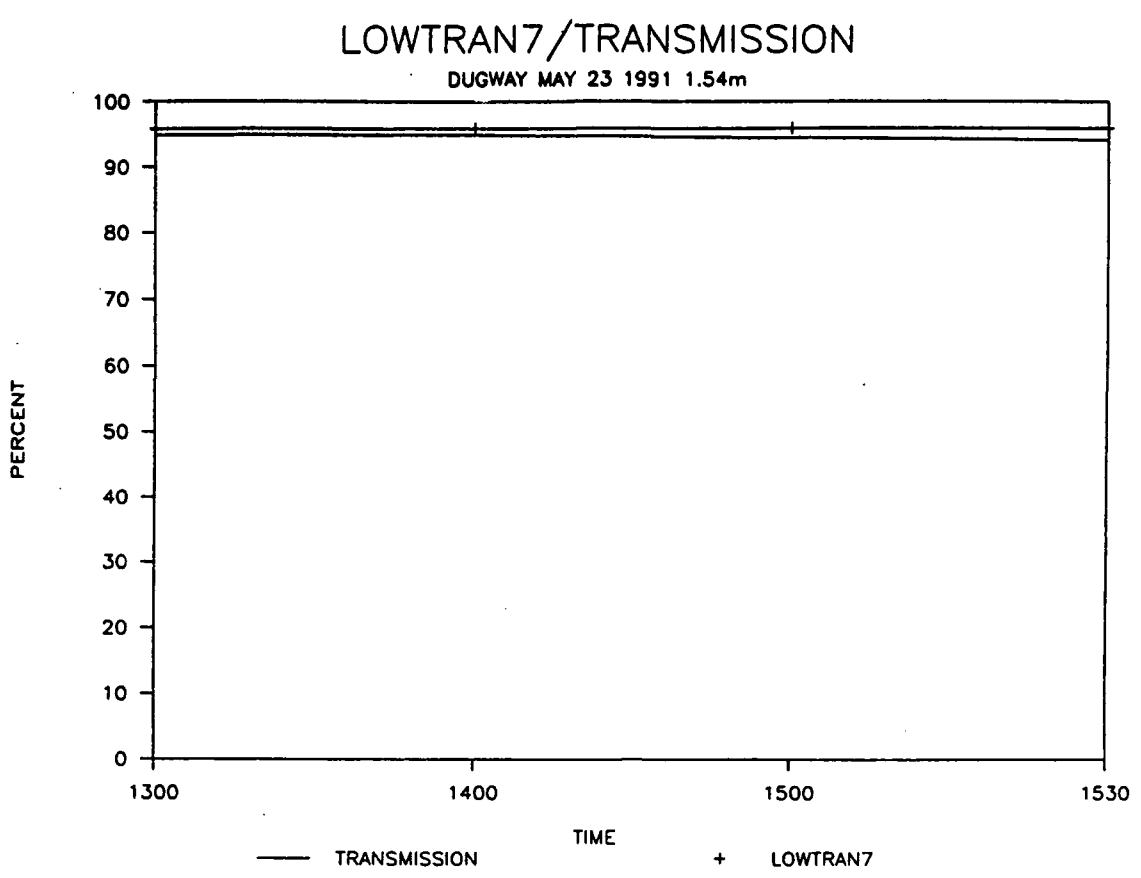

PRESSURE
DUGWAY MAY 23 1991
876
874
872
870
868
866
864
862
860
858
856
854
852
850
MILLIBARS
1300
1400
1500
1530
TIME

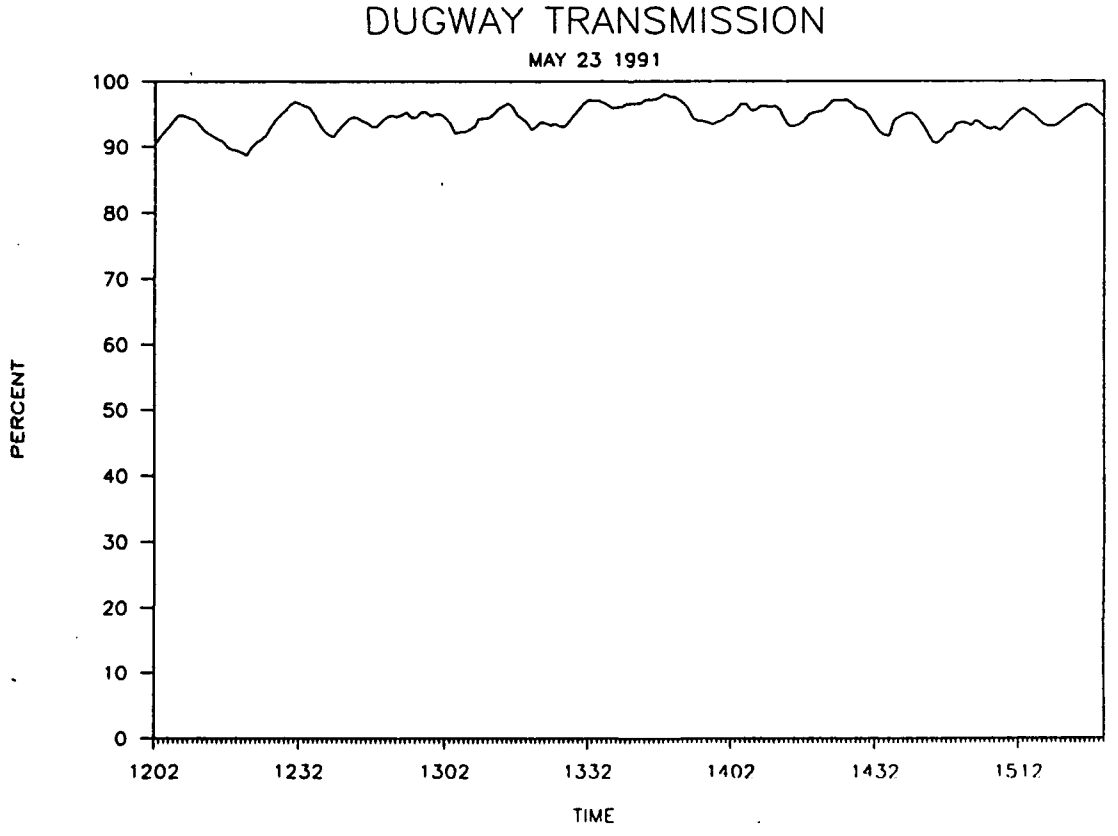

LOWTRAN7/TRANSMISSION
DUGWAY MAY 21 1991 1.54m
PERCENT
100
90
80
70
60
50
40
30
20
10
0
1000
1100
1200
1300
1400
1500
1600
TIME

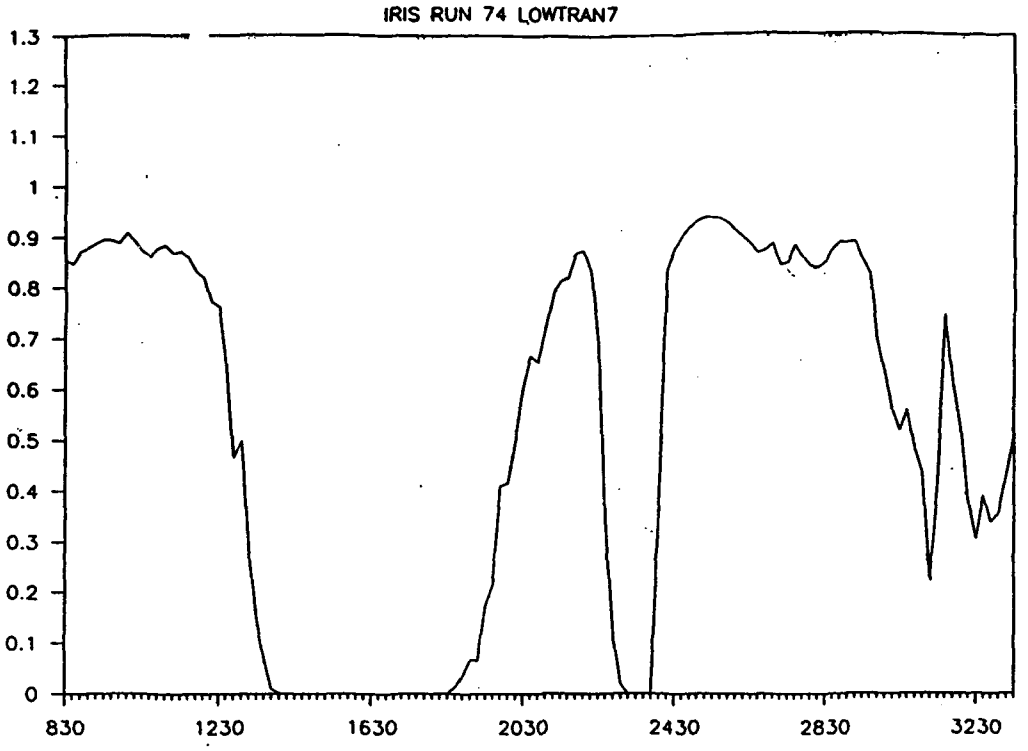

DUGWAY TRANSMISSION
MAY 21 1991
PERCENT
100
90
80
70
60
50
40
30
20
10
0
939
1024
1109
1152
1237
1322
1407
1500
1545
TIME

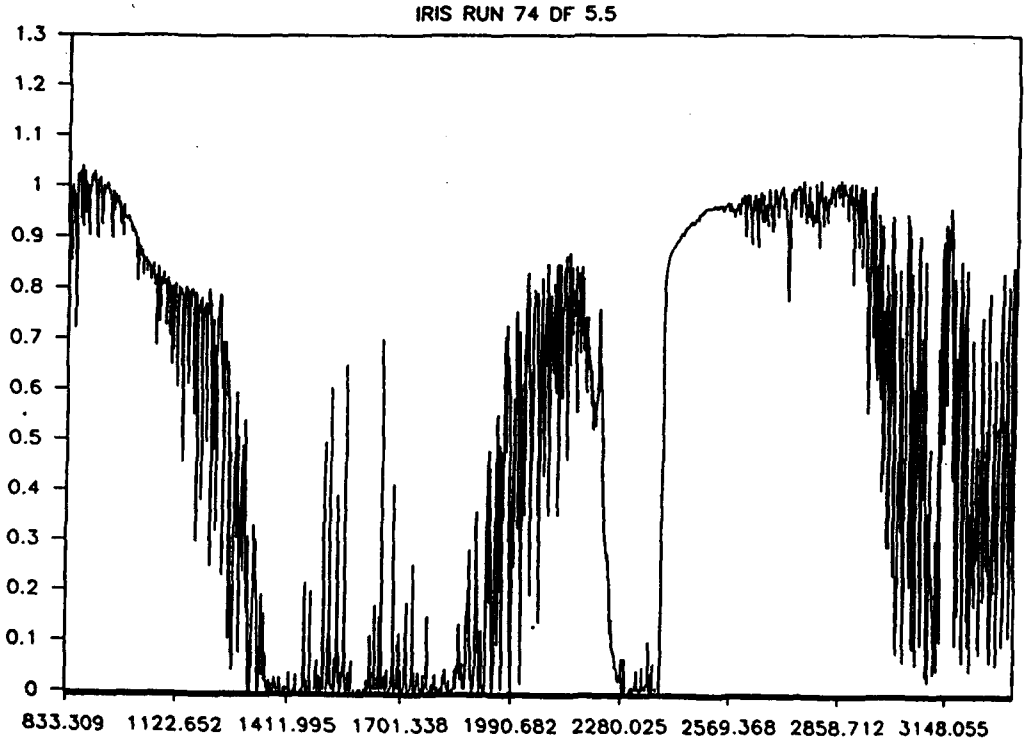

LOWTRAN7/TRANSMISSION
DUGWAY MAY 22 1991 1.54m
PERCENT
100
90
80
70
60
50
40
30
20
10
0
1300
1400
1500
1600
TIME
TRANSMISSION
+ LOWTRAN7

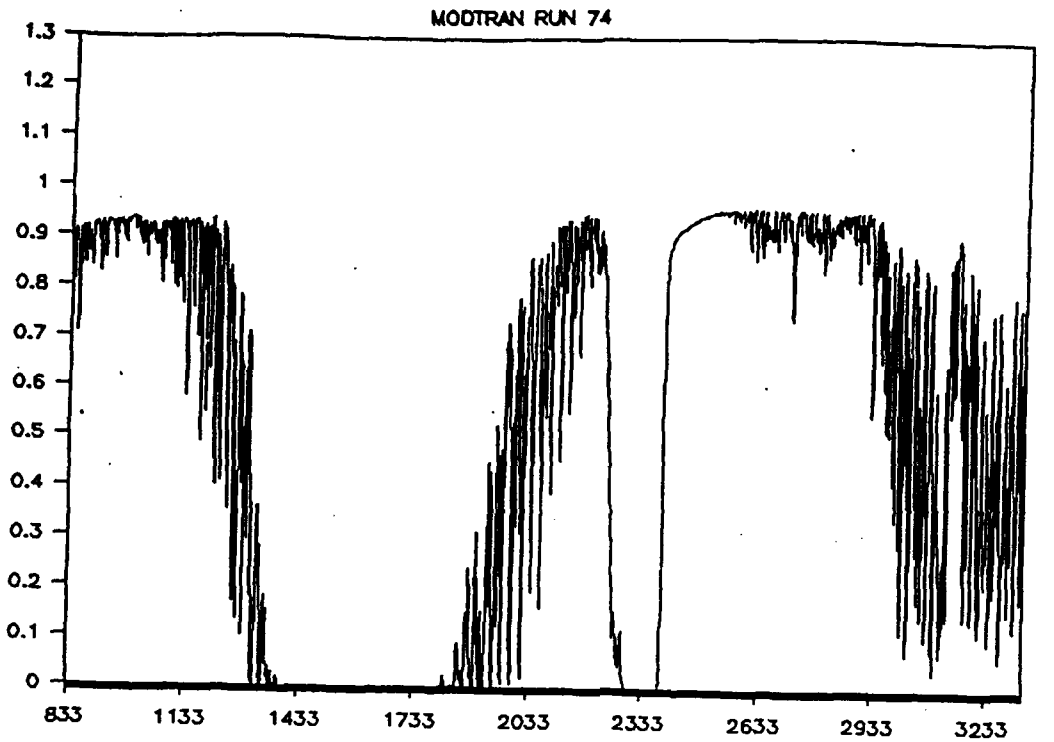

DUGWAY TRANSMISSION
MAY 22 1991
PERCENT
100
90
80
70
60
50
40
30
20
10
0
1232
1301
1329
1359
1428
1458
1528
1558
TIME


LOWTRAN7/TRANSMISSION
DUGWAY MAY 23 1991 1.54m
PERCENT
100
90
80
70
60
50
40
30
20
10
0
1300
1400
1500
1530
TIME
TRANSMISSION
LOWTRAN7


DUGWAY TRANSMISSION
MAY 23 1991
PERCENT
100
90
80
70
60
50
40
30
20
10
0
1202
1232
1302
1332
1402
1432
1512
TIME


IRIS RUN 74 LOWTRAN7
1.3
1.2
1.1
1
0.9
0.8
0.7
0.6
0.5
0.4
0.3
0.2
0.1
0
830
1230
1630
2030
2430
2830
3230


IRIS RUN 74 DF 5.5
1.3
1.2
1.1
1
0.9
0.8
0.7
0.6
0.5
0.4
0.3
0.2
0.1
0
833.309
1122.652
1411.995
1701.338
1990.682
2280.025
2569.368
2858.712
3148.055


MODTRAN RUN 74
1.3
1.2
1.1
1
0.9
0.8
0.7
0.6
0.5
0.4
0.3
0.2
0.1
0
833
1133
1433
1733
2033
2333
2633
2933
3233

SPECTRAL SMOOTHING IN THE FOURIER DOMAIN: A SOFTWARE PACKAGE FOR LINE-BY-LINE CALCULATIONS

W. Gallery
Atmospheric and Environmental Research, Inc., 840 Memorial Drive,
Cambridge, MA 02139

M. Esplin
Stewart Radiance Laboratory, 139 Great Road, Bedford, MA 01730

We have developed a software package which will convolve a spectrum with a spectral scanning function using Fourier transforms. This technique mimics the operation of Fourier transform spectroscopy and preserves the full extent of the scanning function, which is particularly important for functions like sinc. This package has the following features:

1. It gives the user a choice of 5 scanning functions commonly used in Fourier transform spectroscopy, including sinc, $sinc^2$, Hamming, Hanning, and Beer, plus triangle and Gauss, and may be easily modified to include other functions.

2. There is no limitation on the size of the spectrum (a disk-based Fourier transform method is used for spectra exceeding the available memory).

3. If possible, it optimizes the calculation by prescanning the spectrum with a rectangle narrow compared to the scanning function, resulting in significant time and size savings.

4. It has been adapted to read and write FASCODE binary files.

Sample calculations will be shown comparing measured spectra with calculated spectra smoothed using this technique.

Spectral Smoothing in the Fourier Domain: A Software Package for Line-by-Line Calculations

William O. Gallery
*OptiMetrics, Inc.**

Mark Esplin
Stewart Radiance Lab, Bedford, MA

*Now with Atmospheric and Environmental Research, Inc., Cambridge, MA

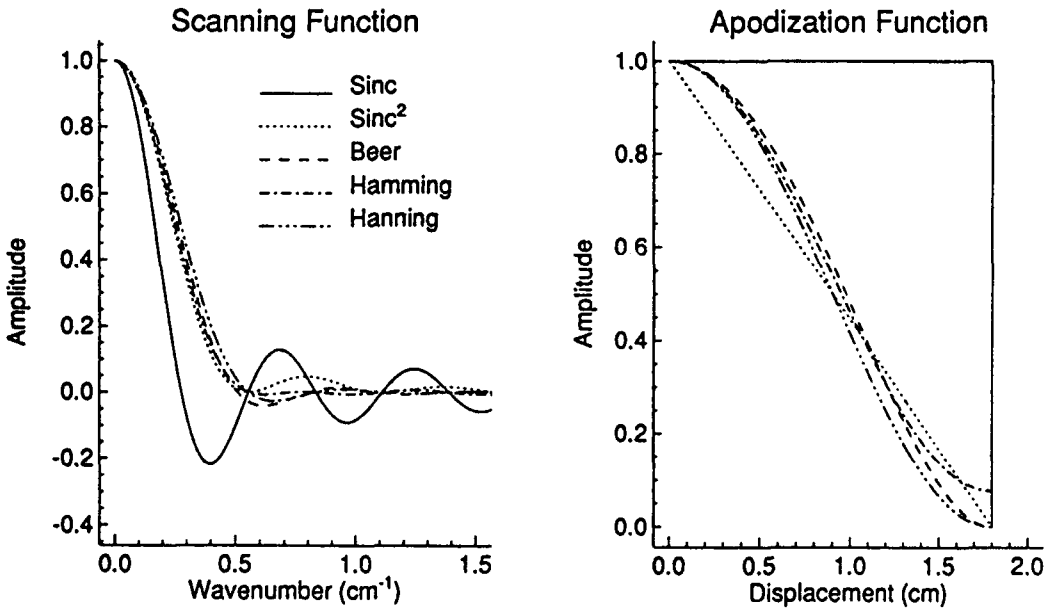
Introduction

- **Line-by-Line Calculation are Often Compared to FTS Measurements**
  - e.g., SCRIBE, CIRRUS, HIS, ATMOS, Lab Measurements
- **Scanning Function is Determined by the Apodization Function Applied to the Interferogram**
- **The Calculation Should Accurately Match the Scanning Function**
  - Extent (Especially Important for Sinc, $Sinc^2$)
  - Shape

Program FFTSCAN

- **A Software Package for Convolving a Spectrum with a Spectral Scanning Function Using Fourier Transforms**
- **Mimics the Operation of a Fourier Transform Spectrometer**
  - Transforms the Calculated Spectrum Into an "Interferogram"
  - Apodized the Interferogram
  - Transforms Back to the Spectral Domain
- **Choice of 5 Common FTS Scanning Functions**
  - Sinc, $Sinc^2$, Hamming, Hanning, Beer
  - Also Triangle, Gauss, and Box

Scanning Functions and Associated Apodization Functions



The Five Scanning Functions and Their Associated Apodization Functions. The functions shown here model the HIS interferometer, with a maximum optical path difference of 1.8 cm.

Program Details

- **Program Reads and Writes Fascode Files**
- **Can Handle Arbitrarily Large Spectra By Using A Disk-Based FFT**
- **Input Spectrum Can be Pre-Scanned with a Boxcar and Deconvoled**
- **Apodization Function Can Be Calculated Either Analytically or As the Fourier Transform of the Scanning Function**

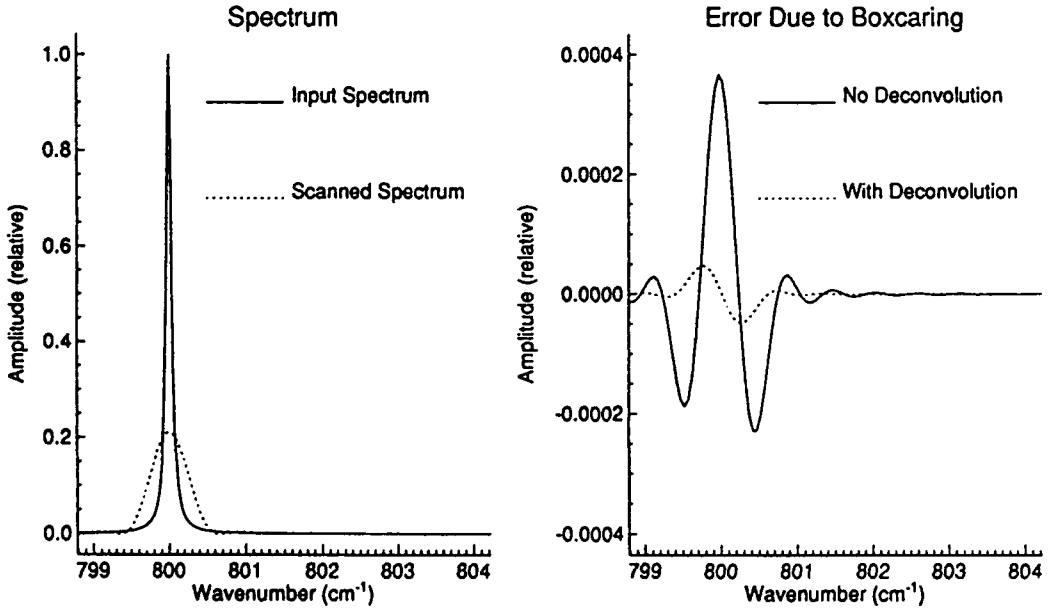
Disk Based FFT

- **Disk Based FFT Courtesy of Mark Esplin, Steward Radiance Lab**
- **If the Number of Points Exceeds the Available Memory, A Disk-Based FFT is Used**
  - Input Data Points Are Sorted Into Blocks and Written To Disk as Direct Access Files
  - Only 2 Blocks Reside in Memory
  - A Standard FFT is Applied to Each Block
  - Data From the Various Blocks is Combined to Obtain the FFT of the Entire Dataset
  - Sorting of Data and Combining of the Blocks is Analogous to the Method of a Standard FFT
- **Time Penalty For a Disk-Based FFT Compared to an In-Memory FFT is 35 % on a Sun 360 Workstation for the Same Total Number of Points**
- **Caution With Virtual Memory**
- **VAX: Direct Access Blocks Blocks Limited to 2048 Points**

Prescanning

- **Prescan Input Spectrum With a Boxcar (Rectangle) If Input $\delta\nu < \alpha/M$**
  - $\delta\nu$ = input frequency spacing, α = scanfunction halfwidth at halfmaximum, M = 5
- **M Points From Input Spectrum Are Averaged To Obtain One Output Point**
- **Prescanning Results In Significant Time and Memory Savings**
- **Smoothing Effect of the Boxcar Can Be (Partially) Reversed By Deconvolving Resampled Spectrum**

Example of Prescanned and Deconvolved Line



Lorenz Line, HWHM = 0.04 cm^{-1}, $d\upsilon$ = 0.01 cm^{-1}, Scanned with a Beer Scanning Function, HWHM = 0.2645 cm^{-1} (HIS Resolution), Prescanned With M = 5 , Output $d\upsilon$ = 0.05 cm^{-1}

- **Resolution:**
  - Half Width at Half Maximum of the Scanning Function, or
  - Maximum Optical Path Difference of an Equivalent Interferometer
- **Frequency Range**
  - Adjusted to Fit Input Spectrum
  - User Must Allow For Edge Effects, Which Can be Quite Extensive For the Sinc Function
- **Transmittance or Radiance**
  - Program Recognizes Different Fascode File Types
- **Scanning Function**
- ***Selectable Options:***
  - Prescanning
  - Deconvolution
  - Apodization Function Calculated as the FFT of the Scanning Function

A COMPARISON OF COMPUTATIONAL APPROACHES FOR THE VOIGT FUNCTION

F. Schreier
DLR - Deutsche Forschungsanstalt für Luft- und Raumfahrt, Institute of Optoelectronics
D-8031 Oberpfaffenhofen (Fed. Rep. Germany)

Several computational procedures for the Voigt function are discussed and compared for accuracy and speed. Vectorization of the codes was applied where possible. This resulted in a variation of computational speed over two orders of magnitude. However, even without vectorization restructuring of the programs can yield a significant acceleration. For applications with least-squares-fitting the evaluation of the complex error function provides an efficient way to calculate both the Voigt function and its partial derivatives.

Annual Review Conference June 1991
on Atmospheric Transmission Models (1991)

A Comparison of Computational Approaches for the Voigt Function

F. Schreier

DLR — Deutsche Forschungsanstalt für Luft- und Raumfahrt
Institute of Optoelectronics
D-8031 Oberpfaffenhofen (Fed. Rep. Germany)

ABSTRACT

Several computational procedures for the Voigt function are discussed and compared for accuracy and speed. Vectorization of the codes was applied where possible. This resulted in a variation of computational speed over two orders of magnitude. However, even without vectorization restructuring of the programs can yield a significant acceleration. For applications with least-squares-fitting the evaluation of the complex error function provides an efficient way to calculate both the Voigt function and its partial derivatives.

The Voigt Function — Definitions

$$g_V = g_L \otimes g_D = \frac{\sqrt{\ln 2/\pi}}{\gamma_D} K(x,y)$$

$$K(x,y) = \frac{y}{\pi} \int_{-\infty}^{+\infty} \frac{e^{-t^2}}{(x-t)^2+y^2}\, dt$$

where

$$x = \sqrt{\ln 2}\, \frac{\tilde{\nu} - \tilde{\nu}_0}{\gamma_D}$$

$$y = \sqrt{\ln 2}\, \frac{\gamma_L}{\gamma_D}$$

and $\tilde{\nu}_0$ line center

γ_L, γ_D Lorentzian and Gaussian half width

representation in complex plane ($z = x + iy$):

$$W(z) = K(x,y) + iL(x,y) = \frac{i}{\pi} \int_{-\infty}^{+\infty} \frac{e^{-t^2}}{z-t}\, dt$$

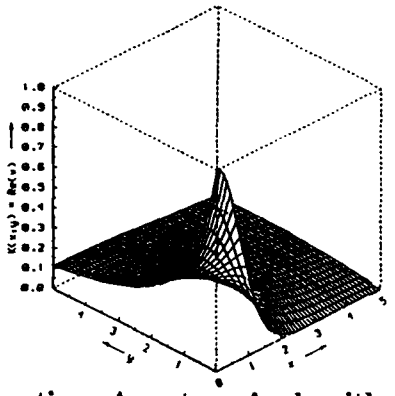
Complex error function:

$$w(z) = e^{-z^2} \left(1 + \frac{2i}{\sqrt{\pi}} \int_0^z e^{t^2}\, dt\right)$$

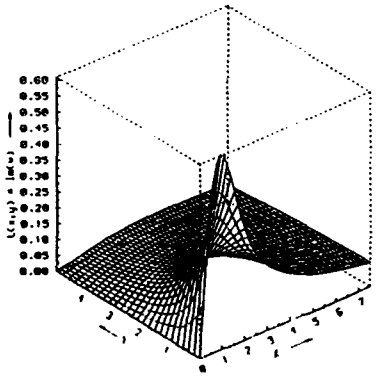
$$= e^{-z^2} \operatorname{erfc}(-iz)$$

$W(z)$ and $w(z)$ are identical for positive y:

$$w(z) = \begin{cases} W(z) & \text{for } y > 0 \\ W(z) + 2e^{-z^2} & \text{for } y < 0 \end{cases}$$



Voigt function: Armstrong's algorithm

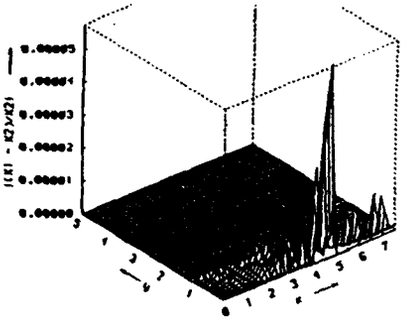


imaginary part of complex error function: Hui's algorithm

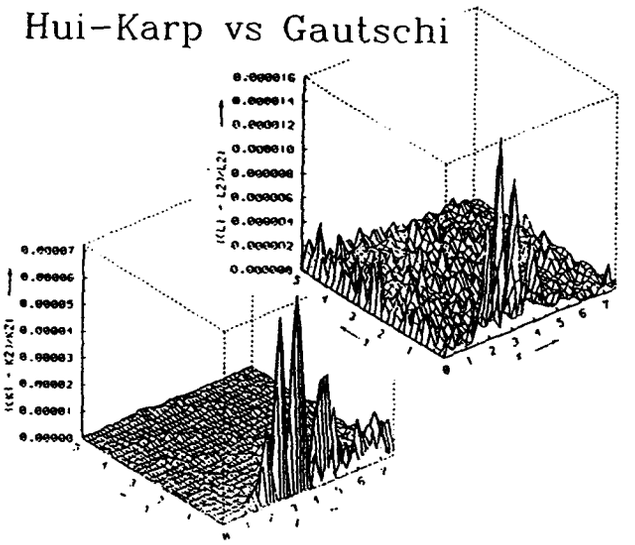
Voigt function: Overview of different algorithms

author(s)	*regions*	*method*	*stated accuracy*
Armstrong (1967)	$y < 1.0,\ x < 4$ or $y < \frac{1.6}{x+1},\ x > 4$ $1 < y < 2.5, x \leq 4$ $y > 2.5,\ x < 4$ or $y > \frac{1.6}{x+1},\ x > 4$	Hummer-Faddeyeva/Terent'ev power series *20-term Gauß-H.-integration of mod. integrand* 20-term Gauß-Hermite-integration	1–2 digits in 6th significant figure
Drayson (1976)	$y < 1.0,\ x < 5 - 0.8y$ $y > 1,\ x < 1.85(3.6 - y)$ else	Taylor expansion, Chebyshev expansion continued fraction 4-term or 2-term Gauß-Hermite-integration	one part in 10^4
Gautschi (1969)	all x, y	truncated Taylor expansion	10 decimal places after decimal point
Hui et al. (1978)	all x, y	rational approximation	rel. error $< 10^{-6}$
Humlicek (1979)	$y > 0.85$ or $\lvert x\rvert < 18.1y + 1.65$ else	rational approximation rational approximation, modified for $\mathcal{R}e(w)$	$2 \cdot 10^{-6}$ for real, $5 \cdot 10^{-6}$ for imag. part
Humlicek (1982)	$\lvert x\rvert + y \geq 15$ $5.5 \leq \lvert x\rvert + y < 15$ $\lvert x\rvert + y < 5.5$ and $y \geq 0.195\lvert x\rvert - 0.176$ else	rational approximations	10^{-4} relative error
Karp (1978)	all x, y	Fourier transform	
Kielkopf (1973)	all x, y	weighted sum of Lorentz and Gauß function	10^{-4} relative to peak value
Pierluissi et al. (1977)	$0 \leq x > 3,\ 0 \leq y < 1.8$ $3 \leq x < 5,\ 1.8 \leq y < 5$ $x \geq 5,\ y \geq 5$	series expansion 6-point Gauß-Hermite integration 4-point Gauß-Hermite integration	peak deviation $\leq 1.4 \cdot 10^{-3}$, RMS deviation $\leq 1.4 \cdot 10^{-5}$
Whiting (1968)	all x, y	weighted sum of Lorentz and Gauß function	5% at worst

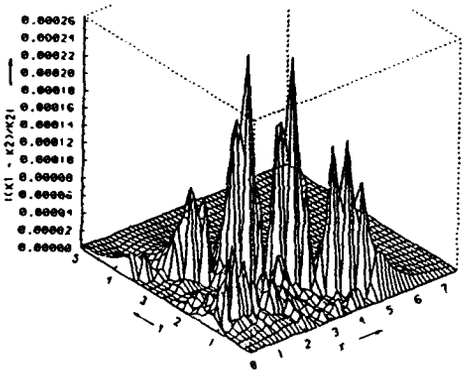
Armstrong vs Gautschi



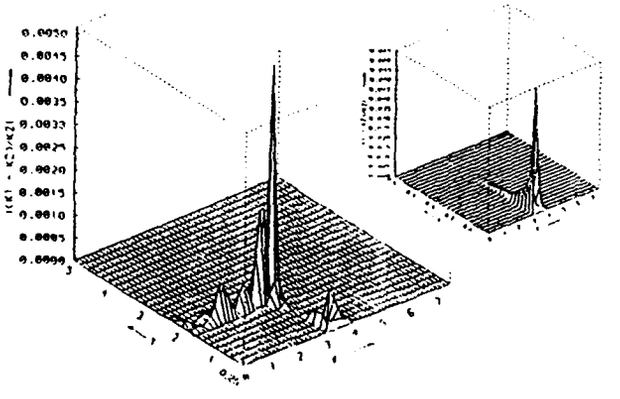
Hui-Karp vs Gautschi



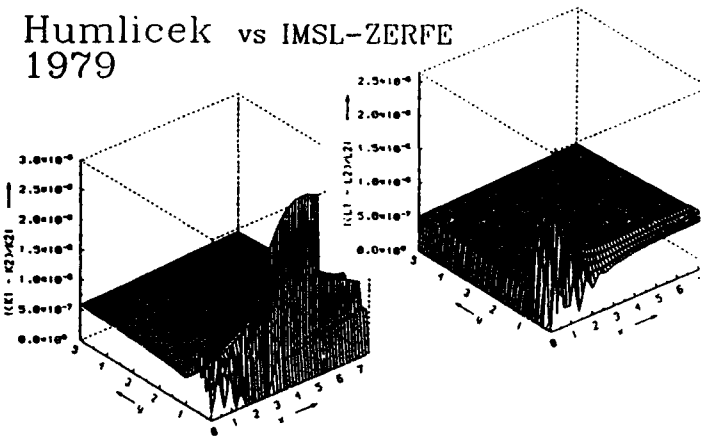
Drayson vs Armstrong



Pierluissi vs Armstrong



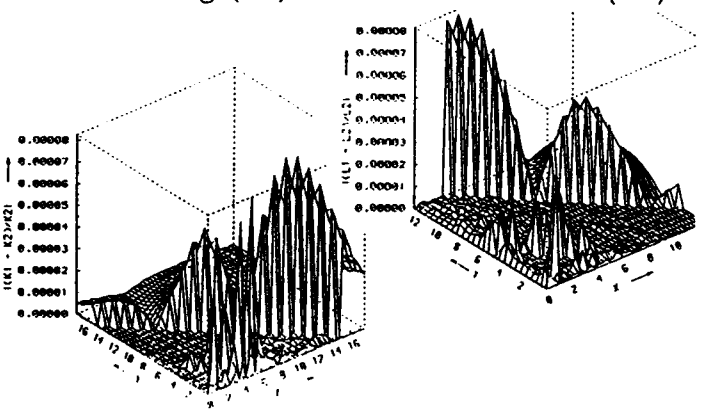
Humlicek vs IMSL-ZERFE
1979

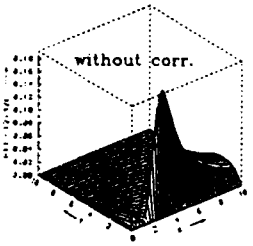


Humlicek 1982

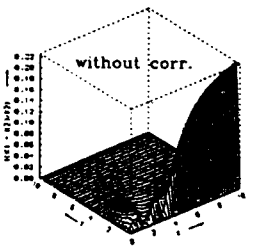
vs Armstrong (Re)

vs IMSL-ZERFE (Im)

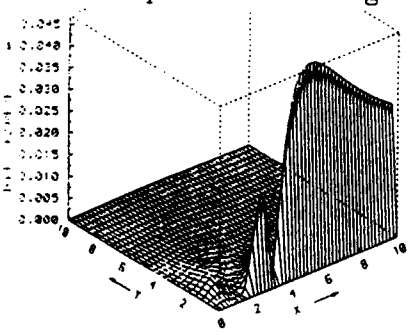




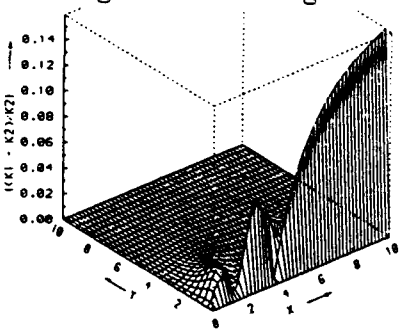
$$K(x,y) \sim \{1-\eta(y)\}G(x)+\eta(y)L(x) + \text{correction}$$



Kielkopf vs Armstrong



Whiting vs Armstrong



Comparison: Computational times

for 1000 x @ 50 y points $(0 < x < 10 \cdot x_{\frac{1}{2}})$

algorithm	time (sec)			
	IBM 3090		CRAY Y-MP2	
	$0 < y < 1$	$1 < y < 10$	$0 < y < 1$	$1 < y < 10$
FUNCTION				
Armstrong	1.26	1.04	1.68	1.49
Drayson	0.38	0.21	1.54	1.39
Hui et al.	0.48	0.48	1.42	1.42
Humlicek 79	0.87	0.76	1.60	1.58
Humlicek 82	0.45	0.29	1.46	1.37
IMSL CERFE *	5.07	3.18	3.75	2.60
Pierluissi et al	0.51	0.24	1.54	1.39
SUBROUTINE				
Hui (vector)	0.093	0.093	0.020	0.020
Kielkopf (vector)	0.051	0.051	0.015	0.015
Kielkopf (novector)	0.17	0.17	0.13	0.13
Whiting (vector)	0.15	0.15	0.036	0.037
Whiting (novector)	0.36	0.36	0.38	0.39

The CPU time used by each function or subroutine has been determined by the IMSL routine CTIME. Jobs were run on a IBM 3090-30S VF(2) under MVS/XA operating system and with VS FORTRAN Version 2 Release 4.0 Compiler. The CRAY Y-MP2/232 runs under UNICOS operating system with a CFT77 compiler. Highest optimization level has been used on both systems.

* implementation of Gautschi algorithm

Vectorization of Hui's algorithm

rational approximation (Hui et al., 1978):

$$w(z) \approx \frac{\sum_{m=0}^{6} a_m (y - ix)^m}{\sum_{n=0}^{7} b_n (y - ix)^n} \quad \text{with} \quad b_7 = 1$$

$\Longrightarrow$ computational effort (for each line and grid point $\tilde{\nu}$):
12 complex multiplications and one complex division,
equivalent to 54 real multiplications and one real division

optimization:
complex polynomial in $\tilde{z} = y - ix$ with real coefficients c_m
$\longleftrightarrow$ polynomial in x with complex coefficients $d_m(y)$

$$\begin{aligned} P(\tilde{z}) &= \sum_{m=0}^{M} c_m \, (y - ix)^m \\ &= \sum_{m=0}^{M} d_m(y) \, x^m \\ &= \sum_{m \text{ even}} d'_m \, x^m + i \sum_{m \text{ odd}} d''_m \, x^m \end{aligned}$$

where

$$d_k = (-i)^k \sum_{l=0}^{M-k} \binom{l+k}{k} c_{l+k} \, y^l$$

$\Longrightarrow$ 21 real multiplications and one real division

Computing times: Hui's algorithm

	time (sec)			
	IBM 3090		CRAY Y-MP2	
	$0 < y < 1$	$1 < y < 10$	$0 < y < 1$	$1 < y < 10$
function	0.48	0.49	1.42	1.43
subroutine (vector)	0.093	0.093	0.020	0.020
optimized subroutine (vector)	0.037	0.037	0.010	0.010
opt. subroutine, novector	0.14	0.14	0.048	0.048
opt. subr., Karp's mod., vector	0.040	0.037	0.010	0.010
opt. subr., Karp, novector	0.145	0.144	0.056	0.048

(Karp's modification is used only for $y \leq 0.1$)

Computing times: Humlicek's algorithm (1979)

	time (sec)			
	IBM 3090		CRAY Y-MP2	
	$0 < y < 1$	$1 < y < 10$	$0 < y < 1$	$1 < y < 10$
function, region I and II, real*4	0.87	0.76	1.60	1.58
function, region I and II	1.29	0.95		
subroutine, only region I	0.18	0.18	0.036	0.036
subroutine, region I and II	0.43	0.18	0.052	0.036
subroutine, I and II, novector	0.95	0.83	0.37	0.25

(Except for the first row double precision arithmetic has been used in the CPF12 routine)

Fourier Transform Methods

advantage: simple Fourier representation of Voigt function

$$K(x,y) = \frac{1}{\sqrt{\pi}} \int_0^\infty e^{-q^2/4-yq} \cos qx \, dq$$

Karp:
- — direct methods: $n_l n_\nu$ evaluations
- — FT methods:
  - only sines, cosines and exponentials for each line
  - and two FFT's for entire frequency range

but: FT method also requires $n_l n_\nu$ evaluations in the Fourier domain plus two FFT's

??? comparable computational effort for direct and FT methods **???**

problems: restriction for the number of grid points to powers of 2
error sources like aliasing

Karp's Fourier Transform Algorithm

total absorption coefficient for n_l lines

$$k(\tilde{\nu}) = \sum_{l=1}^{n_l} S_l \frac{\sqrt{\ln 2/\pi}}{\gamma_l^D} K(x_l, y_l)$$

insert Fourier representation for $K(x,y)$
use $\delta_l \equiv \gamma_l^D/\sqrt{\ln 2}$ and $\lambda_l \equiv \gamma_l^L$,
change of variables $qx_l = p(\tilde{\nu} - \tilde{\nu}_l)$
$\Longrightarrow$

$$k(\tilde{\nu}) = \frac{1}{\pi}\int_0^\infty dp\ \cos p\tilde{\nu} \left[\sum_l S_l\ e^{-(p\delta_l)^2/4 - p\lambda_l} \cos p\tilde{\nu}_l\right] + \frac{1}{\pi}\int_0^\infty dp\ \sin p\tilde{\nu} \left[\sum_l S_l\ e^{-(p\delta_l)^2/4 - p\lambda_l} \sin p\tilde{\nu}_l\right]$$

estimate of computing time

$$t_{[\ldots]} \approx n_l n_p \left(t_{exp} + 2t_{sin} + 6t_{mult} + 3t_{add}\right)$$

equidistant grid points $p_j = j\Delta p$:
recursive relations for exponential and trigonometric functions

$$t_{Karp} = n_l n_p (12t_{mult} + 4t_{add}) + n_l \left(2t_{exp} + 2t_{sin} + 6t_{mult}\right) + 2n_\nu \log_2 n_\nu \tau_{FFT}$$

Absorption coefficient: Hui's rational approximation

total absorption coefficient for n_l lines

$$k(\tilde{\nu}) = \sum_{l=1}^{n_l} \frac{S_l}{\sqrt{\pi}\,\delta_l} \mathcal{R}e \frac{\sum_{m=0}^{6} a_m (y_l - ix_l)^m}{\sum_{n=0}^{7} b_n (y_l - ix_l)^n}$$

requires $n_l n_\nu$ evaluations of $x_l(\tilde{\nu}_i)$ and of fraction of polynomials
define new coefficients for all lines

$$\alpha_{ml} \equiv \frac{S_l a_m}{\sqrt{\pi}\,\delta_l^{m+1}}$$

$$\beta_{nl} \equiv \frac{S_l b_n}{\sqrt{\pi}\,\delta_l^{n+1}}$$

$\Longrightarrow$ absorption coefficient

$$k(\tilde{\nu}) = \sum_{l=1}^{n_l} \mathcal{R}e \frac{\sum_{m=0}^{6} \alpha_{ml}\left(\lambda_l - i(\tilde{\nu} - \tilde{\nu}_l)\right)^m}{\sum_{n=0}^{7} \beta_{nl}\left(\lambda_l - i(\tilde{\nu} - \tilde{\nu}_l)\right)^n}$$

with rearrangement of the complex polynomials

$$t_{Hui} = n_l n_\nu (16t_{mult} + t_{div} + 13t_{add}) + n_l (10t_{mult} + t_{div} + t_{add})$$

Derivatives of the Voigt function

Differential equation ($z = x + iy$)

$$w'(z) = \frac{2i}{\sqrt{\pi}} - 2z\,w(z)$$

use Cauchy-Riemann conditions

or

direct differentation of $K(x,y)$ and partial integration

$\Longrightarrow$

$$\frac{\partial K(x,y)}{\partial x} = -2\,\mathcal{R}e\Big(z\,w(z)\Big)$$
$$\frac{\partial K(x,y)}{\partial y} = +2\,\mathcal{I}m\Big(z\,w(z)\Big) - \frac{2}{\sqrt{\pi}}$$

Voigt function and derivatives calculated simultaneously !!!

numerics:

subtracting two numbers of approximately equal magnitude

Conclusions and Remarks

Accuracy:

sufficient accuracy of most algorithms, but

for applications further aspects are important, too:

- other error sources:
  - — limited accuracy of molecular line parameters
  - — uncertainties from exact temperature dependance of γ_L
  - — deviations from pure Lorentzian line shape
- least-squares-fits in molecular spectroscopy:
  higher accuracy for computation of derivatives

Computational Speed:

- — "black boxes": quick implementation for single applications
  but possibly time consuming otherwise
- — vectorization: significant acceleration (factor 140 for Hui)
- — restructuring: subroutine instead of functions
  invariant code
- — usefulness of imaginary part of $w(z)$

Session 4

Summary of the Topical Session on Spectral Line Shapes

The inclusion of the Topical Session on Spectral Line Shape, as part of the Annual Review Conference on Atmospheric Transmission Models, was an effort to introduce the workshop attendees to some of the basic physics of spectral line shape, to some of the recent research results in this field of study, to the ways those results are manifest in radiative transfer computer codes and to the effects the new results have on the problems of radiative transfer and remote sensing. A particular feature of the topical session was that special consideration was given to providing a tutorial overview of the subject with some emphasis on historical developments.

Within the constraint of time, there were two particular objectives. First, that there should be some presentation in outline tutorial form of the basic physics of spectral line shape. The intention was to stress the physics and not the mathematical theory. The second objective was that there should be detailed consideration of recent research results concerning (1) the shape of far wings of water vapor spectral lines and their aggregate affect on the water vapor continuum, especially in the "window" spectral regions, and (2) the shape of overlapped spectral lines, in particular in the microwave spectrum of oxygen and in the spectrum of carbon dioxide Q branches in the fifteen micron spectral region. The question of the shape of the far wings of water vapor spectral lines is a long standing and much studied theoretical and experimental problem. The questions concerned with the shape of overlapping spectral lines were first addressed almost thirty-five years ago, both theoretically and experimentally in the study of the microwave spectrum of oxygen. However, the discovery, within the last ten years, of line coupling effects in laboratory and atmospheric spectra of many other molecules has brought this effect considerable new attention. Both problems are important to studies related to radiative transfer and remote sensing.

Five invited and five contributed papers composed the topical session. Both invited and contributed papers included original research results. In addition, however, the authors of the invited papers were asked to include tutorial and historical material, related to the general topic of their respective papers. The inclusion of historical material was considered appropriate and was specifically encouraged to address the lack of background knowledge of some of the conference attendees concerning the physics of spectral line shape. In compensation for the added requirement the invited presentations were allotted slightly more time than the contributed papers.

Copies of the transparencies of all of the presentations, both invited and contributed are collected together on the following pages. The authors of the invited papers were asked to prepare and submit summaries of their papers, including references, in particular because these papers contained interesting tutorial and historical materials. Some authors were not able to honor the request, and in part for that reason a very brief description of each paper, along with a few references, is given below.

The first paper, 4a1, "Basis of the Water Vapor Continuum Coefficients in the GL Models" was presented by S.A. Clough (Atmospheric and Environmental Research, Inc. and formerly of the Air Force Geophysics Laboratory). The results of the studies of S.A. Clough, F.X. Kneizys and their co-workers (1), are incorporated in the Geophysics

Directorate's computer code FASCODE. This paper covered some of the general dynamical and statistical considerations for spectral line shape. In particular as they apply to the shape of the far wings of water vapor spectral lines, the frequency dependence of the self and nitrogen broadened Chi-factors and continua. Some of their research is based on the studies of Huber and Van Vleck (2).

The second paper, 4a2, "Water Vapor Continuum Absorption Measurements with Line Shape Interpretations", was presented by M. Thomas (Johns Hopkins University Applied Physics Laboratory). This paper was concerned with the application of a line shape model developed by George Birnbaum (3). Birnbaum's stated objective was to develop a line shape which is applicable from resonance to the far wings. To achieve this he focused his attention on the dipole autocorrelation function, seeking to bridge the gap between the known long and short time behavior of the correlation function with a well chosen empirical interpolation function.

The third paper, 4a3, "Line Coupling for Microwave Oxygen Lines", was presented by P.W. Rosenkranz (Massachusetts Institute of Technology). This paper was concerned with the effect of line mixing in the microwave spectrum of oxygen. The line coupling effect was first observed in the microwave spectrum of oxygen and Rosenkranz was among the first to model the effect (5), employing a perturbation approximation to the line shape matrix. Rosenkranz's presentation included an historical overview of the study of the line coupling effect and recent results for the microwave oxygen band obtained in collaboration with H.J. Liebe (see contributed paper 4b2). Rosenkranz's data analysis technique is unique and differs from that of most other researchers in that the first order perturbation theory line coupling coefficients are inferred directly from the spectral data. Rosenkranz's presentation did not cover the technique but focused on the results of the analysis. However, a discussion of the technique has been presented by Rosenkranz in the literature (6).

The fourth paper, 4a4, "Laboratory Measurements of Line Coupling in CO_2 and N_2O" was presented by L.L. Strow (Univ. of Maryland). This paper considered laboratory measurements and analyses of spectra of carbon dioxide and nitrous oxide which Strow and his co-workers have made. The presentation also included a discussion of the technique most often used to model the line coupling effect in spectral data. Most often rate matrix parameters, and from them line coupling coefficients, are inferred from the spectral line widths, using "gap" laws, for example exponential gap or exponential-power gap laws, to model off diagonal elements of the rate matrix (7,8,9, see also contributed paper 4b3). First or second order perturbation theory is applied to the line shape operator (10) to yield the description in terms of the line coupling parameters (y_i).

The fifth paper, 4a5, "Line Mixing: A Near Wing and Far Wing Problem", was presented by J.M. Hartmann (Ecole Centrale, Paris). This paper, the last of the invited papers, was designed to iterate and tie together some of the basic physical ideas which were presented in the preceding four papers. Hartmann's presentation also illustrates those ideas with some of his and his co-worker's results (11,12) from studies of spectra of water vapor and carbon dioxide.

The sixth paper, 4b1, "Far Wing Line Shape Contribution to the Water Continuum in the Millimeter and Infrared Regions", was presented by R.H. Tipping (Univ. of Alabama). In this paper Tipping presented a theoretical collision broadened line shape, developed in collaboration with Q. Ma (Goddard Instituted for Space Studies) (13). The

theory assumes only the known values of (a) the permanent dipole moment, (b) the rotational constants and (c) the Lennard-Jones potential parameters. Their theory predicts, in particular, the experimentally observed negative temperature dependence of the molecular absorption by water vapor. Their theory partially follows the theoretical studies of Rosenkranz (14).

The seventh paper, 4b2, "Laboratory Measurements of the 60 GHz O_2 Spectrum in Air", was presented by Hans J. Liebe (Institute for Telecommunication Sciences). In this paper Liebe discussed his experimental apparatus which he used to make new measurements of the spectrum of O_2. Liebe also presented some of the experimentally recorded data and some data analyses. Liebe's data were the basis of analyses presented by Rosenkranz (see paper 4a3).

The eighth paper, 4b3, "Line Mixing in Polar and Nonpolar Molecules", was presented by A.S. Pine (National Institute of Standards and Technology; NITS). In this paper Pine presented data of HCN and HCCH which he collected and analyzed in collaboration with J.P. Looney (NITS). Pine reported new measurements and analysis of HCN; their studies of HCCH have been reported previously (15). Pines' presentation compared and contrasted results of data analyses employing various semi-empirical gap laws; an exercise which no one else has to date performed.

The ninth paper, 4b4, "Study of CO_2 Blue Wing in the 4.1 Micron Region", was presented by C.T. Delaye (Applied Physics Laboratory, the Johns Hopkins Univ.) and covered research performed in collaboration with M.E. Thomas (also of the Applied Physics Laboratory); see paper 4a2. Delaye presented interferometric data collected at the Applied Physics Laboratory of carbon dioxide in the 4.3 micron region. Delaye also presented an analysis of this data performed using the same Birnbaum line shape (3) which had been discussed by M. Thomas in paper 4a2. An important result of this study was the applicability of the line shape from the band head region into the far wing of the band and from this the implication that the Birnbaum line shape offered a convenient and accurate expression which would be useful in radiative transfer calculations.

The tenth paper, 4b5, "Theoretical Approach to the Line Wing Problem", was presented by L. Sinitsa (Institute of Atmospheric Optics, Tomsk, USSR). The presentation covered theoretical studies of spectral line shape and approximations with applications to a variety of experimental data from the infrared to the microwave region.

References:

1. S.A. Clough, F.X. Kneizys and R.W. Davies, "Line Shape and the Water Vapor Continuum", Atmospheric Research, 23, 229 (1989).

2. J.H. Van Vleck and D.L. Huber, "Absorption, Emission and Linebreadths: A semihistorical Perspective", Reviews of Modern Physics, 49, 939 (1977).

3. George Birnbaum, "The Shape of Collision Broadened Lines from Resonance to the Far Wings", J.Q.W.S.R.T., 21, 597 (1979).

4. Michel Baranger, "Problem of Overlapping Lines in the Theory of Pressure Broadening", Physical Review, 111, 494 (1958).

5. Philip W. Rosenkranz, "Shape of the 5 mm Oxygen Band in the atmosphere", IEEE Transactions on Antennas and Propagation, Vol. AP-23, 499 (1975).

6. P.W. Rosenkranz, "Interference Coefficients for Overlapping Oxygen Lines in Air", J.Q.S.R.T., 39, 287 (1988).

7. W. Lempert, G.J. Rosasco and W.H. Hurst, "Rotational Collisional Narrowing in the NO Fundamental Q Branch, Studied with CW Stimulated Raman Spectroscopy", J. Chem. Phys., 81, 4241 (1984).

8. L. Larrabee Strow, "Rotational Collisional Narrowing in an Infrared CO_2 Q Branch Studied with a Tunable Diode Laser", J. Chem. Phys., 84, 1149 (1986).

9. A.S. Pine and J.P. Looney, "Decoupling in the Line Mixing of Acetylene Infrared Q Branches", J. Chem. Phys., 93, 6942 (1990).

10. Earl W. Smith, "Absorption and Dispersing in the O_2 Microwave Spectrum at Atmospheric Pressures", J. Chem. Phys., 74, 6658 (1981).

11. J.M. Hartmann, L. Rosenmann and J. Taine, "Temperature and Pressure Dependence of Absorption in the Narrow R_{66}-R_{68} Window of the $^{12}C^{16}O_2v_3$ Band", J.Q.S.R.T., 40, 93 (1988).

12. M.Y. Perrin and J.M. Hartmann, "Temperature Dependent Measurements and Modeling of Absorption by CO_2-N_2 Mixtures in the Far Line Wings of the 4.3 um CO_2 Band", J.Q.S.R.T., 42, 311 (1989).

13. Q. Ma and R.H. Tipping, "A Far Wing Line Shape Theory and its Application to the Water Continuum Absorption in the Infrared Region. I", J. Chem. Phys., 95, 6390 (1991).

14. P.W. Rosenkranz, "Pressure Broadening of Rotational Bands. I. A Statistical Theory", J. Chem. Phys., 83, 6139 (1985).

15. A.S. Pine and J.P. Looney, "Decoupling in the Line Mixing of Acetylene Infrared Q Branches", J. Chem. Phys., 93, 6942 (1990).

BASIS OF THE WATER VAPOR CONTINUUM COEFFICIENTS IN THE GL MODELS

S.A. Clough
Atmospheric and Environmental Research, Inc., 840 Memorial Drive, Cambridge, MA 02139

F.X. Kneizys
Geophysics Directorate, Hanscom AFB, MA 01731

R.W. Davies
GTE Laboratories, Waltham, MA 02154

A formulation is developed in which the contribution of the far wings of collisionally broadened spectral lines to the water vapor continuum absorption is established. The effects of deviations from the impact (Lorentz) line shape due to duration of collision effects are treated semi-empirically to provide agreement with experimental results for the continuum absorption and its temperature-dependence. The continua due to both water-water molecular broadening (self-broadening) and water-air molecular broadening (foreign broadening) are discussed. Several atmospheric validations of the present approach are presented.

Atmospheric Research, 23 (1989) 229-241
Elsevier Science Publishers B.V., Amsterdam — Printed in The Netherlands

Line Shape and the Water Vapor Continuum

S.A. CLOUGH, F.X. KNEIZYS and R.W. DAVIES

Atmospheric and Environmental Research, Inc., Cambridge, MA 02139 (U.S.A.)
Air Force Geophysics Laboratory, Hanscom AFB, MA 01731 (U.S.A.)
GTE Laboratories, Waltham, MA 02154 (U.S.A.)

(Received May 1, 1988; accepted June 1, 1989)

ABSTRACT

Clough, S.A., Kneizys, F.X. and Davies, R.W., 1989. Line shape and the water vapor continuum. Atmos. Res., 23: 229-241.

A formulation is developed in which the contribution of the far wings of collisionally broadened spectral lines to the water vapor continuum absorption is established. The effects of deviations from the impact (Lorentz) line shape due to duration of collision effects are treated semi-empirically to provide agreement with experimental results for the continuum absorption and its temperature-dependence. The continua due to both water-water molecular broadening (self-broadening) and water-air molecular broadening (foreign broadening) are discussed. Several atmospheric validations of the present approach are presented.

RESUME

On développe une formulation dans laquelle on établit la contribution des ailes éloignées des raies élargies par collision au continuum d'absorption de la vapeur d'eau. Les effets des déviations de la forme de raie d'impact (Lorentz) sont traités de façon semi-empirique pour fournir un accord avec les résultats expérimentaux concernant le continuum d'absorption et sa dépendence en température. Les continua dûs à l'effet d'élargissement moléculaire eau-eau (self broadening) et air-eau (foreign broadening) sont discutés. Plusieurs validations atmosphériques de cette approche sont présentées.

INTRODUCTION

The continuum absorption due to water vapor has posed a complex problem for researchers concerned with atmospheric radiative problems. In fact, a universally accepted definition of continuum absorption has not been established making more difficult the discussion of the effect. The regions of the atmospheric spectrum in the microwave and the infrared with the greatest transparency, the windows, are strongly dependent on the water vapor continuum. These spectral regions are at 0 cm^{-1}, 800-1200 cm^{-1} and 2000-3000 cm^{-1}. Laboratory measurements of the water vapor continuum are made difficult by the long path lengths required with conventional spectroscopic techniques or by the complexities encountered with methods of high sensitivity such as spectrophone detection. Atmospheric measurements are adversely affected by the difficulty in adequately characterizing the path, aerosol attenuation, turbulence, scintillation and instrument calibration. From a theoretical point of view, the continuum has posed a comparably complex problem and still lacks a completely satisfactory explanation. The issue of whether the absorption represents an excess or deficiency is fundamentally dependent on the line shape formulation chosen as reference as well as on the frequency regime of interest. A theoretical understanding of this problem entails a satisfactory description of the line shape and its temperature-dependence from line center to the far line wing requiring a proper treatment of the physical processes occurring in the time associated with the duration of collision. Further, an adequate model must also address the issue of collision-induced spectra as well as the possibility of dimer absorption.

0169-8095/89/$03.50 © 1989 Elsevier Science Publishers B.V.

LINE SHAPE FORMULATION

In our consideration of the continuum, we start with a line shape formulation for the absorption coefficient $k(\nu)$ (cm^2/molec.), that is applicable from the microwave to the infrared (Clough et al., 1983):

$$k(\nu)=R(\nu)\langle\phi(\nu)+\phi(-\nu)\rangle \tag{1}$$

with:

$$R(\nu)=\nu\frac{1-e^{-\beta\nu}}{1+e^{-\beta\nu}} \tag{2}$$

$$=\nu\tanh(\beta\nu/2) \tag{3}$$

where ν is the wavenumber value, $R(\nu)$ (cm^{-1}) is a radiation field term at temperature T with $\beta=hc/kT$ (cm), and $\langle\phi(\nu)+\phi(-\nu)\rangle$ is the symmetrized power spectral density function (Van Vleck and Huber, 1977). The term $R(\nu)$ includes the effect of stimulated emission. This formulation has a number of attractive properties: its appropriateness to all spectral domains and the fact that the symmetrized power spectral density function satisfies an important intensity sum rule, the Nyquist theorem. For the application of this formalism to the computation of spectra in terms of line transition data, we obtain:

$$k(\nu)=\nu\tanh(\beta\nu/2)\times\sum_i \tilde{S}_i(T)\frac{1}{\pi}\left[\frac{\alpha_i}{(\nu-\nu_i)^2+\alpha_i^2}\chi(\nu_i-\nu)+\frac{\alpha_i}{(\nu+\nu_i)^2+\alpha_i^2}\chi(\nu+\nu_i)\right] \quad (4)$$

where $\tilde{S}_i$ (cm²/molec.) is the intensity of the transition at wavenumber value ν_i (cm^{-1}) and halfwidth α_i (cm^{-1}). The Lorentz function, $f(\nu-\nu_i)$ (cm):

$$f(\nu-\nu_i)=\frac{1}{\pi}\frac{\alpha_i}{(\nu-\nu_i)^2+\alpha_i^2} \quad (5)$$

is the line shape function appropriate to the impact approximation for which the collision time is assumed to be instantaneous. The χ function is a semi-empirical function applied to the impact result to correct for duration of collision effects and to attain agreement between calculated and measured spectra. With $\chi=1$, this line shape reduces to the Lorentz shape in the infrared, since $R(\nu)\to\nu_i$ for $|\nu-\nu_i|\ll\nu_i$ and to the Van Vleck-Weisskopf shape in the microwave, since $R(\nu)\to\beta\nu^2/2$. We adopt a notation in which a tilde over a quantity indicates that the radiation term, $R(\nu)$, has been excluded from that quantity.

At this stage we define a continuum absorption by excluding from the power spectral density function fast spectral components associated with the line center. The continuum, $\tilde{C}(\nu)$, is given by:

$$\tilde{C}(\nu)=\langle\phi(\nu)+\phi(-\nu)\rangle_c \quad (6)$$

$$=\sum_i \tilde{S}_i[f_c(\nu-\nu_i)\chi(\nu-\nu_i)+f_c(\nu+\nu_i)\chi(\nu+\nu_i)] \quad (7)$$

where f_c is a line shape with the strong central component excluded (Clough et al., 1980). We systematically define f_c ($\nu\mp\nu_i$) in the following way:

$$f_c(\nu\mp\nu_i)=\begin{cases}\dfrac{1}{\pi}\dfrac{\alpha_i}{25^2+\alpha_i^2} & |\nu\mp\nu_i|\le 25\text{ cm}^{-1}\\[2ex] \dfrac{1}{\pi}\dfrac{\alpha_i}{(\nu\mp\nu_i)^2+\alpha_i^2} & |\nu\mp\nu_i|\ge 25\text{ cm}^{-1}\end{cases} \quad (8)$$

The function f_c is indicated schematically in Fig. 1 by the solid curve. Another function that has been used by Burch in some of his work is indicated by the dashed line in Fig. 1. The lack of agreement among researchers on the line shape formulation and on the definition of the function f_c has inhibited the intercomparison and validation of continua. It must be emphasized that the continuum and the details of the line-by-line calculation are inextricably related. The present formulation for the continuum is consistent with the FASCODE line-by-line model (Clough et al., 1986). Similarly, it is important to recognize that band models developed to describe molecular absorption, must also be derived in the context of a consistent treatment of the continuum. To

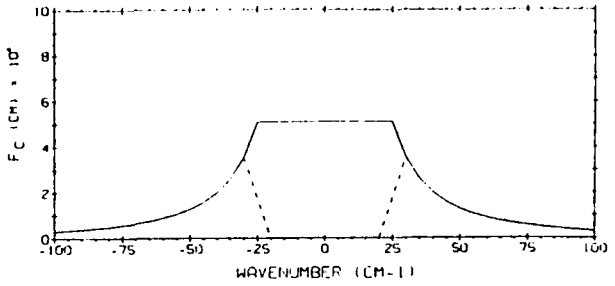


Fig. 1. The line shape function, $f_c(\nu)$, used to develop the continuum (solid curve). The dashed curve represents the function used by Burch.

be more explicit, if a band model is to be used in conjunction with a continuum, then the absorption effects included in the continuum must be excluded from the band model. We should note that the continuum functions have been developed in such a way as to obey Beer's law.

It is an important consideration that the continuum coefficier ., $\tilde{C}(\nu)$, is proportional to collider density, ρ. Since the collision frequency which is proportional to density determines the broadening, density is more appropriate as the dependent variable than pressure. At constant temperature the distinction is not relevant. The values for the self broadened halfwidths, α_i^0, referred to atmospheric density, ρ_0, are of the order of 0.1 cm^{-1} (0.5 cm^{-1} for self-broadened water vapor). With the halfwidth density-dependence given bv:

$$\alpha_i=\alpha_i^0(\rho/\rho_0) \quad (9)$$

the α_i^2 terms in eq. 8 may be dropped and the continuum shape function becomes:

$$f_c(\nu\mp\nu_i)=\begin{cases}\dfrac{1}{\pi}\dfrac{\alpha_i^0(\rho/\rho_0)}{25^2} & |\nu\mp\nu_i|\le 25\text{ cm}^{-1}\\[2ex] \dfrac{1}{\pi}\dfrac{\alpha_i^0(\rho/\rho_0)}{(\nu\mp\nu_i)^2} & |\nu\mp\nu_i|\ge 25\text{ cm}^{-1}\end{cases} \quad (10)$$

The density scaling of the continuum is established as:

$$\tilde{C}(\nu)=\tilde{C}^\circ(\nu)\ (\rho/\rho_0) \quad (11)$$

since f_c is proportional to (ρ/ρ_0) for all values of ν.

The temperature-dependence of the absorption is dependent on the radiation term, $R(\nu)$ in eq. 2, the strength $\tilde{S}_i$, the halfwidth α_i^0, and on the line shape factor χ. The dependence is known theoretically for $R(\nu)$ and for $\tilde{S}_i$ and is

satisfactorily described through an empirical exponent, m, determined from measurements for α, where:

$$\alpha_i(\rho,T)=\alpha_i^0(T/T_0)^m(\rho/\rho_0)$$

For the line shape factor χ the situation is more complicated. Near line center, $|\nu \pm \nu_i| < 5\ \mathrm{cm}^{-1}$, χ is essentially unity for all temperatures. However far from line center the temperature-dependence for χ must be inferred from the temperature of the absorption resulting from many overlapping lines.

WATER VAPOR

We are now in a position to apply the formulation we have developed to water vapor absorption. Performing a line-by-line calculation using the entire set of water vapor lines from 0 cm^{-1} to 10,000 cm^{-1}, we obtain the power spectral density function for self-broadened water vapor shown in Fig. 2. The dotted curve is attained by utilizing the continuum line shape function, f_c, thus excluding from the power spectral density function the contribution of the line centers, and providing a spectrum of low spectral content designated as the continuum. The well known water vapor bands associated with pure rotation (0 cm^{-1}), ν_2 (1600 cm^{-1}), ν_1 of HDO (2720 cm^{-1}), $2\nu_2$ (3100 cm^{-1}), ν_1 (3660 cm^{-1}) and ν_3 (3760 cm^{-1}) are evident in Fig. 2. In Fig. 3 we indicate two

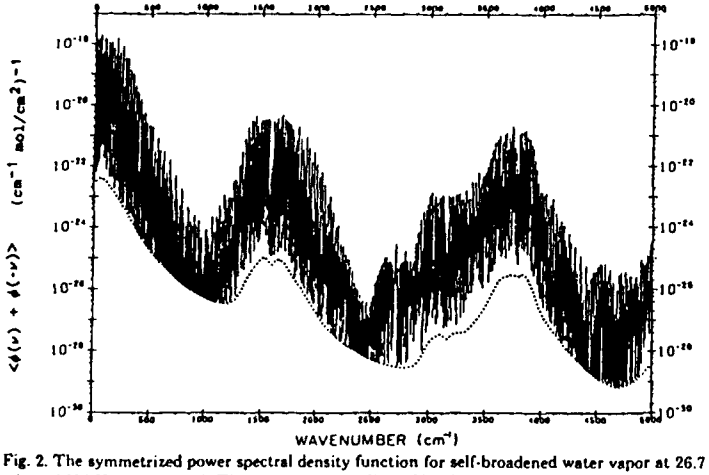


Fig. 2. The symmetrized power spectral density function for self-broadened water vapor at 26.7 mb. and 296 K (solid curve). The continuum is indicated by the dotted curve.

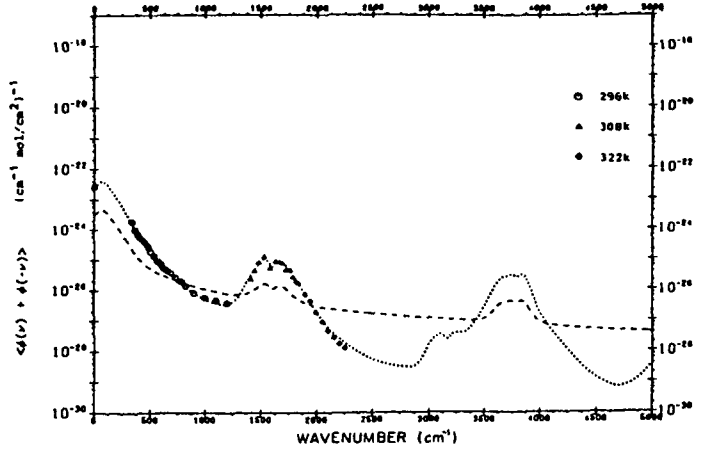


Fig. 3. The continuum for self-broadened water vapor. The dashed line is the impact result and the dotted curve is with the χ function adjusted to fit the experimental data of Burch, 1981. The broadening pressure is ~~1013~~ 26.7 mb.

continua, one obtained using the impact line shape ($\chi=1$), and the other with a function obtained by adjusting the parameters in an empirical χ-function to attain agreement with the indicated spectral results (Burch, 1981; Burch and Alt, 1984; Burch, 1985).

Note that in Fig. 3 the continuum coefficient for self-broadened water vapor, $\tilde{C}_s^0$, exhibits an excess absorption with respect to the reference impact continuum ($\chi=1$) in the center of the bands at 0–500 cm^{-1} and 1400–1800 cm^{-1} and a deficiency between central band absorption regions, 800–1200 cm^{-1} and 1800–3300 cm^{-1}. This result is consistent with theoretical requirements and is a direct consequence of the formulation. The χ function associated with the line shape for self-broadened water vapor, designated χ_s, is shown by the solid curve in Fig. 4. The functional form of χ is given by:

$$\chi=\begin{cases}1-(1-\chi')\dfrac{(\nu\mp\nu_i)^2}{25^2} & |\nu\mp\nu_i|\leqslant 25\ \mathrm{cm}^{-1}\\ \chi' & |\nu\mp\nu_i|\geqslant 25\ \mathrm{cm}^{-1}\end{cases} \tag{12}$$

where for self-broadening χ_s is obtained by setting $\chi'=\chi_s$ with:

$$\chi_s'=8.63\exp(-z_1^2)+(0.83z_2^2+0.033z_2^4)\exp(-|z_2|) \tag{13}$$

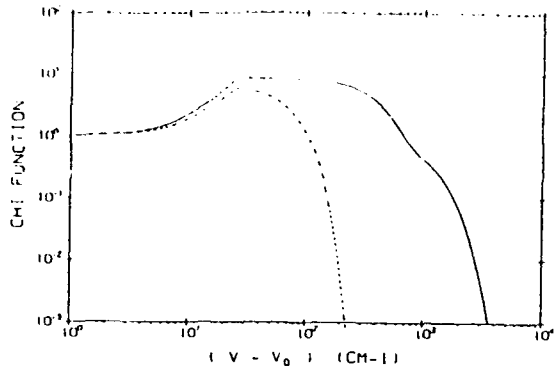


Fig. 4. The χ function for water at 296 K. The solid curve is for self-broadening; the dashed curve is for foreign-broadening.

where $z_1 = (\nu \mp \nu_i)/400$ and $z_2 = (\nu \pm \nu_i)/250$ at 296 K. From eq. 12 and Fig. 4 we note that χ is continuous at 25 cm^{-1}, but that the first derivative is discontinuous. This is a direct consequence of the choice of f_c (eq. 8) but causes no particular problems in the formulation.

The self-continuum for water vapor demonstrates a rather strong temperature-dependence, particularly in the 1000 cm^{-1} window. It is an important shortcoming of the current state of line shape theory for molecular collisions, that the temperature-dependence of the far wings, or alternatively of the continuum in the window regions, is not explained. Rosenkranz (1985, 1987), in two particularly interesting papers, has proposed an alternative formulation to eqs. 1 and 3, which leads to a strong temperature-dependence consistent with observations in the far-wing regions. This proposed formulation warrants additional scrutiny. The dimer has often been postulated as a source of the continuum absorption primarily as a consequence of its simple and attractive temperature-dependence. However, the absence of spectral structure, difficulties in explaining spectral pressure-dependence and the fact that the absorption in the windows as developed in this paper represents an excess with respect to the impact line shape are in direct contradiction with the dimer theory. On the other hand, dimers should be formed under atmospheric conditions so that the central issue becomes the question of dimer lifetime (Suck et al., 1979).

For pragmatic purposes the temperature-dependence of the continuum has been treated as follows: the parameters in an analytical χ function are obtained by least-squares fitting the calculated continuum to the data of Burch at 296 K and 338 K. These parameters for 296 K and 338 K are then extrapolated to

260 K and a continuum for that temperature is calculated. This is potentially a source of error; however, validations for atmospheric measurements have provided remarkably good results. Continua for 338 K, 296 K and 260 K are shown in Fig. 5.

An analogous treatment is performed for air-broadening of water vapor, referred to as foreign broadening. Fig. 6 shows the empirical continuum, $\tilde{C}_f^0$, fit to the data of Burch as well as the continuum for the impact approximation. For the foreign-broadened case, the line wings decay much more rapidly as a function of wavenumber difference from line center than for the self-broadened case. This is reflected in the foreign chi-function, χ_f shown by the dashed curve in Fig. 4. For the foreign continuum χ_f is obtained by setting $\chi' = \chi_f'$ in eq. 12 with:

$$\chi_f' = 6.65 \exp(-z_1^2) \tag{14}$$

where $z_1 = (\nu \pm \nu_i)/75$. For the window regions of the foreign continuum, 1000 cm^{-1} and 2500 cm^{-1} in Fig. 6, an absorption coefficient has been added to the continuum resulting from the present formalism in order to attain agreement with atmospheric measurements (Roberts et al., 1976). The contribution of the foreign continuum is very small in these spectral regions making the measurements particularly difficult. The observed effect may be due to collision

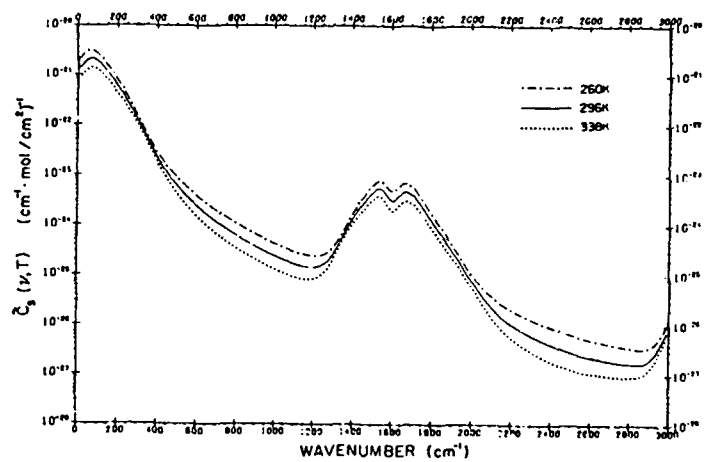


Fig. 5. The self-broadened water vapor continuum at 338 K, 296 K and 260 K. The continua at 338 K and 296 K have been fit to data and the 260 K continua have been extrapolated.

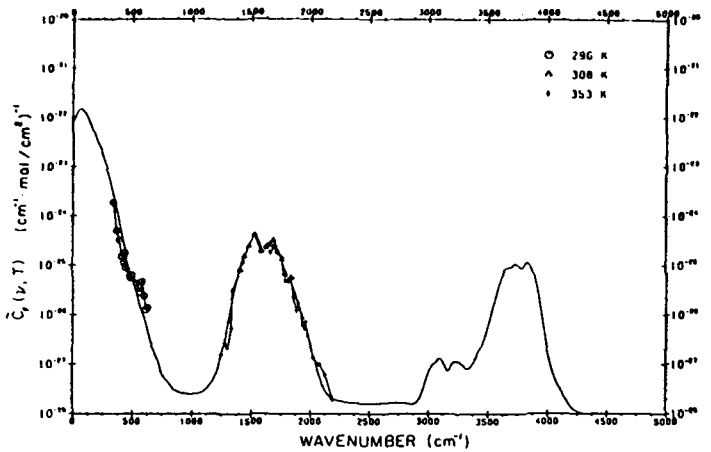


Fig. 6. The continuum for foreign-broadened water vapor. The solid curve is the calculated continuum with the χ function adjusted to fit the experimental data of Burch, 1981. The broadening pressure is 1013 mb.

induced spectra or humidity-dependent aerosols. No significant temperature-dependence has been observed for the foreign continuum.

The total absorption coefficient due to self- and foreign-water-vapor continuum, $k_c(\nu)$, is given by the relation:

$$k_c(\nu) = \nu \tanh(\beta\nu/2)\,[\tilde{C}_s^0(\rho_s/\rho_0) + \tilde{C}_f^0(\rho_f/\rho_0)] \qquad (15)$$

It is an important point that for atmospheric conditions, the foreign continuum is dominant for in-band absorption and the self continuum is dominant for the out-of-band absorption, the window regions of water vapor spectrum.

ATMOSPHERIC VALIDATION

The most important element in the development of an atmospheric transmittance/radiance model is validation with atmospheric data. Since the atmospheric window at 1000 cm^{-1} (10 μm) is of such importance, we consider that spectral region in more detail. The continuum currently being used in FASCOD2 has been adjusted to fit the more recent measurements at 1000 cm^{-1} of Burch and Alt, 1984 (Fig. 7). In Fig. 8 we show a plot of the optical depth for a 1-km path at 990 cm^{-1} as a function of water vapor density from LOWTRAN7 (Kneizys et al., 1988) which incorporates this continuum de-

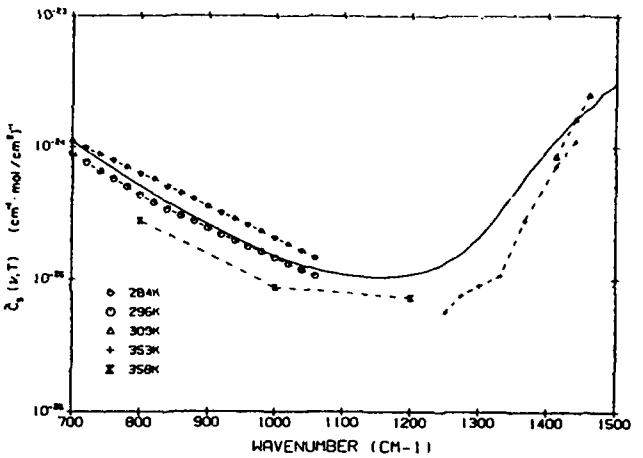


Fig. 7. Details of the self-broadened continuum at 1000 cm^{-1}. The solid line is the calculated continuum at 296 K. The data for 284 K and 296 K are from Burch and Alt (1984); the other data are from Burch (1981).

velopment. We consider two sets of atmospheric measurements: one from the Air Force Wright Aeronautical Laboratories (AFWAL) taken over an 8-km path and for a range of visibilities (Kneizys et al., 1984) and the other from the Technion Institute in Israel over an 8.6-km path (Oppenheim and Lipson, 1986). Both of these sets of measurements were taken with circular variable filter (CVF) spectrometers. Since the atmospheric measurements include extinction due to aerosol effects, the calculated optical depths, which do not include aerosol contributions, are less than those for the atmospheric measurements. The calculations do take into effect the contribution from other molecules (intercept) and from the local water vapor lines. Spectral validation of the continuum model with the Technion measurements for the 8–12 micron window is shown in Fig. 9 and for the 3–5 micron window in Fig. 10. Of particular note is the excellent agreement between calculation and observation obtained at 4.75 μm and 3.2 μm. These two regions demonstrate the predictive capability of the current formulation since there has been no adjustment with data in these spectral regions. With respect to the continua beyond 5000 cm^{-1}, it should be emphasized that the calculations are essentially qualitative and unvalidated. This is particularly the case for the self-broadened continuum, important between the bands.

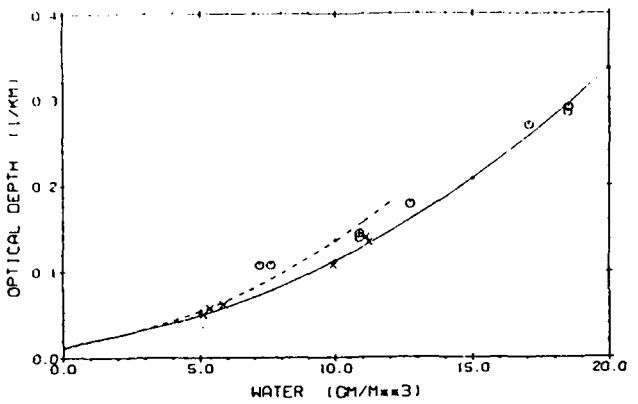


Fig. 8. The optical depth for a 1-km path at 990 cm^{-1} as a function of water vapor density. The calculations are from LOWTRAN with the self-continuum of Fig. 7. The solid curve is for 296 K and the dashed curve is for 284 K. The data are from Kneizys et al., 1984. The X-symbols are for cases with visibilities > 15 km.

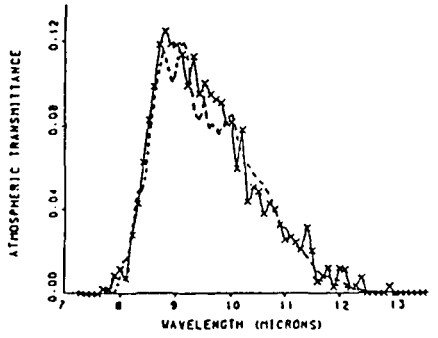


Fig. 9. Spectral comparison between a CVF measurement in the 8-12 micron window over a 8.637-km path by Technion (Oppenheim and Lipson, 1985) and a LOWTRAN calculation with the FASCOD2 continuum (dotted curve). The measurement conditions: $T = 297.5$ K, $P = 1008$ mb., $RH = 85\%$, and visibility = 15 km.

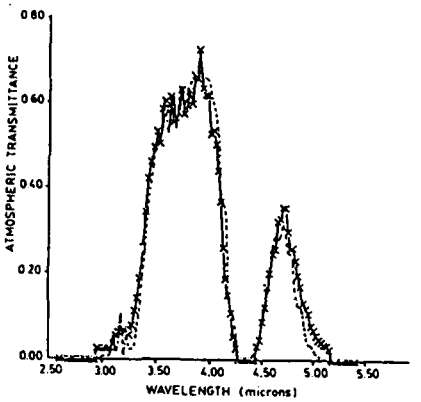


Fig. 10. Spectral comparison between a CVF measurement in the 3-5 micron window over a 10.37-km path by Technion (Oppenheim and Lipson, 1985) and a LOWTRAN6 calculation (dotted curve). The measurement conditions: $T = 283$ K, $P = 899$ mb., $RH = 68\%$ and visibility = 40 km.

SUMMARY

The present discussion is not intended as a comprehensive review of the water vapor continuum problem. It is rather a description of a specific approach that is consistent with the physics of the problem and that has been constrained to provide results consistent with experimental measurements. The choice of measurements used for this discussion has been highly selective. This is related to a need for internal consistency of the observations, our estimation of the accuracy of the measurements and a treatment of the data that is in the context of the current development. The present status should be regarded as useful if not definitive. In order to meet current objectives in atmospheric remote sensing and related phenomena, more observations of high accuracy both in the laboratory and in the atmosphere are required, and significant advances in the theoretical treatment of the effects of collision on molecular line shape need to be achieved. A floppy disk containing a program to calculate continuum absorption coefficients as described here and consistent with FASCOD2 and LOWTRAN7 is available from the authors.

ACKNOWLEDGEMENTS

One of us, S.A.C., would like to acknowledge the invaluable support received while at AFGL during which time most of the work was performed. In particular we wish to recognize the contribution of James Chetwynd for the extensive

calculations leading to the current results. We would also like to thank our many colleagues, experimentalists and theoreticians, for the discussions that have clarified our understanding of a very difficult problem. The discussion and experimental results due to Darrel Burch have been invaluable in reaching the present state of understanding. To our other colleagues not mentioned here, we hope to do greater justice in a more extensive paper in preparation.

REFERENCES

Burch, D.E., 1981. Continuum Absorption by H_2O. AFGL-TR-81-0300.

Burch, D.E., 1985. Absorption by H_2O in Narrow Windows Between 3000-4200 cm^{-1}. AFGL-TR-85-0036.

Burch, D.E. and Alt, R.L., 1984. Continuum Absorption in the 700-1200 cm^{-1} and 2400-2800 cm^{-1} Windows. AFGL-TR-84-0128.

Clough, S.A., Kneizys, F.X., Davies, R.W., Gamache, R. and Tipping, R.H., 1980. Theoretical line shape for H_2O vapor: application to the continuum. In: A. Deepak, T.D. Wilkerson and L.H. Ruhnke (Editors), Atmospheric Water Vapor. Academic Press, London, pp. 25-46.

Clough, S.A., Davies, R.W. and Tipping, R.H., 1983. The line shape for collisionally broadened molecular transitions: a quantum theory satisfying the fluctuation dissipation theorem. Proc. 6th Conf. Spectral Line Shapes. Walter de Gruyter, New York, N.Y., pp. 553-568.

Clough, S.A., Kneizys, F.X., Shettle, E.P. and Anderson, G.P., 1986. Atmospheric radiance and transmittance: FASCOD2. Proc. 6th Conf. Atmospheric Radiance. AMS, Williamsburg, VA, pp. 141-144.

Kneizys, F.X., Gruenzel, R.R., Martin, W.C., Schuwerk, M.J., Gallery, W.O., Clough, S.A., Chetwynd, J.H. and Shettle, E.P., 1984. Comparison of 8 to 12 Micrometer and 3 to 5 Micrometer CVF Transmissometer Data with LOWTRAN Calculations. AFGL-TR-84-0171.

Kneizys, F.X., Shettle, E.P., Abrev, L.W., Chetwynd, J.H., Anderson, G.P., Gallery, W.O., Selby, J.E.A. and Clough, S.A., 1988. User's Guide to LOWTRAN7, AFGL-TR-88-0177.

Oppenheim, U.P. and Lipson, S.G., 1986. Private Communication. See also A. Ben-Shalom, A.D. Devir, S.G. Lipson, U.P. Oppenheim and E. Ribak, 1985. Absorption of IR radiation by atmospheric water vapor in the regions 4.3-5.5 micron and 8-13 micron. Proc. Topical Meeting on Remote Sensing of the Atmosphere, OSA.

Roberts, R.E., Selby, J.E.A. and Biberman, L.M., 1976. Infrared continuum absorption by atmospheric water vapor in the 8-12 μm window. Appl. Opt., 15: 2085.

Rosenkranz, P.W., 1985. Pressure broadening in rotational bands, I. A statistical theory. J. Chem. Phys., 83: 6139.

Rosenkranz, P.W., 1987. Pressure broadening in rotational bands, II. Water vapor from 300 to 1100 cm^{-1}. J. Chem. Phys., 87: 163.

Suck, S.H., Kassner, J.L., Jr. and Yamagushi, Y., 1979. Water cluster interpretation of IR absorption spectra in the 8-14 μm wavelength region. Appl. Opt., 18: 2609.

Van Vleck, J.H. and Huber, D.L., 1977. Absorption, emission and linebreadths: a semihistorical perspective. Rev. Mod. Phys., 49: 939.

WATER VAPOR CONTINUUM ABSORPTION MEASUREMENTS WITH A LINE SHAPE INTERPRETATION

M.E. Thomas, C.T. Delaye
Applied Physics Laboratory, The Johns Hopkins University, Laurel, Maryland 20723

A review of water vapor continuum experimental data is presented as a function of frequency, partial pressures, and temperature for atmospheric windows from the millimeter wave to 1 μm. The millimeter wave and 10 μm regions are the most extensively characterized. The behavior of the continuum can be represented in the form of simple well behaved functions, yet a physical interpretation has been elusive. For the millimeter wave window, the continuum frequency dependence is frequency squared. For infrared windows, the continuum frequency dependence is exponential always decreasing away from strongly absorbing bands for both self and foreign broadening. These observations have lead to line shape interpretations of the water vapor continuum.

A particular line shape of interest has been developed by G. Birnbaum in the late 1970's. It has a closed form solution, has a continuous representation from line center to the far wing and thus is normalizable, has an exponential far wing and is consistent with many line shapes at line center. In short, it is a versatile and practical line shape. Line-by-line calculations based on this line shape are compared to the experimental data base with interesting results. The agreement with experimental data is best when the continuum is at a minimum, but deviates below observation towards the bordering absorption band. However, this formalism does not include line mixing (or coupling) and this is certainly important. Far wings must play some role in continuum absorption, but a definitive model will require a complete theory.

WATER VAPOR CONTINUUM ABSORPTION MEASUREMENTS WITH LINE SHAPE INTERPRETATIONS

Michael E. Thomas and Corinne T. Delaye

The Johns Hopkins University
Applied Physics Laboratory
Laurel, Maryland 20723

Absorption by molecules defines the atmospheric windows and is an important mechanism of tropospheric attenuation at millimeter and infrared wavelengths, especially in the marine environment. Therefore, the understanding and accurate modeling of absorption by atmospheric molecules are important to atmospheric remote sensing, infrared imaging systems, long-path laser propagation, electro-optical systems, radar, and atmospheric meteorology. Figure 1a shows low-resolution infrared transmittance of the atmosphere and demonstrates the importance of water vapor over other atmospheric constituents[1]. The H_2O absorption bands, along with those of CO_2, define the atmospheric window regions in the infrared. At millimeter and microwave wavelengths, O_2 and H_2O determine the window regions.

The main rotational and vibrational bands have been extensively characterized by many investigators[2,3,4]. This work has resulted in a compendium of absorption-line parameters, maintained by the Air Force Geophysics Laboratory [5,6] (AFGL), which represents a significant contribution to absorption calculations. The database also contains parameters for weak absorptions lines in the window regions. However, this information is, in general, not as accurate as that of the main bands.

The comparatively weak absorption that does occur in the window regions can be described as arising from two distinct sources, local line and continuum absorption, as illustrated in the high-resolution computed spectrum of Fig. 1b for the 10 μm window region. Weak absorption bands of CO_2 and HDO, along with other H_2O absorption lines in the window regions, compose the local line contribution. The continuum contributes an additional, gradually varying, frequency-dependent background to the total absorption. A general empirical form for the continuum absorption coefficient used to represent the data[5] is

$$\beta_{cont}(\nu,T,P_{f1}\ldots P_{fi},P_s) = \frac{P_s}{RT}\sum_i\left[C_{Fi}(\nu,T)P_{fi}+C_s(\nu,T)P_s\right] \qquad (1)$$

where C_s is the self-broadening coefficient of the absorbing gas, C_{Fi} is the foreign broadening coefficient due to the i^{th} type foreign gas, and R is the ideal-gas constant. The equation can be conveniently rewritten for $i = 2$ to obtain

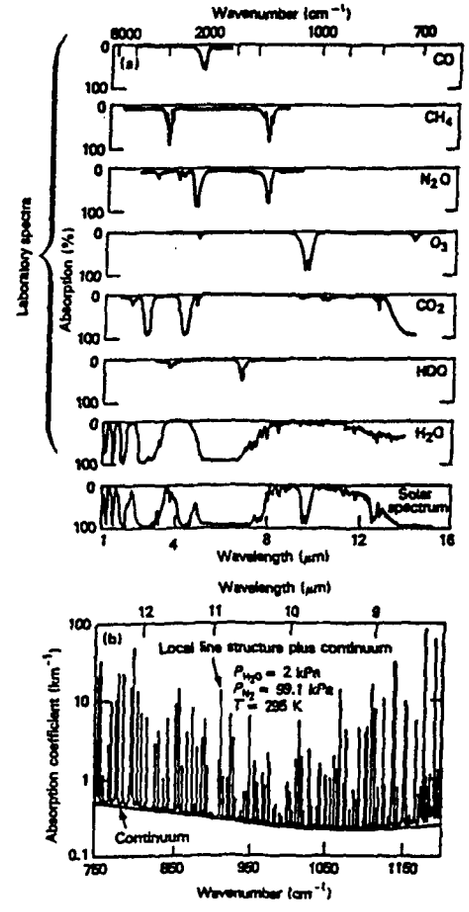


Figure 1. (a) Low-resolution solar spectrum compared with laboratory spectra of atmospheric gases. (b) Local line structure plus continuum in the 10-μm region.

$$\beta_{cont}(\nu,T) = \frac{C_{f1}(\nu,T)}{M} P_a [P_{f1} + F(\nu,T) P_{f2} + B(\nu,T) P_a] \qquad (2)$$

where $F = C_{f2}/C_{f1}$ and $B = C_a/C_{f1}$ are the dimensionless broadening coefficients. Near line center, B has the value of 5 for water vapor relative to nitrogen. In the real atmosphere, the effects of oxygen broadening must also be included. The dimensionless broadening coefficient ξ accounts for oxygen. However, many laboratory experiments ignore the effects of oxygen and use only nitrogen as the broadening gas along with the absorbing gas.

Water vapor absorption

As previously mentioned, molecular absorption in the window regions manifests itself as local line and continuum type absorption. Narrow band systems can avoid local line effects but not continuum absorption. Broad band systems must account for both.

Local lines

Local line structure of the 10- and 4 μm water vapor window regions has been experimentally characterized by *Thomas*[39], and Long and Damon[6b]. The 1 to 1.1 μm local line structure based on experimental data has been reported by Gallery et. al.[6c]. The data demonstrate the importance of local line structure in the case of water vapor. The HITRAN database also represents local line structure based on experimental data and/or theoretical calculations.

Continuum

In 1942, Elsasser[7] recognized a continuum in the 13- to 8- μm window region, which he attributed to the far wings of the strong, nearby rotational and ν_2 vibrational rotational bands of H_2O. Further verification of this nonlocal line absorption feature was provided by Yates and Taylor[8], who studied infra-red attenuation along horizontal paths at sea level. Solar spectra studies also indicated continuum absorption in the 13- to 8- μm window[9-11]. The nature of the continuum, judged by those measurements, was uncertain. It could be due to far wings (far from the band center) of strong absorption bands or to scattering and absorption by particulates.

In an effort to determine the cause of continuum absorption in the 13- to 8 μm window, Bignell[12], in 1963 examined solar spectra while monitoring the atmosphere for aerosol concentrations and studying CO_2 far-wing contributions. He concluded that the amount of continuum absorption observed could not be explained by aerosol attenuation or far-wing absorption by CO_2. An attempt was then made to model the continuum by far wings of the bordering H_2O bands. The important contribution from this initial work was the realization of major water vapor contributions to the continuum. A second paper by Bignell[13] in 1970 described a careful examination of water vapor absorption in the window regions by use of a multiple-traversal absorption cell and grating spectrometer. Two important characteristics of the 13- to 8 μm window were noted: (a) a large ratio of water vapor self-to-foreign-gas broadening ability (see Eq. 2) and (b) a strong negative temperature dependence. Neither of these findings was anticipated

on the basis of the far-wing approaches of Bignell's 1963 paper[12]. Also reported by Bignell[13] was a similar, but much weaker, continuum absorption in the 4 μm region. (The 4 μm region also features a collision-induced absorption band of nitrogen[14,15]. The band is of comparable strength to the water vapor continuum in the earth's atmosphere. It is a smooth absorption band showing no structure; thus, it is often referred to as the nitrogen continuum. Also, a far-wing continuum of CO_2 beyond the ν_3 band head is observed between 4.1 and 4.0 μm[16].)

Since those initial experimental efforts to characterize water vapor continuum absorption, many measurements have been made. They fall into three categories: (a) measurements within the earth's atmosphere or field measurements, (b) laboratory measurements using a long-path cell and a spectrometer, and (c) laboratory measurements using a long-path cell or a photoacoustic cell and a laser. Although continuum absorption was first observed through long-path field measurements, its precise characterization requires control and knowledge of the propagation path. The effects of turbulence, particulate scattering, temperature variations, and partial-pressure variations are difficult to determine in a field measurement. Thus, laboratory measurements are needed to characterize the pressure and temperature dependence of each atmospheric constituent. Spectrometer measurements determine the frequency dependence of the window regions, i.e., local lines and continuum absorption. Laser measurements are limited to discrete frequencies, but because of the laser's higher power and stability, greater accuracy can be obtained; this is particularly true for photoacoustic techniques. Laboratory transmission measurements require very long path lengths ($\approx$1 km or longer) and thus are difficult to obtain. The photoacoustic cell, on the other hand, is compact (about 30 cm) but still maintains considerable sensitivity. Of course, field measurements will have the final say in the validation of atmospheric propagation computer codes.

As a result of these experiments, a good characterization of the commonly used window regions exists today. An excellent review of the field is given by the recent work of Hinderling et al.[17]. They emphasize the 8- to 14- μm window region, which, along with the millimeter-wave window, is the most extensively measured. A review of the current experimental data for all the window regions is given in the next section, followed by a brief review of the theoretical and empirical models used to explain the experimental data.

Millimeter-wave window

Figure 1.3.10 [18-22] shows continuum absorption from 10 to 1000 GHz (total absorption minus local lines). The solid line represents an empirical formula given by Gaut and Reifenstein: [19]

$$\beta_{continuum} = (1.08\times10^{-6})\rho_s \left(\frac{300}{T}\right)^4 \left(\frac{P_T}{101}\right) f^2 \qquad (km^{-1}), \qquad (3)$$

where ρ_s is the water vapor density (g/m^3), P_T is the total pressure (kPa), and f is the frequency (GHz). The plotted points indicate experimental data. The formula correctly demonstrates the frequency dependence of the continuum but not

the temperature and pressure dependence. More recent work by Liebe[23] uses a continuum formula, fitted to experimental data at 138 GHz, of the form

$$\beta_{\text{continuum}} \sim (4.73\times10^{-8})\, f^2 \left(\frac{300}{T}\right)^3 P_a \left[P_f + 31.6 \left(\frac{300}{T}\right)^{7.5} P_a\right] \quad (\text{km}^{-1}), \tag{4}$$

where f is gigahertz, T is in kelvins, and P_a and P_f ($P_f = P_T - P_a$) are in kilopascals. A strong dependence on the water vapor partial pressure is shown ($B \gg 5$). The continuum calculated using Eq. 4 is smaller than that calculated using Eq. 3 because of improved local line modeling. On the basis of the work by Liebe and Layton[24], the parameter B grows as the frequency decreases from 833 to 110 GHz (see Table 1). This dependence is expected based on the far-wing model of Birnbaum[47] and leads to the following empirical model (for $f < 1000$ GHz and in units of km^{-1})[24a]

$$\beta_{\text{continuum}}(f) = (4.73\times10^{-8}) f^2 \theta^4 p_a [p_f + 40.9 e^{-0.0025 f} \theta^{8.5} p_a] \ , \tag{5}$$

where $\theta = (300/T)$ and the other variables have the same units as above.

Table 1. Experimental frequency dependence of B (ν,300)

f (GHz)	ν (cm^{-1})	B (ν, 300)
110	3.7	32
138	4.6	31.6
213	7.1	20
833	27.8	7.4

As Eq. 4 indicates, B is not only a function of frequency but a strong function of temperature as well. Although Liebe[23] chooses to represent his data in a power law form, a comprehensive study at 213 GHz by Llewellyn-Jones[23] shows the data fits an Arrhenius plot with the functional form

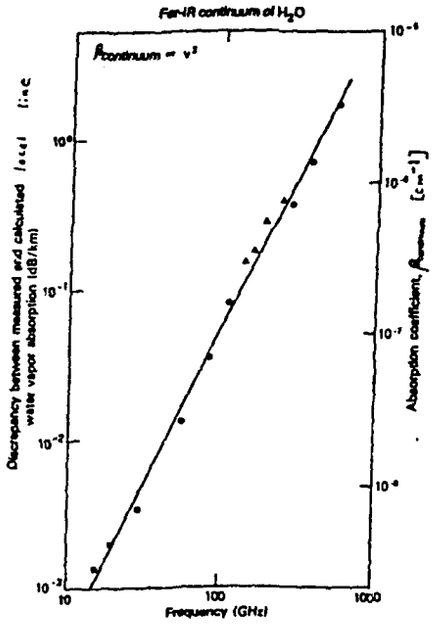


Figure 2. Water vapor continuum absorption coefficient as a function of frequency. The solid line is an empirical fit to the experimental data points as given by Eq. 1.3.92. The plotted points are (▲) [20], (•) [21], and (■) [22] for T = 300 K, P_T = 101 kPa and $\rho_a = 10^{-3}$ kg/m^3.

$$C_a(\nu, T) \propto e^{b/T}, \tag{6}$$

$b = 5 \times 10^4$ K. Again, a strong negative temperature dependence is observed at this frequency as well. Figure 3 illustrates the experimental results of Llewellyn-Jones[25].

In summary, the millimeter-wave water vapor continuum falls off as frequency squared, has an enhanced self-broadening contribution that grows with decreasing frequency, and has a strong negative temperature dependence.

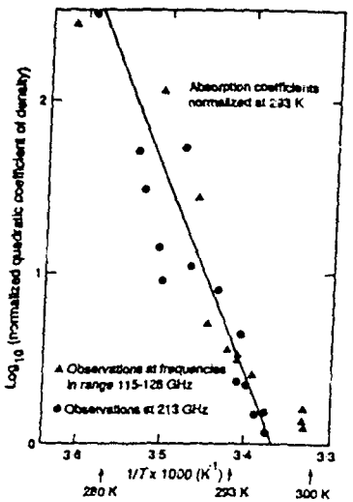


Figure 3. Temperature dependence of millimeter wave water vapor continuum. Solid curve represents empirical fit to data as given by Eq. 6.

The 8- to 12-μm window

Figure 1.4[27] shows the self-broadening water vapor continuum coefficient, C_s, as a function of frequency between 9 and 14 μm at 296 K. The coefficient decreases exponentially as the frequency increases. The same functional dependence is exhibited by C_N, the nitrogen-broadening coefficient, as shown in Fig. 5[27], but the rate of decrease is more rapid. Thus, $B(=C_S/C_N)$ increases as the frequency increases away from the rotational band. Long-path White cell and -photoacoustic laser measurements indicate that B can be quite large. Values ranging from 100 to 600 have been measured in the 10-μm region with CO_2 lasers.[15,28,29] Figure 6 illustrates a laser measurement at 940.548 cm^{-1} as a function of the water vapor partial pressure. The total pressure is maintained at 101 kPa (1 atm) with nitrogen.

The observed temperature dependence at 10.6 μm features a rapid decrease with increasing temperature (Fig. 7), just as in the millimeter window region.[30-33] The temperature dependence has the following functional form over a wide temperature range:

$$C_s(\nu,T) = C_S(\nu,T_0)e^{b(1/T - 1/T_0)}, \qquad (7)$$

where $C_s(940\ cm^{-1},296\ K) = 1.83 \times 10^{-22}$ cm^{-2}/molecule·atm and $b = 1680$ k. This result at 10 μm is also consistent with other measurements in the 10-μm region and at 14.3 μm[15,27].

Based on the data presented and Birnbaum's line shape formula, a simple formula for the nitrogen broadened water vapor continuum absorption coefficient from 700 to 1100 cm^{-1} and for typical atmospheric temperatures is given by [33a]

$$\beta_{continuum} = 6.41\times10^{5}\exp(-0.00839\nu) \times((T_0/T)^3 p_{N2} + 16.96\exp(0.00374\nu + 1680(1/T - 1/T_0)p_{H2O}p_{H2O}/T \quad [km^{-1}] \qquad (8)$$

where p is atmospheres, ν is wave numbers and $T_0 = 296$ K.

An excellent review of experimental measurements in the 10-μm region by Grant[34] makes the following additional points:

1. Oxygen does not broaden as effectively as nitrogen and must be included in a realistic model of the earth's atmosphere. A broadening coefficient of F 0.75 ± 0.1 for oxygen relative to nitrogen was measured by Nordstrom et al.[35] Using Eq. 3, this means air has an effective broadening of 0.95.
2. Understanding the local line structure is critical in determining the true continuum. Line positions are known reasonably well; however, line strength and half-width are not known with enough accuracy.

Long-path field measurements by Devir et al.[36] are in excellent agreement with the laboratory measurements of Burch and Alt[27] and Peterson et al.[28] in this window region concerning the water vapor continuum. The measured spectral range of Devir extends the range covered by Burch and Alt[27] and shows the water vapor continuum increasing with increasing frequency. The minimum occurs at 9.0 μm (1111 cm^{-1}). The nature of 8-12 μm continuum absorption appears to be understood on the basis of the agreement between laboratory and field measurements.

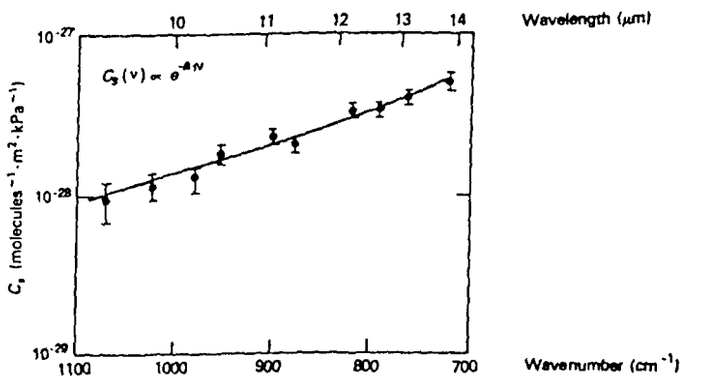


Figure 4. Self-broadening coefficient as a function of wave number from 700 to 1100 cm^{-1} at 296 K.

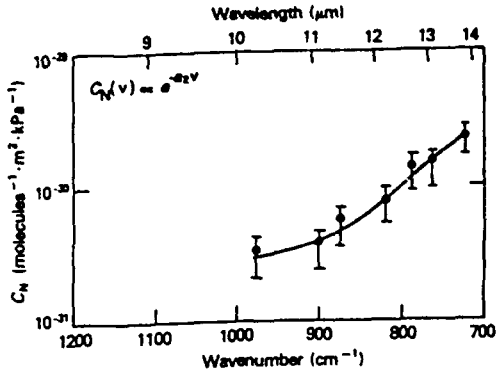


Figure 5. Nitrogen broadening coefficient as a function of wave number from 700 to 1000 cm^{-1} at 296 K.

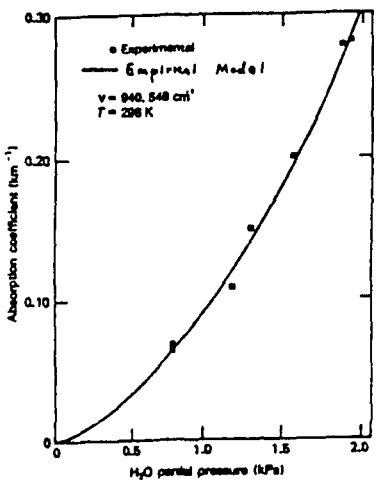


Figure 6. Water vapor partial pressure dependence in the 10 μm region.

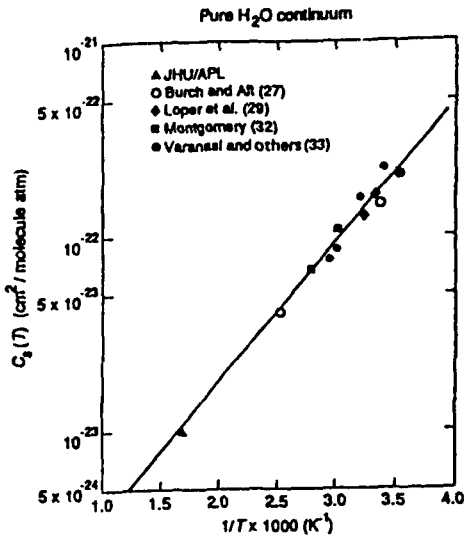


Figure 7. Temperature dependence of self-broadening coefficient in the 10 μm region.

The 3- to 5-μm window

The 3- to 5-μm continuum region has a different frequency dependence compared with the millimeter and 8- to 12-μm regions. Figure 1.3.16b displays a nearly parabolic dependence with a minimum at a wavenumber of 2600 cm^{-1}.[27,37,38] As shown by the spectrometer measurements of Burch and Alt[27] (Fig. 8a), the self-broadening coefficient has an exponential falloff at wavenumbers up to 2550 cm^{-1}, then the falloff rate decreases as the frequency increases. Figure 8b shows long-path White cell DF laser measurements[37] taken under atmospheric conditions, which indicate continuum absorption levels roughly 50% higher than those indicated by Burch and Alt[27]. The level of absorption in the 4-μm region is roughly an order of magnitude less than that in the 10-μm region. Long-path CO, DF, and HF laser measurements near room temperature again indicate large values for B in the continuum region, ranging from 10 to 20 at 5 μm[39] to approximately 50 to 60 at 4 μm[37] and back down to 10 at 3 μm[40].

A strong negative temperature dependence is again observed for the self-broadening coefficient. Figure 9 shows the results of laboratory long-path spectrometer measurements by Burch and Alt[27]. The temperature dependence at 2400 cm^{-1} exhibits exponential falloff similar to that in the 10-μm and millimeter regions. However, the curves at 2500 and 2600 cm^{-1} show double exponential trends. The nature of the water vapor continuum in this window region is more complicated than the other windows previously discussed.

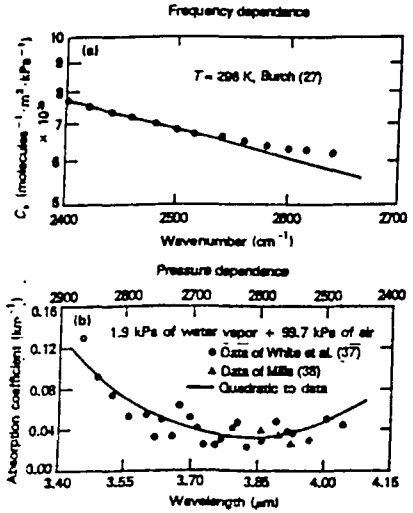


Figure 8. 4 μm water vapor continuum region at T= 296K. (a) C_s vs wave number [27] and (b) absorption coefficient vs wavelength [37,38].

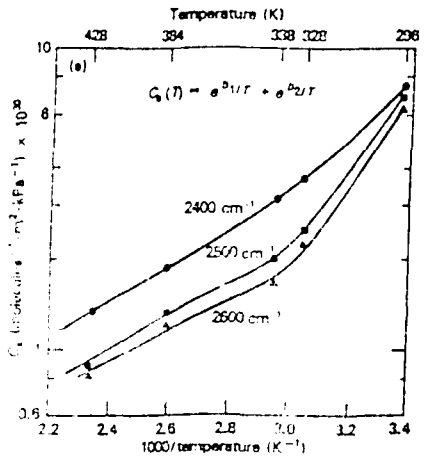


Figure 9. Plots of the water vapor self-broadening coefficients at 2400, 2500 and 2600 cm^{-1} vs reciprocal temperature [27]. The symbols •, ■ and ▲ represent the experimental data points.

More experimental data is needed to generate a meaningful empirical model of the continuum absorption coefficient. An attempt at representing the existing data is given by the following formula for the nitrogen broadened water vapor continuum absorption coefficient valid from 2400 to 2800 cm^{-1} [33a],

$$\beta_{continuum} = 7.34\times10^{26}(p_{H2O}/T)\{C_s(\nu,T)p_{H2O} + C_N(\nu,T)p_{N2}\} \quad [km^{-1}] \qquad (9)$$

where

$$C_s(\nu,T) = 1.77\times10^{-20}\exp(-3.32\times10^{-3}\nu)\exp(1234(1/T - 1/T_0)) + 3.91\times10^{-28}\exp(3.46\times10^{-3}\nu)\exp(2626(1/T - 1/T_0))$$

and

$$C_N(\nu,T) = (296/T)^3\{7.16\times10^{-19}\exp(-6.45\times10^{-3}\nu) + 2.73\times10^{-33}\exp(6.45\times10^{-3}\nu)\}.$$

Again, long-path field measurements by Devir et al.[36] are in good agreement with Burch and Alt[27] in this window region concerning the water vapor continuum. The results of Devir et al.[36] also point out the importance of the water vapor continuum between 4.5 and 5.0 μm. In this region, local line contributions can be significant as well, thus masking to some extent water vapor continuum absorption. CO laser transmission measurements as a function of water vapor partial pressure show an increase in the dimensionless self-broadening coefficient, B, over the near line center value[39]. As observed in the previous window regions, this observation is indicative of continuum absorption.

Field measurements between 4.1 and 3.8 μm reveal that other continuum sources exist. The far blue wing beyond the band head of the fundamental ν_3 band of CO_2[41] and the collision-induced absorption band of nitrogen[36] also contribute to continuum-type absorption in this window region and will be discussed later.

The 2.0- to 2.5-μm window

This window region has not received the same attention as the longer-wavelength windows; as a result, no experimental continuum absorption has been previously reported. Recent measurements[41a], however, indirectly suggest that continuum absorption does exist. Transmission measurements on hot (T = 685 K) high-pressure (up to 4.8 MPa) water vapor show the continuum absorption in the 2.1- and 4-μm regions (Fig. 10). Absorption levels at 4 μm are consistent with the extrapolated values from the curves in Fig. 9. The point to be made is that a similar continuum absorption process occurs in the 2.1-μm region, as shown in Fig. 10. If we assume that an extrapolation to lower temperature follows the same trend as at 4 μm, then a continuum exists in the 2.0- to 2.5-μm window that is very similar to the 3- to 5-μm window under normal atmospheric conditions.

1.7 to 1.5 μm window and beyond

Figure 10 shows the beginning of the continuum centered at 1.6 μm. Again, this suggests a water vapor continuum in this window region at a weaker level than at 4 and 2 μm. Based on this observation, it is expected that every window in the infrared has a water vapor continuum at some absorption level. This level should become weaker as the frequency increases.

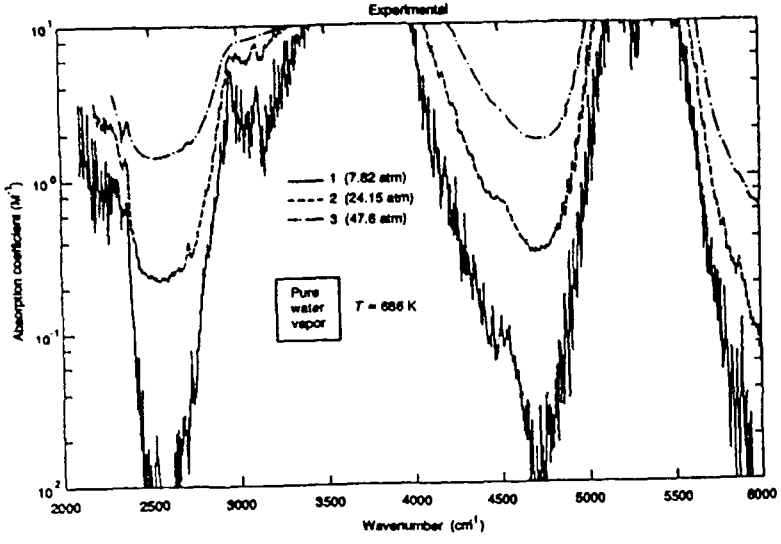


Figure 10. Pure water vapor absorption coefficient at T = 685 K and three different pressures.

The 1 μm window water vapor continuum has been measured by a novel interferometric calorimeter technique[41b]. A pulsed Nd-glass laser is used to heat a nitrogen buffered water vapor sample placed in the arm of He-Ne Mach-Zehnder interferometer. Variations in the index of refraction due to the heating cause measurable fringe shifts proportional to the absorption coefficient. The resulting continuum absorption coefficient measured at 9466 cm^{-1} is $6x10^{-10}$ cm^{-1} for a water vapor partial pressure of 16.5 Torr buffered by nitrogen to a total pressure of 1 atmosphere at 30°C. Thus, the water vapor continuum is roughly two orders of magnitude weaker near 1 μm than at 4 or 2 μm. Further measurements to determine the water vapor partial pressure dependence and temperature dependence are needed.

The tragedy of experimental water vapor continuum characterization is that unlike CO_2[41] and nitrogen[42-46] continuum experiments, it presently cannot be done at high pressure. High-pressure water vapor measurements also require high-temperature and thus a theoretical understanding of the continuum absorption temperature dependence to extrapolate back to atmospheric temperatures.

Concepts and models

No universal interpretation of continuum absorption by water vapor presently exists. Clearly, far wings must play a role in continuum absorption because of the observed frequency dependence observed in every window and this belief has lead to various semi-empirical attempts[47,49,53-55]. Work is continuing to find a line-shape theory valid in the far wing[47-50a]. The major shortcoming

of past line-shape theories is in their failure to predict the observed strong negative temperature dependence characteristic of all the window regions, except for the recent line shape model of Ma and Tipping at the millimeter wave window[50a]. But this weakness is the very strength of an alternative hypothesis to explain the water vapor continuum: the water dimer. The formation of water vapor dimers has a strong negative -temperature dependence that closely matches the temperature dependence of the continuum absorption in the 10-μm region[33,51]. However, this near match does not occur in the microwave window or in the 4-μm window. This approach also requires dimer absorption bands to account for the continuum. However, the hypothesis would require a dimer absorption band in every water vapor window, a condition that has not been experimentally found or theoretically shown[16,52]. Furthermore, measurements on supersaturated water vapor indicate that dimer absorption is an order of magnitude too small to account for the water vapor continuum at 10 μm[16]. In spite of these shortcomings, the dimer hypothesis demonstrates the importance of understanding water-vapor water-vapor interaction to explain the continuum absorption temperature dependence[16].

A semi-empirical line shape model developed by Birnbaum[47] with validity from line center to the far wing (when line mixing can be ignored) predicts an exponential wing as observed experimentally and can be properly normalized. This model has been successfully applied to the CO_2 blue wing of the 4.3 μm band[47]. Application of this line shape to line-by-line calculations indicate that this model is not complete enough to represent the water vapor continuum in near band regions (probably because it lacks line mixing effects). However, the simple models given in the text for the water vapor continuum broadened by nitrogen are based on this formalism.

The continuum models for the popular Air Force Geophysics Laboratory codes FASCODE and LOWTRAN are based on the efforts of Clough et al.[49], who used far-wing concepts to represent the water vapor continuum throughout the entire infrared region. The experimental data previously described are reasonably represented by these codes. The strength of this approach is accounting for spontaneous emission and the fluctuation dissapation theorem in enforcing detailed balance across the entire line shape. This results in a physically meaningful far wing and a more versatile line shape overall.

Although no definitive interpretation of the water vapor continuum exists, the experimental and theoretical evidence indicates that far-wing absorption contributions by the bordering strong water vapor bands play a dominant role. The evidence is based largely on the frequency dependence of the continuum in the first four spectral windows reviewed (i.e., the shape of the continuum as a function of frequency and growth of the dimensionless broadening coefficient, B, away from a band as a function of frequency). The shortcoming of the far-wing approach is predicting the temperature dependence, but the character of a far wing must be driven by close binary interactions much like the creation of a dimer, which does exhibit the observed temperature dependence in the 10-μm window region. This point has been verified by the recent work of Ma and Tipping[50a].

REFERENCES

1. J. H. Shaw, Ohio J. Sci. 53, 258 (1953).
2. W. S. Benedict and R. F. Calfee, Line Parameters for the 1.9 and 6.3 Micron Water Vapor Bands, ESSA Professional Paper 2, U.S. Government Printing Office, Washington, D.C. (Jun 1967).

3. D. M. Gates, R. F. Calfee, D. W. Hansen, and W. S. Benedict, "Line Parameters and Computed Spectra for Water Vapor Bands at 2.7 μm," National Bureau of Standards Monograph 71, U.S. Government Printing Office, Washington, D.C. (1964).

4. C. Camy-Peyret and J. M. Flaud, "Line positions and intensities in the band of H2O," Mol. Phys. 32, 523 (1976).

5. R. A. McClatchey, W. S. Benedict, S. A. Clough, D. E. Burch, R. F. Calfee, K. Fox, L. S. Rothman, and J. S. Garing, AFCRL Atmospheric Absorption Line Parameters Compilation, AFCRL-TR-73-0096, Air Force Cambridge Research Laboratories, Bedford, Mass. (Jan 1973).

6. L. S. Rothman, "AFGL atmospheric absorption line parameters compilation: 1980 version," Appl. Opt. 20, 791 (1981).

6b. R. K. Long and K. K. Damon, " An Atlas of Pure Water Vapor Spectra from 500 to 5000 cm^{-1} Vol. I and II," Ohio State University/Electroscience Laboratory, Report No. 713774-3 (Sept. 1984).

6e. W. O. Gallery, J. L. Manning, D. R. Longtin and L. S. Rothman, "Revised Water Vapor Line Parameters in the 1.8 to 1.1 micrometer Region," Propagation Engineering: Third in a Series, SPIE 1312, (1990).

7. W. M. Elsasser, Heat Transfer by Infrared Radiation in the Atmosphere, Harvard University Press, Cambridge, Mass. (1942).

8. R. M. Yates and J. S. Taylor, Infrared Transmission of the Atmosphere, NRL Report 5453 (1960).

9. A. Adel, Astrophys. J. 89, 1 (1939).

10. R. Anthony, "Atmospheric absorption of solar infrared radiation," Phys. Rev. 85, 874 (1952).

11. W. T. Roach and R. W. Goody, Q. J. R. Meteorol. Soc. 84, 319 (1958).

12. K. Bignell, F. Saiedy, and P. A. Sheppard, "On the atmospheric infrared continuum," J. Opt. Soc. Am. 53, 466 (1963).

13. K. Bignell, Q. J. R. Meteorol. Soc. 96, 390 (1970).

14. M. F. Crawford, H. L. Welsh, and J. L. Locke, "Infrared absorption of oxygen and nitrogen induced by intermolecular forces," Phys. Rev. 75, 1607 (1949).

15. J. Bonshkind and J. E. Searl, "Atmospheric absorption near 2400 cm1," J. Quant. Spectrosc. Radiat. Transfer 18, 381 (1977).

16. D. H. Winters, S. Silverman, and W. S. Benedict, J. Quant. Spec. Rad. Trans. 4, 527 (1964).

17. J. Hinderling, M. W. Sigrist, and F. K. Kneubuhl, "Laser photoacoustic spectroscopy of water-vapor continuum and line-absorption in the 8- to 14-μm atmospheric window," Infrared Phys. 27, 63 (1987).

18. J. W. Waters, Methods of Experimental Physics, Volume 12 Part B Astrophysics Radio Telescopes, M. L. Meeks, ed., Academic Press, New York (1976).

19. E. E. Gast and E. C. Reifenstein III, Environmental Research and Technical Report, No. 13, Lexington, Mass. (1971).

20. G. E. Becker and S. H. Autler, "Water vapor absorption of electromagnetic radiation in the centimeter wavelength range," Phys. Rev. 70, 300 (1946).

21. L. Frankel and D. Woods, "The microwave absorption by H2O vapor and its mixtures with other gases between 100 and 300 Gcps," Proc. IEEE 54, 488 (1966).

22. D. E. Burch, "Absorption of infrared radiant energy by CO2 and H2O. III. Absorption by H2O between 0.5 and 38 cm^{-1} (27μp-2 cm)," J. Opt. Soc. Am. 58, 1383 (1968).

23. H. J. Liebe, "A contribution to modeling atmospheric millimeter-wave properties," FREQUENZ 41, 31 (1987).

24. H. J. Liebe and D. H. Layton, "Experimental and analytical aspects of atmospheric EHF refractivity," in Proc. URSI Commission F 1983 Symposium, Louvain, Belgium (Jun 1983).

24a. M. E. Thomas, "Atmospheric absorption model from 0.01 to 10 wave numbers," SPIE Proceedings, 1312, (April 1990).

25. D. T. Llewellyn-Jones, "Laboratory measurements of absorption by water vapour in the frequency range 100 to 1000 GHz," in Atmospheric Water Vapor, A. Deepak, T. D. Wilkerson, and L. H. Ruhnke, Eds., Academic Press, New York, p. 255 (1980).

26. H. J. Liebe, "An updated model for millimeter wave propagation in moist air," Radio Sci. 20, 1069 (1985).

27. D. E. Burch and R. L. Alt, Continuum Absorption by H2O in the 700-1200 cm^{-1} and 2400-2800 cm^{-1} Windows, AFGL-TR84-0128, Ford Aerospace and Communications Corporation, Aeronutronic Division (May 1984).

28. J. C. Peterson, M. " Thomas, R. J. Bordstrom, E. K. Damon, and R. K. Long, "Water vapor nitrogen absorption at CO2 laser frequencies," Appl. Opt. 18, 834 (1979).

29. G. L. Loper, M. A. O'Neill, and J. A. Golbrecht, "Water-vapor continuum CO2 laser absorption spectra between 27 cf,411,°C and 10cf,411,°C," Appl. Opt. 22, 3701 (1983).

30. J. C. Peterson, A Study of Water Vapor Absorption at CO2 Laser Frequencies Using a Differential Spectrophone and White Cell Dissertation, The Ohio State University (Jun 1978).

31. V. M. Aref'ev and V. I. Dianov-Klokov, "Attenuation of 10.6-μm radiation by water vapor and the role of (H2O)2 dimers," Opt. Spectrosc. 42, 488 (1977).

32. G. P. Montgomery, Jr., "Temperature dependence of infrared absorption by the water vapor continuum near 1200 cm1," Appl. Opt. 17, 2290 (1978).

33. P. S. Varanasi, S. Chou, and S. S. Penner, J. Quant. Spectrosc. Radiat. Transfer 8, 1537 (1968), and P. Varanasi and S. Chudamani, "Self- and N2-broadened spectra of water vapor between 7.5 and 14.5 μm," J. Quant. Spectrosc. Radiat. Transfer 30, 487 (1987).

33a. C. T. Deleye and M. E. Thomas, "Atmospheric continuum absorption models," SPIE Proceedings, 1487 (1991).

34. M. V. Grant, A Critical Review of Measurements of Water Vapor Absorption in the 840 to 1180 cm^{-1} Spectral Region, JPL Publication 87-34, Jet Propulsion Laboratory (Dec 1987).

35. H. J. Bordstrom, M. E. Thomas, J. C. Peterson, E. K. Damon, and R. K. Long, "Effects of oxygen addition on pressure-broadened water vapor absorption in the 10-μm region," Appl. Opt. 17, 2724 (1978).

36. A. D. Devir, A. Ben-Shalom, E. Truthovsky, E. Ras, M. Engel, S. G. Lipson, and U. P. Oppenheim, "Experimental validation of atmospheric transmittance codes," Proc. SPIE, Optical, Infrared, and Millimeter-Wave Propagation Engineering 926 (W. B. Miller and B. B. Lopoths, Eds.), 54 (1988).

37. K. O. White, W. H. Watkins, C. W. Bruce, R. E. Meredith, and F. G. Smith, "Water vapor continuum absorption in the 3.54.0 μm region," Appl. Opt. 17, 2711 (1978).

38. F. S. Mills, Absorption of Deuterium Fluoride Laser Radiation by the Atmosphere, Dissertation, The Ohio State University (Aug 1975).

39. M. E. Thomas, Tropospheric Water Vapor Absorption in the Infrared Window Regions, Dissertation, The Ohio State University (Aug 1978).

40. W. H. Watkins, R. L. Spolliey, K. O. White, B. Z. Sojka, and L. B. Bower, "Water vapor absorption coefficients at HF laser wavelength (2.64 & 2.93 μm)," Appl. Opt. 18, 1362 (1979).

41. T. G. Kyle, D. G. Murcray, F. H. Murcray, and W. J. Williams, "Absorption of solar radiation by atmospheric carbon dioxide," J. Opt. Soc. Am. 55, 1421 (1965).

41a. M. E. Thomas, "Infrared and Millimeter-Wavelength Absorption in the Atmospheric Windows by Water Vapor and Nitrogen: Measurements and Models," Infrared Physics, 30, 181 (1990).

41b. S. F. Fulghum and M. M. Tilleman, "An Interferometric Calorimeter for the Measurement of Water Vapor Absorption," (1991).

42. J. Van Kranendonk "Induced infrared absorption in gases: calculation of the binary absorption coefficients of symmetrical diatomic molecules," Physica 24, 347 (1958).

43. D. T. Cheng and G. E. Ewing, "Collision-induced infrared absorption of gaseous nitrogen at low temperatures," J. Chem. Phys. 55, 5425 (1971).

44. S. P. Reddy and C. W. Cho, "Induced infrared absorption of nitrogen and nitrogen-foreign gas mixtures," Can. J. Phys. 43, 2331 (1965).

45. M. M. Shapiro and H. P. Gush, "The collision-induced fundamental and first overtone bands of oxygen and nitrogen," Can. J. Phys. 44, 949 (1966).

46. N. I. Moskalenko, Yu. A. Ilin, S. B. Parshin, and L. V. Rodionov, "Pressure-induced IR radiation absorption in atmospheres," Izv. Atmos. Ocean Phys. 15, 632 (1979).

47. G. Birnbaum, "The shape of collision broadening lines from resonance to the far wings," J. Quant. Spectrosc. Radiat. Transfer 21, 597 (1979).

48. C. Boulet and D. Robert, "Short time behavior of the dipole autocorrelation function and molecular gases absorption spectrum," J. Chem. Phys. 77, 4288 (1982).

49. S. A. Clough, F. X. Kneizys, R. Davies, R. Gamache, and R. H. Tipping, "Theoretical line shape for H2O vapor; application to the continuum," in Atmospheric Water Vapor, A. Deepak, T. D. Wilkerson, and L. H. Ruhnke, Eds., Academic Press, New York, p. 25 (1980); and S. A. Clough, F. X. Kneizys and R. Davies, "Line shape and the water vapor continuum," Atmospheric Research, 23 229-241 (1989).

50. V. E. Zuev and V. V. Fomin, "Consideration of continuum absorption in the problems of sounding from outer space," Presentation at the Symposium on Remote Sensing of the Atmosphere from Space, Innsbruck, Austria (Jun 13, 1978).

50a. Q. Ma and R. H. Tipping, "Water Vapor continuum in the millimeter Spectral Region," J. Chem. Phys., 93, pp. 6127-6136 (1990) and "The Atmospheric Water Continuum in the Infrared: Extension of the Statistical Theory of Rosenkranz," J. Chem. Phys. 93, pp. 7060-7073 (1990).

51. S. S. Penner, J. Quant. Spectrosc. Radiat. Transfer 13, 383 (1973).

52. R. A. Bohlander, H. J. Emery, D. T. Llewellyn-Jones, G. G. Gimmestad, H. A. Gebbie, O. A. Stegman, J. J. Gallagher, and S. Perkowitz, "Excess absorption by water vapor and comparison with theoretical dimer absorption," in Atmospheric Water Vapor, A. Deepak, T. D. Wilkerson, and L. H. Ruhnke, Eds., Academic Press, New York, p. 241 (1980).

53. M. E. Thomas and R. J. Bordstrom, "The H2-broadened water vapor absorption line shape and infrared continuum absorption I. Theoretical development," J. Quant. Spectrosc. Radiat. Transfer 28, 81 (1982).

54. M. E. Thomas and R. J. Bordstrom, "The H2-broadened water vapor absorption line shape and infrared continuum absorption II. Implementation of the line shape," J. Quant. Spectrosc. Radiat. Transfer 28, 103 (1982).

55. M. E. Thomas and R. J. Bordstrom, "Line shape model for describing infrared absorption by water vapor," Appl. Opt. 24, 3528 (1985).

Prepared for: Annual Review Conference on Atmospheric Transmission Models
Topical Session on Spectral Line Shapes
June 12, 1991
Geophysics Directorate, Phillips Laboratory
Hanscom Air Force Base



WATER VAPOR CONTINUUM ABSORPTION MEASUREMENTS WITH LINE SHAPE INTERPRETATIONS

M. E. Thomas and C. T. Delaye
Applied Physics Laboratory
The Johns Hopkins University
Laurel, Maryland 20723

BIRNBAUM'S LINE SHAPE

IGNORING LINE MIXING, THE ABSORPTION COEFFICIENT IS:

$$\beta(\nu) = \sum_j S_j \frac{\nu}{\nu_j} \frac{\tanh \frac{hc\nu}{2k_BT}}{\tanh \frac{hc\nu_j}{2k_BT}} j(\nu,\nu_j)$$

WHERE S_j IS THE LINE STRENGTH OF THE J^{TH} LINE,

ν IS THE FREQUENCY IN WAVE NUMBERS.

$j(\nu, \nu_j)$ IS THE FOURIER TRANSFORM OF THE DEPENDENT AUTOCORRELATION FUNCTION $C(\tau)$:

$$j(\nu,\nu_j) = \frac{1}{N}\cdot\frac{1}{\pi}\int_0^\infty d\tau \cos 2\pi c\nu\tau \left(e^{j2\pi c\nu_j\tau} C(\tau) + e^{-j2\pi c\nu_j\tau} C^*(\tau)\right)$$

N IS THE NORMALIZATION FACTOR OF THE LINE PROFILE. AT INFRARED FREQUENCIES N = 1.

BIRNBAUM USES THE FOLLOWING SEMI-EMPIRICAL EXPRESSION FOR $C(\tau)$:

$$C_a(\tau) = \exp[\tau_{a2} - (\tau_{a2}^2 + \tau^2 - 2\tau_0\tau)^{1/2}]/\tau_{a1}$$

$$\text{and } C(\tau) = C_a(\tau) \cdot C_b(\tau) \ldots C_m(\tau)$$

WHERE THE SUBSCRIPTS DESIGNATE THE DIFFERENT MOLECULES IN THE SYSTEM.

τ_{A1} AND τ_{A2} REPRESENT THE LONG TIME AND SHORT TIME BEHAVIOR OF THE AUTOCORRELATION FUNCTION RESPECTIVELY.

τ_0 IS A THERMAL TIME DEFINED BY:

$$\tau_o = \frac{h}{4\pi k_B T}$$

IN THE CASE OF PURE GASES, $J(\omega,\omega_j)$ IS WRITTEN (WITH $\omega = 2\pi c\nu$):

$$J(\omega,\omega_j) = \frac{1}{N}\frac{\tau_1}{\pi} e^{\tau_2/\tau_1} \left\{ e^{(\omega-\omega_j)\tau_0} \cdot \frac{Z_- K_1(Z_-)}{1+((\omega-\omega_j)\tau_1)^2} + e^{(\omega+\omega_j)\tau_0} \cdot \frac{Z_+ K_1(Z_+)}{1+((\omega+\omega_j)\tau_1)^2} \right\}$$

WHERE $Z_\pm = (\tau_1^{\,2} + \omega_\pm^{\,2})^{\frac{1}{2}} (\tau_2^{\,2} + \tau_0^{\,2})^{\frac{1}{2}}$ AND

$\omega_\pm = \omega \pm \omega_j$

$K_1(Z)$ IS THE MODIFIED BESSEL FUNCTION OF THE SECOND KIND. τ_1 IS WRITTEN AS

$$\tau_1 = \frac{1}{2\pi c \gamma_i}$$

WHERE γ_i IS THE SELF BROADENED COEFFICIENT FOR EACH ABSORBER MOLECULE I. WE ASSUME THAT τ_2 IS CONSTANT FOR EACH MOLECULE AND FOR EACH STUDIED FREQUENCY RANGE.

Far Wing line shape.

$$g_{FW}(\nu : \nu_j) = \frac{\nu}{\nu_j} \frac{\tanh(hc\nu/2k_BT)}{\tanh(hc\nu_j/2k_BT)} j_{FW}(\nu)$$

and

$$j_{FW}(\nu) = \left(\frac{\tau_{a2}}{2\pi}\right)^{1/2} \frac{1}{\tau_{a1}\sqrt{2\pi c}} \frac{\exp(-2\pi c|\nu - \nu_j|\tau_{a2})}{|\nu - \nu_j|^{1.5}} \exp(2\pi c(\nu - \nu_j)\tau_o)$$

The exponential wing is consistent with experimental observation [13,18]. The general far wing result for a binary mixture can be obtained by solving a convolution integral of the individual line shape functions (j_a and j_b) in the far wing limit. Thus, given

$$j_a(\nu) = \frac{1}{2\pi} \int_{-\infty}^{\infty} d\tau \; e^{-i2\pi c\nu} \; C_a(\tau),$$

$$j_b(\nu) = \frac{1}{2\pi} \int_{-\infty}^{\infty} d\tau \; e^{-i2\pi c\nu} \; C_b(\tau),$$

and

$$j(\nu) = \int_{-\infty}^{\infty} j_a(x) j_b(\nu - \nu_j - x) dx \; .$$

then using contour integration and in the far wing limit

$$j_{FW}(\nu) = \left(\frac{\tau_{a2}}{2\pi}\right)^{1/2} \frac{1}{\tau_{a1}\sqrt{2\pi c}} \frac{\exp(-2\pi c|\nu - \nu_j|\tau_{a2})}{|\nu - \nu_j|^{1.5}} \exp(2\pi c(\nu - \nu_j)\tau_o)$$

$$+ \left(\frac{\tau_{b2}}{2\pi}\right)^{1/2} \frac{1}{\tau_{b1}\sqrt{2\pi c}} \frac{\exp(-2\pi c|\nu - \nu_j|\tau_{b2})}{|\nu - \nu_j|^{1.5}} \exp(2\pi c(\nu - \nu_j)\tau_o).$$

Note:

$$g_{FW}(\nu) \xrightarrow[\nu \to 0]{} \nu^2$$

A general empirical form for the continuum absorption coefficient used to represent the data (5) is

$$\beta_{cont}(\nu, T, P_{f1} \ldots P_{fi}, P_s) = \frac{P_s}{RT} \sum_i \left[C_{fi}(\nu, T) P_{fi} + C_s(\nu, T) P_s \right]$$

where C_s, is the self-broadening coefficient of the absorbing gas, C_{fi}) is the foreign broadening coefficient due to the i^{th} type foreign gas, and R is the ideal-gas constant. The equation can be conveniently rewritten for i = 2 to obtain

$$\beta_{cont}(\nu, T) = \frac{C_{f1}(\nu, T)}{RT} P_s \left[P_{f1} + F(\nu, T) P_{f2} + B(\nu, T) P_s \right]$$

where $F = C_{f2}/C_{f1}$ and $B = C_s/C_{f1}$ are the dimensionless broadening coefficients. Near line center, B has the value of 5 for water vapor relative to nitrogen. In the real atmosphere, the effects of oxygen broadening must also be included. The dimensionless broadening coefficient F accounts for oxygen. However, many laboratory experiments ignore the effects of oxygen and use only nitrogen as the broadening gas along with the absorbing gas.

EXPERIMENTAL WATER VAPOR CONTINUUM DATA

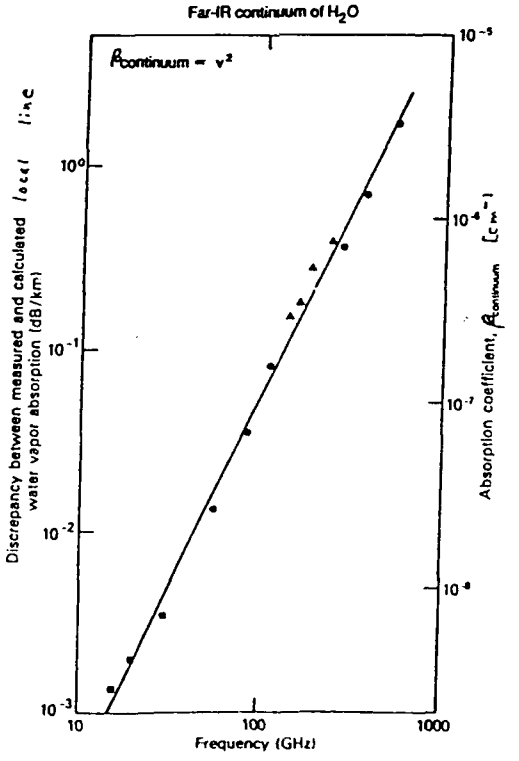


Figure 1.3.10 Water vapor continuum absorption coefficient as a function of frequency. The solid line is an empirical fit to the experimental data points as given by Eq. 1.3.92. The plotted points are (▲) [20], (•) [21], and (■) [22] for T = 300 K, P_t = 101 kPa and $\rho_v = 10^{-3}$ kg/m^3.

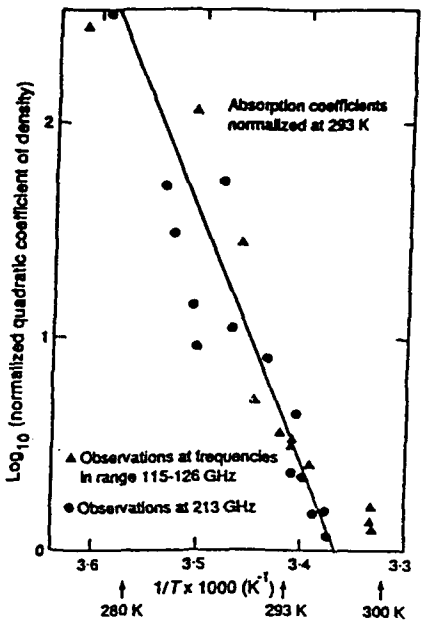


Figure 1.3.11 Temperature dependence of millimeter wave water vapor continuum. Solid curve represents empirical fit to data as given by Eq.

Table 1 Experimental frequency dependence of B (ν,300)

f (GHz)	ν (cm^{-1})	B (ν, 300)
110	3.7	32
138	4.6	31.6
213	7.1	20
833	27.8	7.4

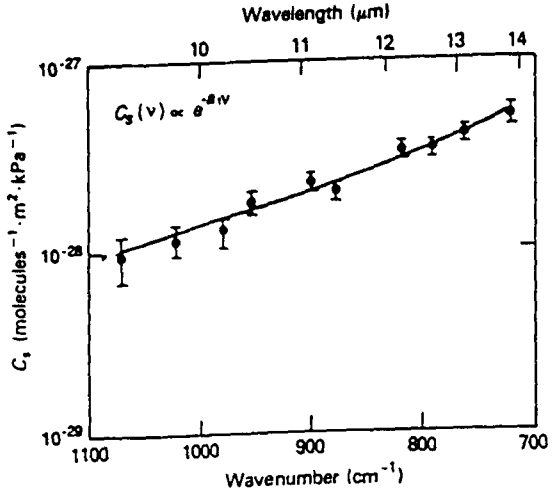


Figure 1.3.12 Self-broadening coefficient as a function of wave number from 700 to 1100 cm^{-1} at 296 K[27].

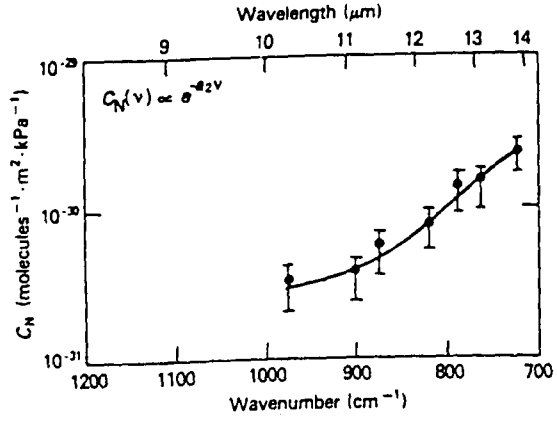


Figure 1.3.13 Nitrogen broadening coefficient as a function of wave number from 700 to 1000 cm^{-1} at 296 K[27].

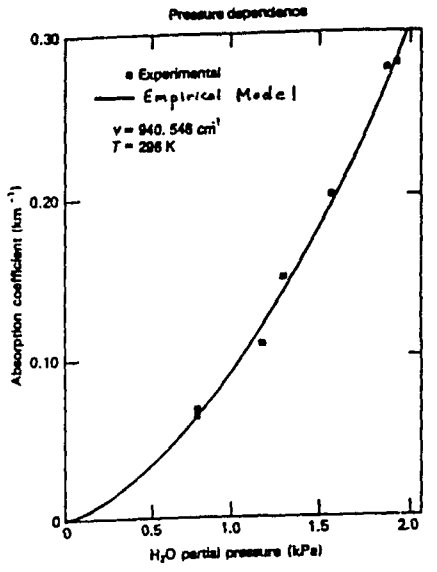


Figure 1.3.14 Water vapor partial pressure dependence in the 10 μm region.

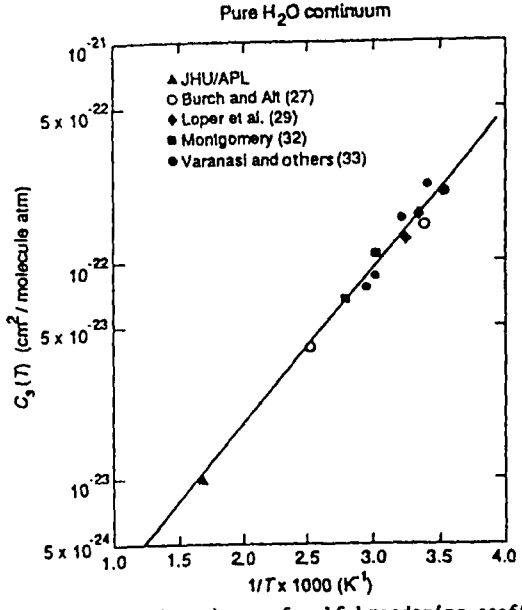


Figure 1.3.15 Temperature dependence of self-broadening coefficient in the 10 μm region.

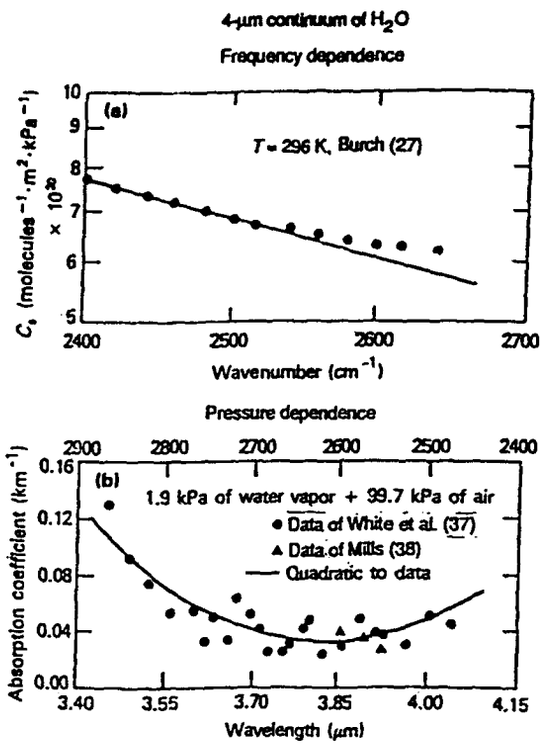


Figure 1.3.16 4 μm water vapor continuum region at T= 296K. (a) C_s vs wave number [27] and (b) absorption coefficient vs wavelength [37,38].

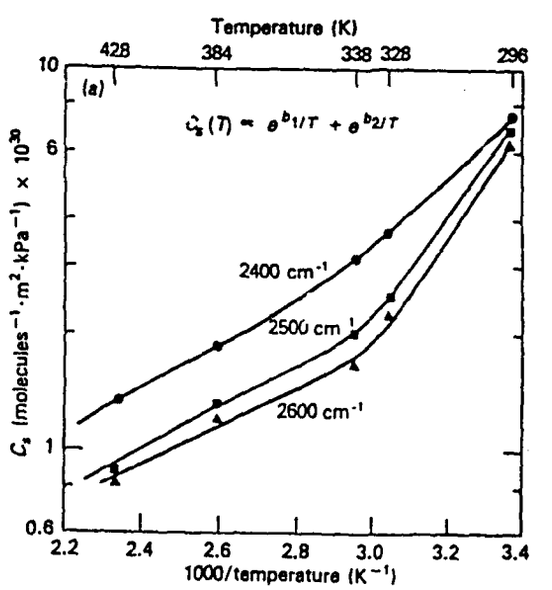
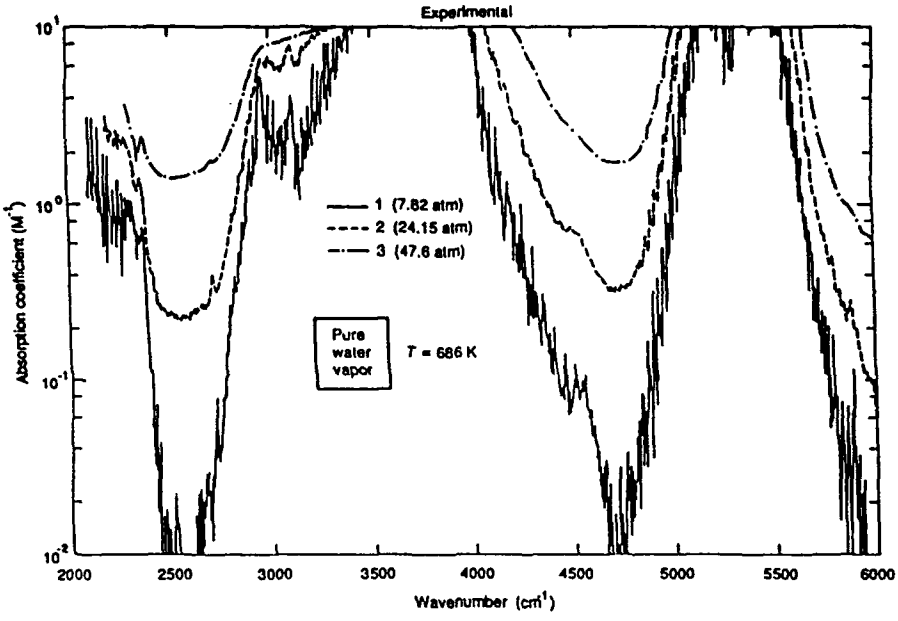


Figure 1.3.17 Plots of the water vapor self-broadening coefficients at 2400, 2500 and 2600 cm^{-1} vs reciprocal temperature [27]. the symbols •, ■ and ▲ represent the experimental data points.



Pure water vapor absorption coefficient at T = 685K and three different pressures.

* The 1 μm window water vapor continuum has been measured by a novel interferometric calorimeter technique.

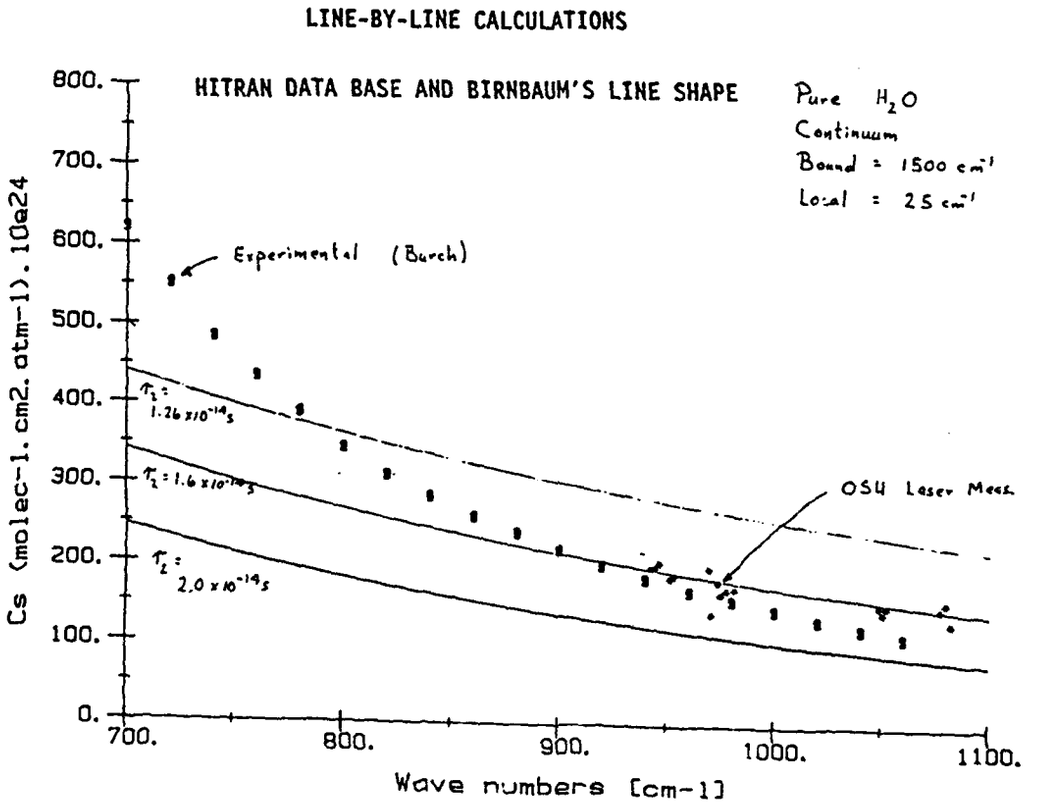
A pulsed Nd-glass laser is used to heat a nitrogen buffered water vapor sample placed in the arm of He-Ne Mach-Zehnder interferometer. Variations in the index of refraction due to the heating cause measurable fringe shifts proportional to the absorption coefficient.

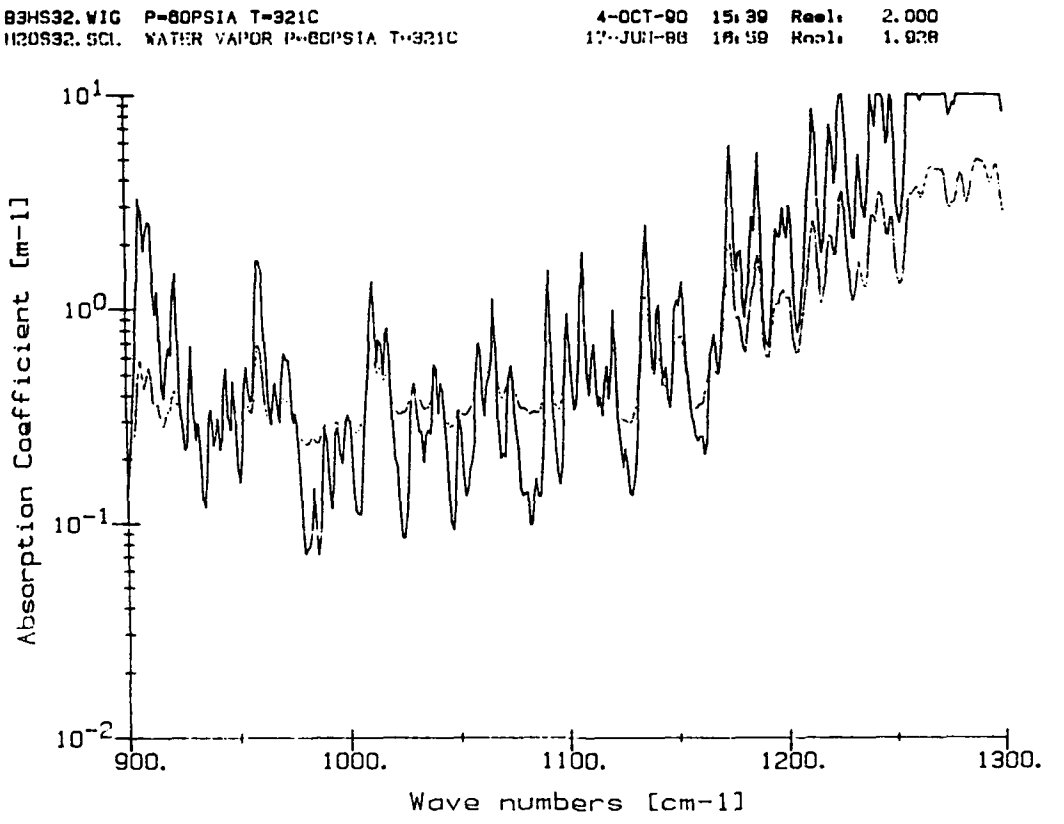
* The resulting continuum absorption coefficient measured at 9466 cm^{-1} is 6×10^{10} cm^{-1} for a water vapor partial pressure of 16.5 Torr buffered by nitrogen to a total pressure of 1 atmosphere at 30°C.

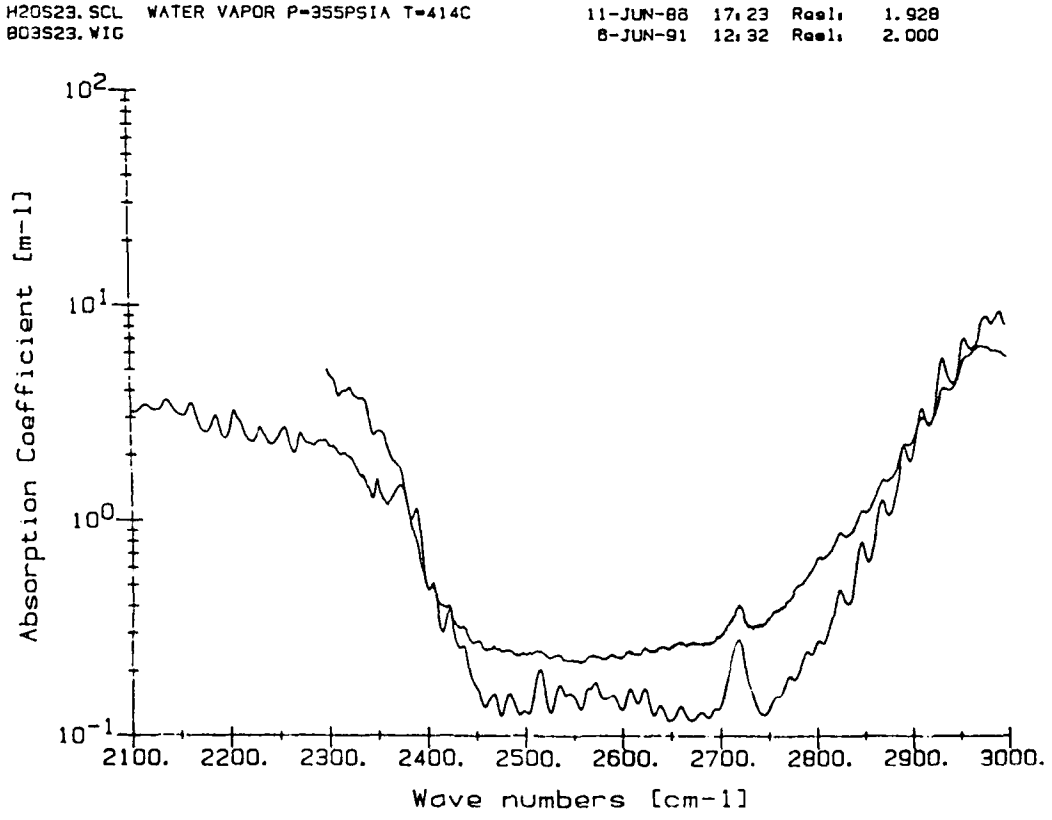
Thus, the water vapor continuum is roughly two orders of magnitude weaker near 1 μm than at 4 or 2 μm.

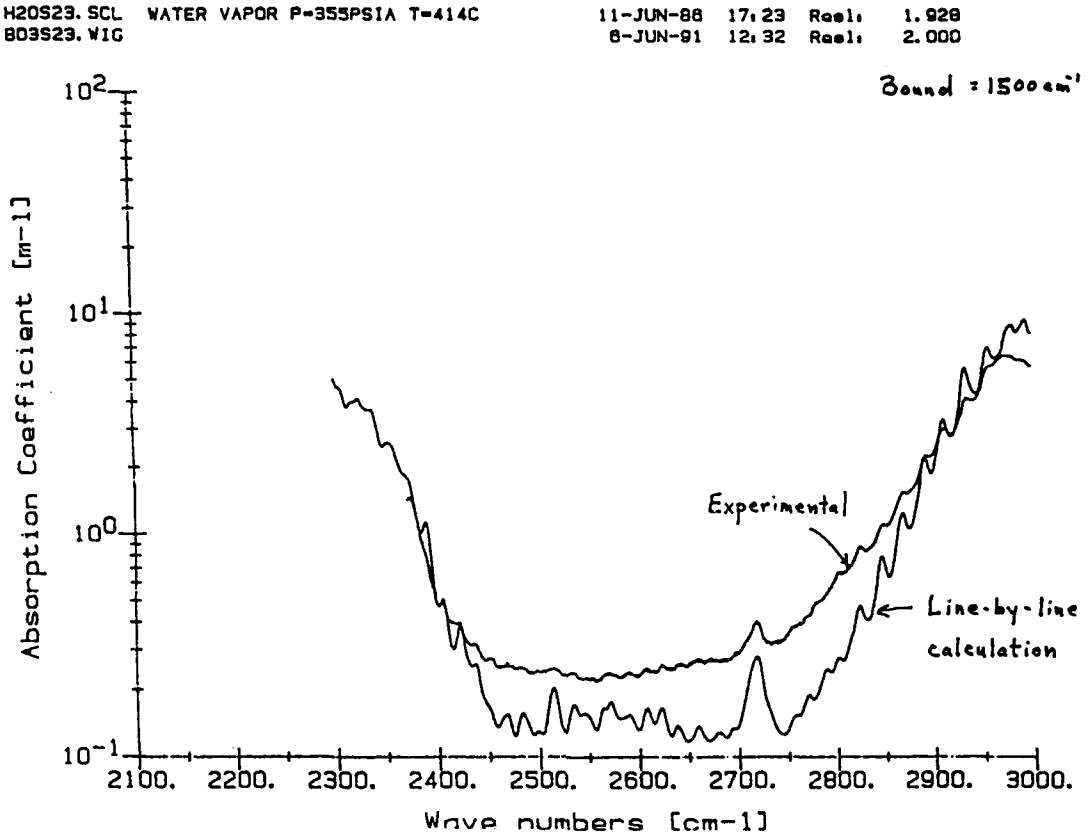
* Further measurements to determine the water vapor partial pressure dependence and temperature dependence are needed.

The tragedy of experimental water vapor continuum characterization is that unlike nitrogen and CO_2 experiments, it presently cannot be done at high pressure. High-pressure water vapor measuremants also require high-temperature and thus a theoretical understanding of the continuum absorption temperature dependence to extrapolate back to atmospheric temperatures.




B3HS32.WIG P=80PSIA T=321C 4-OCT-90 15:39 Real: 2.000
H20S32.SCL WATER VAPOR P=80PSIA T=321C 17-JUN-88 18:59 Real: 1.928
Absorption Coefficient [m-1]
10^1
10^0
10^{-1}
10^{-2}
900.
1000.
1100.
1200.
1300.
Wave numbers [cm-1]


H20S23.SCL WATER VAPOR P=355PSIA T=414C 11-JUN-88 17:23 Real: 1.928
B03S23.WIG 6-JUN-91 12:32 Real: 2.000
Absorption Coefficient [m-1]
10^2
10^1
10^0
10^{-1}
2100.
2200.
2300.
2400.
2500.
2600.
2700.
2800.
2900.
3000.
Wave numbers [cm-1]


H2OS23.SCL WATER VAPOR P=355PSIA T=414C
B03S23.WIG
11-JUN-88 17:23 Real: 1.928
6-JUN-91 12:32 Real: 2.000
Bound = 1500 cm⁻¹
Absorption Coefficient [m-1]
10²
10¹
10⁰
10⁻¹
2100. 2200. 2300. 2400. 2500. 2600. 2700. 2800. 2900. 3000.
Wave numbers [cm-1]
Experimental
Line-by-line calculation

OVERVIEW OF LINE COUPLING IN THE 5 mm BAND OF OXYGEN

P.W. Rosenkranz
Massachusetts Institute of Technology, 77 Massachusetts Avenue, Cambridge, MA 02139

Nearly forty years ago, measurements of microwave absorption in oxygen indicated that pressure broadening became less effective, by approximately a factor of two, at pressures approaching one atmosphere than at lower pressures where the individual lines in the band were resolved. The explanation of this behavior of oxygen by means of overlapping line theory eventually led to methods of calculating absorption by oxygen that could be based on parameters determinable from careful laboratory measurements. Only recently, however, have such measurements explored an extensive range of frequency, pressure and temperature. These measurements (made by H.J. Liebe) are interpreted to determine the variation with temperature of the parameters that characterize line coupling. Possible revisions in transmittances for weather satellite frequencies are discussed.

Overview of Line Coupling in the 5 mm Band of Oxygen

P. W. Rosenkranz
Massachusetts Institute of Technology
Cambridge, MA 02139

Abstract-Nearly forty years ago, measurements of microwave absorption in oxygen indicated that pressure broadening became less effective, by approximately a factor of two, at pressures approaching one atmosphere than at lower pressures where the individual lines in the band were resolved. The explanation of this behavior of oxygen by means of overlapping line theory eventually led to methods of calculating absorption by oxygen that could be based on parameters determinable from careful laboratory measurements. Only recently, however, have such measurements explored an extensive range of frequency, pressure and temperature. These measurements (made by H. J. Liebe) are interpreted to determine the variation with temperature of the parameters that characterize line coupling. Possible revisions in transmittances for weather satellite frequencies are discussed.

When microwave absorption in oxygen began to be measured, it was recognized very early (e.g. Crawford and Hogg, 1956 - Fig. 1) that at pressures near 1 atmosphere where the lines overlapped into a band, pressure broadening seemed to be less effective, by approximately a factor of two, than at much lower pressures where the individual lines were resolved. Meeks and Lilley (1963) proposed the use of the oxygen band for remote measurement of atmospheric temperature from satellites. They also devised a scheme for calculating absorption by assuming that the ratio of linewidth to pressure varied with altitude (Fig. 2). Similar absorption models were devised by Carter, Mitchell and Reber (1968) and Reber (1972). By and large, these models represented atmospheric opacity on the far wings of the oxygen band reasonably well. However, when the Nimbus 5 Microwave Spectrometer was launched into space in 1972, some systematic discrepancies from calculated brightness temperatures were observed, in particular near 58.8 GHz (Waters et al., 1975 - Fig. 3).

Gordon (1967) had already explained the relative narrowness of the oxygen band at high pressures by means of the theory of overlapping lines. This theoretical framework had been originated by Baranger (1958) and Kolb and Griem (1958) and had been further developed by Fano (1963) and Ben-Reuven (1966). In the impact approximation, the pressure-proportional width parameter that applies to an isolated line is replaced, for a band of lines, by a pressure-proportional matrix w whose diagonal elements are width parameters for each line, and whose off-diagonal elements represent the coupling of each pair of lines by collisions. Calculation of the band shape involved the inversion of a complex matrix (Fig. 4); however, a first-order perturbation expansion (Rosenkranz, 1975 - Fig. 5) made it feasible to use the theory for atmospheric radiative-transfer calculations. In the first-order approximation, the influence of the off-diagonal matrix elements occurs through the addition of dispersion-shaped functions to the usual resonant line shapes that describe isolated lines. Because of the way in which the signs of the coefficients associated with the former terms depend on rotational quantum number, the effect is an increase in absorption near the band center, and a decrease on the wings (Fig.6).

Initially these coefficients (of the dispersion-shaped terms) were obtained from a method that estimated the largest of the off-diagonal elements of w. A later refinement (Rosenkranz, 1988) allowed their determination directly from laboratory measurements. Direct calculation of the w matrix has been carried out by Lam (1977) (whose results were revised by Smith, 1981 - Fig. 7), and by Mingelgrin et al. (1972, 1979 - Fig. 8). These calculations obtained agreement with measurements at normal laboratory temperature and at pressures up to at least seven atmospheres (although the exact matrix inversion is required above one atmosphere).

Despite the success of overlapping-line theory in accounting for laboratory measurements of absorption and dispersion as well as atmospheric opacity on the far wings of the band, it has not eliminated all discrepancies between calculations and measurements for satellite-based radiometers. Grody (1983) discusses some of these systematic offsets in data from the Microwave Sounding Unit on NOAA satellites (Fig.9). They reach 1 to 2 K in the channels at 55 and 58 GHz, which measure thermal emisison from the upper troposphere and lower stratosphere. These brightness temperature differences could be explained by an increase in absorption of approximately 10%.

The association of these offsets with the colder parts of the atmosphere suggested that the temperature dependence of the line coupling might be different from that which had been assumed. A recently completed series of measurements by Liebe et al. (1991) on dry air at 279, 303 and 327 K provide the opportunity to test this hypothesis (Fig. 10). Coefficients for the line interference effect have been extracted from these measurements by the method described by Rosenkranz (1988). For the lower rotational quantum levels (1, 3, 5, 7) their temperature dependence is $T^{-0.8}$ (Fig. 11), similar to the line widths. The higher levels have some further variation with temperature, to which a linear function of the reciprocal temperature variable $\theta = 300/T$ was fitted.

Atmospheric absorption can be calculated by extrapolating this fitted temperature dependence, and the new coefficients produce slightly less absorption than previously calculated at 53.7 and 55 GHz. The calculated brightness temperatures at these frequencies

have changed by less than 0.4 K. At 58 GHz there is essentially no change from the older calculation. Possibly, one could choose different functions to represent the variation with temperature that might fit the data equally well over the measured temperature range, yet extrapolate differently to colder temperatures. On the basis of the present laboratory measurements, however, the discrepancies observed by the MSU do not find an explanation.

An aircraft-based radiometer experiment is planned for the summer of 1991. It is hoped that these measurements, in the zenith-observing mode, will provide the lower-temperature test points that could validate (or not validate) the new oxygen-band line parameters.

References

Baranger, M., *Phys. Rev.* **111**, 494-504 (1958).
Ben-Reuven, A., *Phys. Rev.* **145**, 7-22 (1966).
Carter, C. J., R. L. Mitchell, and E. E. Reber, *J. Geophys. Res.* **73**, 3113-3120 (1968).
Crawford, A. B., and D. C. Hogg, *Bell System Tech. J.* **35**, 907-916 (1956).
Fano, U., *Phys. Rev.* **131**, 259-268 (1963).
Gordon, R. G., *J. Chem. Phys.* **46**, 448-455 (1967).
Grody, N. C., *J. Climate and Appl. Meteor.* **22**, 609-625 (1983).
Kolb, A. C., and H. Griem, *Phys. Rev.* **111**, 514-521 (1958).
Lam, K. S., *J. Quant. Spectros. Radiat. Trransfer* **17**, 351-383 (1977).
Liebe, H. J., G. A. Hufford, and R. O. DeBolt, "The Atmospheric 60-GHz Oxygen Spectrum: Modeling and Laboratory Measurements," NTIA Report 91-272, U. S. Dept. of Commerce (1991).
Meeks, M. L., and A. E. Lilley, *J. Geophys. Res.* **68**, 1683-1703 (1963).
Mingelgrin, U., R. G. Gordon, L. Frenkel, and T. E. Sullivan, *J. Chem. Phys.* **57**, 2923-2931 (1972).
Mingelgrin U., and R. G. Gordon, *J. Chem. Phys.* **70**. 3828-3839 (1979).
Reber, E. E., *J. Geophys. Res.* **77**, 3831-3845 (1972).
Rosenkranz, P. W., *IEEE Trans. Antennas Propagat.* **AP-23**, 498-506 (1975).
Rosenkranz, P. W., *J. Quant. Spectros. Radiat. Transfer* **39**, 287-297 (1988).
Smith, E. W., *J. Chem. Phys.* **74**, 6658-6673 (1981).
Waters, J. W., K. F. Kunzi, R. L. Pettyjohn, R. K. L. Poon, and D. H. Staelin, *J. Atmos. Sci.* **32**, 1953-1969 (1975).

Viewgraphs:

1. Absorption in air at sea level, from Crawford and Hogg (1956).

2. Oxygen line-width parameter, from Meeks and Lilley (1963).

3. Calculated minus measured NEMS brightness temperatures at 58.8 GHz, from Waters *et al.*(1975).

4. Complex index of refraction.

5. Absorption at 58.8 GHz, from Rosenkranz (1975).

6. The effect of off-diagonal elements of w.

7. Dispersion at 59.59 GHz, from Smith (1981).

8. O_2 spectrum, from Mingelgrin *et al.* (1972).

9. Measured versus computed MSU brightness temperatures, from Grody (1983).

10. New laboratory measurements on dry air by Liebe *et al.*(1991). Interference coefficients were fitted to the 101 kPa data.

11. Derived interference coefficients at three temperatures. The plotted coefficients are adjusted to 100 kPa pressure and normalized by the factor $\theta^{0.8}$.

Note: Figs. 10 and 11 were revised after the conference.

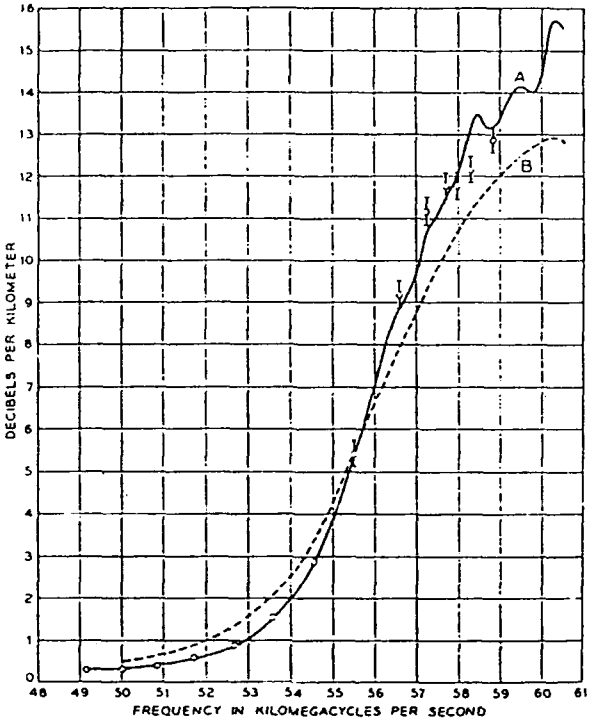
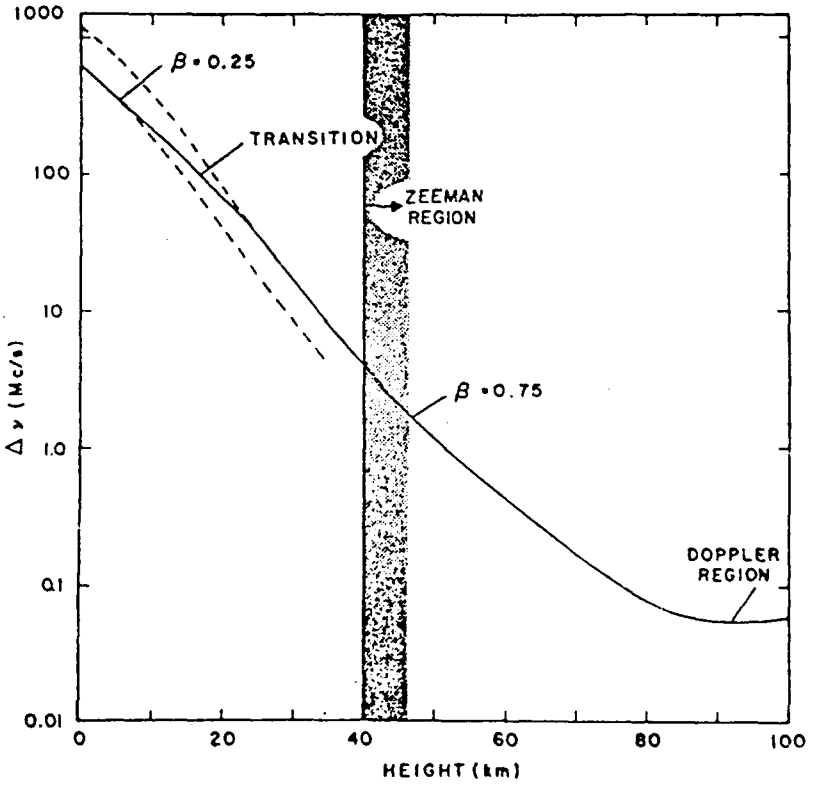
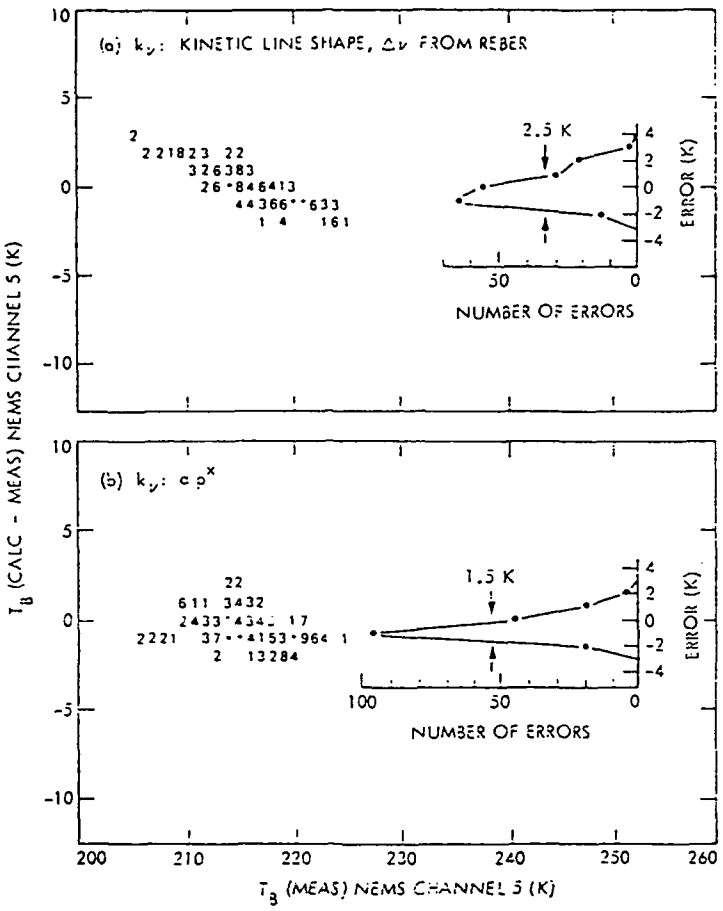


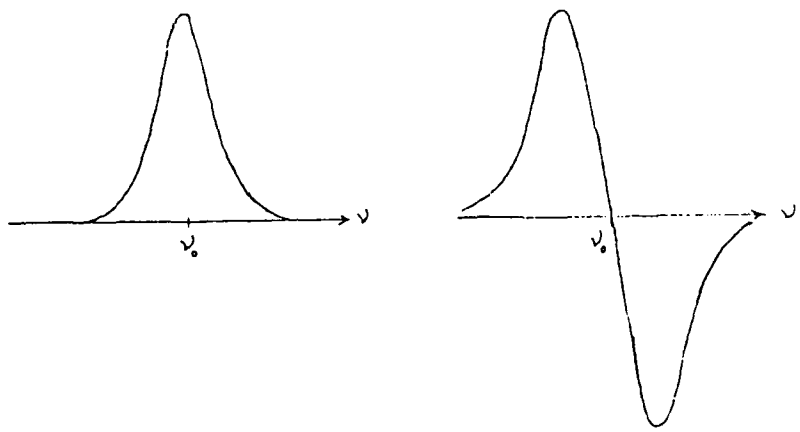
Fig. 8 — Calculated and measured absorption by air at sea level. The dots represent the experimental data; the vertical lines indicate the spread in the measured values. Curves A and B are calculated curves of oxygen absorption using line-breadth constants of 600 and 1200 mc, respectively, and a temperature of 293° K. (Courtesy of T. F. Rogers, Air Force Cambridge Research Center.)

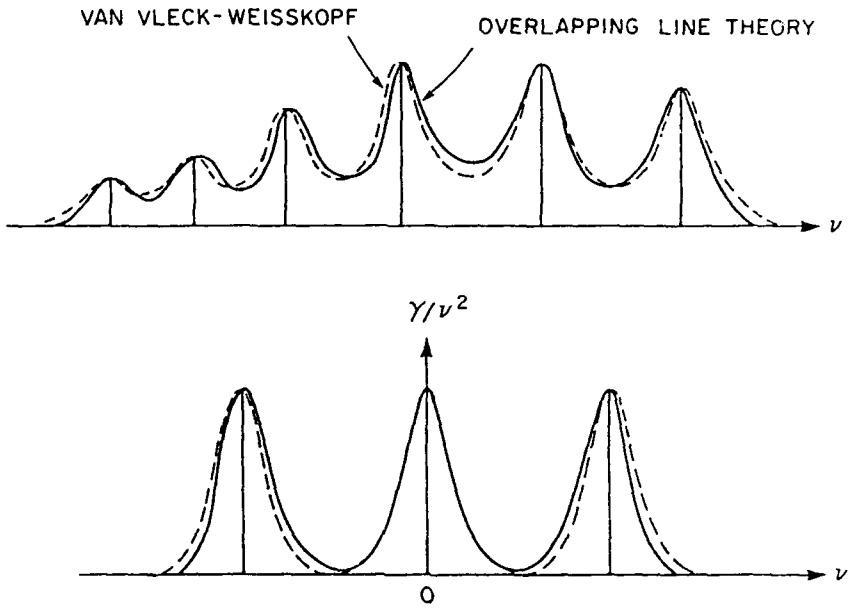




Complex index of refraction:

$$n(\nu) - n(0) = -\frac{8\pi\mu_0^2 N_{O_2}\nu}{3kTQ}\ \underline{\ell}^T\left(\nu - \underline{\underline{\nu}}_0 - i\,\underline{\underline{W}}\right)^{-1}\underline{\underline{\rho}}\,\underline{\ell}$$





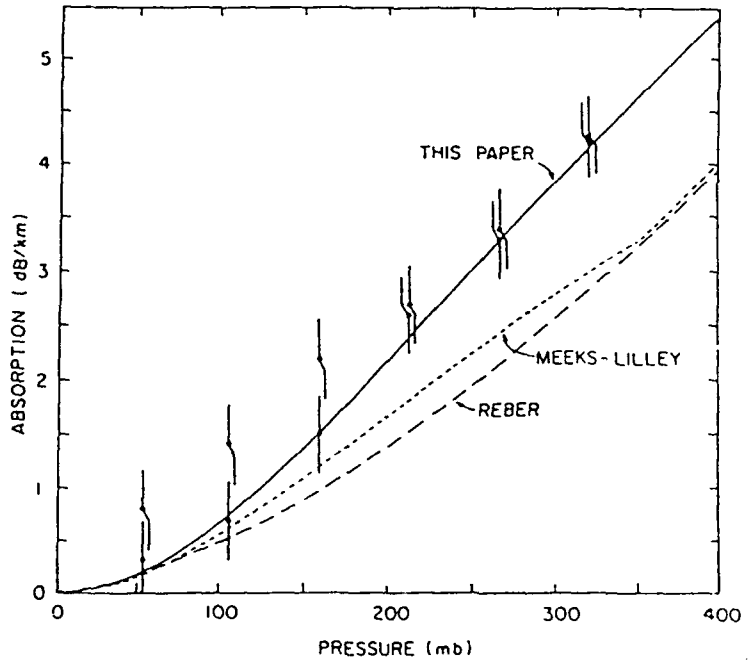


Fig. 3. Absorption in dry air at 58.82 GHz and 295 K, computed for three models. Measurements are by Poon [30].

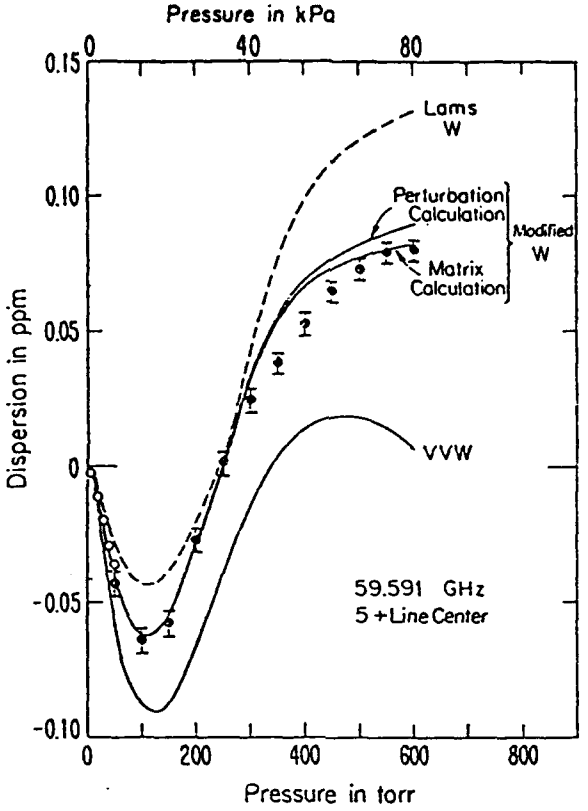


FIG. 8. Dispersion[21] at 59.591 GHz as a function of pressure at a temperature of 300 K. Experimental points, solid and open circles, obtained from two independent unpublished measurements.[6]

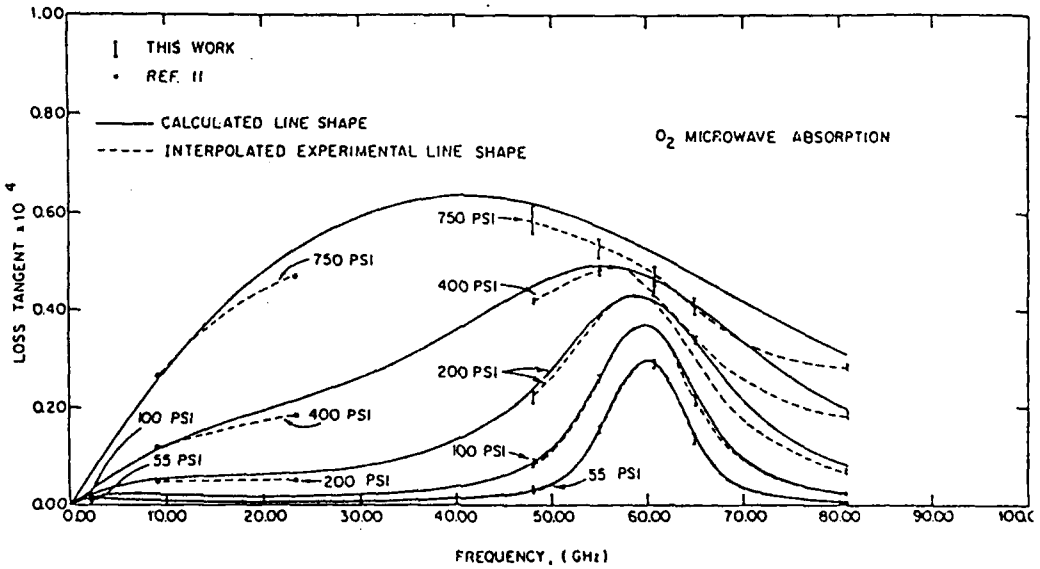
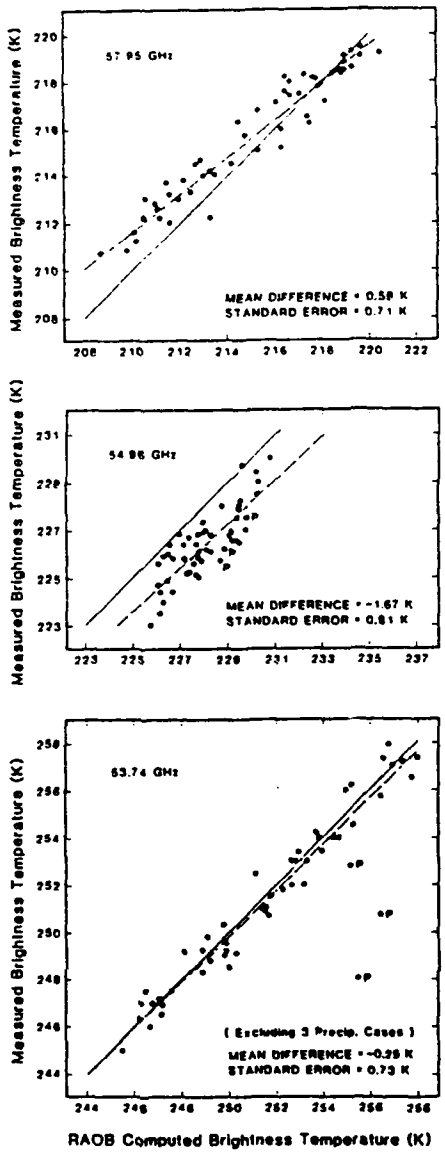
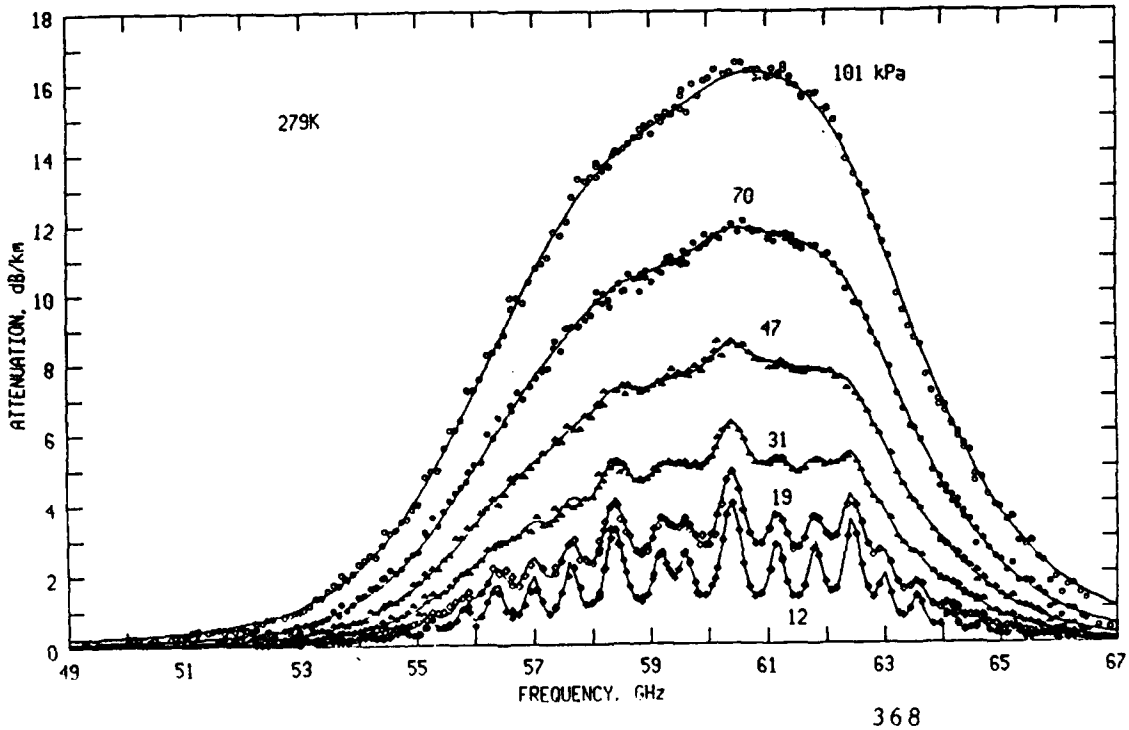
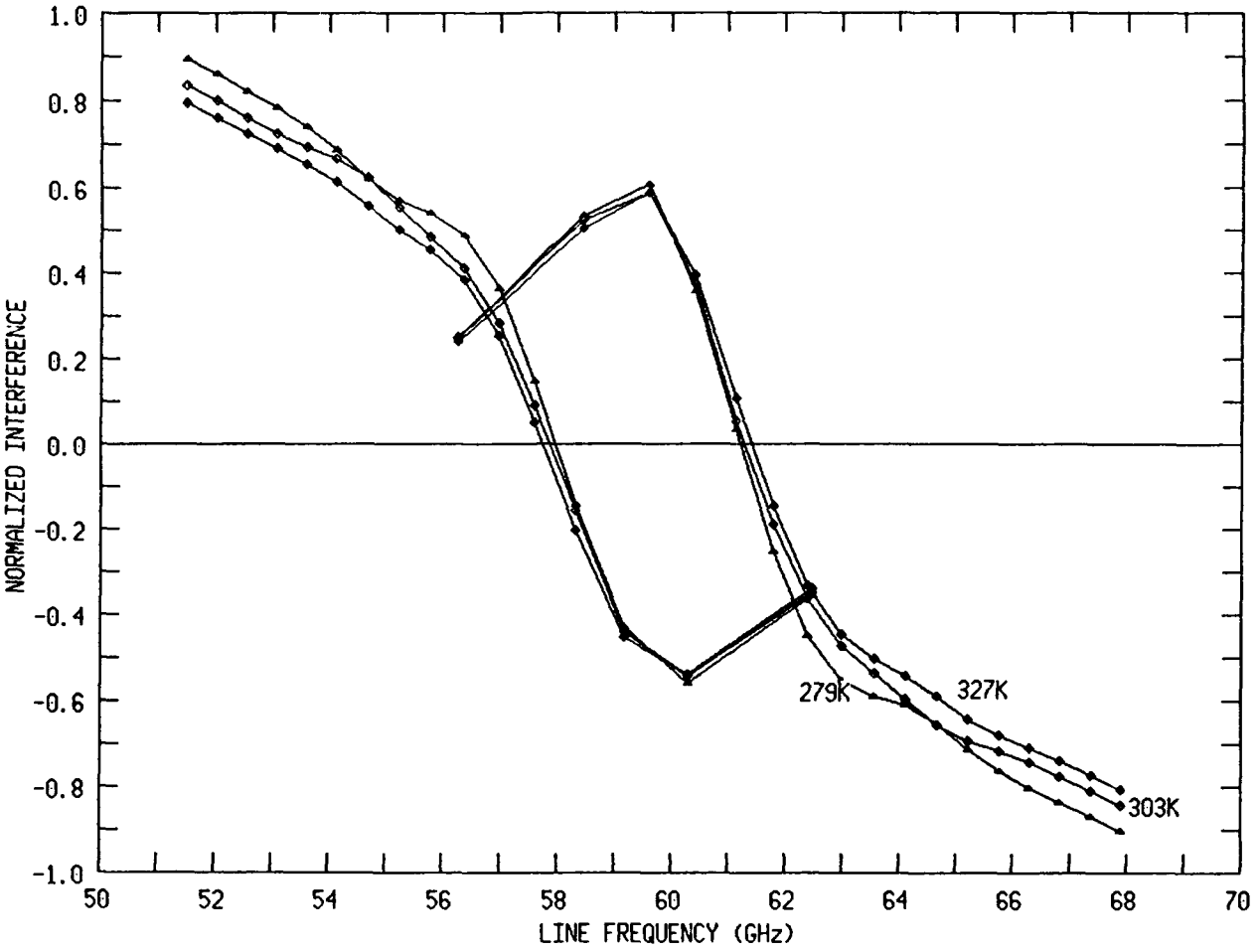


FIG. 7. Calculated vs experimental line shape of pure O_2.


57.95 GHz
MEAN DIFFERENCE = 0.58 K
STANDARD ERROR = 0.71 K
54.96 GHz
MEAN DIFFERENCE = -1.67 K
STANDARD ERROR = 0.81 K
53.74 GHz
(Excluding 3 Precip. Cases)
MEAN DIFFERENCE = -0.25 K
STANDARD ERROR = 0.73 K
Measured Brightness Temperature (K)
RAOB Computed Brightness Temperature (K)


279K
101 kPa
70
47
31
19
12
ATTENUATION, dB/km
FREQUENCY, GHz


1.0
0.8
0.6
0.4
0.2
0.0
-0.2
-0.4
-0.6
-0.8
-1.0
NORMALIZED INTERFERENCE
50
52
54
56
58
60
62
64
66
68
70
LINE FREQUENCY (GHz)
279K
327K
303K

LABORATORY MEASUREMENTS OF LINE COUPLING IN CO_2 AND N_2O

L.L. Strow
Physics Department, University of Maryland Baltimore County, Baltimore, MD 21228

Laboratory studies of line coupling in a number of CO_2 and N_2O Q-branches will be presented. Coupling calculations based on very simple scaling laws for rotational relaxation give good agreement with observation for self-broadened spectra over a wide temperature range (200 to 350K). N_2-broadened CO_2 Q-branches, however, exhibit more line coupling than calculated unless one forces the $f \rightarrow f$ collision rate in the Π state to be larger than the $f \rightarrow e$ collision rate. These two collision rates are approximately equal for self-broadened line coupling. Similar, but more extreme differences in these collision rates have been observed in CO_2 Q-branches broadened by He. Laboratory measurements of line coupling in the Q-branch at the Π–Δ band of CO_2 will also be presented. All previous measurements of Q-branch line coupling in CO_2 have involved Π–Σ bands. Examples of line coupling in N_2O Q-branches will also be presented.

Laboratory Measurements of Line Coupling in CO_2 and N_2O

L. Strow
University of Maryland Baltimore County

- Line Mixing – also known as

  Line Coupling

  Rotational Collisional Narrowing

  Q-branch Collapse

- Previous Work

  Raman – CO_2, NO, N_2, O_2, CO

  1932, 2070 cm^{-1} CO_2 Q branches, self- and N_2-broadened; 667 cm^{-1} 597 cm^{-1} Q-branches, N_2-broad.

  720 cm^{-1} CO_2 Q branch, self-broadened

  N_2O Q branches, self-broadened (1880, 2800 cm^{-1}), N_2-broadened (2800 cm^{-1})

  C_2H_2, HCN, etc. Q branches, self-broadened

  ν_3 R-branch bandhead of CO_2

- Atmospheric Implications

  Temperature Sounding: UARS (CLAES, ISAMS), EOS (AIRS, TES), ATMOS, HIS

Line Coupling Theory

- $\Pi - \Sigma$ band, l=1 in Π state
- Line mixing absorption coefficient given by

$$k(\nu) = \frac{N}{\pi}\mathrm{IM}\left\{\sum_{j,k} d_j \langle\langle j|\left[(\nu-\nu_o) - iP\mathbf{W}\right]^{-1}|k\rangle\rangle d_k \rho_k\right\},$$

- Determine W matrix ($\Pi - \Sigma$ bands) from

$$W_{jj} = -\frac{1}{2}\left(\sum_{j'\neq j} K_{j'j}^{\Sigma(e\leftarrow e)}\right) - \frac{1}{2}\left(\sum_{j'\neq j}^{f\ levels} \beta K_{j'j}^{\Pi(f\leftarrow f)} + \sum_{j'\neq j}^{e\ levels} (1-\beta) K_{j'j}^{\Pi(e\leftarrow f)}\right),$$

  where W_{jj} is the linewidth, and $K_{j'j}$ is modeled with the hybrid power-exponential-gap (PEG) law

$$K_{j'j} = a_1 (T_o/T)^{0.5} \left(\frac{|\Delta E_{j'j}|}{B_o}\right)^{-a_2} \exp\left(\frac{-a_3|\Delta E_{j'j}|}{kT}\right),$$

  for $j' > j$. Detailed balance gives $K_{j'j}$ for $j' < j$. $\Delta E_{j'j} = E_{j'} - E_j$ is the rotational energy gap. For CO_2-CO_2, N_2O-N_2O collisions $\beta \approx 0.50$. For CO_2-N_2 collision $\beta \approx 0.625$, for CO_2-He collisions $\beta \approx 0.75$. W is obtained by letting

$$W_{j'j} = -\beta K_{j'j}^{\Pi(f\leftarrow f)}.$$

- Only β must be determined from spectra exhibiting mixing

Calculational Details

$$k(\nu) = \frac{N}{\pi}\mathrm{IM}\left\{\sum_{j,k} d_j \langle\langle j|\left[(\nu - \nu_o) - iP\mathbf{W}\right]^{-1}|k\rangle\rangle d_k \rho_k\right\},$$

can be rewritten as

$$k(\nu) = \frac{N}{\pi}\mathrm{IM}\left\{\mathbf{d}\cdot\mathbf{G}(\nu)^{-1}\cdot\rho\cdot\mathbf{d}\right\},$$

where

$$\mathbf{G} = \nu - \mathbf{H}, \quad \mathbf{H} = \nu_o + iP\mathbf{W}.$$

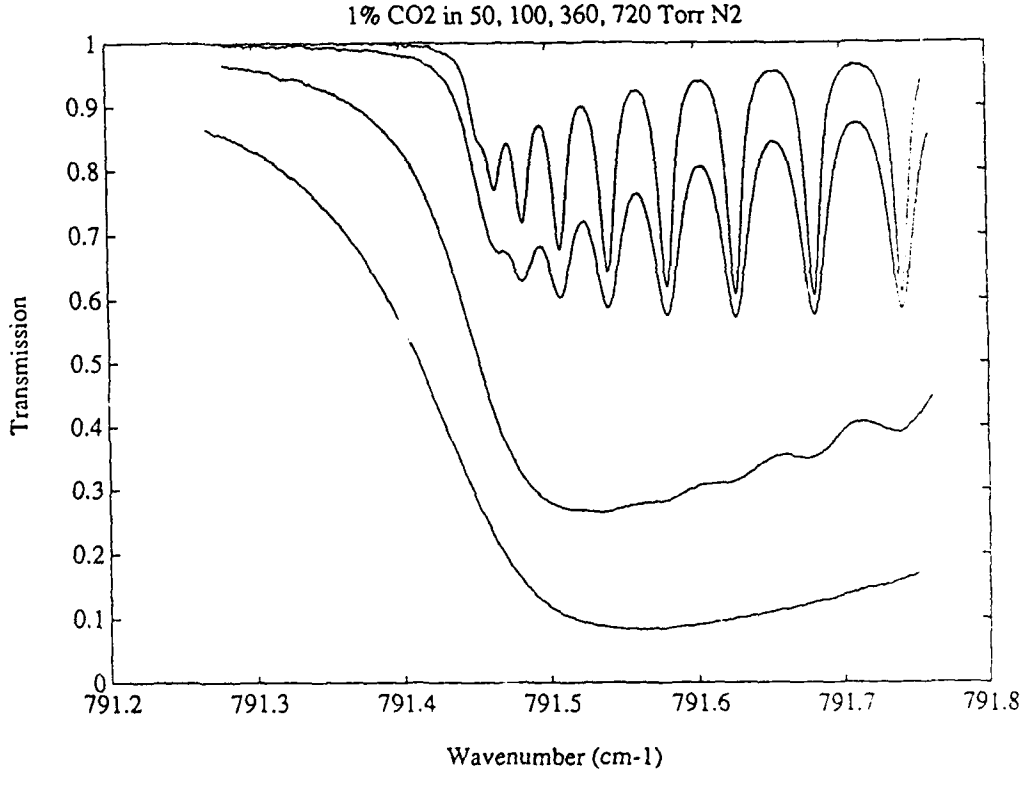
Diagonalizing $\mathbf{H}$ with $\mathbf{L}$

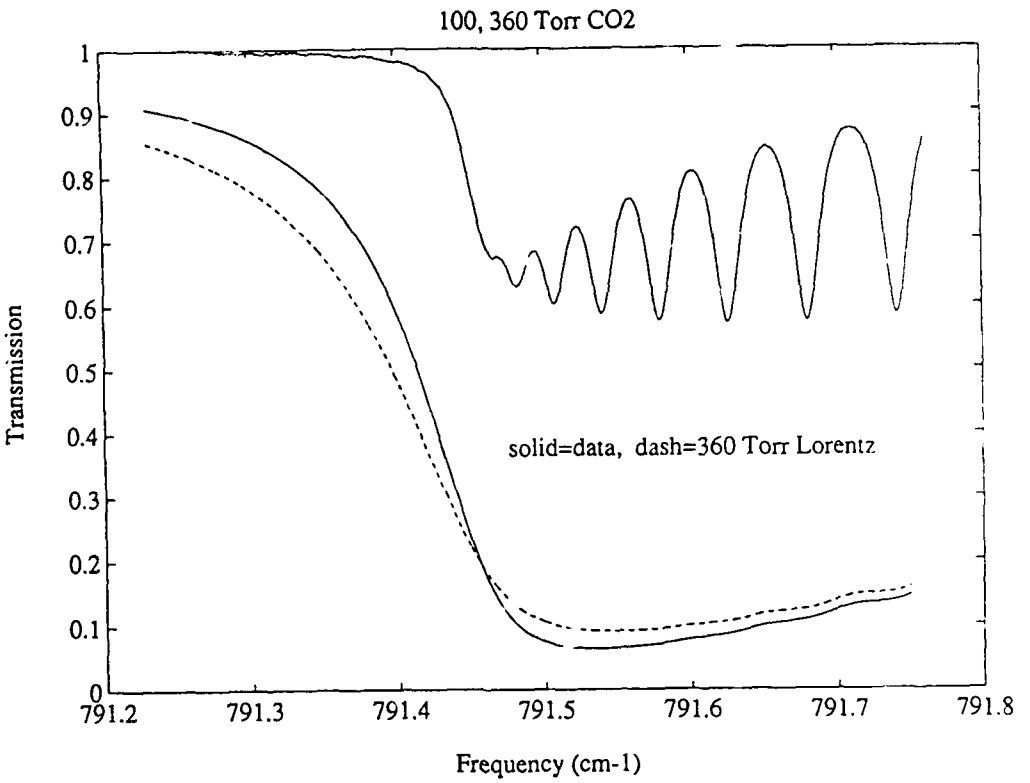
$$\mathbf{A}^{-1}\cdot\mathbf{H}\cdot\mathbf{A} = \mathbf{L}$$

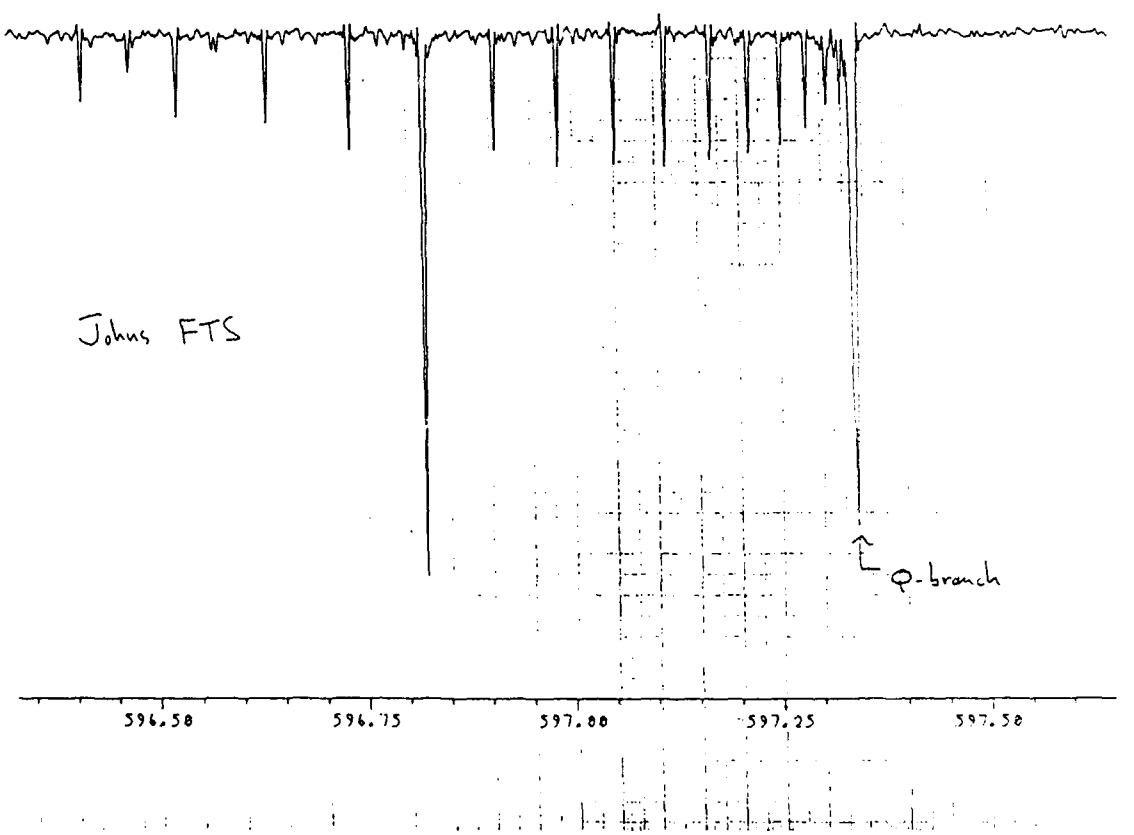
allows $k(\nu)$ to be rewritten

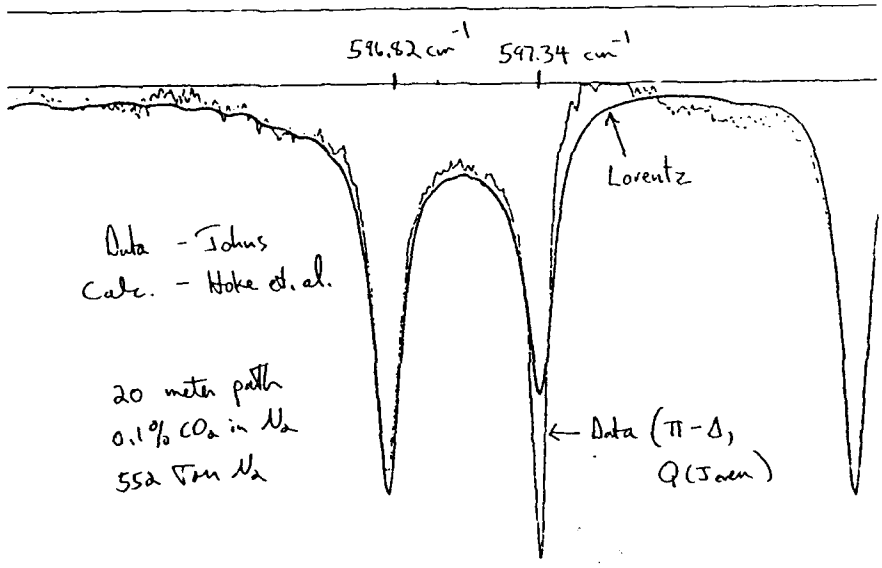
$$k(\nu) = \frac{N}{\pi}\mathrm{IM}\left\{\sum_i \frac{(\mathbf{d}\cdot\mathbf{A})_i(\mathbf{A}^{-1}\cdot\rho\cdot\mathbf{d})_i}{\nu - l_i}\right\}$$

which is an algebraic sum.




100, 360 Torr CO2
Transmission
1
0.9
0.8
0.7
0.6
0.5
0.4
0.3
0.2
0.1
0
791.2
791.3
791.4
791.5
791.6
791.7
791.8
solid=data, dash=360 Torr Lorentz
Frequency (cm-1)


Johns FTS
Q-branch
596.50
596.75
597.00
597.25
597.50



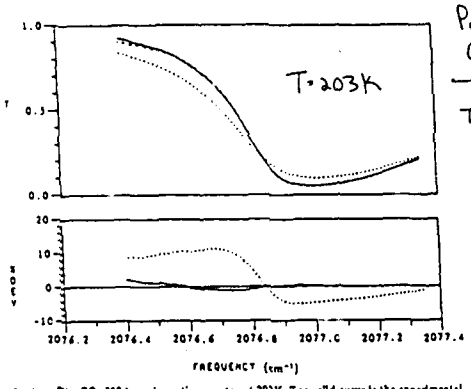


Fig.14a The CO_2 720 torr absorption spectra at 203K. The solid curve is the experimental data taken using the gas cell. The long dashed curve is the mixing calculation. The short dashed curve is the Voigt calculation.

Pure CO_2 / TDL

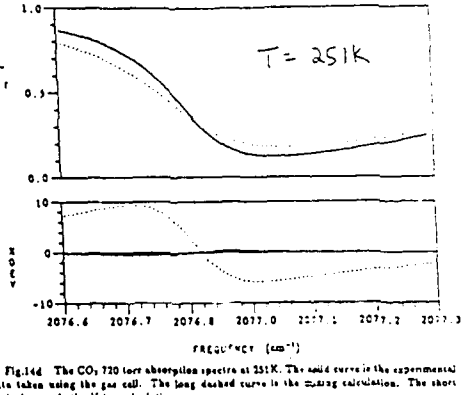


Fig.14d The CO_2 720 torr absorption spectra at 251K. The solid curve is the experimental data taken using the gas cell. The long dashed curve is the mixing calculation. The short dashed curve is the Voigt calculation.

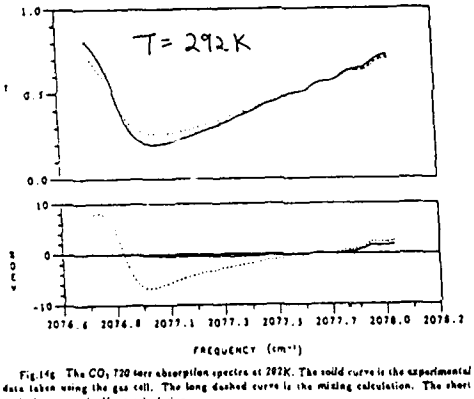


Fig.14g The CO_2 720 torr absorption spectra at 292K. The solid curve is the experimental data taken using the gas cell. The long dashed curve is the mixing calculation. The short dashed curve is the Voigt calculation.

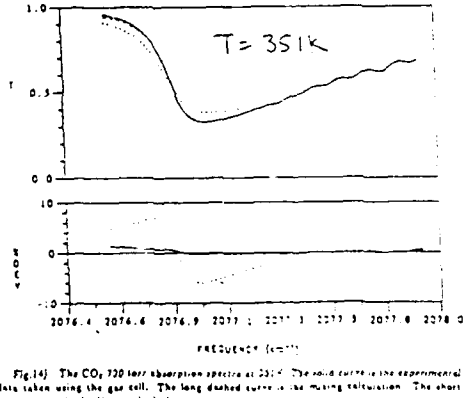
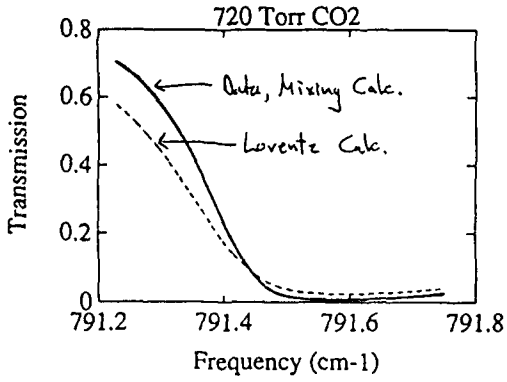
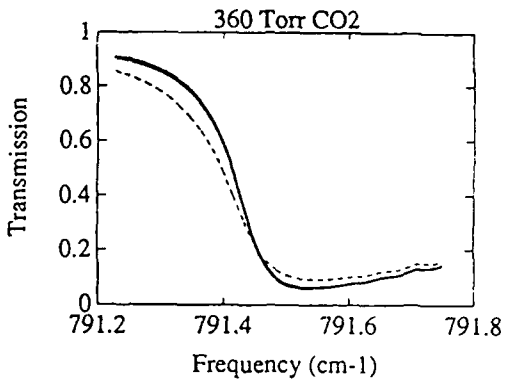
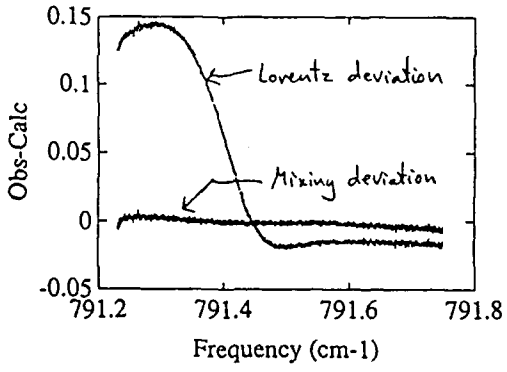
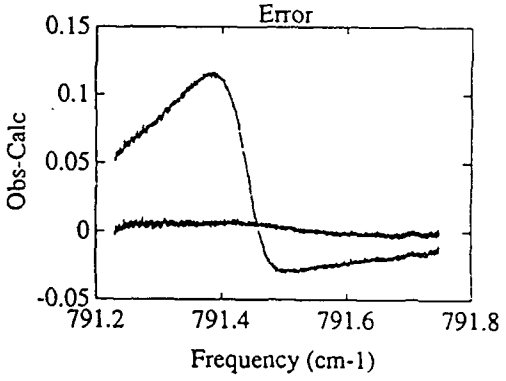


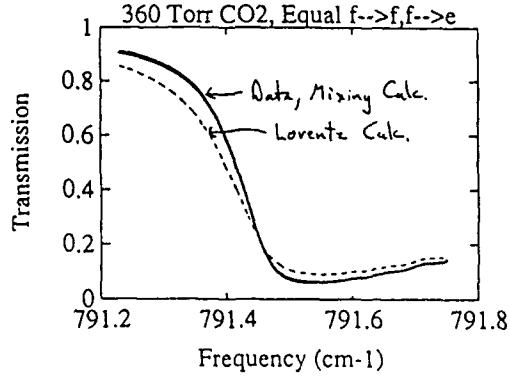
Fig.14j The CO_2 720 torr absorption spectra at 351K. The solid curve is the experimental data taken using the gas cell. The long dashed curve is the mixing calculation. The short dashed curve is the Voigt calculation.

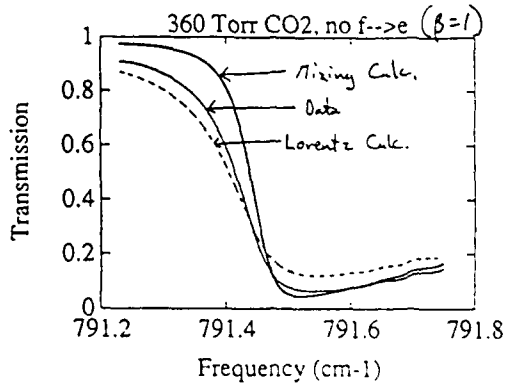

720 Torr CO2
Data, Mixing Calc.
Lorentz Calc.
Transmission
Frequency (cm-1)

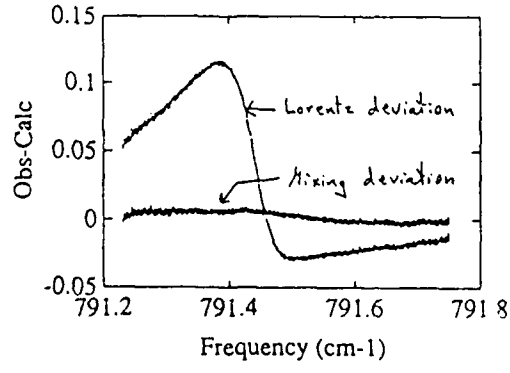

360 Torr CO2
Transmission
Frequency (cm-1)

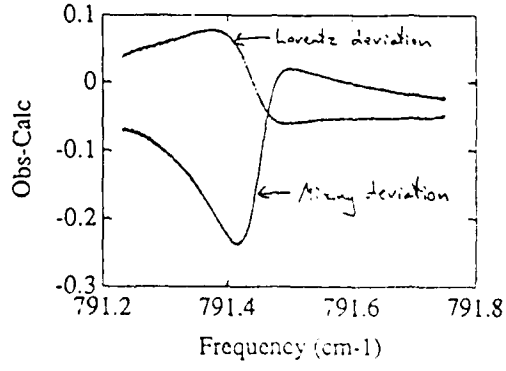

Lorentz deviation
Mixing deviation
Obs-Calc
Frequency (cm-1)

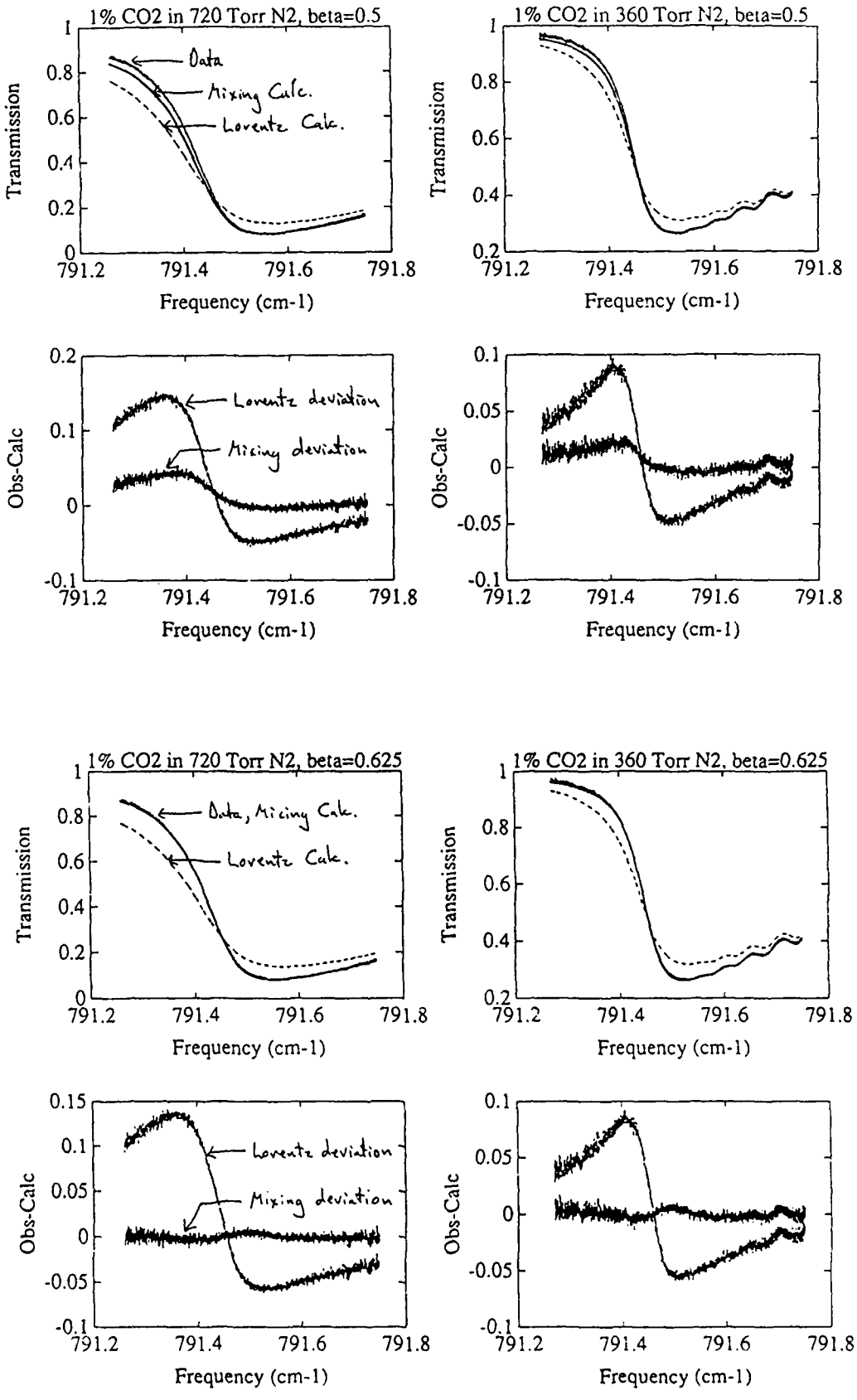

Error
Obs-Calc
Frequency (cm-1)

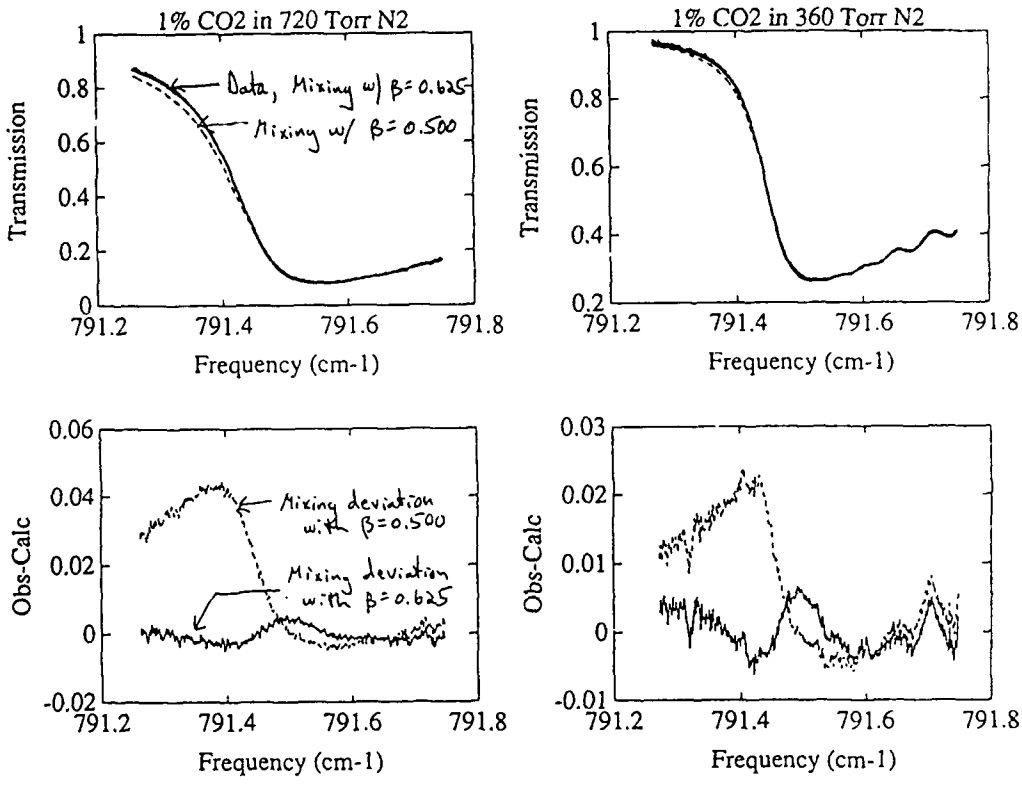

360 Torr CO2, Equal f-->f,f-->e
Data, Mixing Calc.
Lorentz Calc.
Transmission
Frequency (cm-1)

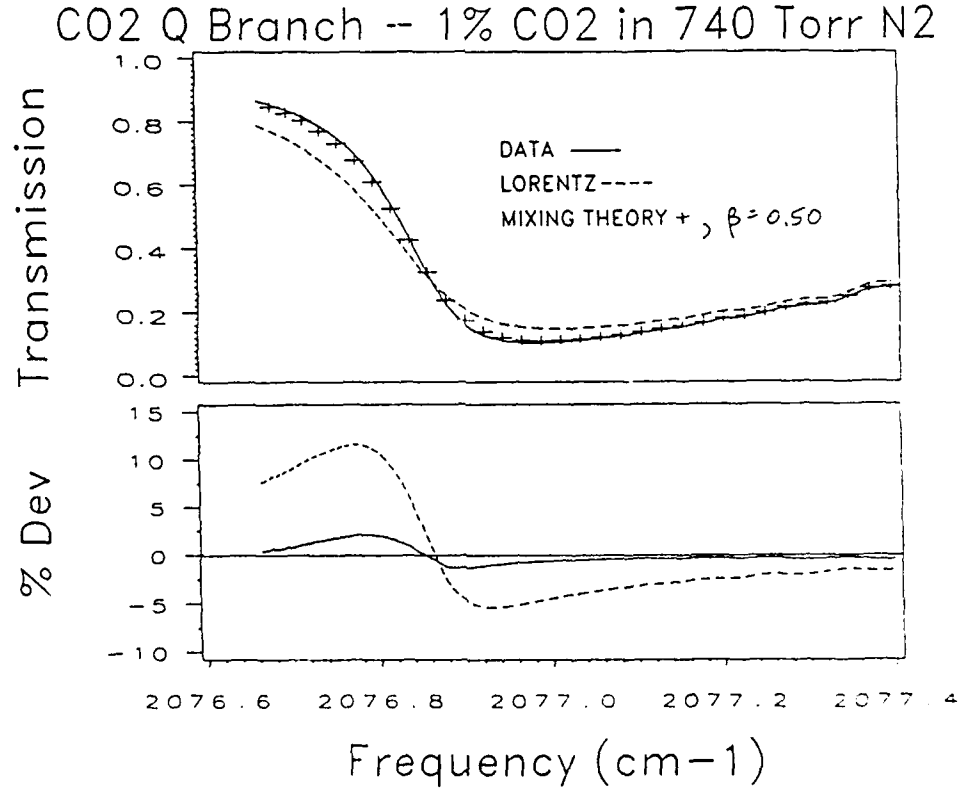

360 Torr CO2, no f-->e (β=1)
Mixing Calc.
Data
Lorentz Calc.
Transmission
Frequency (cm-1)

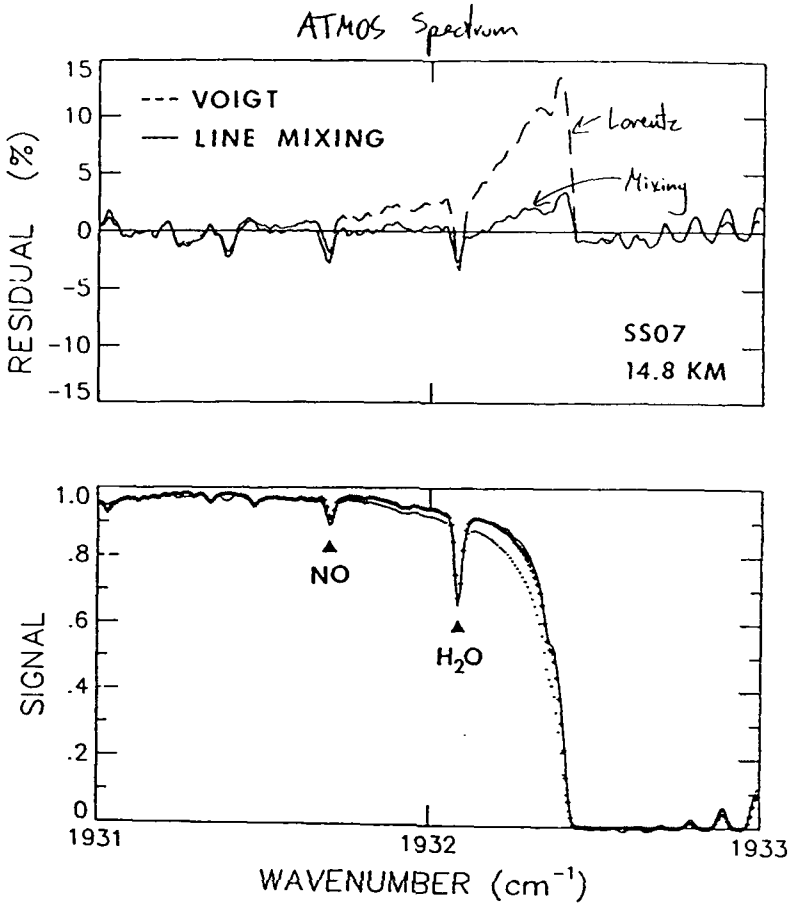

Lorentz deviation
Mixing deviation
Obs-Calc
Frequency (cm-1)

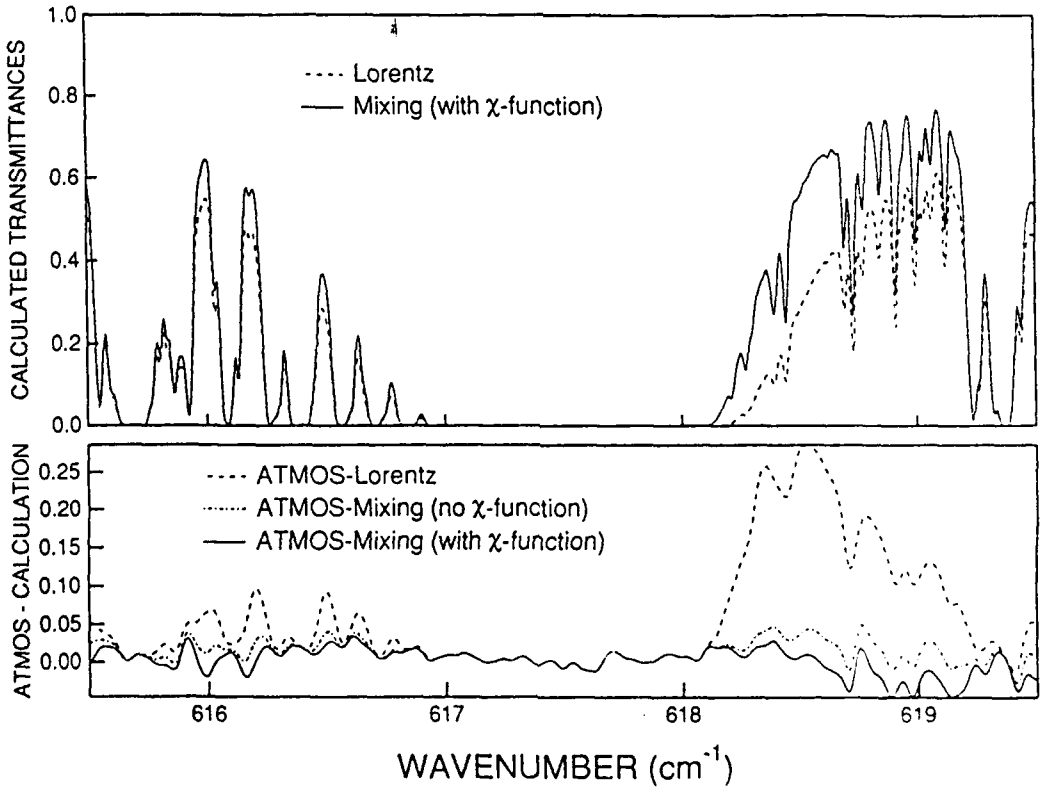

Lorentz deviation
Mixing deviation
Obs-Calc
Frequency (cm-1)

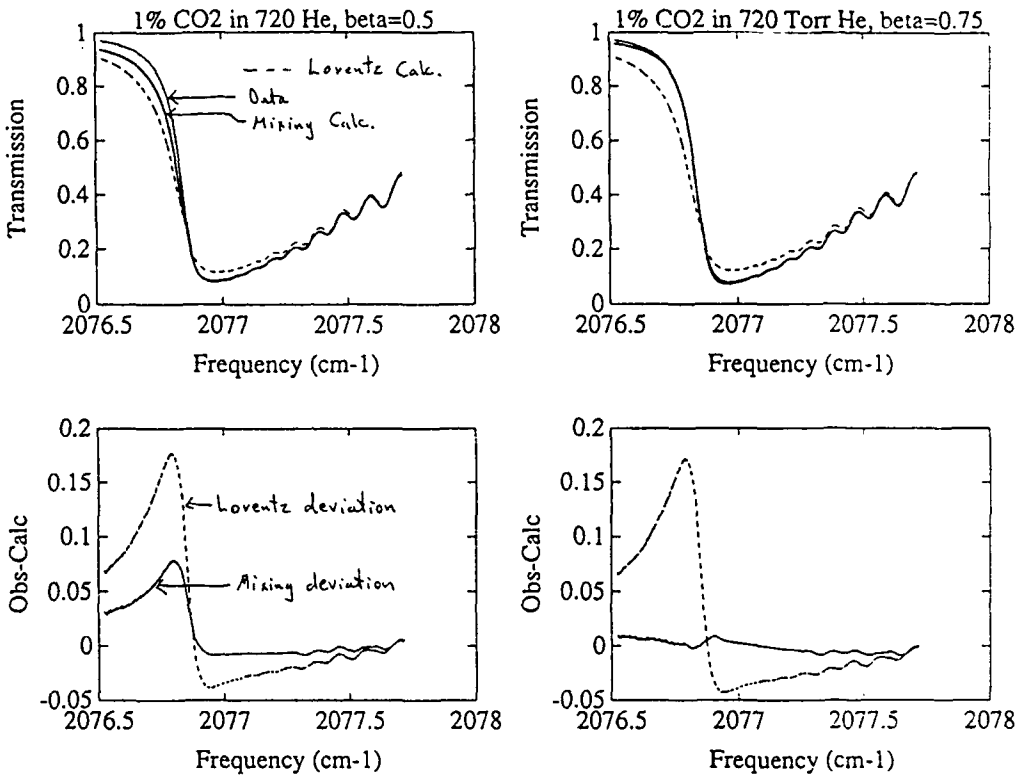

1% CO2 in 720 Torr N2, beta=0.5
Data
Mixing Calc.
Lorentz Calc.
Transmission
Frequency (cm-1)
1% CO2 in 360 Torr N2, beta=0.5
Transmission
Frequency (cm-1)
Lorentz deviation
Mixing deviation
Obs-Calc
Frequency (cm-1)
Obs-Calc
Frequency (cm-1)
1% CO2 in 720 Torr N2, beta=0.625
Data, Mixing Calc.
Lorentz Calc.
Transmission
Frequency (cm-1)
1% CO2 in 360 Torr N2, beta=0.625
Transmission
Frequency (cm-1)
Lorentz deviation
Mixing deviation
Obs-Calc
Frequency (cm-1)
Obs-Calc
Frequency (cm-1)

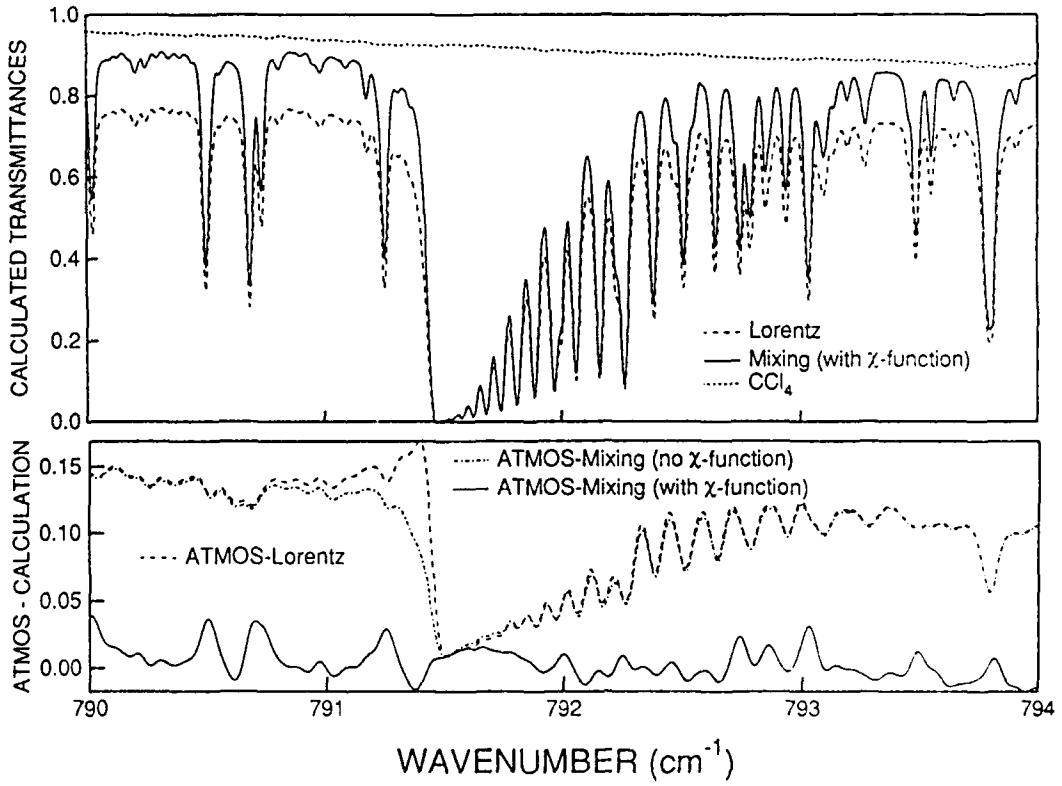

1% CO2 in 720 Torr N2
Data, Mixing w/ β=0.625
Mixing w/ β=0.500
Transmission
Frequency (cm-1)
1% CO2 in 360 Torr N2
Transmission
Frequency (cm-1)
Mixing deviation with β=0.500
Mixing deviation with β=0.625
Obs-Calc
Frequency (cm-1)
Obs-Calc
Frequency (cm-1)

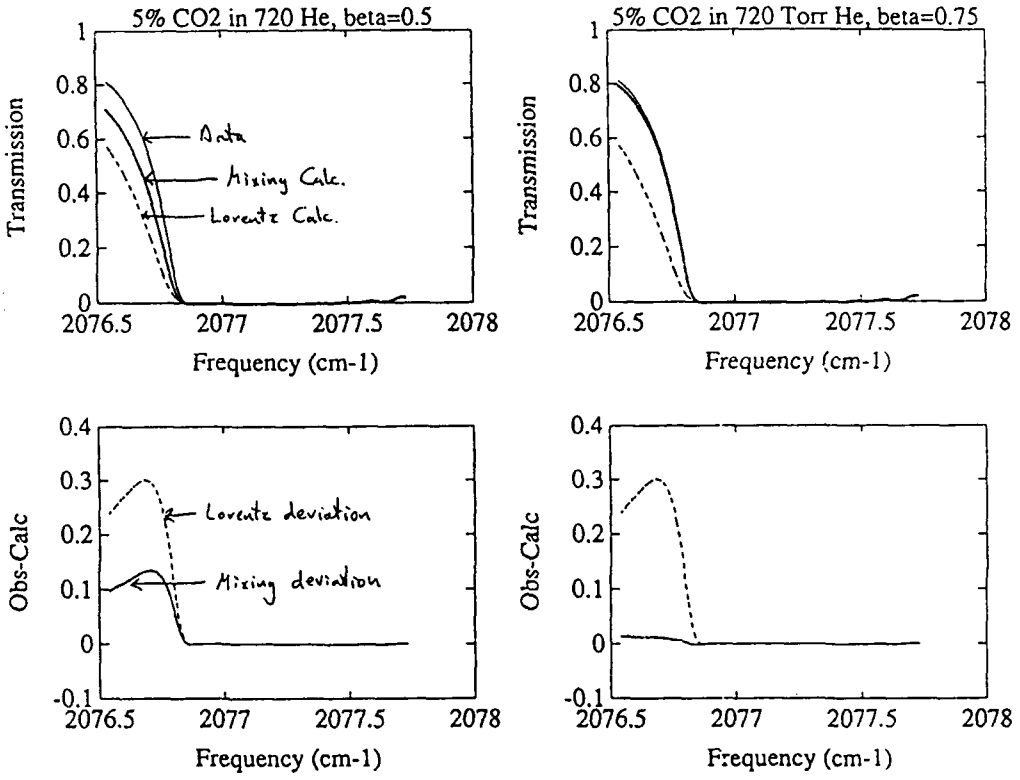

CO2 Q Branch -- 1% CO2 in 740 Torr N2
DATA
LORENTZ----
MIXING THEORY +, β=0.50
Transmission
% Dev
Frequency (cm-1)


ATMOS Spectrum
--- VOIGT
— LINE MIXING
Lorentz
Mixing
RESIDUAL (%)
15
10
5
0
-5
-10
-15
SS07
14.8 KM
1.0
.8
.6
.4
.2
0
SIGNAL
NO
H_2O
1931
1932
1933
WAVENUMBER (cm^{-1})

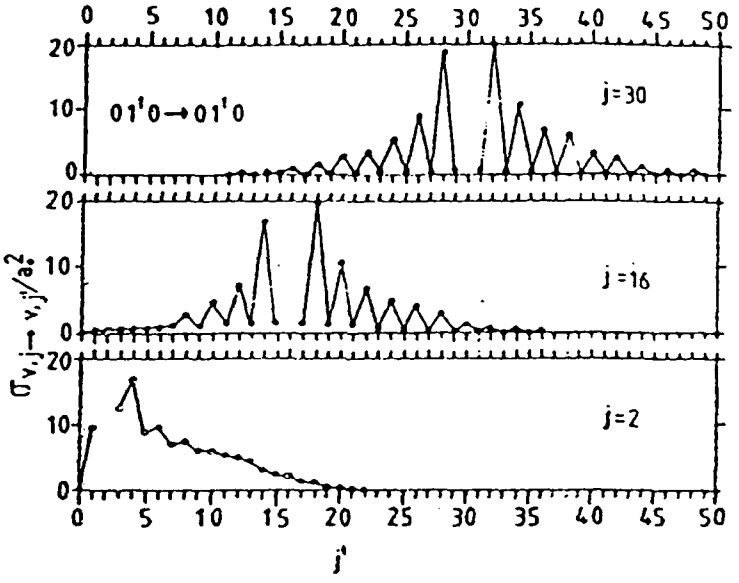

---- Lorentz
— Mixing (with χ-function)
CALCULATED TRANSMITTANCES
1.0
0.8
0.6
0.4
0.2
0.0
---- ATMOS-Lorentz
..... ATMOS-Mixing (no χ-function)
— ATMOS-Mixing (with χ-function)
ATMOS - CALCULATION
0.25
0.20
0.15
0.10
0.05
0.00
616
617
618
619
WAVENUMBER (cm^{-1})

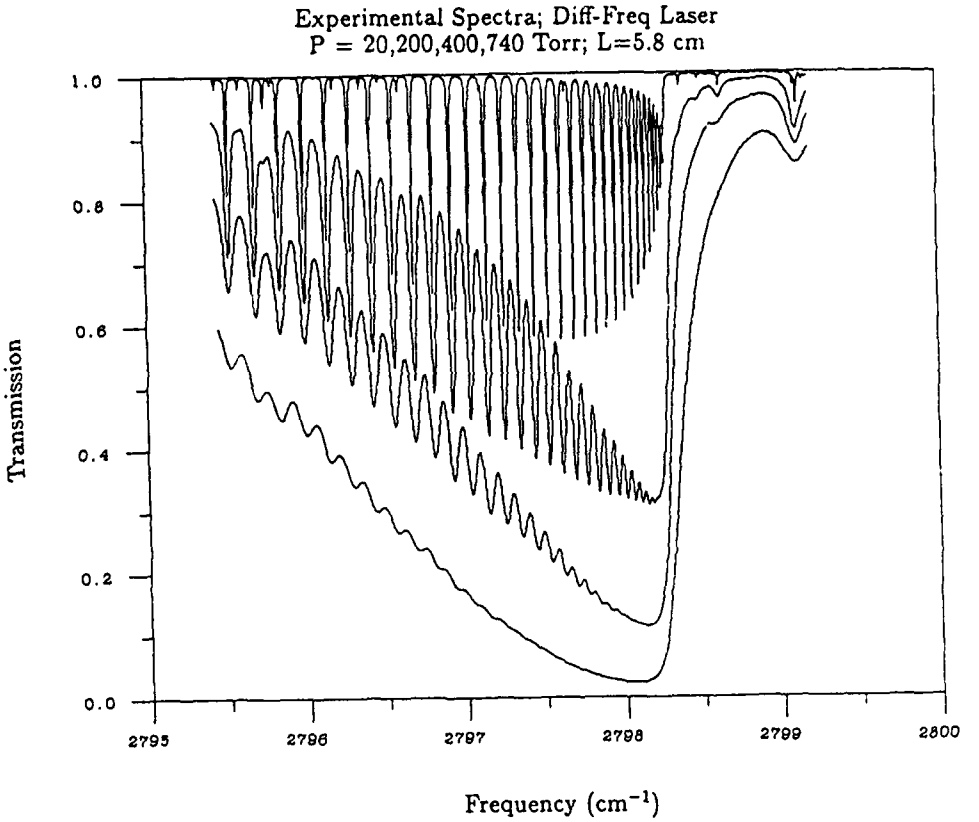

1% CO2 in 720 He, beta=0.5
1% CO2 in 720 Torr He, beta=0.75
Lorentz Calc.
Data
Mixing Calc.
Transmission
Frequency (cm-1)
Lorentz deviation
Mixing deviation
Obs-Calc
2076.5
2077
2077.5
2078

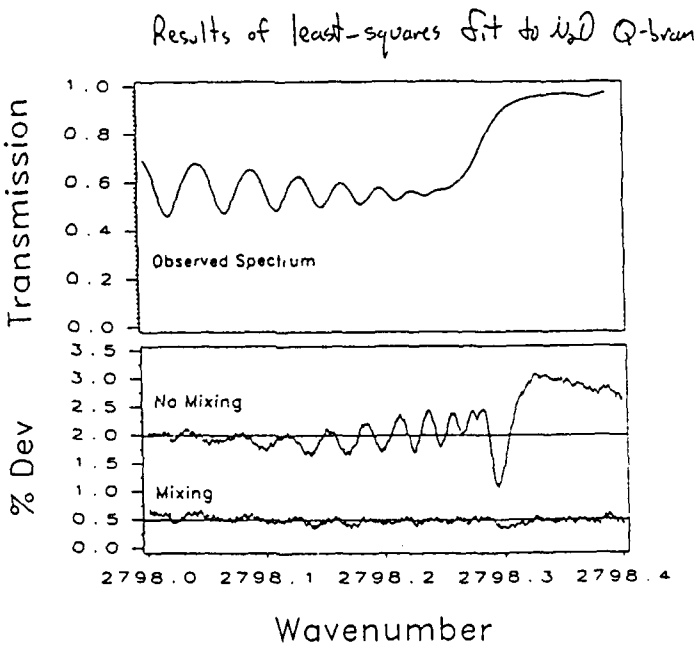

CALCULATED TRANSMITTANCES
Lorentz
Mixing (with χ-function)
CCl4
ATMOS - CALCULATION
ATMOS-Mixing (no χ-function)
ATMOS-Mixing (with χ-function)
ATMOS-Lorentz
790
791
792
793
794
WAVENUMBER (cm-1)

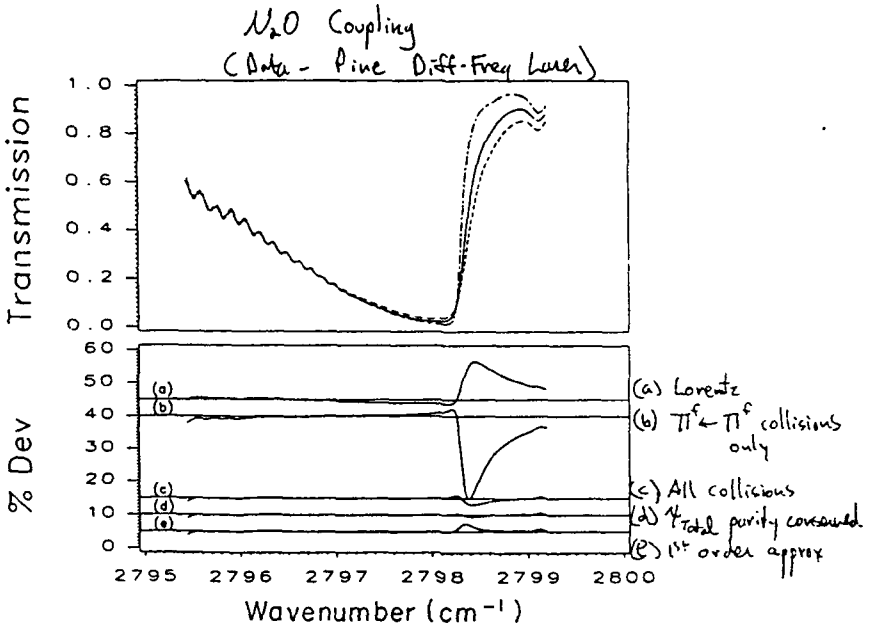


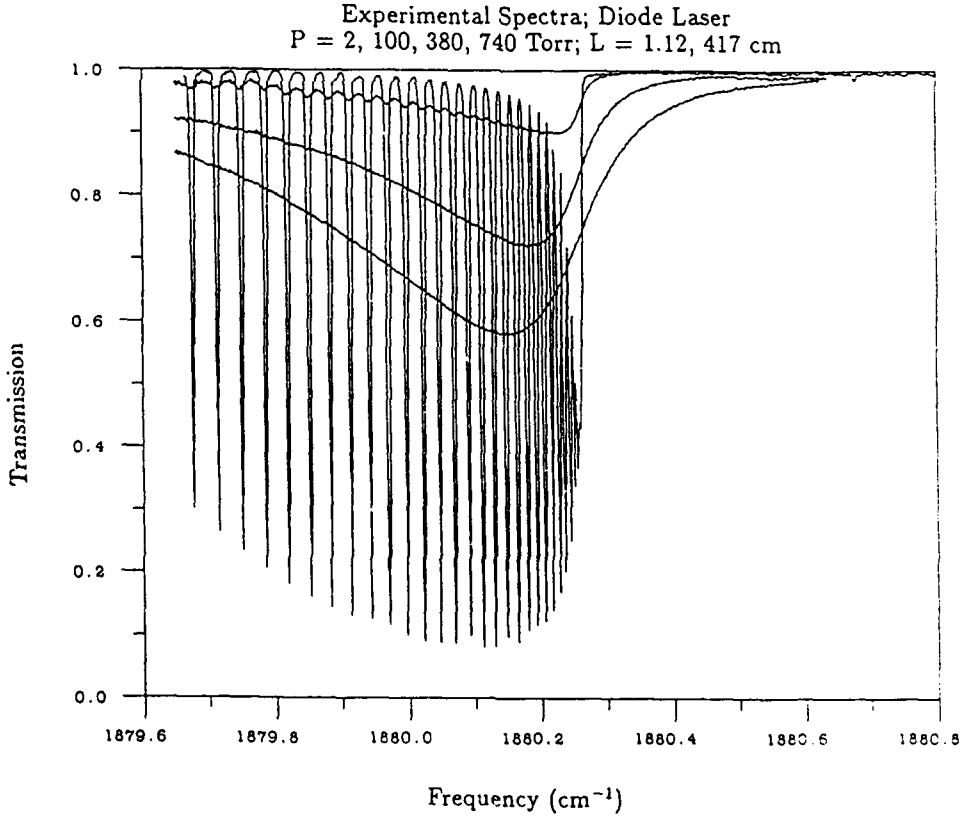
Alexander + Clary, Chem Phys Lett., 96, 319 (1983)

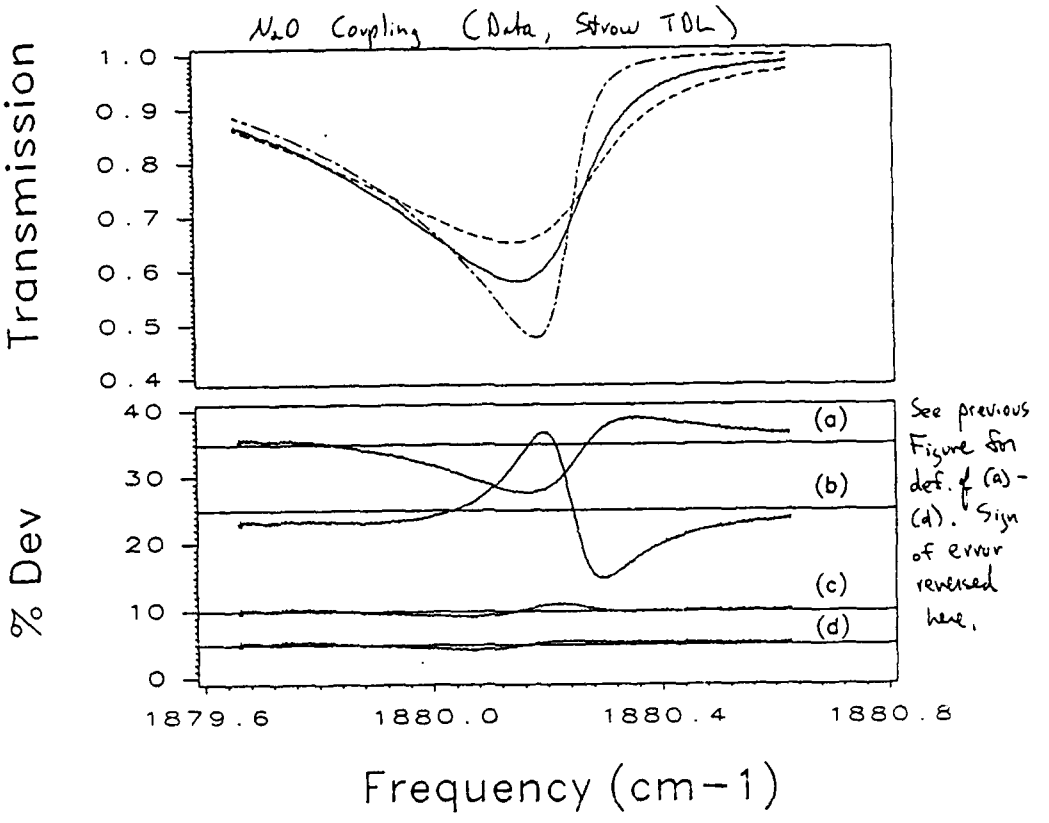


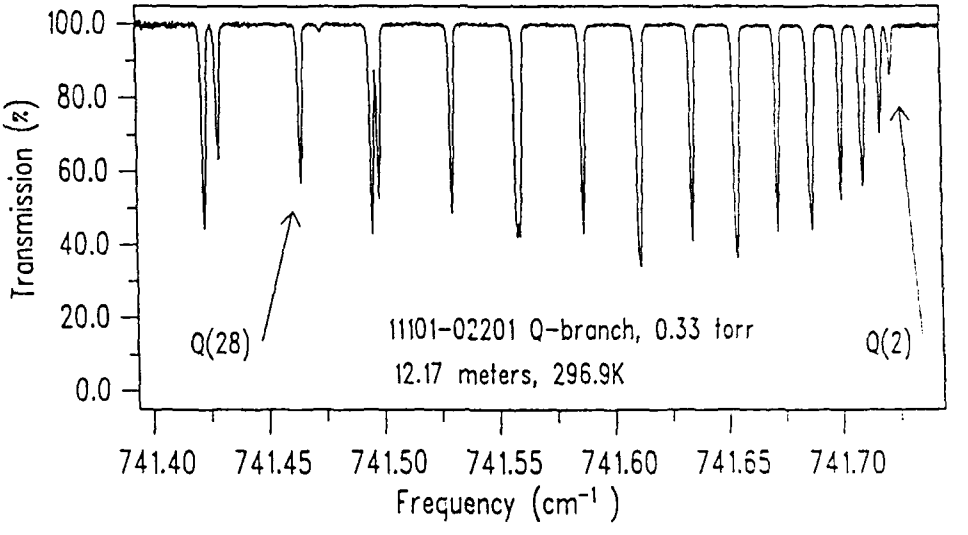

Experimental Spectra; Diff-Freq Laser
P = 20,200,400,740 Torr; L=5.8 cm
Transmission
1.0
0.8
0.6
0.4
0.2
0.0
2795
2796
2797
2798
2799
2800
Frequency (cm^{-1})

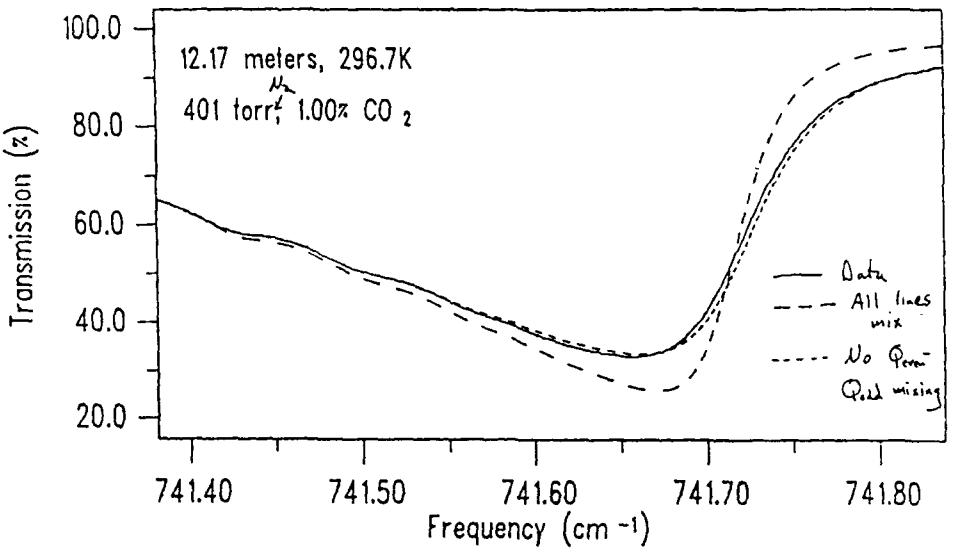

Results of least-squares fit to N_2O Q-branch
Transmission
Observed Spectrum
% Dev
No Mixing
Mixing
2798.0
2798.1
2798.2
2798.3
2798.4
Wavenumber

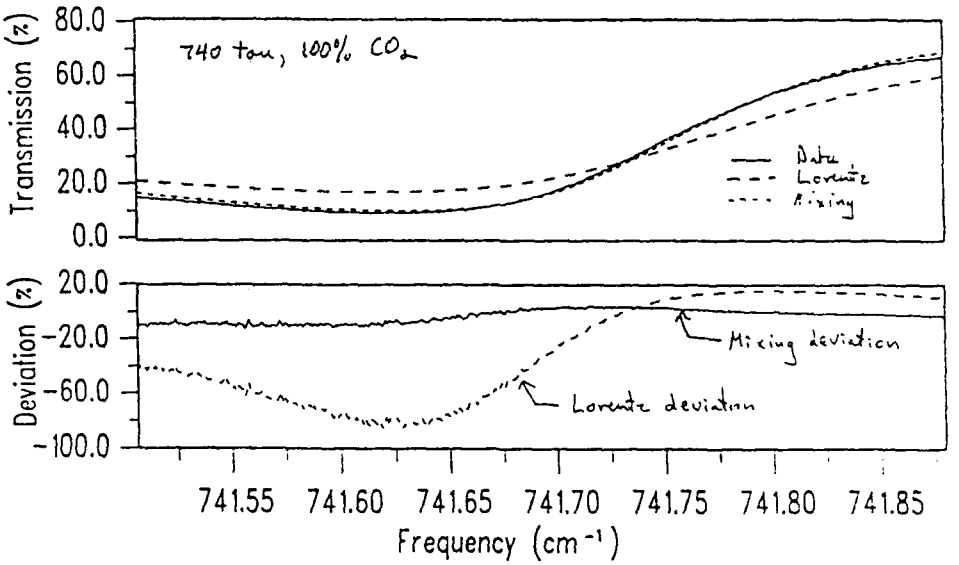

N_2O Coupling
(Data - Pine Diff-Freq Laser)
Transmission
% Dev
(a) Lorentz
(b) $\Pi^f \leftarrow \Pi^f$ collisions only
(c) All collisions
(d) Total parity conserved
(e) 1st order approx
Wavenumber (cm^{-1})


Experimental Spectra; Diode Laser
P = 2, 100, 380, 740 Torr; L = 1.12, 417 cm
Transmission
Frequency (cm^{-1})


N_2O Coupling (Data, Straw TDL)
Transmission
1.0
0.9
0.8
0.7
0.6
0.5
0.4
% Dev
40
30
20
10
0
(a)
(b)
(c)
(d)
See previous Figure for def. of (a)-(d). Sign of error reversed here.
1879.6
1880.0
1880.4
1880.8
Frequency (cm-1)


Transmission (%)
100.0
80.0
60.0
40.0
20.0
0.0
Q(28)
11101-02201 Q-branch, 0.33 torr
12.17 meters, 296.9K
Q(2)
741.40
741.45
741.50
741.55
741.60
741.65
741.70
Frequency (cm-1)


12.17 meters, 296.7K
401 torr, 1.00% CO 2
Transmission (%)
100.0
80.0
60.0
40.0
20.0
741.40
741.50
741.60
741.70
741.80
Frequency (cm -1)
Data
All lines mix
No Q mix


740 torr, 100% CO2
Transmission (%)
80.0
60.0
40.0
20.0
0.0
Data
Lorentz
Mixing
Deviation (%)
20.0
-20.0
-60.0
-100.0
Mixing deviation
Lorentz deviation
741.55
741.60
741.65
741.70
741.75
741.80
741.85
Frequency (cm -1)

Line Coupling in the ν_3 Bandhead of CO_2 at 4.3 μm

- Line coupling accounts for much of the sub-Lorentz absorption in the bandhead region which is used for temperature sounding
- Duration-of-collision effects may also be important inside the bandhead
- Trade-offs between high-J behavior of rotational relaxation (is the scaling law any good at high J?) and the duration-of-collision parameter give good results for room-temperature spectra of pure CO_2

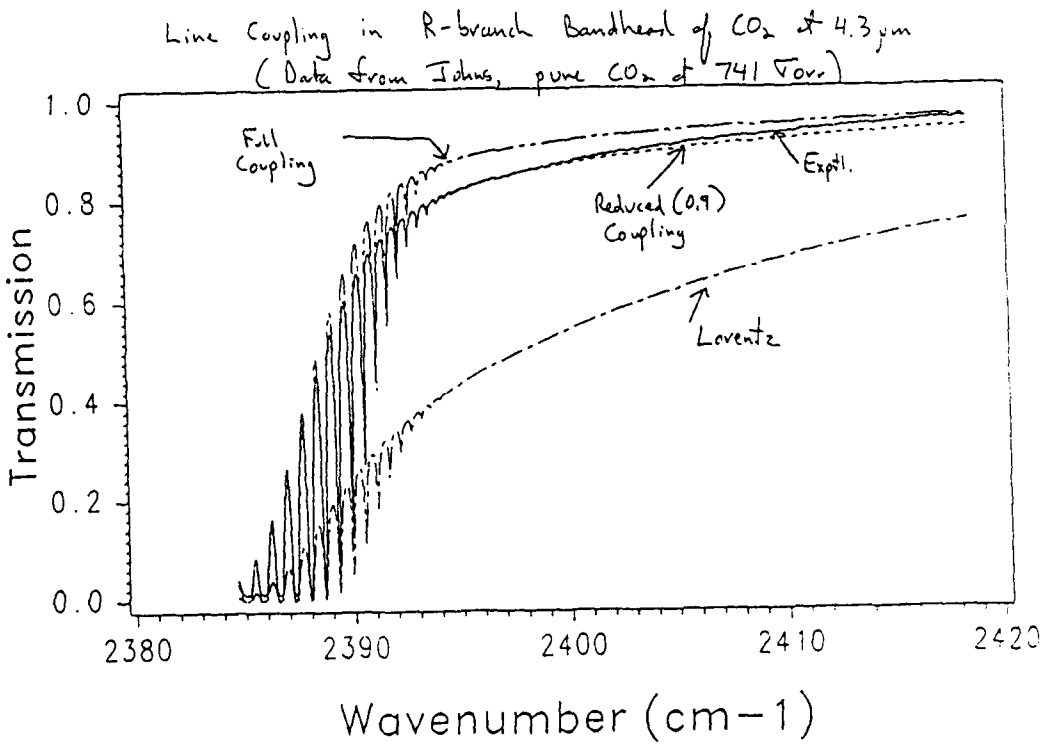
We use a semi-empirical lineshape in this region

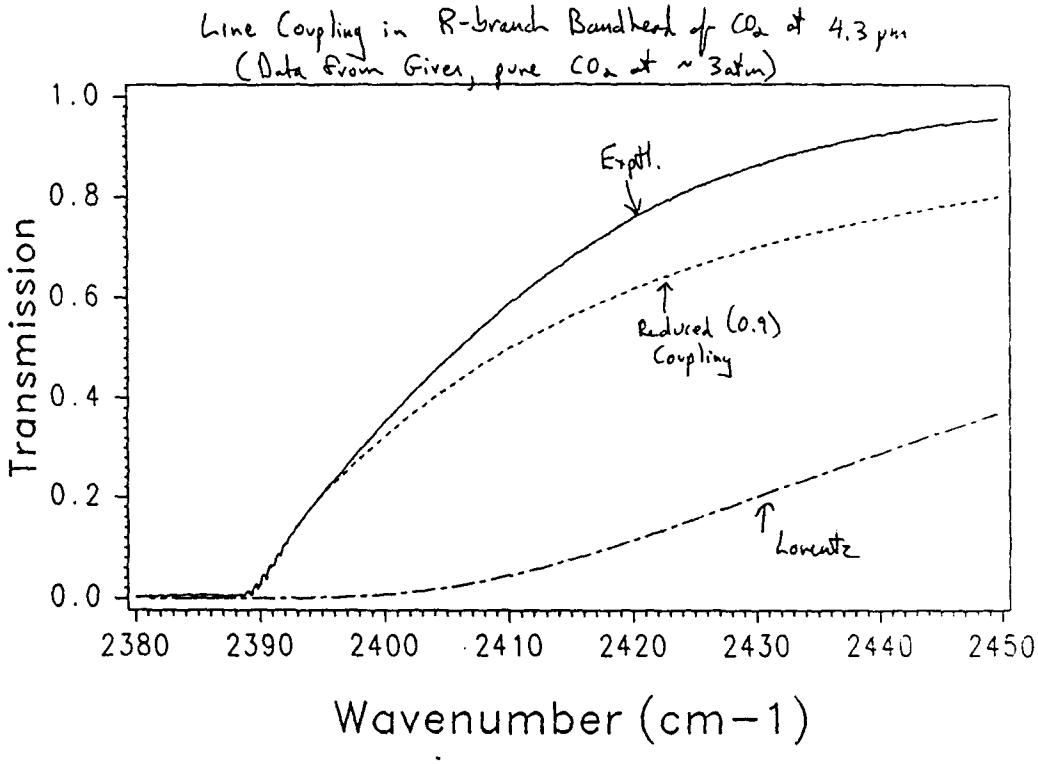
$$k(\nu)_{empirical} = k_{mixing}(\nu) * \chi(\Delta\nu), \quad \Delta\nu_i = \nu - \nu_i.$$

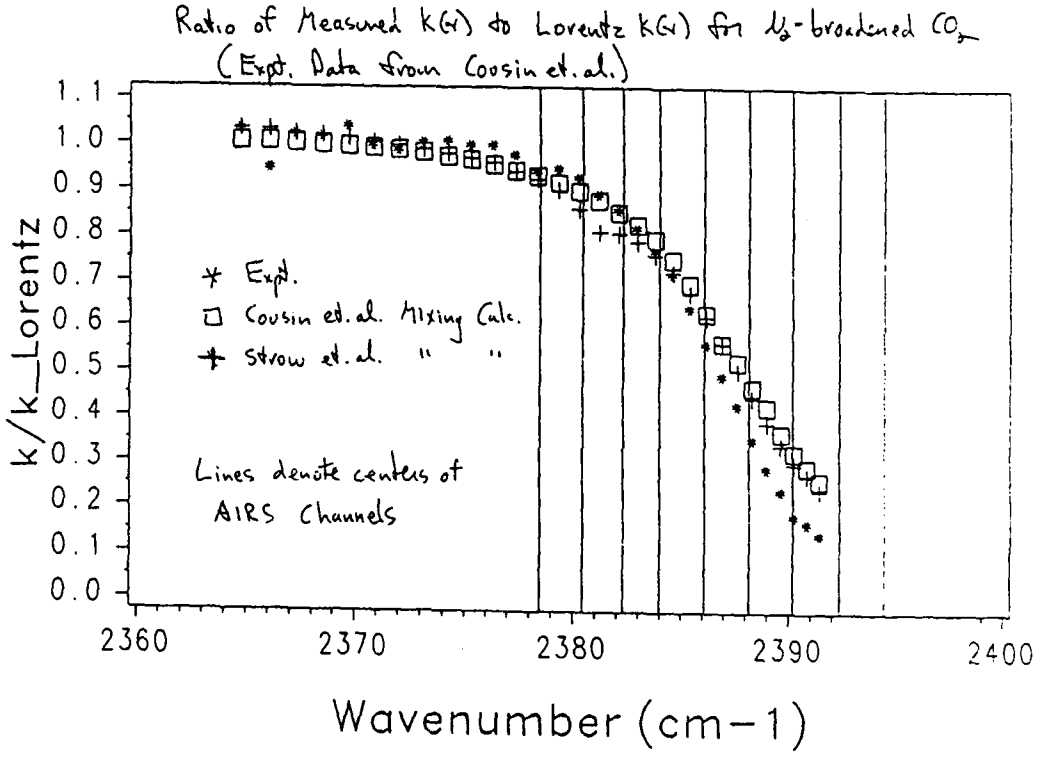
$$\chi_i = z_i K_1(z_i) exp(\tau_2 \alpha_{L_i} + \tau_o \Delta\nu_i),$$

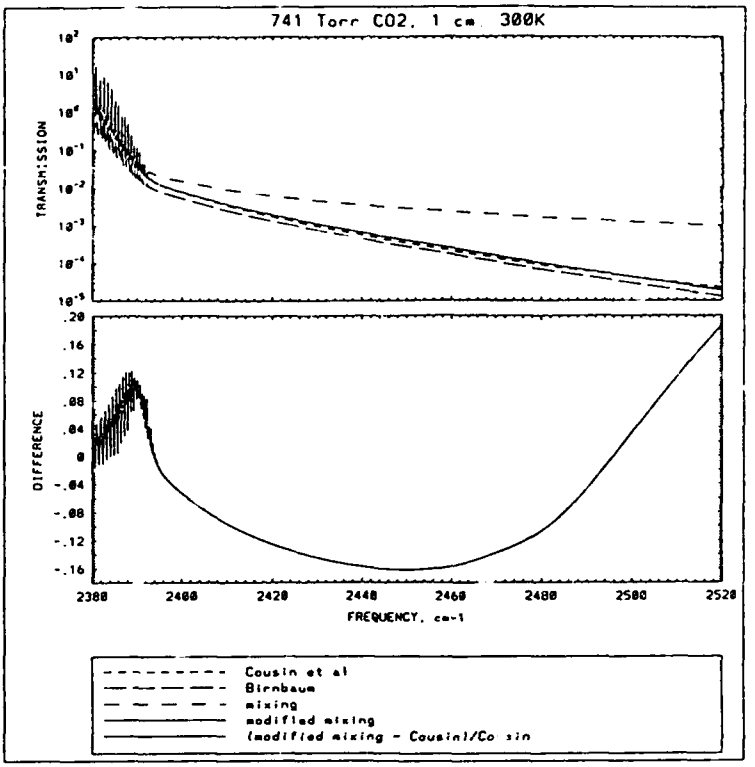
where

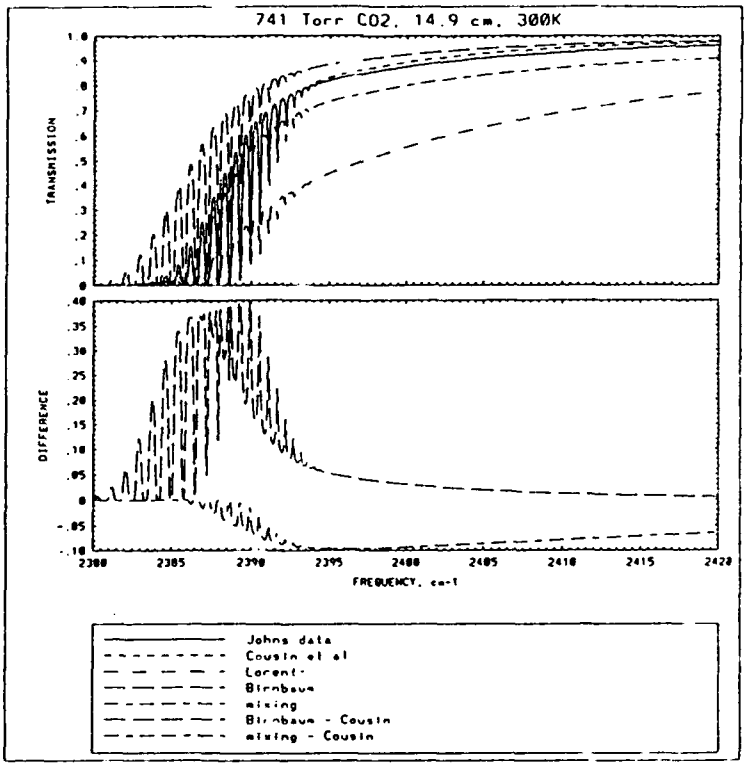
$$z_i = \sqrt{(\alpha_{L_i}^2 + \Delta\nu_i^2)(\tau_o^2 + \tau_2^2)}, \quad \tau_o = \frac{0.72}{T}, \quad \tau_2 \sim 0.0275.$$

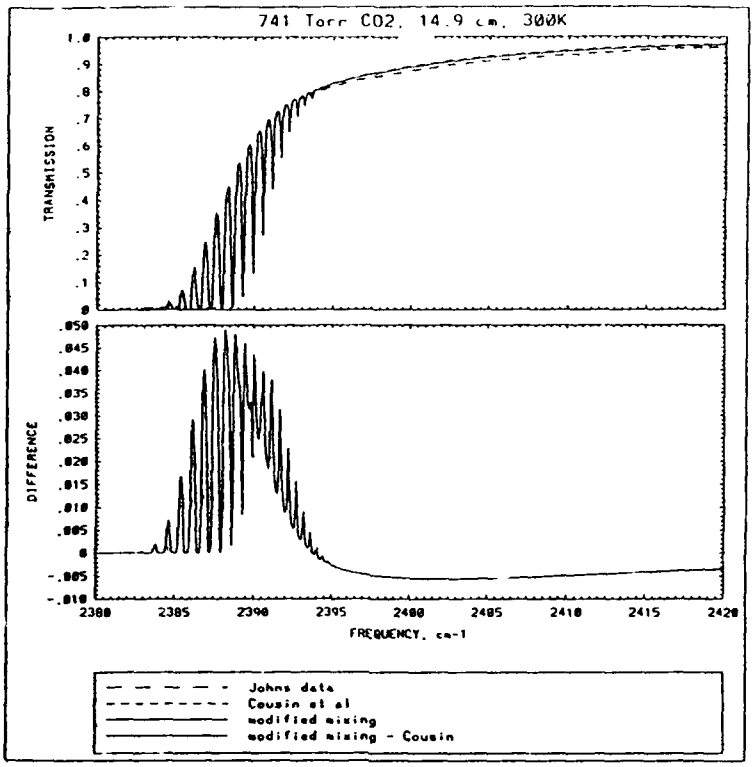



Line Coupling in R-branch Bandhead of CO_2 at 4.3 μm
(Data from Giver, pure CO_2 at ~3atm)
Transmission
1.0
0.8
0.6
0.4
0.2
0.0
Expt.
Reduced (0.9) Coupling
Lorentz
2380
2390
2400
2410
2420
2430
2440
2450
Wavenumber (cm−1)


Ratio of Measured k(ν) to Lorentz k(ν) for N_2-broadened CO_2
(Expt. Data from Cousin et. al.)
k/k_Lorentz
1.1
1.0
0.9
0.8
0.7
0.6
0.5
0.4
0.3
0.2
0.1
0.0
* Expt.
□ Cousin et. al. Mixing Calc.
+ Strow et. al. " "
Lines denote centers of AIRS Channels
2360
2370
2380
2390
2400
Wavenumber (cm−1)


741 Torr CO2, 1 cm, 300K
TRANSMISSION
DIFFERENCE
FREQUENCY, cm-1
Cousin et al
Birnbaum
mixing
modified mixing
(modified mixing - Cousin)/Co sin


741 Torr CO2, 14.9 cm, 300K
TRANSMISSION
DIFFERENCE
FREQUENCY, cm-1
Johns data
Cousin et al
Lorent-
Birnbaum
mixing
Birnbaum - Cousin
mixing - Cousin



Conclusions

- CO_2–N_2 calculations predict less coupling than observed indicating some propensity to conserve vibrational angular momentum, this propensity is more pronounced for CO_2-He collisions
- CO_2 self-broadening models also very accurate over a wide temperature range
- Line coupling models sufficiently accurate for Q-branches important for CLAES, AIRS, HIS retrievals
- Atmospheric measurements (ATMOS, HIS) indicate that temperature dependence of line coupling is in relatively good shape for air–broadening
- More parameters needed to model Π-Δ Q-branches at 740 and 797 cm^{-1}?
- One N_2-broadened N_2O study shows good agreement using self-broadened collision model ($\beta = 0.50$), some further work warranted on other bands, and with O_2–broadening
- Good progress made with R–branch coupling at 4.3 μm. Further work with N_2–broadening, low temperature, high–resolution spectra required for AIRS temperature sounder which operates inside the R–branch

LINE-MIXING: A NEAR AND FAR LINE WING PROBLEM

J.-M. Hartmann
Laboratoire E.M2.C., de CNRS (UPR288) et de l'Ecole Centrale Paris,
Grand voie des vignes, 92295 Chatenay-Malabry Cedex, France

Line mixing is a problem of crucial importance for modeling of gas absorption spectra. For this reason, much experimental and theoretical studies have been made in the infrared and Raman domains. In particular, absorption in Q-branches and troughs between lines of P and R-branches, which are affected by line-interferences at moderate densities have been widely investigated. Various models have been proposed for the modeling of such phenomenon, which are generally based on the impact approximation. Studies of absorption at elevated density and in the very far wings of lines have demonstrated that these models can be very inaccurate. Other approaches, which account for the finite collision duration, have been proposed quite recently which lead to satisfactory results.

The author will try to present a comprehensive revue of experimental and theoretical results connected with the influence of line-mixing on absorption spectra. The advantages and limits of approaches based on the impact approximation will be discussed. The state of the art and perspectives for measurements and calculations of high density spectra and continuum absorption will be discussed.

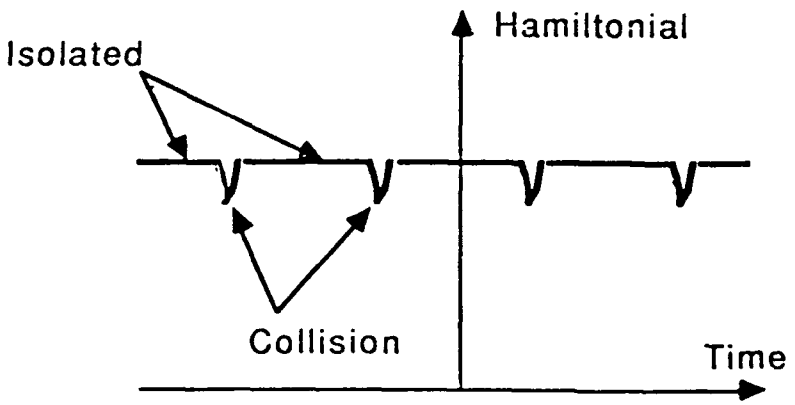
LINE - MIXING : NEAR AND FAR LINE - WING PROBLEMS

Jean-Michel HARTMANN
Laboratoire E.M2.C, Ecole Centrale
France.

- WHAT HAPPENS?
- IMPACT APPROXIMATION
  - MODELLING
  - REMAINING PROBLEMS
- FAR WING

COLLISIONAL BROADENING : WHAT IS HAPPENING

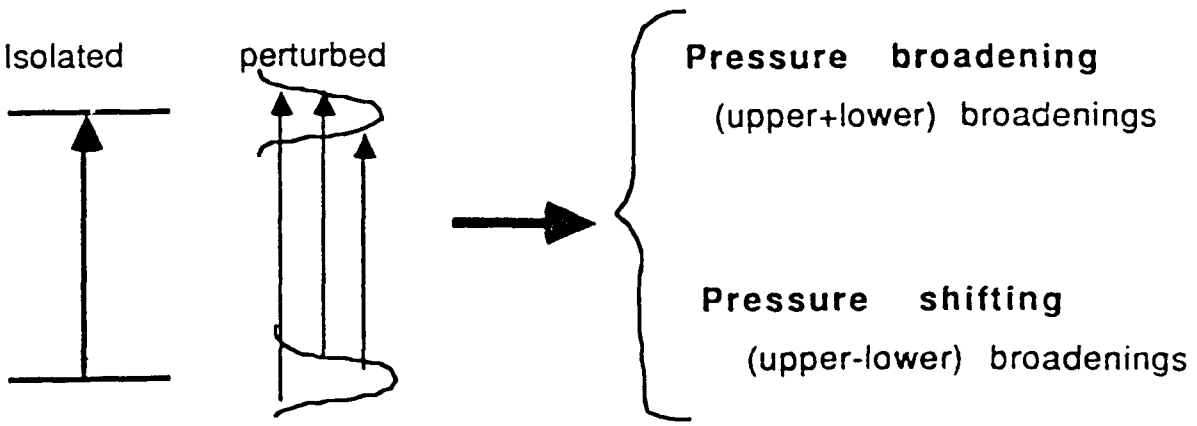
Hamiltonial



The hamiltonian of the isolated molecule is perturbated *during* each collision. The energy levels of the molecule are then modified and functions of time

---

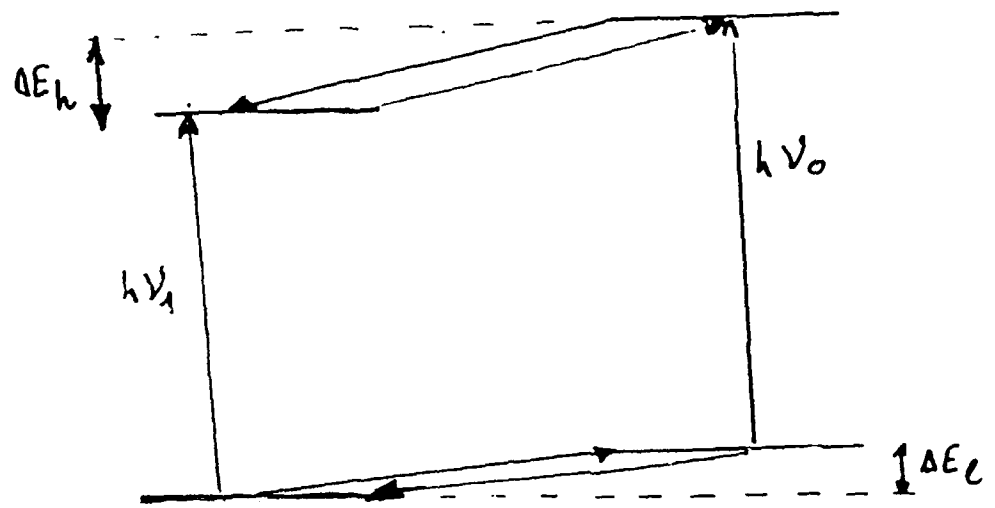
Transitions



All the more important that the interaction potential is large and spread (long range), and that the collision duration is long (low T)

LINE-MIXING : what happens ?

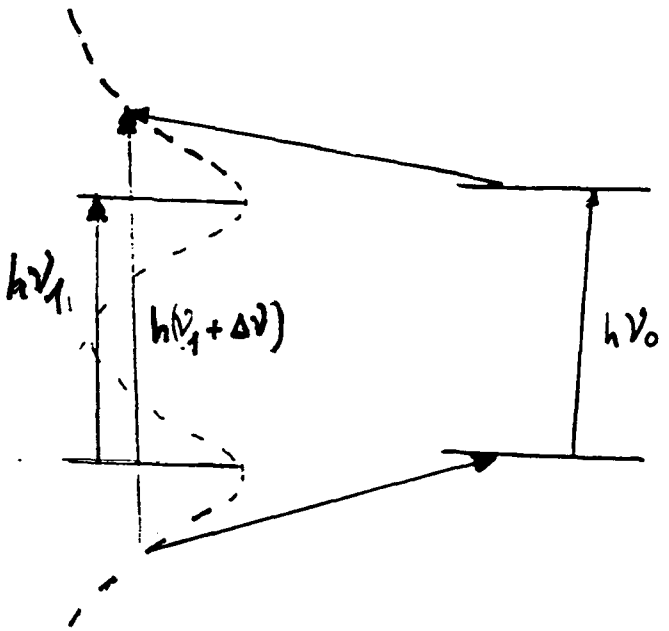
NEAR LINE CENTER



- Energy of collisional process : $|\Delta E| = |\Delta\mathcal{E}_\ell - \Delta\mathcal{E}_h| = h(\nu_1 - \nu_0)$
  → efficient if $\underline{|\nu_0 - \nu_1| \ll \gamma}$
- Dominant process : $\rho_0 \sigma_{0\to1} = \rho_1 \sigma_{1\to0}$
  → if ($\rho_0 > \rho_1$, i.e. $S_0 > S_1$) $\sigma_{1\to0}$ more efficient
  → molecules which are on ν_0 absorb at ν_1
  → intensity taken from weak lines given to strong lines

Conclusion : from line-center to line center
- only if $\gamma \gg |\nu_0 - \nu_1|$ (→ large pressure)
- only if ≠ populations on the levels (low T)
- from weak to strong lines

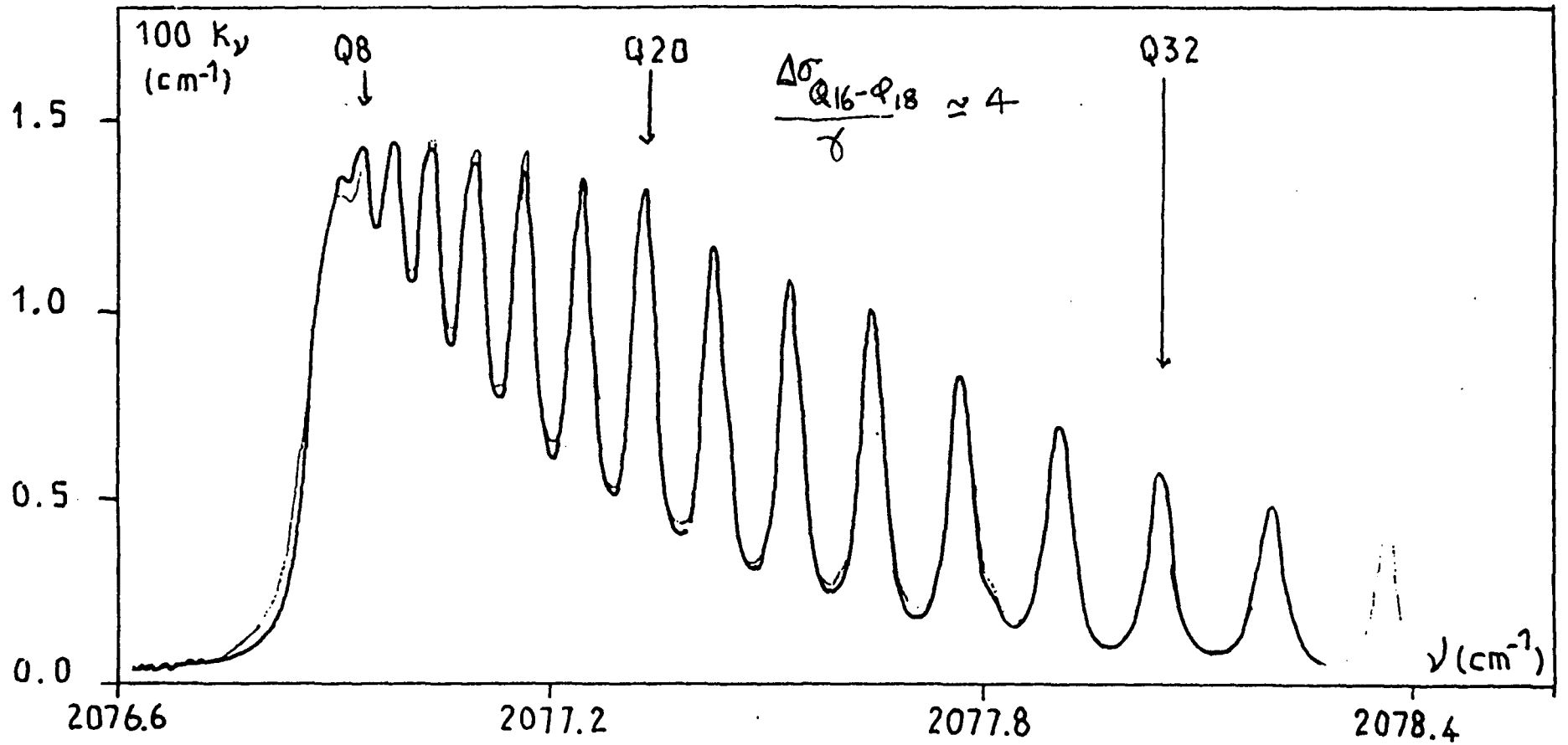
χ IN THE WINGS



- Energy $|\Delta E| = |h(\nu_0 - \nu_1 + \Delta\nu)|$
- efficiency : when $|\nu_0 - \nu_1| << \Delta\nu$
  the jump is $\Delta\nu$ → as efficient as the broadening up to $\Delta\nu$

→ Take intensity in the wings to give to line centers

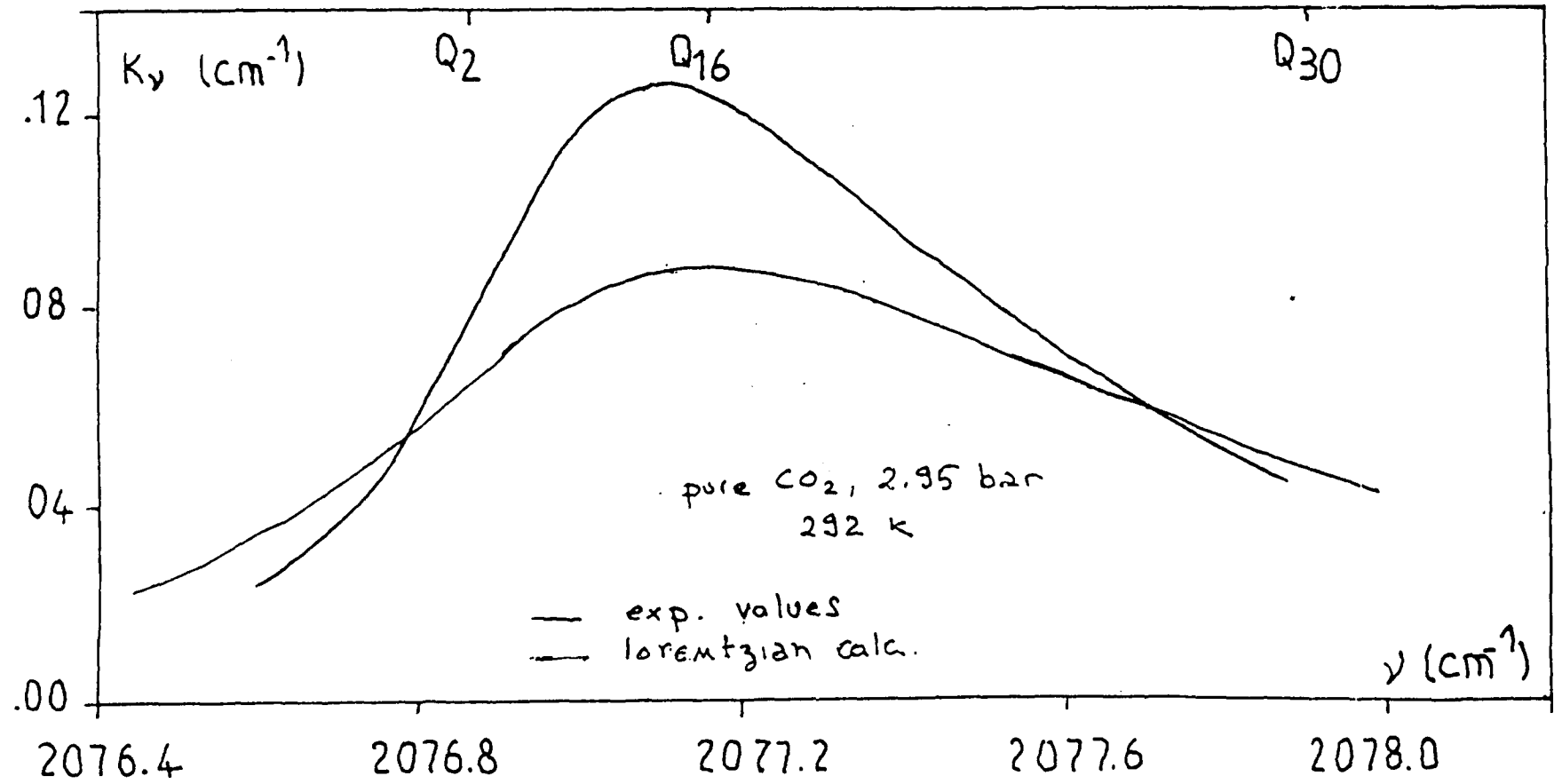
- absorption will go to zero in far wing



pure CO_2, 0.2 bar, 293 K, Q branch of $(11^10)_I \leftarrow (00^00)$

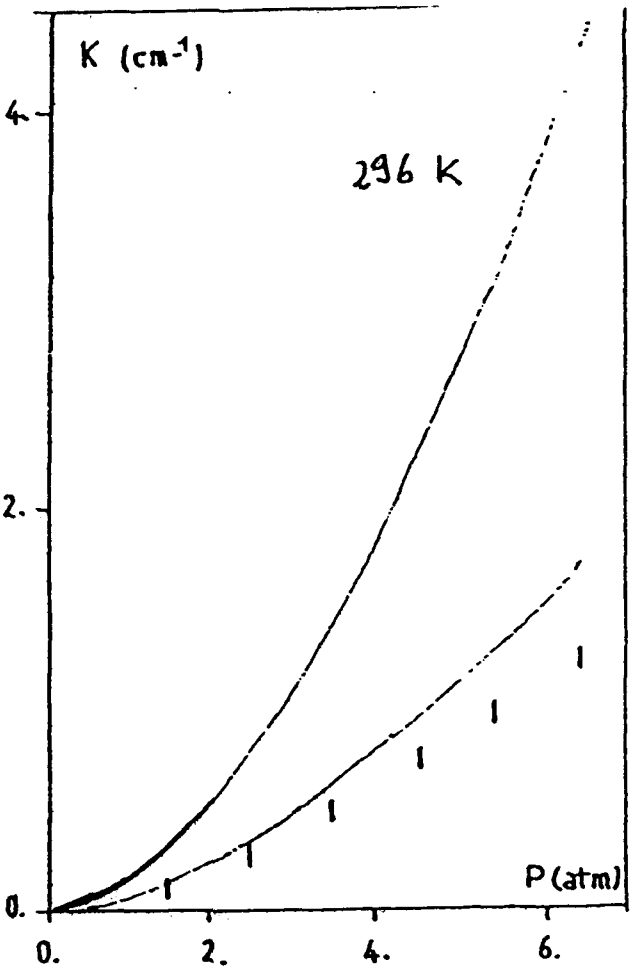
— exp. values
—·· lorentzian calculation

Hartmann et al. 1988

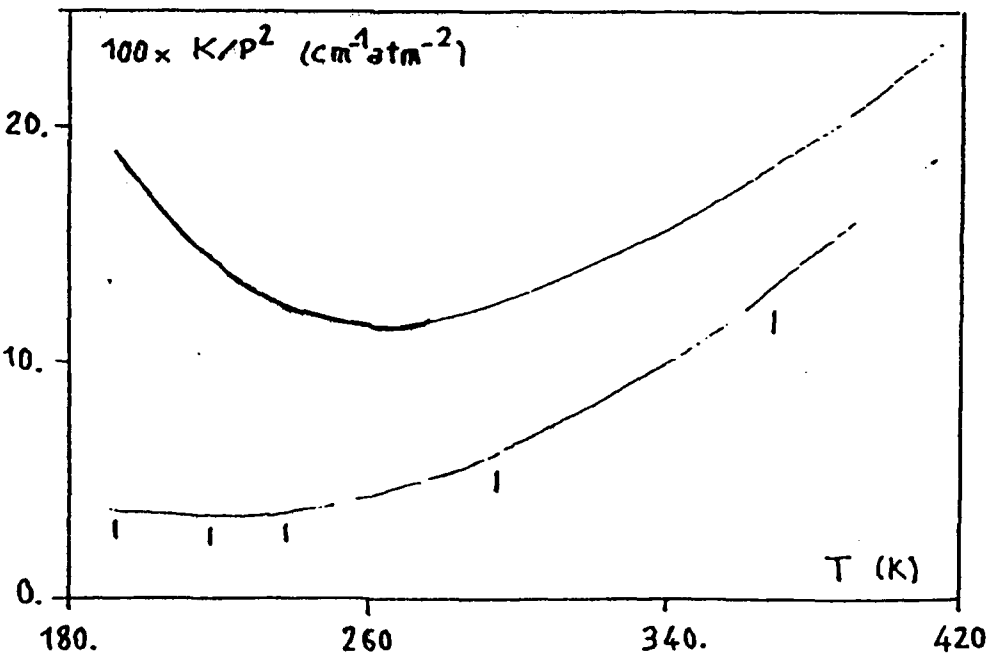


Similar results in N_2O, CO_2 Hartmann et al. 1988

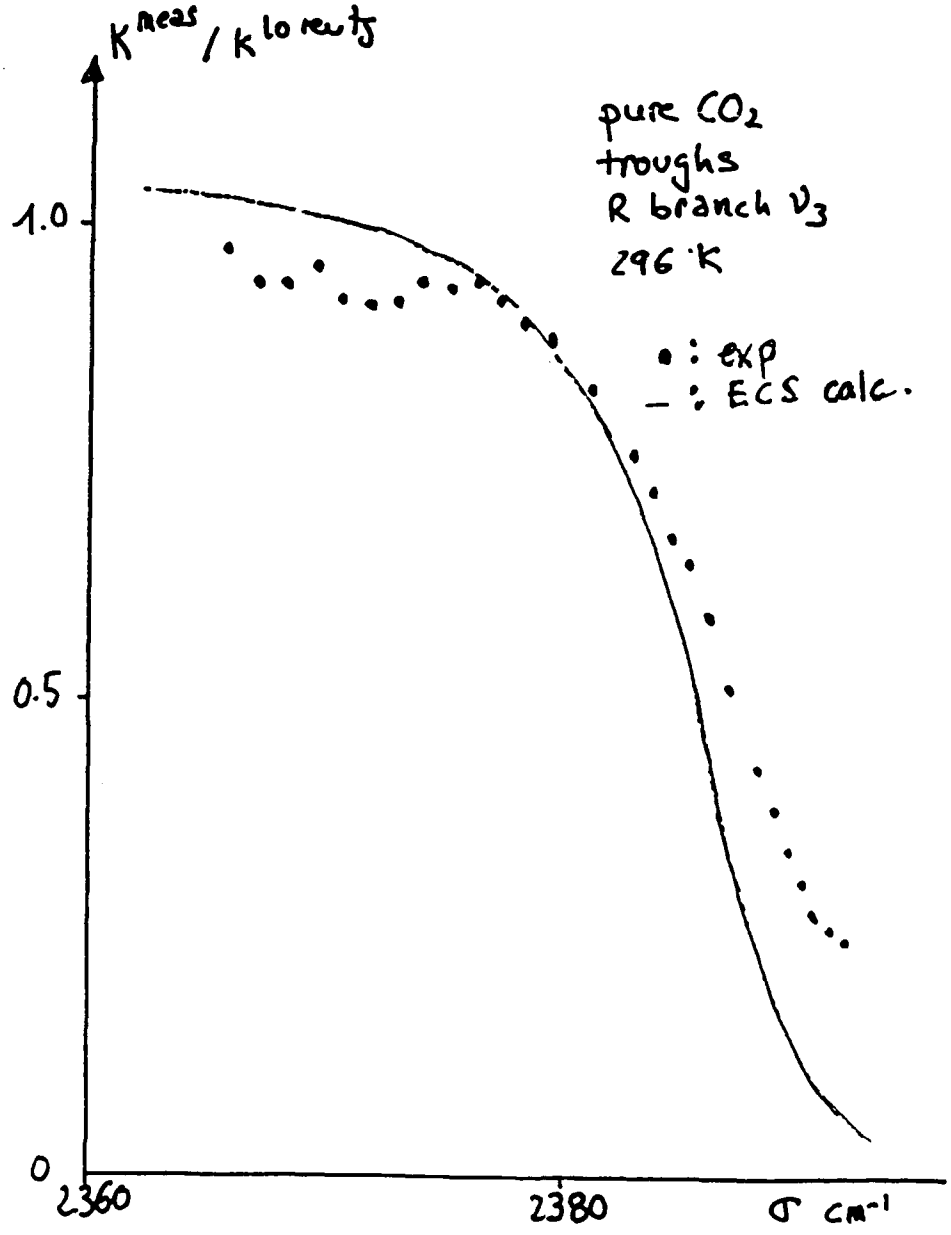
strow et al. Margottin et al.



I : experimental
— : Lorentzian calculation
-- : EGL fitting low line-mixing calculation.



Trough Between R_{66} - R_{68} CO_2 lines CO_2 - N_2



C. Boulet et al.

Similar results for CO, N_2O ....

Bubarin et al.

$$\alpha(\sigma) = \frac{8\pi^3\sigma}{3h\pi c} N_a \sum_{if} [\rho_i - \rho_f] d_{if} \frac{\sinh[hc\sigma/2kT]}{\sinh[hc\sigma_{if}/2kT]}$$

$$\times \left\{ \sum_{i'f'} d_{i'f'} \, Im\left[\langle\langle if \| [\tilde{\sigma} - \tilde{\sigma}_{lines} - i N_a \tilde{W}(\sigma)]^{-1} \| i'f' \rangle\rangle \right\} \right]$$

$\tilde{W}$: relaxation operator - All the influence of collisions.

- $\underline{2\pi c |\sigma - \sigma_{if}| \tau_c \ll 1} \rightarrow \tilde{W}$ indépendant de σ
  (Impact approximation)

- $\tilde{W}$ diagonal → Lorentz shape
  $\langle\langle if \| \tilde{W} \| if \rangle\rangle = \gamma_{if} - i\Delta_{if}$

- In Raman (isotropic)

$$\sum_{i'f' \neq if} \langle\langle if \| \tilde{W} \| i'f' \rangle\rangle = - \langle\langle if \| \tilde{W} \| if \rangle\rangle$$

- In infrared (within IOSA)

$$\sum_{i'f' \neq if} \frac{d_{i'f'}}{d_{if}} \langle\langle if | \tilde{W} | i'f' \rangle\rangle = \langle\langle if | \tilde{W} | if \rangle\rangle$$

LINE MIXING MODELS

W(= :)

Statistically based **FITTING LAWS**

$$\ll if \| W(0) \| i'f' \gg_{if \neq i'f'} = F(i,i')$$

Exponential Gap Law $= \rho_{i'} \cdot \exp\left[-\alpha |E_i - E_{i'}|\right]$

Polynomial Energy Gap Law $= \rho_{i'} \left(\sum_k \alpha_k |E_i - E_{i'}|^{-k} \right)$

Isotropic Raman Sum Rule

$$\sum_{i'f' \neq if} \ll if \| W(0) \| i'f' \gg = - \ll if | W(0) | if \gg$$

Widely used in Raman (Greenhalgh, Hall, Rosasco, Robert, Bonamy, ...)

in IR (Strow, Gentry, Lacome, Boulet, Hargottin-Macloux, ...)

Dynamically based **SCALING LAWS** (De Pristo, Rabitz, 1979)
(IOS, ECS)

$$\langle if | W(0) | i'f' \rangle \propto \sum_L \underbrace{F(i,i',f,f',L)}_{\substack{\text{Angular momenta} \\ \text{Energy corrections} \\ \text{Detailed Balance}}} \sigma_{0 \to L}$$

Direct calculation (IOS, CS, CC) (Green, Boulet 1989)

Inversion from broadening (De Pristo, Rabitz Bonamy, Robert 1989

More accurate than fitting laws. Correct J dependence (interbranch mixing)

MODELS within the IMPACT APPROX

Absorption coefficients

$$K_\nu^{LC}(T,P) = \mathrm{Im}\{P\,(8\pi^2\nu)/(3hc)\,[1-\exp(-h\nu/kT)]\sum_{IF}\rho_I(T)\,d_{IF} \times \Big[\sum_{I'F'} d_{I'F'}\,\langle IF|(\nu-\nu_{IF}-iP\mathbf{W}(T))^{-1}|I'F'\rangle\Big]\}$$

W(T) : relaxation operator. Contains all the influence of collisions. Relation with line-broadening:

$$\langle IF|W(T)|IF\rangle = \gamma_{IF}(T) - i\Delta_{IF}(T)]$$

No line-mixings--> W diagonal --> lorentzian shape.

$$K_\nu^{LR}(T,P) = \sum_{IF}[PS_{IF}(T)][P\gamma_{IF}(T)]/\{\pi[[\nu-\nu_{IF}-P\Delta_{IF}(T)]^2 + [P\,\gamma_{IF}(T)]^2]\}$$

Problem : Model the off-diagonal elements of W

Fitting laws

$$\langle IF|W(T)|I'F'\rangle = f(a_1,a_2,..,a_n,I,I') \qquad (I\neq I')$$

Exponential Gap Law) : ρ_I, a $\exp(-b|E_I-E_{I'}|)$

parameters deduced from isotropic Raman sum rule :

$$\sum \langle IF|W(T)|I'F'\rangle = -\langle IF|W(T)|IF\rangle$$

Scaling relations (Energy Corrected Sudden Approximation).

$$(j_i'j_f'|W^{ECS}|j_ij_f) = -(Nv/2\pi c)\,A(j_i,j_i')\,A(j_f,j_f')\exp[(E_{ji}-E_{ji>})/kT]\sum_{L\neq 0}\{F_1(j_i'j_f'|j_ij_f|L00)\,A(L,0)^{-2}\,(2L+1)\,\sigma_{OL}$$

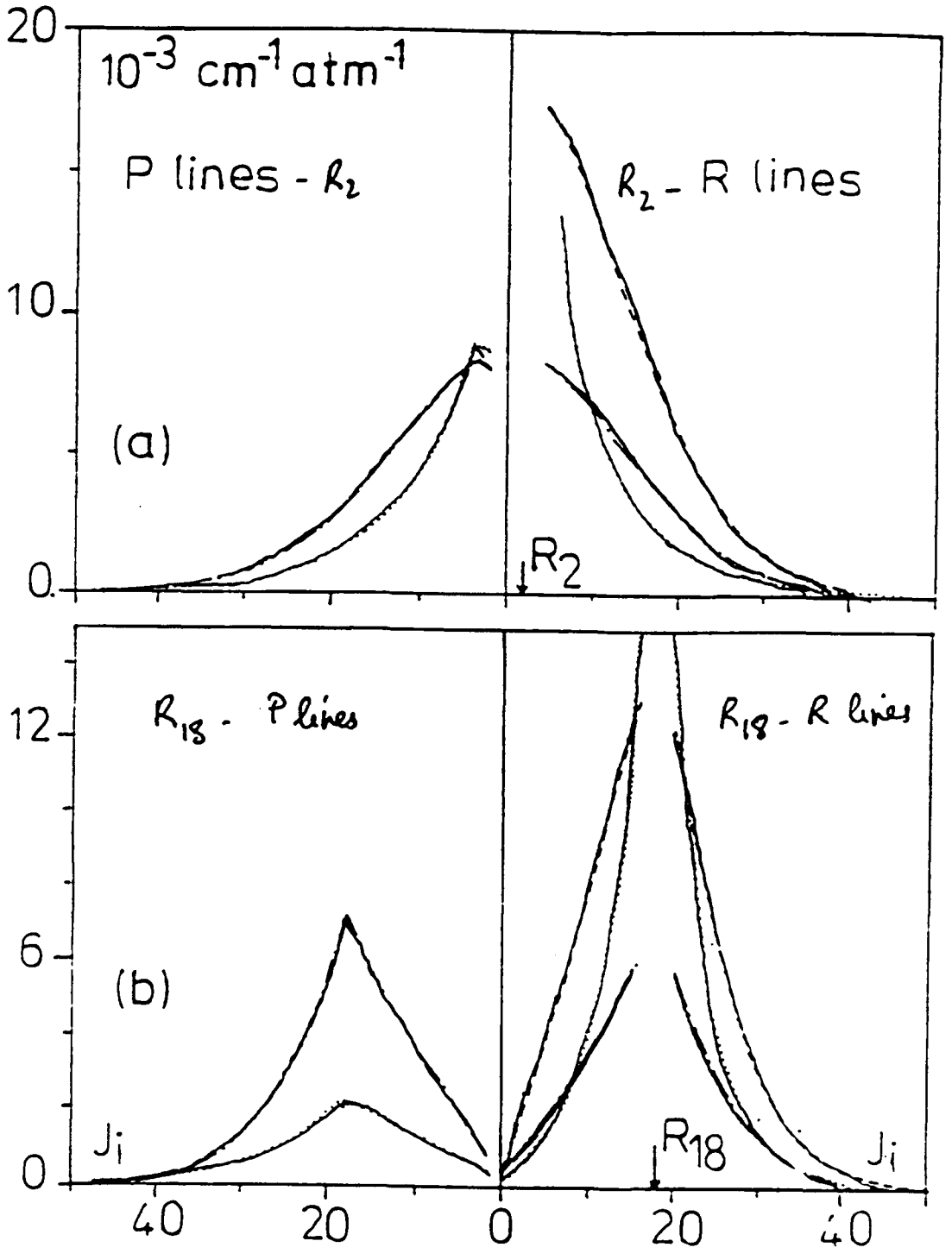
$$F_1(j_i'j_f'|j_ij_f|L00) = (-1)^{n+++j_f+j_f'+L}(2j_i'+1)\sqrt{(2j_f+1)(2j_f'+1)}\begin{Bmatrix} j_i & j_f & n \\ j_f' & j_i' & L\end{Bmatrix}\begin{pmatrix} j_i' & L & j_i \\ 0 & 0 & 0\end{pmatrix}\begin{pmatrix} j_f' & L & j_f \\ 0 & 0 & 0\end{pmatrix}$$

$$A(j,j') = [\,1 + (\Omega(j,j')\,\ell_c/v\,)^2/24]^{-1}\,, \quad (\ell_c \text{ scaling length})$$

calculation or analytical law for σ_{OL} (exemple : $A\,[L(L+1)]^{-\alpha}$)

parameters (including ℓ_c) deduced from line-broadening :

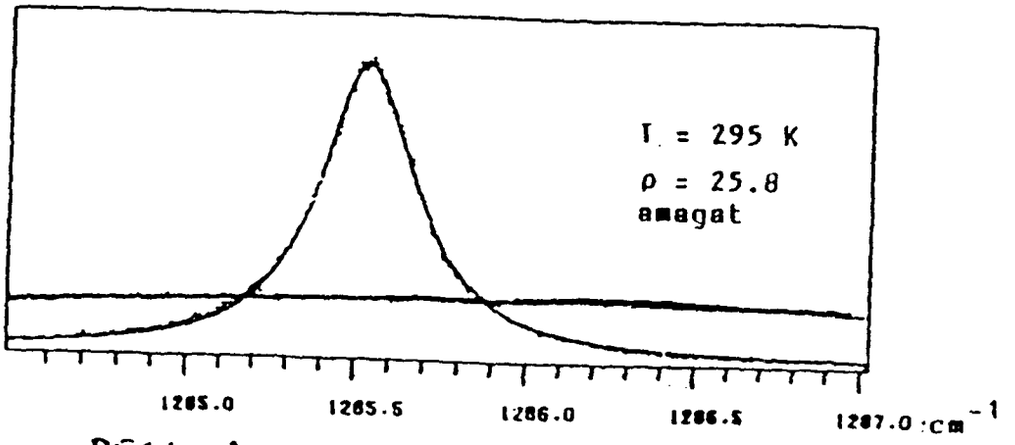
$$(j_ij_f|W^{ECS}|j_ij_f) = \gamma_{j_ij_f} = (Nv/2\pi c)\,A(j_i,j_i)A(j_f,j_f)\Big(\sum_{L\neq 0} 1 - [F_n(j_ij_f|j_ij_f|L00)\,A(L,0)^{-2}\,(2L+1)\,\sigma_{OL}$$



— ECS
— MEGL only intra-branch
— MEGL intra + inter branch

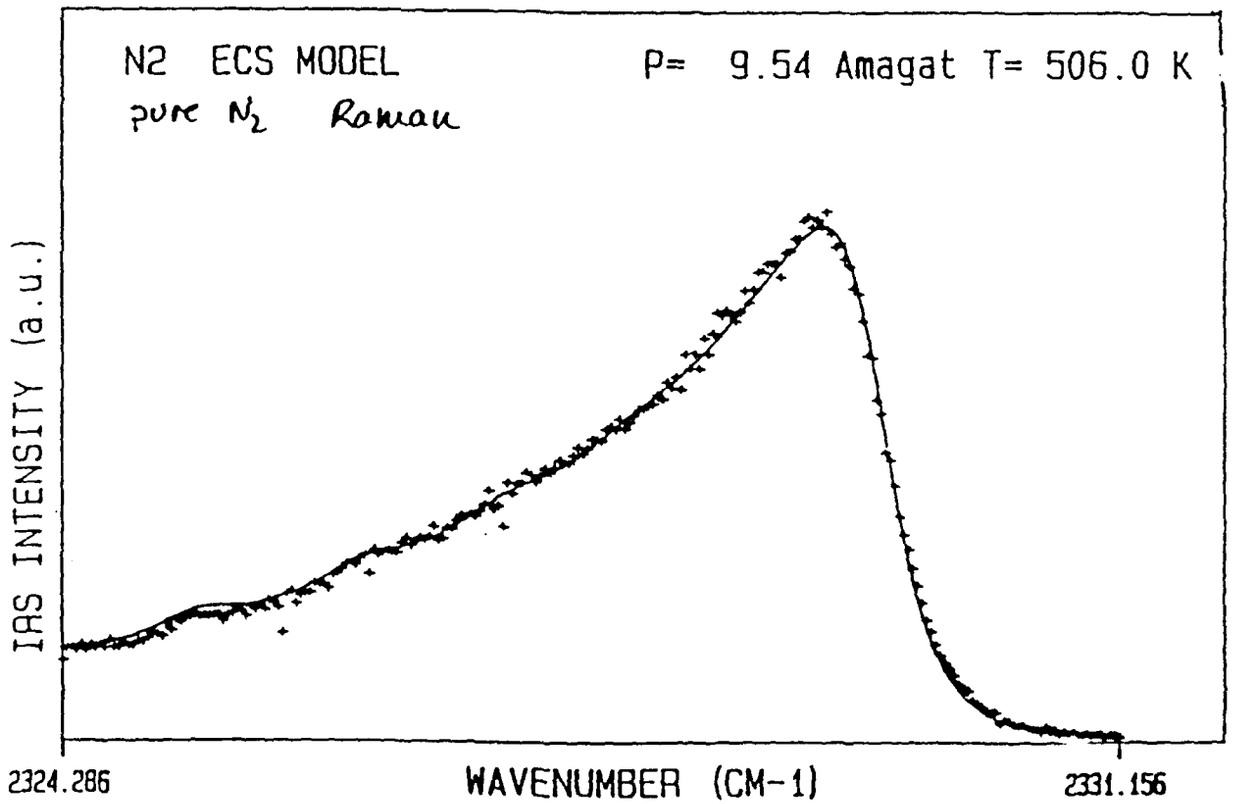
Pure CO_2 296 K : $\langle\langle e \| W(0) \| e' \rangle\rangle$

pure CO_2 ν_1 band Raman Q branch



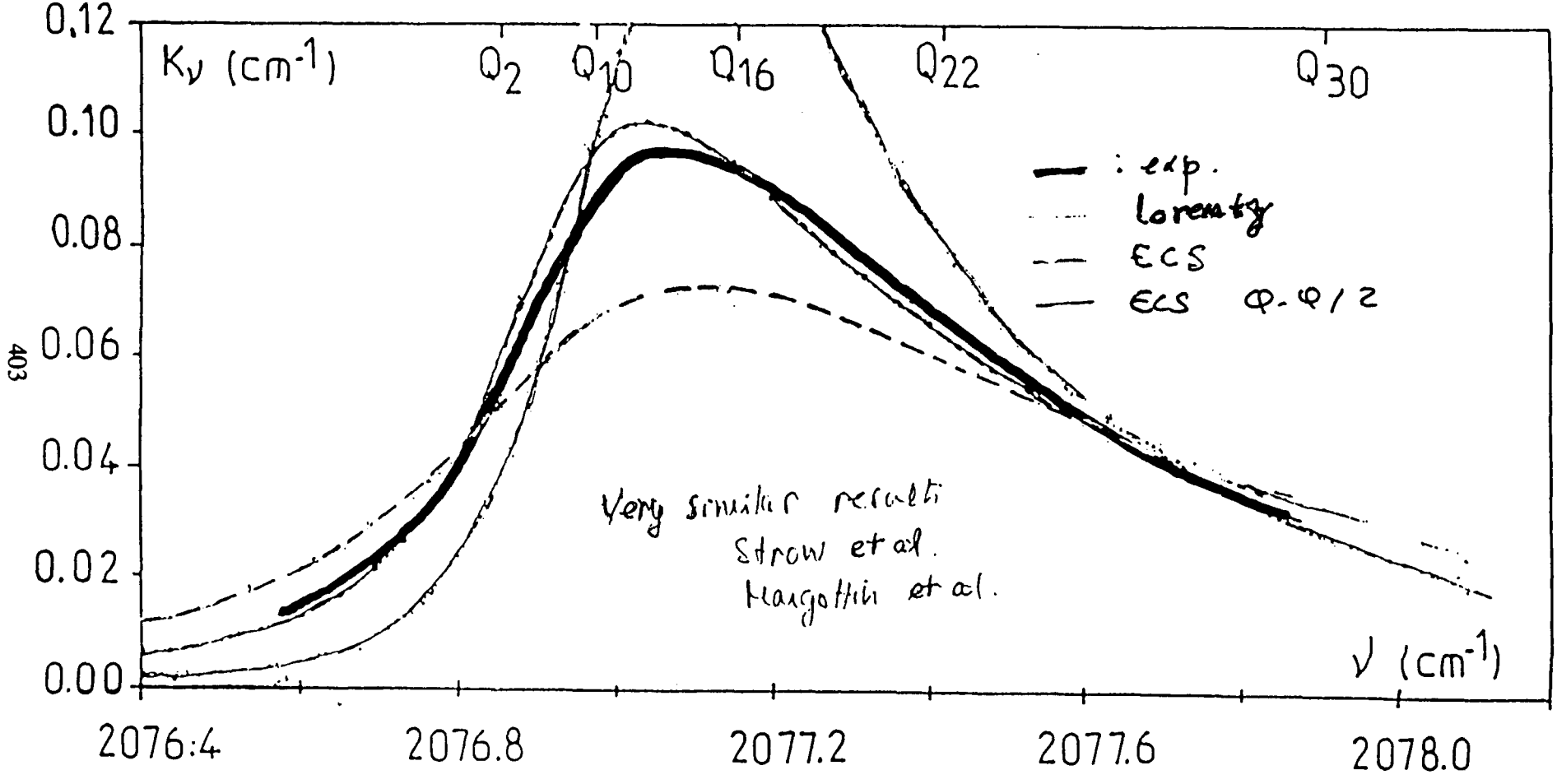
— PEGL line-mixing
— lorentzian

Millot et al. 1987



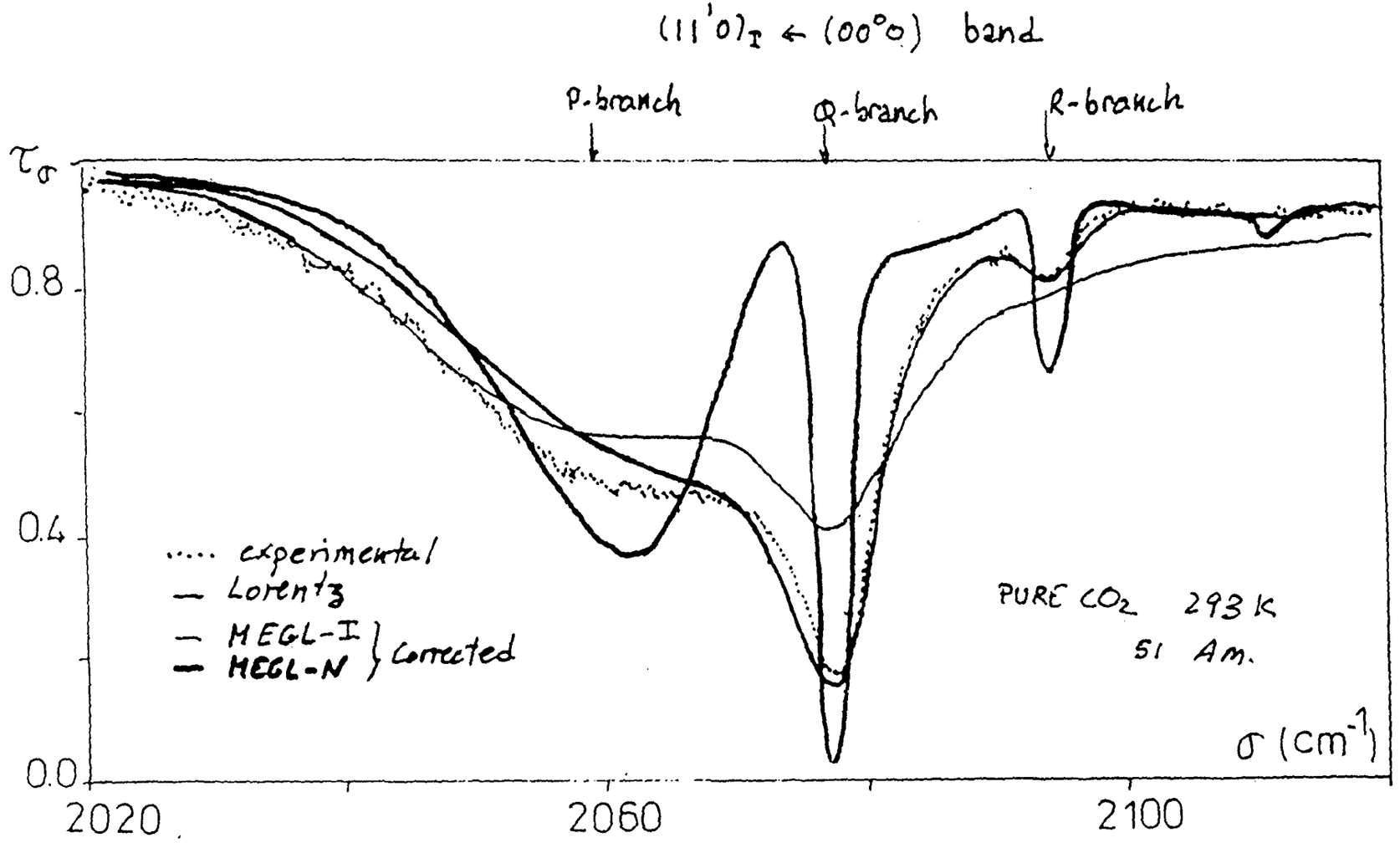
Bonamy et al., Berger et al 1989

PURE CO_2 IR Q-Branch 296 K, 30 atm



403

→ Still Problems in IR Q-branch
(Q-P, Q-R mixing)



404

J. H. Hartmann et al. FIGURE 12d

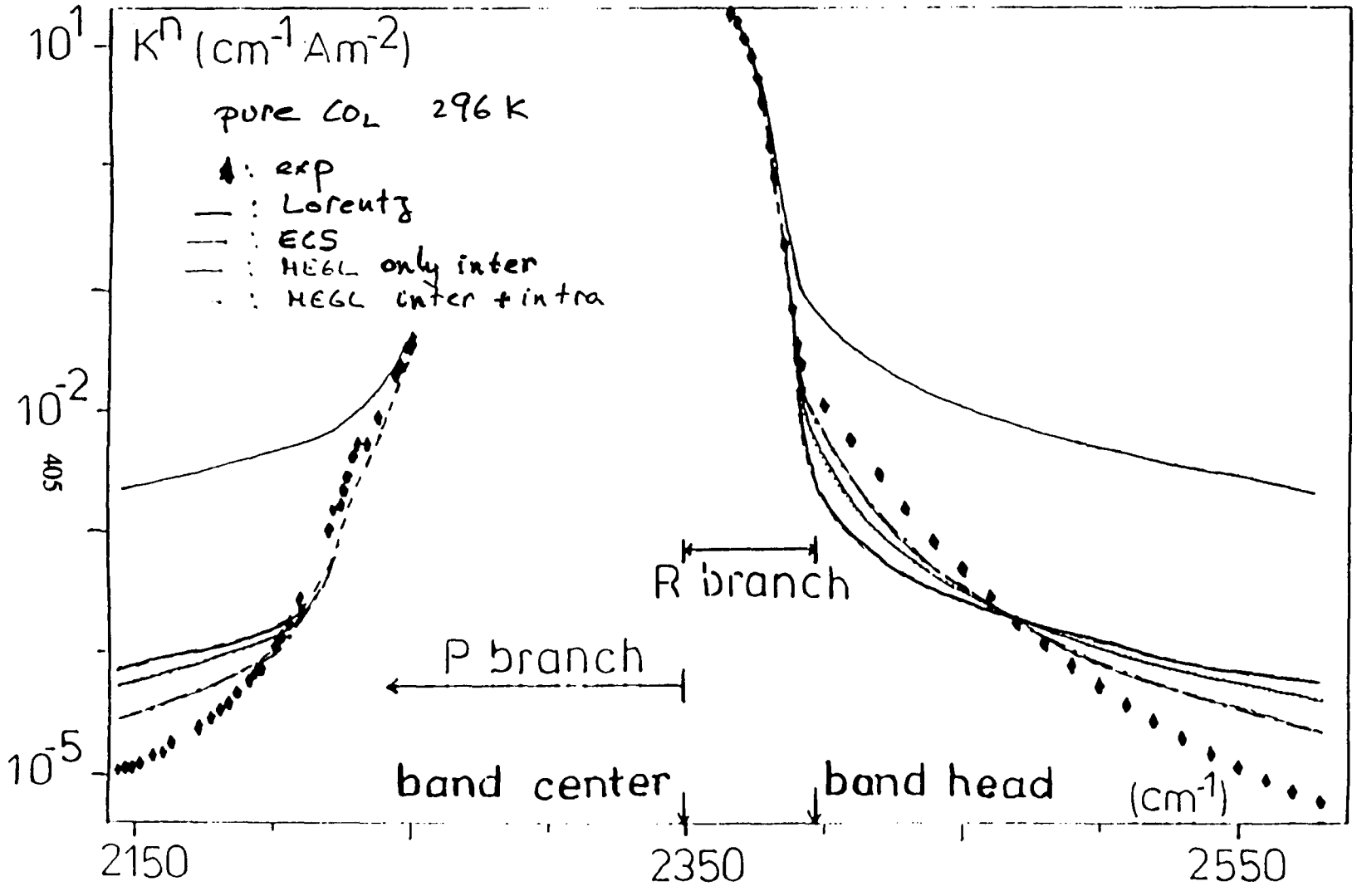
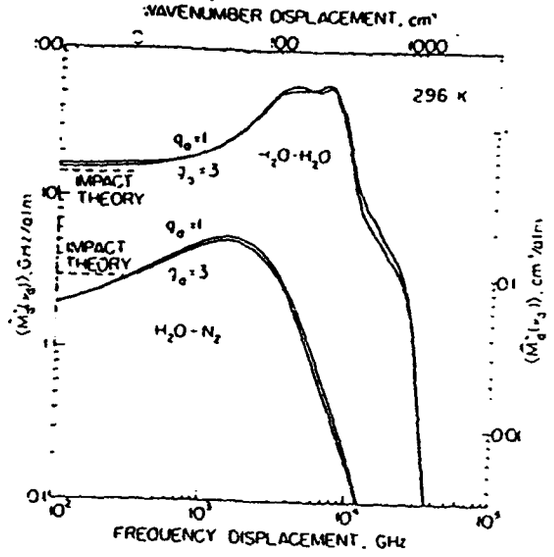
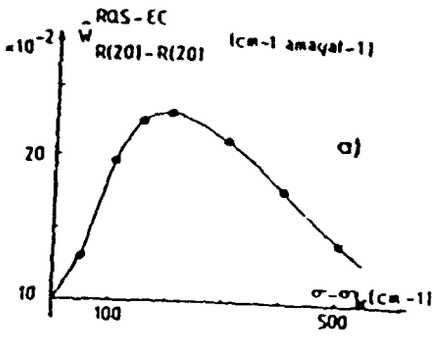

10^1
K^n ($cm^{-1}Am^{-2}$)
pure CO_L 296 K
: exp
: Lorentz
: ECS
: HEGL only inter
: HEGL inter + intra
10^{-2}
405
10^{-5}
R branch
P branch
band center
band head
(cm^{-1})
2150
2350
2550

Figure 8



H_2O

Tipping



CO_2-Ar

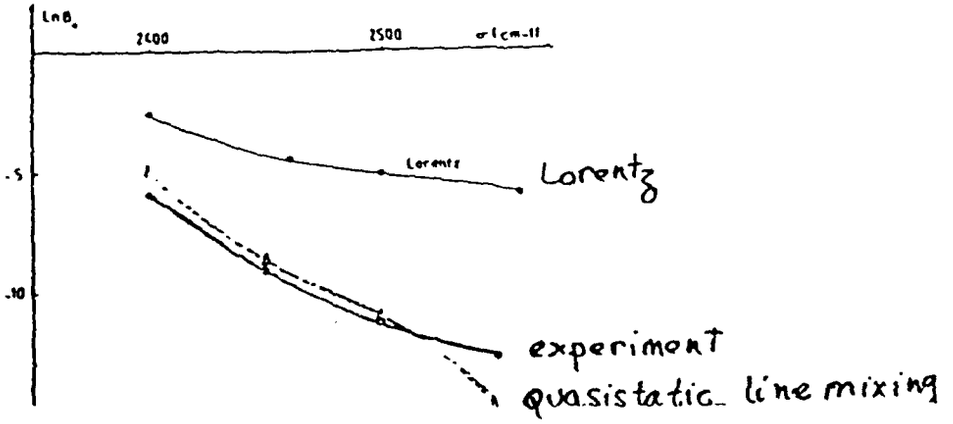
Boulet et al

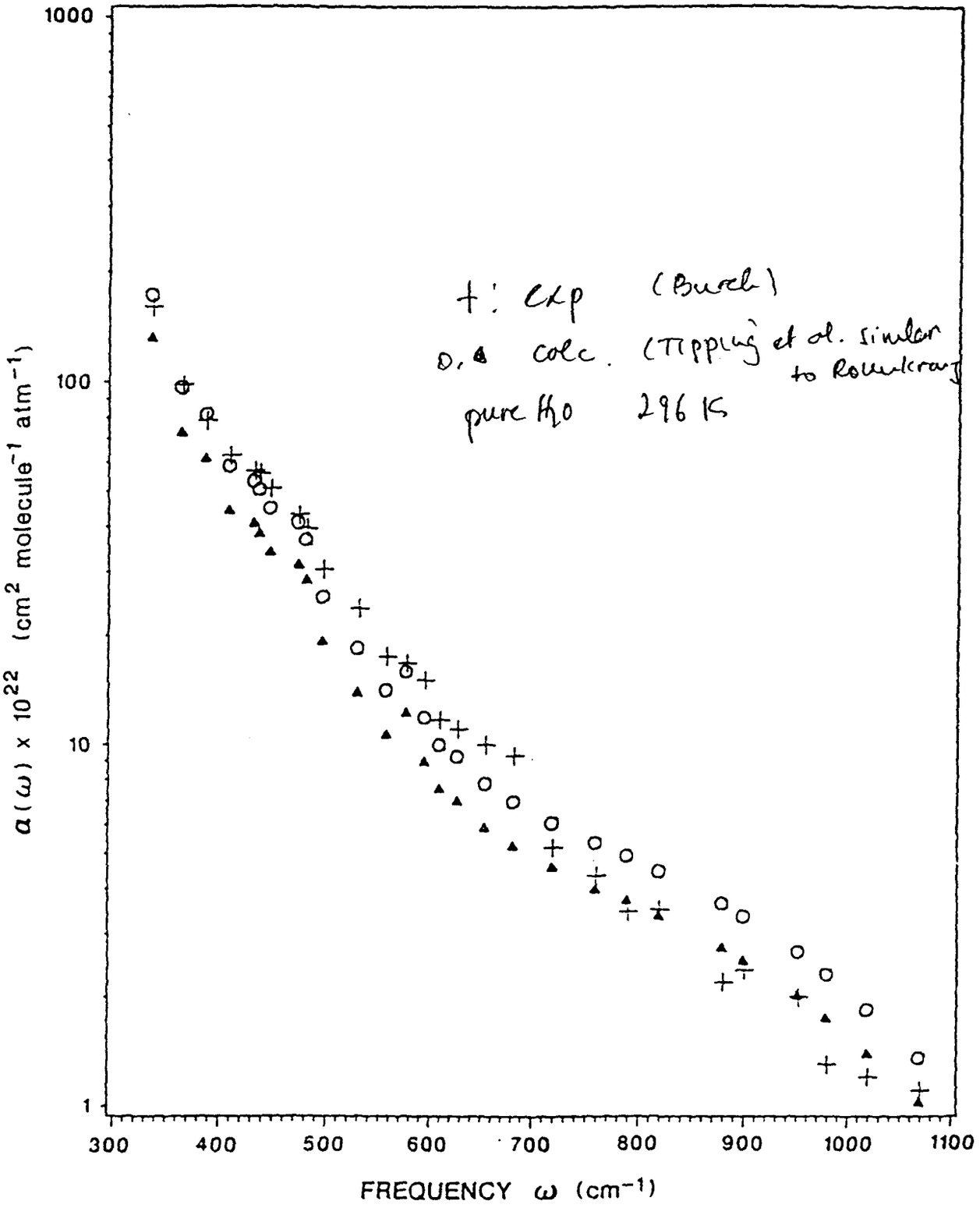
Statistical quasistatic approach

- Danes et al.)
- From first principles

CO_2-Ar 296 K IR

Boulet et al




1000
100
10
1
$\alpha(\omega) \times 10^{22}$ (cm^2 molecule^{-1} atm^{-1})
300
400
500
600
700
800
900
1000
1100
FREQUENCY ω (cm^{-1})
+: exp (Burch)
o, ▲ calc. (Tipping et al. similar to Rosenkranz
pure H$_2$O 296 K

CONCLUSION

Impact Models

- QUITE ACCURATE BY USING EMPIRICAL FACTORS FOR INTER/INTRA BRANCH OR e/f LEVELS
- STILL PROBLEMS : WHY INTRA BRANCH MIXING HAS TO BE LOWERED IN THE IR (OK IN RAI EVEN WITH MODELS (IOS, ECS) WHICH SHOULD ACCOUNT CORRECTLY FOR COUPLING BETWEEN LEVELS OF ≠ SYMMETRY
- EFFORTS ON Q-branches (CO_2-He ? Close Coupling ?

FAR WING

- VERY DIFFICULT PROBLEM
- RESULTS ARE VERY SENSITIVE TO THE INTERACTION POTENTIAL (particularly in far wing → short range interactions)
- THEORY ONLY FOR VERY FAR WING (QUASISTATIC) : HOW TO CONNECT WITH IMPACT
- STILL QUITE UNTRACTABLE FOR MOLECULE-MOLECULE WITH MANY LEVELS AND MULTI-COMPONENT INTERACTION

FAR-WING LINESHAPE CONTRIBUTION TO THE WATER CONTINUUM IN THE MILLIMETER AND INFRARED REGIONS

R.H. Tipping
Department of Physics and Astronomy, University of Alabama, Tuscaloosa, AL 35487

Q. Ma
Center for the Study of Global Habitability, Columbia University and Institute of Space Studies, Goddard Space Flight Center, New York, NY 10025

Theoretical calculations of the contributions from the far wings of allowed transitions to the continuous absorption by water vapor have been carried out for both the millimeter and infrared spectral regions. The theory is based on the quasistatic approximation and assumes as input only the known rotational constants and dipole moment matrix elements, and two Lennard-Jones potential parameters describing the isotropic interaction between two molecules. Results will be compared to recent laboratory data, and the implications for atmospheric applications discussed.

FAR WING LINESHAPE CONTRIBUTION TO THE WATER CONTINUUM IN THE MILLIMETER AND INFRARED REGIONS

R. H. Tipping

University of Alabama

Q. Ma

Goddard Institute for Space Studies

INTRODUCTION

1.1) IMPORTANCE OF MILLIMETER AND INFRARED RADIATION IN ATMOSPHERES

(1) Controls the energy balance and affects the climate of the Earth.

(2) Widely used in remote sensing, atmospheric communications, etc.

(3) To determine characteristics of planetary atmospheres from experiment data.

1.2) ATMOSPHERIC WINDOWS AND CONTINUUM ABSORPTION

OPAQUE REGIONS AND WINDOWS:

The opaque regions are mainly determined by H_2O lines, along with O_2 and CO_2 lines. Between them there are "WINDOWS".

THE WEAK ABSORPTION IN WINDOWS:

(1) Some weak local lines of H_2O, O_2 and CO_2.

(2) A gradually varying background, i.e. continuum absorption.

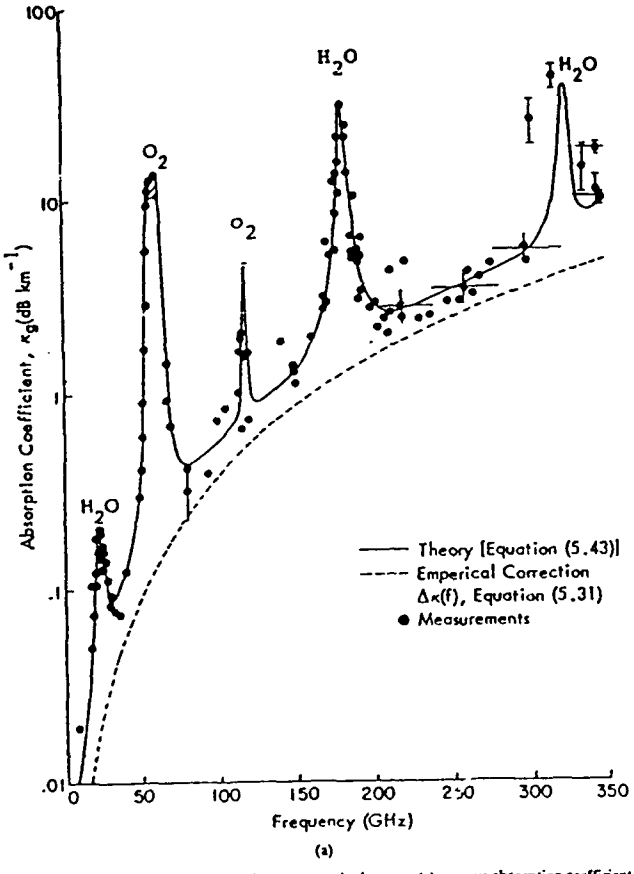


Fig. 5.7 Microwave absorption due to atmospheric gases: (a) gaseous absorption coefficient $\kappa_g(f)$ at sea level and (b) zenith opacity, both for the surface conditions $P_0 = 1013$ mbar, $T_0 = 293$ K, and $\rho_0 = 7.5$ g cm^{-3}. Solid curves are calculated according to theory, and dots are measured

SEMANTIC/NOTATIONAL

1. "CONTINUUM" - ABSORPTION NOT ASSOCIATED WITH NEARBY LINES. THIS DOES NOT IMPLY THAT IT IS ASSOCIATED WITH UNBOUND STATES.

2. EXCESS ABSORPTION OR DEFICIENT ABSORPTION?

1.3) BASIC CHARACTERISTICS OF CONTINUA

There are two kinds of water continua:

(1) H_2O - H_2O (self) continuum

(2) H_2O - N_2, O_2 (foreign) continuum

Usually, the self-continuum is dominant.

CHACTERISTICS OF THE SELF-CONTINUUM:

(1) Varies smoothly with frequency.

(2) Proportional to n^2.

(3) Very strong negative temperature dependence.

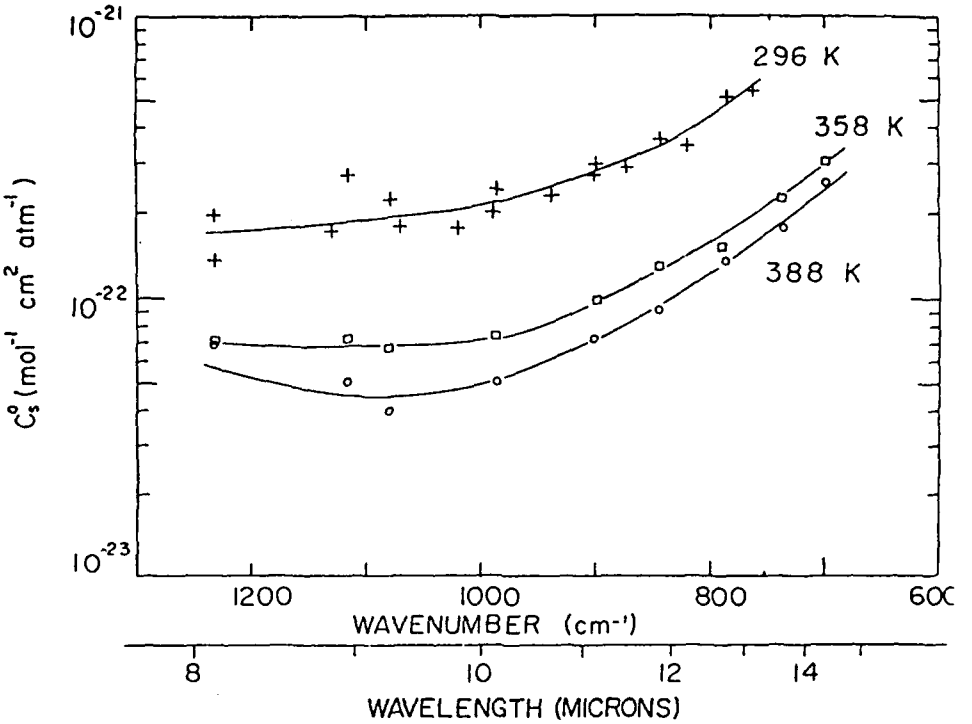


FIG. 3-4. Comparison of the continuum absorption coefficient at three temperatures.

1.4) MAIN THEORIES OF WATER CONTINUUM

THREE MECHANISMS FOR SELF-CONTINUUM:

(1) Collision broadened far-wings of allowed water vapor lines.

(2) Collision-induced absorption.

(3) Water dimers.

All three mechanisms vary as n^2, but there are large differences in the temperature dependencies and in the magnitudes of the absorption.

BRIEF HISTORY OF COLLISION-BROADENING MECHANISM FOR THE WATER CONTINUUM:

(1) In 1938, Elsasser first proposed that the water continuum was due to far-wings of allowed lines.

(2) Anderson-type theories with the impact approximation.

(3) Clough et al. considered the finite duration of collisions.

(4) Boulet and Robert, Birnbaum, etc. obtained exponential-like far wings.

(5) Rosenkranz's quasistatic method based on two approximations:
   (a) the far wing limit: $\omega \gg \omega_{fi}$
   (b) the narrow band approximation: $\omega \gg \Delta\omega_{fi}$.

RESULTS:

In the IR, the temperature dependence and the magnitude of $\alpha(\omega)$ were in reasonable agreement with experiment

BUT

there are significant differences in some regions, and this method is NOT APPLICABLE IN THE MILLIMETER REGION.

THEORY MILLIMETER REGION

$$\alpha(\omega) = \frac{4\pi^2}{3\hbar c}\,\omega\,\tanh(\beta\hbar\omega/2)\,[F(\omega) + F(-\omega)]$$

$$= \frac{4\pi^2}{3\hbar c}\,\omega\,(e^{\beta\hbar\omega} - 1)\,F(\omega)$$

$$F(\omega) = (2\pi)^{-1} \int_{-\infty}^{+\infty} e^{i\omega t} \langle\vec{\mu}(0)\cdot\vec{\mu}(t)\rangle\, dt$$

$$\langle\vec{\mu}(0)\cdot\vec{\mu}(t)\rangle \equiv \sum_i \rho_i \langle i|\vec{\mu}(0)\cdot\vec{\mu}(t)|i\rangle$$

$$F(\omega) = -(\pi)^{-1}\,\mathrm{Im}\,\mathrm{Tr}\,\left(\vec{\mu}(0)\,\frac{1}{\omega - \mathcal{F}}\,\rho\vec{\mu}(0)\right)$$

APPROXIMATIONS

1. BINARY COLLISIONS
2. PAIR POTENTIAL

   $V = V_{ISO} + V_{d\text{-}d}$
3. QUASISTATIC

INPUT DATA

A, B, C, μ

S_{if}, ϵ, σ

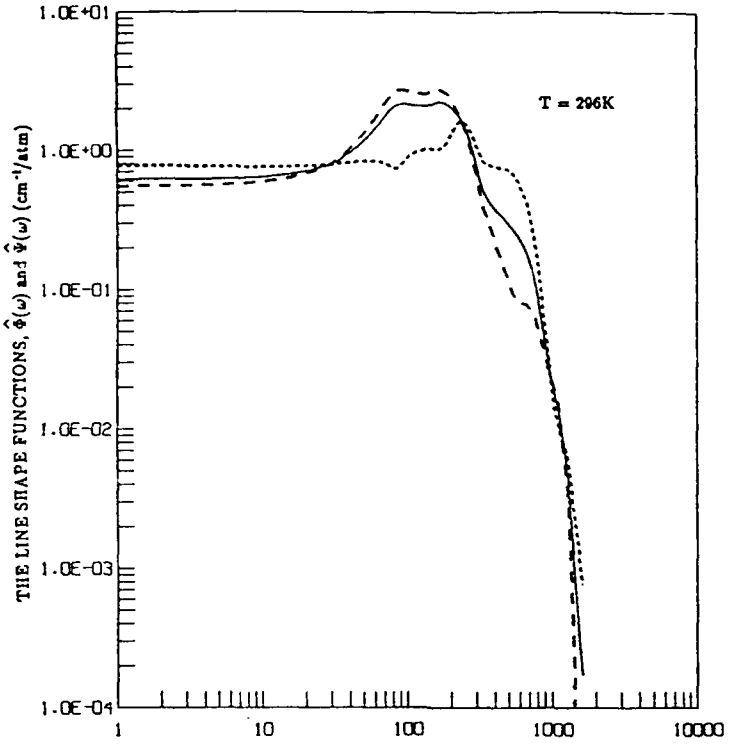
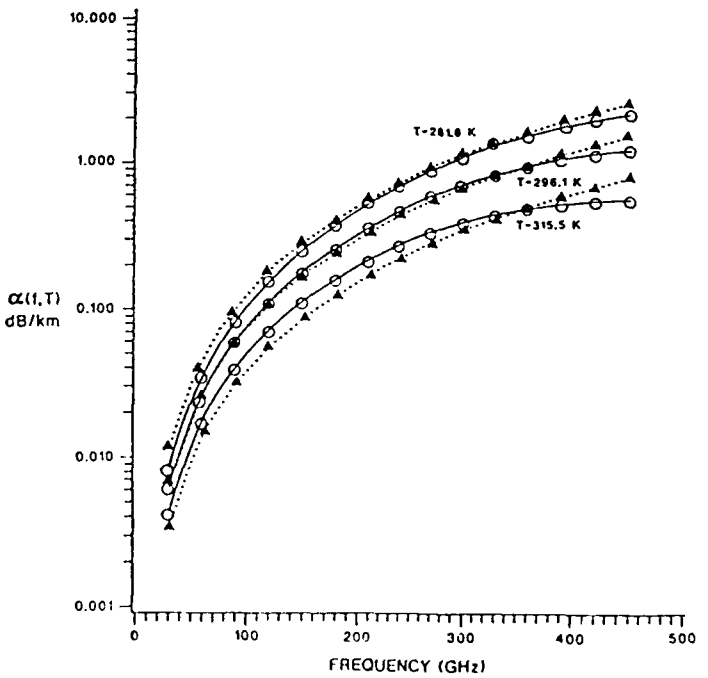
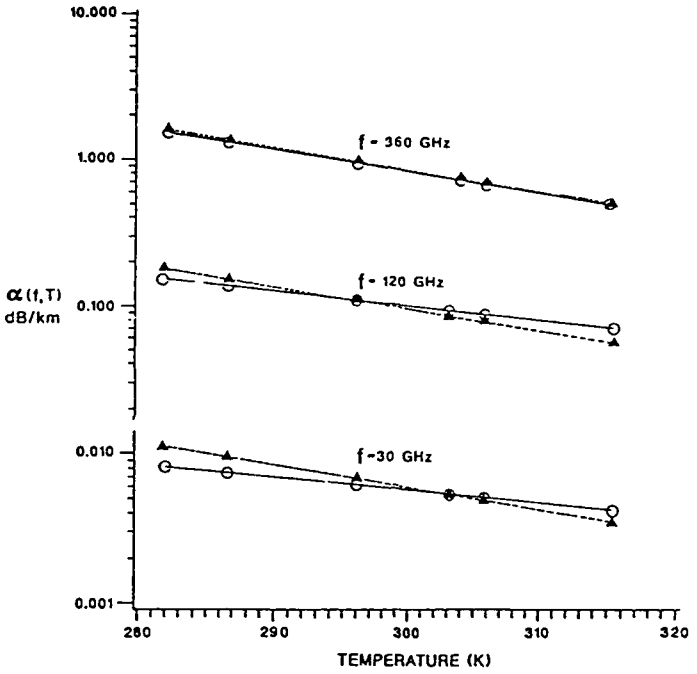

1.0E+01
1.0E+00
1.0E-01
1.0E-02
1.0E-03
1.0E-04
THE LINE SHAPE FUNCTIONS, $\hat{\Phi}(\omega)$ and $\hat{\Psi}(\omega)$ (cm^{-1}/atm)
T = 296K
1
10
100
1000
10000
FREQUENCY ω (cm^{-1})

FIG. (1)


10.000
1.000
0.100
0.010
0.001
α(f,T)
dB/km
T=281.8 K
T=296.1 K
T=315.5 K
0
100
200
300
400
500
FREQUENCY (GHz)


10.000
1.000
0.100
0.010
0.001
α (f,T)
dB/km
f = 360 GHz
f = 120 GHz
f =30 GHz
280
290
300
310
320
TEMPERATURE (K)

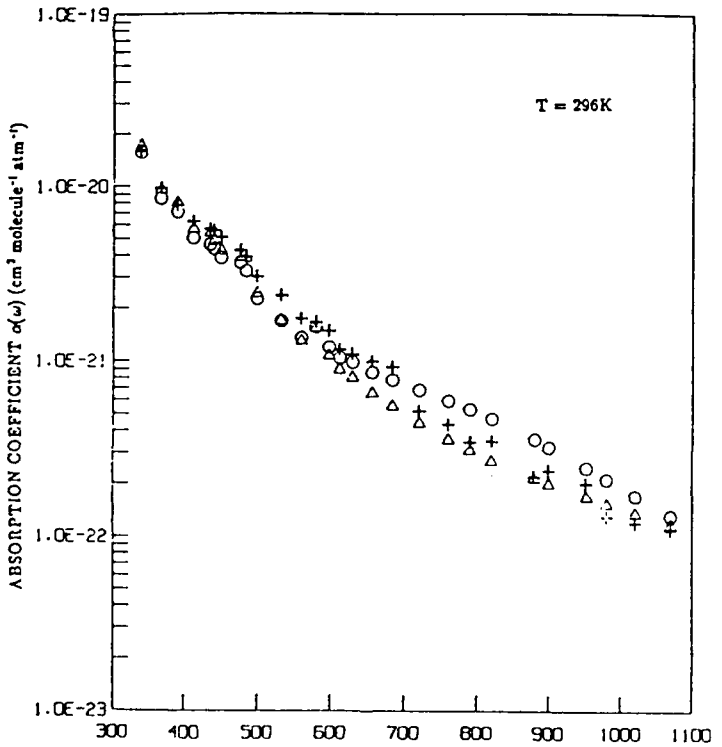

1.0E-19
1.0E-20
1.0E-21
1.0E-22
1.0E-23
ABSORPTION COEFFICIENT σ(ω) (cm² molecule⁻¹ atm⁻¹)
T = 296K
300
400
500
600
700
800
900
1000
1100
FREQUENCY ω (cm⁻¹)

FIG. (4)

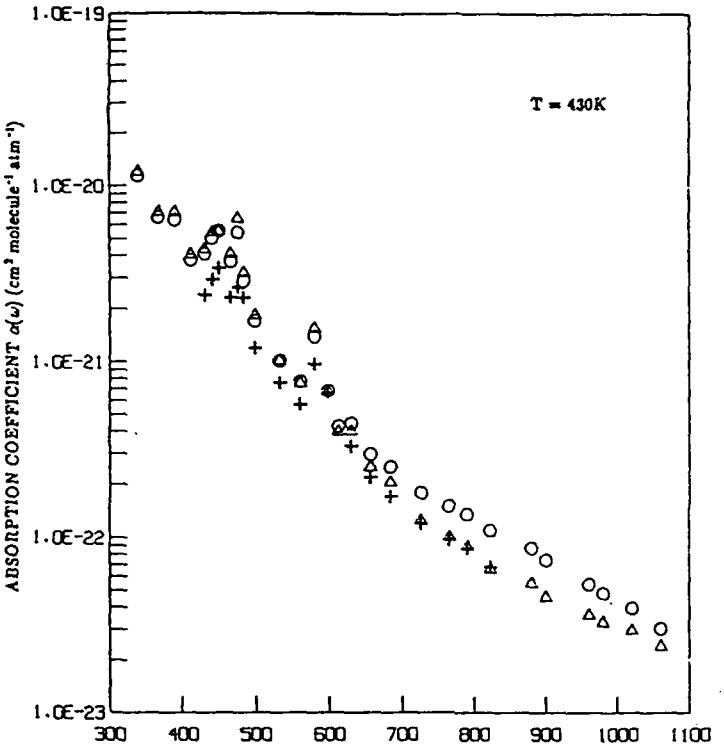

T = 430K
ABSORPTION COEFFICIENT α(ω) (cm² molecule⁻¹ atm⁻¹)
1.0E-19
1.0E-20
1.0E-21
1.0E-22
1.0E-23
300
400
500
600
700
800
900
1000
1100
FREQUENCY ω (cm⁻¹)

FIG. (6)

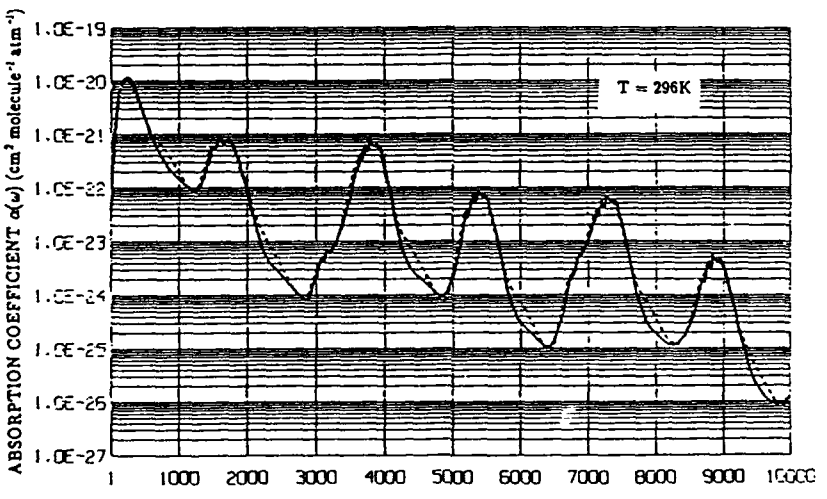

T = 296K
ABSORPTION COEFFICIENT α(ω) (cm² molecule⁻¹ atm⁻¹)
1.0E-19
1.0E-20
1.0E-21
1.0E-22
1.0E-23
1.0E-24
1.0E-25
1.0E-26
1.0E-27
1
1000
2000
3000
4000
5000
6000
7000
8000
9000
FREQUENCY ω (cm⁻¹)

FIG. (4)

LABORATORY MEASUREMENTS OF THE 60-GHz O_2 SPECTRUM IN AIR

H.J. Liebe
Institute for Telecommunication Sciences, National Telecommunications and Information Administration, U.S. Department of Commerce, NTIA/ITS.S1, 325 Broadway, Boulder, CO 80303

The O_2-spectrum of dry air was studied with a resonance spectrometer under controlled laboratory conditions. Key parts of the instrumentation were an automatic network analyzer and a one-port Fabry-Pérot resonator affording an effective path length of 240 m. Measurements were made at frequencies between 49.3 and 67.2 GHz in 0.1 GHz increments for eleven pressure steps (1-100 kPa) and three different temperatures (7-30-53°C). More than $5X10^6$ data points (S_{11} parameters) have been recorded and reduced to about 5,000 absorption values α (dB/km). Measurement uncertainties were estimated to be typically the worse of ±0.05 dB/km or 2 percent. The collective spectral behavior of 38 pressure-broadened O_2 lines is described by the model MPM (NTIA Report 91-**272**, March 1991). A comparison of the absorption results with MPM predictions reveals systematic differences which correlate with O_2 line width and overlap parameters. An interpretation of the extensive data set with *Rosenkranz*'s overlap theory [JQSRT **39**(4), 287-297, 1988] is underway.

14th Annual Review Conf. on *Atmospheric Transmission Models*

AFSC, Hanscom AFB, MA 01731 11-12 June 1991

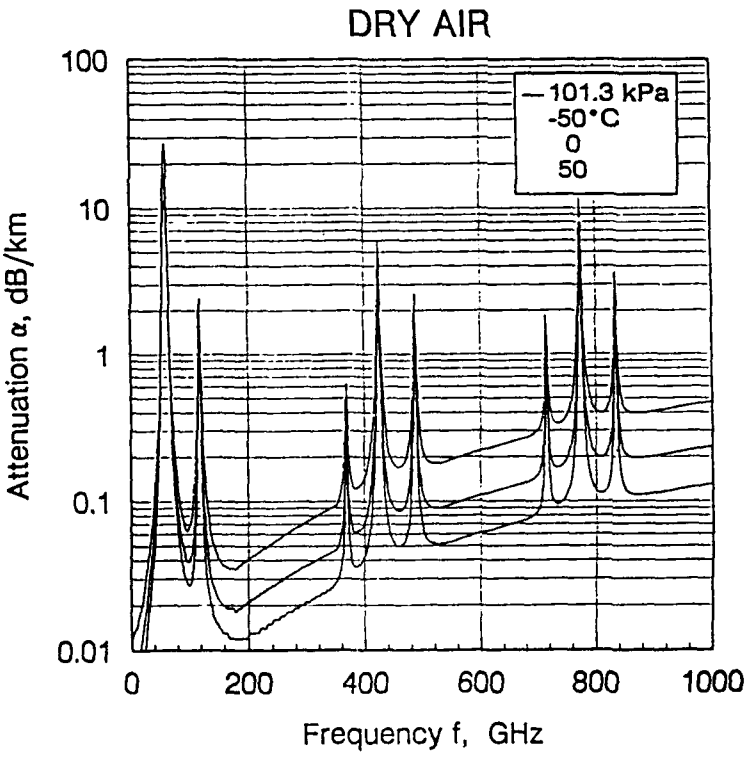
LABORATORY MEASUREMENTS OF THE 60-GHz O_2 SPECTRUM IN AIR

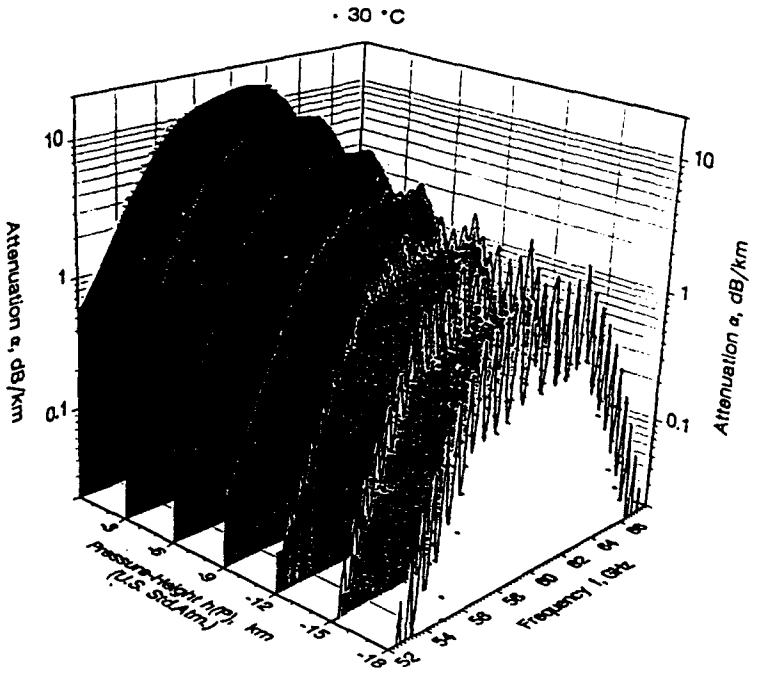
Hans J. Liebe

Institute for Telecommunication Sciences

National Telecommunications and Information Administration
U.S. Department of Commerce

NTIA/ITS.S1, 325 Broadway, Boulder, CO 80303, USA





Microwave Line Spectrum of Dry Air

Line-by-line summation of 40 O_2 transitions (K^2 = 1 to 39) to yield the complex refractivity (6 × 40 = "240-parameter" problem),

$$N_f = \sum_k S_k F_k \qquad \text{ppm}$$

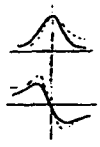
where the line strength is

$$S_k = a_1 P \theta^3 \exp[a_2(1-\theta)] \qquad \text{kHz}$$

and F_k is a complex shape function in GHz^{-1}. The Van Vleck-Weisskopf shape function of a pressure-broadened line was modified by Rosenkranz (1988) to account for overlap interferences,

$$F(f) = \frac{f}{\nu_k}\left[\frac{1+jY_k}{\nu_k - f + j\gamma_k} - \frac{1-jY_k}{\nu_k + f - j\gamma_k}\right]$$

which rationalizes to absorption (F'') and dispersion (F') profiles



$$F''(f) = A(X+Y) - Y_k[(1-B)X + (1+B)Y]$$

and

$$F'(f) = (1-B)X - (1+B)Y + Y_k A(X-Y),$$

with the abbreviations

$$A = \gamma_k/\nu_k, \qquad B = f/\nu_k,$$

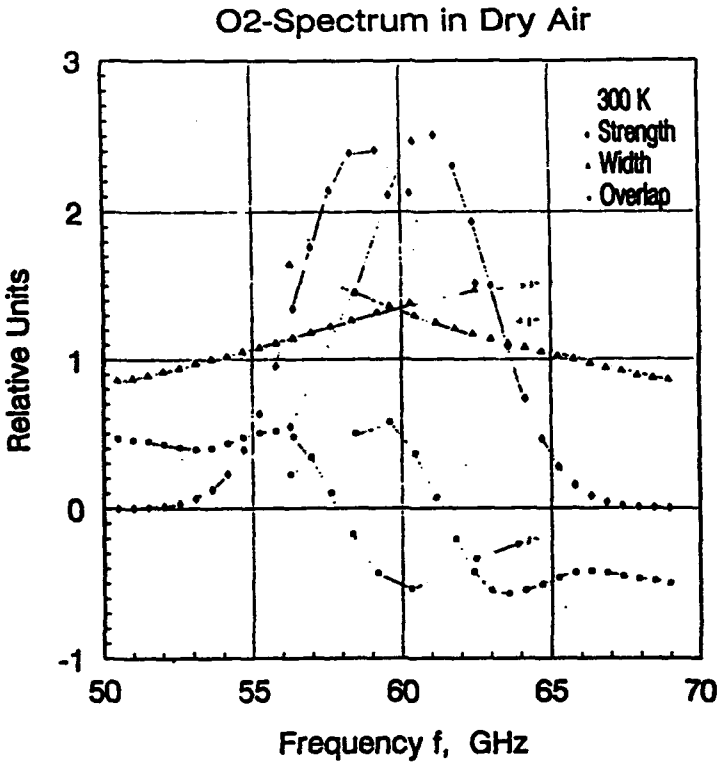
$$X = f/[(\nu_k - f)^2 + \gamma_k^2], \qquad Y = f/[(\nu_k + f)^2 + \gamma_k^2].$$

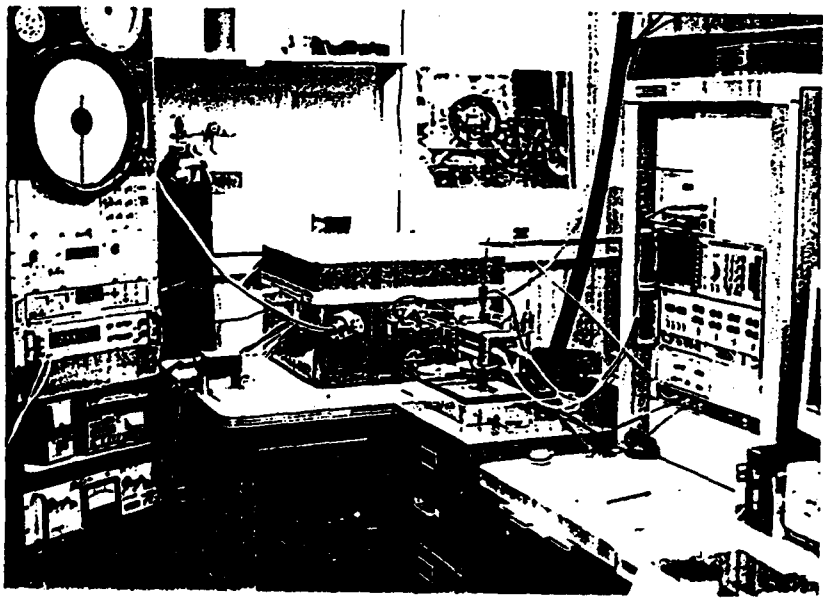
Width and interference parameters are for O_2 lines in air,

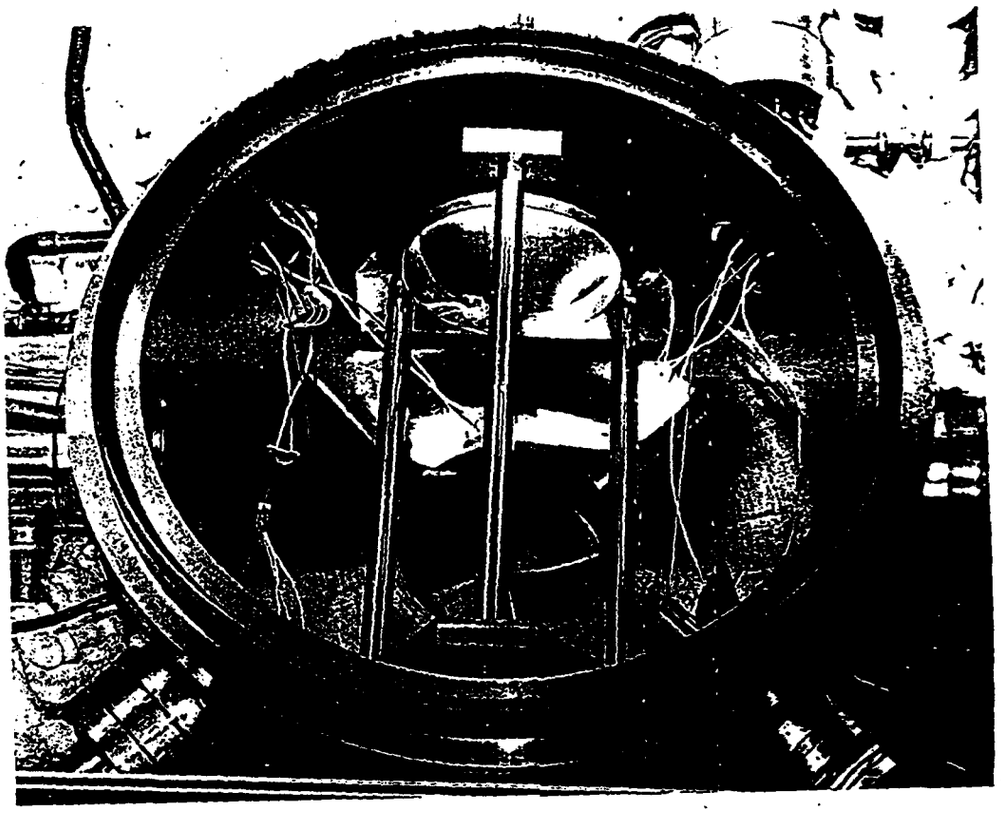
$$\gamma_k = a_3 P \theta^{(0.8 - a_4)} [1 + \underline{\quad}] \qquad \text{GHz} \qquad \text{for } f < 0.8$$

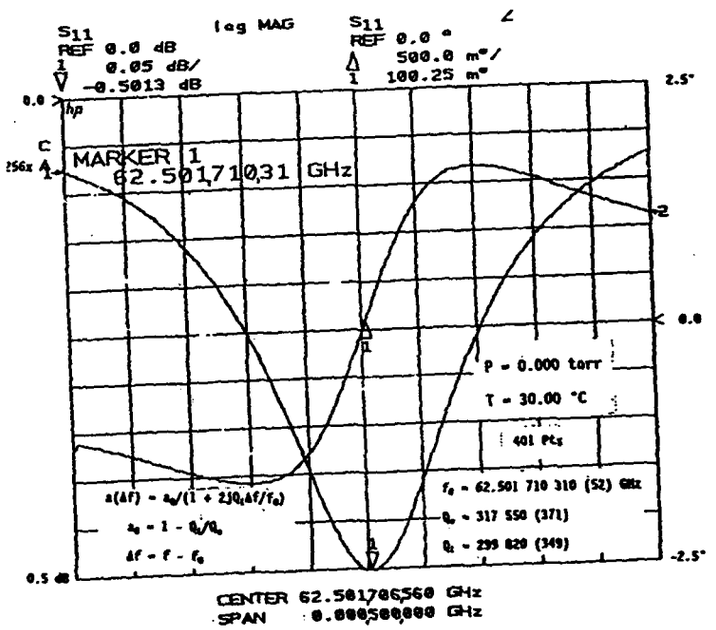
and

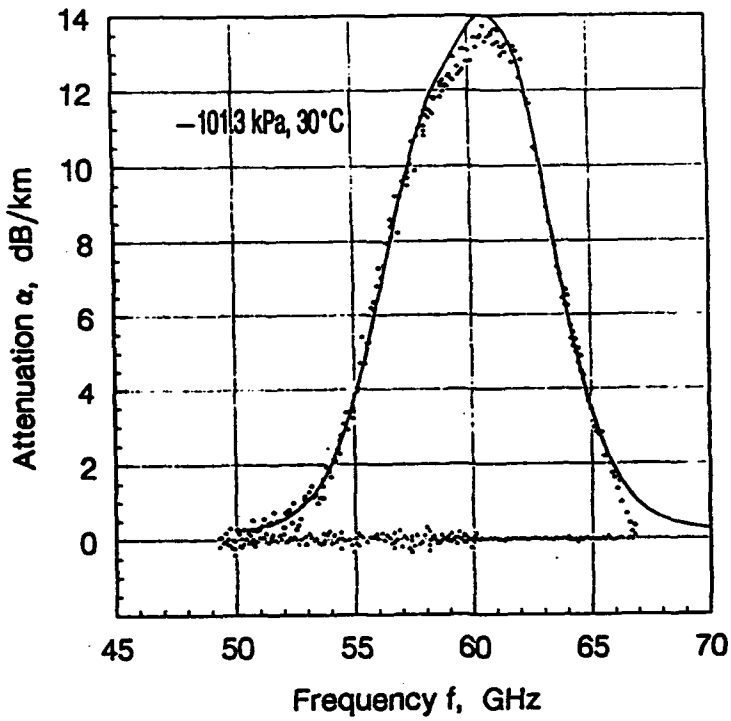
$$Y_k = (a_5 + a_6[\underline{\quad}]\theta)P\theta^{0.8} \qquad \text{for } f < 0.8$$

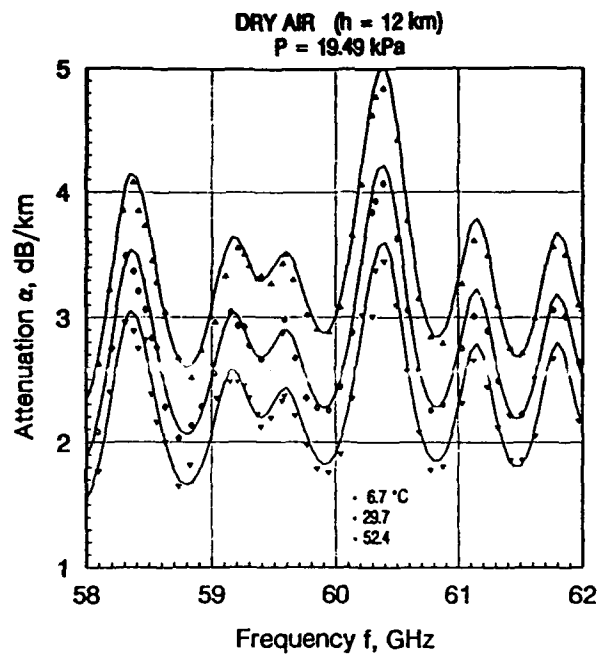

O2-Spectrum in Dry Air
300 K
Strength
Width
Overlap
Relative Units
3
2
1
0
-1
50
55
60
65
70
Frequency f, GHz

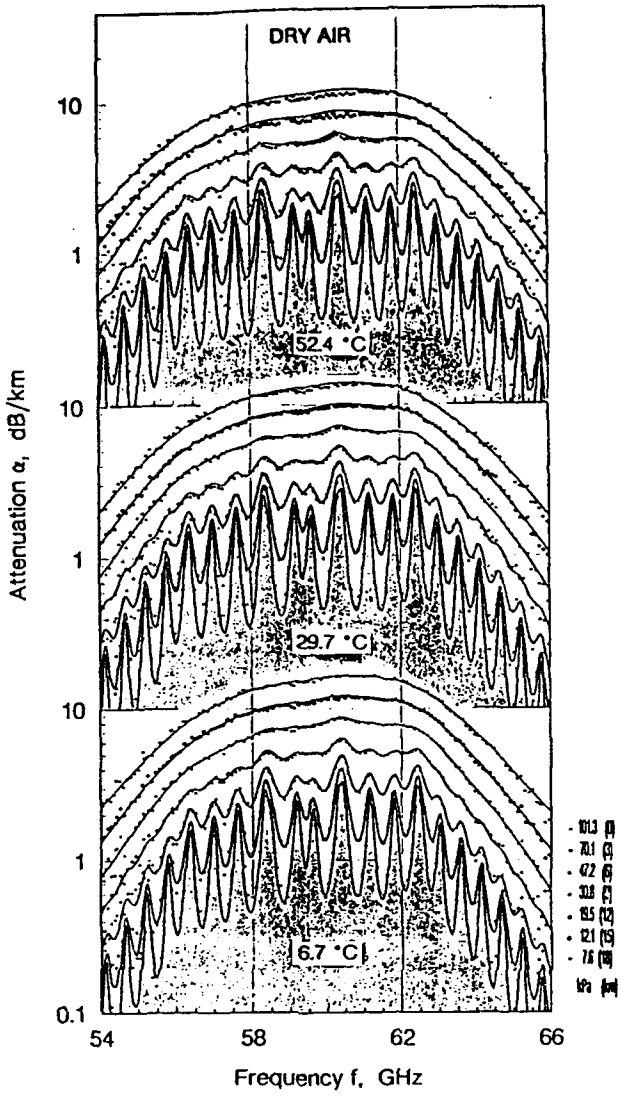


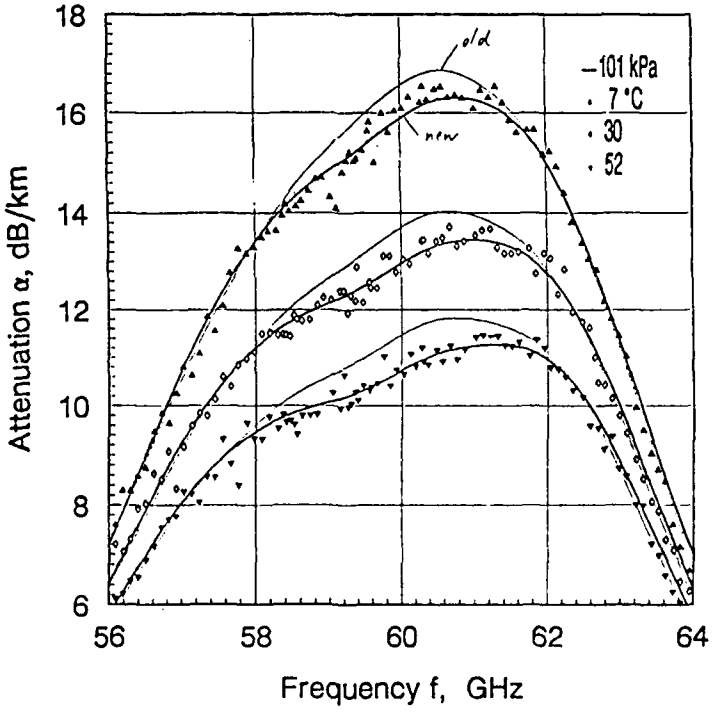


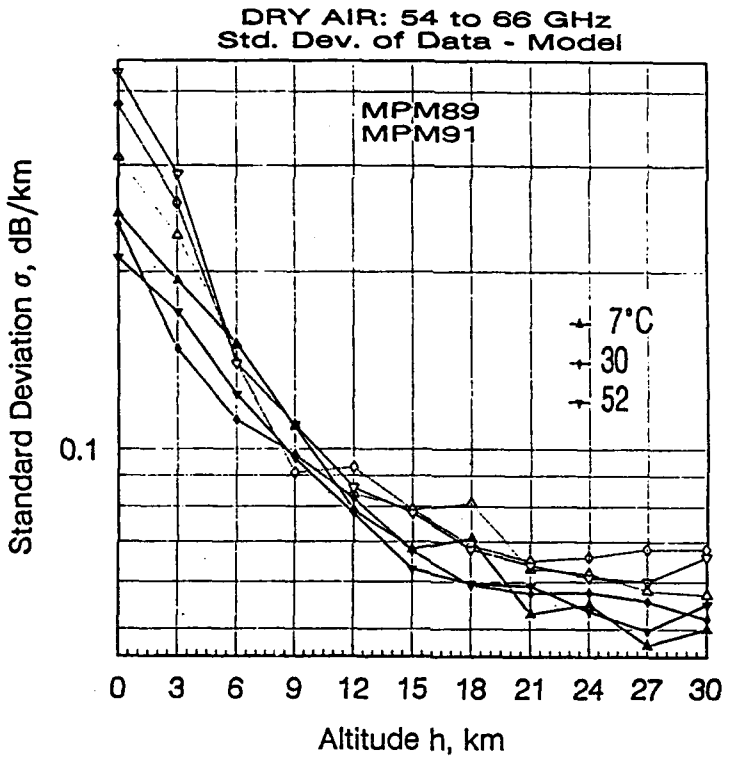

S11
REF 0.0 dB
1 0.05 dB/
-0.5013 dB
log MAG
S11
REF 0.0 °
500.0 m°/
1 100.25 m°
MARKER 1
62.501710,31 GHz
P = 0.000 torr
T = 30.00 °C
401 Pts
CENTER 62.501706,560 GHz
SPAN 0.000500000 GHz

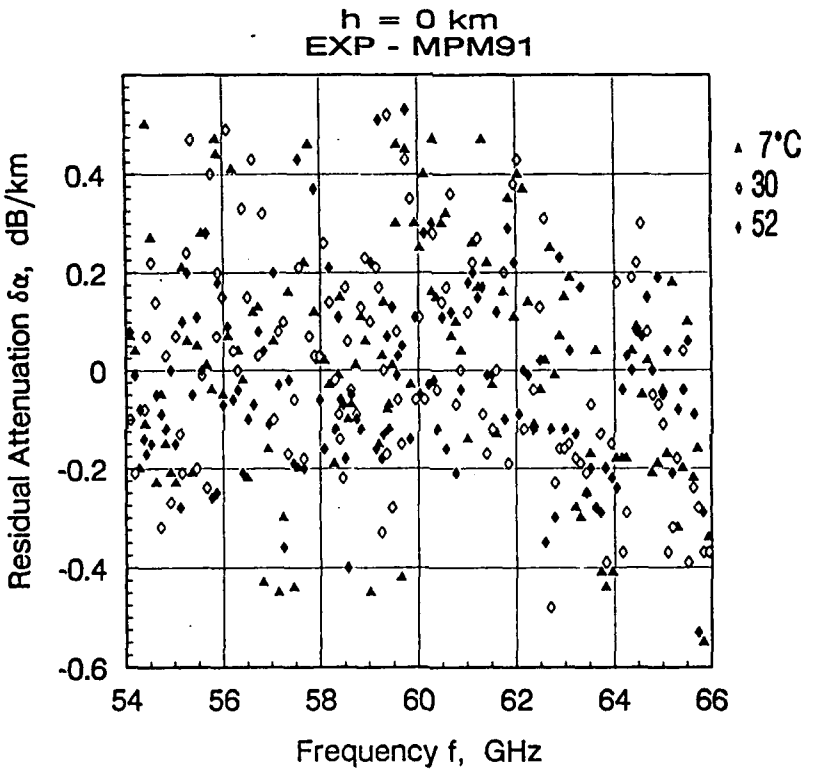

14
12
10
8
6
4
2
0
Attenuation α, dB/km
–101.3 kPa, 30°C
45
50
55
60
65
70
Frequency f, GHz

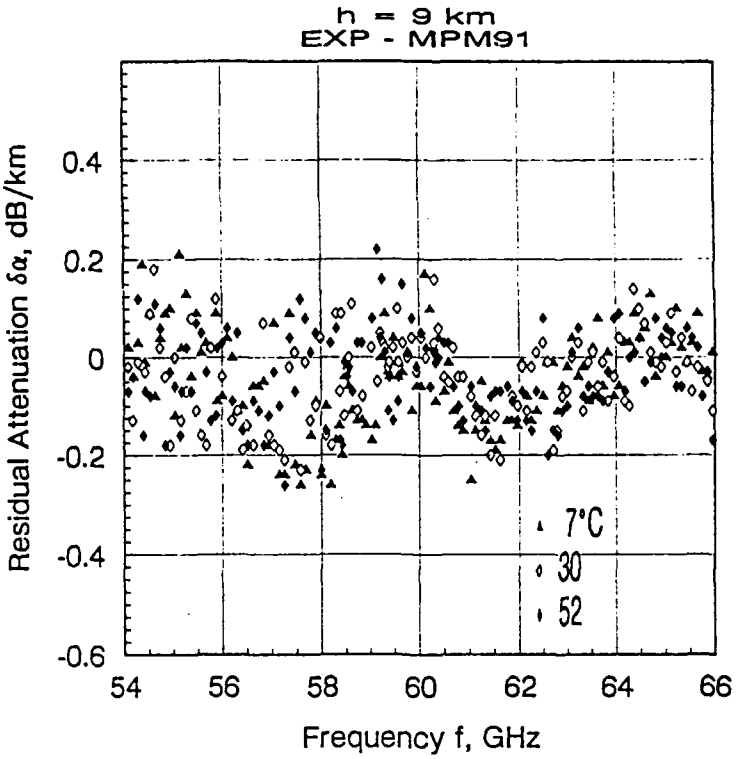

DRY AIR (h = 12 km)
P = 19.49 kPa
5
4
3
2
1
Attenuation α, dB/km
· 6.7 °C
· 29.7
· 52.4
58
59
60
61
62
Frequency f, GHz

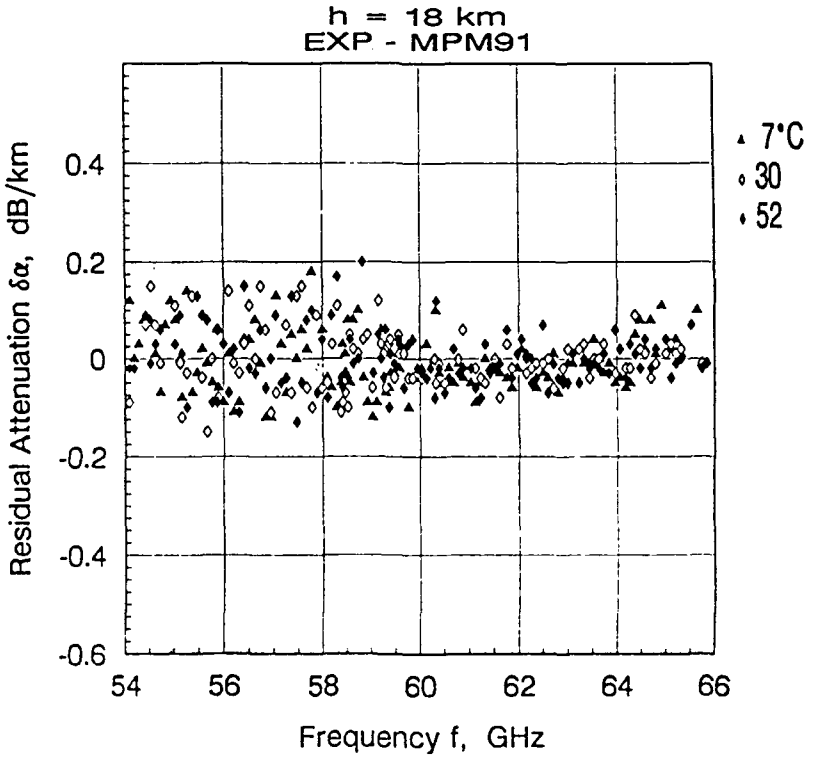

DRY AIR
52.4 °C
29.7 °C
6.7 °C
Attenuation α, dB/km
Frequency f, GHz

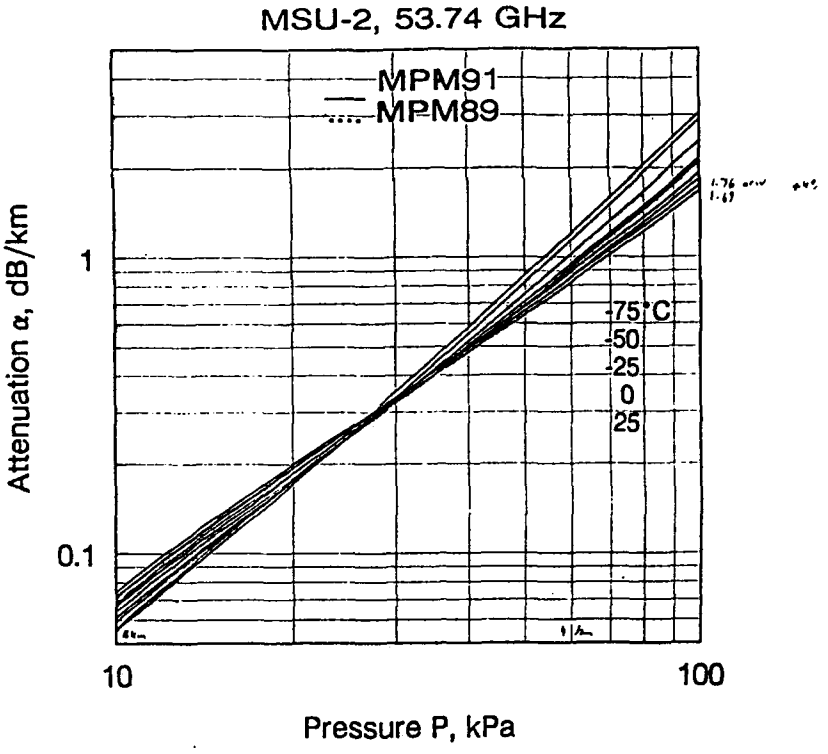

old
new
101 kPa
7 °C
30
52
Attenuation α, dB/km
Frequency f, GHz


DRY AIR: 54 to 66 GHz
Std. Dev. of Data - Model
MPM89
MPM91
7°C
30
52
Standard Deviation σ, dB/km
0.1
0 3 6 9 12 15 18 21 24 27 30
Altitude h, km


h = 0 km
EXP - MPM91
7°C
30
52
Residual Attenuation δα, dB/km
0.4
0.2
0
-0.2
-0.4
-0.6
54 56 58 60 62 64 66
Frequency f, GHz


h = 9 km
EXP - MPM91
Residual Attenuation δα, dB/km
0.4
0.2
0
-0.2
-0.4
-0.6
54
56
58
60
62
64
66
Frequency f, GHz
7°C
30
52


h = 18 km
EXP - MPM91
Residual Attenuation δα, dB/km
0.4
0.2
0
-0.2
-0.4
-0.6
54
56
58
60
62
64
66
Frequency f, GHz
7°C
30
52


MSU-2, 53.74 GHz
MPM91
MPM89
Attenuation α, dB/km
1
0.1
-75°C
-50
-25
0
25
10
100
Pressure P, kPa

LINE MIXING IN POLAR AND NONPOLAR MOLECULES

A.S. Pine, J.P. Looney
Molecular Physics and Thermophysics Divisions, National Institute of Standards and Technology, Gaithersburg, MD 20899

Line mixing has been observed for three infrared Q branches of HCN and HCCH, self-broadened at subatmospheric pressures, using a difference-frequency laser spectrometer. Broadening coefficients and line-coupling effects are independent of vibration in these species. The broadening coefficients monotonically decrease with J for HCCH whereas they peak near the Boltzmann population maximum for HCN. Empirical energy-gap rate laws adequately describe the broadening and line mixing in HCCH provided that a decoupling factor, representing collisional cross relaxation between the e and f levels of the Π bending vibrations, be included. These rate laws do not fit the line mixing in HCN whereas an energy-corrected-sudden (ECS) scaling law does. Here the cross relaxation decoupling is smaller than for HCCH, indicating a slight propensity for preserving vibrational angular momentum in polar molecule collisions.

LINE MIXING IN POLAR AND NONPOLAR MOLECULES

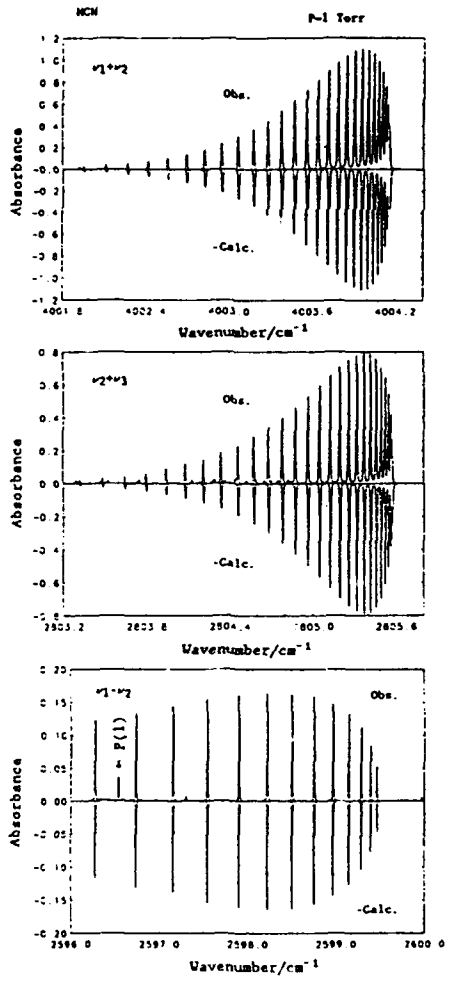
(HCN) (HCCH)

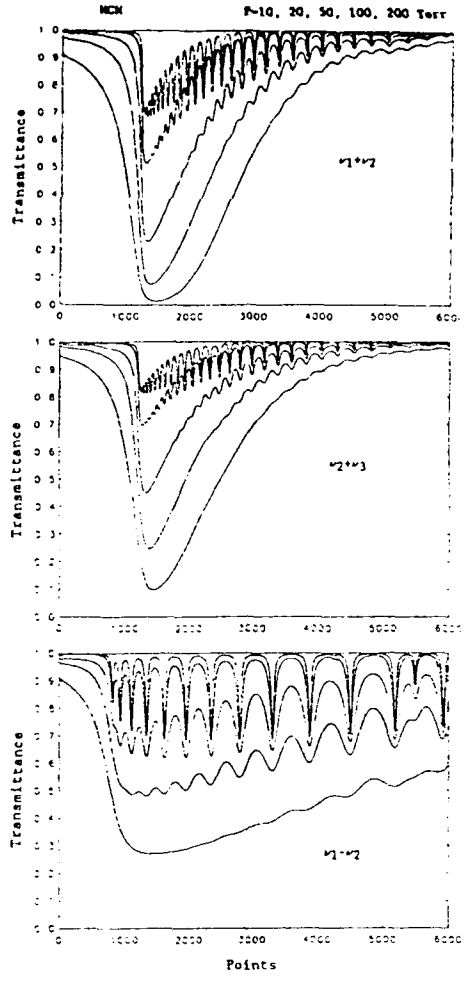
A. S. Pine and J. P. Looney

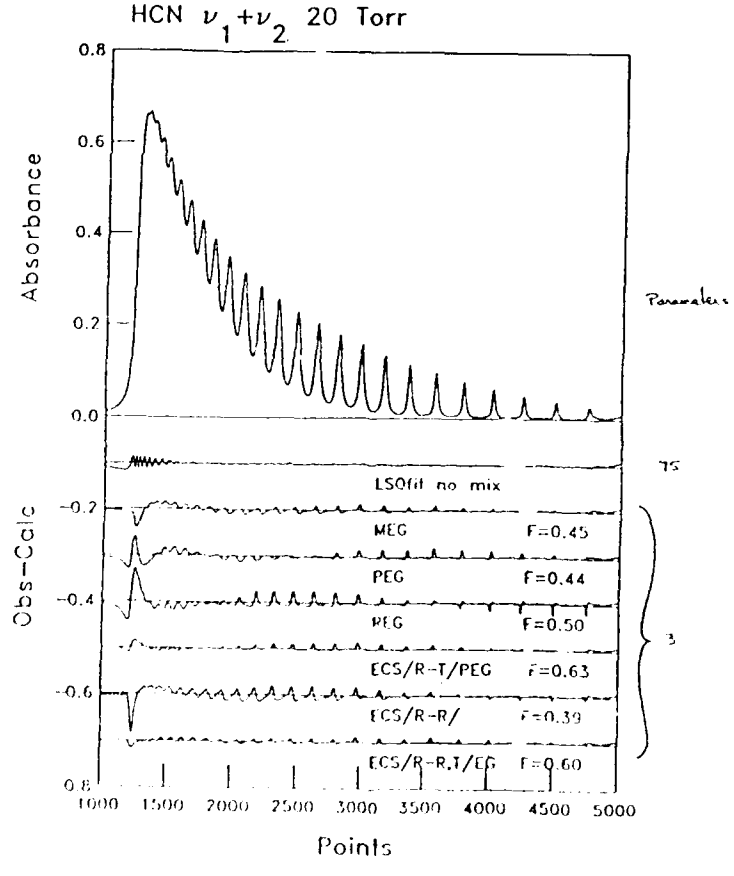
Molecular Physics and Thermophysics Divisions

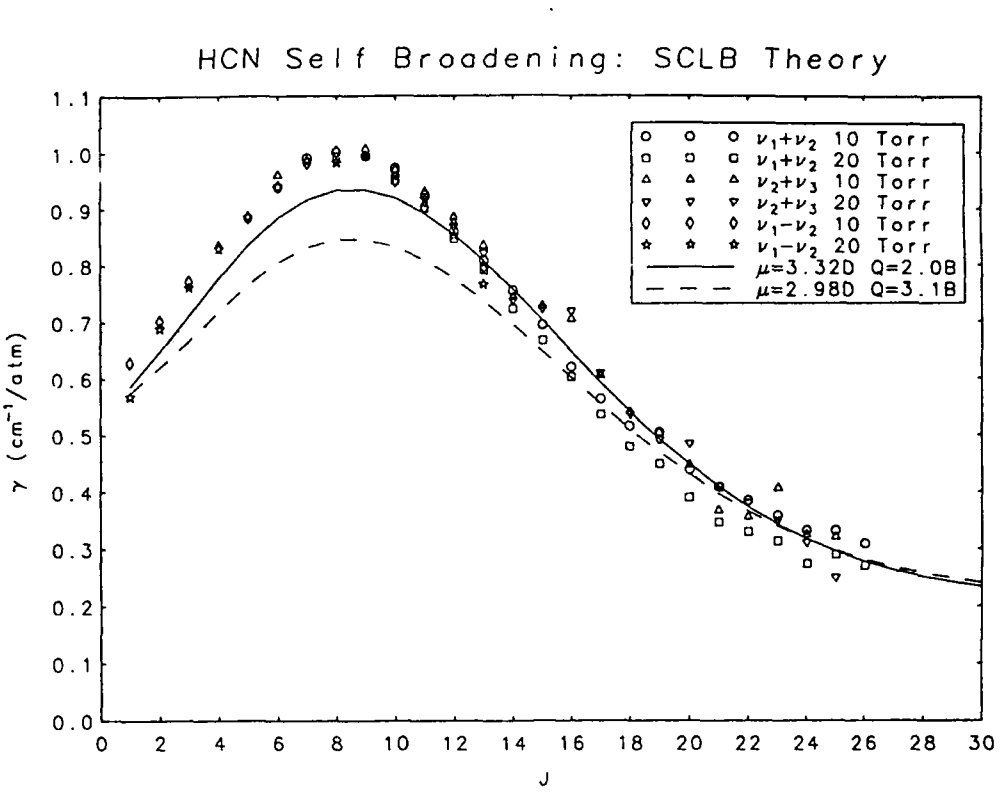
National Institute of Standards and Technology

Gaithersburg, MD 20899




HCN
P=10, 20, 50, 100, 200 Torr
Transmittance
Points


HCN $\nu_1+\nu_2$ 20 Torr
Absorbance
Obs-Calc
LSQfit no mix
MEG F=0.45
PEG F=0.44
REG F=0.50
ECS/R-T/PEG F=0.63
ECS/R-R/ F=0.39
ECS/R-R,T/EG F=0.60
Points



EMPIRICAL COLLISION RATE FITTING LAWS

R-T Hybrid Power-Exponential-Gap (PEG) Law

$$R_{J\to K} = a_1 (E_{KJ}/B)^{-a_2} \exp(-a_3 E_{KJ}/kT)$$

where $E_{KJ} = E_K - E_J$ and $k = k_B/hc$

R-T Modified-Exponential-Gap (MEG) Law

$$R_{J\to K} = a_1 \frac{[1+1.5(E_J/a_2 kT)]}{[1+1.5(E_J/kT)]} \exp(-a_3 E_{KJ}/kT)$$

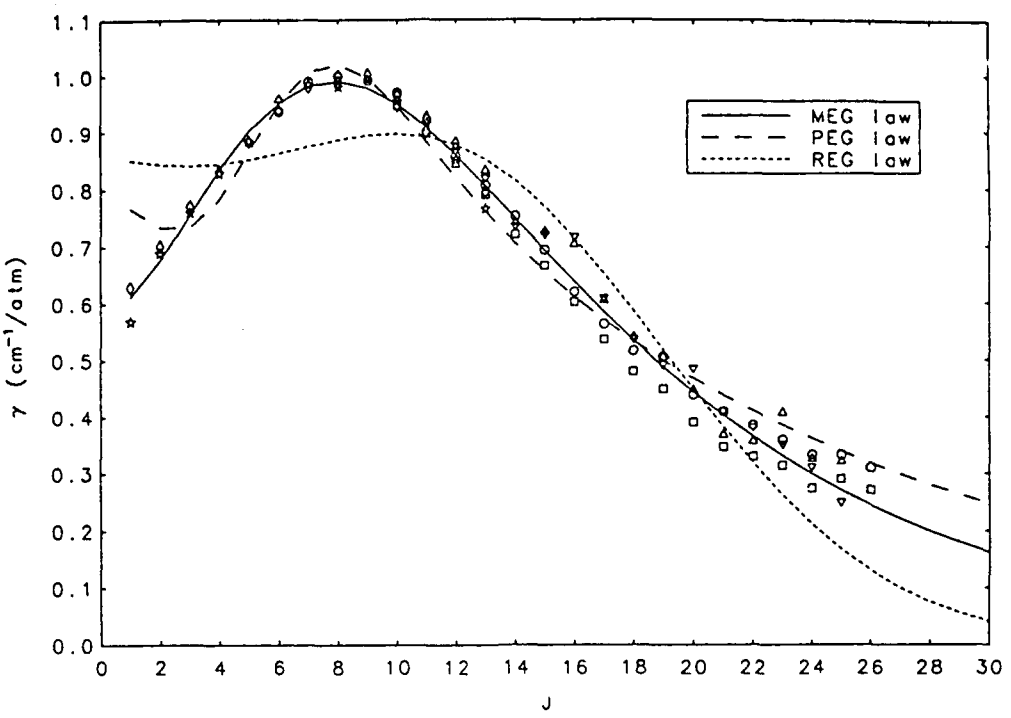
R-R Resonant-Exponential-Gap (REG) Law

$$R_{J\to K} = a_1 \rho_K \Sigma_{LM} \rho_L \rho_M \exp(-a_3 |E_{KJ}+E_{ML}|/kT)$$

where $\rho_J = g_J(2J+1)\exp(-E_J/kT)/Z_R$

for upward collisional transitions, $K > J$.

Downward transitions related by detailed balance, $R_{K\to J} = R_{J\to K}\, \rho_J/\rho_K$.



ENERGY-CORRECTED-SUDDEN (ECS) SCALING LAWS

R-T Inelastic Collision Rates

$$R_{J\to K} = (2K+1)\exp(-E_{KJ}/kT)\,\Sigma_L(2L+1)\begin{pmatrix} J & K & L \\ 0 & 0 & 0 \end{pmatrix}^2 R_{L\to 0}$$

$$\times\,[1+(a_4E_{L-})^2/BkT]^2/[1+(a_4E_{K-})^2/BkT]^2$$

where $E_{KJ} = E_K - E_J$ and $k = k_B/hc$,

$E_{K-} = E_K - E_{K-I}$ for I = 1 (dipole) or I = 2 (quadrupole),

$R_{L\to 0} = a1\,(E_L/B)^{-a2}\exp(-a_3E_L/kT)$ (PEG)

R-R Inelastic Collision Rates

$$R_{J\to K} = a_1(2K+1)\,\Sigma_L\,\rho_L\exp(-\Delta E/kT)\begin{pmatrix} J & K & I \\ 0 & 0 & 0 \end{pmatrix}^2\begin{pmatrix} L & M & I \\ 0 & 0 & 0 \end{pmatrix}^2$$

$$\times\,(2M+1)(2I+1)/[1+(a_4(E_{KJ}+E_{ML}))^2/BkT]^2$$

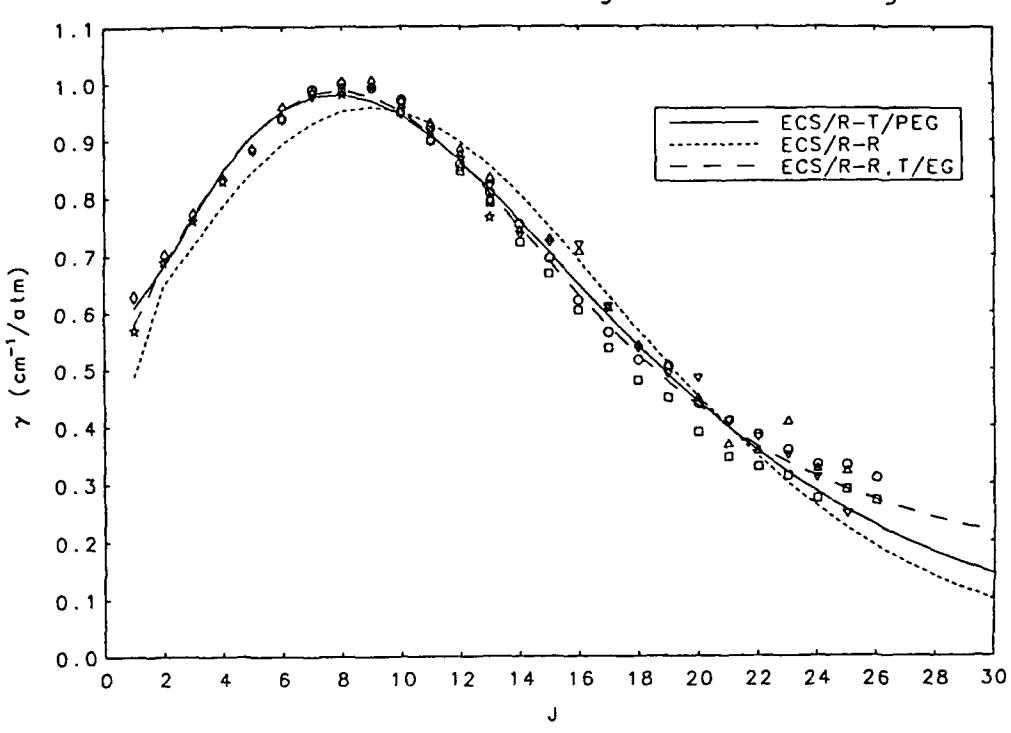
where $\rho_L = g_L(2L+1)\exp(-E_L/kT)/Z_R$,

$K = J+I$, $M = L-I$, for I = 1 or 2,

$\Delta E = E_{KJ}+E_{ML}$ if > 0 or $= 0$ if ≤ 0

for upward collisional transitions, $K > J$.

Downward transitions related by detailed balance, $R_{K\to J} = R_{J\to K}\,\rho_J/\rho_K$.



LINE COUPLING or LINE MIXING

Absorption Coefficient (impact approximation)

$$\kappa(\nu) = (N/\pi)\ \mathrm{Im}\{\ \Sigma_J (d\cdot A)_J (A^{-1}\cdot\rho\cdot d)_J/(\nu-\omega_J)\ \}$$

where

$$d_J = \mu_v\ [1+\alpha_{HW} J(J+1)]^{\frac{1}{2}}$$

$$\rho_{JJ'} = \delta_{JJ'}\ g_J\ (2J+1)\ \exp(-hcE''(J)/k_BT)$$

ω_J *are complex eigenvalues of complex matrix*

$$H = \nu_o + iPW$$

whose eigenvectors are columns of matrix A

$$A^{-1}\cdot H\cdot A = \Omega \quad \text{where} \quad \Omega_{JJ'} = \delta_{JJ'}\ \omega_J$$

ν_o is a diagonal matrix of transition frequencies, ν_J

W is relaxation matrix whose diagonal elements are broadening coefficients and off-diagonal elements are line-coupling coefficients.

RELAXATION MATRIX

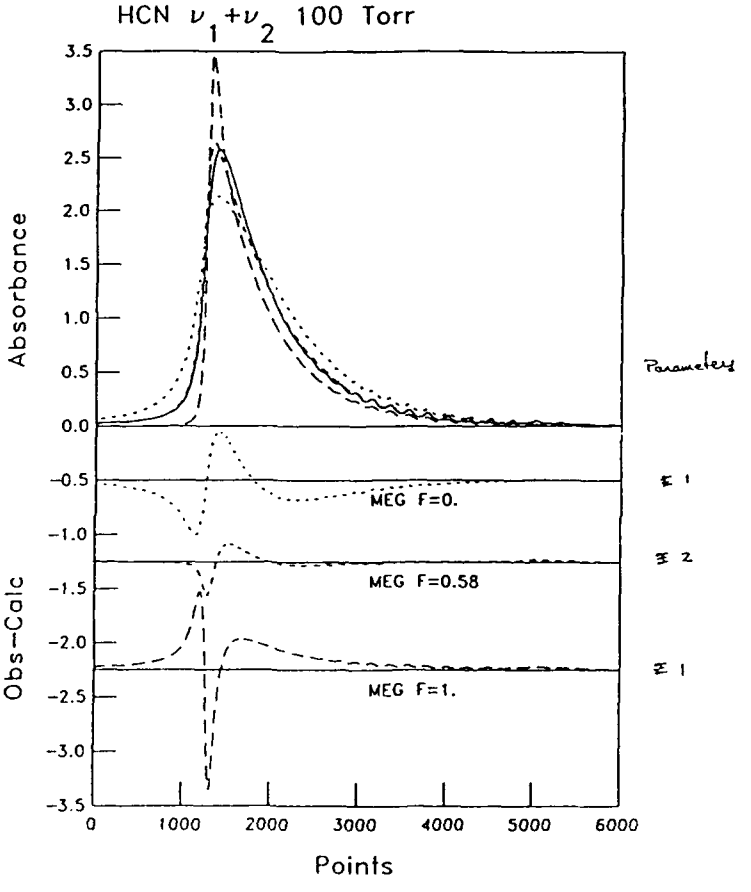
Diagonal Elements (Broadening)

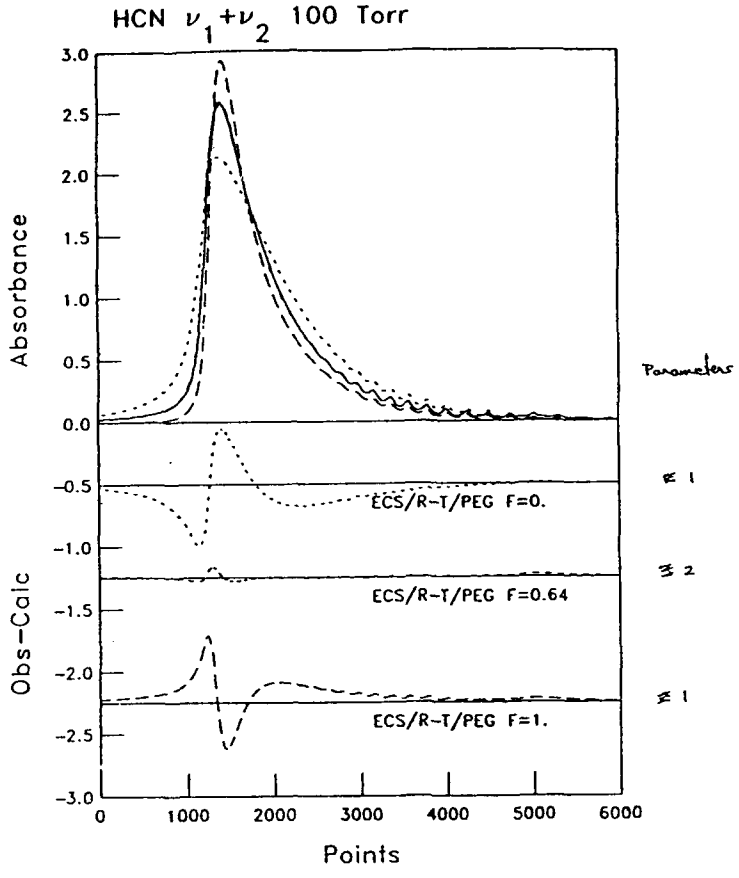
$$W_{JJ} = \tfrac{1}{2} \Sigma_{K \neq J} [(R_{J \to K}(\Sigma, e \to e) + R_{J \to K}(\Pi, f \to f) + R_{J \to K}(\Pi, f \to e)]$$

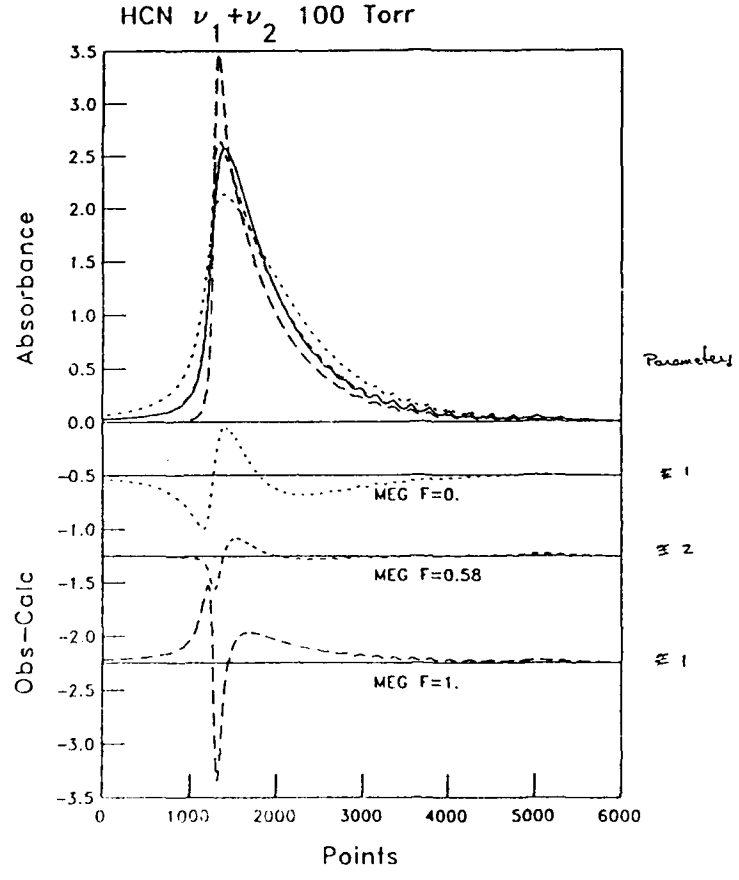
Off-Diagonal Elements (Coupling)

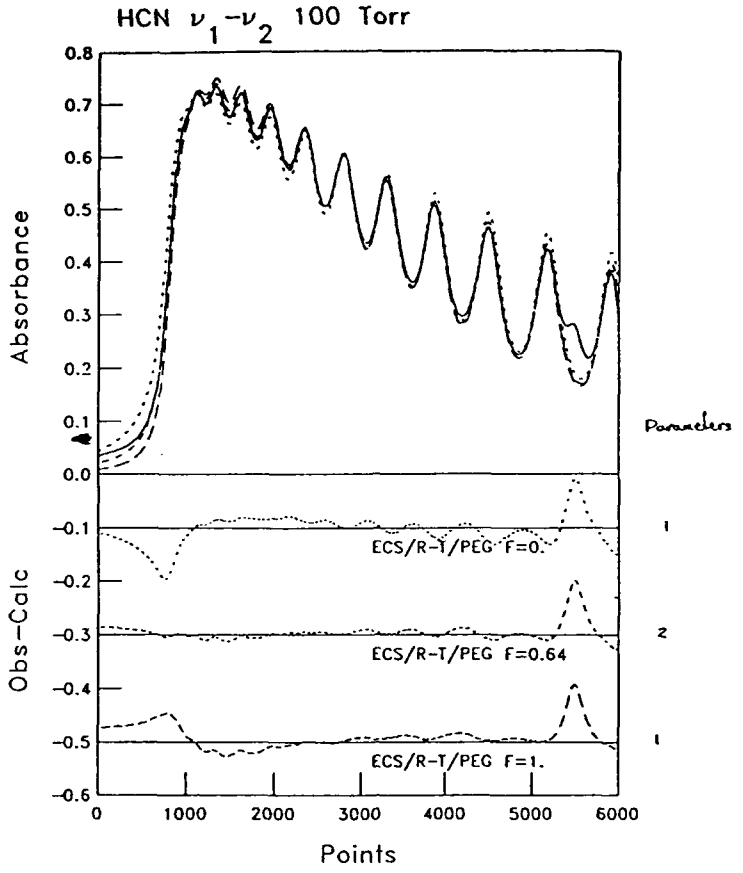
$$W_{JK} = -F\, R_{J \to K}(\Pi, f \to f)$$

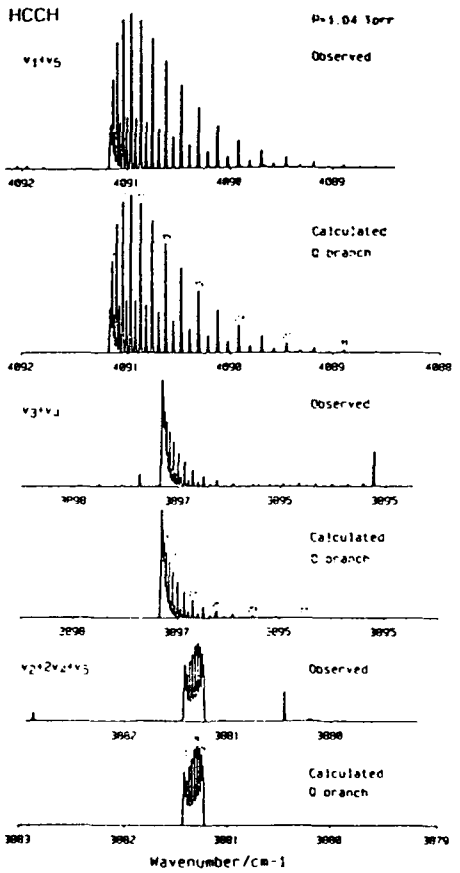
F is an empirical coupling factor.

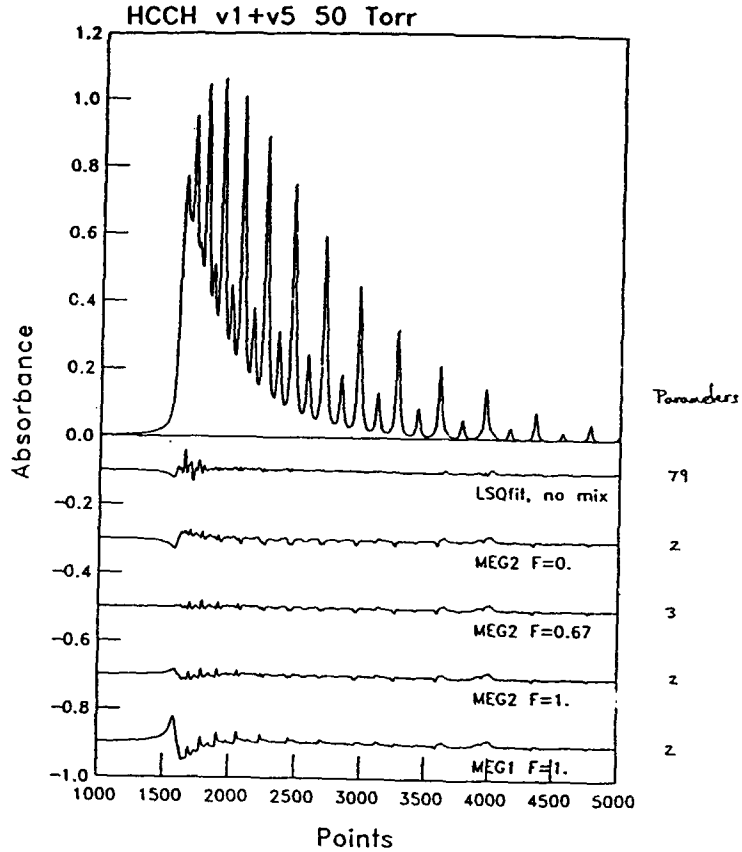


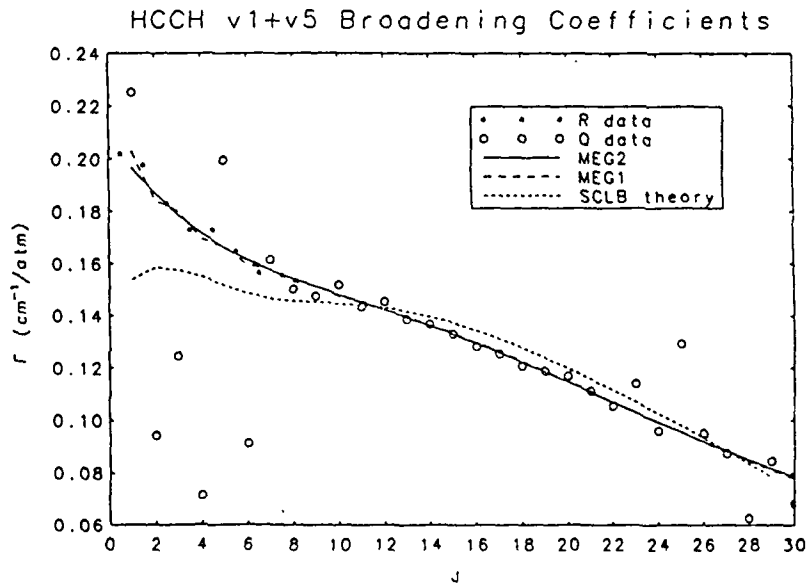

HCN $\nu_1+\nu_2$ 100 Torr
Absorbance
Obs−Calc
Points
Parameters
ECS/R-T/PEG F=0.
ECS/R-T/PEG F=0.64
ECS/R-T/PEG F=1.
≡ 1
≡ 2
≡ 1

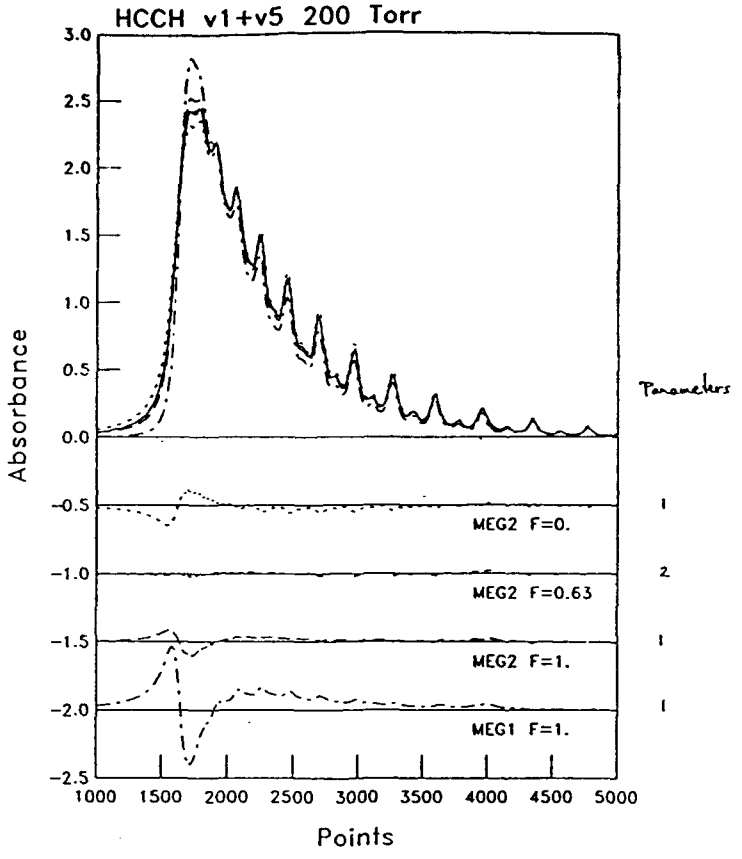

HCN $\nu_1+\nu_2$ 100 Torr
Absorbance
Obs−Calc
Points
Parameters
MEG F=0.
MEG F=0.58
MEG F=1.
≡ 1
≡ 2
≡ 1

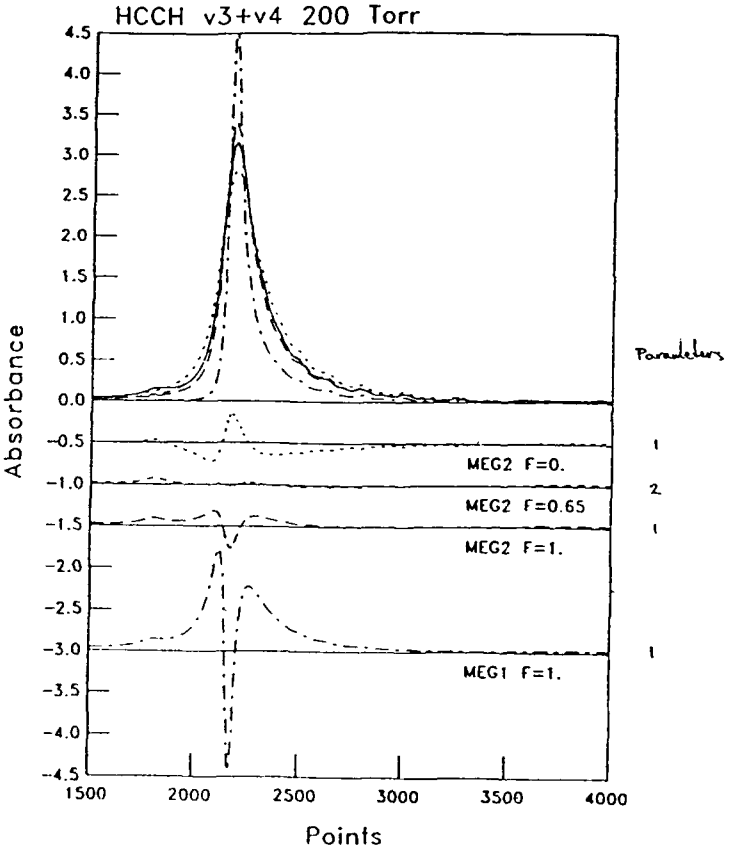

HCN $\nu_1-\nu_2$ 100 Torr
Absorbance
Obs−Calc
Parameters
ECS/R-T/PEG F=0.
ECS/R-T/PEG F=0.64
ECS/R-T/PEG F=1.
Points

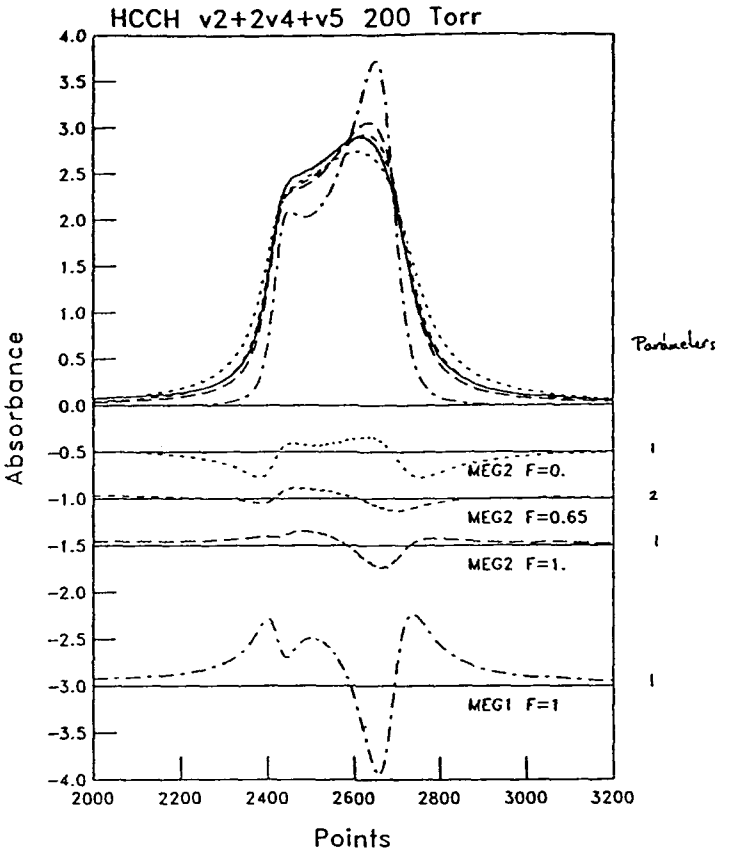

HCCH
Observed
Calculated
Q branch
Wavenumber/cm-1


HCCH v1+v5 50 Torr
Absorbance
Points
Residuals
LSQfit, no mix
MEG2 F=0.
MEG2 F=0.67
MEG2 F=1.
MEG1 F=1.


HCCH v1+v5 Broadening Coefficients
R data
Q data
MEG2
MEG1
SCLB theory
Γ (cm⁻¹/atm)
J


HCCH v1+v5 200 Torr
Absorbance
Points
Parameters
MEG2 F=0.
MEG2 F=0.63
MEG2 F=1.
MEG1 F=1.
1
2
1
1


HCCH v3+v4 200 Torr
Absorbance
Points
Parameters
MEG2 F=0.
MEG2 F=0.65
MEG2 F=1.
MEG1 F=1.
1
2
1
1


HCCH v2+2v4+v5 200 Torr
Absorbance
Points
Parameters
MEG2 F=0.
MEG2 F=0.65
MEG2 F=1.
MEG1 F=1
1
2
1
1
4.0
3.5
3.0
2.5
2.0
1.5
1.0
0.5
0.0
-0.5
-1.0
-1.5
-2.0
-2.5
-3.0
-3.5
-4.0
2000
2200
2400
2600
2800
3000
3200

STUDY OF THE CO_2 BLUE WING IN THE 4.1 μM REGION

C.T. Delaye, M.E. Thomas
Applied Physics Laboratory, The Johns Hopkins University, Laurel, MD 20723

In the 4.1 μm region, continuum type absorption by CO_2 is the blue wing of the υ_3 fundamental band. Correct modeling of absorption in the wings of CO_2 vibrational bands is required to calculate the shape of atmospheric windows.

Birnbaum's line shape is used to calculate absorption coefficients beyond 2380 cm^{-1}. This line shape allows a continuous representation from local calculations near resonance to continuum calculations in the far wings. It is incorporated in a line by line calculation, where it can be used with up to date spectroscopic databases. The calculation duplicates the shape of the wing, but not the magnitude. Line mixing effects are not taken into account in this model and an empirical scaling factor is required to match the model with the experimental data. This scaling factor remains constant below 1 atmosphere and increases, as expected, with increasing density. However, it is not possible to deduce a relation between this coefficient and the pressure. At high pressure, collision induced absorption (CIA) bands appear, which are forbidden, in the infrared. These bands are centered at 2669 cm^{-1} and at 3015 cm^{-1}, and they modify the shape of the far wing. Beyond 2380 cm^{-1}, no strong temperature dependence has been observed. Experimental data have been obtained with a 10 meter long White cell and with a 30 cm long high pressure high temperature cell. Comparisons with calculations are presented.



STUDY OF CO_2 BLUE WING IN THE 4.1 μm REGION

C. T. Delaye and M. E. Thomas
Applied Physics Laboratory
The Johns Hopkins University
Laurel, Maryland 20723

STUDY OF CONTINUUM ABSORPTION

- RADAR
- ELECTRO-OPTICAL SYSTEMS
- ATMOSPHERIC REMOTE SENSING
- INFRARED IMAGING SYSTEMS
- ATMOSPHERIC METEOROLOGY ...

CO_2

4.1 μm REGION [2380 - 2600] cm^{-1}

$CO_2 - N_2$

BIRNBAUM'S MODEL

EFFECTS OF LINE MIXING → EMPIRICAL SCALE FACTOR

In the far wing

$$g_{FW}(\omega) = \frac{i}{\pi} \left\{ \sum_i \frac{\rho_i d_i^2}{\Delta_i^2} B_{ii}(\Delta_i) + \sum_i \sum_{k \neq i} \frac{\rho_i d_k d_i}{\Delta_i \Delta_k} B_{ki}(\Delta_i) \right\}$$

$\Delta_i = \omega_i - \omega$

ρ_i POPULATION OF THE ACTIVE MOLECULE

d_i REDUCED DIPOLE MATRIX ELEMENT

$B_{ii}(\Delta_i)$ FREQUENCY DEPENDENT LINE WIDTH

$B_{ki}(\Delta_i)$ FREQUENCY DEPENDENT CROSS-RELAXATION FUNCTION WHICH PRODUCES LINE INTERFERENCE

BIRNBAUM'S MODEL:

$$B_{ii}(\Delta_i) = \gamma_{ii}\, h_{ii}(\Delta_i)$$

$$B_{ki}(\Delta_i) = \gamma_{ki}\, h_{ki}(\Delta_i)$$

$$h_{ki}(\Delta_i) = \frac{H_{ki}(\Delta_i)}{H_{ki}(0)}$$

$$H_{ki}(\Delta_i) = \frac{1}{2} \frac{\pi^{1/2}}{\Gamma(3/2)} e^{\frac{\beta \hbar \Delta_i}{2}} \cdot \frac{\tau_{ki} x K_1(x)}{1 + (\tau_0/\tau_{ki})^2}$$

$$x = |\Delta_i| [\tau_{ki}^2 + \tau_0^2]^{1/2}$$

approximations → $h_{ki}(\Delta_i) = h_{ii}(\Delta_i)$

→ $\tau_{ki} = \tau_1$

→ $\Delta_k = \Delta_i + \delta\omega$

sum rule $- \sum_{i \neq k} \rho_i d_k d_i \gamma_{ki} = \rho_i d_i^2 \gamma_{ii}$

$$g_{FW}(\omega) = \frac{1}{\pi} \left\{ \sum_i \frac{\rho_i d_i^2 \gamma_{ii}}{\Delta_i^2} h_{ii}(\Delta_i) \left[1 - (1 - \frac{\delta\omega}{\Delta_i}) \right] \right\}$$

scale factor

$$\alpha = \frac{\delta\omega}{\Delta_i}$$

MIXTURE CO_2 - N_2

$$\tau_2(CO_2 - CO_2) = \tau_2(CO_2 - N_2)$$

$$\gamma_{ij} = \gamma_{ij\,CO_2-CO_2} + \gamma_{ij\,CO_2-N_2}$$

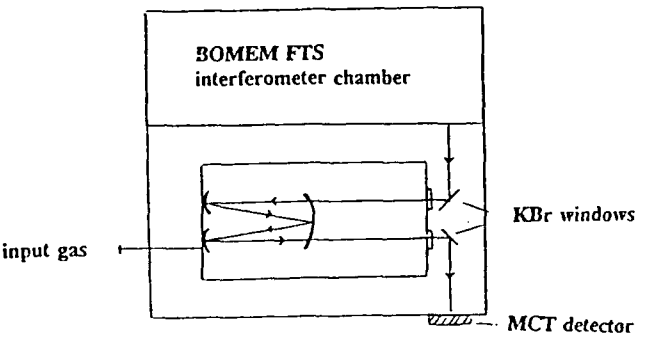
$$\rightarrow g_{FW}(\omega) = \frac{1}{\pi}\left\{\sum_j \frac{\rho_j d_j^2 \gamma_{ij}}{\Delta_j^2} h_{ij}(\Delta_j)\right\} \cdot \alpha$$

- ABSORPTION CELL

  10 M WHITE CELL
  (40 TRAVERSALS)

  P < 1 ATM

  ROOM TEMPERATURE

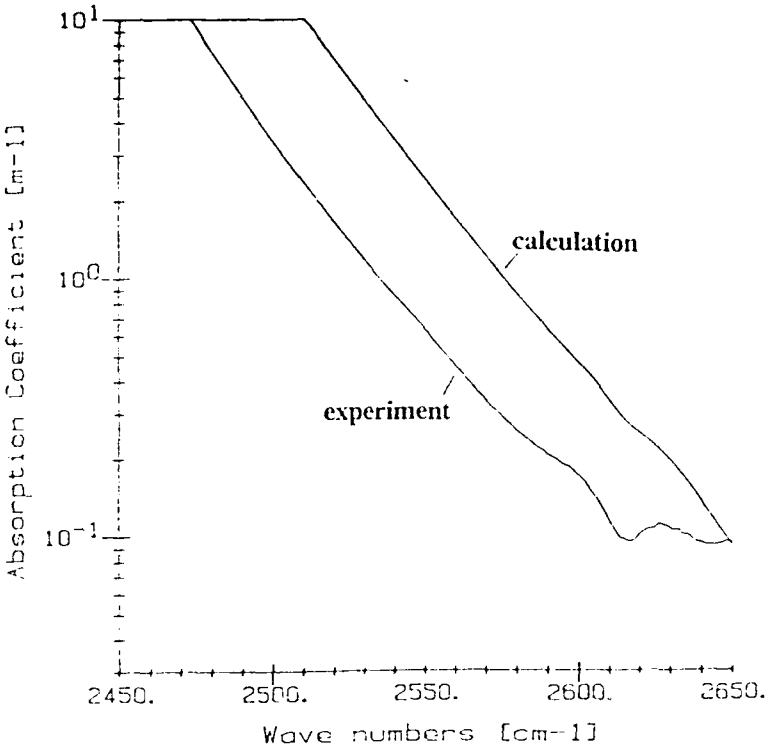


- HIGH PRESSURE - HIGH TEMPERATURE CELL

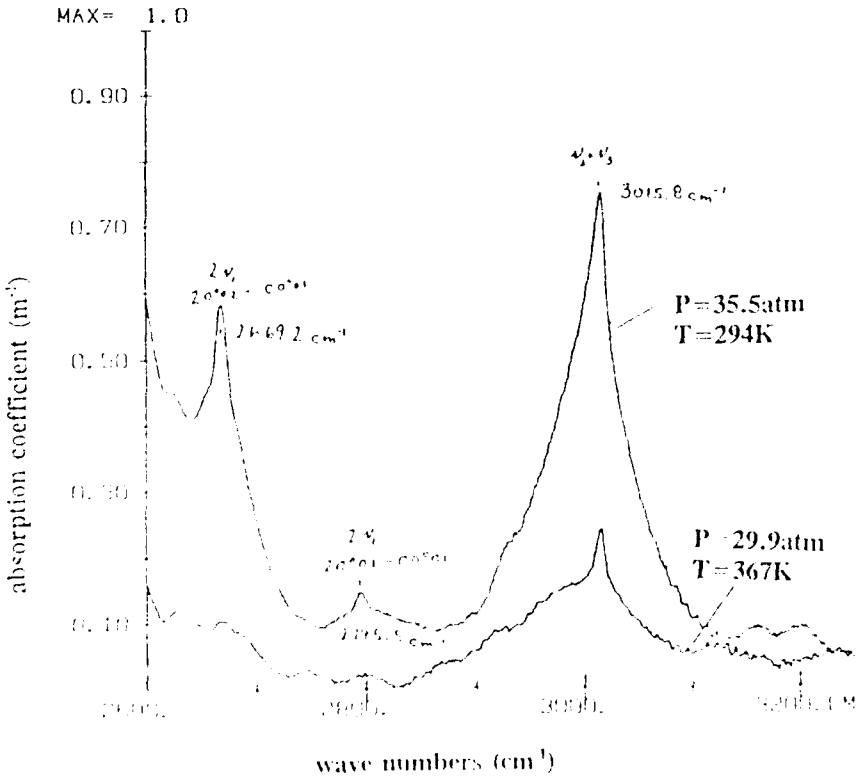
  L = 30 CM

  P = 1 ATM - 35 ATM

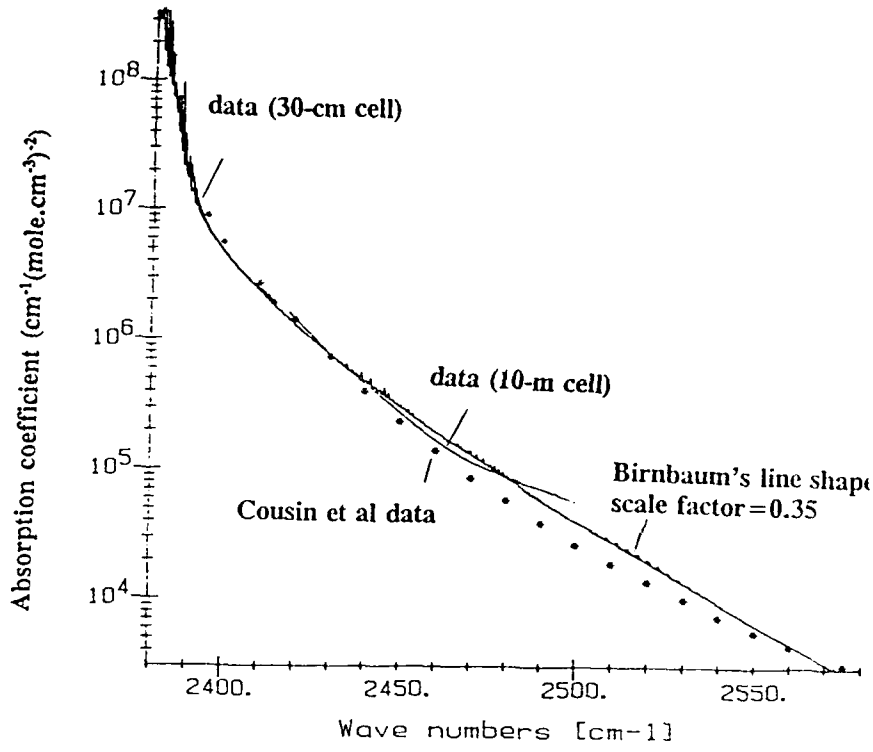
  T = 296K - 370K



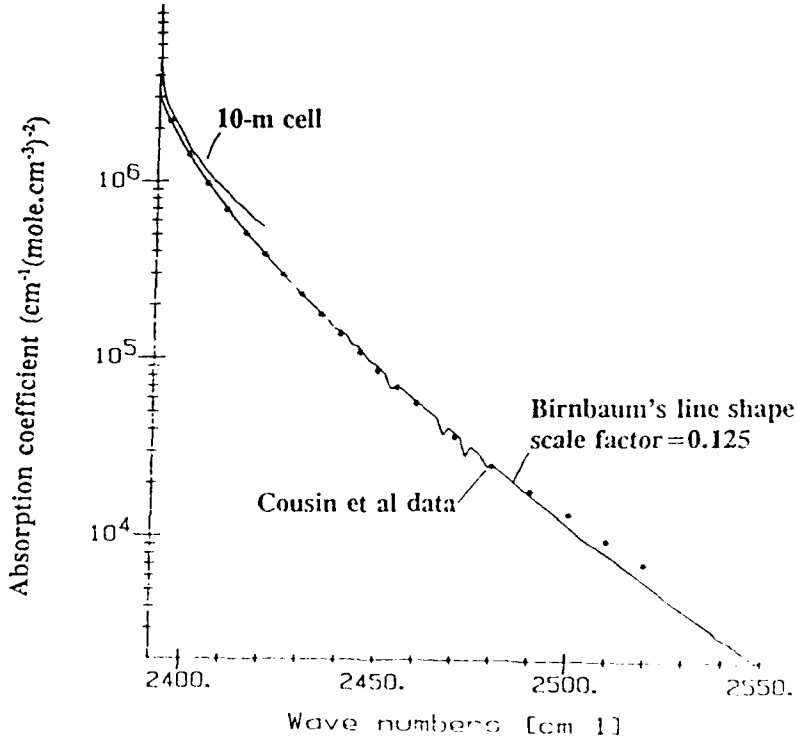
CO_2 absorption coefficient in m^{-1} at T=329K and p=28.9atm.



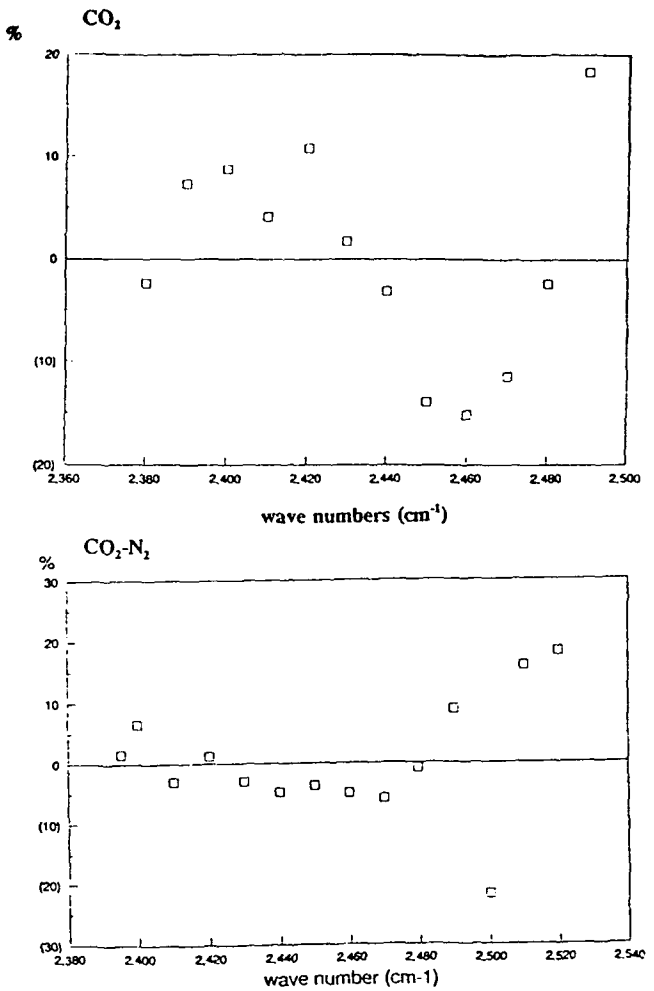
CO_2 absorption coefficient in m^{-1} at 295K and p=35.5atm and at T=367K and p=29.9atm.



CO_2 absorption coefficient in $(cm^{-1}(mole.cm^{-3})^{-2})$ at 295K.



CO_2-N_2 absorption coefficient in $(cm^{-1}(mole.cm^{-3})^{-2})$ at 295K.



Relative difference in percent between experimental and calculated data.

CO_2

T =	296K	329K	367K	534K	627K
α	0.35	0.25	0.19	0.22	0.14

CO_2-N_2

T =	296K	550K	643K
α	0.125	0.08	0.25

Scale factor α for CO_2 and CO_2-N_2 at different temperatures.

CONCLUSIONS

BIRNBAUM'S LINESHAPE

VERSATILE LINE SHAPE (H_2O,CH_4,...)

EASILY UTILIZED IN A LINE-BY-LINE CALCULATION

AGREEMENT WITH EXPERIMENTAL DATA AT ROOM TEMPERATURE FOR CO_2 AND CO_2-N_2

UNDERSTANDING OF TEMPERATURE DEPENDENCE OF THE CONTINUUM ABSORPTION
(TEMPERATURE DEPENDENCE OF THE SCALE FACTOR)

THEORETICAL APPROACH TO THE LINE WING PROBLEM

L. Sinitsa
Institute of Atmospheric Optics
Tomsk, USSR

THEORETICAL APPROACH TO THE LINE WING PROBLEM

Presented by

L. Sinitsa

Institute of Atmospheric Optics

Tomsk, USSR

Theoretical approach to the line wing problem

$$H = H_S + H_{OR} = (H_1 + H_2 + H_3 + U) + H_{OR} \qquad (1)$$

H_1 – absorbing molecule } dynamic subsystem ρ_1

H_2 – surrounding molecules } dissipative subsystem ρ_2

H_3 – kinetic energy of mass centers } dissipative subsystem ρ_3

U – intermolecular interation } interaction between subsystems Φ

⇩

First order perturbation theory in H_{OR}

$$\varkappa \sim Re \int dt e^{i\omega t} Sp\rho S^{-1}(t) M e^{-i\frac{\omega}{c}\vec{K}_0\vec{r}} \int_{\Delta V} d\vec{s}\,\delta(\vec{s}-\vec{r}) S(t) M e^{i\frac{\omega}{c}\vec{K}_0\vec{r}} \qquad (2)$$

M – dipole moment of absorbing molecule

$$ih\frac{\partial S}{\partial t} = H_S S \;,\; S(0) = 1 \;,\; \rho = \frac{1}{Z} e^{-H_S/kT}$$

⇩

Long-wave approximation

$$\varkappa \sim Re \int_0^\infty e^{i\omega t} F(t)\, dt \qquad (3)$$

⇩

Kinetic equation, semiclassical description

$$F = Sp\rho MM(t) = Sp_1 MQ \;,\; M(t) = S^{-1}MS \;,\; Q = Sp_{23}\rho M(t)$$

(ρ: U; M: U)

$$\rho = \rho_1\rho_2\Phi(V) \;,\; V = Sp_{12}\rho_1\rho_2 U$$

"classical" intermolecular potential

$$i(\omega-\omega_{mn})Q_{mn} + (M\rho_1)_{mn} = (\omega-\omega_{mn})^2 I_{mn} + J_{mn} \qquad (4)$$

(I_{mn}: $\Phi(V)$, U; J_{mn}: U)

Theoretical approach to the line wing problem

$$H = H_S + H_{OR} = (H_1 + H_2 + H_3 + U) + H_{OR} \qquad (1)$$

H_1 – absorbing molecule } dynamic subsystem ρ_1

H_2 – surrounding molecules } dissipative subsystem ρ_2

H_3 – kinetic energy of mass centers } dissipative subsystem ρ_3

U – intermolecular interation } interaction between subsystems Φ

⇩

First order perturbation theory in H_{OR}

$$\varkappa \sim Re \int dt e^{i\omega t} S_{pp} S^{-1}(t) M e^{-i\frac{\omega}{c}\bar{K}_0\bar{r}} \int_{\Delta V} d\bar{s}\,\delta(\bar{s}-\bar{r}) S(t) M e^{i\frac{\omega}{c}\bar{K}_0\bar{r}} \qquad (2)$$

M – dipole moment of absorbing molecule

$$i\hbar \frac{\partial S}{\partial t} = H_S S \;,\; S(0) = 1 \;,\; \rho = \frac{1}{Z} e^{-H_S/kT}$$

⇩

Long-wave approximation

$$\varkappa \sim Re \int_0^{\infty} e^{i\omega t} F(t)\, dt \qquad (3)$$

⇩

Kinetic equation, semiclassical description

$$F = Sp_{\rho} \rho M M(t) = Sp_1 MQ \;,\; M(t) = S^{-1} M S \;,\; Q = Sp_{23} \rho M(t)$$

(ρ: U, U)

$$\rho = \rho_1 \rho_2 \Phi(V) \;,\; V = Sp_{12} \rho_1 \rho_2 U$$

"classical" intermolecular potential

$$i(\omega - \omega_{mn}) Q_{mn} + (M\rho_1)_{mn} = (\omega - \omega_{mn})^2 I_{mn} + J_{mn} \qquad (4)$$

(I_{mn}: $\Phi(V)$, U; J_{mn}: U)

$$i(\omega - \omega_{mn}) Q_{mn} + (M\rho_1)_{mn} = (\omega - \omega_{mn})^2 I_{mn} + J_{mn} \qquad (4)$$

(I_{mn}: $\Phi(V)$, U; J_{mn}: U)

Asymptotic cases

small $\Delta\omega$	large $\Delta\omega$	
~~$(\omega - \omega_{mn})^2 I_{mn}$~~	~~J_{mn}~~	Line wing theory

$$\varkappa \sim \sum \frac{\gamma}{\gamma^2 + \Delta\omega^2} \qquad \varkappa = D_a \Sigma S_{\Delta} \omega^{-1-3/a} F(R(\Delta\omega), T) \qquad (5)$$

(F: $\Phi(V)$, U)

$$F(R(\Delta\omega), T) = \frac{1}{R_i} \int_0^{R_i} dR e^{-V(R)/kT} R (R_i^2 - R^2)^{1/2} \qquad (6)$$

(V, U)

$$R_i = C_a \Delta\omega^{-1/a} \qquad (7)$$

(R_i: U)

R_i – the root of the Equation

$$\Delta E_{mn} = \hbar\omega \qquad (8)$$

$$\Delta E_{mn} \sim \frac{C_a}{R^a} \qquad (9)$$

$$i(\omega-\omega_{mn})a_{mn}+(M\rho_1)_{mn}=(\omega-\omega_{mn})^2 I_{mn}+J_{mn} \qquad (4)$$

$I_{mn} \to \Phi(V), U$; $J_{mn} \to U$

Asymptotic cases

small $\Delta\omega$	large $\Delta\omega$	Line wing theory
~~$(\omega-\omega_{mn})^2 I_{mn}$~~	~~J_{mn}~~	

$$\varkappa \sim \sum \frac{\gamma'}{\gamma^2+\Delta\omega^2} \qquad \varkappa = D_a \Sigma S \Delta\omega^{-1-3/a} F(R(\Delta\omega),T) \qquad (5)$$

$F \to \Phi(V), U$

$$F(R(\Delta\omega),T)=\frac{1}{R_i}\int_0^{R_i} dR e^{-V(R)/kT} R(R_i^2-R^2)^{1/2} \qquad (6)$$

V, U

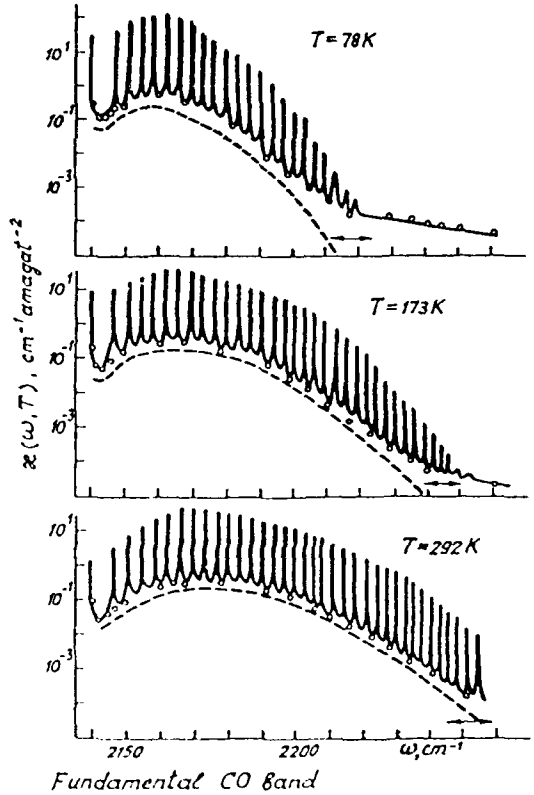
$$R_i = Ca\,\Delta\omega^{-1/a} \qquad (7)$$

$R_i \to U$

R_i - the root of the Equation

$$\Delta E_{mn}=\hbar\omega \qquad (8)$$

$$\Delta E_{mn} \sim \frac{Ca}{R^a} \qquad (9)$$

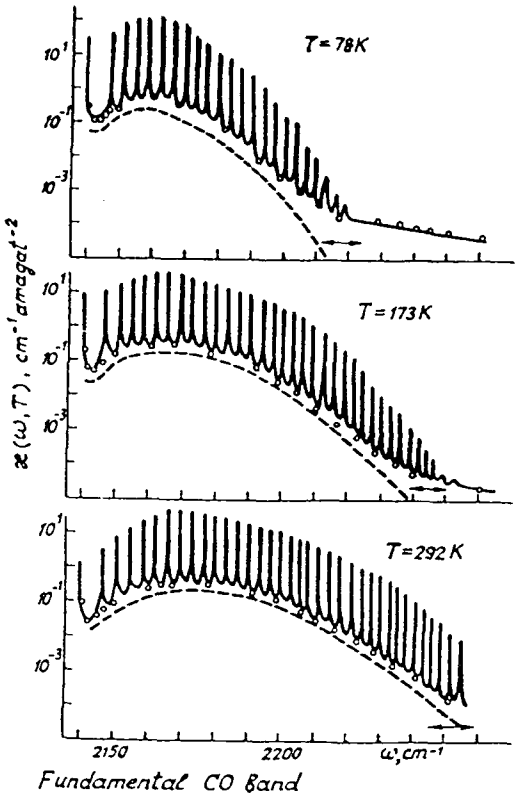


Fundamental CO Band

experiment : o - Bulanin et al (1984)

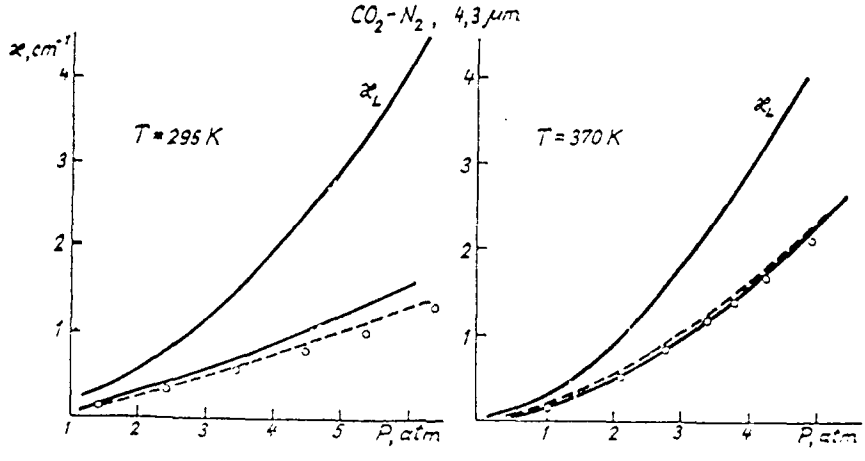
calculation : —— - line wing theory (1988)

--- calculations using four nearest lines with Lorentz profile

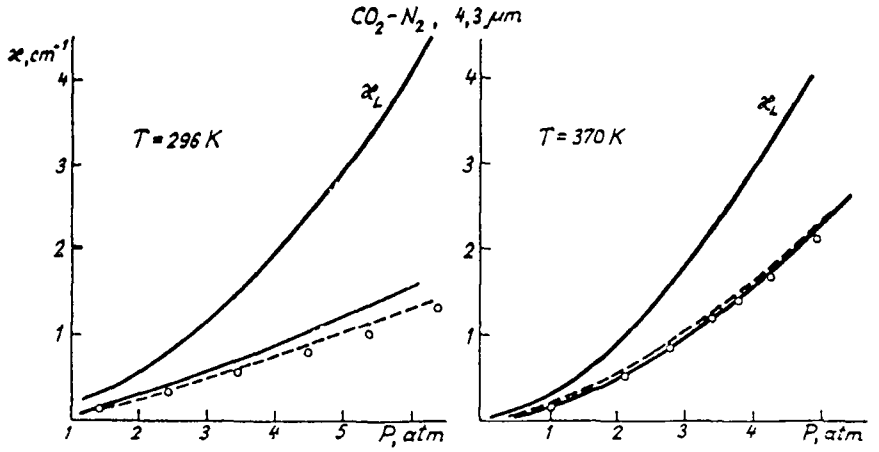


Fundamental CO Band

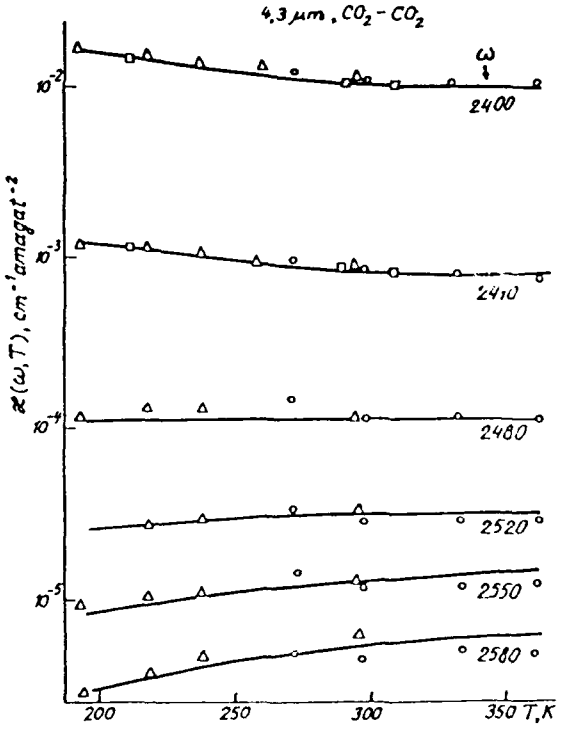
experiment : ∘ - Bulanin et al (1984)
calculation : —— line wing theory (1989)
--- calculations using four nearest lines with Lorentz profile



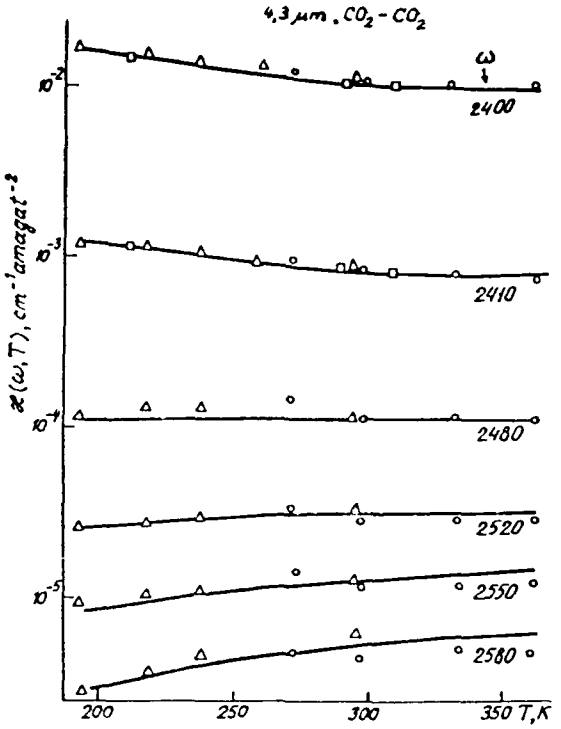
experiment between the R_{66} and R_{68} lines: ∘ } Hartman et al (1988)
calculation —— line mixing theory
--- line wing theory (1989)



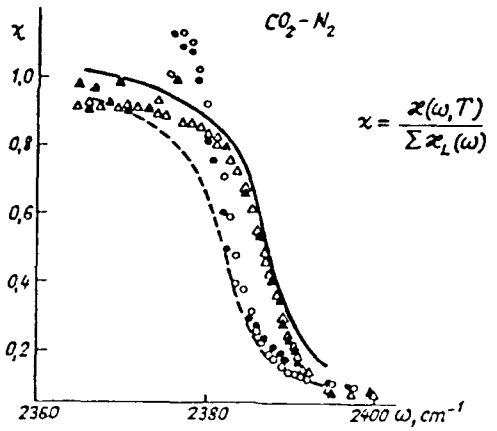
experiment between the R_{66} and R_{68} lines: ○ } Hartman et al (1988)
calculation — line mixing theory
--- line wing theory (1989)

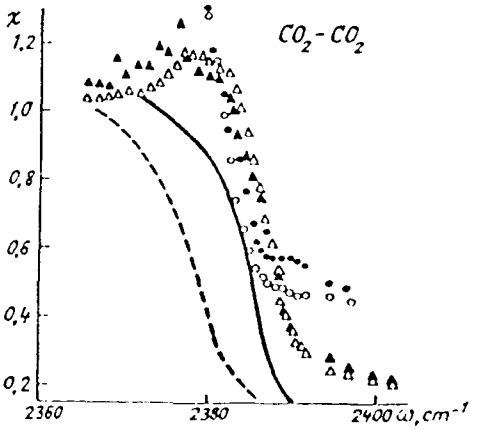


experiment : △ Le Doucen et al. (1985)
○ Gaitsev et al. (1984)
□ Bulanin et al. (1976)
calculation, line wing theory (1987)

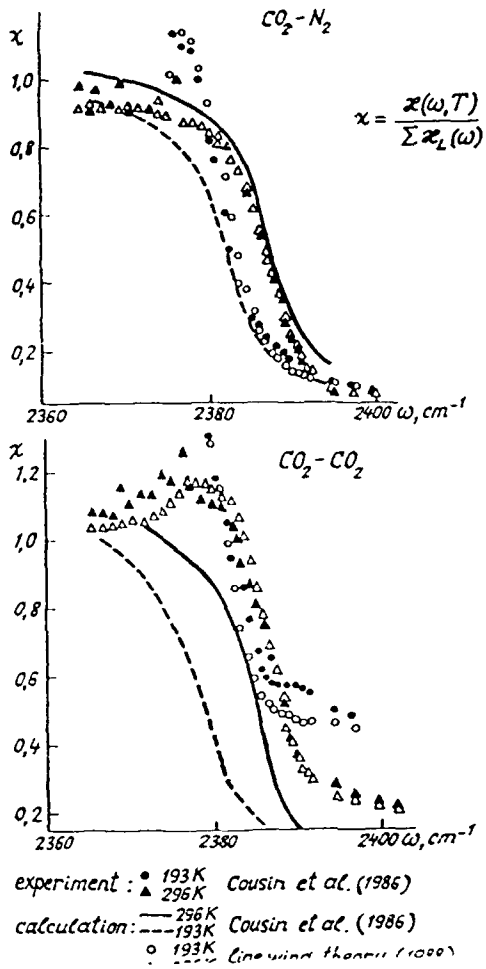


experiment : △ Le Doucen et al. (1985)
○ Galtsev et al. (1984)
□ Bulanin et al. (1976)
calculation , line wing theory (1987)





experiment : ● 193K ▲ 296K Cousin et al. (1986)
calculation : —— 296K ---- 193K Cousin et al. (1986)
○ 193K line wing theory (1988)


$CO_2 - N_2$
$\chi = \frac{\varkappa(\omega,T)}{\sum \varkappa_L(\omega)}$
χ
1,0
0,8
0,6
0,4
0,2
2360
2380
2400 ω, cm^{-1}
$CO_2 - CO_2$
1,2
1,0
0,8
0,6
0,4
0,2
2360
2380
2400 ω, cm^{-1}
experiment : 193 K 296 K Cousin et al. (1986)
calculation: 296 K 193 K Cousin et al. (1986)
193 K

DEPARTMENT OF THE AIR FORCE
GEOPHYSICS LABORATORY (AFSC)
HANSCOM AIR FORCE BASE, MASSACHUSETTS 01731-5000

REPLY TO ATTN OF: OPS/F.X. Kneizys, 617-377-3654/L.W. Abreu, 617-377-2337 28 January 1991

SUBJECT Annual Review Conference on Atmospheric Transmission Models

TO DISTRIBUTION

1. The extended DoD Plan for Atmospheric Transmission Research and Development tasks the Air Force to conduct an annual review conference to provide for tri-service discussion of model deficiencies and recommend corrective action.

2. The 14th Annual Review Conference will be held at the Geophysics Laboratory (now designated the Geophysics Directorate, Phillips Laboratory), Hanscom Air Force Base, Bedford, Massachusetts during the second week in June (11-12 June 1991). The objectives of the meeting are to review the current status of transmittance/radiance models and in hearing your recommendation regarding how we can overcome any identified deficiencies.

3. Areas of interest include molecular and aerosol effects on atmospheric radiative transfer, lidar, turbulence, remote sensing, the impact of trace atmospheric constituents on climate, and the general topic of spectral line shapes including both continua and line coupling effects.

4. This letter is intended to solicit contributions to this conference. If you would like to present a paper, please provide an unclassified abstract which should be double-spaced and no more than 12 lines. Please send abstracts to L.W. Abreu, GL/OPS (AFSC), HANSCOM AFB, MA 01731-5000 by 19 April 1991 (Telephone 617-377-2337).

5. Note all sessions will be open, and it is anticipated that foreign nationals will be permitted to attend. Allow sufficient time to obtain the necessary clearances for your papers. Immediately following this meeting, on 13-14 June the workshop on the HITRAN database will be held. For those interested in also attending this workshop, contact L.S. Rothman, GL/OPS, Hanscom AFB, MA 01731 (Telephone 617-377-2336).

6. If you plan to participate in the conference, but not make a presentation, please notify us in writing, by 19 April 1991 (non-US citizens should allow at least 6 weeks for visit approval). Send your letter to L.W. Abreu, GL/OPS (AFSC), Hanscom AFB, MA 01731-5000. (Telephone 617-377-2337). If you have any questions contact us at the numbers listed. AUTOVON prefix for Hanscom AFB is 478.

FRANCIS X. KNEIZYS
Simulation Branch
Optical Environment Division

LEONARD W. ABREU
Simulation Branch
Optical Environment Division

DEPARTMENT OF THE AIR FORCE
GEOPHYSICS LABORATORY (AFSC)
HANSCOM AIR FORCE BASE, MASSACHUSETTS 01731-5000

REPLY TO ATTN OF: OPS/F. Kneizys/617-377-3654/L.W. Abreu/617-377-2337 1 May 1991

SUBJECT: Annual Review Conference on Atmospheric Models (11-12 June 91) (OPS Ltr, 28 Jan 91, same subject)

TO: DISTRIBUTION

1. On the basis of responses to our January 28th letter announcing the Annual Review Conference on Atmospheric Transmission Models, we have constructed the enclosed tentative agenda for a two-day meeting on 11-12 June 1991. In general, we have reduced some initial time requests slightly to allow for adequate discussion. Speakers should plan on a maximum total presentation time of 15 minutes. Viewgraphs are preferable as visual aids in the talks. The meeting will be unclassified.

2. We ask that all conference speakers provide us with hard copies of viewgraphs used in your presentation at the meeting. You can either mail them to L.W. Abreu GL/CPS, Hanscom AFB, MA 01731-5000, or bring a copy to the meeting.

3. We will meet on 11-12 June (starting at 0845 on the 11th and 0830 on the 12th in the GL Science Center, Bldg 1106, Hanscom AFB. (See attached map). Please plan to arrive by 0830 on the eleventh to allow time for registration on the first day.

4. We do not intend to make motel reservations for any participants, but we have enclosed a list of motels which are reasonably close to Hanscom AFB (although you will need a car for transportation). On-base government quarters are limited, so if you require VOQ accommodations, please make your reservations early by calling 617-377-2112. The AUTOVON prefix for Hanscom AFB is 478.

Francis X. Kneizys
FRANCIS X. KNEIZYS
Simulation Branch
Optical Environment Division

Leonard W. Abreu
LEONARD W. ABREU
Simulation Branch
Optical Environment Division

3 Atchs
1. Agenda
2. Map
3. List of Motels

ANNUAL REVIEW CONFERENCE ON ATMOSPHERIC TRANSMISSION MODELS

11-12 June 1991

Geophysics Directorate, Phillips Laboratory
Hanscom Air Force Base
Science Center, Building 1106

PROGRAM

Tuesday, 11 June 1991
(0845 - 1200)

WELCOME - R.E. Good, OP/Geophysics Directorate

KEYNOTE - Col. G. Aufderhaar, USAF (OUSDA)

SESSION 1 - AEROSOLS AND CLOUDS
(Co-Chairpersons: E.P. Shettle (NRL) and J.R. Hummel (SPARTA)

"Boundary Layer Illumination Radiation Balance Model: BLIRB"
A. Zardecki (Science and Technology Corporation)

"Relations Between Giant Aerosols Near the Surface and Solar Aureole Brightness"
F.E. Volz (Geophysics Directorate)

COFFEE BREAK (1000 - 1015)

"The Computation of Radiative Transfer Through the Atmosphere Incorporating Various Aerosol Scenarios"
L.C. Rosen (University of California, Lawrence Livermore National Laboratory)

"BACKSCAT Lidar Backscatter Simulation: Version 2.0"
J.R. Hummel, D.R. Longtin, N.L. Paul, J.R. Jones (SPARTA, Inc.)

"Cirrus Cloud Transmission Modelling"
W.M. Cornette, J.G. Shanks (Photon Research Associates, Inc.)

"ICE-CLOUD - A Model for IR Transmittance Through Cirrus Cloud"
W.T. Kreiss, R. Vik (Horizons Technology, Inc.)

"The Status of the Navy Oceanic Vertical Aerosol Model"
S. Gathman (Naval Ocean Systems Center)

LUNCH (1130 - 1330)

Tuesday, 11 June 1991
(1330 - 1700)

SESSION 2 - ATMOSPHERIC PROPAGATION MODELS
Co-Chairpersons: L.W. Abreu (PL), R. Shirkey (ASL) and J.E.A. Selby (Grumman)

"MODTRAN/LOWTRAN: Current Status, Future Plans"
L.W. Abreu, F.X. Kneizys, G.P. Anderson, J.H. Chetwynd (Geophysics Directorate)

"FASCODE3: An Update"
G.P. Anderson, F.X. Kneizys, J.H. Chetwynd, L.W. Abreu, M. Hoke (Geophysics Directorate), S.A. Clough, R.D. Worsham (Atmospheric and Environmental Research, Inc.), E.P. Shettle (Naval Research Laboratory)

"EOSAEL92"
A.E. Wetmore (U.S. Army Atmospheric Sciences Laboratory)

"HITRAN'91: The Contemporary Spectroscopic Molecular Database"
L.S. Rothman (Geophysics Directorate)

"SHARC, An Atmospheric Radiation and Transmittance Code for Altitudes from 50 to 300 km"
D. Robertson, L. Bernstein, J. Duff, J. Gruninger, R. Sundberg (Spectral Sciences, Inc.), R. Sharma (Geophysics Directorate), R. Healey (Yap Analytics, Inc.)

"Recent Developments of the GENLN2 Line-by-Line Model: Studies in Support of the UARS Project"
D.P. Edwards (National Center for Atmospheric Research)

COFFEE BREAK (1500 - 1515)

"Present Status of Transmittances and Radiances Modelling at L.M.D."
N.A. Scott, A. Chédin, F. Chéruy, B. Tournier (ARA/LMD - Ecole Polytechnique)

"AURIC (Atmospheric Ultraviolet Radiance Integrated Code): an Update"
R. Huguenin, R. Hickey, K. Minschwaner (Aerodyne Research, Inc.), G.P. Anderson, L.A. Hall, R.E Huffman (Phillips Laboratory)

"Ontar's PC Compatible LOWTRAN Package"
J. Schroeder, P. Noah (Ontar Corporation)

"Coupling Atmosphere and Background Effects"
W.M. Cornette (Photon Research Associates, Inc.)

Tuesday, 11 June 1991
(1330 - 1700)

SESSION 2 - ATMOSPHERIC PROPAGATION MODELS (continued)
Co-Chairpersons: L.W. Abreu (PL), R. Shirkey (ASL) and J.E.A. Selby (Grumman)

"SENTRAN7: A Sensitivity Analysis Package for LOWTRAN7 and MODTRAN"
D.R. Longtin, F.M. Pagliughi, N.L. Paul (SPARTA, Inc.)

"Atmospheric Models in the Strategic Scene Generation Model"
W.M. Cornette, D.C. Anding (Photon Research Associates, Inc.)

"Review of the Chemical Kinetic Rate Constants Used in the SHARC Model"
V.I. Lang, A.T. Pritt, Jr., (The Aerospace Corporation)

SOCIAL HOUR/DINNER

Wednesday, 12 June 1991
(0830 - 1200)

SESSION 3 - MEASUREMENTS AND MODELS
Co-Chairpersons: G.P. Anderson (PL), R. Smith (TECOM) and H. Revercomb (Univ. of Wisconsin)

"Atmospheric Ultraviolet Radiance and its Variations"
R. Link, D.J. Strickland and D.E. Anderson Jr. (Computational Physics, Inc.)

"Photoabsorption Cross Sections in the Transmission Window Regions of the Schumann-Runge Bands of Oxygen"
K. Yoshino, J.R. Esmond, D.E. Freeman, W.H. Parkinson (Harvard-Smithsonian Center for Astrophysics), A.S-C. Cheung (Chemistry Department - University of Hong Kong)

"Incorporation of LOWTRAN7 into the ACQUIRE Model"
S.G. O'Brien (Las Cruces Scientific Consulting)

"High-resolution Spectral Measurements of Upwelling and Downwelling Atmospheric Infrared Emission with Michelson Interferometers"
H.E. Revercomb (University of Wisconsin - SSEC)

"Validation of HIS Spectral Measurements with the FASCODE Line-by-Line Model"
S.A. Clough, R.D. Worsham (Atmospheric and Environmental Research, Inc.), W.L. Smith, H.E. Revercomb, R.O. Knuteson, H.M. Woolf (U. of Wisconsin), G.P. Anderson, M.L. Hoke, F.X. Kneizys (Geophysics Directorate), M.V. Wagner, R.M. Goody (Harvard University)

"Improved HNO_3 Band Model Parameters"
N. Jones, A. Goldman, D. Murcray, F. Murcray, W. Williams (University of Denver, Department of Physics)

COFFEE BREAK (1000 - 1015)

"Line-by-line Calculations of Atmospheric Fluxes and Heating Rates"
S.A. Clough, M.J. Iacono, J.-L. Moncet (Atmospheric and Environmental Research, Inc.)

"Comparison of FASCOD2 and LOWTRAN7 Models with FIT Spectral Transmittance Measurements in the 3-12μm Region"
J.M. Thériault (DREV-Defense Research Establishment Valcartier)

"Spectral Solar Radiation Modeling, Measurement, and Data Base Activities at the Solar Energy Research Institute"
C.J. Riordan, R.L. Hulstrom (Solar Energy Research Institute)

Wednesday, 12 June 1991
(0830 - 1200)

SESSION 3 - MEASUREMENTS AND MODELS (continued)
Co-Chairpersons: G.P. Anderson (PL), R. Smith (TECOM) and H. Revercomb (Univ. of Wisconsin)

"LOWTRAN 7 Comparisons with Field Measurements"
R. Smith, N. McNabb, K. Hammerdorfer, T. Corbin (TECOM Fort Belvoir Met Team)

"Spectral Smoothing in the Fourier Domain: A Software Package for Line-by-Line Calculations"
W. Gallery (Atmospheric and Environmental Research, Inc.), M. Esplin (Stewart Radiance Lab)

"A Comparison of Computational Approaches for the Voigt Function"
F. Schreier (Deutsche Forscungsanstalt fur Luft- und Raumfahrt, Institute of Optoelectronics)

LUNCH (1200 - 1330)

Wednesday, 12 June 1991
(1330 - 1700)

SESSION 4 - TOPICAL SESSION ON SPECTRAL LINE SHAPES
Chairperson: M.L. Hoke (PL)

SESSION 4a - INVITED PAPERS

"Basis of the Water Vapor Continuum Coefficients in the GL Models"
S.A. Clough (Atmospheric and Environmental Research, Inc.)

"Water Vapor Continuum Absorption Measurements with Line Shape Interpretations"
M. Thomas (Johns Hopkins University)

"Line Coupling for Microwave Oxygen Lines"
P.W. Rosenkranz (Massachusetts Institute of Technology)

"Laboratory Measurements of Line Coupling in CO_2 and N_2O"
L.L. Strow (University of Maryland)

COFFEE BREAK (1500 - 1515)

"Line Mixing: A Near Wing and Far Wing Problem"
J.-M. Hartmann (Ecole Centrale Paris)

SESSION 4b - CONTRIBUTED PAPERS

"Far-wing Lineshape Contribution to the Water Continuum in the Millimeter and Infrared Regions"
R.H. Tipping (University of Alabama), Q. Ma (Goddard Space Flight Center)

"Laboratory Measurements of the 60-GHz O_2 Spectrum in Air"
H.J. Liebe (U.S. Department of Commerce)

"Line Coupling in Polar and Nonpolar Molecules"
A.S. Pine and J.P. Looney (NITS)

"Study of CO_2 Blue Wing in the 4.1 μm Region"
C. Delaye, M. Thomas (Johns Hopkins University)

Annual Review Conference on Atmospheric Transmission Models
11-12 June 1991
Attendance List

Name	Affiliation	Phone Number
Lt. Col. Mike Abel	ESD/WE Hanscom AFB, MA 01731-5000	617-377-3237
Mr. Leonard Abreu	PL/OPS Hanscom AFB, MA 01731-5000	617-377-2337
Mr. Donald E. Anderson, Jr.	Computer Physics, Inc. PO Box 360 Anandale, VA 22003	703-642-8728
Gail P. Anderson	PL/OPS Hanscom AFB, MA 01731-5000	617-377-2335
Stacy Angle	Loral IRIS 2 Forbes Road, Mail Stop 391 Lexington, MA 02173	617-863-3918
Roblin Antoine	ONERA(FR)	
Col. Grant Aufderhaer	OUSDA (R&AT/E&LS) The Pentagon/Room 3D129 Washington, DC 20301	703-695-9604
Stuart D. Augustin	Scitec, Inc. 100 Wall Street Princeton, NJ 08540	609-921-3892
Dr. Robert R. Beland	PL/OPA Hanscom AFB, MA 01731-5000	617-377-4604
Capt. Leslie O. Belsma	AFSD/AWS-OL-F Los Angeles AFS, CA 90009	213-416-7720
Dr. Larry Bernstein	Spectral Sciences, Inc. 111 S. Bedford Street Burlington, MA 01803	617-273-4770
Ron Bieniek	U. Missouri Rolla 102 Physics Rossa, MS 05401	314-341-4786
Dr. W. A. M. Blumberg	GL/OPS Hanscom AFB, MA 01731	617-377-3688

Annual Review Conference on Atmospheric Transmission Models
11-12 June 1991
Attendance List

Name	Affiliation	Phone Number
Barry W. Bryant	Nichols Research Corporation 251 Edgewater Drive Wakefield, MD 01880	617-246-4200
Mr. James T. Bunting	PL/LYS Hanscom AFB, MA 01731-5000	617-377-3495
Georgette Burgen	MIT/Lincoln Lab P.O. Box 73 Lexington, MA 02173-0073	617-981-2870
Mark Caccui	York University 4700 Keele Street North York, Toronto Canada M3J 1P3	416-736-2100
Dr. Ken Champion	PL/LY Hanscom AFB, MA 01731	617-377-3033
Dr. Kelly Chance	Harvard Smithsonian Center for Astrophysics 60 Garden Street Cambridge, MA 02138	617-495-7389
Frederique Cheruy	Centre National de la Recherche Scientifique Ecole Polytechnique Palaiseau Cedex F-91128 France	331-693-34533
Mr. James H. Chetwynd	PL/OPS Hanscom AFB, MA 01731-5000	617-377-2613
Robert W. Cleary	USA-Materials Technology Lab Tecom Watertown, MA 02172	617-923-5440
Marianne Clinarella	Creative Optics, Inc. One DeAngelo Drive Bedford, MA 01730	617-275-8823
Dr. William M. Cornette	Photon Research Associates, Inc. 9393 Town Center Drive San Diego, CA 92121	619-455-9741

Annual Review Conference on Atmospheric Transmission Models
11-12 June 1991
Attendance List

Name	Affiliation	Phone Number
Willam T. Creoss	Horizons Technology, Inc. 3990 Ruffin Road San Diego, CA 92123	619-292-8331
Lt. Kevin M. Crupi	Det. 10 2nd Weather Sqdn. Eglin AFB, FL 32542	904-882-5960
Frank DelGreco	PL/LIM Hanscom AFB, MA 01731	617-377-4758
John DeVore	Physical Research Inc. 350 South Hope Avenue Suite A201, PO Box 30129 Santa Barbara, CA 93130	805-682-1605
Dr. Edmond Dewan	PL/OPS Hanscom AFB, MA 01731-5000	617-377-4401
Paul Dorian	General Electric Building A, Room 37A30 PO Box 8048 Philadelphia, PA 19101	215-531-3863
Dr. Laila Dzelzkalns	GL/OPS Hanscom AFB, MA 01731	617-377-3671
Dr. John F. Ebersole	Creative Optics, Inc. One DeAngelo Drive Bedford, MA 01730	617-275-8823
Dr. David Edwards	NCAR/GOMOT Box 3000 Boulder, CO 80307	303-497-1467
Dr. Paul Eitner	General Electric Building A, Room 37A30 PO Box 8048 Philadelphia, PA 19101	215-531-1195
Vin Falcone	GP/LYS Hanscom AFB, MA 01731	617-377-4029
Hans Fast	AES (ARQX) 495 Dufferin Street Downsview, Ontario M3H 5T4 Canada	416-739-4627

Annual Review Conference on Atmospheric Transmission Models
11-12 June 1991
Attendance List

Name	Affiliation	Phone Number
Patrick Freeman	Science & Technology Corp. 555 Telshor Blvd., Suite 200 Las Cruces, NM 88001	505-678-8013
Stuart Friedenreich	NOAA/GFDL PO Box 308 Princeton, NJ 08542	609-452-6645
William O. Gallery	Atmospheric and Environmental Research, Inc. 840 Memorial Drive Cambridge, MA 02139	617-547-6207
Margaret E. Gardner	Visidyne 10 Corporate Place South Bedford Street Burlington, MA 01803	617-273-2820
Dr. Dennis Garvey	ARMY Atmospheric Sciences Laboratory White Sands Missile Range, NM 88002	505-678-5677
Stuart Gathman	NOSC, Code 4320 Naval Research Laboratory Washington, DC 20375	619-553-1418
Mimi Gerstell	Center for Earth and Planetary Physics Harvard University 29 Oxford Street Cambridge, MA 02139	617-846-9117
Dr. James R. Gillis	Boeing Aerospace PO Box 3999 MS 87-08 Seattle, WA 98124-2499	206-773-9956
Dr. R. Earl Good	PL/OP Hanscom AFB, MA 01731-5000	617-377-2951
Melanie Gouviea	STX 109 Massachusetts Avenue Lexington, MA 021378	617-862-0405
Allen S. Grossman	Lawrence Livermore National Laboratory P.O. Box 808 Livermore, CA 94550	510-423-6371

Annual Review Conference on Atmospheric Transmission Models
11-12 June 1991
Attendance List

Name	Affiliation	Phone Number
Dr. L. A. Hall	PL/LIU Hanscom AFB, MA 01731	617-377-3322
J. Hartney	MIT/Lincoln Laboratory P.O. Box 73 Lexington, MA 02173-0073	617-981-4727
Mr. Robert Hawkins	PL/OPS Hanscom AFB, MA 01731-5000	617-377-3614
Rebecca Healey	Yap Analytics 594 Marrett Road Lexington, MA 02173	617-863-1599
Mr. Glenn J. Higgins	TASC 33 Walkers Brook Drive Reading, MA 01867	617-942-2000
Don Hirst	AFTAC/Advanced Systems Patrick AFB, FL 32925-6001	407-494-2531
Helen Hoover	MIT/Lincoln Laboratory P.O. Box 73 Lexington, MA 02173-0073	617-981-2869
Mr. Robert E. Huffman	PL/LIU Hanscom AFB, MA 01731-5000	617-377-3311
Robert L. Huguenin	Aerodyne Research Inc. 45 Manning Road Billerica, MA 01821	508-663-9500
Dr. John R. Hummel	SPARTA, Inc. 24 Hartwell Avenue Lexington, MA 02173	617-863-1060
Dr. Nicole Husson	Laboratoire de Meteorologie Dynamique C.N.R.S. Ecole Polytechnique 91128 Palaiseau France	33 16933h02
Priscilla Ip	Mission Research Corporation 1 Tara Boulevard, Suite 302 Nashua, NH 03062-2801	603-891-0070

Appendix

Annual Review Conference on Atmospheric Transmission Models
11-12 June 1991
Attendance List

Name	Affiliation	Phone Number
Ronald G. Isaacs	Atmospheric and Environmental Research, Inc. 840 Memorial Drive Cambridge, MA 02139	617-547-6207
Douglas R. Jensen	Naval Ocean Systems Center San Diego, CA 92152	619-553-1415
Rana Jones	MIT	617-981-2970
Dr. Frank Kantrowitz	U.S. Army Atmospheric Sciences Lab Attn: SLCAS-AA-A White Sands Missile Range, NM 88002	505-678-1526
Dieter Klaes	PL/LYS Hanscom AFB, MA 01731	617-377-3317
Mr. Francis X. Kneizys	PL/OPS Hanscom AFB, MA 01731-5000	617-377-3654
Dr. Olga Lado-Bordowsky	Ecole Nationale Superieure de Sciences Appliques et de Technologie Universite de Rennes 6 Reude Kerampont 22305 Lannion FRANCE	33-96465030
Capt. Bob Lawconnell	USAFA, FJSRL/NP Colorado Springs, CO 80840-6528	719-472-3503
Dr. Edward Lee	GL/PL Hanscom AFB, MA 01731	617-377-2338
Dr. Hans Liebe	NTIA/TIS.S3 Boulder, CO 80303	303-497-3310
Mr. David R. Longtin	SPARTA, Inc. 24 Hartwell Avenue Lexington, MA 02173	617-863-1060
Charles LoPresti	Battelle Pacific Northwest Labs PO Box 999 MS K7-34 Richland, WA 99352	509-375-3923

Annual Review Conference on Atmospheric Transmission Models
11-12 June 1991
Attendance List

Name	Affiliation	Phone Number
Qiancheng Ma	The Goddard Institute for Space Studies 2880 Broadway New York, NY 10025	212-678-5574
Arvind S. Marathay	PL/OPS Hanscom AFB, MA 01731	617-377-2810
William R. Mark	Det 1, HQAWS SAF/SS Pentagon Room 4C, 1052 Washington DC 20330-1000	703-614-1772
Mary Martin	Complex Systems Research Center SERB University of New Hampshire Durham, NH 08324	603-862-4098
Prof. Arthur Mason	Univ. of Tennessee Space Institute Tullahoma, TN 37388	615-455-0631
Ms. Susan M. McKenzie	Atmospheric & Space Sciences Division Mission Research Corporation 1 Tara Boulevard, Suite 302 Nashua, NH 03062-2801	603-891-1986
John L. Mergenthaler	Lockheed P. A. Research Lab Org: 97-90 Bldg. 201 3251 Hanover St. Palo Alto, CA 94304	415-424-2483
Ken Minschwaner	Harvard University Center for Astrophysics 60 Garden Street Cambridge, MA 02138	617-496-8318
H. Nebel	Alfred University Dept. of Geology Alfred, NY 14802	607-871-2208
Dr. Flemming M. Nicolaisen	University of Copenhagen The H.C. Orsted Institute Universitetsparker 5 DK-2100 Kobenhavn DENMARK	

Annual Review Conference on Atmospheric Transmission Models
11-12 June 1991
Attendance List

Name	Affiliation	Phone Number
Mr. Edward R. Niple	Aerodyne Research, Inc. 45 Manning Road The Research Center at Manning Park Billerica, MA 01821-3976	508-663-9500
Paul Noah	Ontar Corp. 129 University Rd. Brookline, MA 02146	617-739-6607
Dr. Sean G. O'Brien	L.C. Scientific Consultants 3373 Solar Ridge St. Las Cruces, NM 88001	505-382-0285
Valdar Oinas	NASA Goddard Institute for Space Studies 2880 Broadway New York, NY 10025	212-778-5528
Armand J. Paboojian	ARCON Corp. 260 Bear Hill Rd. Waltham, MA 02154	617-377-2262
Ms. Nanette L. Paul	SPARTA, Inc. 24 Hartwell Avenue Lexington, MA 02173	617-863-1060
Dr. Richard H. Picard	PL/OPS Hanscom AFB, MA 01731-5000	617-377-2222
Ms. Angela Phillips	E-O & Data Systems Group Hughes Aircraft Company P.O. Box 902 El Segundo, CA 90245	213-616-0124
Damon J. Phillips	MIT/Lincoln Laboratory P.O. Box 73 Lexington, M^ 02173-0073	617-981-4716
William J. Phillips	Sverdrup Technology AEDC Group MS 900 Arnold AFS, TN 37389	615-454-4664
Chuck Pritt	Aerospace Corp. P. O. Box 92957 Los Angeles, CA 90009	213-396-6701

Appendix

Annual Review Conference on Atmospheric Transmission Models
11-12 June 1991
Attendance List

Name	Affiliation	Phone Number
Dr. Anthony Ratkowski	PL/OPS Hanscom AFB, MA 01731-5000	617-377-3655
Kenneth W. Reese	DET 3 AWS Okizaka CA	
Mr. H.E. Revercomb	Cooperative Institute for Satellite University of Wisconsin 1225 W. Dayton Street Madison, WI 53706	608-263-6758
Ms. Carol J. Riordan	Solar Energy Research Institute 1617 Cole Boulevard Golden, CO 80401-3393	303-231-1344
Dr. Rolando Rizzi	European Centre for Med. Range Weather Forecasting Shinfield Park, Reading RG2 9AX UNITED KINGDOM	447-344-99080
Dr. David C. Robertson	Spectral Sciences, Inc. 111 S. Bedford Street Burlington, MA 01803	617-273-4770
Mr. Ron Rodney	Wright Laboratory - Staff Metoeorology WRDC/WEA WPAFB, OH 45433-6543	513-255-1978
Dr. L. C. Rosen	Lawrence Livermore National Laboratory P.O. Box 808 Livermore, CA 94550	415-422-1834
P.W. Rosenkranz	Massachusetts Institute of Technology 77 Massachusetts Avenue Cambridge, MA 02139	617-253-3073
Sam Rosenzweig	SAIC 6 Fortune Drive Billerica, MA 01821	617-275-2200
Dr. Laurence S. Rothman	GL/OPS Hanscom AFB, MA 01731-5000	617-377-2336
Robert Rubio	U.S. Army Atmospheric Science Lab White Sands Missile Range, NM 88002	505-678-2926

Appendix

Annual Review Conference on Atmospheric Transmission Models
11-12 June 1991
Attendance List

Name	Affiliation	Phone Number
Ms. Crystal Schaaf	GL/LYA Hanscom AFB, MA 01731-5000	617-377-2963
Franz Schreier	DFVLR, Institut fur Optoelectronik 8031 Oberpfaffenhofen Post Wessling Federal Republic of Germany	8153 28777
Dr. John Schroeder	ONTAR Corporation 129 University Road Brookline, MA 02146	617-739-6607
Dr. Bertram D. Schurin	MS E-55-MS/G-223 Hughes Aircraft Company P.O. Box 902 El Segundo, CA 90245	213-616-6978
Noelle A. Scott	Centre National de la Recherche Scientifique Ecole Polytechnique Palaiseau Cedex F-91128 France	33-1-69334532
Dr. John E. A. Selby	Research Department, MS A08-35 Grumman Aerospace Corporation South Oyster Bay Road Bethpage, NY 11714	516-575-6608
Lt. Scott Shannon	GL/OPS Hanscom AFB, MA 01731-5000	617-377-7396
Mr. Eric P. Shettle	NRL, Code 6522 Washington, DC 20375	202-404-8152
Mr. Richard C. Shirkey	Atmospheric Sciences Laboratory DELAS-EO-S White Sands Missile Range, NM 88002	505-678-5470
Dr. Lewis L. Smith	Mail Stop A01-26 Grumman Corporate Research Center Bethpage, NY 11714-3580	516-575-2196

Appendix

Annual Review Conference on Atmospheric Transmission Models
11-12 June 1991
Attendance List

Name	Affiliation	Phone Number
Shaoann Shon	MIT/Lincoln Laboratory P.O. Box 73 Lexington, MA 02173-0073	617-275-0111
M.O. Shyluf	NOAA/GFDL PO Box 308 Princeton, NJ 08542	609-452-6521
Robert W. Smith	Chief, TECOM Ft. Belvoir Met Team AMSTE-TC-AM (BE) CCNVEO Fort Belvoir, VA 22060	703-664-1188
Dr. J. William Snow	GL/LYS Hanscom AFB, MA 01731-5000	617-377-3496
Doug Strickland	Computer Physics, Inc. PO Box 360 Anandale, VA 22003	703-642-8728
L. Larrabee Strow	University of Maryland 5401 Wilkins Avenue Baltimore, MD 21228	301-455-2528
Mr. Frank Suprin	PL/OPA Hanscom AFB, MA 01731-5000	
Capt. Andrew Terzakis	WL/WE Kirtland AFB, NM 87117-608	505-846-4722
Jean-Marc Theriault	DREV P.O. Box 8800 Courcelette, Quebec GOA 1RO Canada	418-844-4335
Patrice Y. Thrash	MIT/Lincoln Lab P.O. Box 73 Lexington, MA 02173-0073	617-981-2870
Dr. Richard H. Tipping	University of Alabama Dept. of Physics & Astronomy 206 Gallalee Box 870324 Tuscaloosa, AL 35487	205-348-3799

Appendix

Annual Review Conference on Atmospheric Transmission Models
11-12 June 1991
Attendance List

Name	Affiliation	Phone Number
C.N. Touart	STX 109 Massachusetts Avenue Lexington, MA 021378	617-862-0405
D. Shawn Turner	Atmospheric Environment Service Attn: ARMA 4905 Dufferin Street Downsview, Ontario CANADA M3H 5T4	416-739-4885
Capt. Glen Van Knowe	RL/WE Griffiss AFB, NY 13441	DSN-587-9836
Marty Venner	PL/RFT Hanscom AFB, MA 01731	805-275-5584
R.C. Vik	Horizons Technology, Inc. 3990 Ruffin Road San Diego, CA 92123	619-453-7024
Dr. Fred Volz	PL/OPS Hanscom AFB, MA 01731-5000	377-3666
R. J. Waldeon	Aerospace Corporation P. O. Box 92957 Los Angeles, CA 90009	213-416-7324
James Wallace	Far Field, Inc. 6 Thoreau Way Sudbury, MA 01776	508-443-9214
Dr. Alan E. Wetmore	Atmospheric Sciences Laboratory White Sands Missile Range, NM 88002-5501	505-678-5563
Gerald Wetzel	Institute for Meteorologie und Klimaforschung Karlsruhe Postfach 3640 D-7500 Karlsruhe 1 Federal Republic of Germany	49 07247-5947
Mr. P. P. Wintersteiner	ARCON Corporation 260 Bear Hill Road Waltham, MA 02154	617-890-3330

Appendix

Annual Review Conference on Atmospheric Transmission Models
11-12 June 1991
Attendance List

Name	Affiliation	Phone Number
Mr. Robertt D. Worsham	Atmospheric and Environmental Research, Inc. 840 Memorial Drive Cambridge, MA 02139	617-547-6207
Dr. Al S. Zachor	Atmospheric Radiation Consultants 59 High Street Acton, MA 01720	508-263-1931
Dr. Andrew Zardecki	Science & Technology Corp. 555 Telshor Blvd., Suite 200 Las Cruces, NM 88001	505-678-8013
Gerald J. Zdyb	PL/OP Hanscom AFB, MA 01731	617-377-2089

AUTHOR INDEX

Abreu, Leonard W. 64, 73
Anderson, Donald E., Jr. 202
Anderson, Gail P. 64, 73, 130, 231
Anding, David C. 173
Bernstein, Larry 107
Chédin, Alain 129
Chéruy, Frederique 129
Chetwynd, James H. 64, 73
Cheung, A.S-C. 203
Clough, Shepard A. 73, 231, 249, 333
Corbin, Ted 282
Cornette, William M. 34, 152, 173
Davies, R.W. 333
Delaye, Corinne T. 341, 441
Duff, James 107
Edwards, David P. 119
Esmond, J.R. 203
Esplin, Mark 314
Freeman, D.E. 203
Gallery, William O. 314
Gathman, Stuart 54
Goldman, Aaron 242
Goody, Richard M. 231
Gruninger, John 107
Hall, L.A. 130
Hammerdorfer, Karl 282
Hartmann, Jean-Michel 389
Healey, Rebecca 107
Hickey, R. 130
Hoke, Michael L. 73, 231
Huffman, Robert E. 130
Hugeunin, Robert L. 130
Hulstrom, Roland L. 276
Hummel, John R. 28
Iacono, Michael J. 249
Jones, James R. 28
Jones, Nicholas 242
Kneizys, Francis X. 64, 73, 231, 333
Kreiss, William T. 47
Lang, V.I. 188
Liebe, Hans J. 419
Link, R. 202
Longtin, David R. 28, 165
Looney, J.P. 429
McNabb, Norman 282
Ma, Qiancheng 409
Minschwaner, Ken 130
Moncet, Jean-Luc 249
Murcray, D. 242
Murcray, Frank 242
Noah, Paul V. 143
O'Brien, Sean G. 211
Pagliughi, Frank M. 165
Parkinson, W.H. 203
Paul, Nanette L. 28, 165
Pine, A.S. 429
Pritt, A.T., Jr. 188
Revercomb, Henry E. 215
Riordan, Carol J. 276
Roberson, David C. 107
Rosen, L.C. 17
Rosenkranz, P. W. 361
Rothman, Laurence S. 98
Schreier, Franz 320
Schroeder, John 143
Scott, Noelle A. 129
Shanks, Joseph G. 34
Sharma, R. 107
Shettle, Eric P. 73
Sinitsa, L. 449
Smith, Robert W. 282
Strickland, Douglas J. 202
Strow, Larry L. 370
Sundberg, Robert 107
Thériault, Jean-Marc 263
Thomas, Michael E. 341, 441
Tipping, Richard H. 409
Tournier, B. 129
Vik, R.C. 47
Volz, Fred E. 14
Wagner, M.W. 231
Wetmore, Alan E. 86
Williams, Walter 242
Worsham, Robert D. 73, 231
Yoshino, A. 203
Zardecki, Andrew 2